

METABOLOMIC PROFILING OF ANTIBIOFILM COMPOUNDS FROM FUNGAL
ENDOPHYTES DERIVED FROM SCOTTISH SEaweEDS

A THESIS PRESENTED FOR THE DEGREE OF DOCTOR OF PHILOSOPHY IN

THE FACULTY OF SCIENCE

THE UNIVERSITY OF STRATHCLYDE

BY

SAIF ALDEEN MOHAMMAD FAYIZ JABER

B.Sc., M.Sc.

Strathclyde Institute of Pharmacy and Biomedical Sciences

University of Strathclyde

161 Cathedral Street

Glasgow

G4 0RE

United Kingdom

This thesis is the result of the author's original research. It composed by the author and has not been previously submitted for examination which has led to award of the degree.

The copyright of the thesis belongs to the author under the terms of the United Kingdom Copyright Acts as qualified by the University of Strathclyde regulation 3.50. Due acknowledgment must always be made of the use of any material contained in or derived from this thesis.

Signed:

Date:

Acknowledgments

First, I like to show my deep thanks and how I am gratefully to Allah giving me the power to finish and to be with me in my PhD journey especially through the tough times during Covid-19 situation. I wouldn't become what I am now without the caring and the blessing from Allah.

I would like to share my gratitude to my supervisor Dr RuAngelie Edrada-Ebel for giving me the opportunity to be one of her students and for her immense knowledge, patience, support, and guidance. I owe her for helping me in growing as a researcher. No word can describe how much I am thankful to her for the time she spent on me teaching me and show me the right way in my research. In my opinion she's the best supervisor ever. I would also thank Mrs Louise Young for her help and guidance in the biological assay work and for letting me work in her lab as one of her students. In addition, I would like to thank Kirsty Neilson for helping me in collecting and identifying the seaweeds used in this study. I also would like to thank Chandani Priyadarshika Kumarapel for working directly under my supervision to assist the fractionation of *D. salina* extract scaled up on malt extract broth and the purification one of the novel compounds.

I would like to thank Dr Rothwell Tate for helping me in PCR and ITS gene sequencing. Also, I would thank Mr Craig Irving for allowing me to use their NMR facility in the pure and applied chemistry.

I am extremely grateful to Middle East University for funding me generously and being in contact with me to support me for any needs during my PhD.

I thank my fellow lab mates in the Natural Products Metabolomic Group: Dr Yahia Tabaza, Dr Mohammed Sebak, Dr Bela, Dr Marie, Dana, Chandani, Ahmad, Cora, Benjamin, Katharina, Flor for their friendship and help. I have enjoyed the times with them.

I would like to give a special thanks to Dr. Noorwini Mazlan for showing me how to work with flash chromatography instruments.

A very special gratitude goes to Dr Steve, Dr Ibrahim and Uncle Abu Ali for helping me in moving to this lovely City of Glasgow and for all my friends in the city.

I dedicated my heartfelt thanks to my dad, Dr Mohammad Jaber, my mom, Mrs Najwa Alkhatib and for my wife, Qamar AbuHassan and my brothers Omar, Mutaz, Yazan, and Ameer for their

wishes and prayer to Allah and for their support in finishing my PhD. The life without them means nothing.

A very special thanks and gratitude to my wife my second half my soulmate for supporting me and for being the happiest part of my life. She was very patience with when I was doing my lab work, writing and under stress she was standing with me specially during Covid-19. I will not forget how she was the creative mind at my home to make everything's easy to get the best of me. No words can describe how I am grateful for being her husband. The best gift from Allah was Qamar. I will pray to Allah to make me able to stand with her and support her till the rest of my life.

Table of Contents

1 General Introduction	28
1.1 Hypothesis and study aims	28
1.2 Drug discovery	29
1.2.1 Natural source for drug discovery	30
1.2.2 Combinatorial drug discovery	31
1.2.3 Computer-based drug discovery (CBDD)	33
1.3 Natural products	34
1.3.1 Anti-cancer compounds isolated from natural sources.	39
1.3.2 Anti-diabetic compounds isolated from natural sources	43
1.3.3 Anti-bacterial compounds isolated from natural sources	44
1.3.4 Advantages of natural products for drug discovery	48
1.3.5 Disadvantages of natural products for drug discovery	48
1.3.6 New approaches and technologies in utilising natural products for drug discovery ...	48
1.4 Marine environment as a source of bioactive compounds	49
1.4.1 Marine endophytes as a source of bioactive compounds	50
1.4.2 Antimicrobial agents isolated from marine endophytic fungi	54
1.5 Fungal endophytes as sources of bioactive compounds	56
1.6 Limitations of working on fungal endophytes	58
2 Materials and methods	59
2.1 Isolation and identification of endophytic fungi from collected seaweeds	59
2.1.1 Materials and equipment	59
2.1.2. Seaweed Collection	61
2.2 Microbiological Methods	62
2.2.1 Preparation of malt extract agar media and fungal inoculation from seaweeds	62
2.2.2 Initial inoculation of endophytic fungi from seaweeds	62
2.2.3 Fungal culture purification step.	62
2.2.4 Fungal extracts for screening	63
2.2.5 Taxonomical identification of antimicrobial active endophytic fungi by ITS gene sequencing	66
2.2.6 Media optimization.	68
2.3 Chemical analysis: Extraction, chromatographic separation and structure elucidation ...	73
2.3.1 Scaled-up fermentation and extraction	73

2.3.2	LC-HRMS.....	78
2.3.3	NMR spectroscopy	78
2.3.4	Medium pressure liquid chromatography (MPLC).....	79
2.3.5	Thin layer chromatography (TLC) and preparative thin layer chromatography (PTLC) 83	
2.4	The metabolomics approach used in this study.....	86
2.4.1	Chemometrics and multivariate analysis.....	88
2.4.2	Applications of metabolomics in natural product research	91
2.4.3	Multivariate analysis of spectral data	92
3	<i>Isolation and Screening of Fungal Endophytes</i>	94
3.1	Literature background on selected seaweeds for this study.....	94
3.1.1	<i>Ascophyllum nodosum</i> source of natural products	94
3.1.2	<i>Laminaria hyperborea</i> source of natural products	94
3.1.3	<i>Ulva intestinalis</i> source of natural products.....	96
3.1.4	<i>Ulva lactuca</i> source of bioactive metabolites.....	96
3.1.5	<i>Fucus vesiculosus</i> source of natural products.....	98
3.1.6	<i>Fucus spiralis</i> source of bioactive metabolites	99
3.1.7	<i>Fucus serratus</i> source of natural products.....	100
3.1.8	<i>Himanthalia elongata</i> source of natural products	100
3.2	Seaweed collection.....	101
3.3	Isolation of endophytic fungi.....	102
3.4	Fungal extraction.	104
3.5	Bioassay screening of fungal extracts.....	107
3.5.1	Alamarblue® Assay of fungal extracts:	107
3.5.2	Planktonic assay of fungal extracts:	109
3.5.3	Minimum inhibitory concentration (MIC) and Minimum biofilm eradication bacteria (MBEC) assay.....	111
3.6	NMR analysis of fungal extracts.....	112
3.7	Multivariate analysis of LC-HRMS data.....	117
3.8	ITS gene sequencing	123
3.9	Summary of the preliminary screening results	124
4	<i>Optimising the production of bioactive fungal extracts</i>	125
4.1	Optimising the production of anti-biofilm bioactive metabolites in <i>Dendryphiella salina</i>	127
4.1.1	Extract yields on different media.....	127
4.1.2	NMR spectroscopy for <i>D. salina</i> extracts.....	130
4.1.3	Anti-biofilm biological assay	139
4.1.4	Multivariate analysis of ¹ H NMR spectral data	147

4.1.5	Multivariate analysis of LC-HRMS data	149
4.2	Optimising the production of anti-biofilm bioactive metabolites produced by <i>Marianna elegance</i>	153
4.2.1	Extract yields on different media.....	153
4.2.2	NMR spectroscopy for <i>M. elegance</i> extracts.....	156
4.2.3	Anti-biofilm biological assay	165
4.2.4	Multivariate analysis of NMR data	173
4.2.5	Multivariate analysis of LC-HRMS data	176
4.3	Optimising the production of anti-biofilm bioactive metabolites produced by <i>Hypoxylon rubiginosum</i>	180
4.3.1	Extract yields on different media.....	180
4.3.2	NMR spectroscopy for <i>H. rubiginosum</i> extracts	182
4.3.3	Anti-biofilm biological assay	191
4.3.4	Multivariate analysis of NMR data	200
4.3.5	Multivariate analysis of LC-HRMS data.....	202
4.4	Summary of the media optimisation results for selected fungi	208
4.4.1	<i>Dendryphiella salina</i> optimisation.....	209
4.4.2	<i>Marianna elegance</i> optimisation	210
4.4.3	<i>Hypoxylon rubiginosum</i> optimisation	211
5	<i>Dendryphiella salina</i> scale up and isolation of antimicrobial compounds.	212
5.1.	Literature background on the endophytic fungi <i>D.salina</i>	212
5.2.	<i>Dendryphiella salina</i> on Malt Extract Broth Media with Sea Salt.....	212
5.2.1	Crude extracts and extract yields	212
5.2.2	Fractionation of the Extract and Multivariate analysis	214
5.2.3	Biological assay results of fractions	216
5.2.4	NMR spectroscopy of <i>D. salina</i> fractions.....	217
5.2.5	LC-HRMS analysis of <i>D. salina</i> MPLC fractions	220
5.2.6	Pure compounds isolation	228
5.3	<i>Dendryphiella salina</i> on Oat Solid Media without sea salt.....	251
5.3.1	Crude extracts and extract yields.....	251
5.3.2	Fractionation of the Extract.....	253
5.3.3	Antimicrobial assay results	254
5.3.4	¹ H NMR spectroscopy.....	255
5.3.5	LC-HRMS data analysis.....	261
5.3.6	Pure compounds isolation and structure elucidation	265
5.4	Biological assay results for purified fractions and isolated compounds	305
6	General Discussion	308

6.1	Metabolomics-guided and bioassay-assisted isolation of antimicrobial compounds	308
6.2	Proposed biosynthetic pathways of the isolated compounds.....	314
6.2.1	Polyketide biosynthetic pathway for orcinol, orsellinic acid and 2,5-dihydroxy-6-hydroxymethyl) benzoic acid.	314
6.2.2	Proposed biosynthetic pathway of linoleic acid and its derivatives.....	315
6.2.3	Proposed biosynthetic pathway of turnagainolide A	318
6.3	Significance of anti-biofilm activity.....	319
7	<i>General Conclusion, Future Work, and Recommendations</i>	327
8	References.....	337
9	Appendix.....	354

Abbreviations

¹³C	Carbon NMR
¹H	Proton NMR
ACN	Acetonitrile
BLAST	Basic Local Alignment Search Tool
Cosy	Correlation spectroscopy
DCM	Dichloromethane
DMSO	Dimethyl sulfoxide
DNA	Deoxyribonucleic acid
DNP	Dictionary of Natural Products
ELSD	Evaporative Light Scattering Detector
EtoAc	Ethyl acetate
FC	Flash chromatography
HMBC	Heteronuclear Multiple-Bond Correlation
HMQC	Heteronuclear Multiple Quantum Correlation
HPLC	High Performance Liquid Chromatography
HSQC	Heteronuclear Single Quantum Correlation
ITS	Internal Transcribed Spacer
JMod	J-Modulated Spin
LC-HRMS	Liquid Chromatography-High Resolution Mass Spectroscopy
MA	Malt Agar
MeOH	Methanol
min	Minute
MPLC	Medium Pressure Liquid Chromatography
MW	Molecular Weight
NCBI	National Center for Biotechnology
NMR	Nuclear Magnetic Resonance
O2-PLS	Modified Orthogonal Projections to Latent Structures
OPLS-DA	Orthogonal Partial Least squares Discriminant Analysis
OSMAC	One Strain Many Compounds
PC	Principal Component
PCA	Principal Component Analysis
PCR	Polymerase Chain Reaction
PLS-DA	Partial Least Squares, or Projections to Latent Structures-Discriminant Analysis
PTLC	Preparative Thin Layer Chromatography
SIMCA	Soft Independent Modelling by Class Analogy
TBE	TrisBorateEDTA
TLC	Thin Layer Chromatography
Tocsy	Total Correlation Spectroscopy
UK	United Kingdom
US	United States
UV	Ultraviolet

List of Figures

Figure number	Figure title
Figure 1.1	Important compounds isolated from natural sources. (1): acetylsalicylic acid, (2): salicin, (3): morphine, (4): digitoxin, (5): quinin, (6): pilocarpine and (7): penicillin.
Figure 1.2	CBDD position in drug discovery process flowchart(Gopalakrishnan et al., 2005).
Figure 1.3(A)	Examples of natural products used or modified to be used as pharmaceutical preparations.
Figure 1.3 (B):	Examples of natural products used or modified to be used as pharmaceutical preparations.
Figure 1.4	All new approved drugs 1981 – 2014; <i>n</i> = 1562, B: Biological macromolecule, 1997, N: Unaltered natural product, 1997, NB: Botanical drug (defined mixture), 2012, ND: Natural product derivative, 1997, S: Synthetic drug, 1997, S*: Synthetic drug (NP pharmacophore), 1997, V: Vaccine, 2003, /NM: Mimic of natural product, 2003 (Newman and Cragg, 2016).
Figure 1.5:	Anti-cancer chemical agents isolated from plants (Sacks et al., 1973, Williams et al., 1987, Creemers et al., 1996, Cragg et al., 1997, Kelland, 2000)
Figure 1.6:	Anti-cancer chemical agents isolated from microorganism (Sacks et al., 1973, Williams et al., 1987, Creemers et al., 1996, Cragg et al., 1997, Kelland, 2000).
Figure 1.7:	Chemical compounds isolated from natural sources used to reduce blood glucose level in DM patient.
Figure 1.8:	Timeline represents the discovery of novel antimicrobial compounds from natural source (Walsh, 2003).
Figure 1.9:	Examples of antibiotic compounds isolated from natural sources.
Figure 1.10	First bioactive compounds isolated from a marine source.
Figure 1.11	Examples of chemical compounds isolated from endophytic microorganisms.
Figure 1.12	Chemical structures of known bioactive compounds isolated from marine endophytes.
Figure 1.13	Chemical structure of novel compounds isolated from endophytes isolated from marine source.
Figure 1.14	Anti-microbial compounds produced by endophytic fungi.
Figure 1.15	Bioactive compounds isolated from endophytic fungi; anti-cancer bioactive compounds (1-3), anti-oxidant compounds (4-6), immunomodulatory compounds (7-8) and anti-bacterial compounds (9-11) (Strobel et al., 2002, Harper et al., 2003, Puri et al., 2005, Kour et al., 2008, Kusari et al., 2009, Zhao et al., 2012).
Figure 2.1	Schematic diagram for the preparation of crude fungal extracts.
Figure 2.2	Map representing samples on gel electrophoresis plate.
Figure 2.3	Schematic diagram for media optimisation work.
Figure 2.4	Schematic diagram represents extraction procedure for both liquid and solid medias.
Figure 2.5	Workflow for sample analysis.

Figure 2.6	Workflow for scale-up fermentation to pure compounds isolation.
Figure 2.7	Preparation of crude extracts of <i>D. salina</i> for liquid-liquid partitioning.
Figure 2.8	Schematic diagram of liquid-liquid partitioning of <i>D. salina</i> extract grown on malt extract with sea salt.
Figure 2.9	Schematic diagram showing the isolation of pure compounds produced by <i>D. salina</i> grown on malt extract media with sea salt.
Figure 2.10	Schematic diagram of liquid-liquid partitioning of <i>D. salina</i> extract grown on oat media.
Figure 2.11	Schematic diagram showing the isolation of pure compounds produced by <i>D. salina</i> grown on oat media without sea salt.
Figure 2.12	The omics flow (Dettmer et al., 2007).
Figure 2.13	“A data matrix of size $I \times K$ is reduced to smaller matrices of size $I \times A$ and $A \times K$ ($A \ll \min(I, K)$), which are easier to interpret and understand, and contain all the relevant information. Noise and other disturbances are left in the residual matrix of size $I \times K$. A general name for the reduced data is latent variables”. Example of metabolomics (Geladi, 2003).
Figure 2.14	Examples of scores plots for two PCs (Geladi, 2003). As the figure depicts, cluster A shows less variation, as it is denser than the spread-out in cluster B which reveals more variation. In some situations, outliers and a gradient between the pure classes A and B might be observed.
Figure 3.1	Examples of compounds isolated from <i>A. nodosum</i> (Kadam et al., 2015)
Figure 3.2	Chemical structure of alginate hydrocolloidal compounds isolated from <i>L. hyperborea</i> .
Figure 3.3	Chemical structure of (1,3)- β -D-glucan building unit of laminarin compounds isolated from <i>L. hyperborea</i> .
Figure 3.4	Ulvan polysaccharides isolated from <i>U. intestinalis</i> .
Figure 3.5	Chemical structure of some compounds produced by <i>U. lactuca</i>
Figure 3.6	Chemical structures of some reported bioactive compounds isolated from <i>Fucus vesiculosus</i>
Figure 3.7	Some phenolic compounds produced by <i>F. spiralis</i> seaweed.
Figure 3.8	Chemical structure of some compounds produced by <i>H. elongata</i> .
Figure 3.9	Yield of extracts produced by isolated endophytic fungi. A: Fast- and B: slow-growing fungi. The red columns represent the bioactive extracts against both biofilm-forming <i>S. aureus</i> and <i>P. aeruginosa</i> .
Figure 3.10	AlamarBlue® Assay results of 100 μ g/mL of fungal extracts against biofilm-forming <i>S. aureus</i> and <i>P. aeruginosa</i> .
Figure 3.11	Planktonic assay results after applying 100 μ g/mL of each fungal extracts against both biofilm-forming <i>S. aureus</i> and <i>P. aeruginosa</i> .
Figure 3.12	MIC results of active fungal extracts against biofilm-forming <i>S. aureus</i> and <i>P. aeruginosa</i> .
Figure 3.13	MBEC results of active fungal extracts against biofilm-forming <i>S. aureus</i> and <i>P. aeruginosa</i> .
Figure 3.14	Stacked ^1H NMR data of fungal extracts obtained from isolated endophytic fungi from some Scottish seaweeds along with MA blank. A: a blank extraction followed by fungal extracts from 12 endophytes and B: a blank

	extract and 13 fungal extracts. Sample's concentration is 5mg/600µl of DMSO- <i>d</i> ₆ (400MHz).
Figure 3.15	Stacked H ¹ NMR spectrum of bioactive fungal extracts along with MA blank in the bottom. Sample concentration was at 5mg/600µl of DMSO- <i>d</i> ₆ (400MHz). Highlighted peaks are resonances belonging to the MA medium.
Figure 3.16	PCA scatter plot of the NMR spectral data of the respective fungal extracts.
Figure 3.17	OPLS-DA scatter plot of the NMR spectral data of the fungal extracts grouped according to their antimicrobial assay result against both biofilm-forming <i>S. aureus</i> and <i>P. aeruginosa</i> .
Figure 3.18	OPLS-DA loadings plot NMR spectral data of the fungal extracts grouped according to their antimicrobial assay result against both biofilm-forming <i>S. aureus</i> and <i>P. aeruginosa</i> .
Figure 3.19:	PCA scatter plot of the mass spectral data obtained for the respective fungal extracts.
Figure 3.20	OPLS-DA scatter plot of the mass spectral data of the fungal extracts grouped according to their antimicrobial assay results against both biofilm-forming <i>S. aureus</i> and <i>P. aeruginosa</i> .
Figure 3.21	OPLS-DA loadings plot of the mass spectral data of the fungal extracts grouped according to their antimicrobial assay results against both biofilm-forming <i>S. aureus</i> and <i>P. aeruginosa</i> . Encircled in red are the discriminating features for the bioactive extracts found in the respective quadrants of the scatter plot (Figure 3.20).
Figure 3.22	Putatively dereplicated compounds afforded by antimicrobial active fungal extracts
Figure 3.23	Variable trend of the known discriminating features assigned on OPLS-DA loading plot.
Figure 3.24	Total Ion Chromatogram (TIC) of both positive and negative modes produced from blank and active extracts. Yellow line represents blank media.
Figure 3.25	Electrophoresis gel image of the PCR results of two fungal samples with a blank sample to quality control the DNA amplification procedure.
Figure 4.1	Chemical structure of compounds earlier isolated from selected fungi for optimisation.
Figure 4.2	Histogram of extract yields obtained from various liquid (A) and solid (B) media used to incubate <i>D. salina</i> extracts at 7-, 15-, and 30-days.
Figure 4.3	Proton NMR spectra of fungal extracts obtained from ME with salt (A) and without sea salt (B). Spectrum 1 at the bottom of each of the stack represents the blank followed by three incubation periods of 7, 15 and 30 days, respectively. Differences are shown in blue boxes.
Figure 4.4	Proton NMR spectra for fungal extracts obtained from Wickersham liquid with salt (A) and without sea salt (B). Spectrum 1 at the bottom of each stack represents the blank followed by the three incubations periods of 7, 15 and 30 days, respectively. Differences are indicated in blue boxes.
Figure 4.5	Proton NMR spectra of extracts obtained from marine broth extracts and blank media; blank followed by the three incubation periods at 7, 15, and 30 days, respectively. Observed differences are shown in blue boxes.
Figure 4.6	Proton NMR spectra of fungal extracts obtained from rice media with salt (A) and without sea salt (B). Spectrum 1 from each stack represents the blank followed by three incubation periods of 7, 15 and 30 days respectively.

Figure 4.7	Proton NMR spectra obtained from both oat media with salt (A) and without sea salt (B). Spectrum 1 at the bottom of the stack represents the blank followed by the three incubation periods at 7, 15, and 30 days, respectively. Differences are shown in blue boxes.
Figure 4.8	Percentage bacterial inhibition of biofilm-forming <i>S. aureus</i> with 100µg/mL of <i>D. salina</i> extracts obtained from various A : liquid and B : solid media.
Figure 4.9	Percentage bacterial inhibition of biofilm-forming <i>P. aeruginosa</i> with 100µg/mL of <i>D. salina</i> extracts obtained from various A : liquid and B : solid media.
Figure 4.10	Percentage biofilm inhibition for <i>S. aureus</i> by 100µg/mL of <i>D. salina</i> extracts obtained from various A : liquid and B : solid media.
Figure 4.11	Percentage biofilm inhibition of <i>P. aeruginosa</i> bacteria against 100µg/mL of <i>D. salina</i> extracts obtained from various A : liquid and B : solid media.
Figure 4.12	MIC results of active <i>D. salina</i> extracts against <i>S. aureus</i> . A : <i>D. salina</i> malt extract without sea salt, B : <i>D. salina</i> malt extract with sea salt, C : <i>D. salina</i> oat extract without sea salt, and D : <i>D. salina</i> oat extracts with sea salt.
Figure 4.13	MIC results of active <i>D. salina</i> extracts against <i>P. aeruginosa</i> . A : <i>D. salina</i> malt extract without sea salt, B : <i>D. salina</i> malt extract with sea salt, C : <i>D. salina</i> oat extracts without sea salt, and D : <i>D. salina</i> oat extracts with sea salt.
Figure 4.14	MBEC results of active <i>D. salina</i> extracts against <i>S. aureus</i> . A : <i>D. salina</i> malt extract without sea salt, B : <i>D. salina</i> malt extracts with sea salt, C : <i>D. salina</i> oat extract without sea salt, and D : <i>D. salina</i> oat extract with sea salt.
Figure 4.15	MBEC results of active <i>D. salina</i> extracts against <i>P. aeruginosa</i> . A : <i>D. salina</i> malt extracts without sea salt, B : <i>D. salina</i> malt extracts with sea salt, C : <i>D. salina</i> oat extracts without sea salt, and D : <i>D. salina</i> oat extracts with sea salt.
Figure 4.16	PCA scatter plot of proton NMR spectral of <i>D. salina</i> extracts from various media incubated at 7, 15, and 30 days. ME-s: malt extract without sea salt, ME+s: malt extract with sea salt, W-s: Wickersham broth without sea salt, W+s: Wickersham with sea salt, MB: marine broth, R-s: rice without sea salt, R+s: rice with sea salt, O-s: oat without sea salt and O+s: oat with sea salt. Each media extract acronym followed by its incubation duration.
Figure 4.17	OPLS-DA scatter and loadings plots of the NMR spectral data of various fungal extracts classified according to their AlamarBlue® and planktonic assay results.
Figure 4.18	PCA scatter plot of LC-HRMS data of fungal extracts from various media.
Figure 4.19	OPLS-DA scatter and loading plots of LC-HRMS data of fungal extracts grouped according to their antibacterial activity against both biofilms forming <i>S. aureus</i> and <i>P. aeruginosa</i> .
Figure 4.20	Putative structures of dereplicated target bioactive metabolites found in the anti-microbial extracts obtained from the oat media.
Figure 4.21	Total Ion Chromatogram (TIC) of the active media extracts. The ion peaks that represent the discriminating features listed in Table 4.6 have been labelled

Figure 4.22	Diagrams represent the weights of fungal extracts obtained from : (A) liquid and (B) solid media on 15 and 30 days of incubation periods at 27C°.
Figure 4.23	Stacked ¹ H NMR spectra of fungal extracts obtained from malt extract liquid media with (A) and without sea salt (B). Spectrum 1 at the bottom of each of the stack represents the blank followed by those incubated at 15 and 30 days, respectively. The differences are highlighted in blue boxes.
Figure 4.24	Stacked ¹ H NMR spectra of fungal extracts obtained from Wickersham liquid media with (A) and without sea salt (B). Spectrum 1 at the bottom of each of the stack represents the blank followed by those incubated at 15 and 30 days, respectively. The differences are highlighted in blue boxes.
Figure 4.25	Stacked ¹ H NMR spectra of <i>M. elegance</i> extracts obtained from marine broth media. Spectrum 1 at the bottom of the stack represents the blank followed by those incubated at 15 and 30 days, respectively. The differences are highlighted in blue boxes.
Figure 4.26	Stacked ¹ H NMR spectra of fungal extracts obtained from rice media with (A) and without sea salt (B). Spectrum 1 at the bottom of each of the stack represents the blank followed by those incubated at 15 and 30 days, respectively. The differences are highlighted in blue boxes.
Figure 4.27	Stacked ¹ H NMR spectra of fungal extracts obtained from oat media with (A) and without sea salt (B). Spectrum 1 at the bottom of each of the stack represents the blank followed by those incubated at 15 and 30 days, respectively. The differences are highlighted in blue boxes and circles.
Figure 4.28	Percentage bacterial inhibition of biofilm-forming <i>S. aureus</i> with 100µg/mL of <i>M. elegance</i> extracts obtained from various A: liquid and B: solid media.
Figure 4.29	Percentage bacterial viability of biofilm-forming <i>P. aeruginosa</i> with 100µg/mL of <i>M. elegance</i> extracts obtained from various A: liquid and B: solid media.
Figure 4.30	Percentage biofilm inhibition of biofilm-forming <i>S. aureus</i> with 100µg/mL of <i>M. elegance</i> extracts obtained from various A: liquid and B: solid media.
Figure 4.31	Percentage biofilm inhibition of biofilm-forming <i>P. aeruginosa</i> with 100µg/mL of <i>M. elegance</i> extracts obtained from various A: liquid and B: solid media.
Figure 4.32	MIC results of active <i>M. elegance</i> extracts against <i>S. aureus</i> . A: MIC of <i>M. elegance</i> growing malt extracts without sea salt, B: MIC of <i>M. elegance</i> growing on malt extracts with sea salt, C: MIC of <i>M. elegance</i> growing on oat extracts without sea salt, and D: MIC of <i>M. elegance</i> growing on oat extracts with sea salt.
Figure 4.33	MIC results of active <i>M. elegance</i> extracts against <i>P. aeruginosa</i> . A: MIC of <i>M. elegance</i> growing malt extracts without sea salt, B: MIC of <i>M. elegance</i> growing on malt extracts with sea salt, C: MIC of <i>M. elegance</i> growing on oat extracts without sea salt, and D: MIC of <i>M. elegance</i> growing on oat extracts with sea salt.
Figure 4.34	MBEC results of active <i>M. elegance</i> extracts against <i>S. aureus</i> . A: MIC of <i>M. elegance</i> growing malt extracts without sea salt, B: MIC of <i>M. elegance</i> growing on malt extracts with sea salt, C: MIC of <i>M. elegance</i> growing on oat extracts without sea salt, and D: MIC of <i>M. elegance</i> growing on oat extracts with sea salt.

Figure 4.35	MBEC results of active <i>M. elegans</i> extracts against <i>P. aeruginosa</i> . A: MIC of <i>M. elegans</i> growing malt extracts without sea salt, B: MIC of <i>M. elegans</i> growing on malt extracts with sea salt, C: MIC of <i>M. elegans</i> growing on oat extracts without sea salt, and D: MIC of <i>M. elegans</i> growing on oat extracts with sea salt.
Figure 4.36	PCA scatter plot of NMR spectral data of <i>M. elegans</i> extracts obtained from various growth media incubated at 15 and 30 days.
Figure 4.37	OPLS-DA scatter (A) and loading (B) plots of the NMR spectral data of <i>M. elegans</i> extracts obtained from various growth media incubated at 15 and 30 days. Extracts were classified according to their antimicrobial activity against both biofilm-forming <i>S. aureus</i> and <i>P. aeruginosa</i> .
Figure 4.38	PCA scatter plot obtained from LC-HRMS data of <i>M. elegans</i> extracts obtained from various media incubated for 15 and 30 days.
Figure 4.39	OPLS-DA scatter plot of LC-HRMS data of <i>M. elegans</i> extracts obtained from various media incubated at 15 and 30 days. Extracts were grouped according to their antimicrobial activity against both biofilm-forming <i>S. aureus</i> and <i>P. aeruginosa</i> .
Figure 4.40	OPLS-DA loadings plot of LC-HRMS data of <i>M. elegans</i> extracts obtained from various media incubated at 15 and 30 days. Group of discriminating features for antimicrobial active extracts is encircled in red.
Figure 4.41	Total Ion Chromatogram (TIC) of the active fraction. The ion peaks that represent the discriminating features listed in Table 4.12 have been labelled.
Figure 4.42	Histogram of extract weights of <i>H. rubiginosum</i> obtained from various (A) liquid and (B) solid media incubated for 15 and 30 days.
Figure 4.43	Stacked ¹ H NMR spectra of <i>H. rubiginosum</i> extracts obtained from malt extract liquid media with (A) and without sea salt (B). Spectrum 1 at the bottom of each of the stack represents the blank followed by those incubated at 15 and 30 days, respectively. The differences are highlighted in blue boxes.
Figure 4.44	Stacked ¹ H NMR spectra of <i>H. rubiginosum</i> extracts obtained from Wickersham liquid media with (A) and without sea salt (B). Spectrum 1 at the bottom of each of the stack represents the blank followed by those incubated at 15 and 30 days, respectively. The differences are highlighted in blue boxes.
Figure 4.45	Stacked ¹ H NMR spectra of <i>H. rubiginosum</i> extracts obtained from marine broth media. Spectrum 1 at the bottom of the stack represents the blank followed by those incubated at 15 and 30 days, respectively. The differences are highlighted in blue boxes.
Figure 4.46	Stacked ¹ H NMR spectra of <i>H. rubiginosum</i> extracts obtained from rice media with (A) and without sea salt (B). Spectrum 1 at the bottom of each of the stack represents the blank followed by those incubated at 15 and 30 days, respectively. The differences are highlighted in blue boxes.
Figure 4.47	Stacked ¹ H NMR spectra of <i>H. rubiginosum</i> extracts obtained from oat media with (A) and without sea salt (B). Spectrum 1 at the bottom of each

	of the stack represents the blank followed by those incubated at 15 and 30 days, respectively. The differences are highlighted in blue boxes.
Figure 4.48	Percentage bacterial inhibition of biofilm-forming <i>S. aureus</i> with 100µg/mL of <i>H. rubiginosum</i> extracts obtained from various A : liquid and B : solid media.
Figure 4.49	Percentage bacterial inhibition of biofilm-forming <i>P. aeruginosa</i> with 100µg/mL <i>H. rubiginosum</i> extracts obtained from various A : liquid and B : solid media.
Figure 4.50	Percentage biofilm inhibition of biofilm-forming <i>S. aureus</i> with 100µg/mL of <i>H. rubiginosum</i> extracts obtained from various A : liquid and B : solid media.
Figure 4.51	Percentage bacterial inhibition of biofilm-forming <i>P. aeruginosa</i> with 100µg/mL <i>H. rubiginosum</i> extracts obtained from various A : liquid and B : solid media.
Figure 4.52	MIC results of antibacterial <i>H. rubiginosum</i> extracts against <i>S. aureus</i> . A: MIC of <i>H. rubiginosum</i> growing rice media without sea salt, B: MIC of <i>H. rubiginosum</i> growing on rice media with sea salt, C: MIC of <i>H. rubiginosum</i> growing on oat extracts without sea salt, and D: MIC of <i>H. rubiginosum</i> growing on oat extracts with sea salt.
Figure 4.53	MIC results of antibacterial <i>H. rubiginosum</i> extracts against <i>P. aeruginosa</i> . A: MIC of <i>H. rubiginosum</i> growing rice media without sea salt, B: MIC of <i>H. rubiginosum</i> growing on rice media with sea salt, C: MIC of <i>H. rubiginosum</i> growing on oat extracts without sea salt, and D: MIC of <i>H. rubiginosum</i> growing on oat extracts with sea salt.
Figure 4.54	MBEC results obtained from antibacterial <i>H. rubiginosum</i> extracts against <i>S. aureus</i> by planktonic assay. A: MIC of <i>H. rubiginosum</i> growing rice media without sea salt, B: MIC of <i>H. rubiginosum</i> growing on rice media with sea salt, C: MIC of <i>H. rubiginosum</i> growing on oat extracts without sea salt, and D: MIC of <i>H. rubiginosum</i> growing on oat extracts with sea salt.
Figure 4.55	MBEC results obtained from antibacterial <i>H. rubiginosum</i> extracts against <i>P. aeruginosa</i> . A: MIC of <i>H. rubiginosum</i> growing rice media without sea salt, B: MIC of <i>H. rubiginosum</i> growing on rice media with sea salt, C: MIC of <i>H. rubiginosum</i> growing on oat extracts without sea salt, and D: MIC of <i>H. rubiginosum</i> growing on oat extracts with sea salt.
Figure 4.56	PCA scatter plot of proton NMR spectral data of <i>H. rubiginosum</i> extracts obtained from various media incubated for 15 and 30 days.
Figure 4.57	OPLS-DA scatter (A) and loadings (B) plots of the ¹ H NMR spectral data of <i>H. rubiginosum</i> extracts obtained from various media incubated at 15 and 30 days. Extracts were grouped according to their antimicrobial activity against both biofilm-forming <i>S. aureus</i> and <i>P. aeruginosa</i> .
Figure 4.58	(A) PCA scatter and (B) loading plots of the LC-HRMS data of <i>H. rubiginosum</i> extracts obtained from various media incubated for 15 and 30 days.
Figure 4.59	OPLS-DA scatter plot of LC-HRMS data of <i>H. rubiginosum</i> extracts obtained from various media incubated at 15 and 30 days. Extracts were grouped according to their antimicrobial activity against both biofilm-forming <i>S. aureus</i> and <i>P. aeruginosa</i> .

Figure 4.60	OPLS-DA loadings plot of LC-HRMS data of <i>H. rubiginosum</i> extracts obtained from various media incubated at 15 and 30 days. Extracts were grouped according to their antimicrobial activity against both biofilms forming <i>S. aureus</i> and <i>P.aeruginosa</i> .
Figure 4.61	Putative structures of dereplicated target bioactive metabolites found in the anti-microbial extracts of <i>H. rubiginosum</i> .
Figure 4.62	Total Ion Chromatogram (TIC) of the active fraction. The ion peaks that represent the discriminating features listed in Table 4.18 have been labelled
Figure 5.1	Chemical structure of metabolites produced by degradative enzymes in <i>D. salina</i> grown on various media.
Figure 5.2	Antimicrobial assay of crude fractions from liquid-liquid partitioning of total crude extract of <i>D. salina</i> grown on malt extract broth using AlamarBlue® assay and planktonic assay as indicated by the % bacterial growth after treatment with respective extracts shown.
Figure 5.3	MPLC system and flasks used to collect fractions.
Figure 5.4	Summary TLC plates for the pooled fractions after spraying with anisaldehyde reagent
Figure 5.5	AlamarBlue® and planktonic assays of <i>D. salina</i> fractions
Figure 5.6	Stacked ¹ H NMR spectra of 15 MPLC fractions. Highlighted spectra represent the bioactive fractions
Figure 5.7	(A) PCA scatter and (B) loading plots of the NMR spectral data of the MPLC fractions. The R ² X and Q ² X values were 1.00 and 0.99, respectively.
Figure 5.8	DMod X results to test the occurrence of true outliers. Variables above the red line are the true outliers that includes Fractions 1, 6, and 13.
Figure 5.9	OPLS-DA scatter (A) and loadings (B) plots of the NMR spectral data of the MPLC fractions grouped according to their antimicrobial activity against biofilm-forming <i>S. aureus</i> and <i>P. aeruginosa</i> . R ² X and Q ² X values were 0.999 and 0.802, respectively. While The difference within group R ² X _o is equal to 23% and the difference between groups (R ² X[1]) is equal to 13%.
Figure 5.10A	PCA scatter plot of the mass spectral data of the MPLC fractions.
Figure 5.10B	OPLS-DA loadings plot of the mass spectral data of the MPLC fractions. R ² X, R ² Y and Q ² X values are equal to 0.743, 1.00 and 0.759 respectively.
Figure 5.11A	OPLS-DA scatter plot of the mass spectral data of the MPLC fractions. Fractions are grouped according to their antimicrobial activity against both biofilms forming <i>S. aureus</i> and <i>P. aeruginosa</i> .
Figure 5.11B	OPLS-DA loadings plot of LC-HRMS data. Discriminatory features for antimicrobial active fractions are encircled and labelled with their MW. Their relative abundance in the respective fractions are shown in the bar graph.
Figure 5.12A	Compound hits for discriminatory feature P_2626 with a RT of 5.9 min, a molecular weight of 184.073 Da, and a molecular formula of C ₉ H ₁₂ O ₄ .
Figure 5.12B	Compound hits for discriminatory feature P_1491 with a RT of 19.4 min, a molecular weight of 234.125 Da, and a molecular formula of C ₁₄ H ₁₈ O ₃ .
Figure 5.13	Total Ion Chromatogram (TIC) of the active fraction. The ion peaks that represent the discriminating features listed in Table 5.5 have been labelled.

Figure 5.14	TLC of bioactive fractions of <i>D. salina</i> grown on malt extract.
Figure 5.15	Preparative TLC of MPLC fraction 2 from crude extract of <i>D. salina</i> grown on malt extract media with sea salts.
Figure 5.16	(A) Stacked proton NMR spectra of fraction 2 subfractions and (B) fraction F2-1 proton NMR spectra with integration and chemical shifts
Figure 5.17	High-resolution mass spectral data for linoleic acid.
Figure 5.18	¹ H NMR spectrum of Compound 2-1 structurally elucidated as linoleic acid.
Figure 5.19	COSY NMR spectrum of Compound 2-1 structurally elucidated as linoleic acid
Figure 5.20:	TLC of fraction 4 developed in 95:5 DCM and MeOH.
Figure 5.21:	Stacked H ¹ NMR spectrum of the preparative TLC bands targeted for further analysis and structure elucidation.
Figure 5.22:	¹ H NMR of Fraction 4-1.
Figure 5.23	High-resolution mass spectral data for orsellinic acid.
Figure 5.24	¹ H and ¹³ C NMR spectra of orsellinic acid in DMSO-d ₆ at 400 and 100 MHz, respectively.
Figure 5.25	HMBC spectrum of orsellinic acid in DMSO-d ₆ . Blue connecting lines represent the CH direct signals.
Figure 5.26	¹ H and ¹³ C NMR spectra of orcinol in DMSO-d ₆ at 400 and 100 MHz, respectively.
Figure 5.27	HMQC (above) and HMBC (below) spectrum of orcinol in DMSO-d ₆ .
Figure 5.28	2,6-dimethoxy-1,4-benzoquinone chemical previously reported from <i>D. salina</i> (Bramhachari et al., 2019)
Figure 5.29	High-resolution mass spectral data for F4-6. Inset shows the relative abundance of F4-6 in the different fractions that is highest in Fraction 6.
Figure 5.30	Hypothetical oxidation of compound F4-6 during isolation work.
Figure 5.31A	¹ H NMR spectrum of F4-6 in DMSO-d ₆ at 500 MHz.
Figure 5.31B	¹ H- ¹ H COSY NMR spectrum of F4-6 in DMSO-d ₆ at 400 MHz.
Figure 5.32	¹³ C NMR spectrum of F4-6 in DMSO-d ₆ at 500 MHz.
Figure 5.33	HMQC spectrum of F4-6 in DMSO-d ₆ at 500 MHz.
Figure 5.34	HMBC spectrum of F4-6 in DMSO-d ₆ at 500 MHz.
Figure 5.35	Chemical structure of 2,5-dihydroxy-3-(hydroxymethyl) benzoic acid (F4-6) and orsellinic acid.
Figure 5.36	Structures of oenostacin and a synthetic precursor analogue (Srivastava et al., 2007).
Figure 5.37	AlamarBlue® and planktonic assays of liquid-liquid partitioning extract against biofilm-forming <i>S. aureus</i> and <i>P. aeruginosa</i> .
Figure 5.38	Summary TLC plate of MPLC fractions of fungal extract obtained from the oat media. TLC was developed in MeOH:DCM 2:98.
Figure 5.39	AlamarBlue® and planktonic assay results of MPLC fractions of <i>D. salina</i> grown on oat solid media fractions.
Figure 5.40	Stacked ¹ H NMR spectrum of MPLC fractions of <i>D. salina</i> grown on oat solid media. Highlighted spectra represent the bioactive fractions
Figure 5.41	PCA scatter plot of the ¹ H NMR spectral data of (A) all MPLC fractions and (B) with the exception fraction-12 of the EtOAc extract of <i>D. salina</i> grown on oat solid media.
Figure 5.42	PCA loadings plot (A) of the ¹ H NMR spectral data of the MPLC fractions with the exception fraction-12 of the EtOAc extract of <i>D. salina</i> grown on

	oat solid media. The relative abundance of the discriminating peaks for Fraction-2 (B) and Fraction-9 (C).
Figure 5.43	OPLS-DA scatter (A) and loadings (B) plots of ¹ H NMR spectral data of the MPLC fractions grouped according to their antimicrobial activity. Encircled in red are the discriminatory features for the antimicrobial-active fractions. R ² and Q ² are 1.00 and 0.37, respectively, for 9 components.
Figure 5.44	PCA (A) and OPLS-DA (B) scatter plot of the LC-HRMS data of the MPLC fractions of the extracts of <i>D.salina</i> grown on oat solid media.
Figure 5.45	(A) OPLS-DA loadings of the LC-HRMS data of the MPLC fractions obtain from the extract of <i>D.salina</i> grown on oat solid media crude extracts fractions. (B) Peak areas showing the relative abundance of discriminatory features of the antimicrobial fractions. (C) VIP plot of top 10 features differentiating the active and inactive fractions. The red bars represent the features from the antimicrobial fractions.
Figure 5.46	Total Ion Chromatogram (TIC) of the active fraction. The ion peaks that represent the discriminating features listed in Table 5.15 have been labelled.
Figure 5.47	Total Ion Chromatogram (TIC) of fraction 2 with assigned [M+H] and [M-H] of the major peaks: [M+H] values are in blue boxes and [M-H] value in red box.
Figure 5.48	Summary TLC plate developed with MP of DCM:MeOH 99:1.
Figure 5.49	Stacked ¹ H NMR spectra of the fraction-2-subfractions obtained by flash chromatography equipped with an evaporative light scattering detector (ELSD).
Figure 5.50	Stacked ¹ H NMR spectra of preparative-TLC subfractions from the pooled fractions 2-1 and 2-2.
Figure 5.51	¹ H spectra of compounds F2-2-2 and F4-6.
Figure 5.52	Stacked ¹ H NMR spectra of fraction-3-subfractions obtained by flash chromatography.
Figure 5.53	Chemical structure of compound F3-1
Figure 5.54	Extracted ion chromatogram for the mass spectral data of F3-1 at the ion peak <i>m/z</i> 393.29934 [M-H].
Figure 5.55	¹ H NMR spectrum of compound F3-1 in DMSO- <i>d</i> ₆ measured at 400 MHz.
Figure 5.56	Correlation (2D-COSY) NMR spectrum of compound F3-1 in DMSO- <i>d</i> ₆ .
Figure 5.57	HSQC NMR spectrum of compound F3-1 in DMSO- <i>d</i> ₆ at 500 MHz.
Figure 5.58	HMBC NMR spectrum of compound F3-1 in DMSO- <i>d</i> ₆ at 500 MHz.
Figure 5.59	Chemical structure of Compound F3-3
Figure 5.60	Extracted ion chromatogram for the mass spectral data of F3-3 at the ion peak <i>m/z</i> 355.28425 [M+H].
Figure 5.61	¹ H NMR spectrum of compound F3-3 in DMSO- <i>d</i> ₆ at 400 MHz.
Figure 5.62	Correlation (2D-COSY) NMR spectrum of compound F3-3 in DMSO- <i>d</i> ₆ .
Figure 5.63	¹³ C, DEPT and HMQC NMR spectra of compound F3-3 in DMSO- <i>d</i> ₆ .
Figure 5.64	HMBC NMR spectrum of compound F3-3 in DMSO- <i>d</i> ₆ .
Figure 5.65	Summary TLC plate for fraction 10 fractionation.
Figure 5.66	Stacked ¹ H NMR spectra of the MPLC sub-fractions of fraction 10 in DMSO- <i>d</i> ₆ recorded at 400 MHz.
Figure 5.67	Chemical structure of compound F10-2 (turnagainolide A)
Figure 5.68	Extracted ion chromatogram for the mass spectral data of F10-2 at the ion peak <i>m/z</i> 557.33406 [M+H].

Figure 5.69	Structures of dereplicated compound hits for ion peak at m/z 557.33406 [M+H] for the molecular formula $C_{30}H_{44}N_4O_6$.
Figure 5.70	1H NMR spectrum of Compound 10-2 in DMSO- d_6 at 500 MHz.
Figure 5.71	COSY spectrum of Compound 10-2 in DMSO- d_6 at 400 MHz.
Figure 5.72	HMBC spectrum of Compound 10-2 in DMSO- d_6 at 500 MHz.
Figure 5.73	HSQC spectrum of Compound 10-2 in DMSO- d_6 at 500 MHz. Red correlations are CHs and CH_3 s while blue are CH_2 s.
Figure 5.74	(A) TOCSY spectrum of F10-2 in DMSO- d_6 at 400 MHz. (B) Carbonyl region of the HMBC spectrum of F10-2 at 500 MHz. (C) Important HMBC correlations to establish the amino acid sequence in the peptide structure of F10-2.
Figure 5.75	Chemical structure of compound F10-8 (1- <i>O</i> -(9 <i>Z</i> ,12 <i>Z</i> -octadecadienoyl) glycerol-3- <i>O</i> -[<i>D</i> -galactopyranosyl-(1→6) α - <i>D</i> -galactopyranoside]
Figure 5.76	Extracted ion chromatogram for the mass spectral data of F10-8 at the ion peak m/z 679.3900 [M+H].
Figure 5.77	Compound hits for the molecular formula $C_{33}H_{58}O_{14}$ dereplicated from the DNP.
Figure 5.78	1H and ^{13}C NMR spectra of Compound 10-8 in DMSO- d_6 at 500 MHz
Figure 5.79	2D COSY and TOCSY spectra of Compound 10-8 in DMSO- d_6 at 500 MHz
Figure 5.80	2D HMBC spectrum of Compound 10-8 in DMSO- d_6 at 500 MHz illustrating the connectivity (H to C) of the three moieties in its structure with bold arrows.
Figure 5.81	2D HSQC spectrum of Compound 10-8 in DMSO- d_6 at 500 MHz highlighting the sugar region.
Figure 6.1A	Compounds isolated from the fungal extract of <i>D. salina</i> grown on malt extract broth media with sea salt.
Figure 6.1B	Compounds isolated from the fungal extract of <i>D. salina</i> grown on oat media without sea salt.
Figure 6.2	Distribution of the isolated compounds between the active and inactive quadrant by OPLS-DA. Positive projection are the predicted compounds with antimicrobial activity and compounds on the negative projection are predicted to be inactive. Ion peaks with the same retention time but ionises in both modes were plotted twice.
Figure 6.3	Relative abundance of the isolated compounds in various MPLC fractions.
Figure 6.4	OPLS-DA score contribution plot of active features in antimicrobial extracts and corresponding outlying fractions. Y-axis is the weighed VIP scores in the active quadrant. X-axis is the feature number arranged according to m/z . Colour range blue to red is from low to high m/z . A) Active extract obtained from <i>D. salina</i> incubated for 30 days on malt extract media with sea salt. B) Active extract obtained from <i>D. salina</i> incubated for 30 days on oat media without sea salt. C) Outlying active Fraction-6 obtained from scaled-up fungal extract derived from malt extract media. D) Outlying active Fraction-5 obtained from scaled-up fungal extract derived from oat media. Asterisk (*) on ion peak at m/z 265.107 signifies similar ion peak detected from antimicrobial-active fungal extract obtained malt extract agar plates.

Figure 6.5	Proposed biosynthetic pathway of orsellinic acid, orcinol and 2,5-dihydroxy-6-hydroxymethyl benzoic acid isolated from <i>D. salina</i> grown on malt extract broth with sea salt (adapted from Chooi et al., 2008).
Figure 6.6A	Proposed biosynthetic pathway of linoleic acid and its derivatives isolated from <i>D. salina</i> grown on malt extract broth and oat solid media, respectively. (Adapted from Akpınar-Bayızit, 2014 and Gajewski et al., 2017)
Figure 6.6-B	Proposed biosynthetic pathway of linoleic acid and its derivatives isolated from <i>D. salina</i> grown on malt extract broth and oat solid media, respectively.
Figure 6.7	Proposed biosynthetic pathway of turnagainolide A isolated from <i>D. salina</i> grown on oat solid media.
Figure 6.8A	Chemical structure of bioactive compounds isolated from marine source against biofilm-forming microbes.
Figure 6.8-B	Chemical structures of bioactive compounds isolated from marine source against biofilm-forming microbes.
Figure 6.9	Some compounds responsible for quorum sensing in biofilm-forming microbes.
Figure 7.1	Schematic diagram representing the integration of molecular and cultivational approaches on silent gene cluster to increase the biodiversity and the yield of the produced compounds.

List of tables

Table number	Table title
Table 1.1	Number of drugs based on natural source in different developments stages.
Table 1.2	Active anti-cancer agents derived from natural source (Sacks et al., 1973, Williams et al., 1987, Creemers et al., 1996, Cragg et al., 1997, Kelland, 2000).
Table 1.3	Some examples of biological active compounds isolated from marine microorganism.
Table 1.4	Some examples of novel compounds isolated from marine endophytes.
Table 2.1	Required concentration of sample for screening.
Table 2.2	Polymerase reaction and amplification steps.
Table 2.3	Elution gradient used for LC-HRMS. Acetonitrile (solvent A) and water (solvent B)
Table 2.4	Elution gradient for the fractionation of <i>D. salina</i> crude extract obtained from malt extract broth with sea salt.
Table 2.5	Elution gradient for the fractionation of <i>D. salina</i> crude extract obtained from oat media without sea salt.
Table 2.6	Elution gradient for the fractionation of <i>D. salina</i> secondary metabolites.
Table 2.7	Mobile phase % used in sub-fractionation of <i>D. salina</i> secondary fraction 10.
Table 2.8	The components of anisaldehyde/sulfuric acid spray reagent.
Table 2.9	Approaches used in multivariate analysis (Wiklund, 2008).
Table 3.1	Seaweeds used to isolate endophytes for the study.
Table 3.2	Fungal endophytes isolated from collected seaweeds.
Table 3.3	Average yields of respective fungal extracts based on their triplicates.
Table 3.4	AlamarBlue® bacterial viability assay results of 100µg/mL of fungal extracts. Highlighted rows represent the bioactive extracts.
Table 3.5	Planktonic biofilm viability assay results for 100µg/mL of fungal extracts. Highlighted rows represent the bioactive extracts.
Table 3.6	MIC of active fungal extracts against <i>S. aureus</i> and <i>P. aeruginosa</i> .
Table 3.7	MBEC of active fungal extracts against biofilm-forming <i>S. aureus</i> and <i>P. aeruginosa</i> .
Table 3.8	Dereplication of 3 known possible bioactive metabolites with <i>p</i> -values < 0.05.
Table 3.9	Identified active fungal strains.
Table 4.1	Weights of Extracts Obtained from <i>D. salina</i> Cultures on Different Media.
Table 4.2	AlamarBlue® bacterial viability assay results of 100µg/mL of fungal extracts.
Table 4.3	Planktonic assay biofilm viability assay results of 100µg/mL of <i>D. salina</i> extracts obtained from various media.
Table 4.4	MIC of active <i>D. salina</i> extracts against <i>S. aureus</i> and <i>P. aeruginosa</i> .
Table 4.5	MBEC of active <i>D. salina</i> extracts against both biofilm-forming <i>S. aureus</i> and <i>P. aeruginosa</i> .
Table 4.6	Dereplication of six target bioactive metabolites found in active extracts, with P values < 0.05 as obtained from the OPLS-DA S-plot.

Table 4.7	Weights of <i>M. elegans</i> extracts obtained by cultivation on various media at different incubation periods.
Table 4.8	AlamarBlue® bacterial viability assay results of 100µg/mL of <i>M. elegance</i> extracts obtained from various media incubated at 15 and 30 days.
Table 4.9	Planktonic biofilm viability assay results of 100µg/mL extracts of <i>M. elegance</i> inoculated on various media incubated at 15 and 30 days.
Table 4.10	MIC of antibacterial <i>M. elegance</i> extracts against <i>S. aureus</i> and <i>P. aeruginosa</i> .
Table 4.11	MBEC of antibacterial <i>M. elegance</i> extracts against <i>S. aureus</i> and <i>P. aeruginosa</i> .
Table 4.12	Dereplication of six target bioactive metabolites found in active extracts, with P values < 0.05 as obtained from the OPLS-DA S-plot.
Table 4.13	Extract weights of <i>H. rubiginosum</i> obtained by cultivation on different media.
Table 4.14	AlamarBlue® bacterial viability assay results of 100µg/mL of <i>H. rubiginosum</i> extracts obtained from various media.
Table 4.15	Planktonic biofilm viability assay results of 100µg/mL of <i>H. rubiginosum</i> extracts obtained from various media.
Table 4.16	MIC values of antibacterial <i>H. rubiginosum</i> extracts against <i>S. aureus</i> and <i>P. aeruginosa</i> .
Table 4.17	MBEC of antibacterial <i>H. rubiginosum</i> extracts against <i>S. aureus</i> and <i>P. aeruginosa</i> .
Table 4.18	Dereplication of six target bioactive metabolites found in active extracts, with P values < 0.05 as obtained from the OPLS-DA S-plot.
Table 5.1	Antimicrobial assay of liquid-liquid partitioning extracts obtained from <i>D. salina</i> grown on malt extract broth media.
Table 5.2	Weights of extracts after pooling similar fractions.
Table 5.3	AlamarBlue® and planktonic assay results of <i>D. salina</i> fractions against biofilm-forming <i>S. aureus</i> and <i>P. aeruginosa</i> . Highlighted rows represent the bioactive fractions.
Table 5.4	Discriminatory features for the outlying variable Fraction 6.
Table 5.5	Top 10 VIP (Variable Importance in Projection) dereplicated metabolites that define the discriminating features of antimicrobial active fractions. The compounds are arranged according to their <i>p</i> -values. Similar features with identical MW and a RT difference of less 0.25 minutes were excluded, including only the one with the highest peak area and <i>p</i> -value. TIC is shown in Figure 5.13.
Table 5.6	weights of the three major band from fraction 2.
Table 5.7	NMR spectral data for linoleic acid (F2-1) measured in DMSO-d ₆ with COSY correlations as indicated by the atom numbers in Figure 5.21.
Table 5.8	Subfraction yield for major bands of fraction 4 of <i>D. salina</i> grown on malt extract media crude extract.
Table 5.9	NMR spectral data for orsellinic acid (F4-1A) measured in DMSO-d ₆ with HMBC correlations as indicated by the arrows in the figure below.
Table 5.10	NMR data for orcinol (F4-1B) of Fraction 4-1 measured in DMSO-d ₆
Table 5.11	NMR spectral data for compound F4-6 measured in DMSO-d ₆ with HMBC correlations as indicated by the arrows in the figure below.
Table 5.12	Antimicrobial assay of liquid-liquid partitioning extracts obtained from <i>D. salina</i> grown on oat solid media.
Table 5.13	Fraction weights obtained after fractionation of crude extracts produced from <i>D. salina</i> grown on oat solid media.

Table 5.14	AlamarBlue® and planktonic assay results of <i>D. salina</i> fractions against both biofilm-forming <i>S. aureus</i> and <i>P. aeruginosa</i> . Highlighted rows are the antimicrobial active fractions at a threshold of 75% growth inhibition or 25% bacterial viability.
Table 5.15	Discriminatory features for the antimicrobial active fractions under the top 10 VIP (Variable Importance in Projection). Features are arranged according to increasing FDR (False Discovery Rate).
Table 5.16	Yields of subfractions of fraction 2 obtained by Reveleris flash chromatography.
Table 5.17	Yields of preparative-TLC subfractions from the pooled fractions 2-1 and 2-2.
Table 5.18	Yields of subfractions of fraction 3 obtained by flash chromatography.
Table 5.19	NMR spectral data for compound F3-1 in comparison to synthesized 1,2-acetonide-3-(9,12-octadecadienoyl)glycerol (Fraser et al., 2007).
Table 5.20	NMR spectral data for compound F3-3 in comparison to F3-1 in DMSO-d ₆ in 400 MHz for ¹ H _δ and 100 MHz for ¹³ C _δ .
Table 5.21	Yield of pooled MPLC sub-fractions of fraction 10
Table 5.22	NMR spectral data for compound F10-2 in DMSO-d ₆ in 500 MHz.
Table 5.23	NMR spectral data for compound F10-8 in MeOD at 500 MHz for δH and at 125 MHz for δC.
Table 5.24	¹³ C NMR spectral data for compound F10-8 measured at 125 MHz in comparison to literature at 67.5 MHz (Yoshikawa et al 1994).
Table 5.25	¹³ C NMR spectral comparison from Glycosciences.DB with a match score of 72.50% (http://www.glycosciences.de/).
Table 5.26	AlamarBlue® and planktonic assay results against biofilm-forming <i>S. aureus</i> and <i>P. aeruginosa</i> for 100µg/ml concentration of bioactive subfractions obtained from <i>D. salina</i> grown on malt extract broth. Highlighted rows represent bioactive fractions at a threshold of less than 30% viability.
Table 5.27	AlamarBlue® and planktonic assay results against biofilm-forming <i>S. aureus</i> and <i>P. aeruginosa</i> for 100µg/ml concentration of subfractions obtained from <i>D. salina</i> grown on oat solid media. Highlighted rows represent bioactive fractions at a threshold of less than 30% viability.
Table 5.28	MIC and MBEC results of isolated compounds from <i>D. salina</i> extracts against biofilm-forming <i>S. aureus</i> and <i>P. aeruginosa</i> . Gentamicin was used as positive control.
Table 6.1	List of active antibiofilm compounds isolated from marine environment. Structures of compounds are illustrated in Figures 6.8-A and -B

Publications and conferences' presentations

1st and 2nd November 2018:

4th Scottish Metabolomics Network Symposium 2019

Dundee, UK.

Poster presentation: "Implementing metabolomics for drug discovery".

Saif Aldeen Jaber, ^{1,2*} Louise Young, ¹ Kirsty Black, ³ Rothwelle Tate, ¹ and RuAngelie Edrada-Ebel ¹

1st – 5th September 2019:

XVI International Symposium on Marine Natural Products | XI European Conference on Marine Natural Products

Peniche, Portugal

and

14th and 15th November 2019:

5th Scottish Metabolomics Network Symposium 2019.

Glasgow, UK.

Poster presentation: "Implementing metabolomics tools to optimise the production of anti-biofilm metabolites of endophytic fungi from Scottish seaweeds".

Saif Aldeen Jaber, ^{1,2*} Louise Young, ¹ Kirsty Black, ³ Rothwelle Tate, ¹ and RuAngelie Edrada-Ebel ¹

27th-29th October 2020

16th Annual Conference of the Metabolomics Society

Online

Poster presentation: "Implementing metabolomic tools to optimise the production of anti-biofilm metabolites of endophytic *Hypoxylon rubiginosum* isolated from Scottish marine *Fucus vesiculosus*".

Saif Aldeen Jaber, ^{1,2*} Louise Young, ¹ Kirsty Black, ³ Rothwelle Tate, ¹ and RuAngelie Edrada-Ebel ¹

¹Strathclyde Institution of Pharmacy and Biomedical Sciences, University of Strathclyde, 161 Cathedral Street, Glasgow, United Kingdom

²Middle East University, Amman, Jordan

³Marine Biopolymers Ltd, Unit 54, Heathfield Industrial Park, Boundary Road, Ayr, KA8 9DJ, United Kingdom

Abstract

In the search for a new antimicrobial bioactive compound from natural source against both biofilm-forming *Staphylococcus aureus* and *Pseudomonas aeruginosa*, endophytic fungi associated with seaweeds are an interesting source of bioactive secondary metabolites. Twenty-four endophytes were isolated from eight different Scottish seaweeds namely; *Ascophyllum nodosum*, *Laminaria hyperborean*, *Ulva intestinalis*, *Ulva lactuca*, *Himanthalia elongata*, *Fucus vesiculosus*, *Fucus serratus*, and *Fucus spiralis*. Endophytes responsible for producing bioactive compounds were identified using internal transcribed spacer (ITS) gene sequencing. Depending on their biological activity and chemical profiles, three endophytic fungi, namely; *Dendryphiella salina* (*D. salina*), *Hypoxyton rubiginosum* (*H. rubiginosum*), and *Mariannaea elegans* (*M. elegans*) were identified and subjected for media optimisation studies on five liquid media and four solid media in three different incubation periods. For liquid media; this included: malt extract broth with and without sea salt, Wickersham liquid media with and without sea salt and lastly, marine broth. While for the solid media, rice and oat, both with and without sea salt were used. The chemical profile for each extract was monitored using Liquid Chromatography-High Resolution Mass Spectrometry (LC-HRMS) and nuclear magnetic resonance spectroscopy (NMR). Antimicrobial activity was monitored using both AlamarBlue® and planktonic assays. The appropriate medium and the incubation period were chosen for a scale-up of the selected endophytic fungus according to the following factors: 1) higher yield, 2) improved antimicrobial activity, and 3) diverse chemical profile. Based on these factors, *D. salina* was chosen for scale-up and isolation work.

D. salina was grown on malt extract with salt and oat without salt. The scaled-up extracts of *D. salina* were subjected to liquid-liquid partitioning followed by fractionation using either medium pressure flash chromatography or flash chromatographic technique. The first fractionation of the scaled-up extracts was tested against both biofilm-forming *S. aureus* and *P. aeruginosa* and analysed using ¹H NMR and LC-HRMS. The HRMS data was processed using MZmine followed by dereplication using an in-house method then subjected to orthogonal partial least square-discriminant analysis (OPLS-DA). OPLS-DA results were used to determine the antimicrobial active secondary metabolites. As a result, eight compounds were isolated from the bioactive fractions of *D. salina*. *D. salina* grown on malt extract broth yielded linoleic acid, orsellinic acid, orcinol and 2,5-dihydroxy-3-(hydroxymethyl)benzoic acid. While *D. salina* inoculated on oat solid media afforded the acetonide and glycerylglycoside derivatives of linoleic acid along with the peptide turnagainolide A. All isolated compounds,

except for linoleic acid and its glycerol congener, displayed antibiofilm activity with MBEC (Minimum Biofilm Eradication Concentration) values between 45 and 360 μM concentrations against biofilm-forming bacteria *S. aureus* and *P. aeruginosa*. F10-2 (turnagainolide A) and F10-8 (gingerglycolipid B stereoisomer) displayed the highest potency with MIC and MBEC values between 45 and 75 μM concentrations.

Conclusion: Endophytic *D. salina* derived from Scottish seaweed *L. hyperborea* grown on malt extract broth and oat solid media showed the ability to produce compounds with antimicrobial bioactivity against biofilm-forming bacteria. In addition, three new antimicrobial natural products: 2,5-dihydroxy-3-(hydroxymethyl)benzoic acid along with an acetonide and glycerylglycoside derivatives of linoleic acid were isolated from *D. salina* extracts. Thus, marine endophytic fungi are promising source of bioactive compounds.

1 General Introduction

1.1 Hypothesis and study aims

The question of the study: Are endophytic fungi derived from Scottish seaweeds good sources of new bioactive compounds with antimicrobial activity against biofilm-forming *S. aureus* and *P. aeruginosa*?

Hypothesis: Applying metabolomics processes, specifically PCA and OPLS-DA, to search for antimicrobial bioactive compounds from endophytic fungi associated with Scottish seaweeds will aid in pinpointing the biologically active compounds in the first fractionation step, thus saving time typically consumed in the traditional bioassay-guided isolation process. These compounds will be targeted, isolated, identified, and tested to ensure their activity as antimicrobial compounds. Moreover, early-stage dereplication will help isolate new compounds.

The aim of this study is to isolate active antimicrobial compounds from seaweed-associated endophytes. Eight Scottish seaweeds, *Ascophyllum nodosum*, *Laminaria hyperborean*, *Ulva intestinalis*, *Himanthalia elongata*, *Fucus serratus*, *Fucus vesiculosus*, *Ulva lactuca*, and *Fucus spiralis*, were chosen for this purpose. The following research objectives will be accomplished:

1. Endophytic fungi will be isolated from the seaweeds and identified using ITS gene sequencing.
2. The obtained endophytic fungi will be screened for antimicrobial activity. A selected endophyte will be scaled-up based on their biological activity and chemistry.
3. A specific type of media will be used for the scaling-up process. Thus, media optimisation will be done for each of the endophytic fungus. The medium which will facilitate the best yield, the most chemically diverse extract, and the most potent biological activity for each endophytic fungus, will be chosen for the scaling-up processes.
4. A metabolomic bioassay-guided approach will be designed for each of the scaled-up endophytes, to identify the biologically active compounds against microbial growth and their effects on biofilm formation.

5. Fractionation will be accomplished to isolate the targeted antimicrobial active compounds.
6. NMR and LC-HRMS will be used to identify the isolated compounds.
7. The isolated compounds will be tested against methicillin sensitive *Staphylococcus aureus* and *Pseudomonas aeruginosa*.

1.2 Drug discovery

The demands for novel chemical compounds to be used as therapeutic agents are increasing every day. These demands have been motivated by many reasons such as the emerging of new diseases and infections, plus the advances in the instruments used for analysis. The increasing incidence of multi-drug resistant microbes, which cause deathly infections is one of these reasons that are boosting the field of discovering new chemical compounds that can overcome these infections (Strobel, 2003, Yu et al., 2010, Alvin et al., 2014, Wu et al., 2015). Furthermore, life-threatening diseases, such as cancer and microbial infections are playing important role on keeping drug discovery processes moving on (Alvin et al., 2014).

Drug discovery can be accomplished by three different pathways depending on the source, type and classes of compounds. The first pathway of discovering new bioactive compounds is by exploring various natural sources. These chemical compounds are produced by both macro and microorganisms through different biosynthetic routes (Alvin et al., 2014). While the second pathway is by computer-based drug design (CBDD), where the chemical compound is designed *in-silico* by a computer software to fit and interact with a specific active site or receptor (Mandal et al., 2009). Finally, there is the utilisation of combinatorial chemistry, where libraries are produced by large number of synthesised compounds to be tested against specific targets, then followed by data analysis for the most potent drugs between the various congeners (Gallop et al., 1994, Liu et al., 2017a).

Recently, pharmaceutical companies and research centres have been interested in employing the 2nd and the 3rd pathways (CBDD and combinatorial drug discovery) of drug discovery by involving new technologies such as 3D X-ray crystallography, drug-docking, and computer-based tools in their favour (Muller, 2009). However, computer-based drug design and combinatorial drug discovery have been facing difficulties as well. These difficulties involve the need for knowledge on the mechanism of elucidating target receptors (Barry and Blanchard, 2010). In addition, most of these chemically-synthesised compounds pose many side effects

and environmental concerns (Strobel and Daisy, 2003). Even more, the high cost to discover novel compounds and marketing them later are adding more pressure on these pathways of drug discovery (Alvin et al., 2014).

1.2.1 Natural source for drug discovery

Natural products (NP) are chemical compounds produced by a living macro or microorganism, such as animals, plants, seaweeds, bacteria and fungi. Plants are the biggest source of natural compounds between all sources. Even though, marine sources, especially marine endophytes, have yielded many of the biologically active secondary metabolites (Harvey, 2008, Sarker and Nahar, 2012, Alvin et al., 2014).

Natural products are divided into two groups of compounds that include primary and secondary metabolites. Primary metabolites such as glucose, amino acids and some fatty acids are compounds produced by living organisms and are essential for its life cycle and its physical activity. Whereas secondary metabolites are low or high molecular weight compounds that are produced by the organism to adapt to a specific situation or environment and are produced by a gene translation process. (Harvey et al., 2015, Nisa et al., 2015).

Records on the utilisation of natural products date back before 2600 BC by using oils of *Cupressus sempervirens* and *Commiphora* species (myrrh) (Cragg and Newman, 2005b). These oils were used by people in Mesopotamia for the treatments of cough and inflammation (Cragg and Newman, 2005b). The Eber papyrus from 2900 BC is an Egyptian pharmaceutical record of 700 plant-based drugs ranging from many drug formulation such as gargles, pills, infusions, to ointments (Dias et al., 2012). In addition, in 1100 BC, the Chinese Materia Medica had documented 52 prescriptions. Furthermore, Shennong Herbalrom from 100 BC recorded 365 drugs, and the Tang Herbal at 659 AD recorded 850 drugs (Cragg and Newman, 2005b). All therapeutic preparations mentioned before were produced from a plant source. On the other hand, microorganisms have also been used before as a source of natural medicinal preparations. A first example is the fungus *Piptoporus betulinus*, which grows in birches, it was incorporated in charcoal to be used as an antiseptic and disinfectant (Swanton, 1914). In addition, *P. betulinus* strips were earlier used as corn pads for staunching bleeding (Swanton, 1932). A second example is *Agaricus campestris* found in the Caribbean, which was reported to be used for throat cancer by stewing the fungi in milk (Hatfield, 1994). Furthermore, lichens have also been utilised such as *Usnea dillenius* that was used for scalp diseases, and sold as an ingredient for anti-dandruff shampoo while it was also described to treat sore eyes in Ireland (Zavarzina

and Zavarzin, 2006). Many famous examples of medicines based on traditional basis or natural products are still being used nowadays. A famous example is the anti-inflammatory agent, acetylsalicylic acid which was derived from the natural product salicin isolated from the willow tree (Süntar, 2019). As well as, opium poppy which produced the commercially and clinically important analgesic drug morphine (Süntar, 2019). Another example of a drug based from a natural source is the cardiotoxic glycoside digitoxin isolated from *Digitalis purpurea* L., and it could be traced back to Europe in the 10th century, but was only discovered after 1700 to improve cardiac conditions, especially with patients facing heart failure (Süntar, 2019). Likewise, quinine drugs isolated from *Cinchona succirubra* Pav. were used for many diseases such as malaria, fever, indigestion, mouth and throat diseases as well as cancer (Süntar, 2019). Additionally, L-histidine derivative of pilocarpine isolated from *Pilocarpus jaborandi* have been used for the treatment of different glaucoma cases (Süntar, 2019). Finally, the antibiotic penicillin isolated from *Penicillium* mould was the beginning of the golden era of antibiotics to treat microbial infections.

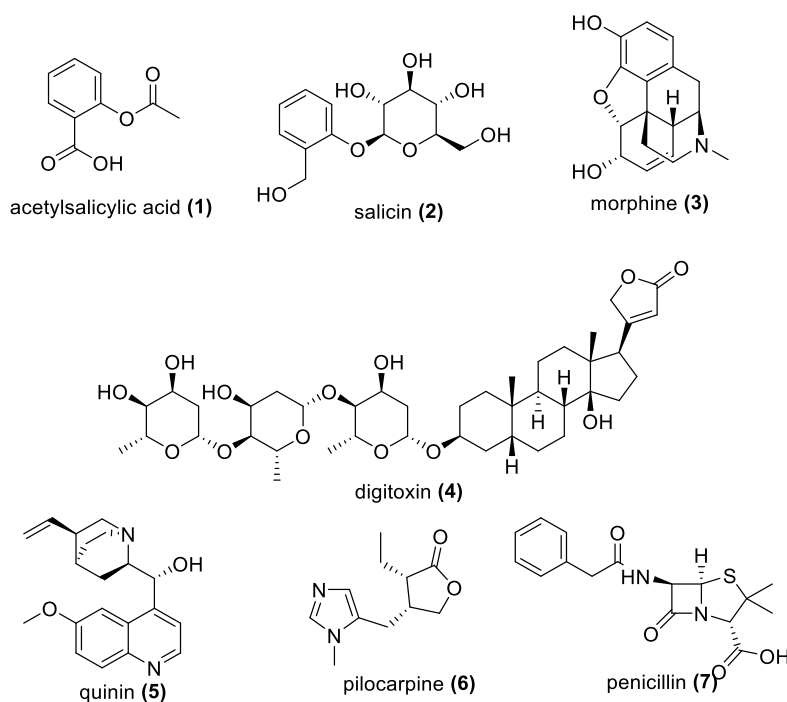


Figure 1.1: Important compounds isolated from natural sources. (1): acetylsalicylic acid, (2): salicin, (3): morphine, (4): digitoxin, (5): quinin, (6): pilocarpine and (7): penicillin.

1.2.2 Combinatorial drug discovery

Combinatorial drug discovery involves the generation of huge numbers of structurally diverse compounds from different chemical groups, which are called compound libraries. Such

libraries would catalogue compounds according to their physicochemical properties such as, solubility, permeability, type of interaction, easiness of formulation and fitting with the binding cavity of the targeted enzymes (Liu et al., 2017b). Active chemical compounds would be categorised on their biological activity and mechanism of action (Liu et al., 2017b). Combinatorial chemistry was introduced in the 1980's during the invention of Geysen's multi-pin technology (Houghten, 1985). The compounds in the libraries can be screened by two ways, as follows:

Virtual screening is based on computer simulations, by predicting the interaction between compounds and a target receptor or structurally-related compounds (Liu et al., 2017b). Virtual screening can be done by three methods that included molecular docking, pharmacopeia mapping and quantitative structure-activity relationship (Liu et al., 2017b). The major problem with virtual screening is the inability to exclude real biological activity testing of these compounds (Liu et al., 2017b). Virtual screening is fundamentally done in a dry lab environment.

Experimental screening is accomplished in a wet lab (Liu et al., 2017b). The invention of the high-throughput screening (THS) made the screening methodology easier and faster, in which hundreds of thousands of compounds could be tested providing a real-time result in a short period with least effort (Liu et al., 2017b). Even though, there is a time advantage through THS, it actually still needs plenty of time to set-up and is considered to be more time consuming than virtual screening (Liu et al., 2017b).

Structural information provided by the different libraries on molecular binding between compounds and receptors guided the rational selection for the best compounds in the library, which lead also to affect the design of the library (Terrett et al., 1995). Many examples on combinatorial drug discovery were found to be successful. For instance, plasmid relaxation assay was used from a solution phase library (Marcon et al., 2010). This afforded the discovery of an antiprotozoal compound (such as, fluorophenyl ethers) against *Leishmania donovani* with no toxicity to the normal mammalian cells (Marcon et al., 2010). Another example is the OBOC peptidomimetic library (Guan et al., 2012), that utilised a cell binding assay for $\alpha_4\beta_1$ integrin ligand screening and generated the development of the drug LLP2A-alendronate for the treatment of osteoporosis (Guan et al., 2012)

1.2.3 Computer-based drug discovery (CBDD)

Computer-based drug discovery and development processes has been getting more implementable, extensive, and popular (Kapetanovic, 2008). Many names are used to describe computer-based drug discovery, such as computer-aided molecular design (CAMD), computer-aided molecular modelling (CAMP), rational drug design, *in-silico* drug design and computer-aided drug design (Kapetanovic, 2008). Computer-based drug discovery (CBDD) involves the following objectives:

- 1- To streamline drug discovery and development process using computing abilities (Kapetanovic, 2008).
- 2- To provide a strong source of chemical and biological information about the legends and/or targets, which would aid in the identification and the optimisation of new drugs synthesis (Kapetanovic, 2008).
- 3- To eliminate compounds with low interest for further drug development due to their inept physicochemical and biological properties, such as (absorption, distribution and metabolism) and (excretion, toxicity and biological activity) respectively (Kapetanovic, 2008).

The increased interest in CBDD had pushed companies to upgrade the needed software to be specifically used for drug design and identification of molecular targets coupled to a publicly available database to target protein structure (Kapetanovic, 2008). Furthermore, this improvement in the software led computer companies to improve their hardware power and sophistication (Kapetanovic, 2008). Biological activity testing of the selected compounds would be done in two ways similar to combinatorial drug discovery, which would either be by virtual or real-time screening (Kapetanovic, 2008). CBDD has been enrolled in important pathways for drug discovery as presented in the workflow shown in Figure 1.2. The advantage of using CBDD over a natural source and combinatorial chemistry for drug discovery is the ability to increase the hit rates for novel compounds (Sliwoski et al., 2014). In addition, CBDD has a higher capability to predict the biological activity on a molecular basis along with the plausible derivatives that would enhance the biological activity of the selected compounds (Abagyan et al., 1994).

Many drugs and mechanisms of actions have been discovered using CADDD with potent bioactivity against specific target like the discovery of Tip60 (Gao et al., 2014). Another

example of CADD was the using of virtual screening of thymidine monophosphate kinase inhibitor, as antitubercular agents by Gopalakrishnan et al., 2005 (Gopalakrishnan et al., 2005).

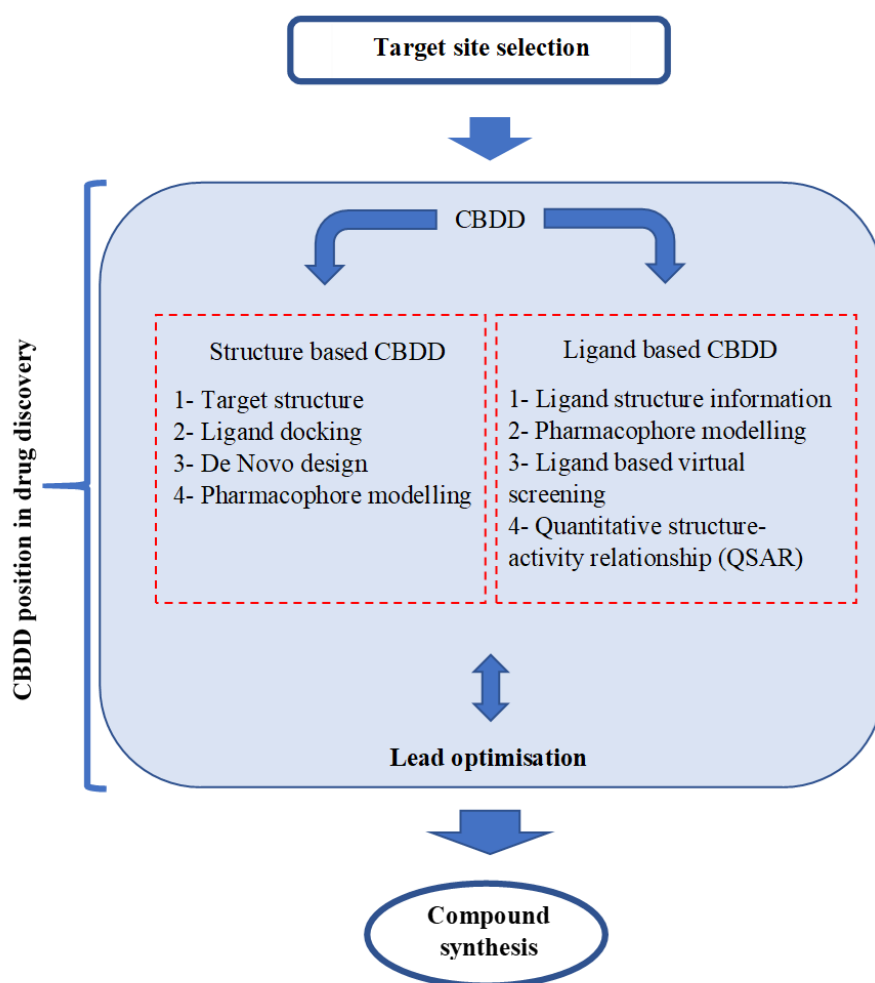


Figure 1.2: CBDD position in drug discovery process flowchart(Gopalakrishnan et al., 2005).

1.3 Natural products

Natural environments have been used as a source of many pharmacologically active compounds used as medicines from the old ages until now (Harvey, 2008). The information provided by research centres, educational institutions, and pharmaceutical manufacturers show that approximately half of the approved drugs between 1981 and 2007 are from natural source or derived from natural products (Newman and Cragg, 2016). Many of these compounds were isolated from plants, microbial or animal sources, such as elliptinium, galantamine and

huperzine from plants, daptomycin from microbes, and exenatide as well as ziconotide from animals (Harvey, 2008). In addition, many synthetic and semi-synthetic compounds were produced based on natural compounds such as tigecycline, everolimus, telithromycin, micafungin and caspofungin (Harvey, 2008).

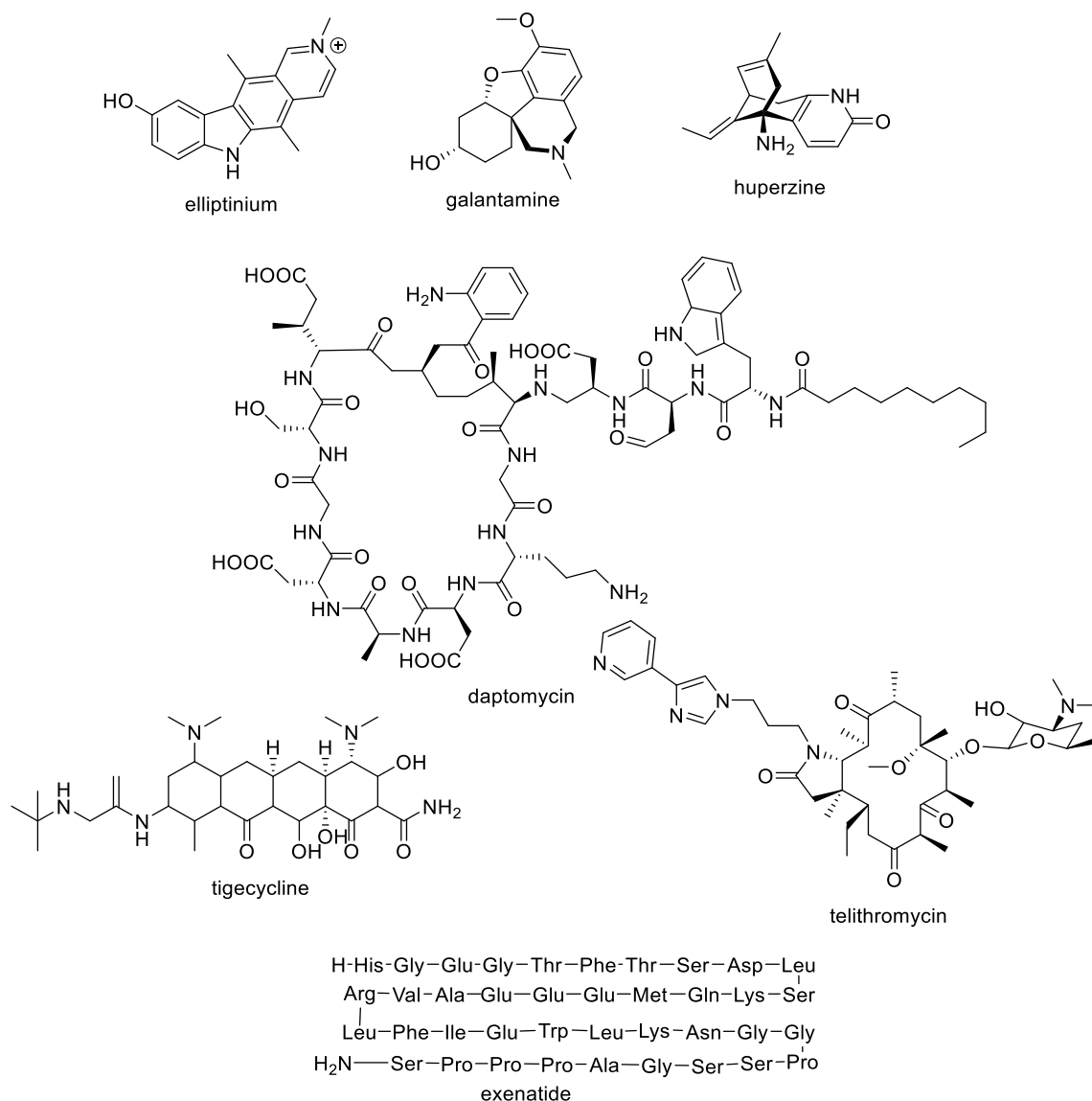


Figure 1.3(A): Examples of natural products used or modified to be used as pharmaceutical preparations (Harvey, 2008).

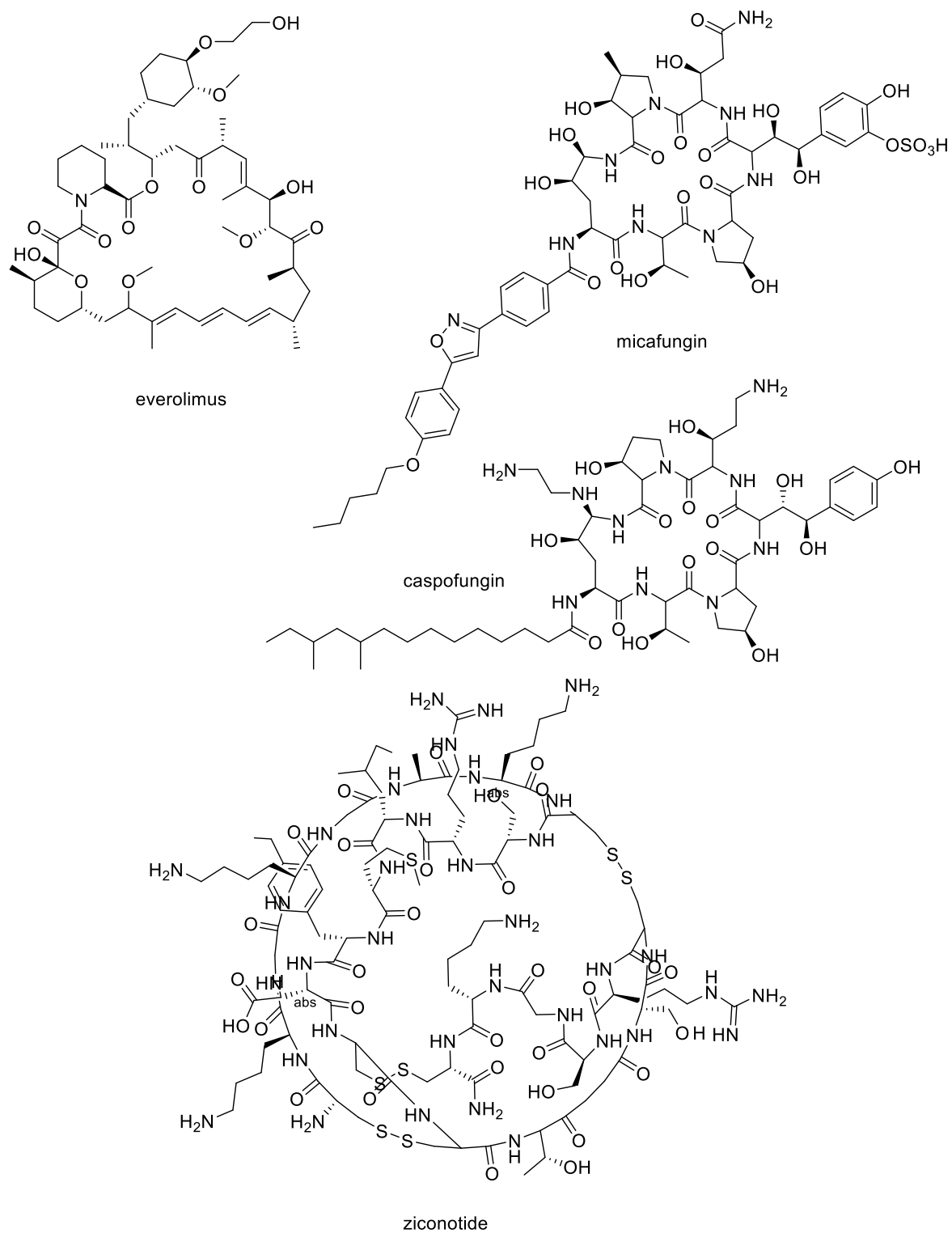


Figure 1.3 (B): Examples of natural products used or modified to be used as pharmaceutical preparations.

Table 1.1: Number of drugs based on natural sources in different developments stages.

Development stage	Plants	Bacteria	Fungi	Animals	Natural products-derived compounds	Total
Pre-clinical	46	12	7	7	27	99
Phase 1	14	5	0	3	8	30
Phase 2	41	4	0	10	11	66
Phase 3	5	4	0	4	13	26
Pre-registration	2	0	0	0	2	4
Total	108	25	7	24	61	225

Source: pharmaprojects database (dated: March 2008)

As presented in Table 1.1, 255 drugs have been afforded directly or derived from a natural source (Harvey, 2008). As demonstrated in Table 1.1, plants and microbes are considered to be the most popular provider for natural lead compounds (Butler, 2008).

Advances provided by the improvements of existing chromatographic technologies such as counter-current chromatography and high-resolution analytical instruments in mass spectroscopy (MS), and nuclear magnetic resonance (NMR) aided the fractionation strategies and purification of natural compounds as well as the elucidation of chemical structures (Singh and Barrett, 2006, Harvey, 2007, Simoben et al., 2018). In addition, the high-throughput capability of screening mixtures of natural compounds or extracts has made the work with natural products less time-consuming and more successful (Singh and Barrett, 2006). Furthermore, these advances in analytical and chromatographic instrumentation have improved the duration of isolating target compounds to less than two weeks as well as from extracts obtained from a broth media (Simoben et al., 2018). Thus, research groups from around the globe working with natural products could currently produce and screen libraries of highly diverse compounds isolated from the natural sources. The Dictionary of Natural products (DNP) published by CRC Press, a member of the Taylor & Francis Group has provided evidence of the availability of highly diverse bioactive compounds and thereby has further aided drug discovery from the natural compounds (Simoben et al., 2018). Unfortunately, compound libraries as such have been facing some problems in their maintenance and curation especially from the cost-point of view (Simoben et al., 2018).

Despite advancements toward computer-based or combinatorial drug discovery, Newman and Cragg stated in 2016 that over 34 years between 1981 and 2014, 44% of all new approved

drugs in the market were either biological macromolecules, unaltered natural products, botanical natural products (define mixture) or natural products derivatives. As well as 21% of these new drugs were synthesised to mimic natural product (Figure 2). Furthermore, in spite of the essential role of combinatorial chemistry in drug discovery, natural product-like library is still of importance (Newman and Cragg, 2016).

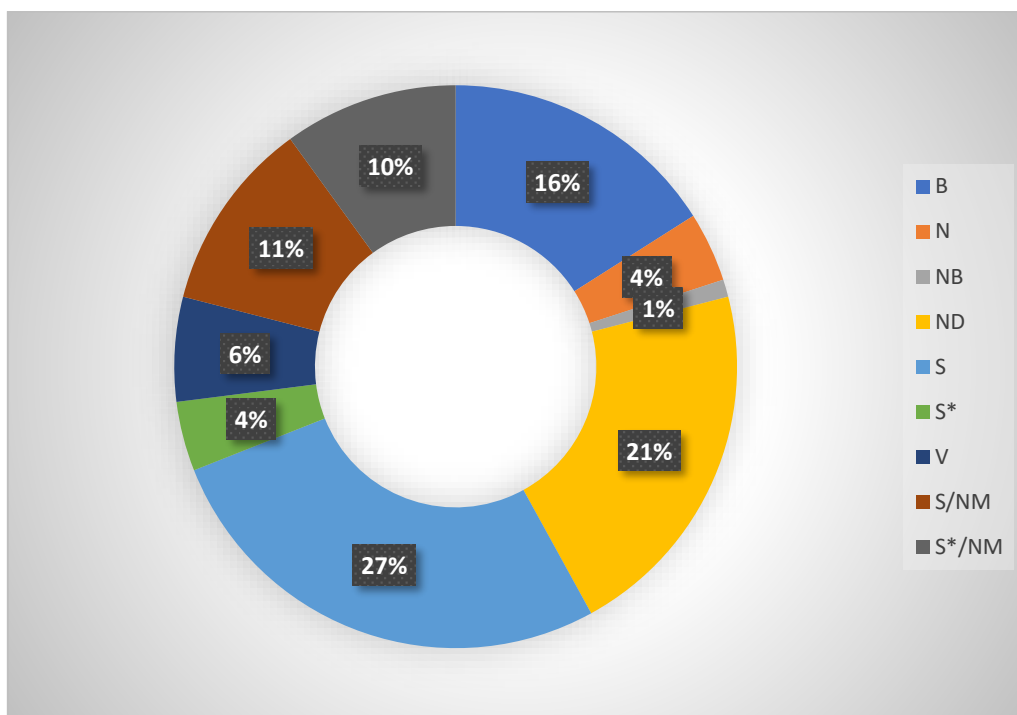


Figure 1.4: All new approved drugs 1981 – 2014; $n = 1562$, B: Biological macromolecule, 1997, N: Unaltered natural product, 1997, NB: Botanical drug (defined mixture), 2012, ND: Natural product derivative, 1997, S: Synthetic drug, 1997, S*: Synthetic drug (NP pharmacophore), 1997, V: Vaccine, 2003, /NM: Mimic of natural product, 2003 (Newman and Cragg, 2016).

Cancer, microbial infections, and diabetes are the main causes of deaths globally (Harvey, 2008, Harvey et al., 2015). Curing these diseases have been the potential target for novel natural products by providing a huge diversity of chemical profiles (Harvey, 2008). Half of the newly approved antitumor, antibacterial, and antifungal drugs between 2006 and 2010 were natural products or derived from natural products (Newman and Cragg, 2012). As well as, from the thirteen natural products, derived drugs that were approved between 2005 and 2007, five of

them were from a novel family of chemical classes as shown in Figure 1.3 (Harvey, 2008). All this confirms the great role of natural products to provide new bioactive lead compounds for drug discovery. As mentioned before, natural source of chemical compounds is an attractive source of new therapeutic agents because of the huge diversity of these chemical compounds due to millions of species involved in the production of these compounds (da Rocha et al., 2001). As mentioned before, the development of novel drugs from natural source is not easy and this is because of many drawbacks related to the natural source of bioactive compounds. This includes the inability to biosynthesise large amounts of these secondary metabolites, challenging access to the natural source of the active compounds, expensive isolation scheme to afford purified active compounds, and the elucidation of a complex chemical structure, which made the exploitation of natural compounds in pharmaceutical industries to be economically not sustainable (da Rocha et al., 2001). But the emergence of new technologies in analysis and biological screening procedures made drug discovery from natural source more feasible.

1.3.1 Anti-cancer compounds isolated from natural sources.

The first search of anti-cancer agents from natural source started in the beginning of 1950's (Cragg and Newman, 2005a). The first active compounds, vinblastine and vincristine were isolated from the plant Madagascar periwinkle leaf (*Catharanthus roseus*) (Roepke et al., 2010). Due to the low yield production of vinblastine and vincristine by *C. roseus*, an endophytic *Fusarium oxysporum* was isolated from the plant and was found to produce both compounds in good yield to be available clinically (Kumar et al., 2013). On the other hand, another group of compounds (Taxol) exhibited bioactivity in various cancer cell lines like paclitaxel isolated from the bark of *Taxus brevifolia*. Paclitaxel was found active against ovarian, breast and adenocarcinoma (Shah et al., 2013). Another taxol compound was derived from the needles of *Taxus baccata*, docetaxel, which was used for the treatment of different types of cell carcinoma (Shah et al., 2013). The advances in the analytical instrumentation resulted in the isolation of many compounds either from plants or marine environment. Some of these compounds have been introduced for clinical studies and/or approved for medicinal use as listed in Table 1.2 (Schwartzmann, 2000, Schwartzmann et al., 2001).

Table 1.2: Active anti-cancer agents derived from natural source (Sacks et al., 1973, Williams et al., 1987, Creemers et al., 1996, Cragg et al., 1997, Kelland, 2000).

Source	Compound
Plant source	
<i>Catharanthus roseus</i>	vincristine
<i>Catharanthus roseus</i>	vinblastine
<i>Taxus brevifolia</i>	paclitaxel
<i>Taxus baccata</i>	docetaxel
<i>Camptotheca acuminata</i>	topotecan
<i>Camptotheca acuminata</i>	irinotecan
<i>Dysoxylum binectariferum</i>	flavopiridol
<i>Brucea antidysenterica</i>	bruceantin
<i>Scutellaria baicalensis</i>	thalicarpin
<i>Microbial source</i>	
<i>Streptomyces sp.</i>	actinomycin D
<i>Soil fungus Streptomyces</i>	bleomycin
<i>Streptomyces sp.</i>	daunomycin
<i>Streptomyces sp.</i>	doxorubicin
<i>Streptomyces sp.</i>	epirubicin
<i>Streptomyces sp.</i>	streptazocin
<i>Streptomyces sp.</i>	mitomycin C

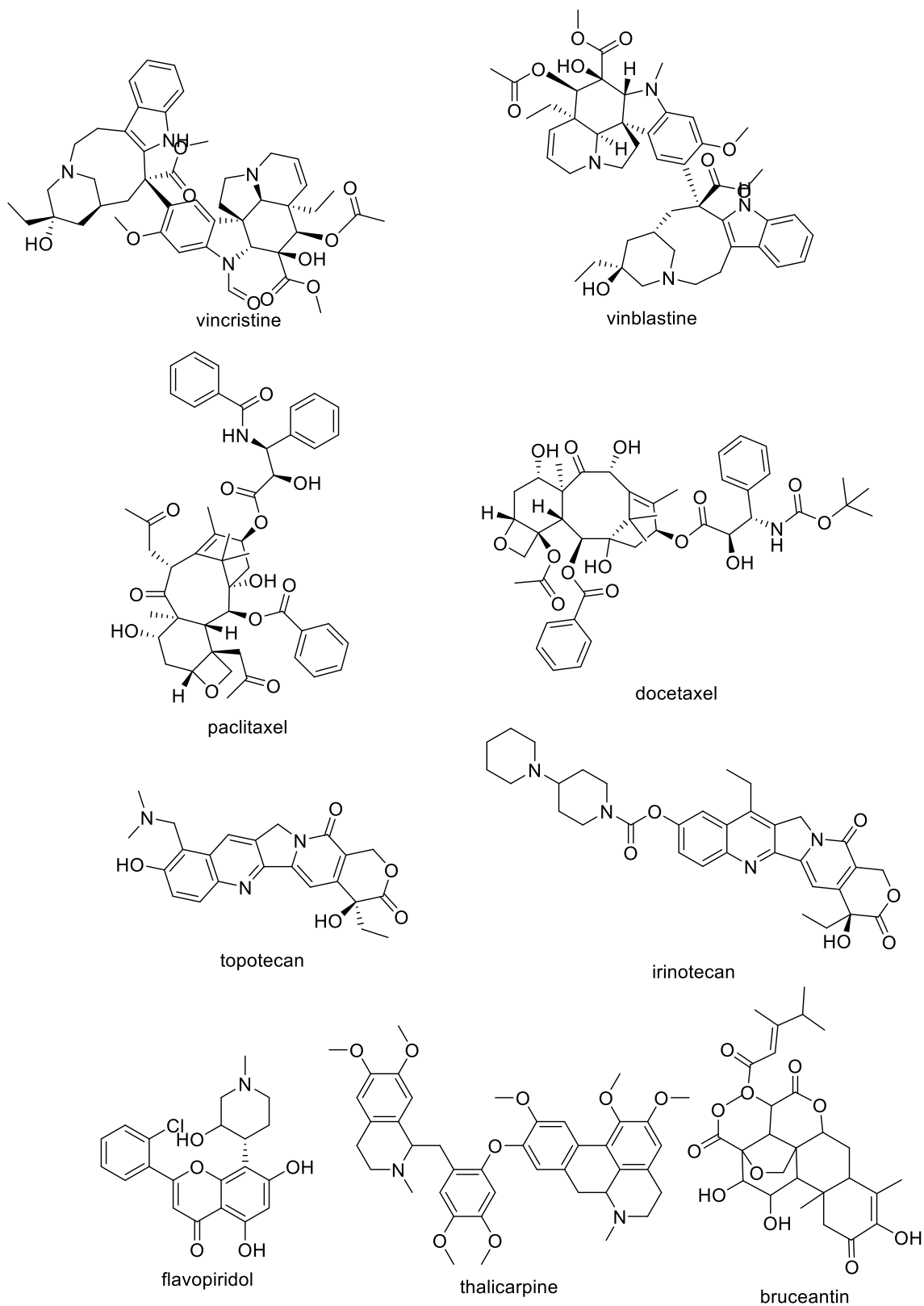


Figure 1.5: Anti-cancer chemical agents isolated from plants (Sacks et al., 1973, Williams et al., 1987, Creemers et al., 1996, Cragg et al., 1997, Kelland, 2000).

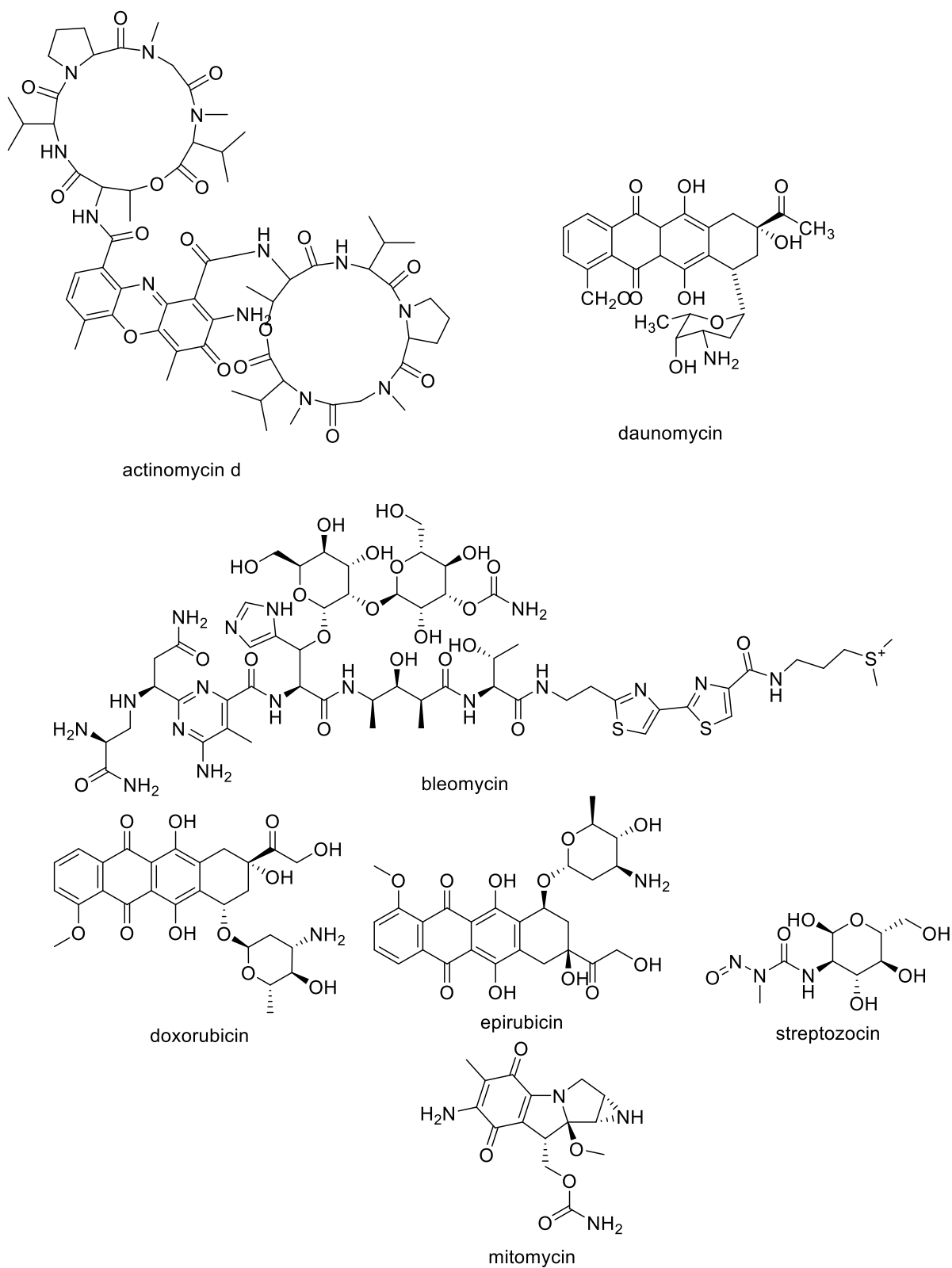


Figure 1.6: Anti-cancer chemical agents isolated from microorganism (Sacks et al., 1973, Williams et al., 1987, Creemers et al., 1996, Cragg et al., 1997, Kelland, 2000).

1.3.2 Anti-diabetic compounds isolated from natural sources

Diabetes mellitus (DM) is a chronic disease that causes elevation in blood glucose level due to either a problem with insulin secretions from pancreas or the inability of insulin to work properly in the human body (Xu et al., 2018). The number of patients with DM is more than 422 million to date, and this number will increase to be 592 million in 2035 (Xu et al., 2018). Lifestyle and synthetic drugs are used to reduce the symptoms coupled with DM (Beccuti et al., 2017). However, lifestyle and synthetic drugs are not enough to control DM due to the poor acceptability and compliance of diabetic patients (Xu et al., 2018). Many evidences have been found to confirm the successful convenient management of DM with herbal medicines exhibiting high activity and low toxicity in patients (Xu et al., 2018). Flavonoids, polyphenols, terpenoids, saponins, alkaloids, and quinones are different groups of compounds used to reduce the symptoms of DM. More specific examples include quercetin and rutin flavonoids, epigallocatechin gallate, resveratrol, abscisic acid, andrographolide, berberine, and jatrorrhizine (Jung et al., 2006, Lee et al., 2006, Lin and Lin, 2008, Fernandes et al., 2010, Soyoung et al., 2011, Ding et al., 2014, Fu et al., 2014, Magnone et al., 2015, Chen et al., 2016).

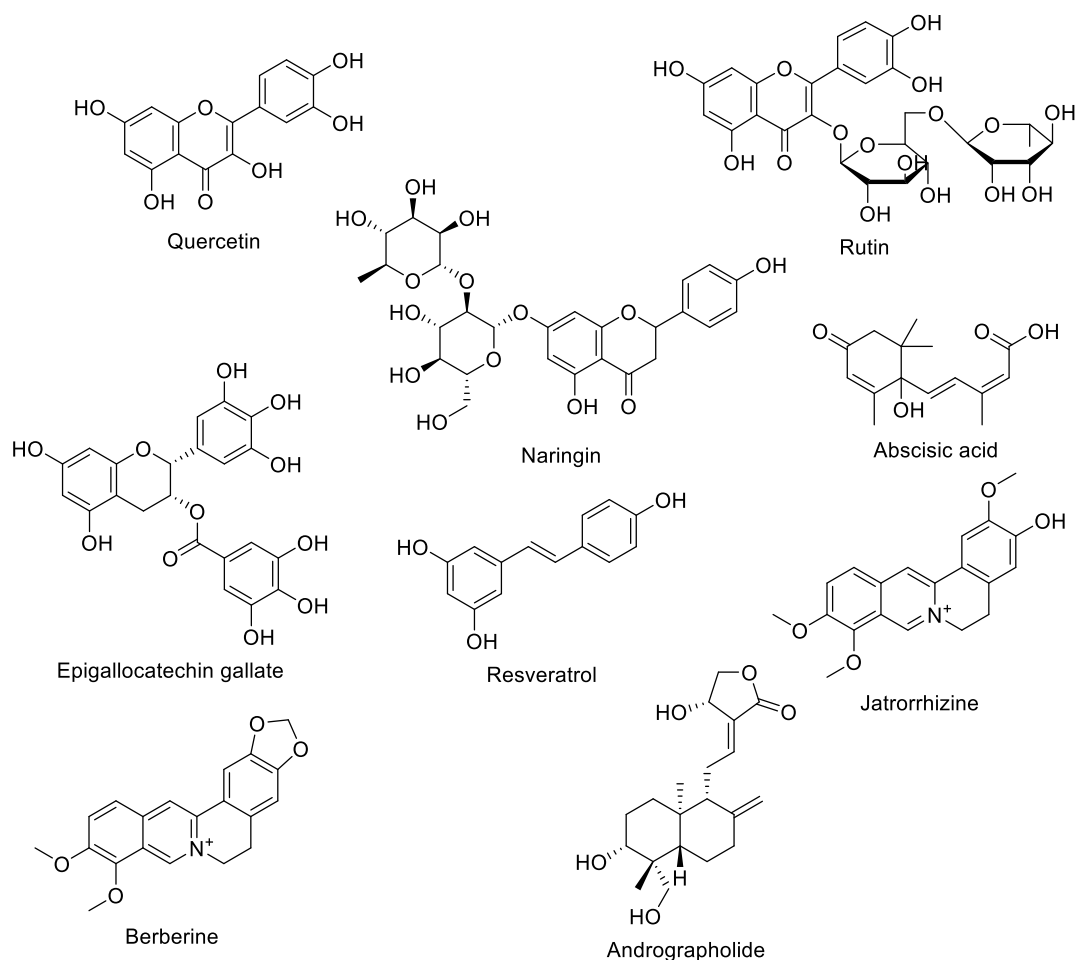


Figure 1.7: Chemical compounds isolated from natural sources used to reduce blood glucose level in DM patient.

1.3.3 Anti-bacterial compounds isolated from natural sources

Amongst the first type of antibacterial compounds were the sulpha-drugs, which was reported to be used in 1936, followed by the discovery of the β -lactam compound penicillin between 1929 and 1941, which was the golden age of antibiotic discovery (Walsh, 2003). However, the occurrence of multi-resistance microbes to the antimicrobial compound based on the β -lactam ring compelled scientists to isolate other antimicrobials, one of which were the phenylpropanoid compounds, such as chloramphenicol in 1946 (Walsh, 2003). The need of new type of antibiotics led to the discovery of the polyketides group, such as tetracycline in 1949, followed by the isolation of aminoglycosides like streptomycin between 1946 and 1950 (Walsh, 2003). While macrolides like erythromycin was discovered in 1952, followed by the isolation of glycopeptides, such as vancomycin between 1956 and 1975 (Walsh, 2003).

Quinolones, 2nd generation β -lactams, streptogramins, 3rd generation β -lactams, oxazolidinones, and daptomycin have been discovered between 1960 and 2003 as represented in Figure 1.8 (Walsh, 2003).

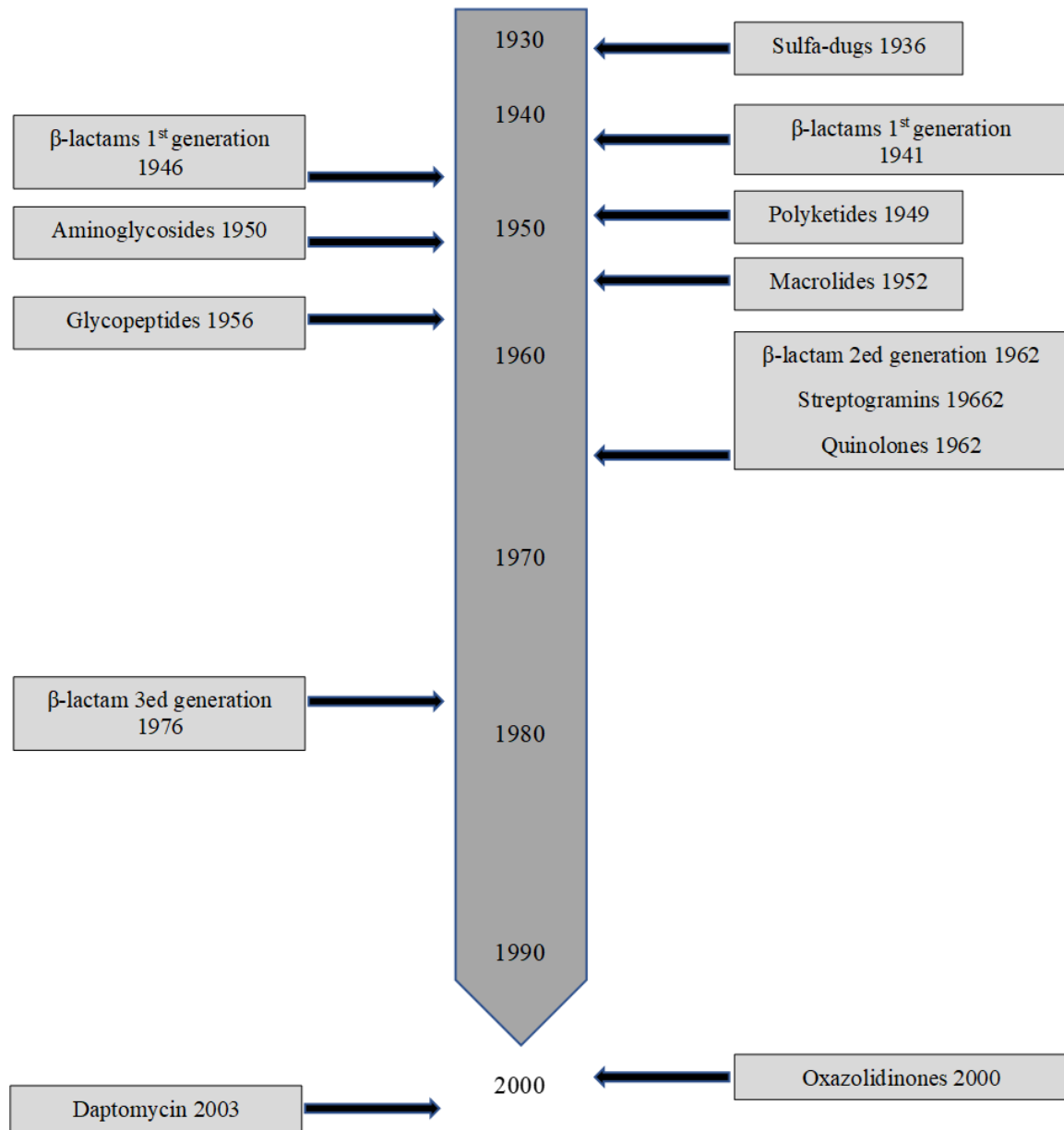


Figure 1.8: Timeline represents the discovery of novel antimicrobial compounds from natural source (Walsh, 2003).

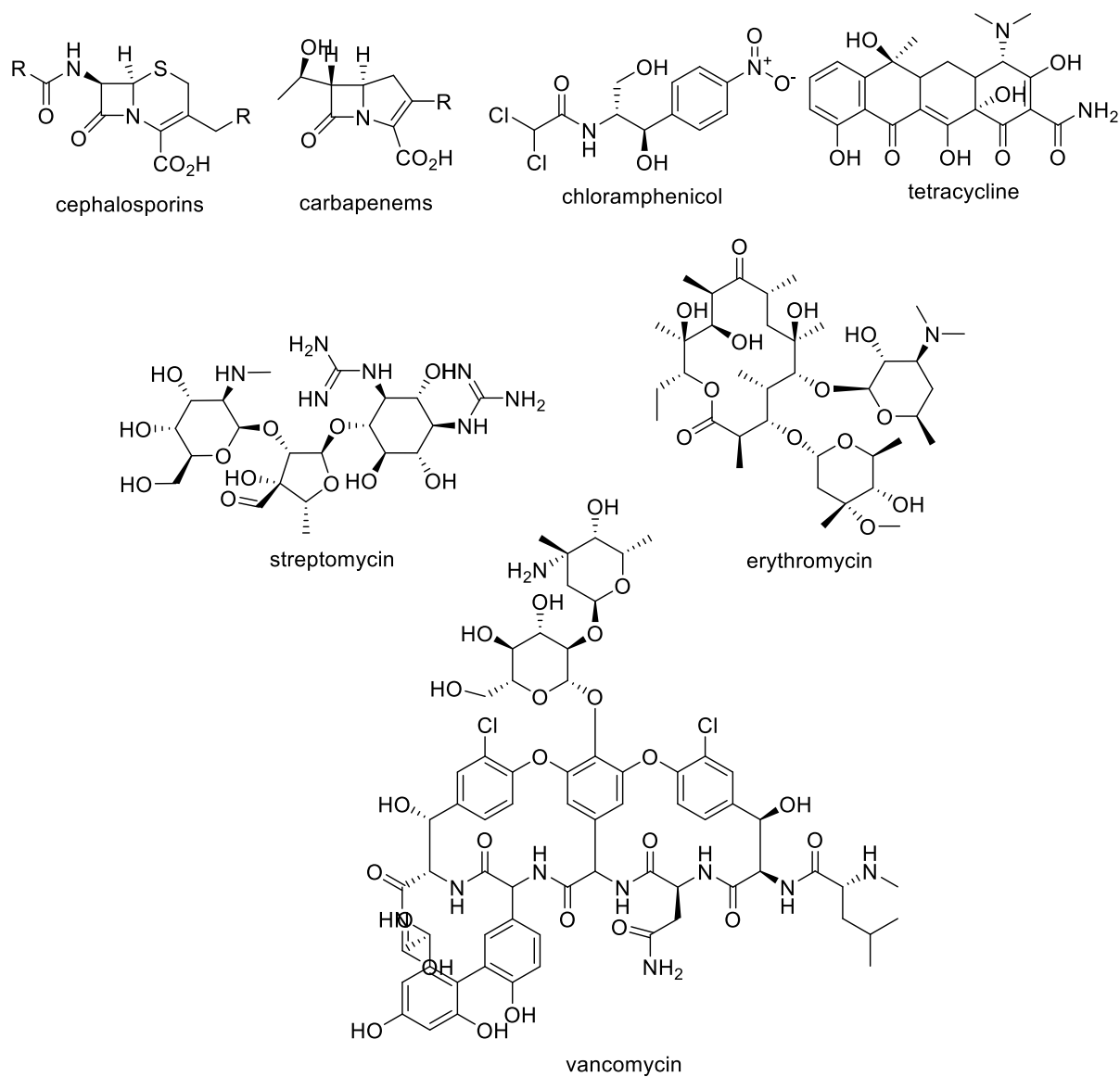
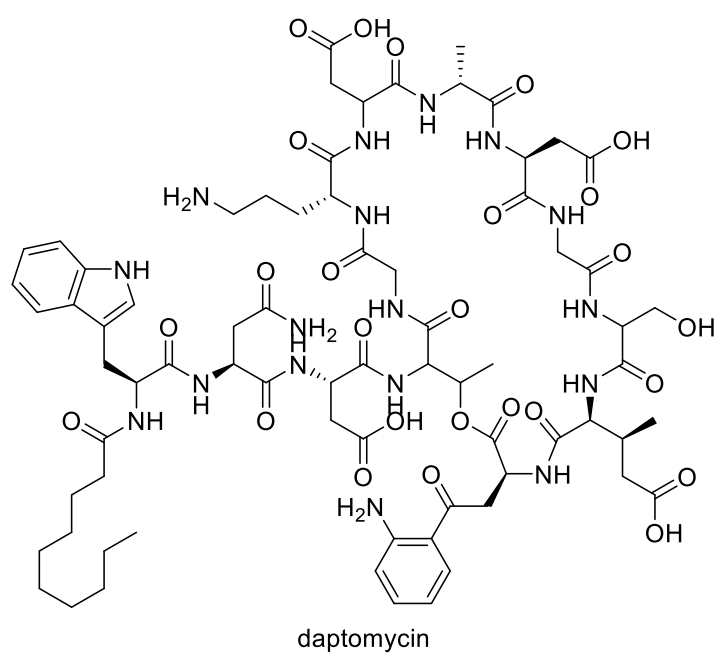
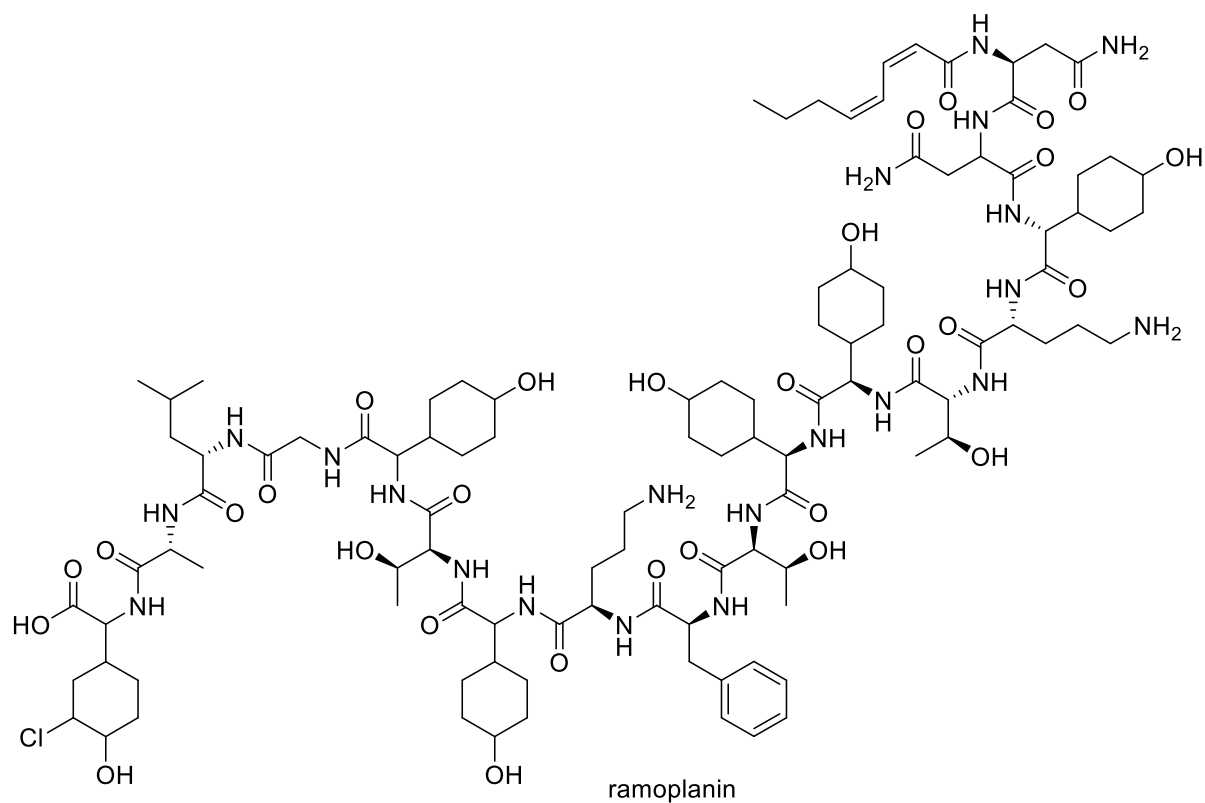


Figure 1.9: Examples of antibiotic compounds isolated from natural sources.



Continued to Figure 1.9: Examples of antibiotic compounds isolated from natural sources.

1.3.4 Advantages of natural products for drug discovery

Natural products afford structural diversity to fit specific targets and receptors, as well as provide models for drug design in terms of selectivity and specificity (Chen et al., 2017). In addition, the diverse range of pharmacophores and unique complex stereochemistry offered by natural products, enabled interaction with targets, like those with the more challenging protein-protein interface (Drewry and Macarron, 2010, Gray et al., 2012). Moreover, cellular transport of natural products through a physiological membrane can offer the ability to act intracellularly, which would improve targeting the active sites and enhance bioavailability (Harvey et al., 2015, Chatzikonstantinou et al., 2018). The chemical space occupied by the natural compounds could suggest novel potential interaction with the biological space on many of their targets (Gray et al., 2012, Harvey et al., 2015). Furthermore, natural products that follow the Lipinski's rule of five in terms of their physicochemical and structural properties would have the ability to be absorbed readily from the gastrointestinal tract, as well as provide wider pharmacokinetic interaction (Quinn et al., 2008).

1.3.5 Disadvantages of natural products for drug discovery

Because of the structural complexity of natural products, which may include properties such as low solubility and stability as mentioned above, a huge difficulty can be encountered in formulating compounds to drug dosage form particularly in parenteral preparations (Harvey, 2008, Chen et al., 2015). However, these challenges which are related to pharmaceutical manufacturing can be eliminated by the improvement of their physicochemical property, stability and selectivity through chemical and structural modifications of these natural products as a lead compound (Chen et al., 2015). In some cases, the presence of lead compounds needs specific conditions to be produced by microbial endophytes, so such conditions must be stipulated to produce the targeted compound (McChesney et al., 2007). In addition, the complexity of these natural products makes the preparation of them in scientific laboratories could be difficult or impossible in some cases (da Rocha et al., 2001).

1.3.6 New approaches and technologies in utilising natural products for drug discovery

The conventional bioassay-guided isolation of bioactive natural products is continually being modified. Strategies for high-throughput screening have enhanced the usability of natural products by pharmaceutical companies. Moreover, applying metabolomics and chemometrics-coupled with functional pharmacology has augmented natural product-based drug discovery (Harvey, 2008, Yuliana et al., 2011). Metabolomics is the science of dealing with the

phenotypic ability of an organism to synthesise secondary metabolites. A metabolomics-based approach uses statistical tools to establish the suitable situation for the production of metabolites at the end of a biological process (Harvey et al., 2015). Multivariate analysis has become an efficient means of targeting the bioactive component(s) to prioritise the active fractions for further isolation and purification work. Similar approaches have been also used to determine the optimum cultivation conditions that could affect the production of secondary metabolites in microorganisms, and for the prediction of precursors that can enrich the biosynthesis of the targeted compounds (Bochner, 2009, Tawfike et al., 2013, Macintyre et al., 2014, Harvey et al., 2015). Molecular biology and genetic engineering have introduced new approaches which can augment microorganism's ability to produce a specific type of natural compound (Chang and Keasling, 2006, Watanabe and Oikawa, 2007). In addition, a metagenomics-based approach of cloning a specific DNA gene from an endophytic microorganism in a host has been used to produce a target bioactive compound (Gillespie et al., 2002). Furthermore, a mutasynthetic method combines both synthetic and enzymatic pathways to produce natural bioactive compounds has been used to improve the ability to isolate novel bioactive compounds (Kopp and Marahiel, 2007).

1.4 Marine environment as a source of bioactive compounds

While plants, fungi and bacteria are the major sources of natural bioactive compounds, the isolation of biologically active compounds from marine sources has significantly increased in the last decades (Altmann, 2017). This is not surprising because the ocean covers more than 65% of the earth, and represents 95% of its biosphere (Agranoff et al., 1969). The huge diversity provided by the marine environment is expected to be a source of highly diverse secondary metabolites (Pye et al., 2017). Thousands of compounds have been isolated from marine sources each year since 2008, and the total number recorded in 2015 was about 27000 compounds (Bergmann and BURKE, 1955). The first drugs developed from a marine source are the arabinose-nucleosides spongothymidine and spongouridine (Figure 1.10), which were isolated from the sponge *Tectitethya crypta* in 1950's (Bergmann and BURKE, 1955).

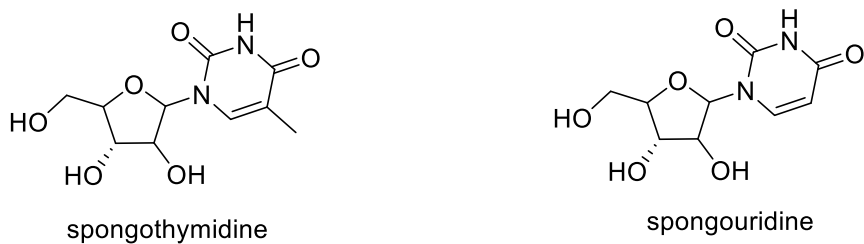


Figure 1.10: First bioactive compounds isolated from a marine source.

Marine organisms are considered to be one of the sources of a wide-range of biologically active compounds (Molinski et al., 2009). Seaweeds have been widely studied in traditional and folk medicines over more than 2000 years (Sarasan et al., 2017). Algal-derived compounds have been earlier described for their antimicrobial and antifungal activity, as well as for other purposes (Bhadury and Wright, 2004). In addition, algal compounds were used in cosmetics and antifouling preparations (Bhadury and Wright, 2004).

1.4.1 Marine endophytes as a source of bioactive compounds

Microbes can easily adapt and respond to their environment and defend their existence by the production of a specific type of secondary metabolites, to aid their adaptation and maintain their defence mechanism (Zhang et al., 2005). Terrestrial fungal endophytes have proven their effects on plant growth and defence mechanism, as well as improved the ability of plants to adapt to environmental stress by producing certain types of compounds (Sturz and Nowak, 2000). Endophytic association with a host organism had yielded novel secondary metabolites with pharmacological and industrial interest (Strobel, 2002). Fungi derived from different marine sources, such as: fish, sponges, mangroves and both micro- and macro-algae have attracted further research because of their ability to produce novel bioactive compounds due to their exposure to varied environmental factors (Zainuddin et al., 2010, Giddings and Newman, 2015, Bajpai, 2016, Di Camillo et al., 2017). As of the last decade, 272 new compounds have been reported from marine fungi until 2002, from these 272 new compounds 85% were derived from epi/endophytes (Zhang et al., 2009). The rise of bacterial resistance, lack of bioactive antimicrobial agents, and the side effects associated with some antimicrobial agents; all these have driven for further research to discover novel bioactive compounds from endophytic microorganisms (Doshi et al., 2011, Pimentel et al., 2011).

Microorganisms like bacteria and fungi are of great importance as a source of a novel bioactive metabolites (Kjer et al., 2010). These bioactive metabolites are used by pharmaceutical

companies as potential drug leads to cure specific types of diseases (König et al., 2006, Zhang et al., 2006). Fungi isolated from the marine environment are considered to be a promising source of biological active metabolites of high chemical diversity (Bugni and Ireland, 2004). Cephalosporins (Figure 1.12) were first isolated by G. Brotzu in 1945 from the marine-derived fungus *Acremonium chrysogenum* (Newton and Abraham, 1955). More recently, a marine sponge-associated *Penicillium chrysogenum* afforded sorbicillactone (Figure 1.11), an alkaloid that showed promising biological activity against leukaemia (Kjer et al., 2010).

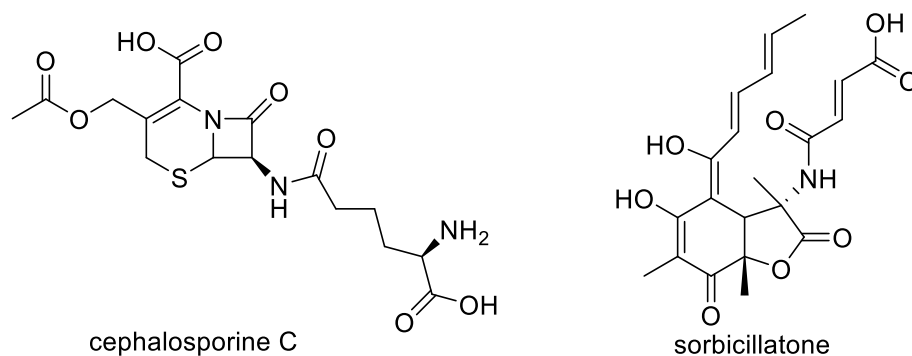


Figure 1.11: Examples of chemical compounds isolated from endophytic microorganisms.

Fungi are considered to be one of the most distinct life forms hence yielding chemically diverse metabolites (Hyde, 2001). Endophytes are microorganisms living in the internal tissues of a host organism without causing any physical damage (Stone et al., 2000). The production of secondary metabolites is directly affected by three correlations which include: 1) endophyte with its host organism, 2) endophyte with its surrounding environment and 3) between various endophytic species (Schulz et al., 2002). Various classes of compounds have been isolated from endophytic fungi such as phenols, xanthenes, terpenoids and quinones (Dos Santos et al., 2003, Schulz and Boyle, 2005). Endophytic fungi are considered to be a source of natural products, which can be optimised to yield a certain biologically active metabolite for a specific type of disease (Tenguria et al., 2011). Like endophytes derived from plants, fungi have also been described to associate with marine organisms such as sponges, or algae and these endophytes were found to produce highly chemically diverse metabolites (Bugni and Ireland, 2004, Paz et al., 2010, Rateb and Ebel, 2011). The interest on marine-derived fungi as a source of novel bioactive compounds has been increasing as implicated by the increasing number of publications since the beginning of the 21st century (Debbab et al., 2011). Numerous novel bioactive compounds have been isolated from marine microbes and were found to be anti-infective, cytotoxic, anti-inflammatory, rheumatoid arthritis and cystic fibrosis as examples are

presented on Table 1.3 and Figure 1.12 (Arunpanichlert et al., 2010, Elsebai et al., 2010, Isaka et al., 2010, Wang et al., 2010). Many endophytes isolated from host marine sources have been responsible for the synthesis of novel compounds and are presented in Table 1.4 and Figure 1.13 (Oliveira et al., 2012).

Table 1.3: Some examples of biological active compounds isolated from marine microorganism.

Microorganism	Compound	Reference
<i>Talaromyces</i>	7-epiaustdiol	(Liu et al., 2010)
<i>Xylaria</i>	mairetolide F	(Isaka et al., 2010)
<i>Streptomyces sp</i>	methylelaiophylin	(Wu et al., 2013)
<i>Streptomyces koyangensis</i>	neoabyssomicins A ₂	(Huang et al., 2018)
<i>Hansfordia sinuosae</i>	hansforesters A	(Wu et al., 2018)
<i>Dendrodochium sp.</i>	dendrodolides M	(Sun et al., 2013)
<i>Penicillium sumatrense</i>	sumalactones B	(Wu et al., 2017)
<i>Aspergillus ochraceus</i>	asperochrins C	(Liu et al., 2015)

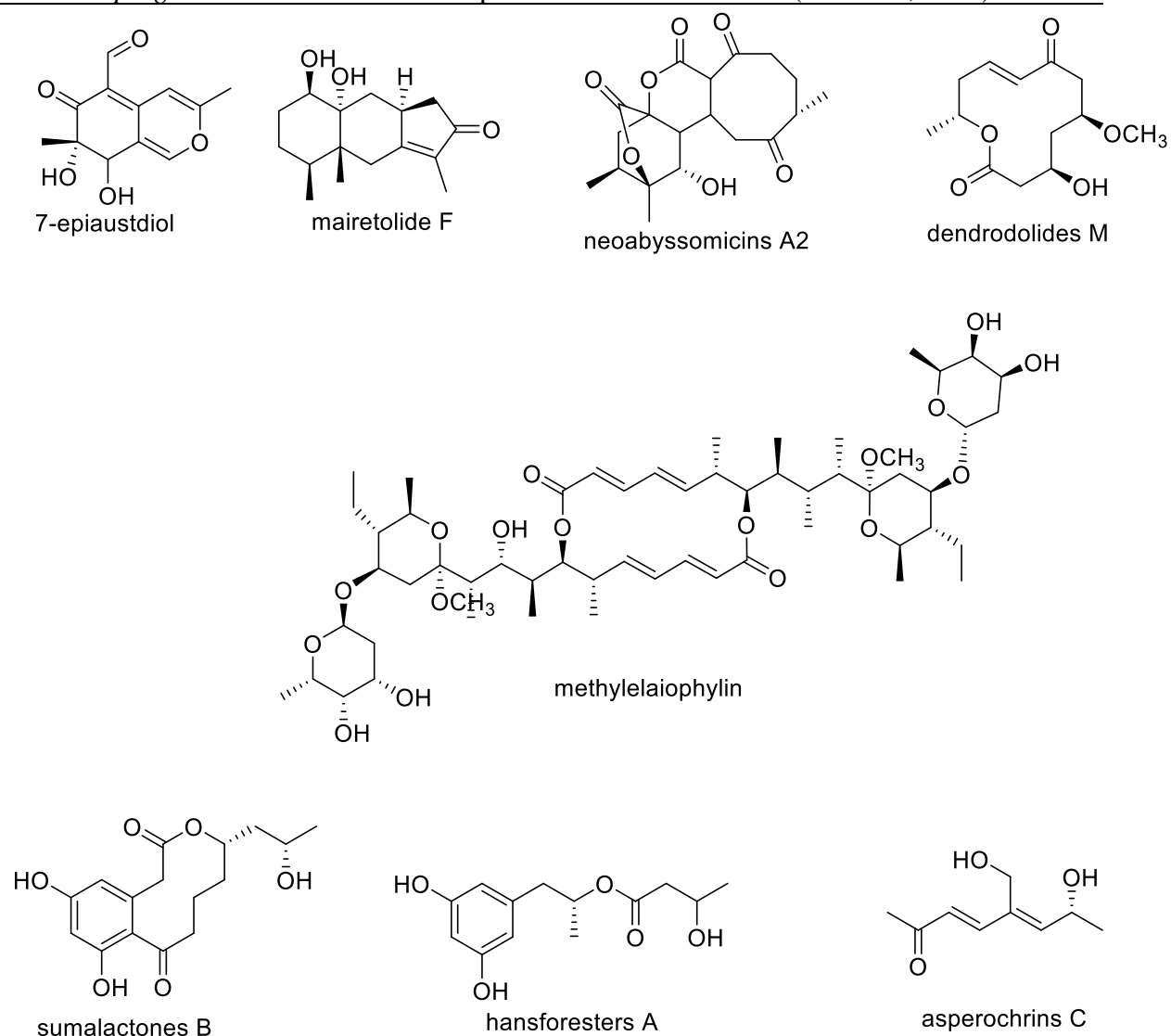


Figure 1.12: Chemical structures of known bioactive compounds isolated from marine endophytes.

Table 1.4: Some examples of novel compounds isolated from marine endophytes.

Host marine source	Endophyte	Structure number	Reference
<i>Blidingia minima</i>	<i>Penicillium sp.</i>	1	(Zhu et al., 2009)
<i>Valsa ceratosperma</i>	<i>Codium fragile</i>	2	(El-Beih et al., 2007)
<i>Enteromorpha sp.</i>	<i>Cadophora malorum</i>	3-5	(Almeida et al., 2010)
<i>Enteromorpha sp.</i>	<i>Coniothyrium cereale</i>	6-8	(Elsebai et al., 2011)
<i>Ulva sp.</i>	<i>Ascochyta salicorniae</i>	9	(Osterhage et al., 2000)
<i>Ulva sp.</i>	<i>Penicillium sp.</i>	10	(Gamal-Eldeen et al., 2009)
<i>Fucus spiralis L.</i>	<i>Phoma tropica</i>	11	(Osterhage et al., 2002)
<i>Fucus vesiculosus L.</i>	<i>Epicoccum sp.</i>	12	(Abdel-Lateff et al., 2003)

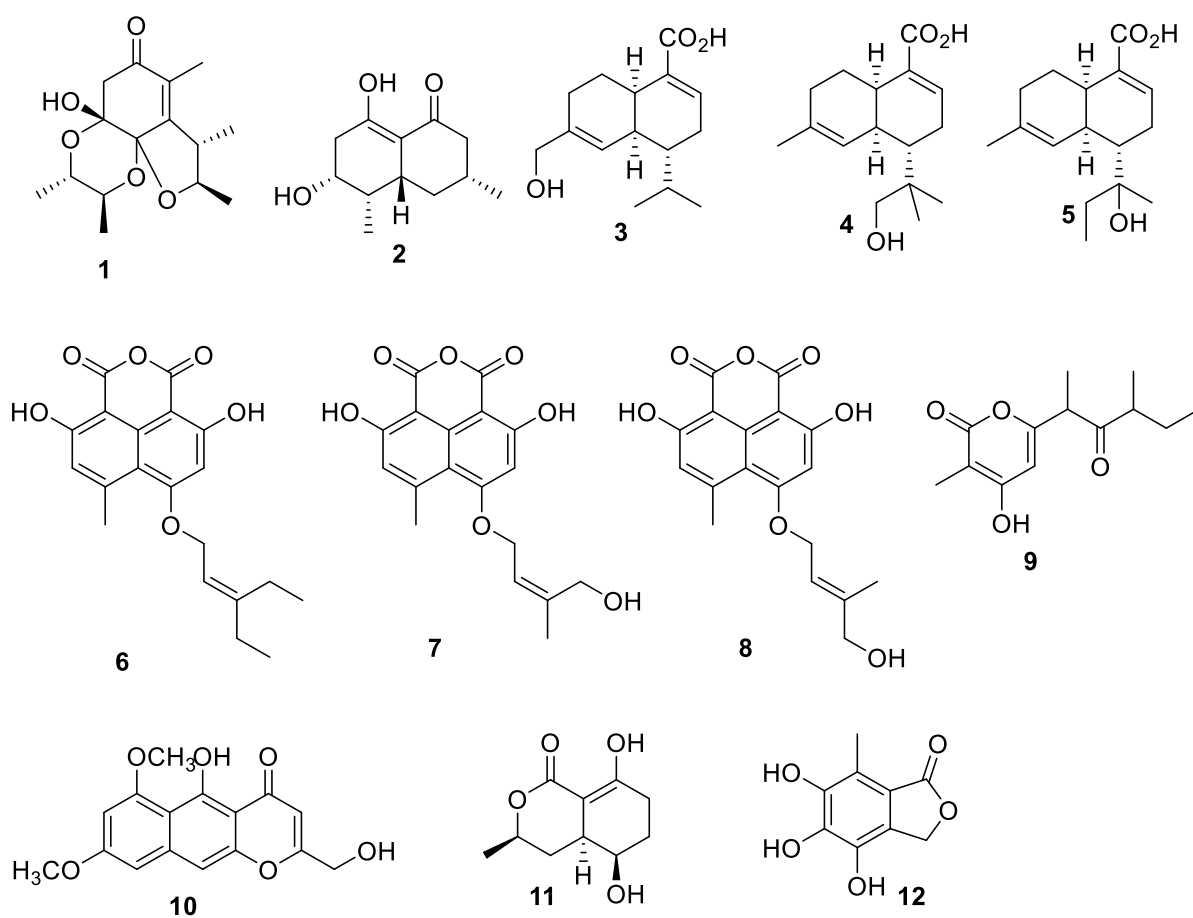


Figure 1.13: Chemical structure of novel compounds isolated from endophytes isolated from marine source.

1.4.2 Antimicrobial agents isolated from marine endophytic fungi

Many novel bioactive compounds isolated from marine endophytes were found to be active against different types of microbial infections (Debbab et al., 2010). Some examples are presented in Figure 1.14. Dihydroxychlorofusareilin B was a new polyoxygenated compounds isolated from a fungus of the *Trichocomaceae* family (to which the genus *Aspergillus* belongs to), which was derived from the Korean brown algae *Sargassum horneri* (Debbab et al., 2010). This polyoxygenated compound showed mild activity against *Staphylococcus aureus*, methicillin-resistance *S. aureus* (MRSA), and multi-drug resistance *S. aureus* (Debbab et al., 2010). Usually compounds produced from fungi associated with brown algae have been described to display antifungal and antioxidant activities (Oliveira et al., 2012). Another example are 1-(2,6-dihydroxyphenyl) pentan-1-one and (Z)-1-2-(2-butyryl-3-hydroxyphenoxy)-6-hydroxyphenyl)-3-hydroxybut-2-en-1-one, compounds produced by *Cryptosporiopsis* sps., from *Clidamia hirta* (Habbu et al., 2016). 1-(2,6-dihydroxyphenyl) pentan-1-one was found active against microbial pathogens with IC₅₀s between 18 and 30 µg/ml. While (Z)-1-2-(2-butyryl-3-hydroxyphenoxy)-6-hydroxyphenyl)-3-hydroxybut-2-en-1-one exhibited activity against *Pseudomonas fluorescens*, with an IC₅₀ of 6 µg/mL (Zilla et al., 2013). A new antimicrobial diketopiperazine (eurocristatine) compound was isolated from the sponge-associated fungus *Eurotium cristatum* (Gomes et al., 2012). α -Campholene aldehyde and lucenin-2 were two novel compounds isolated from a sponge-associated *Aspergillus ochraceus*. Both compounds displayed activity against microbial human pathogens (Meenupriya and Thangaraj, 2011). Furthermore, *Curvularia lunata* was another sponge-derived endophytic fungus that yielded two anthraquinone compounds, lunatin and cytoskyrin-A that were found active against *S. aureus*, *Escherechia coli* and *Bacillus subtilis* (Jadulco et al., 2002). Another active antimicrobial compound was varixanthone isolated from the endophytic fungus *Emericella variecolor* (Malmstrøm et al., 2002). Varixanthone was found active against a wide range of bacteria (Malmstrøm et al., 2002).

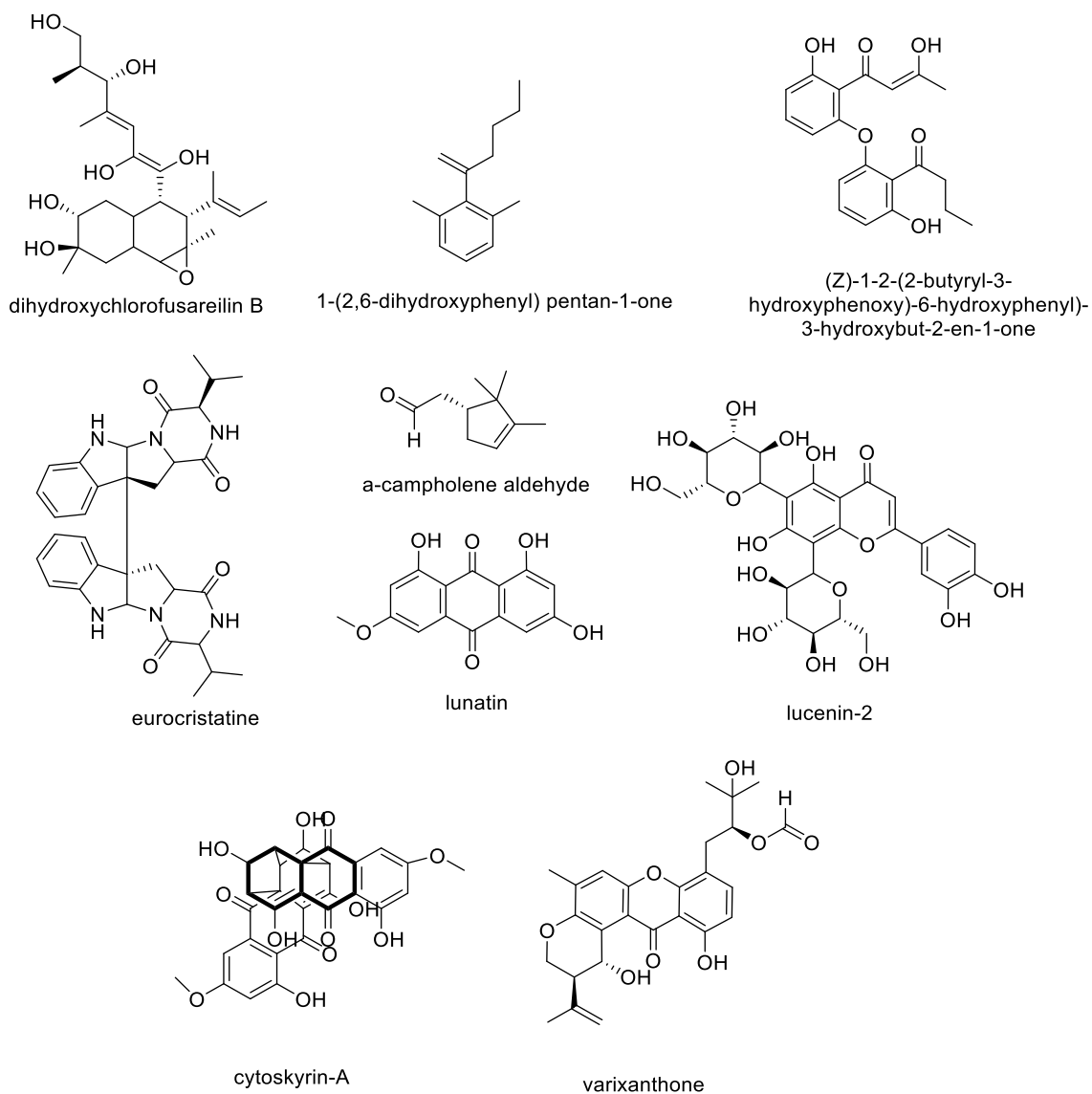


Figure 1.14: Anti-microbial compounds produced by endophytic fungi.

1.5 Fungal endophytes as sources of bioactive compounds

Natural bioactive compounds are chemical compounds produced from a natural source as a result of a metabolic process in organism, such as plant, animals and microorganism (Strobel and Daisy, 2003). As mentioned above, about 68% of antimicrobial agents and 34% of the anti-cancer agents are derived from natural sources (Newman and Cragg, 2007). There has been a strong need to find novel and sustainable sources of bioactive compounds to overcome emerging new diseases and microbial resistance (Kaul et al., 2012). One of the sources of biologically active compounds which can overcome supply problems are endophytic fungi and bacteria (Kaul et al., 2012). Endophytes are microorganism either both bacteria and/or fungi, which live inside a living host organism such as plants, animal and seaweeds without causing any disease to the host organism (Bacon and White, 2000). Endophyte-organism association is a beneficial relationship. Endophytes afford chemical defence compounds to protect the host organism from any attack of other microorganisms and pests (Strobel and Daisy, 2003). Host organisms can be beneficial to endophytes by supplying them with primary and secondary metabolites to be used for the synthesis of compounds needed for the endophyte's adaptation (Bacon and White, 2000). Endophytic fungi have been considered to be the most generous provider of secondary metabolites amongst endophytic microorganisms (Zhang et al., 2006). Compounds produced by endophytic fungi have afforded a broad spectrum of biological activity from diverse chemical groups (Figure 1.15) that include alkaloids, steroids, terpenoids, flavonoids, glycosides, isocoumarins and many more (Zhang et al., 2006). Studies on the endophytic secondary metabolites are considered to be small, which indicates the high possibility for the discovery of novel biologically active compounds (Kaul et al., 2012).

Fungi relate with their host organism either by parasitic or saprobic and asymptomatic association (Suryanarayanan, 2012). Parasitic association causes host cell damage with the production of toxic compounds (Suryanarayanan, 2012). Saprobiic or asymptomatic association do not cause any damage to the host organism but affords biologically active compounds that are not harmful to the host (Suryanarayanan, 2012).

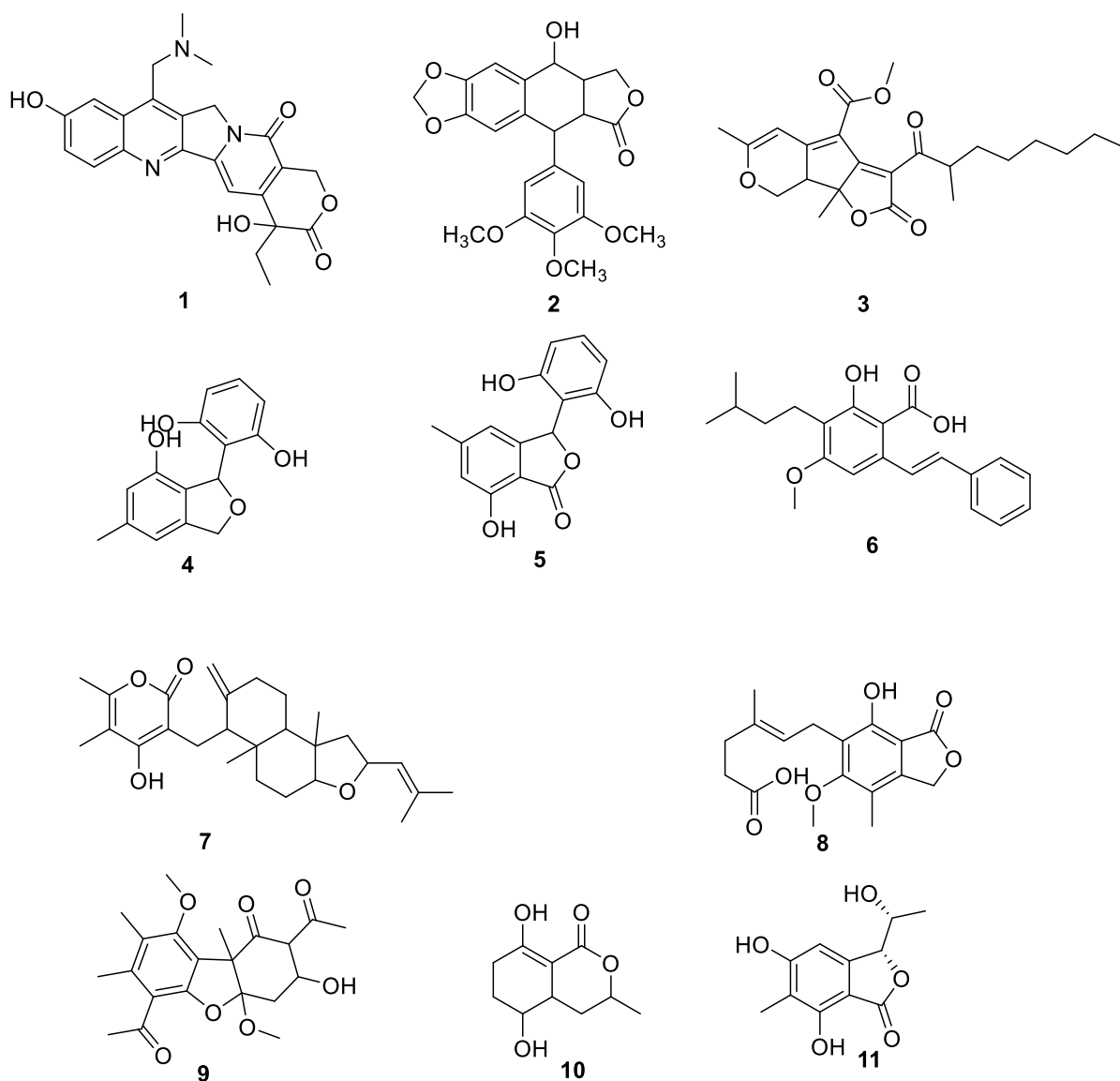


Figure 1.15: Bioactive compounds isolated from endophytic fungi; anti-cancer bioactive compounds (**1-3**), anti-oxidant compounds (**4-6**), immunomodulatory compounds (**7-8**) and anti-bacterial compounds (**9-11**) (Strobel et al., 2002, Harper et al., 2003, Puri et al., 2005, Kour et al., 2008, Kusari et al., 2009, Zhao et al., 2012).

1.6 Limitations of working on fungal endophytes

Working on endophytes as a source of novel bioactive compounds can be greatly valuable for drug discovery, but the following technical difficulties must be overcome:

1. Fungi have a highly diverse morphological traits that a traditional taxonomical method alone is insufficient for their identification. Correct identification must be accomplished through molecular biological methods, which requires an internal transcribed spacer (ITS) for gene sequencing (Kusari et al., 2014, Gardes and Bruns, 1993, Horton and Bruns, 2001). The ITS is unique for every organism that is used to taxonomically identify respective genus within a family or even species within a genus. ITS gene sequencing requires only a small amount of DNA to facilitate amplification reactions. All fungi have a specific DNA priming site that can be used to find certain types of fungi, so it could be well conserved by the primers (Peay et al., 2008).
2. A consistent expressions of the genes responsible for the biosynthesis of a bioactive compound in the endophyte could be difficult to reproducibly obtain because genes can change very quickly during the fermentation process.
3. Repeated sub-culturing could repress the expression of the genes responsible for the biosynthesis of the bioactive compounds, and thus decrease the amount of the bioactive compounds that are produced by the endophyte (Scherlach and Hertweck, 2009, Kusari et al., 2014).

2 Materials and methods

2.1 Isolation and identification of endophytic fungi from collected seaweeds

2.1.1 Materials and equipment

Media for the inoculation of the endophytic fungi was prepared from malt extract (ME) powder and nutrient agar, both were purchased from Oxoid, Manchester, UK. Chloramphenicol obtained from Acros Organics, Geel, Belgium was used as an antibacterial agent in the initial inoculation step. A solution of 70% of isopropanol was prepared by mixing HPLC grade isopropanol from Sigma-Aldrich, Poznań, Poland with sterile water. Sagrotan® spray from Sagrotan, Heidelberg, Germany was used as a disinfectant for the microbial safety cabinet.

Adjustment of media pH was done by using sodium hydroxide (NaOH) purchased from Sigma-Aldrich Poznań, Poland. The pH has been monitored using pH meter obtained from Jenway, Staffordshire, UK. Magnetic mixer from Stuart, Stone, UK and Vortex Genie 2 from Scientific Industries Inc, London, UK were used for multi-purpose mixing or solubilization either during media or sample preparation and fractions produced by preparative thin layer chromatography (TLC) extraction. Inoculated media used for screening, media-optimisation and scale-up were incubated at 27C° using an incubator from Vindon scientific, Oldham Lancashire, UK. Petri dishes used to initially grow the fungi were purchased from Thermo Scientific, Massachusetts, USA. The laminar flow (BioMAT²) was obtained from Medical Air Technology, Manchester, UK. Thirty strains were obtained after inoculation of seaweed internal tissues on malt agar plates. For endophytes identification, Internal transcribed spacer (ITS) region that stand between 16s and 23s rRNA genes of endophytes were used. Successful ITS gene sequencing was done by preparing electrophoresis gel plates containing UltraPure™ TBE buffer 10X from Life technologies, Cramlington, UK, ethidium bromide 10mg/ml from Sigma-Aldrich, Continental, USA and Agarose-Molecular Grade, from Camarillo, Bioline, US. While the samples for polymerase chain reaction (PCR) were prepared using Water-Molecular Biology reagent, REExtract-N-Amp™ PCR ReadyMix™, Extraction and Dilution solution purchased from Sigma-Aldrich, St. Louis, USA. In addition, ITS primers; ITS1 {5'-TCC-GTA-GGT-GAA-CCT-GCG-G-3'}a and ITS4 {5'-TCC-TCC-GCT-TAT-TGA-TAT-GC-3'} used in PCR were obtained from Integrated DNA Technologies, Coralville, USA. The HyperLadder II and sample loading buffer used for processing the electrophoresis experiments were purchased from Bioline, Camarillo, USA.

For DNA extraction and DNA amplification Two thermal cyclers were used including, Primus 96 Thermal Cycler from MWG AG Biotech, Ebersberg, Germany and DNA Thermal Cycler 480 Manual from Perkin Elmer, Waltham, USA. Electrophoresis plates were purchased from Bioscience Services, London UK. While the voltage source used for amplified DNA movements in electrophoresis gel plate was a BioMax MBP300 from Kodak, New Jersey USA. Gel imaging for the plates was done using INGENIUS gel documentation system from Syngene, Cambridge, UK.

GenElute™ Gel Extraction Kit from Sigma-Aldrich, St. Louis, USA was used to extract the DNA after PCR of the DNA samples from electrophoresis gel. Washing solution, gel solubilization solution, column preparation solution, elution solution, GenElute™ binding column G and collection Tube were all obtained with a GenElute extraction kit. The solubilization of agarose gel containing DNA was done using a dry block DRI-BLOCK® DB-2A from Techne, Chelmsford, UK. Centrifugation of the samples after each DNA extraction step was done using 5415 D Centrifuge from Eppendorf, Hamburg, Germany. DNA concentration of each sample was measured using Nanodrop 2000c Spectrophotometer from Thermo Scientific, Massachusetts, USA. While the processing of the PCR results was done using FinchTV 1.4.0 software developed by Geospiza, and the data produced was compared with data obtained by Basic Local Alignment Search Tool (BLAST) that is available online from the National Centre for Biotechnology (NCBI), Maryland, USA.

Crude extract produced during screening, media optimization and scale up were extracted using (HPLC) grade ethyl acetate (EtOAc) from Sigma-Aldrich, Poznań, Poland were used as extraction solvent. Different solvents were used either for LC-HRMS, HPLC-grade acetonitrile (ACN) and formic acid both from Sigma-Aldrich, Poznań, Poland were used. For MPLC, HPLC-grade dichloromethane (DCM), n-hexane, acetone, and methanol (MeOH) from Sigma-Aldrich, Poznań, Poland were purchased. While analytical-grade acetone from VWR, Fontenay-sous-Bois Cede, France was used for multi-purpose work. Homogenization of incubated media was done with a T18 basic ULTRA-TURRAX from IKA, Anhalt-Bitterfeld, Germany. While crude extracts in EtOAc were concentrated and dried under vacuo using a rotary evaporator R-110 from Buchi, Flawil, Switzerland. Concentrated extracts were reconstituted in EtOAc and dried under nitrogen in a Heating Block SBH130D/3 and sample concentrator SBHCONC/1 from Stuart, Stone, UK. During the extraction process an ultra-wave sonicator from Scientific Laboratory Supplies, Nottingham, UK was used to enhance

solubilization. In addition, ultrapure water for solvent and media preparation was generated using a Direct-Q® water purification system from Merck Millipore, Massachusetts, USA.

For extracts and fractions, samples were run on an Accela HPLC (Thermo Scientific, Germany) coupled to an Exactive mass spectrometer (Orbitrap, Germany). Data were processed with “Xcalibur 2.2” released by Thermo Scientific, Heidelberg, Germany. In addition, data splitting was done with ProteoWizard (<https://sourceforge.net/projects/teowizard/>), USA to separate the data between the negative and positive ionization files (Kessner et al., 2008). While splitted data analysis was done with MZmine 2.4.2 followed by an in-house excel sheet called Macro which coupled with Dictionary of Natural Products (DNP version 2021) database published by CRC Press, Boca Raton, USA (Pluskal et al., 2010, Macintyre et al., 2014). The NMR samples have been dissolved using deteriorated dimethyl sulfoxide (DMSO-d₆) purchased from Sigma-Aldrich, Poznań, Poland and transferred to NMR tubes obtained from Norell, New York, USA. NMR samples were measured in a 400 MHz Jeol-LA400 FT-NMR spectrometer system equipped with a 40TH5AT/FG probe. In addition, an AVANCE-III 600 instrument with a 14.1 T Bruker UltraShield magnet from the Department of Pure and Applied Chemistry was used as well. It has a 24 position autosampler, 3 channel console, is DQD and Waveform-equipped and can use either a BBO-z-ATMA-[³¹P-183W/1H] probe or a TBI-z-[¹H, ¹³C, ³¹P-¹⁵N] probe from Bruker, Rheinstetten, Germany. All NMR spectra were processed with MestReNova 14.2 developed Mestrelab Research, Santiago de Compostela, Spain.

2.1.2. Seaweed Collection

Eight seaweeds namely: *Ascophyllum nodosum*, *Laminaria hyperborea*, *Ulva intestinalis*, *Ulva lactuca*, *Fucus vesiculosus*, *Fucus serratus*, *Fucus spiralis*, and *Himanthalia elongata* were collected from Culzean coast, Ayr, Scotland, United Kingdom and were identified by Kirsty Blake from Marine Biopolymers Ltd (MBL). Seaweeds were collected at least five meters from both sides the dry coastline at low tide. GPS collection location was at 55.3546966, -4.7891084. The seaweeds were placed in 50ml falcon tubes and stored in fridge at 2-8C° until used for inoculation work.

2.2 Microbiological Methods

2.2.1 Preparation of malt extract agar media and fungal inoculation from seaweeds.

Malt agar (MA) media was prepared with 7.5g of malt extract powder mixed with 7.5g of agar followed by addition of 0.1g of chloramphenicol in a 500ml bottle. The mixture solubilized in 500ml of ultrapure water and pH of the mixture was adjusted to between 7.4 and 7.8 with 0.1M sodium hydroxide. A pH meter was used to monitor the pH of the media. The prepared media were then autoclaved. The autoclaving was done for 1h and 30mins at 121°C under 15psi. The autoclaved agar-based media was poured into 100mm×15mm Petri dishes plates in a laminar flow safety cabinet hood.

The laminar flow was cleaned and disinfected using both physical sterilization through UV light for 30min and chemical sterilization using 70% isopropanol and Sagrotan spray to ensure sterility. A small cut (1×1cm) of a seaweed frond was rinsed with 70% isopropanol to get rid of the epiphytes living on the surface of it, followed by rinsing with sterile water to get rid of any isopropanol residues. Each seaweed was divided to three or four parts (1×1cm) and each part was added into an agar plate with the cut in direct contact with the media. All inoculated plates were incubated at 27C° until fungal growth could be observed.

2.2.2 Initial inoculation of endophytic fungi from seaweeds

MEA plates were again prepared as described above but 3x of the volume in section 2.2.1. A small cut of each of the fungal colony from the incubated plates from section 2.2.1 were transferred to the new MEA plates. The re-inoculated plates were labelled according to their host origin. The colour and morphology of each transferred colony were recorded. The newly incubated plates were again incubated at 27C° until enough biomass was available for the 2nd inoculation for further purification.

2.2.3 Fungal culture purification step.

MEA plates were again prepared as in section 2.2.2 but without adding chloramphenicol. An aliquot cut of each of the pure fungal colonies from section 2.2.2 were re-inoculated on new plates and were incubated at 27C°. Enough plates were inoculated for chemical profiling, biological screening, voucher storage and taxonomical identification. The isolated endophytes have been coded according to their host seaweeds and morphology.

2.2.4 Fungal extracts for screening.

2.2.4.1 Preparation of crude fungal extracts

Each purified fungus was re-inoculated on nine MEA plates as prepared in section 2.2.3 to make a triplicate from each fungal extract. Every extract was prepared from three plates. According to their growth rates, the triplicates were categorised into slow and fast-growing groups. The fast-growing fungi were incubated for 15 days, while the slow-growing endophytes were incubated for 30 days. After incubation, the fungal cultures were transferred to a 250ml Erlenmeyer flask to which 100ml of EtOAc was added and left to macerate for 24h under fume hood. After 24h, each flask of fungal culture in EtOAc was then homogenized for 30 min and filtered. The homogenized flasks have been subjected to extraction producer using a buchner funnel. While the mycelia were extracted for another 2 times using 100ml of EtOAc as presented in Figure 2.1. Extracts was dried using rotary evaporator and placed in tared vials. The dried extracts were stored at 2-5C° until further use for chemical profiling with NMR and MS, as well as prior to the biological assays.

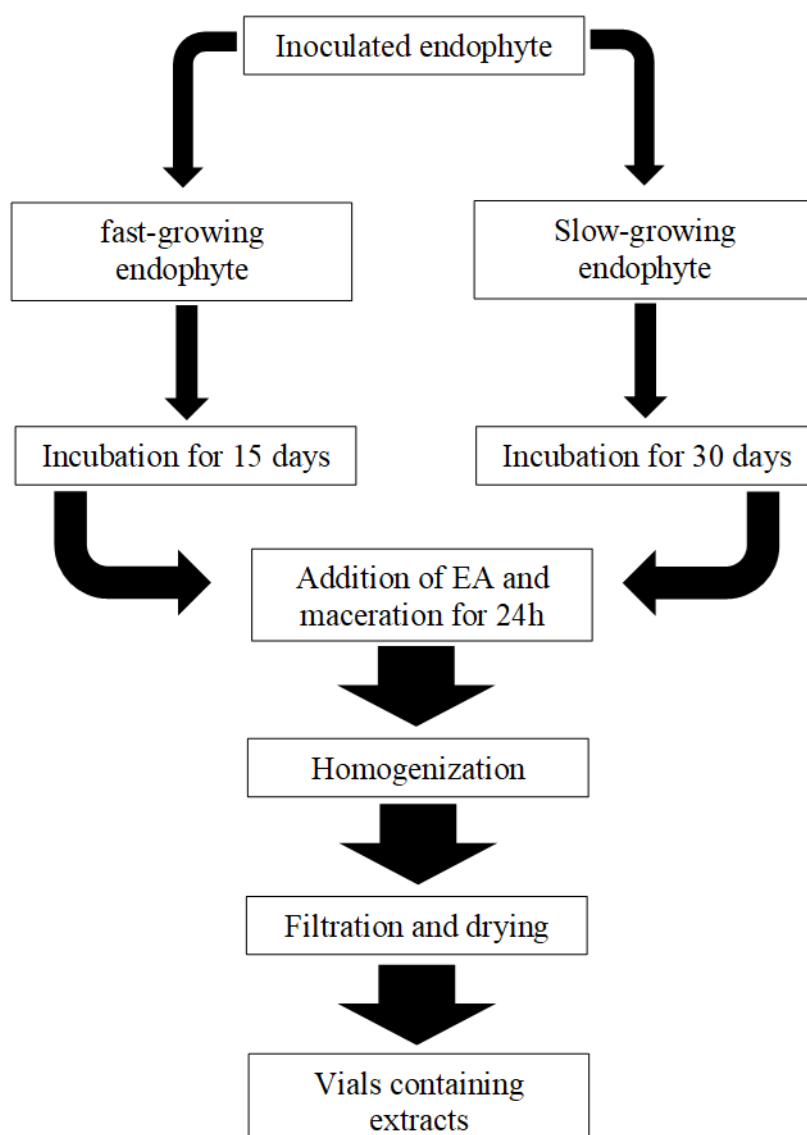


Figure 2.1: Schematic diagram for the preparation of crude fungal extracts.

2.2.4.2 Sample preparation of fungal crude extracts for screening.

The crude fungal extracts were subjected to three screening tests. The three screening tests included nuclear magnetic resonance spectroscopy (NMR), high performance liquid chromatography coupled with high-resolution mass spectrometry (LC-HRMS) and antibiofilm assay. The spectral data was processed and subjected to multivariate analysis using the SIMCA software. Sample concentrations for each screening test is summarised in Table 2.1.

Table 2.1: Required concentration of sample for screening.

Screening test	Concentration	Solvent used
LC-HRMS	1 mg/mL	Methanol
NMR	5 mg/600 μ L	DMSO- <i>d</i> ₆
Bioassay	10 mg/mL	DMSO

2.2.4.3 Anti-biofilm biological assay.

2.2.4.3.1 Bacterial concentration preparation:

Both biofilm-forming *Staphylococcus aureus* (ATCC 29213) and *Pseudomonas aeruginosa* (ATCC 27853) were prepared by inoculating a loop of each bacteria in three different 25 cm² of tissue culture flasks containing 5ml of (Lysogeny broth) LB broth with a total of six flasks. The six flasks were prepared to be used in AlamarBlue® and planktonic assays, three flasks for each. The inoculated flasks were incubated for 16h at 37C°. This was done to let *S. aureus* and *P. aeruginosa* reach stationary growth phase. This was followed to the transfer of 100 μ l from the flasks to a new 6 flasks containing a fresh media and incubated for 6h to grow again and reach log phase. Optical density was measured at 600nm wavelength, the density of each bacterial culture was calculated, and each culture was diluted to a final concentration of 1 \times 10⁷cfu/ml.

2.2.4.3.2 Stock solutions and dilution plates:

Stock solutions of each of the extracts and fractions were prepared with 100 μ g of the samples dissolved in 100 μ l of biological-grade DMSO. The dilution plate for extracts, fractions, and pure compounds was prepared to have a final concentration of 1000 μ g/ml by diluting 4 μ l of 10mg/ml extract with 36 μ l of LB broth.

2.2.4.3.3 AlamarBlue® biofilm viability assay:

Assay plates were prepared by mixing 10 μ l of the sample stock solutions in the dilution plate with 90 μ l of LB broth pre-inoculated with the bacteria to give a final concentration of the sample at 100 μ g/ml. Gentamicin was used as a standard with which the reference curve was prepared using a concentration range of 10-0.039 μ g/ml. The plates were incubated at 37C° in a shake incubator at a speed of 150rpm for 16h. A 10 μ l volume of Alamarblue® solution was added to each well. The plates were further incubated for 4h in a shake incubator at 37C°. Absorbance reading was taken at 560nm excitation wavelength and 590nm emission

wavelength every 30 mins after 2h of incubation. The readings were processed in excel sheet and final graphs were produced after processing the results with GraphPad prism 5.

2.2.4.3.4 Planktonic assay:

Assay plates were similarly prepared and inoculated as in the AlamarBlue® assay. In the planktonic assay, the wells were emptied and washed twice with 100µl of phosphate buffer saline (PBS) after the incubation period. Absorbance readings for the plates were measured to determine the ability of the extracts to inhibit biofilm formation at wavelength of 600nm.

2.2.4.3.5 Minimum biofilm eradication Concentration (MBEC) and Minimum inhibitory concentration (MIC) assay:

The active fungal extracts with a minimum of 80% with a concentration of 100µg/ml against bacterial growth and biofilm formation were again tested in both AlamarBlue® and planktonic assays to calculate the MBEC, and MIC of each of the active extracts. A dilution plate was prepared for each extract with a concentration range of 3.91 to 1mg/ml by serial dilution method. Assay plates were prepared as described above in the AlamarBlue® and planktonic assays in section 2.2.4.3.3 and 2.2.4.3.4 respectively.

After finishing the data analysis of the screening tests, the results along with the spectral data of the samples were subjected to multivariate analysis using SIMCA to obtain the corresponding OPLS-DA scatter and loadings plots.

2.2.5 Taxonomical identification of antimicrobial active endophytic fungi by ITS gene sequencing.

A small cut of each of the fungal cultures devoid of any trace of the solid media were transferred to 1.5ml Eppendorf tube, followed by an addition of 100µl of DNA extraction solution and mixed vigorously on a vortex. The mixture was placed in a DNA thermal cycler 480 Manual at 95C° for 10 min to denature the DNA strands. 100µl of DNA dilution solution was added to each Eppendorf tubes containing the DNA and stored at 2-8C° for the next step. Polymerase chain reaction (PCR) and gene amplification were done for each of the endophytic fungus by mixing 4µl of a solution of denatured DNA with 25 µL of REExtract-N-Amp™ PCR ReadyMix™, 3 µL of the forward primer ITS1, 3 µL of the reverse primer ITS4 and 18 µL of

water-molecular biology reagent. The resulting mixture from each of the fungus was amplified and subjected to PCR using Primus 96 Thermal Cycler as summarised in Table 2.2.

Table 2.2: Polymerase reaction and amplification steps.

Step	Temperature (°C)	Duration (min)	Cycles
Initial denaturation	95	3	1
Denaturation	95	1	-
Annealing	56	1	35
Extension	72	1	-
Final extension	72	10	1
Hold	4	-	-

Gel electrophoresis plates were prepared by dissolving 0.5g of agarose powder in 50ml of 1x TrisBorateEDTA (TBE) buffer. The mixture was heated using a full power microwave for 1-2 min to ensure full solubilization. The weight loss during microwaving was recovered by the addition of ultrapure water. A 2µl volume of ethidium bromide was added under the fume hood followed by pouring the mixture in an empty gel electrophoresis plate and the plate was left to stand for 20min until the mixture solidified. A volume of 1x TBE buffer was added to the plate to enhance the migration of fungal DNA in the plate. A 6µl volume of hyperLadder II, 45µl of blank sample and amplified DNA samples were applied on the prepared gel electrophoresis plate and partitioned at three positions as shown in Figure 2.2.

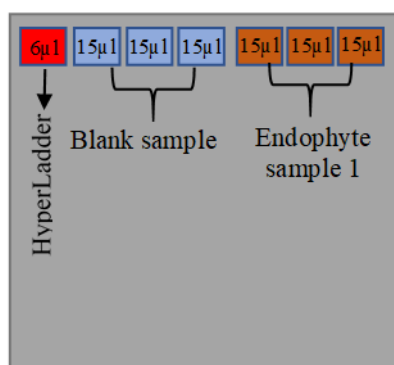


Figure 2.2: Map representing samples on gel electrophoresis plate.

The gel electrophoresis plate was subjected to 50 volts for 1h for the DNA to migrate in the gel electrophoresis plate. After 1h, gel imaging was accomplished for documentation then DNA bands for each of the fungus were cut out with a scalpel and stored in 1.5mL Eppendorf tube

and stored at -20C° until extraction. DNA was extracted from the agarose gel with a GenElute extraction kit using the kit protocol. The agarose gel pieces that contained the gene fragments were weighed for each sample. Then the solubilisation solution was added, which was three times the volume of the DNA solution. Subsequently, the mixture was incubated in DRI-BLOCK® for 10 min with occasional mixing on a vortex. Then, equal volumes of isopropanol were added to the solubilised gene-agarose mixture and again homogenised with a vortex. Meanwhile, the GenElute™ Binding Columns were prepared. Each binding column was placed in a 2 mL collection tube, to which 500 µL of column preparation solution was added to each binding column then centrifuged for 1 min. The preparation solution was drained into the collection tube and discarded. The solubilized gel solution mixture was loaded into the binding column and again centrifuged for 1 min. After centrifugation, the solution was collected into the collection tube then discarded. While 700 µL of the wash solution was added to the binding column. This was followed again centrifuged for 1 min. After finishing, the solution was discarded along with the collection tubes. Next, the binding columns were placed in a new collection tubes, with 25 µL of previously heated Elution Solution added into them and centrifuged for 1 min. Then the binding columns were discarded, and the genes were solubilised in the Elution Solution and collected in the collection tubes. Each tube containing the genes was stored in -20C° freezer until they were submitted for sequencing. Only the fungus that afforded antimicrobial active extracts were submitted for sequencing. The sequencing results were processed with the FinchTV software and compared to database hits available on the Basic Local Alignment Search Tool (<http://blast.ncbi.nlm.nih.gov/Blast.cgi>).

2.2.6 Media optimization.

Three of the four antimicrobial active fungal extracts were selected for further optimisation on nine different media to obtain a higher yield and improved biological activity of the extracts as shown in Figure 2.3. Depending on the extract yield and the biological assay results as well as the uniqueness of the chemical profiles of the crude extracts obtained from the malt agar extract, *D. salina*, *M. elegance*, and *H. rubiginosum* were selected for media optimisation work.

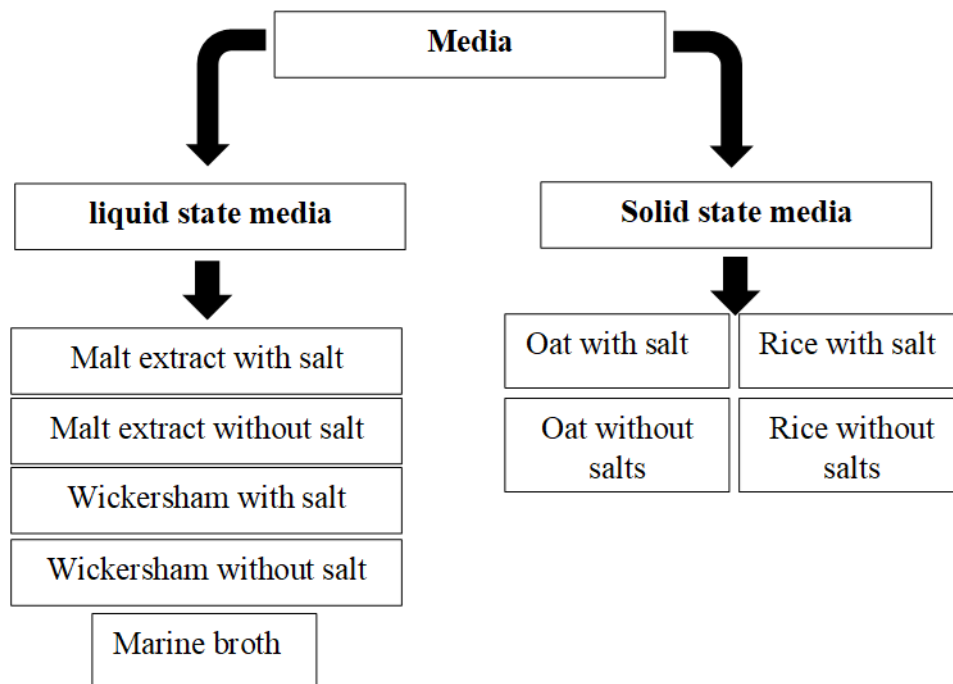


Figure 2.3: Schematic diagram for media optimisation work.

2.2.6.1 Preparation of fungal inoculum for media optimisation.

Fungal stock cultures in 30% glycerol and 70% malt extract broth were initially inoculated on petri dish plates of MEA media and incubated for 10 days at 27C°. At one vial per plate, three plates were prepared for each fungus. After 10 days, fungal cultures were re-inoculated on fresh MEA plates and incubated for another 10 days at 27C°.

2.2.6.2 Media preparation to optimise the production of active crude extract.

2.2.6.2.1 Malt extract broth media with and without sea salt:

Malt extract broth without sea salt was prepared by mixing 1.5g of malt extract powder with 100ml of ultrapure water in 250ml Erlenmeyer flask. The pH of the mixture was adjusted to 7.4 using 0.1M NaOH. The prepared media was then autoclaved. In parallel, malt extract broth with sea salt was prepared with 2.5g of sea salt.

2.2.6.2.2 Wickersham broth with and without sea salt:

Wickersham broth without sea salt was prepared by mixing 0.3g of malt extract and 0.3g of yeast extract powder (Oxoid) with 0.5g of peptone (Oxoid) with 100ml of ultrapure water in 250ml Erlenmeyer flask. The pH was adjusted to 7.4 with 0.1M NaOH then autoclaved. Wickersham liquid broth with sea salt was prepared with 2.5g of sea salt.

2.2.6.2.3 Marine broth media:

Marine broth was prepared by dissolving 3.74g of marine broth powder (Oxoid) in 100ml of ultrapure water in a 250ml Erlenmeyer flask. The pH was adjusted to 7.4 with 0.1M NaOH then autoclaved.

2.2.6.2.4 Rice media with and without sea salt:

Rice (long grain) media without sea salt was prepared by mixing 100g of rice purchased from Aldi store. UK with 150ml of ultrapure water in 500ml Erlenmeyer flask then autoclaved. Alternatively, rice media with sea salt was prepared by mixing 100g of rice with 3.75g of sea salt in 150ml of ultrapure water.

2.2.6.2.5 Oat media with and without sea salt:

For oat (Scott's Porage Oats) media without sea salt a 100 %w/v of oat was prepared by mixing 100g of oat with 100ml of ultrapure water in 250ml Erlenmeyer flask then autoclaved. While for oat solid media with sea salt, a 100 %w/v of oat was prepared with 2.5 %w/v of sea salt.

2.2.6.3 Fungal inoculation.

One-third of the petri dish fungal culture was added to the respective media described above. The inoculated media were incubated at 27C° in three time periods at 7, 15, and 30 days. Each sample at different incubation periods were prepared in triplicates.

2.2.6.4 Preparation of extracts from fungal cultures.

Fungal cultures were extracted with EtoAc by macerating the cultures in 100 ml of the solvent for 24h then homogenized for 30 min to lyses the fungal cells and filtered. For the

EtOAc extracts from the liquid media, the filtrate was added into a separatory funnel to achieve further extraction of the aqueous layer with EtOAc by solvent partitioning. EtOAc was added 3-4 times during liquid-liquid extraction for exhaustive extraction. The several volumes of pooled organic phase were then concentrated under vacuo by rotary evaporation. For the fungal culture from the solid media, the homogenate was also extracted several times with EtOAc, decanted and filtered. The pooled filtrates were then concentrated under vacuo. The concentrated extracts were transferred to tared vials and stored at 2 to 5C° until further analysis. A summary of the extraction procedure is presented in Figure 2.4.

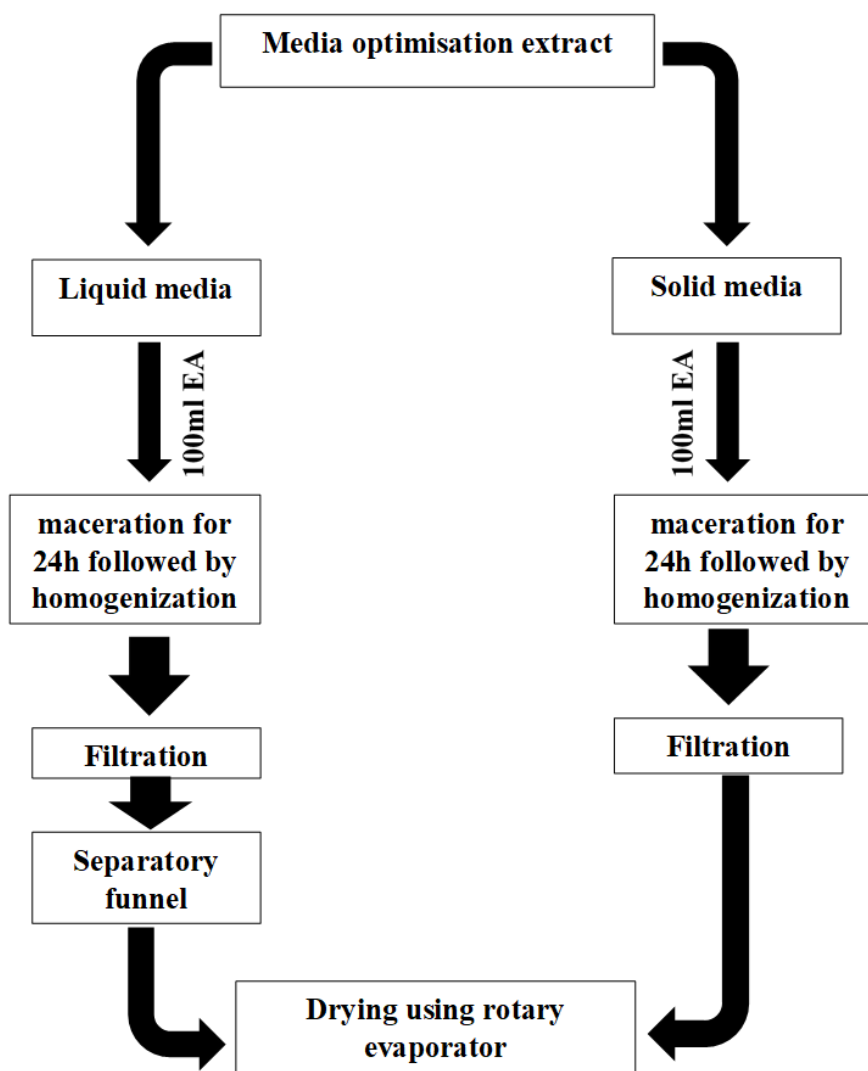


Figure 2.4: Schematic diagram represents extraction procedure for both liquid and solid medias.

2.2.6.5 Sample Preparation

NMR, LC-HRMS, and bioassay samples were prepared to provide the spectral and biological data necessary to select the media for the scale-up work. The samples were prepared as summarised above in Table 2.1. The generated spectral data was processed then subjected to multivariate analysis using the software SIMCA as shown in Figure 2.5.

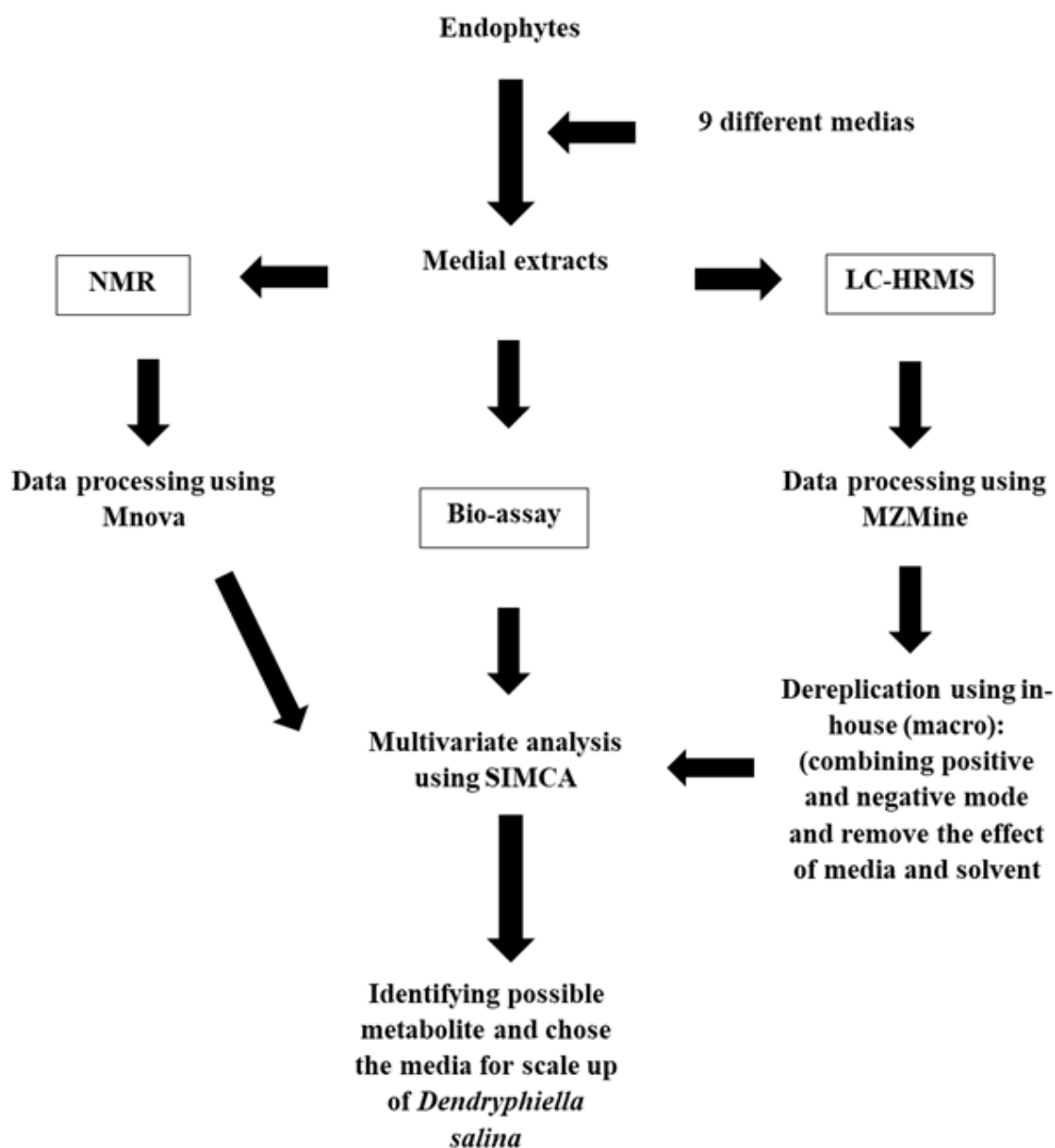


Figure 2.5: Workflow for sample analysis.

2.3 Chemical analysis: Extraction, chromatographic separation and structure elucidation

2.3.1 Scaled-up fermentation and extraction

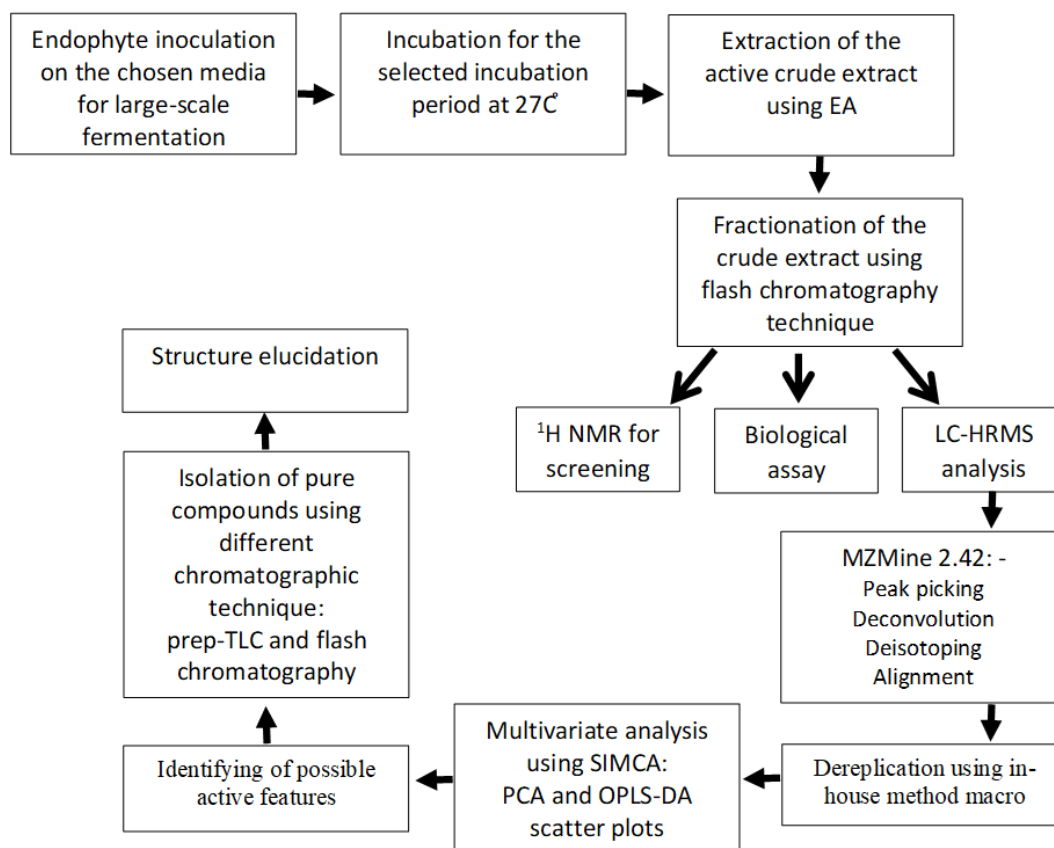


Figure 2.6: Workflow for scale-up fermentation to pure compounds isolation.

Malt extract liquid broth with sea salt and oat solid media without sea salt were chosen to scale-up the crude extract yield from *D. salina*. Media were prepared following a scaled-up protocol as further outlined below.

For malt extract broth media with sea salt, 20 flasks were prepared with 15g of malt extract powder and 25g of sea salt in 1000ml of ultrapure water in a 2000ml Erlenmeyer flask. The pH was adjusted to 7.4 with 0.1M sodium hydroxide then the media flasks were autoclaved. For oat media without sea salt, 20 flasks were prepared with 500g of oat with 1000ml of ultrapure water in a 2000ml Erlenmeyer flasks then autoclaved.

Fungal inoculum for scale-up cultures of *D. salina* was prepared as described in section 2.2.6.1. and inoculation was accomplished as described in section 2.2.6.3. The inoculated 1-litre media were incubated as stand cultures at 27°C for 30 days.

For extraction, 800ml of EtOAc was added to each flask and again macerated for 24h to stop *D. salina* growth and other metabolic processes. After 24h, the culture flasks were homogenised for 30min. For *D. salina* growing on malt extract broth, the organic EtOAc phase layer was separated from the aqueous phase with a separatory funnel. Liquid-liquid extraction was done exhaustively with EtOAc. The multiple batches of EtOAc extracts were pooled, concentrated under vacuo and transferred to a tared vial for storage until fractionation. For *D. salina* growing on oat media, the same steps were followed except the solvent partitioning step. After homogenisation, EtOAc was repeatedly added on the mycelia growing on the oat and the solvent was instead decanted and filtered at the end.

The crude extracts afforded by the two-culture media were subjected further to preliminary fractionation by liquid-liquid partitioning. The crude extracts were reconstituted with 200ml of 10% aqueous methanol and extracted thrice with equal volumes of n-hexane to eliminate fatty acids and lipids. Then successively, the 10% Aq methanol layer was solvent extracted three times with equal volumes of EtOAc as well. The crude fractions of hexane, EtOAc, and aqueous methanol were concentrated, dried, and subjected to chemical profiling and antimicrobial assay screening. Extraction workflow for both fungal extracts generated from two media is presented below in Figure 2.7. A schematic diagram of liquid-liquid partitioning of crude extracts of *D. salina* grown on malt extract with sea salt is shown in Figure 2.8/2.9 and those grown in oat media is in Figure 2.9/2.10.

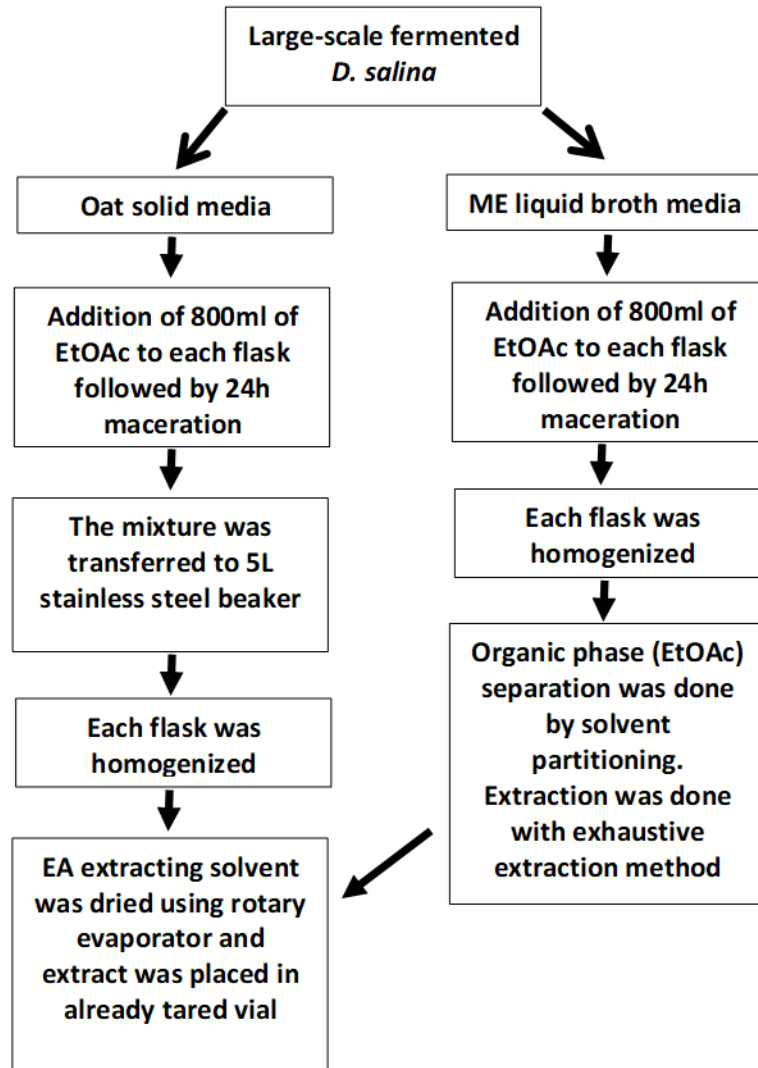


Figure 2.7: Preparation of crude extracts of *D. salina* for liquid-liquid partitioning.

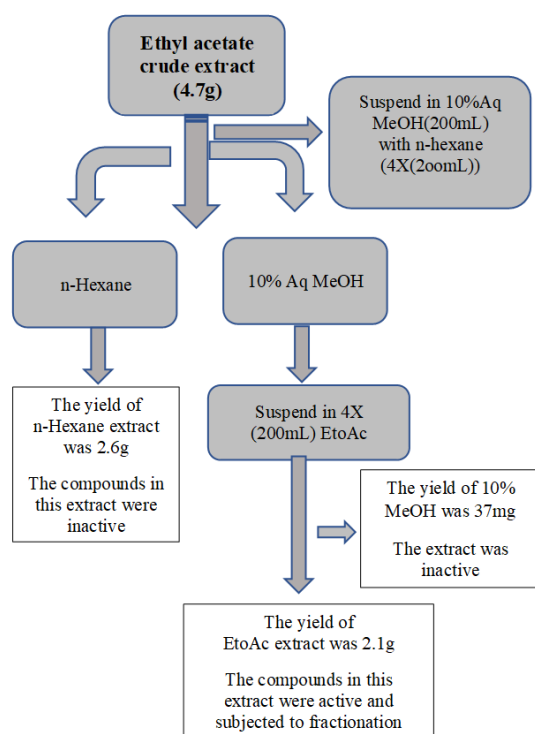


Figure 2.8: Schematic diagram of liquid-liquid partitioning of *D. salina* extract grown on malt extract with sea salt.

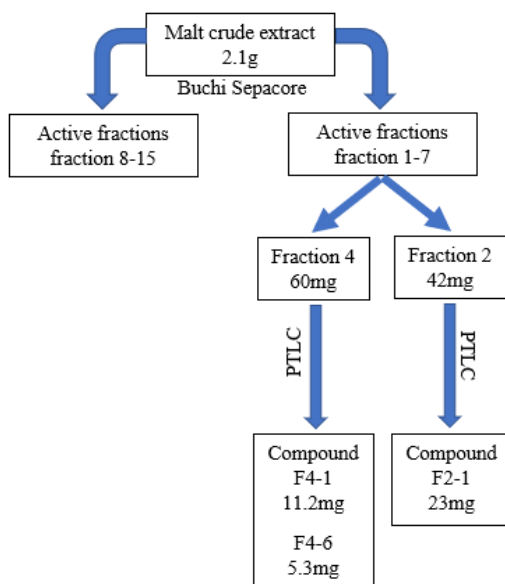


Figure 2.9: Schematic diagram showing the isolation of pure compounds produced by *D. salina* grown on malt extract media with sea salt.

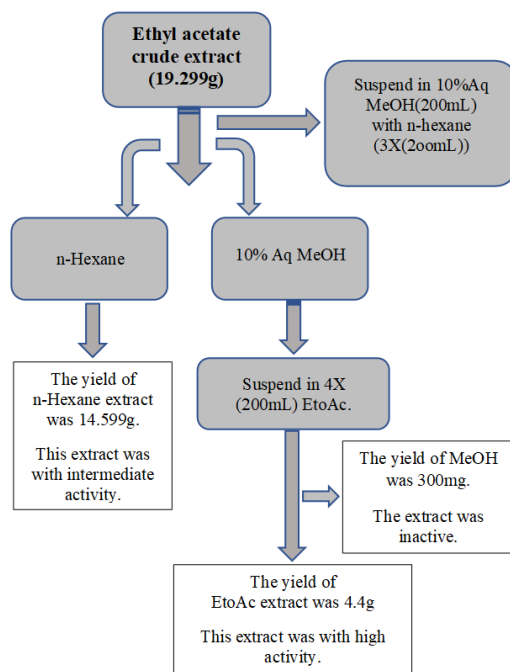


Figure 2.10: Schematic diagram of liquid-liquid partitioning of *D. salina* extract grown on oat media.

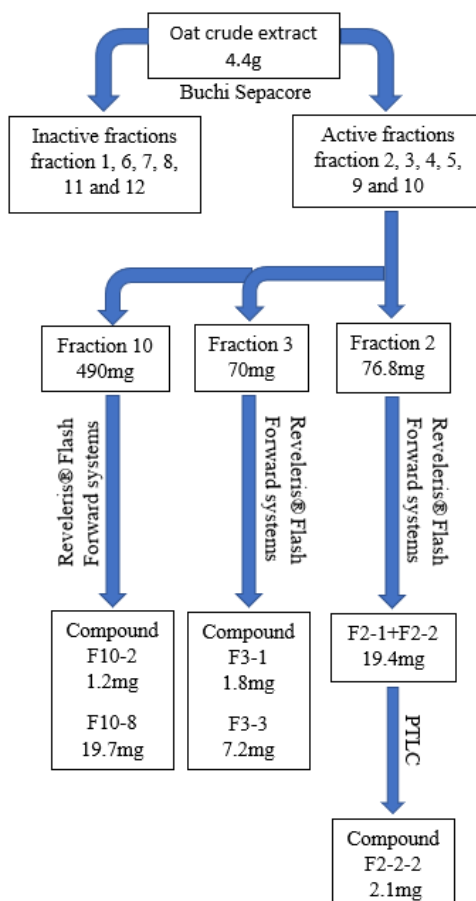


Figure 2.11: Schematic diagram showing the isolation of pure compounds produced by *D. salina* grown on oat media without sea salt.

2.3.2 LC-HRMS

Each sample was weighed and dissolved in methanol to prepare a concentration of 1 mg/mL for LC-HRMS analysis. Methanol was used as a media blank. ACE 5 C18 column was used. Solvent system was made up of acetonitrile (solvent A) and water (solvent B), both with 0.1% formic acid. The injection volume was 10 μ L, the flow rate was at 300 μ L/min. The standard gradient is presented in Table 2.3. High resolution mass spectrometry analysis was performed in both positive and negative modes in a mass range that varied from m/z 150 to 1500. The spray voltage was 4.5 kV. The capillary temperature was 320°C.

Table 2.3: Elution gradient used for LC-HRMS. Acetonitrile (solvent A) and water (solvent B)

Time (minutes)	% A	% B
0	90	10
30	0	100
35	0	100
36	90	10
45	90	10

The LC-HRMS chromatograms and spectra were viewed in Thermo Xcalibur 2.2.

2.3.3 NMR spectroscopy

Samples were dissolved in 600 μ L of DMSO- d_6 and transferred to NMR tubes. 5 mg were used for fractions, while the entire amount obtained (up to 30 mg) was used for pure compounds. Quantities less than 5 mg were dissolved in 300 μ L DMSO- d_6 and transferred to capillary NMR tubes. For structure elucidation, all compounds were submitted to applied chemistry department to use their 500MHz Bruker NMR instruments. This was done to perform HMBC, HSQC, and C¹³ especially for compounds with low yield (less than 5mg). The rest of the experiments (COSY, TOCSY, ¹H and HMQC) were done at Strathclyde Institution of Pharmacy and Biomedical Science (SIPBS) using 400MHz NMR instrument. All experiments were processed using MestReNova 14.2. For Proton Spectra, smoothing with Whittaker Smoother, baseline correction with Whittaker Smoother, apodization with Gaussian 1.00 and manual phase correction were carried out in MestReNova. While COSY analysis, smoothing with Whittaker Smoother, reducing t1 noise and symmetrizing as COSY-like were done.

2.3.4 Medium pressure liquid chromatography (MPLC)

MPLC or flash chromatography (FC) is a separation technique that is very similar to open column chromatography; however, a pressure is applied to elute the sample faster from the column. The solvent system was chosen after it was optimised on a TLC plate.

In both Buchi Sepacore and Reveleris® Flash Forward systems, normal phase columns were used and conditioned with the starting solvent system before loading the dry samples that were mixed with celite. For the initial fractionation of the crude extract with the Buchi Sepacore system, fractions were collected manually in 100 mL Erlenmeyer flasks at a rate of 100 ml/min. With Reveleris® Flash Forward system, samples were collected automatically in test tubes at lower flow rates. TLC analysis was done for all fractions so the similar ones would be pooled together.

2.3.4.1 Fractionation of *D. salina* extract obtained from malt extract broth with sea salt.

The crude extract (2.1g) was reconstituted in 6mL of EtOAc or in other appropriate solvent at the minimum amount possible and added to 7.5g of celite. The concentrated extract solution was added to the celite drop-wise to obtain homogeneous mixing then dried overnight under the fume hood. A prepacked column of silica was used as a stationary phase with 40x150mm (width x height) dimension. The main solvent used was DCM and MeOH. The percentage of MeOH in the mobile phase must not exceed 80%, to avoid the solvation of silica from the pre-packed column. Prior to chromatographic separation, the column was equilibrated with 100% DCM for 10 min at a slower flow rate of 50 mL/min with a total volume of (500ml) because DCM could be abrasive on the piston pump seals. The chromatographic separation was accomplished by step-wise gradient elution using a very gradual slope with increasing ratio of MeOH from 1 to 20% in 160 min at a flow rate of 100 ml/min. The column was washed with 70:30 acetone and MeOH. The selected mobile phase for fractionation was optimised by TLC and the elution gradient is presented in Table 2.4.

Table 2.4: Elution gradient for the fractionation of *D. salina* crude extract obtained from malt extract broth with sea salt.

Time (min)	Mobile phase %			Flow rate mL/min
	DCM	MeOH	Acetone	
0	100	0	0	50
10	100	0	0	50
40	99	1	0	100
70	97	3	0	100
130	95	5	0	100
160	80	20	0	100
180	0	30	70	100
200	0	30	70	100

2.3.4.2 Fractionation of *D. salina* extract obtained from oat media without sea salt.

The crude extract (4.4g) was reconstituted in 10mL of EtOAc and added to 9g of celite drop-wise to obtain a homogeneous mixture then left to dry overnight under the fume hood. A prepacked column of silica was used as a stationary phase solvent. The column was also equilibrated with 100% DCM for 10 min at a flow rate of 50 mL/min. The chromatographic separation was accomplished by step-wise gradient elution with increasing ratios of MeOH from 1 to 20% in 130 min at a flow rate of 100 ml/min. The column was washed with 70:30 acetone and MeOH. The selected mobile phase for fractionation was also optimised by TLC and the elution gradient is presented in Table 2.5.

Table 2.5: Elution gradient for the fractionation of *D. salina* crude extract obtained from oat media without sea salt.

Time (min)	Mobile phase %			Flow rate mL/min
	DCM	MeOH	Acetone	
0	100	0	0	50
10	100	0	0	50
40	99	1	0	100
70	97	3	0	100
100	95	5	0	100
130	80	20	0	100
120	0	30	70	100
140	0	30	70	100

2.3.4.3 Purification of Fraction 2 obtained from *D. salina* grown on oat media

Fraction 2 (76.8g) was dissolved in 2ml of EtOAc and added drop-wise to 2g of celite with thorough mixing. The mixture was left to dry under the fume hood over a weekend prior to loading on a pre-packed 12g silica column for a Grace Reveleris flash chromatography system. For fractionation, a gradient mobile phase system of DCM and EtOAc was used by starting with 100% DCM and ending with 100% EtOAc in 2h.

2.3.4.4 Purification of fraction 3 obtained from *D. salina* grown on oat media

Fraction 3 (70mg) was dissolved in 2ml of EtOAc and added drop-wise to 2g of celite powder with thorough mixing. The mixture was left to dry under the fume hood over the weekend. The dried sample-celite mixture was added to a loader for a 12g silica column for the Reveleris flash chromatography system. DCM and MeOH were used as the solvent system for fractionation as shown in Table 2.6 below. The sub-fractions were collected automatically by peaks monitored with both ELSD and UV detectors. The wavelengths used in the UV detector were at 254 and 280nm. Column was washed using a mixture of acetone and MeOH (70:30).

Table 2.6: Elution gradient for the fractionation of *D. salina* secondary metabolites.

Time (min)	Mobile phase %			Flow rate mL/min
	DCM	MeOH	Acetone	
0	100	0	0	25
10	100	0	0	25
15	100	0	0	15
25	99	1	0	15
35	98	2	0	15
45	97	3	0	15
55	95	5	0	15
65	90	10	0	15
70	85	15	0	15
75	80	20	0	15
95	0	30	70	15
100	0	30	70	15

2.3.4.5 Purification of fraction 10 obtained from *D. salina* grown on oat media

Fraction 10 (490mg) was dissolved in 5ml of EtOAc and incorporated to a 4g of celite powder. The mixture was left to dry over the weekend. The dried sample-celite mixture was added to a loader for a 12g silica column for the Reveleris flash chromatography system. Ratios of n-hexane and EtOAc were used as the mobile phase as summarised in Table 2.7 below. The sub-fractions were collected by peaks monitored with both ELSD and UV detectors. The UV wavelengths used were at 254 and 280nm. Column was washed as above using a mixture of acetone and MeOH (70:30).

Table 2.7: Mobile phase % used in sub-fractionation of *D. salina* secondary fraction 10.

Time (mins)	Mobile phase %				Flow rate mL/min
	n-Hexane	EtOAc	MeOH	Acetone	
0	100	0	0	0	25
10	100	0	0	0	25
15	100	0	0	0	25
25	95	5	0	0	25
35	90	10	0	0	25
55	80	20	0	0	25
75	70	30	0	0	25
95	60	40	0	0	25
125	50	50	0	0	25
130	0	0	0	100	25
150	0	0	30	70	25
170	0	0	30	70	25

2.3.5 Thin layer chromatography (TLC) and preparative thin layer chromatography (PTLC)

Thin layer chromatography (TLC) was used as an analytical tool to identify compounds based on their R_f value and colour either under UV light or upon reaction with different spraying reagents. Moreover, it was used to determine the purity of a sample and to estimate the number of compounds in a mixture. Furthermore, it was used to determine the suitability of solvent systems for column chromatography. In addition to all of that, it was used as a preparative tool to purify compounds.

Mobile phases used in the MPLC/Flash chromatography system were chosen after they were optimised on TLC plates (TLC silica gel 60 F254 plates) obtained from Merck, Darmstadt, Germany to ensure a proper separation of compounds on the column. The appropriate mobile phase was chosen based on is the R_f value of first eluting component. The R_f value of the spots should be between 0.3 and 0.5 to avoid a fast elution rate of the various components in the crude extract, which will lead to inferior separation if the R_f value is more than 0.5. The elution rate is quite slow when the R_f value of a component is less than 0.3.

For analytical TLC purposes, fractions were all dissolved in acetone and spotted 1 cm above the bottom edge of the TLC plate. The TLC chamber was equilibrated with the mobile phase to which the plates were added and left to develop. The run of the plates was 5 – 6 cm (the

plate size was 2×8cm). The eluted spots were detected under short and long UV lights. Compounds that quenched fluorescence or phosphorescence could be detected as dark spots under the short UV light. Conjugated double bond systems and aromatics could be detected as coloured spots under short UV wavelengths as well. Alkaloids, flavonoids and other analytes could be detected under long UV light (Wall, 2005). TLC plates were also sprayed with anisaldehyde/sulfuric acid reagent (Table 2.8) and heated to 200°C with a heat gun. This spraying reagent is used to detect many natural products like essential oil components, steroids, terpenes, sugars, phenolic compounds, and sapogenins (Wall, 2005). The mobile phases used are mentioned under the results and discussion in Chapter 5.

For PTLC, 10 mg of sample was dissolved in 150µL of acetone and applied to each plate (TLC silica gel 60 F254 on 20x20 cm aluminium sheets) as a band, 2 cm above the bottom edge of the plate. Few spots were applied to the TLC plate at both sides as a reference. Prior to the development of the PTLC plates, filter papers were placed inside TLC chamber for equilibration. This is very important, otherwise, the solvent front would evaporate from the plates, decreasing their volatility causing the solvent front to be uneven and concavely shaped. After the mobile phase had developed the plates, the bands were viewed under UV light. Prior to using a spray reagent, 90% of the plate area was covered with an aluminium foil, allowing the edges to be exposed and sprayed with anisaldehyde/sulfuric acid reagent. The bands were marked with a pencil, cut, and recovered with acetone. The mobile phases used are mentioned under results and discussion in Chapter 5.

Table 2.8: The components of anisaldehyde/sulfuric acid spray reagent.

Component	Volume (mL)
anisaldehyde	0.5
methanol	85
glacial acetic acid	10
concentrated sulfuric acid	5

2.3.5.1 Thin layer chromatography (TLC) of *D. salina* crude extracts.

Various mobile phases were tested to select the optimum solvent system for MPLC. The best mobile phase was 99:1 of DCM:MeOH that generated R_f values of less than 0.5. However,

0.1% MeOH was not enough to elute all compounds, which means using a higher percentage MeOH was necessary to elute all compounds. When using 3% MeOH, the R_f value was higher than 0.5 for the first two eluate but this percentage was still not enough to elute all the components. After using 5% of MeOH, the R_f value of most compounds was higher than 0.5, but again it failed to elute the most polar compounds. Different ratios of DCM and MeOH were then used in the MPLC separation procedures for the respective extracts and fractions. However, the columns were always washed with acetone and MeOH at a ratio of 70:30 at the end of each chromatographic run.

2.3.5.2 Purification of fraction 2 from D. salina extract obtained from malt extract broth.

Preparative TLC was chosen for the sub fractionation of fraction 2 due to its low yield of 42mg. The fraction was dissolved in 600µl of EtOAc. A volume of 150µl was loaded as a band on every 20×20cm silica TLC using four TLC plates in total. DCM and MeOH (95:5) was used as mobile phase. TLC plates were developed twice to ensure the maximum separation between bands.

2.3.5.3 Purification of fraction 4 from D. salina extract obtained from malt extract broth.

Like fraction 2, fraction 4 was subjected to fractionation by preparative TLC. Fraction 4 (60mg) was dissolved in 900µl of EtOAc and divided to six smaller volumes of 150µl. The sample was loaded on six 20×20cm silica TLC plates. The plates were developed twice in DCM and MeOH (95:5).

2.3.5.4 Purification of fraction 2-2(1+2) from D. salina extract obtained from oat media.

Fractions 1 and 2 produced from the sub-fractionation of fraction 2 from *D. salina* extract obtained from oat media were pooled together due to their similar chemical profiles. Both fractions F2-1 and F2-2 resulted in a yield of 19.4mg. The pooled fraction F2-2(1+2) was dissolved in 300µl of EtOAc and divided to two portions of 150µl. The sample portions were loaded on two 20×20cm silica TLC plate and also developed twice with DCM and MeOH (97:3).

2.4 The metabolomics approach used in this study

Metabolomics is defined as a holistic approach, which can be used as a qualitative and quantitative technique for all metabolites found in an organism or as part of an organism at specific times and in particular environments (Rochfort, 2005, Maree et al., 2014, Harvey et al., 2015). This approach can also be used for the end product of the gene expression process as well as to monitor gene function and the biochemical status of an organism (Yuliana et al., 2011).

Metabolomics-based studies can be divided into two types:

1. Non-targeted studies

These studies examine all measurable analytes in the extracts. They should be coupled with chemometrics-based methods to analyse the compounds, including compounds at low concentrations when within the limit of detection (Griffiths et al., 2010).

2. Targeted studies

Targeted studies would only search within the pathway that provided the selected metabolites or known and predefined metabolites (Griffiths et al., 2010).

As illustrated on Figure 2.12, The “-omics” flow includes proteomics, genomics, and transcriptomics that all either utilises or supports metabolomics (Rochfort, 2005, Dettmer et al., 2007). However, studying gene functions by transcriptomic and proteomic methods is a limiting process. This is because changes in proteomes and transcriptomes do not always result in biochemical phenotype changes. Furthermore, translated proteins could be less active than enzymes. Moreover, mRNA identifications and protein depend on the similarity of sequence and database matching. Thus, any lack in database resources will affect the identification process. Accordingly, the most functional “-omics” approach is the metabolomics-based method (Sumner et al., 2003, Rochfort, 2005, Yuliana et al., 2011).

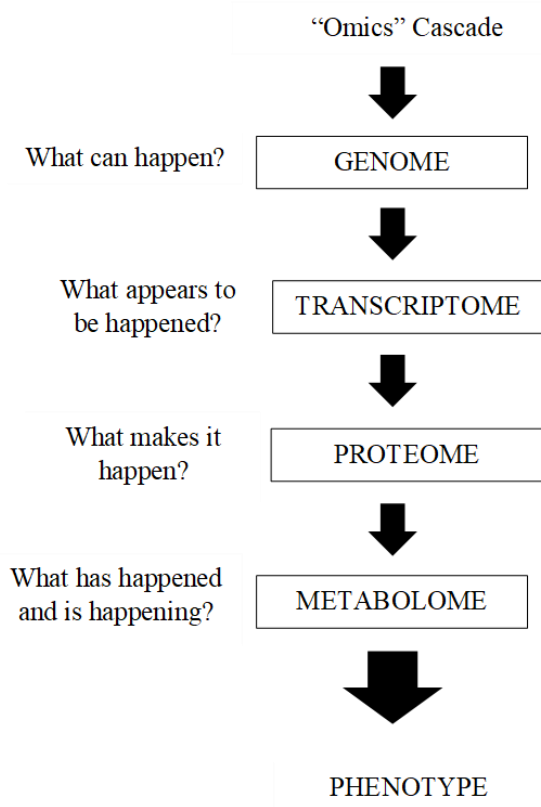


Figure 2.12: The omics flow (Dettmer et al., 2007).

Secondary metabolites demonstrate a huge degree of diversity in their structural complexities and physicochemical properties; as a result, it is challenging to identify and quantify secondary metabolites which are present in certain natural sources. Hence, robust and selective analytical methods must be chosen to overcome these challenges (Tawfike et al., 2013, Stuart et al., 2020). Liquid chromatography, coupled with high-resolution mass spectroscopy (LC-HRMS) and NMR spectroscopy, are the instruments mostly used in metabolomics processes. Because crude extracts are used in the first screening to guide metabolomics, LC-HRMS is more effective than NMR due to the higher sensitivity of LC-HRMS; it can detect compounds which are presented as femtogram levels in the extracts. Furthermore, the compound dereplication can be accomplished using exact mass and fragmentation patterns, as well as the specific retention time can enhance the identification. However, the ionisation capability of the isolated compound can affect the metabolite identification (Griffiths et al., 2010, Tawfike et al., 2013, Krug and Müller, 2014). Reproducible methods, like NMR, and its ability for structural elucidation can be valuable. However, NMR can miss compounds with low concentrations and cause problems in dereplication processes.

Dereplication applies spectroscopical analysis to identify known compounds, especially in the early stages of their fractionation and isolation processes (Krug and Müller, 2014, Harvey et al., 2015). It can be carried out using LC-HRMS, where hits with specific m/z values are compared to databases, such as the AntiMarin and the Dictionary of Natural Products (DNP). This comparison is used in parallel with multivariate analysis, which pinpoints active metabolites and facilitates an improved selection of fractions, which can be used for further purification. As a result, this can save time and money in the novel bioactive metabolite isolation process. Merging data provided by both LC-HRMS and NMR with multivariate data analysis tools allows researchers to make comparisons and detect differential metabolites in biological extracts and fractions, thus narrowing the search for potential biomarkers and avoiding chemical redundancy at the very beginning of the study (Wu et al., 2015). This reflects the ability of metabolomics data to be analysed and visualised by incorporating multivariate analysis, to simplify and identify significant correlations which lie within the dataset (Covington et al., 2017).

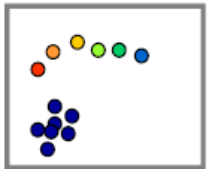

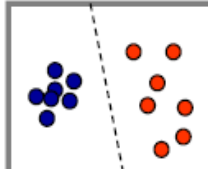
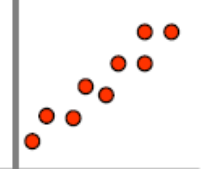
2.4.1 Chemometrics and multivariate analysis

Chemometrics is described by Wold and Sjöström as the “art of extracting chemically relevant information from data produced in chemical experiments, and is heavily dependent on the use of different kinds of mathematical models. The major concern is to modulate the chemical problem to a form that can be expressed as a mathematical relation. It is how to get chemically relevant information out of measured chemical data, how to represent and display this information and how to get such information into data” (Wold and Sjöström, 1998). It incorporates the use of both numerical and statistical techniques to recover more data from complex datasets and could be used as a way to clear up patterns in complicated chemical matrices (Wold and Sjöström, 1998, Mok and Chau, 2006, Maree et al., 2014).

Multivariate data analysis is a chemometrics-based method which provides interpretable data from a complex collected data matrix of an experiment, thereby examining the data and allowing the estimation of its outcomes. High-resolution analytical instruments produce multivariate colinear data, determining variables, which describe the system and provides information similarity in the information content. These colinear variables which describe the system, and thus the data structure, could be incorporated and defined by fewer factors, which are called latent variables or principal components (Rajalahti and Kvalheim, 2011).

Approaches in multivariate analysis include principal component analysis (PCA), soft independent modelling by class analogy (SIMCA), partial least squares (or projections to latent structures) discriminant analysis (PLS-DA), orthogonal partial least squares discriminant analysis (OPLS-DA) and modified orthogonal projections to latent structures (O2-PLS). Those approaches are summarised in Table 2.9 (Wiklund, 2008).

Table 2.9: Approaches used in multivariate analysis (Wiklund, 2008).

PCA: Overview	SIMCA: Classification	PLS-DA and OPLS- DA: Discrimination	O2-PLS: Regression
Trends	Pattern recognition	Discriminating between groups	Comparing blocks of omics data
Outliers	Diagnostics	Biomarker candidates	Metabolomic vs proteomic vs genomic
Quality control	Healthy/diseased	Comparing studies or instrumentation	Correlation spectroscopy
Biological diversity	Toxicity mechanisms		
Patient monitoring	Disease progression		
			

Two of the most commonly used multivariate approaches for metabolomics data analysis are PCA and OPLS-DA (Covington et al., 2017). For example, measuring "K" number of variables for "I" number of objects; will result in a big data matrix $I \times K$ in size (as shown in Figure 2.13). Using PCA could reduce this matrix to the smaller matrices $I \times A$ and $A \times K$, which are easier to interpret and understand (Geladi, 2003). PCA converts the large data space that is present in the $I \times K$ matrix into a smaller space (as shown in Figure 2.13), where $X = I \times K = I \times A + A \times K + E$. Each term ($I \times A$ and $A \times K$), is called a PC or a latent variable, and E represents the residual matrix. Usually, many PCs are obtained; however, two could be sufficient to represent the data in an efficient and descriptive way.

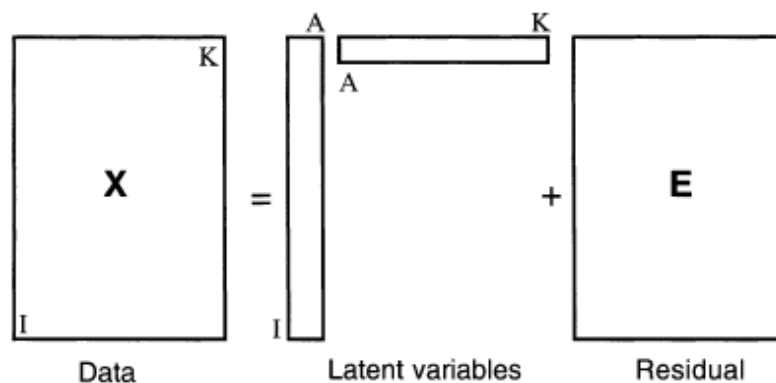


Figure 2.13: “A data matrix of size $I \times K$ is reduced to smaller matrices of size $I \times A$ and $A \times K$ ($A \ll \min(I, K)$), which are easier to interpret and understand, and contain all the relevant information. Noise and other disturbances are left in the residual matrix of size $I \times K$. A general name for the reduced data is latent variables”. Example of metabolomics (Geladi, 2003).

Two types of plots are used for PCA: the scores plot and the loadings plot. The scores plot (Figure 2.14) summarises observations (crude extracts or fractions), and the loadings plot summarises the variables (mass ion peaks, m/z or chemical shifts, ppm) responsible for the pattern of observations in the scores plot (Geladi, 2003).

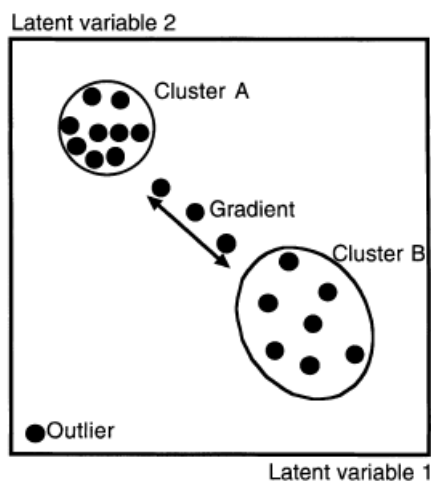


Figure 2.14: Examples of scores plots for two PCs (Geladi, 2003). As the figure depicts, cluster A shows less variation, as it is denser than the spread-out in cluster B which reveals more variation. In some situations, outliers and a gradient between the pure classes A and B might be observed.

PCA is an unsupervised approach which does not make assumptions about the data and identifies the sources of variation among the observations; thus, observations are classified in scores plots according to the variables in the loading's plots (Covington et al., 2017). In contrast, the PLS-DA approach is supervised. Thus, separate groups of observations are defined by the researcher and are clustered accordingly in the scores plot, while variables in the loadings plot are grouped so that they are responsible for the observation groups in the scores plot (Covington et al., 2017). Enhanced separation between predictive and nonpredictive variations, can be done by applying orthogonal signal corrections to PLS regressions (Bylesjö et al., 2006).

2.4.2 Applications of metabolomics in natural product research

In examining natural products for drug discovery purposes, metabolomics has introduced important applications, both in tracking novel compounds and active metabolites, and in optimising the production of secondary metabolites. Both PCA and OPLS-DA could be used to guide the isolation of compounds and to prioritise fractions for further work, which will save time and resources and direct fractionation and purification toward the novel and bioactive compounds (Raheem et al., 2019, Tawfike et al., 2019, Mazlan et al., 2020). This effect is a result of the ability of a metabolomics processes to compare and screen secondary metabolites extracted from endophytic fermentations, rapidly revealing outliers, differences, and biomarkers among experimental extracts, either from different sources or from different fractions related to the same extract. This would aid in tracking the possible novel and bioactive metabolites and biomarkers present from the early stages of research to the end (Sebak et al., 2020, Stuart et al., 2020, Santiago et al., 2021) . Then, such biomarkers could be isolated, and their structural information (provided by NMR or LC-HRMS) are compared with database or library information to serve as a dereplication process and conserve time in defining the target metabolites (Wu et al., 2015). If the core structure of the biomarker is known, but its functional groups are not, then two-dimensional NMR and fragmentation patterns from MS/MS spectra combined with molecular networking evaluation processes could be used to identify the compound in question. However, if its nucleus is novel, then a full de novo NMR structural characterisation is needed (Tawfike et al., 2013).

Furthermore, metabolomics processes could be used to optimise fermentation conditions and to detect and sustain the production of interesting secondary metabolites during the scaling-up process (Schulz et al., 2002, Harvey et al., 2015). Furthermore, studying, exploring, and

validating relationships between culture methods, diversity, bioactivity, and metabolome evaluation in the microbial isolate could be aided by real time-metabolomics (Jordà et al., 2012, Zhu et al., 2013, Abdelmohsen et al., 2014, Hubert et al., 2014). When certain fermentation parameters are changed, the secondary metabolite production could be checked by metabolomics processes. This gives the metabolomics processes the ability to work as quality control tools (Tawfike et al., 2013, Toya and Shimizu, 2013, Wu et al., 2015). Metabolomics processes could also be used as quality control tools in phytomedicine. Interspecies variations, adulterations, environmental changes, post harvesting treatments, and extraction methods may all lead to change in the metabolic profiles and affect the activity of the resulting isolated compounds. Any change of these could be detected by PCA (Yuliana et al., 2011). In addition, metabolomics could be used to link the chemical profiles and bioactivity patterns of certain phytomedicines, where the activity of these phytomedicines is a result of the synergism of many individually inactive chemical constituents. In such cases, the combination of these constituents is monitored to maintain the biological activity (Yuliana et al., 2011). Further, metabolomics data can be mined in searches for biosynthetic precursors, which could be used to increase the production of a certain bioactive secondary metabolite (Harvey et al., 2015).

2.4.3. Multivariate analysis of spectral data

The LC-HRMS files were splitted into positive or negative ionisation mode files with MassConvert by Proteowizard before they were imported to MZmine 2.42 for processing. The splitting was essential due to the inability of MZmine to process both negative and positive data modes sets at together (Pluskal et al., 2010).

Mzmine parameters followed those put together by Macintyre et al, 2014, the centroid mass detector was used for peak detection where the noise level set to $1.0E^4$ and the MS level to 1(Macintyre et al., 2014). The chromatogram builder function was set to a minimum time span of 0.2 min, minimum height of $1.0E^4$ and m/z tolerance of 0.001 m/z or 5.0 ppm. Local minimum search algorithm was used for chromatogram deconvolution. The chromatographic threshold was set to 5.0%, the search minimum in t_R range to 0.4 minutes, the minimum relative height to 5.0%, the minimum absolute height to 10000, the minimum ratio of peak top/edge to 3 and the peak duration range to 0.2 – 5.0 min. Isotopic peak grouper was used for detecting isotopes. The tolerances of both t_R and m/z were set to 0.1 min and 0.001 m/z , respectively. The maximum charge was set to 2 and the representative isotope chosen was the most intense. After

that, the chromatograms were cropped to 5.0 – 40.0 min using the peak list row filtering function. Then, join aligner was used to align the peak list, in which, m/z tolerance was set to 0.001 m/z or 5 ppm, weight for m/z to 20, t_R tolerance to 5 relative % and weight for t_R and m/z to 20. Later, gap filling took place where the m/z tolerance was set to 0.001 m/z too, intensity tolerance to 30%, t_R tolerance to 0.5 minutes and m/z tolerance to 0.001 m/z or 5 ppm. Adduct search was performed with t_R tolerance of 0.2 min, m/z tolerance of 0.001 m/z or 5 ppm and maximum relative adduct peak height of 30%. The adducts searched for were Na, K, NH_4 in positive mode and format in negative mode. ACN was searched for in both modes. Furthermore, a complex searched was performed using $[\text{M}+\text{H}]^+$ for the positive mode and $[\text{M}-\text{H}]^-$ for the negative mode. The tolerance of t_R was set to 0.2 min, m/z tolerance of 0.001 m/z or 5 ppm and maximum complex peak height to 50%. Moreover, the formula prediction function was used to search for unknowns where again m/z tolerance was 0.001 m/z or 5 ppm. Finally, the data was exported as a CSV excel file for further clean up using the *in-house* developed macro. The exported parameters were Row ID, m/z , t_R , identification method, predicted chemical formula and the peak area. In macro, data preparation took place where both positive and negative outputs were combined again in one data set. This was followed by the removal of media and solvent effects and dereplication. This resulted in a data set prepared to be analysed using SIMCA-P software. The data was imported into SIMCA. Polarity and MZmine ID were merged and set to be the primary identifier and m/z , t_R , molecular formula and molecular weight (MWt) were selected as secondary identifiers. Both Principal Component Analysis (PCA) and Orthogonal Partial Least Squares Discriminant Analysis (OPLS-DA) was performed depending on the purpose of the study. Scores, loadings and S-plots were then generated (Macintyre et al., 2014). Permutation test was performed for OPLS-DA models. This test calculates the model's fitness (R^2) and predictive power (Q^2). A strong model has its R^2 and Q^2 values close to 1, its R^2Y intercept must be less than 0.4 and Q^2Y intercept less than 0.05 (Ali et al., 2013).

3 Isolation and Screening of Fungal Endophytes

3.1 Literature background on selected seaweeds for this study

3.1.1. *Ascophyllum nodosum* source of natural products

Ascophyllum nodosum (*A. nodosum*) is a brown seaweed that belongs to the *Fucales* family (Jiménez et al., 2010). Previous reports indicated the presence of bioactive metabolites, which affect different macro and micro-organisms (Jiménez et al., 2010). Macroalgae-derived extracts have been used extensively by the cosmetic industry for skincare products (Jiménez et al., 2010). Extracts of *A. nodosum* exhibited antioxidant and immunomodulatory activities both *in vitro* and *in vivo* (Turner et al., 2002). The crude extract of *A. nodosum* was also shown to be a good food additive to reduce the growth of pathogens and has improved the performance of livestock grazing animals (Allen et al., 2001). The acetone crude extract of *A. nodosum* exerted good anti-oxidant, anti-microbial and tyrosine inhibitor activities (Jiménez et al., 2010). *A. nodosum* was also a good source of fucoidan, alginates, ascophyllan, laminarins and polyphenolic compounds (Kadam et al., 2015). Some of these examples are shown in Figure 3.1.

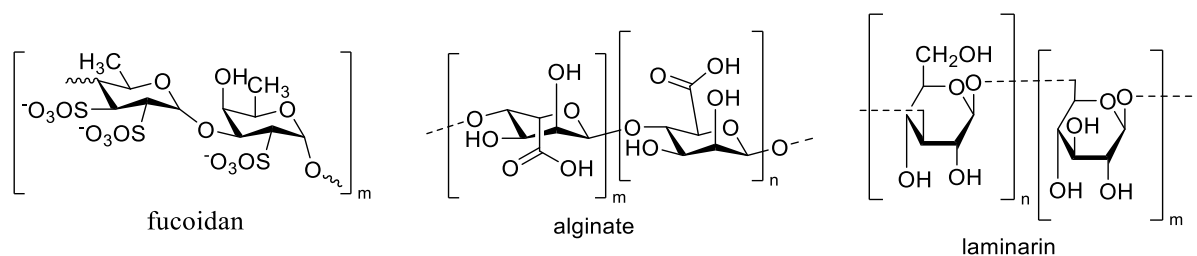


Figure 3.1: Examples of compounds isolated from *A. nodosum* (Kadam et al., 2015)

3.1.2 *Laminaria hyperborea* source of natural products

Laminaria hyperborea (*L. hyperborea*) is a brown seaweed listed under Laminariaceae species, which is likely to be found on the coast of Scotland, Ireland and Norway (Kadam et al., 2015). *L. hyperborea* is commonly utilised in the hydrocolloidal industry for their high yields of various alginate-like compounds as shown in Figure 3.2 (Werner and Kraan, 2004).

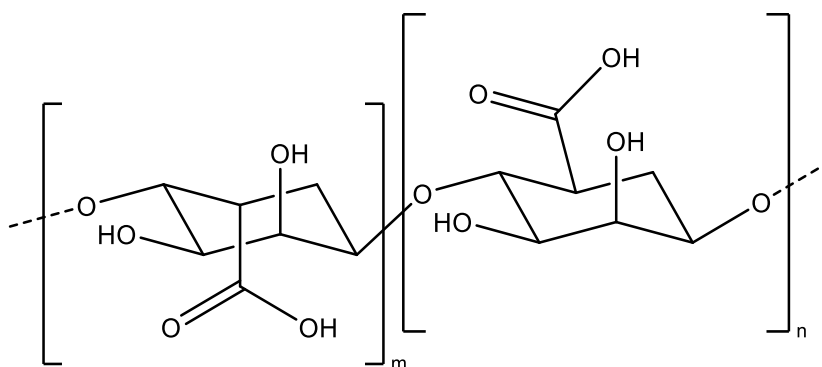


Figure 3.2: Chemical structure of alginate hydrocolloidal compounds isolated from *L. hyperborea*.

In addition, the crude extracts of *L. hyperborea* are rich with phenolic compounds and β -glucan polysaccharide, known as laminarins which can enhance various biological activities (Murphy et al., 2013, Kadam et al., 2015). Laminarins consist of (1,3)- β -D-glucopyranose residues (Figure 3.3) with some 6-*O*-branching in the main chain and/or some β -(1,6)-intrachain links (Rioux et al., 2007, Kadam et al., 2015). The physicochemical property of laminarin compounds depends on the degree of branching of each compound, which can also affect the biological activity of these polysaccharides (Rioux et al., 2007, Kadam et al., 2015).

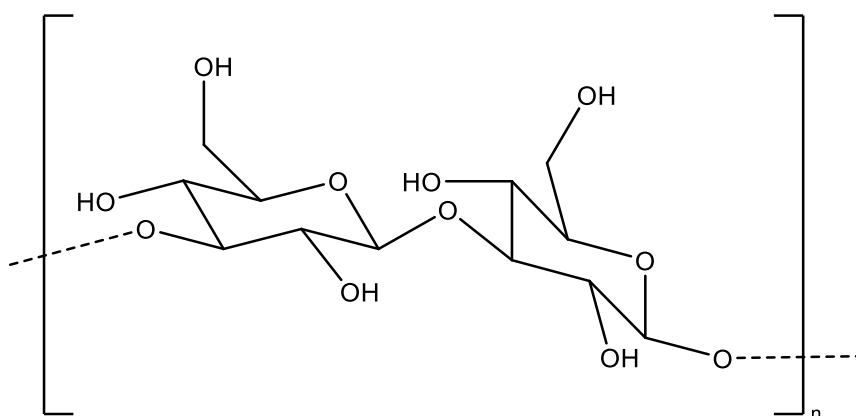


Figure 3.3: Chemical structure of (1,3)- β -D-glucan building unit of laminarin compounds isolated from *L. hyperborea*.

3.1.3 *Ulva intestinalis* source of natural products

Ulva intestinalis is a marine green microalga growing in rockpools (Larsson et al., 1997). Crude extracts of *U. intestinalis* was also found to exhibit anti-microbial activity (Sahnouni et al., 2016). *U. intestinalis* was describe to yield ulvan polysaccharides with building blocks such as glucouronic acid, rhamnose 3-sulfate, xylose, xylose 2-sulfate and iduronic acid, as presented in Figure 3.4 (Brading et al., 1954, Tavernier et al., 2008).

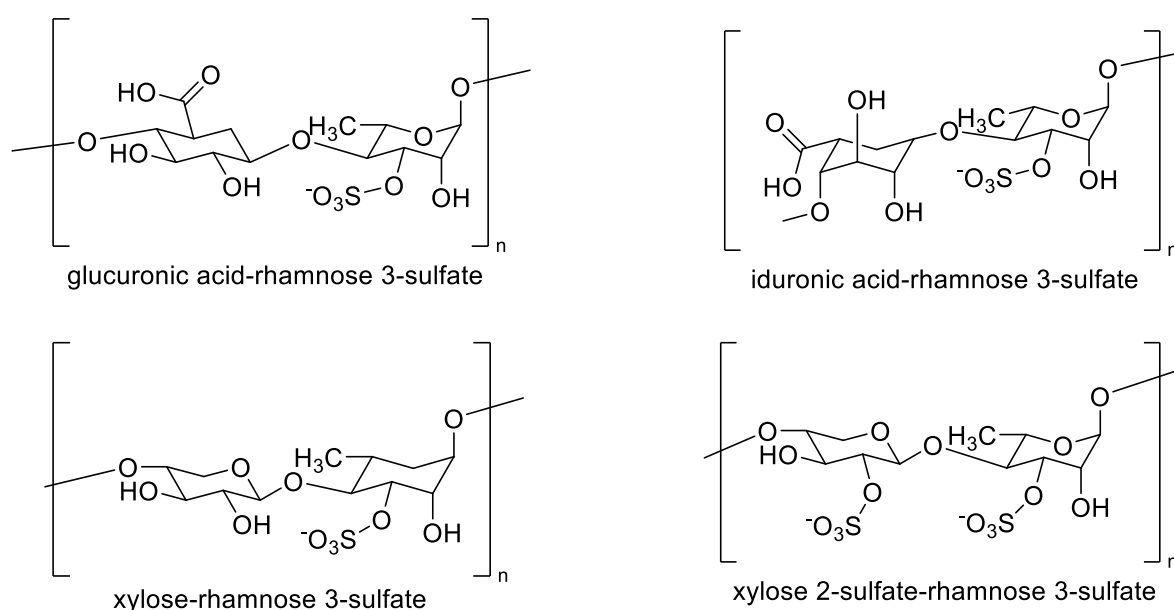
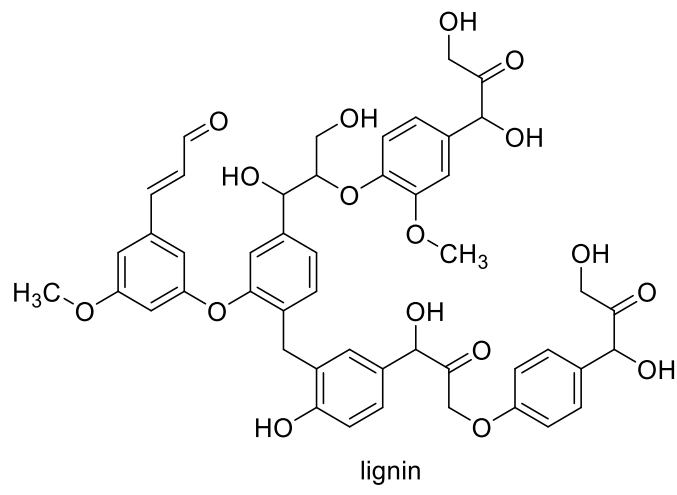
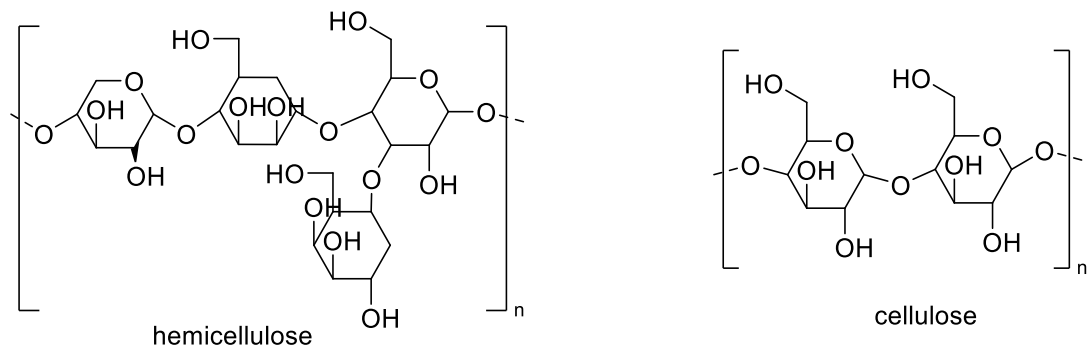


Figure 3.4: Ulvan polysaccharides isolated from *U. intestinalis*.

3.1.4 *Ulva lactuca* source of bioactive metabolites

Ulva lactuca (*U. lactuca*) is a green edible seaweed under the *Ulvaceae* family and is commonly known as sea lettuce (Fotadar, 2011). *U. lactuca* was able to produce metabolites that can be used by the seaweed itself and/or by its endophytes (Yaich et al., 2011). As illustrated in Figure 3.5, metabolites found in *U. lactuca* were related to different families of compounds like amino acids, polyphenolics, polysaccharides, and fatty acids (Yaich et al., 2011).



polyphenolic compound

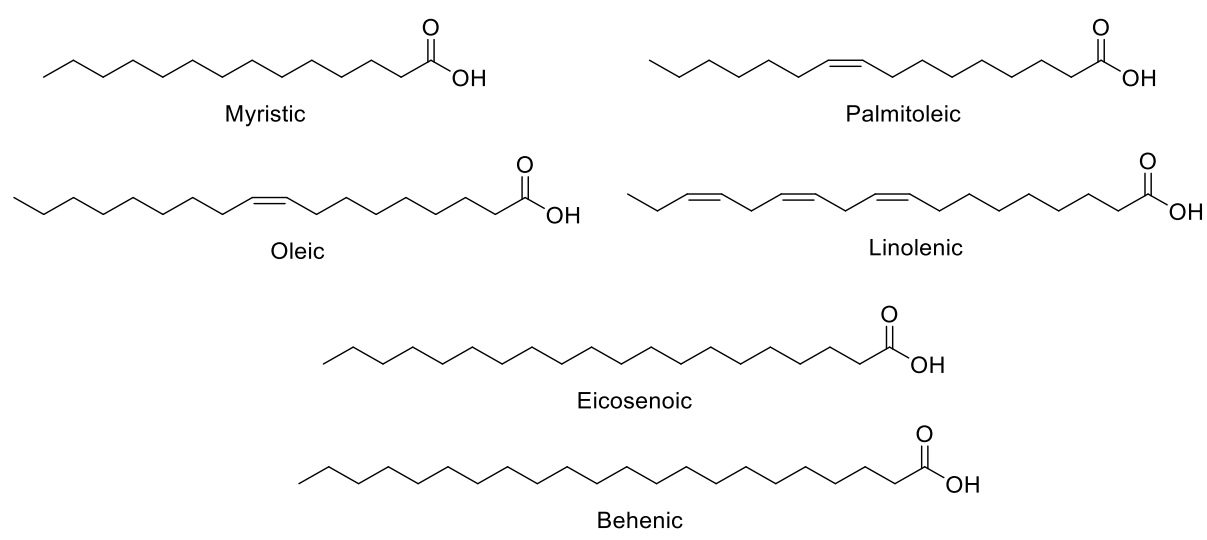


Figure 3.5: Chemical structure of some compounds produced by *U. lactuca*

3.1.5 *Fucus vesiculosus* source of natural products

Fucus vesiculosus is a brown alga usually found in the north Atlantic ocean, Baltic sea (Craigie et al., 1977). Brown alga has been widely reported in the literature to produce active antimicrobial metabolites (Buedenbender et al., 2020). These reported compounds were found to exhibit inhibitory effect against gram+ bacteria like *S. aureus* and *Bacillus subtilis* (*B. subtilis*) (Narayani et al., 2011, Pérez et al., 2016). Antimicrobial compounds from various chemical groups have been isolated from brown alga such as phenolics, carotenoids, polysaccharide and lipids (Pérez et al., 2016). Only a few number of research papers have reported the biological activity of the isolated pure compounds (Figure 3.6), while the majority of the publications described the biological activity of the crude extracts (Buedenbender et al., 2020). From the reported compounds, a polyhydroxylated fucophlorethol was found to be active against *E. coli* and *S. aureus* growing on the surface of the seaweeds (Sandsdalen et al., 2003). Another compound under the carotenoid group was fucoxanthin that e to be active exhibited antimicrobial activity against four different types of bacteria (*Pseudoalteromonas sp.*, *Ulvibacter littoralis*, *Bacillus aquimaris*, *Cytophaga KT0804*) growing on algal surface at a concentration of 0.9-10mg/cm³ (Saha et al., 2011). In addition, galactolipid compounds were also found to be active against *S. aureus* (DSM346) (Buedenbender et al., 2020). The production of phenolic compounds was higher in the summer, while galactolipids production was higher in the winter and both were active against *S. aureus* (Buedenbender et al., 2020).

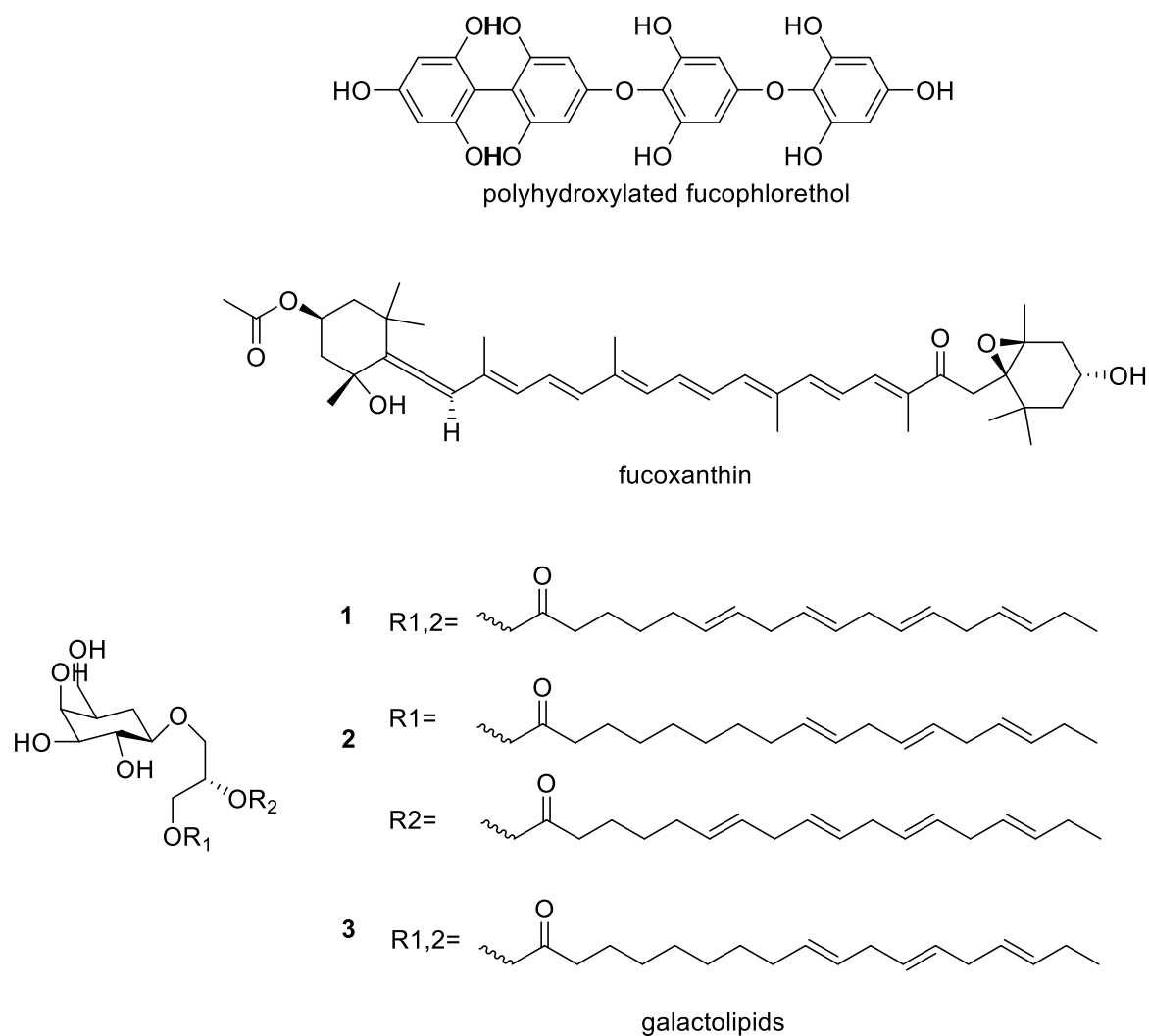


Figure 3.6: Chemical structures of some reported bioactive compounds isolated from *Fucus vesiculosus*

3.1.6 *Fucus spiralis* source of bioactive metabolites

Fucus spiralis (*F. spiralis*) is a brown algae that usually thrives at the intertidal zones of marine environments (Schmid et al., 2017). *F. spiralis* has been reported as a valuable source of nutritional and bioactive metabolites (Neto et al., 2006). These bioactive metabolites like phlorotannins have a potential impact on human health (Paiva et al., 2016, Catarino et al., 2017, Paiva et al., 2017). *F. spiralis* displayed good antioxidant activity due to the polyphenolic compounds produced by these seaweeds (Paiva et al., 2018). Many phenolic compounds have been reported to be produced by *F. spiralis*, like gallic acid, caffeic acid, vanillic acid and gentistic acid, as presented in Figure 3.7 (Fernando et al., 2016).

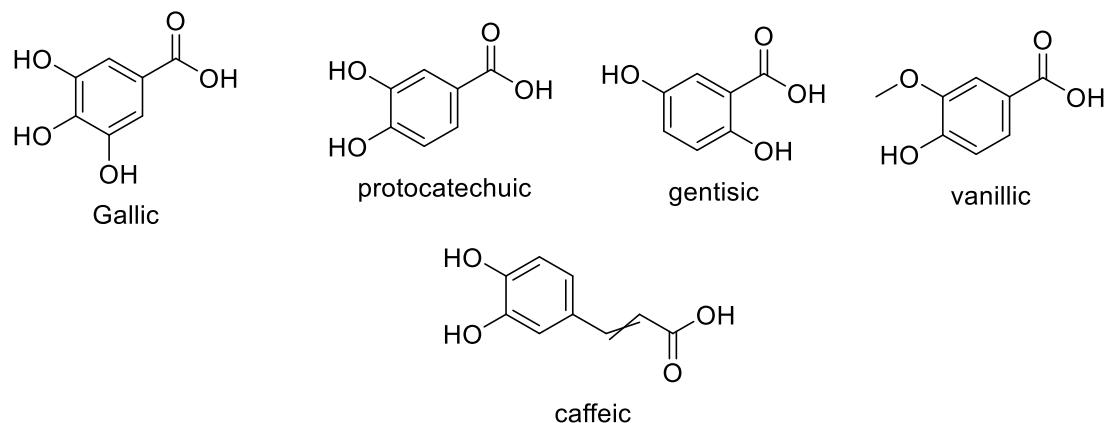


Figure 3.7: Some phenolic compounds produced by *F. spiralis* seaweed.

3.1.7 *Fucus serratus* source of natural products

Fucus serratus (*F. serratus*) is a brown alga that belongs to the same family as *Fucus vesiculosus* and *spiralis* (Major, 1977). *F. serratus* is usually found at the Atlantic coast of European Canary Islands and on the shores of north-east America (Taylor and Rao, 1957, Ryzhik et al., 2014). Most of the compounds produced by *A. nodosum* and *F. vesiculosus* have also been described in *F. serratus* (Le Tutour et al., 1998).

3.1.8 *Himanthalia elongata* source of natural products

Himanthalia elongata (*H. elongata*), also known as thongweed, seathong or sea spaghetti, is also a brown algae that belongs to the Order *Fucales* (Costello et al., 2013). *H. elongata* flourishes in the north east Atlantic Ocean and the North sea (Costello et al., 2013). The soluble lipids produced by *H. elongata* were found to increase the antioxidant activity of vitamin E by at least 45% (Le Tutour et al., 1998). *H. elongata* yielded α -tocopherol and other compounds, like ethylenecholesterol and cholesterol, as presented in Figure 3.8 (Sánchez-Machado et al., 2004). These chemical compounds can be used as a precursor for the synthesis of new secondary metabolites, either by *H. elongata* or its microbial endophytes.

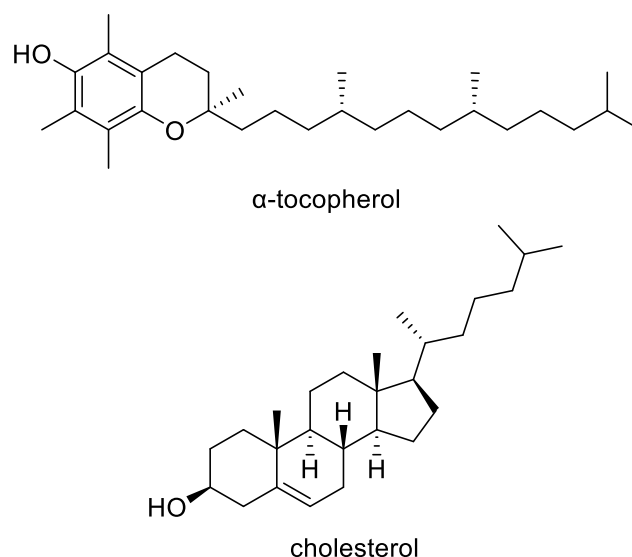




Figure 3.8: Chemical structure of some compounds produced by *H. elongata*.







3.2 Seaweed collection

Seaweeds used in this study as a source of endophytic fungi were collected from Culzean coast, Ayr, Scotland, United Kingdom. A photograph of each seaweed is presented in Table 3.1. Collection and identification were done in May 2018 with Kirsty Black, the Product Development Manager from Marine Biopolymer (MBL) Limited.

Table 3.1: Seaweeds used to isolate endophytes for the study.

Seaweed #	Seaweed name	Seaweed picture
1	<i>Ascophyllum nodosum</i>	
2	<i>Laminaria hyperborean</i>	

Continued Table 3.3: Seaweeds used to isolate endophytes for the study.

Seaweed #	Seaweed name	Seaweed picture
3	<i>Ulva intestinalis</i>	
4	<i>Himanthalia elongata</i>	
5	<i>Fucus serratus</i>	
6	<i>Fucus vesiculosus</i>	
7	<i>Ulva lactuca</i>	
8	<i>Fucus spiralis</i>	

3.3 Isolation of endophytic fungi.

Forty endophytic fungi were isolated from internal tissues of seaweeds (refer to section 2.2.4 for detailed procedure). In this study, the internal tissues of respective seaweeds were

inoculated on malt agar to grow and isolate endophytic fungi for further chemical analysis and antimicrobial work. Malt extract agar was chosen to grow the endophytic fungal isolates due to the type of the primary metabolites provided by this media (like sugars and peptides) to be a source of carbon and nitrogen needed in the synthesis of secondary metabolites. Chloramphenicol was used in the first inoculation step of the seaweeds tissues to prevent the growth of the endophytic bacteria because in this study only endophytic fungi were targeted. The seaweeds were rinsed and surface-sterilised with 70% isopropanol to prevent the possible contamination of epiphytes. The second inoculation of the respective isolated fungi in malt extract agar media were grown in the absence of chloramphenicol. The presence of chloramphenicol can mask the identification of low yielding bioactive metabolites when analysing the chemical profile and the biological activity of the fungal extracts, which could give misleading results.

Many of the isolated endophytes in this study, showed similar morphological features. Fungal colonies from the same host seaweed and those exhibiting identical morphological characteristics were excluded. The reason of excluding these strains is due to the lower probability of producing unique secondary metabolites between isolates when the main source of their primary metabolites was deduced from the same seaweed. In this case, further study was only accomplished on the fungal sample affording the highest biomass and this one representative strain was selected. On the other hand, fungal isolates with the same morphological features but derived from different seaweed sources were kept and used for further screening and profiling. These fungal strains were expected to have a higher probability to yield different sets of natural products because their primary metabolites that could be utilised for their biosynthesis were derived from different host seaweeds. After excluding identical strains isolated from the same seaweed source, 26 endophytic fungi were isolated, purified by repeated inoculation, and coded according to seaweed source as well as their morphological features as listed in Table 3.2.

Table 3.2: Fungal endophytes isolated from collected seaweeds.

Seaweed #	Seaweed name	Fungal morphology	Code
1	<i>Fucus serratus</i>	Green fast-growing	1/1
2	<i>Laminaria hyperborean</i>	Brown powdered	2/1
		Fluffy white with brown dots	2/2

		Brown mass with obvious gland	2/3
		Orange mass with white surrounding	2/4
		Light brown with white dots	2/5
		Fast grown green	2/6
3	<i>Ulva lactuca</i>	Green small biomass	3/1
4	<i>Fucus spiralis</i>	White huge mass	4/1
		Green fast-growing	4/2
		Green fast-growing large biomass	5/1
		Grey small biomass	5/2
5	<i>Fucus vesiculosus</i>	White and orange circles biomass	5/3
		Dark red small biomass	5/4
		White fluffy biomass	5/5
6	<i>Ascophyllum nodosum</i>	Green with orange crystals	6/1
		Small green biomass	6/2
		White small circle with light background	7/1
		White with grey background	7/2
7	<i>Himanthalia elongata</i>	Orange with white hair like shape	7/3
		Green fast-growing biomass	7/4
		Small green mass with white dots	7/5
		White biomass	8/1
8	<i>Ulva intestinalis</i>	Light brown biomass	8/2
		White biomass with orange dots	8/3
		Grey mass with brown dots	8/4

3.4 Fungal extraction.

Due to the growth rate differences between isolated fungal strains, twenty-six fungi were classified as fast- and slow-growing fungus depending on their growth rates. Each fungus was inoculated on nine malt agar plates with a dimension of 100×15mm. Every three plates of MA media containing fungus was used to prepare a one extract. Average yields of the extracts from each of the triplicates were recorded and listed in Table 3.3.

Table 3.3: Average yields of respective fungal extracts based on their triplicates.

Endophyte code	Weight	Endophyte code	Weight
1/1	3.7mg	2/1 (<i>D. salina</i>)	7.5mg
2/2	6.6mg	2/3	6.2mg

2/4	8.2mg	2/5 (<i>G. candidum</i>)	4.8mg
2/6	4.2mg	3/1	7.3mg
4/1	5.7mg	4/2	3.1mg
5/1	8.1mg	5/2	6.9mg
5/3 (<i>M. elegance</i>)	16.9mg	5/4 (<i>H. rubiginosum</i>)	22.1mg
5/5	6.7mg	6/1	6.8mg
6/2	7.4mg	7/1	6.1mg
7/2	5.1mg	7/3	4.7mg
7/4	6.3mg	7/5	6.1mg
8/1	5.1mg	8/2	7.2mg
8/3	7.1mg	8/4	5.7mg
Blank	5.3mg		

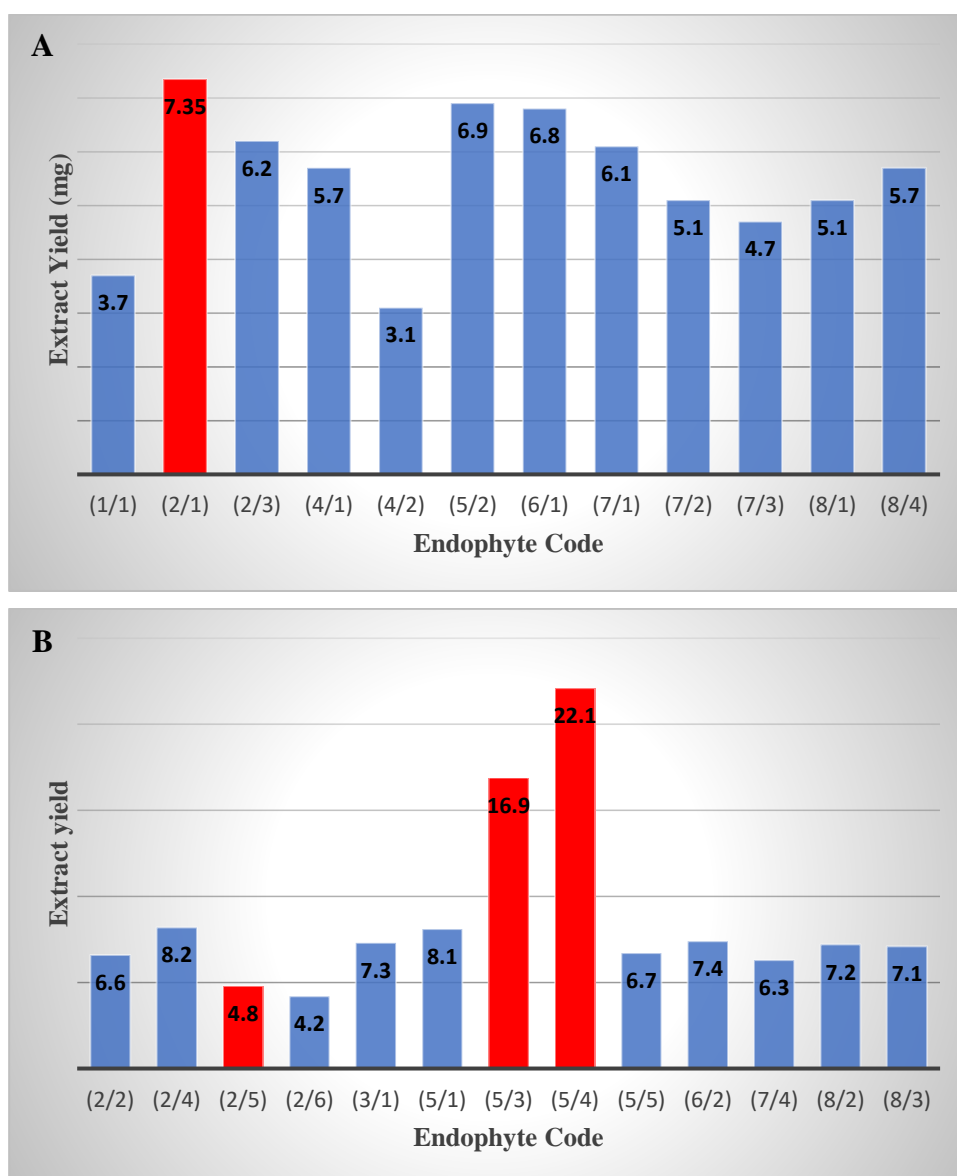


Figure 3.9: Yield of extracts produced by isolated endophytic fungi. **A:** Fast- and **B:** slow-growing fungi. The red columns represent the bioactive extracts against both biofilm-forming *S. aureus* and *P. aeruginosa*.

The slow-growing fungi were incubated for 30 days to ensure enough extract yield could be subjected for further chemical profiling and microbial assay procedures. Whereas, the fast-growing fungal isolates were incubated for only 15 days to avoid biomass overgrowth, which could lead to the consumption of its own secondary metabolites. However, the yields of the fungal extracts were generally very low with only a maximum yield of 22.1mg for fungal strain #5/4 from the three 10-cm malt extract agar plates. The endophytes have been grouped depending on the growth rate.

To safeguard good practice for metabolomics data analysis, a media blank was also incubated for both incubation durations to be compared with the extracts afforded by the screened fungal isolates. In addition, all replicates from both incubation periods were analysed using LC-HRMS and tested against the biofilm-forming *S. aureus* and *P. aeruginosa*.

3.5 Bioassay screening of fungal extracts.

The extracts were tested to screen their biological activity against bacterial growth of biofilm-forming bacteria *S. aureus* and *P. aeruginosa*. Due to the high possibility for the presence of a biofilm forming bacteria on seaweeds (Steinberg and De Nys, 2002), which is the host organism in this study, antimicrobial assays were chosen for biological activity screening of the extracts of the isolated endophytic fungal strains. AlamarBlue® and planktonic assay methods were used to test the ability of the fungal extracts to inhibit bacterial growth and biofilm formation, respectively. Screening for antibiofilm activity has been essential to combat bacterial resistance through biofilm formation.

3.5.1 Alamarblue® Assay of fungal extracts:

After applying 100µg/mL of each of the fungal extracts in 96-well plates inoculated with biofilm-forming *S. aureus* and *P. aeruginosa*, four of the extracts exhibited more than 90% biological activity. These four bioactive extracts were afforded by endophytic fungi *M. elegance* (5/3), *D. salina* (2/1), *G. candidum* (2/5), and *H. rubiginosum* (5/4). The highest biological activity was obtained from *D. salina* extracts with a biological activity of 97% and 98% against *S. aureus* and *P. aeruginosa*, respectively. On the other hand, extract 8/4 displayed no antimicrobial activity against *S. aureus* and *P. aeruginosa* at -3% and 1% growth inhibition, respectively. Some fungal extracts were able to produce weak antimicrobial activity between 40 and 60% bacterial growth inhibition, which were however not enough to be chosen for further isolation and bioprospecting work.

Table 3.4: AlamarBlue® bacterial viability assay results of 100µg/mL of fungal extracts. Highlighted rows represent the bioactive extracts.

Liquid media extract	% of bacterial viability <i>S. aureus</i> & <i>P. aeruginosa</i>	Solid media extract	% of bacterial viability <i>S. aureus</i> & <i>P. aeruginosa</i>
1/1	78.82 & 84.12	<i>D. salina</i> (2/1)	2.79 & 1.76
2/2	67.69 & 72.10	2/3	70.49 & 68.84
2/4	86.75 & 92.68	<i>G. candidum</i> (2/5)	8.69 & 7.61
2/6	57.38 & 60.97	3/1	44.92 & 43.50
4/1	39.60 & 41.77	4/2	55.34 & 53.83
5/1	86.32 & 92.23	5/2	63.57 & 61.99
<i>M. elegance</i> (5/3)	8.58 & 8.27	5/4	95.34 & 93.46
5/5	63.55 & 67.64	<i>H. rubiginosum</i> (5/4)	3.95 & 2.92
6/2	91.18 & 97.47	6/1	77.60 & 75.88
7/2	76.78 & 81.92	7/1	56.93 & 55.41
7/4	66.21 & 70.50	7/3	80.71 & 78.97
8/1	55.15 & 58.56	7/5	58.73 & 57.19
8/3	74.05 & 78.98	8/2	67.86 & 66.24
8/4	103.12 & 98.84		

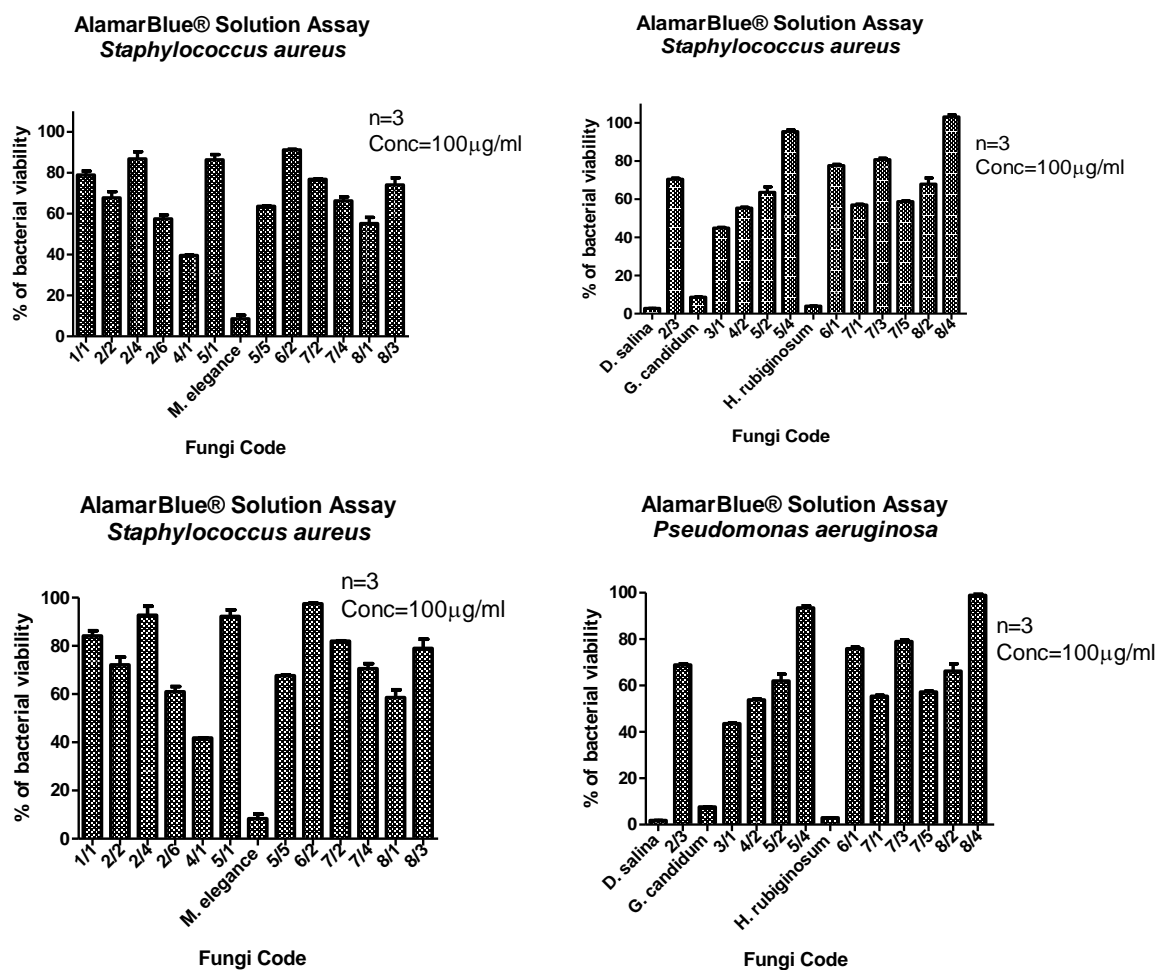


Figure 3.10: AlamarBlue® Assay results of 100µg/mL of fungal extracts against biofilm-forming *S. aureus* and *P. aeruginosa*.

3.5.2 Planktonic assay of fungal extracts:

Comparable to the AlamarBlue® assay results, an identical set of four endophytic extracts exhibited superior biological activity in inhibiting biofilm formation by *S. aureus* and *P. aeruginosa*. These extracts were from *M. elegance* (5/3), *D. salina* (2/1), *G. candidum* (2/5), and *H. rubiginosum* (5/4). The highest % of anti-biofilm activity was obtained with *H. rubiginosum* at 98 and 95% inhibition against *S. aureus* and *P. aeruginosa*, respectively.

Table 3.5: Planktonic biofilm viability assay results for 100µg/mL of fungal extracts. Highlighted rows represent the bioactive extracts.

Fungi code	% of biofilms viability <i>S. aureus</i> & <i>P. aeruginosa</i>	Fungi code	% of biofilms viability <i>S. aureus</i> & <i>P. aeruginosa</i>
1/1	34.27 & 40.15	<i>D. salina</i> (2/1)	5.36 & 8.89
2/2	40.69 & 46.01	2/3	16.97 & 21.35
2/4	53.14 & 58.97	<i>G. candidum</i> (2/5)	9.75 & 13.84
2/6	53.31 & 59.15	3/1	22.72 & 27.33
4/1	46.92 & 52.49	4/2	40.14 & 45.44
5/1	53.78 & 59.63	5/2	56.00 & 61.93
<i>M. elegans</i> (5/3)	10.16 & 7.27	<i>H. rubiginosum</i> (5/4)	1.43 & 5.18
5/5	98.80 & 94.45	6/1	67.01 & 73.39
6/2	35.94 & 41.07	7/1	47.90 & 53.52
7/2	93.87 & 101.33	7/3	55.25 & 61.16
7/4	60.95 & 67.09	7/5	47.06 & 52.64
8/1	67.30 & 73.69	8/2	49.68 & 55.37
8/3	58.45 & 64.49	8/4	54.88 & 60.77

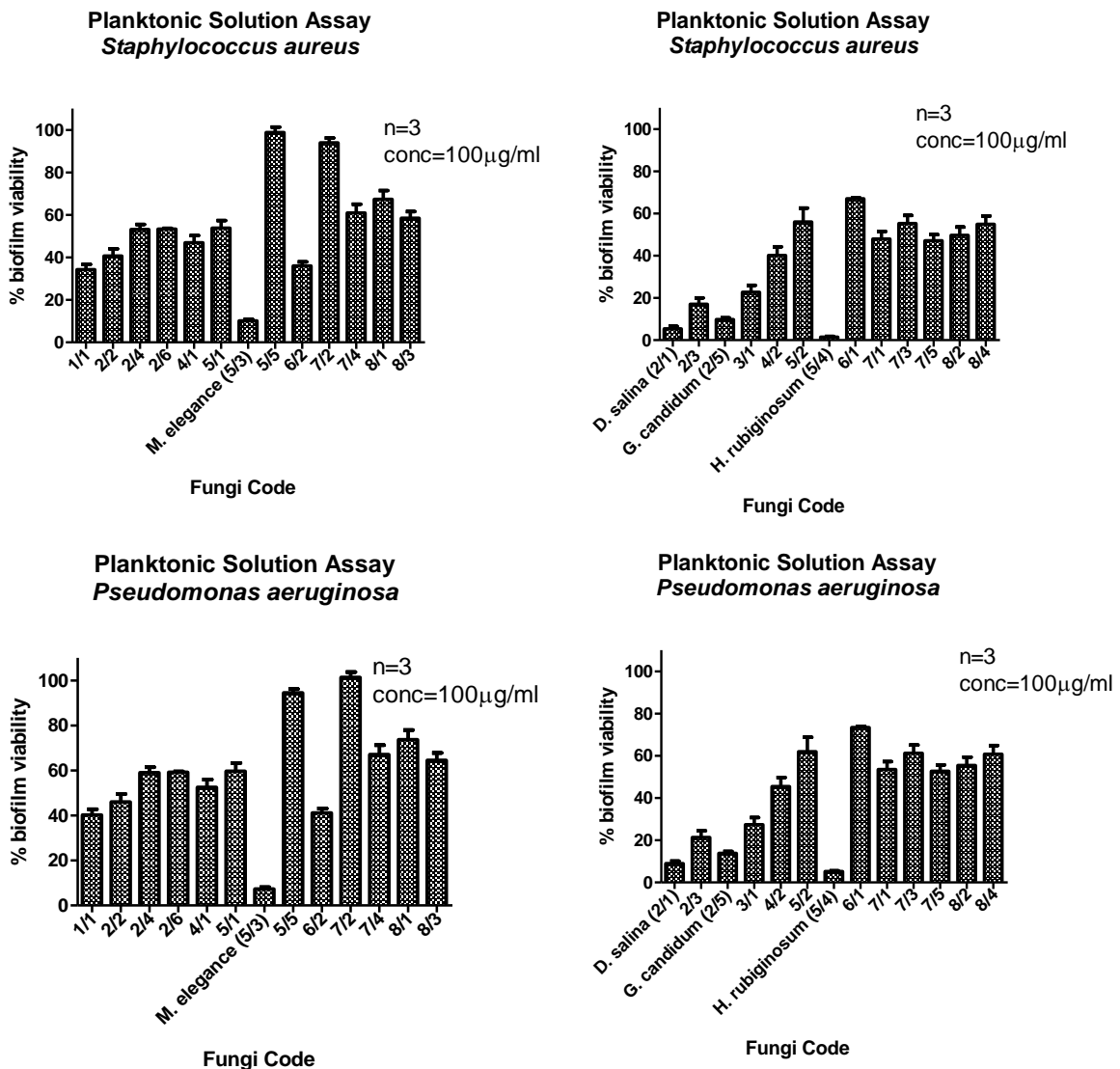


Figure 3.11: Planktonic assay results after applying 100µg/mL of each fungal extracts against both biofilm-forming *S. aureus* and *P. aeruginosa*.

3.5.3 Minimum inhibitory concentration (MIC) and Minimum biofilm eradication bacteria (MBEC) assay.

MIC and MBEC were calculated for the four antimicrobial extracts. All MIC were less than 35 $\mu\text{g}/\text{mL}$. The lowest MIC values were obtained with *M. elegance* extract at 18.50 and 23.20 $\mu\text{g}/\text{mL}$ against *S. aureus* and *P. aeruginosa*, respectively. While highest MIC values of 29.78 and 32.61 $\mu\text{g}/\text{mL}$, respectively were acquired from *H. rubiginosum* extract. On the other hand, the lowest MBEC values of 15.52 and 22.43 $\mu\text{g}/\text{mL}$ were obtained with *G. candidum* and *M. elegance* against *S. aureus* and *P. aeruginosa*, respectively. The highest MBEC values of 28.72 and 31.61 $\mu\text{g}/\text{mL}$ were attained with *D. salina* and *H. rubiginosum* extracts against *S. aureus* and *P. aeruginosa*, respectively.

Table 3.6: MIC of active fungal extracts against *S. aureus* and *P. aeruginosa*.

Medial extract	MIC $\mu\text{g}/\text{mL}$ against <i>S. aureus</i>	MIC $\mu\text{g}/\text{mL}$ against <i>P. aeruginosa</i>
<i>D. salina</i>	27.37	24.51
<i>M. elegance</i>	18.50	23.20
<i>H. rubiginosum</i>	29.78	32.61
<i>G. candidum</i>	28.72	30.63

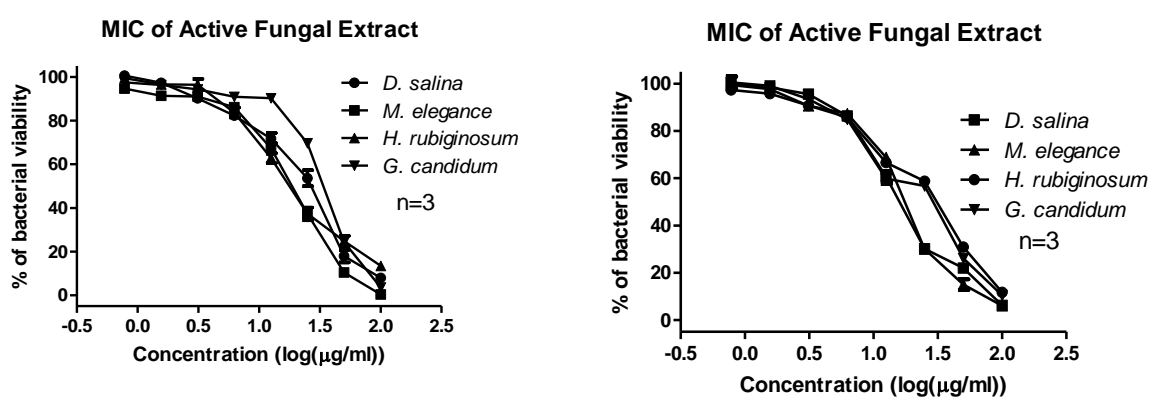


Figure 3.12: MIC results of active fungal extracts against biofilm-forming *S. aureus* and *P. aeruginosa*.

Table 3.7: MBEC of active fungal extracts against biofilm-forming *S. aureus* and *P. aeruginosa*.

Medial extract	MBEC $\mu\text{g}/\text{ml}$ against <i>S. aureus</i>	MBEC $\mu\text{g}/\text{ml}$ against <i>P. aeruginosa</i>
<i>D. salina</i>	28.72	23.66
<i>M. elegance</i>	26.77	22.43
<i>H. rubiginosum</i>	18.91	31.61
<i>G. candidum</i>	15.52	29.49

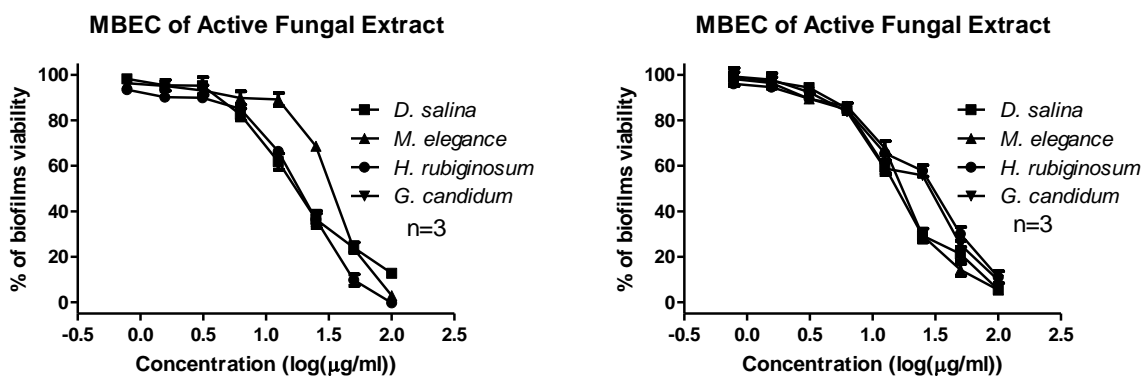


Figure 3.13: MBEC results of active fungal extracts against biofilm-forming *S. aureus* and *P. aeruginosa*.

3.6 NMR analysis of fungal extracts

As illustrated in Figure 3.14, there was quite a small change between NMR spectra of the fungal and blank media extracts. No major changes can be detected due to two reasons:

- 1- Low yield of extracts, which was less than 5mg from many of the fungal cultures. In addition, for extracts with yield less than 5mg, a 3mm NMR tubes were used with 300μl of DMSO_{d6} to improve NMR spectrum resolution.
- 2- NMR spectroscopy as a method is of lower sensitivity compared to mass spectrometry, which led to the inability to detect all peaks for low yielding secondary metabolites.

A high ratio of peaks at the aliphatic region between 0.00 and 3.50 ppm was afforded by all fungal extracts. This could be due to the marine nature of the endophytic fungi, which were known to produce high yield of fatty acids (Devi et al., 2006). However, according to the stacked ¹H NMR spectra of the fungal extracts with the blank media presented in Figure 3.15, there was an obvious difference between spectrum of the blank extract and those of the bioactive extracts especially those produced by *D. salina* and *H. rubiginosum*. *H. rubiginosum* seems to deplete the medium in comparison with the rest of the other active extracts where resonances belonging from the media blank could be perceived. However, *D. salina* afforded higher intensity resonances in the region between 0.5 and 4.5 ppm when compared to the media peaks.

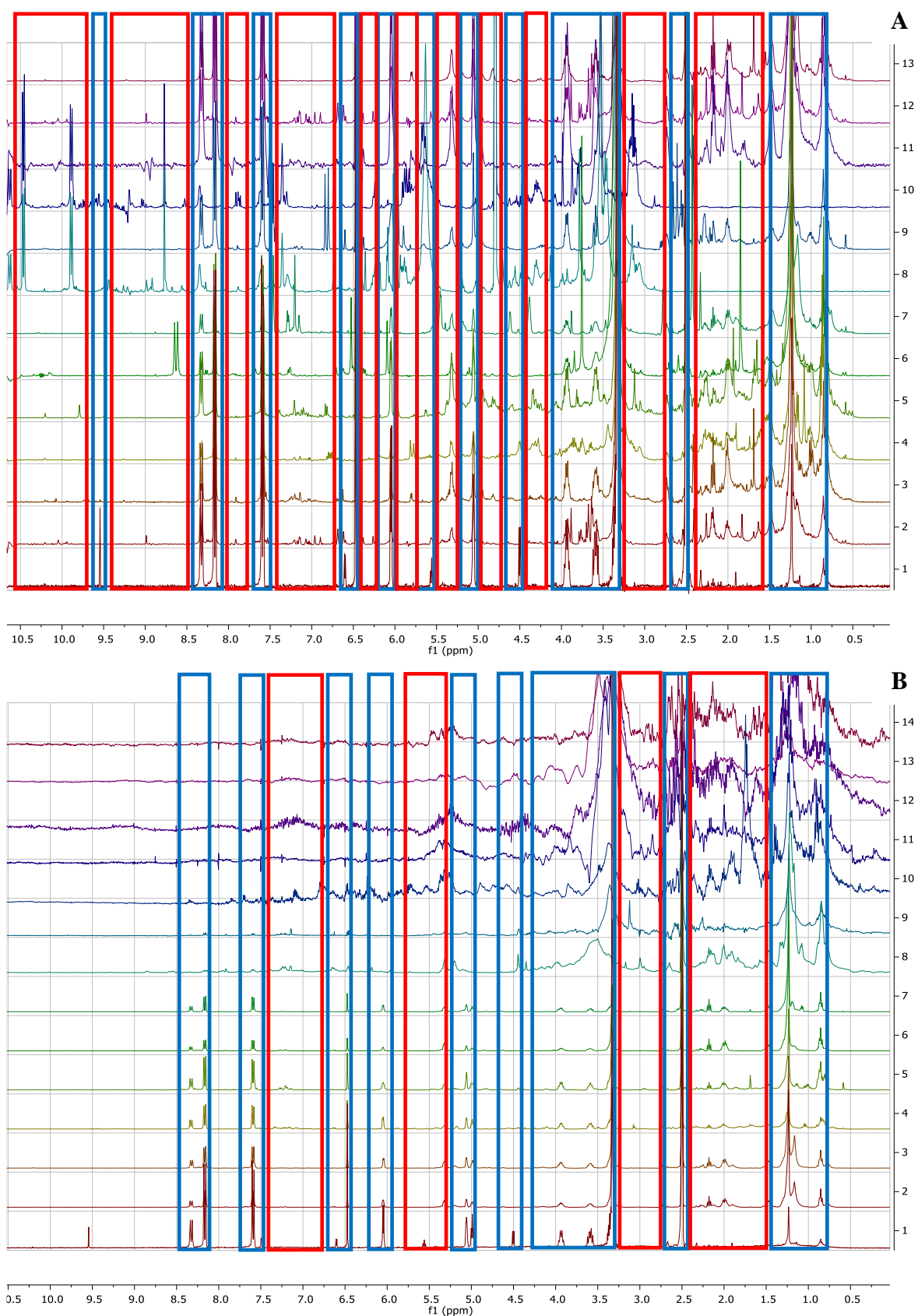


Figure 3.14: Stacked H^1 NMR data of fungal extracts obtained from isolated endophytic fungi from some Scottish seaweeds along with MA blank. A: a blank extraction followed by fungal extracts from 12 endophytes and B: a blank extract and 13 fungal extracts. Sample's concentration is 5mg/600 μl of $\text{DMSO-}d_6$ (400MHz).

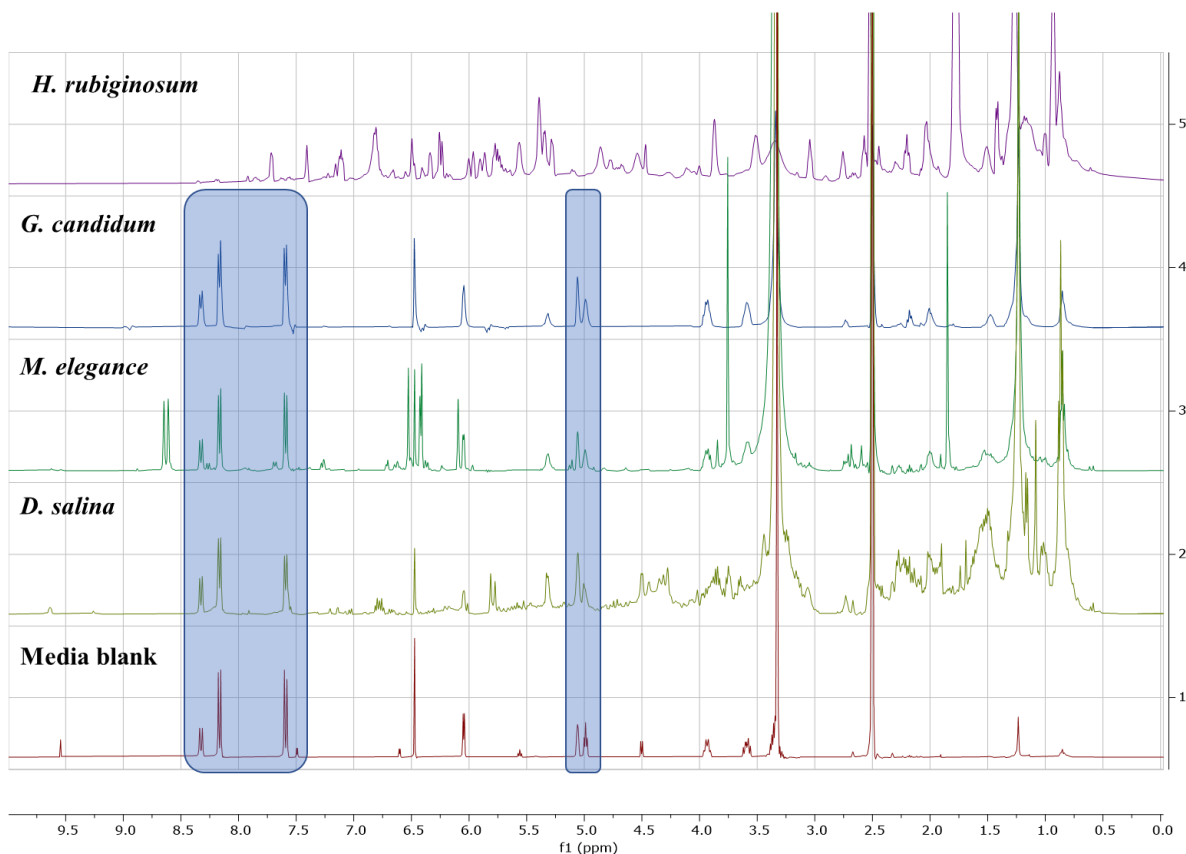


Figure 3.15: Stacked H^1 NMR spectrum of bioactive fungal extracts along with MA blank in the bottom. Sample concentration was at 5mg/600 μ l of DMSO- d_6 (400MHz). Highlighted peaks are resonances belonging to the MA medium.

In general, the NMR spectral data of the various fungal extracts displayed resonating peaks at a wide range of chemical shifts from the aliphatic to aromatic region with a higher ratio of hydroxylated and aliphatic peaks.

The PCA scatter plot of the NMR spectral data of the fungal extracts indicated a unique chemical profile for *D. salina*, which was positioned as an outlier. In addition, *M. elegance* and *H. rubiginosum* produced different chemical profile from most of the other extracts and located on the right quadrants of the plot. On the other hand, *G. candidum*, which produced a low yield of extract was more similar to the inactive extracts and the media blank. PCA scatter plot of the NMR data is presented on Figure 3.16.

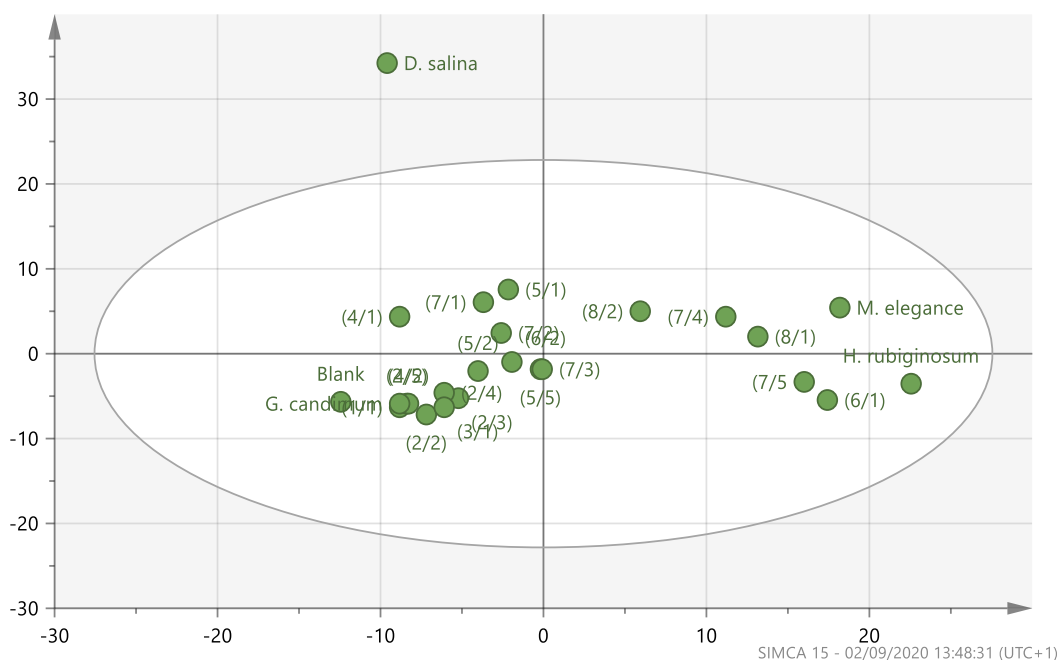


Figure 3.16: PCA scatter plot of the NMR spectral data of the respective fungal extracts.

When incorporating the antimicrobial assay results to the multivariate analysis data, the active secondary metabolites were located at the right side of the OPLS-DA scatter plot (Figure 3.20), while the inactive extracts accumulated at the left side of the plot. The chemical profiles afforded by the active *D. salina* and *G. candidum* extracts were quite similar as indicated by their close proximity on upper right quadrant of the scatter plot (Figure 3.17) as well as signified by their relatively very comparable spectra (Figure 3.15). The NMR spectral similarity of extracts obtained from *D. salina* and *G. candidum* could be due to their low yield being masked by the signals exhibited by the media blank (Figure 3.15).

On the other hand, albeit a non-identical spectra (Figure 3.18) for *M. elegance* and *H. rubiginosum* extracts, their respective chemical profiles were more comparable to each other as displayed by their position on the lower right quadrant of the scatter plot. The OPLS-DA scatter plot of the NMR spectral data showed some similarities in the entire range of chemical shifts (0.00 – 10.00 ppm) exhibited by the extracts provided by *M. elegance* and *H. rubiginosum*.

As presented by the OPLS-DA loadings plot in Figure 3.18, a higher ratio of aromatic signals at 6.00 to 10.00 ppm were produced by *G. candidum* and *D. salina* extracts. Alternatively, *H. rubiginosum* and *M. elegance* extracts yielded a higher ratio of aliphatic signals at chemical shifts between 0.00 and 5.50 ppm.

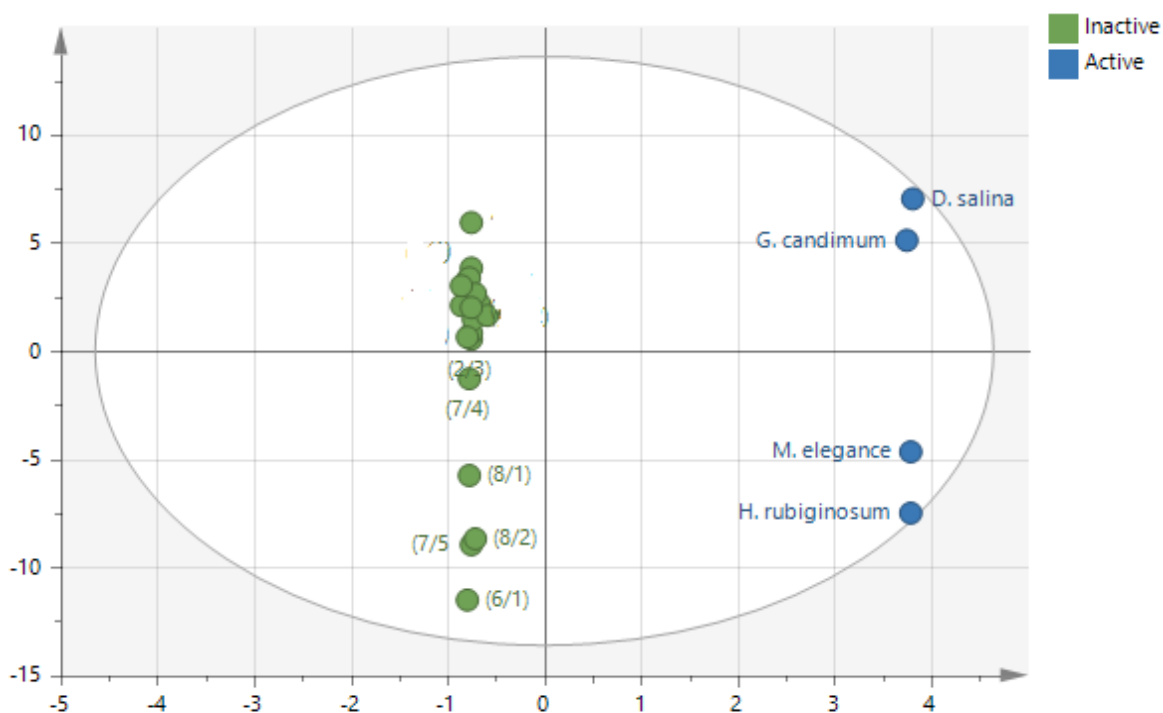


Figure 3.17: OPLS-DA scatter plot of the NMR spectral data of the fungal extracts grouped according to their antimicrobial assay result against both biofilm-forming *S. aureus* and *P. aeruginosa*. $R2X = 14.9\%$ and $R2Xo = 12.7\%$

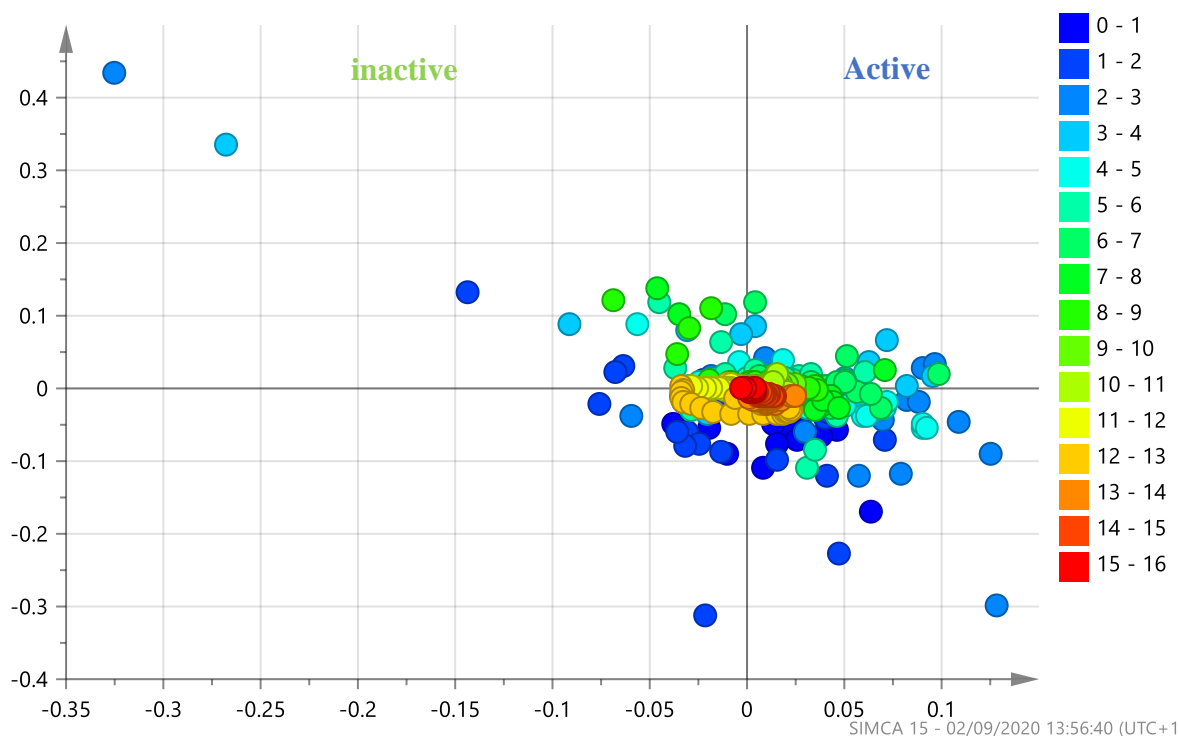


Figure 3.18: OPLS-DA loadings plot NMR spectral data of the fungal extracts grouped according to their antimicrobial assay result against both biofilm-forming *S. aureus* and *P. aeruginosa*.

3.7 Multivariate analysis of LC-HRMS data

The PCA scatter plot of the LC-HRMS data for the fungal extracts, as shown in Figure 3.19, displayed *H. rubiginosum* and *D. salina* as outliers indicating their unique chemical profiles. The rest of the fungal extracts overlappingly clustered together that indicated high similarity and with no huge difference in their chemical profiles. This could have also been affected by the small yield of the extracts that exhibited the media components at the forefront of the chromatograms.

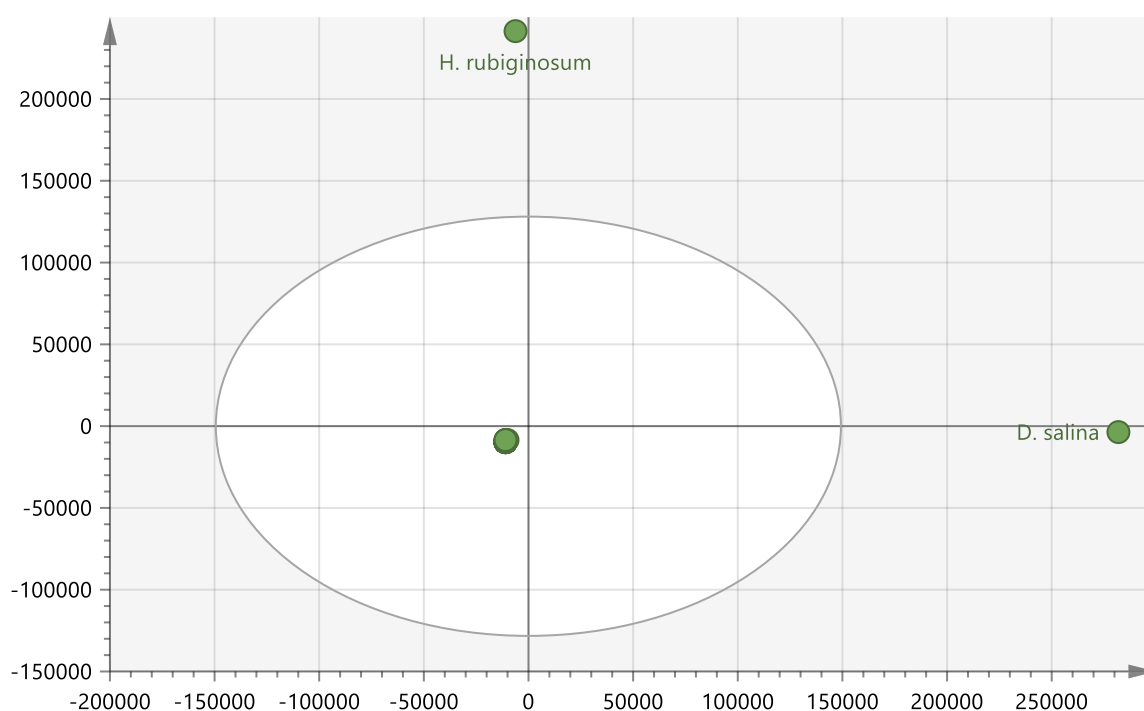


Figure 3.19: PCA scatter plot of the mass spectral data obtained for the respective fungal extracts.

Integrating the antimicrobial assay results with the LC-HRMS data in Figure 3.20, the active endophytes were dispersedly distributed at the right side of the OPLS-DA scatter plot. While the inactive endophytes were overlapping and closely clustered at the left side of the scatter plot as in the PCA plot in Figure 3.20. Extracts produced by *G. candidum* and *M. elegans* signified a more comparable or identical chemical profile. In parallel, the *M. elegans* and *G. candidum* extracts were not able to exhibit any discriminating features in the OPLS-DA loadings plot presented in Figure 3.21.

Whereas, the outlying extracts afforded by *D. salina* and *H. rubiginosum* indicated the occurrence of more unique chemical profiles and indicated the high possibility of isolating

novel compounds in the next stages of bioprospecting. *D. salina* and *H. rubiginosum* extracts were able to categorise their discriminating metabolites in the OPLS-DA loadings plot (Figure 3.21). The outlying *D. salina* extract was discriminated by metabolites with a wide MW range between 150 and 2000 Da. Alternatively, *H. rubiginosum* extract was categorised as an outlier by metabolites with lower molecular weights between 150 and 698 Da. Discriminating metabolites encircled in red gave p -values < 0.05 , which indicated a strong model with a confidence interval of more than 95%. Three metabolites with mzMine IDs N_1890, P_9719, and N_1962 were found at m/z 342.14012, 265.104272, and 271.06112 were dereplicated from the DNP database as citridone B, oxosorbicillinol, and griseoxanthone C (Broadbent et al., 1975, Abe et al., 2000, Fukuda et al., 2005), citridone B, oxosorbicillinol, and griseoxanthone C the three known discriminating features have been isolated *Penicillium roseopurpureum*, *Penicillium chrysogenum*, and *Fusarium equiseti* from respectively (Broadbent et al., 1975, Abe et al., 2000, Fukuda et al., 2005). All these three known compounds and their respective derivatives were earlier described as antimicrobial agents ((Fukuda et al., 2014, V Simoben et al., 2015). The rest of the encircled discriminating metabolites gave no hits. According to the variable trend histogram in figure 3.22, oxosorbicillinol was found to be produced by *D. salina* while citridone B and griseoxanthone C were produced by *H. rubiginosum* The encircled discriminating features are listed in Table 3.8.

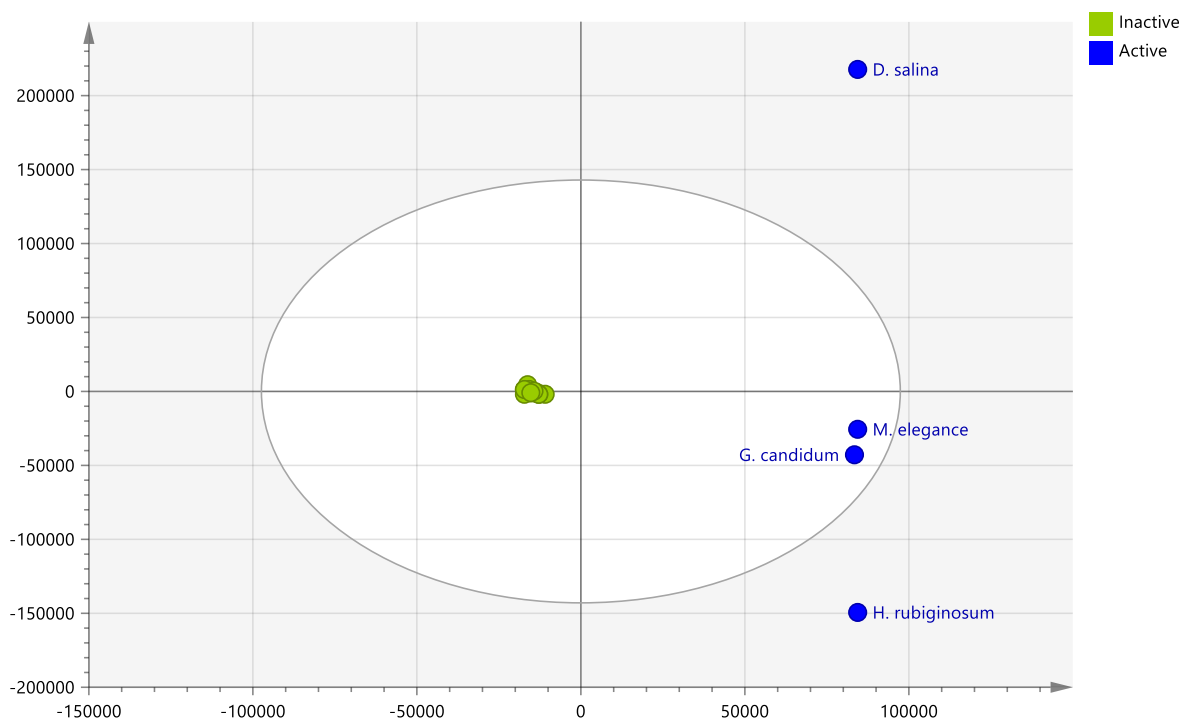


Figure 3.20: OPLS-DA scatter plot of the mass spectral data of the fungal extracts grouped according to their antimicrobial assay results against both biofilm-forming *S. aureus* and *P. aeruginosa*.

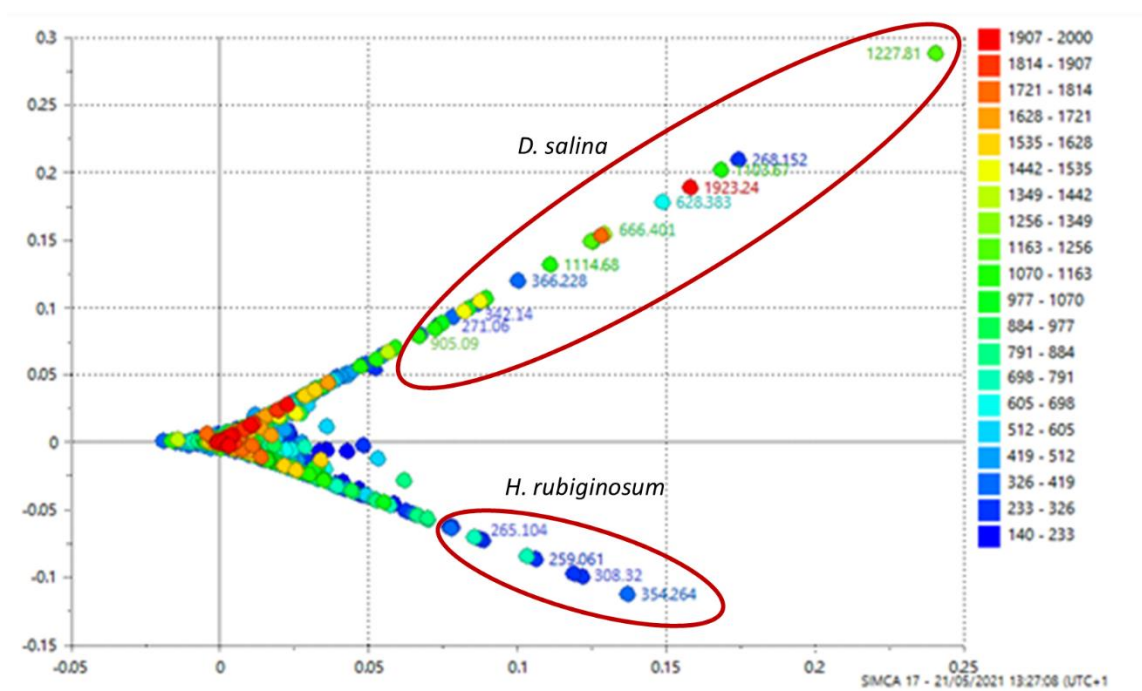
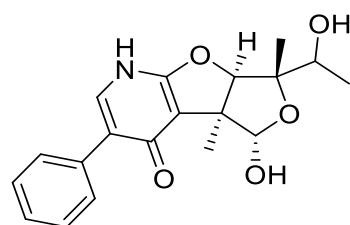


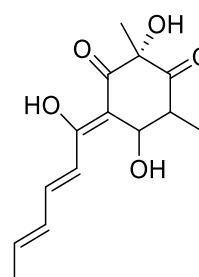
Figure 3.21: OPLS-DA loadings plot of the mass spectral data of the fungal extracts grouped according to their antimicrobial assay results against both biofilm-forming *S. aureus* and *P. aeruginosa*. Encircled in red are the discriminating features for the bioactive extracts found in the respective quadrants of the scatter plot (Figure 3.14).

Table 3.8: Dereplication of 3 known possible bioactive metabolites with *p*-values < 0.05.

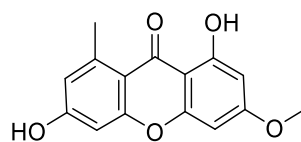
MZmine ID	Rt (min)	<i>p</i> -value	FDR	Molecular weight (Da)	Chemical formula (DBE)	Compound hits
N_1890	17.80	0.0377	0.0230	343.14117	C ₁₉ H ₂₁ NO ₃ (10)	citridone B
P_9719	12.22	0.0477	0.0423	264.1000	C ₁₄ H ₁₆ O ₅ (7)	oxosorbicillinol
N_1962	19.05	0.0408	0.0307	272.068475	C ₁₅ H ₁₂ O ₅ (10)	griseoxanthone C
N_2094	21.01	0.0206	0.0115	1702.562	C ₁₁₂ H ₁₆₀ N ₁₄ (40)	No hit
P_8404	19.70	0.0257	0.0192	1517.0837	C ₁₀₄ H ₁₁₃ N ₁₁ (54)	No hit
P_13433	19.71	0.0447	0.0346	1085.0400	no prediction	No hit
P_12858	16.42	0.0224	0.0153	904.30354	C ₆₂ H ₄₀ N ₄ O ₄ (45) C ₆₁ H ₄₄ O ₈ (40)	No hit
P_6368	13.67	0.0107	0.0038	855.0792	C ₄₃ H ₁₇ N ₇ O ₁₄ (39)	No hit
N_1886	19.06	0.0145	0.0076	721.0200	no prediction	No hit
P_11293	14.26	0.0468	0.0384	665.39387	C ₃₄ H ₅₁ N ₉ O ₅ (14)	No hit



citridone B



oxosorbicillinol



griseoxanthone C

Figure 3.22: Putatively dereplicated compounds afforded by antimicrobial active fungal extracts

According to the variable trend results provided by SMICA, citridone B was found in *D. salina* extract. While both oxosorbicillinol, and griseoxanthone C were found to be in *H. rubiginosum* extract as presented in figure 3.23.

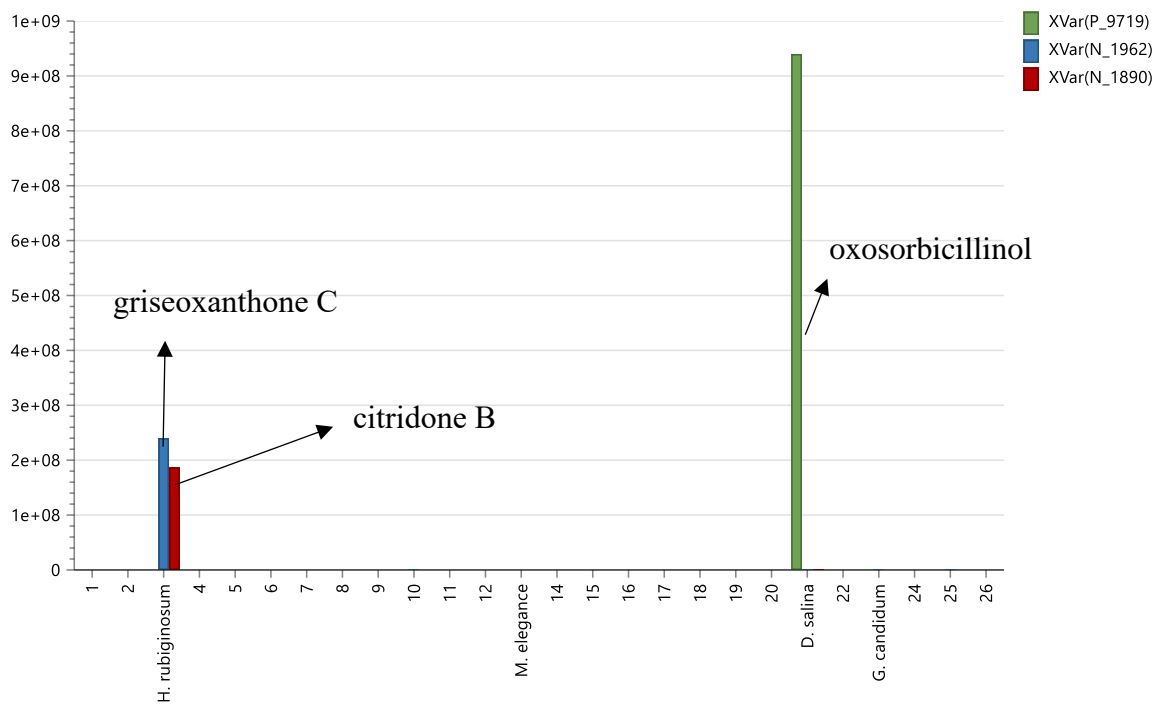


Figure 3.23: Variable trend of the known discriminating features assigned on OPLS-DA loading plot.

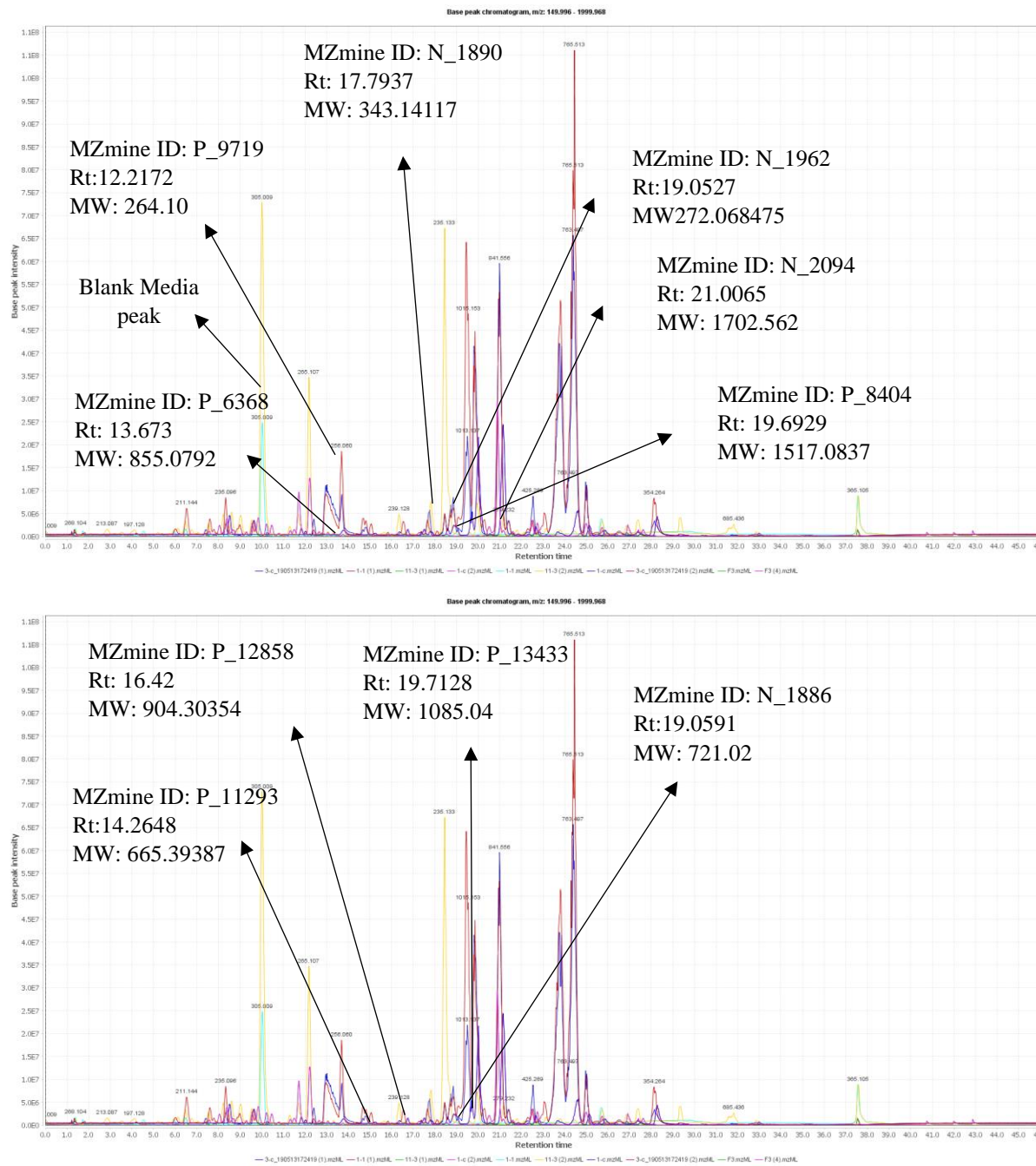


Figure 3.24: Total Ion Chromatogram (TIC) of both positive and negative modes produced from blank and active extracts. Yellow line represents blank media.

3.8 ITS gene sequencing

ITS gene sequencing was used to taxonomically identify each of the isolated endophytic fungi. Twenty-four fungi showed the presence of DNA bands upon visualising the gel electrophoresis plates under the UV. However, two fungal samples did not exhibit any band under UV. Due to the sensitivity of ITS gene sequencing to any contaminant, a blank sample was prepared as described in section 2.2.5 and run alongside the fungi samples for quality control. The blank sample should show no presence of any contamination as presented in Figure 3.25.

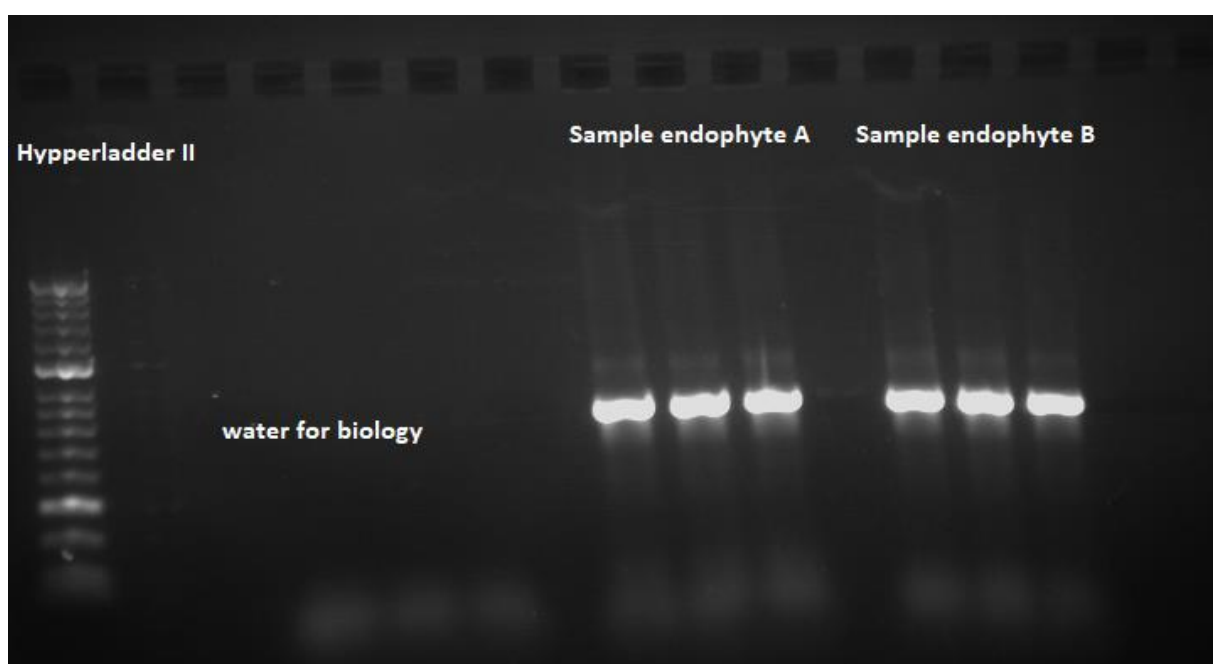


Figure 3.25: Electrophoresis gel image of the PCR results of two fungal samples with a blank sample to quality control the DNA amplification procedure.

Depending on the antimicrobial assay results, extracted DNA of four active fungal strains were submitted for ITS gene sequencing. Results of the BLAST sequence comparison is presented under the Appendix in Figures 9.2 and 9.3. The ITS gene sequencing results were processed using FinchTV then the data was compared with NCBI-blast database.

Table 3.9: Identified active fungal strains.

Sample ID	Concentration ng/ μ l	Source	Endophyte
2/1	19.7	<i>Laminaria hyperborea</i>	<i>Dendryphiella salina</i> (<i>D. salina</i>)
5/3	18.3	<i>Fucus vesiculosus</i>	<i>Hypoxyton rubiginosum</i> (<i>H. rubiginosum</i>)
2/6	12.1	<i>Fucus vesiculosus</i>	<i>Galactomyces candidum</i> (<i>G. candidum</i>)
5/4	8.2	<i>Fucus vesiculosus</i>	<i>Mariannaea elegans</i> (<i>M. elegance</i>)

3.9 Summary of the preliminary screening results

Only four fungal isolates (*D. salina*, *H. rubiginosum*, *M. elegance* and *G. candidum*) were able to produce the desired antimicrobial active extracts with high ability to inhibit bacterial growth and biofilm formation at more than 90%. In choosing the fungal isolate for further scale up and fractionation, MIC and MBEC were calculated. However, there was no huge difference in the MIC and MBEC values of the antimicrobial active fungal extracts. All evaluated antimicrobial extracts afforded an MIC and MBEC of less than 35 μ g/ml.

For further scale up and fractionation work, vital factors need to be considered. Besides the antimicrobial activity, this also included the extract yield and uniqueness or novelty of the chemistry of predicted biologically active target metabolites. *G. candidum* was excluded due to the low yield of its extracts. Both *D. salina* and *H. rubiginosum* afforded the extracts with the most unique chemical profiles as indicated by the multivariate analysis of their NMR and mass spectral datasets. In the antimicrobial assays, particularly considering the MIC and MBEC values, *D. salina* and *M. elegance* were the most potent.

D. salina, *H. rubiginosum* and *M. elegance* were chosen for further scale-up optimization work based on potent biological activity, high extract yield, and uniqueness of chemical profiles of the respective extracts.

4 Optimising the production of bioactive fungal extracts

The emergence of drug resistant pathogens has motivated researchers to explore for new sources of bioactive compounds (Deka and Jha, 2018). Endophytic microorganisms are considered to be one of the promising sources of potential bioactive metabolites (Krabel et al., 2013). Since the isolation of penicillin from fungi, by Alexander Fleming in 1928, microorganisms have been used as a source of novel bioactive compounds which can offer an easy way to scale up the production of these bioactive compounds by different types of cultivation or fermentation methods (Fatima et al., 2016). The association between a host organism and an endophyte can result in a beneficial relationship, which can aid the survival of both host organism and microorganism (Fatima et al., 2016). Survival of both organisms can be aided by the production of secondary metabolites from one or both organisms, protecting each other against the stress provided by their surrounding environment (Strobel, 2003, Owen and Hundley, 2004). Various factors like temperature, salinity, incubation periods, and nutrient source are playing important roles in the production of various bioactive metabolites (Thakur et al., 2009, Bhattacharyya and Jha, 2011).

The aim of this study is to optimize the production yield of bioactive metabolites afforded by *Dendryphiella salina* (*D. salina*), *Mariannaea elegans* (*M. elegance*) and, *Hypoxylon rubiginosum* (*H. rubiginosum*). *D. salina* is a fungi species usually collected from an intertidal zones of both tropical and subtropical coasts (Kohlmeyer and Kohlmeyer, 1979). *D. salina* has been widely studied for its eco-physical and morphological adaptation to salinity in the marine environment (Clipson and Jennings, 1992, Edwards et al., 1998). *M. elegance* is a harmless fungi, which is found mainly on rotting wood and soil environment (Söderström and Bååth, 1978). Reports regarding the chemical composition of the extracts afforded by *Mariannaea* genus are few (Ishiuchi et al., 2020). Three compounds were recently isolated from *M. elegance* namely; mariannaeapyrone and mariannamides A and B (Fabian et al., 2001, Ishiuchi et al., 2020). *H. rubiginosum* is one of 150 species under the genus *Hypoxylon* (*Xylariaceae*) (Mühlbauer et al., 2002). Many compounds have been isolated from various species related to the genus *Hypoxylon*, while three compounds, which are entonaemin A, daldinin C, and orsellinic acid have been described from methanolic extracts of *H. rubiginosum* (HASHIMOTO et al., 1994, Buchanan et al., 1995, Hashimoto and ASAKAWA, 1998, Jayaprakasha and Rao, 2000).

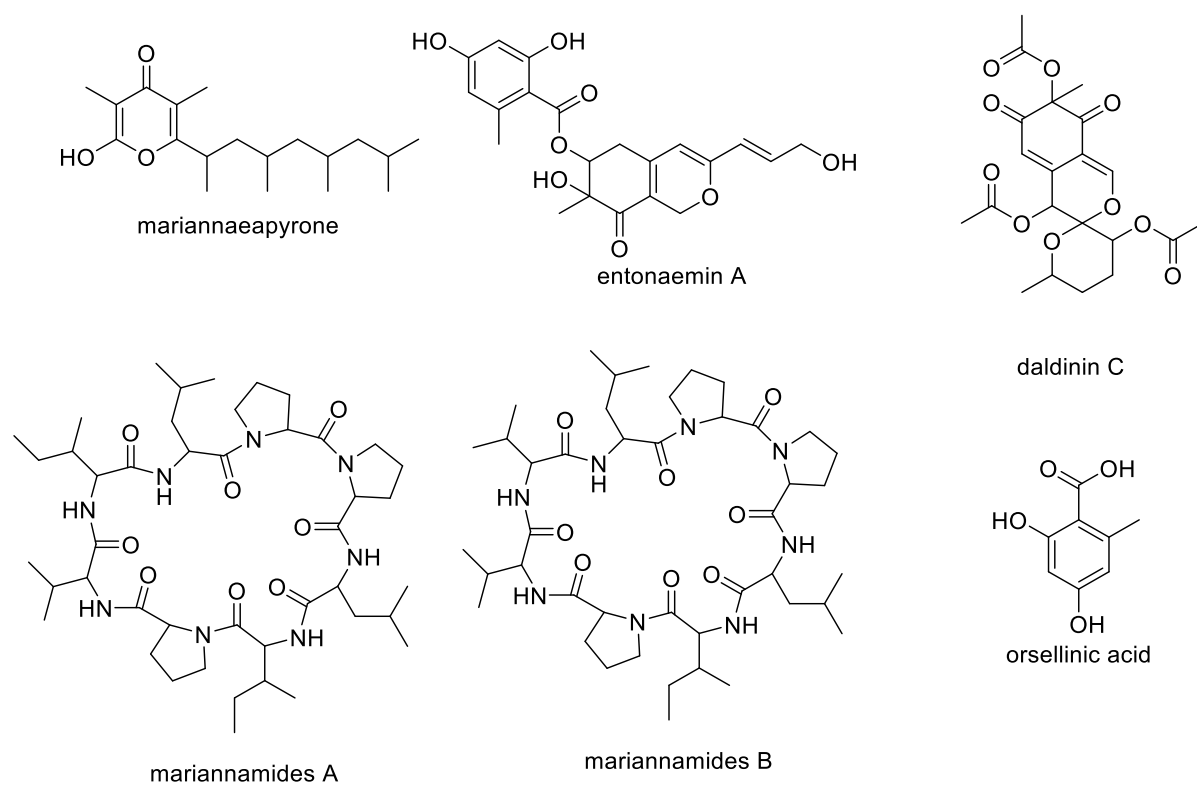


Figure 4.1: Chemical structure of compounds earlier isolated from selected fungi for optimisation.

4.1 Optimising the production of anti-biofilm bioactive metabolites in *Dendryphiella salina*

4.1.1 Extract yields on different media.

Solid media either with or without sea salt were able to afford higher yields than those obtained from liquid media with and without sea salt. The highest yield of *D. salina* extract was obtained from oat media without sea salt while the lowest extract yield was obtained on Wickersham liquid media, both were incubated for 7 days, as shown in Table 4.1. All cultures were incubated at 27°C as stand cultures.

Table 4.1: Weights of Extracts Obtained from *D. salina* Cultures on Different Media.

Liquid Media				
Type of Media	Incubation Period			Blank Media
	7 Days	15 Days	30 Days	
Malt Extract without Sea Salt	21.0mg	23.4mg	25.6mg	4.21mg
Malt Extract with Sea Salt	18.7mg	24.5mg	89.8mg	5.34mg
Wickersham Media without Sea Salt	15.7mg	62.1mg	46.4mg	2.78mg
Wickersham Media with Sea Salt	27.9mg	68.1mg	18.4mg	3.51mg
Marine Broth	16.3mg	17.7mg	15.8mg	1.27mg
Solid Media				
Type of Media	Incubation Period			Blank
	7 Days	15 Days	30 Days	
Rice Media without Sea Salt	193mg	206mg	157mg	12.7mg
Rice Media with Sea Salt	230mg	143mg	193mg	13.4mg
Oat Media without Sea Salt	695mg	648mg	593mg	83.7mg
Oat Media with Sea Salt	673mg	623mg	570mg	95.3mg

The histogram below (Figure 4.2) shows the weight of the extracts of *D. salina* at 7-, 15-, and 30-days of incubation on nine different media. After 30 days of incubation in malt extract (ME) broth with and without sea salt, *D. salina* has reached the height of its log growth phase going into the stationary as shown in Figure 4.1A. On the other hand, the extract yields started to decline on the 30th day of incubation on Wickersham broth with and without sea salt as well as in marine broth, which indicated the end of the stationary phase and beginning of the death phase.

From the rice media without sea salt, the extract yield decreased after 15 days of incubation indicating a changeover from the stationary growth to death phase of the fungus (Figure 4.1B). Alternatively, the extract yield from rice media with sea salt gained optimum yield on the 7th day of incubation then underwent a fluctuational decrease thereafter as the fungus started to transition to its death phase on the 15th day. Similarly, on oat media with and without sea salt, optimum extract yields were also afforded on the 7th day, which indicated the peak of the log growth phase as the fungus moved into its stationary phase, while a steady decline of the extract yields was observed from the 15th day of incubation as the fungal growth went into its death phase (Figure 4.1B).

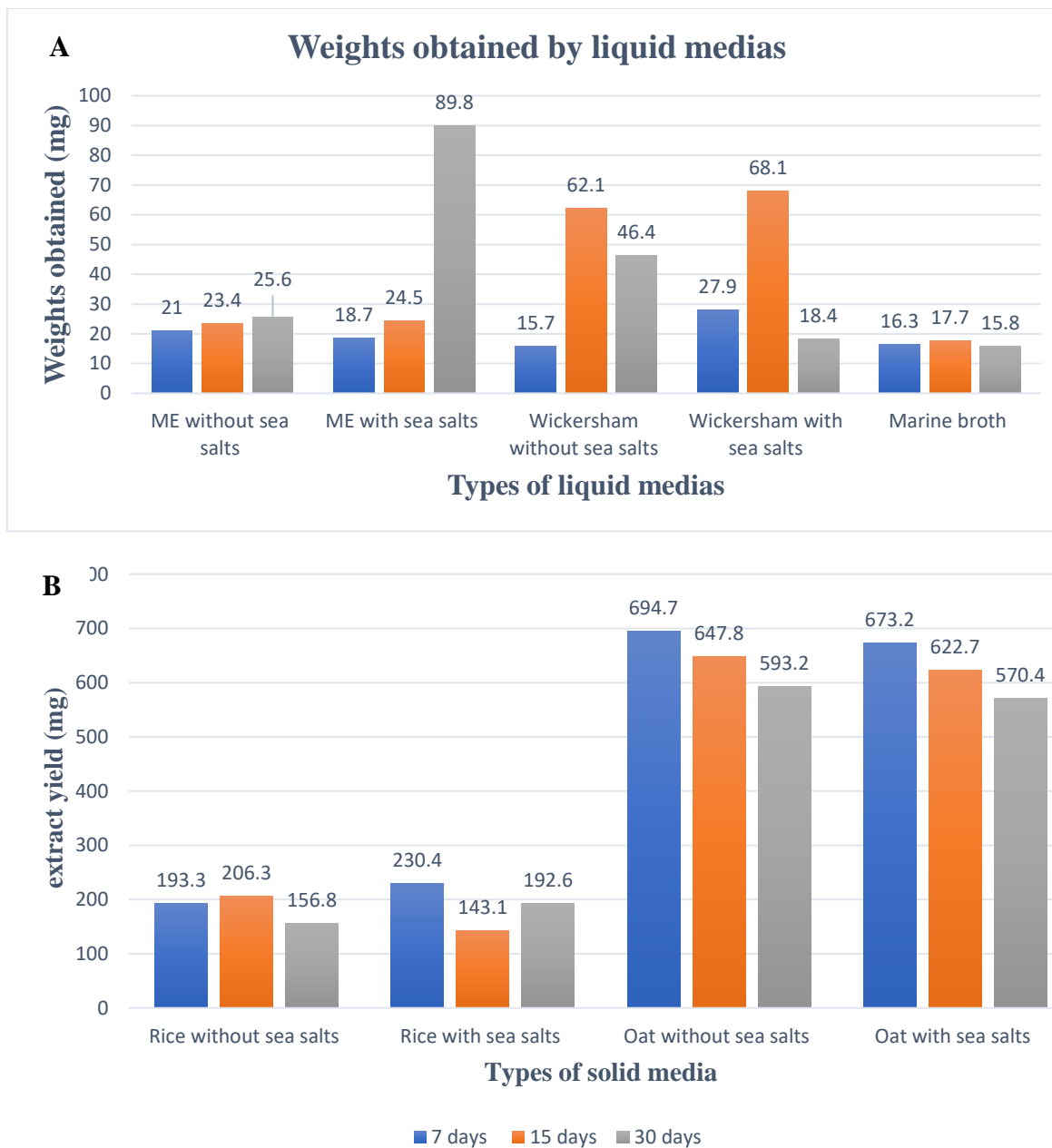


Figure 4.2: Histogram of extract yields obtained from various liquid (A) and solid (B) media used to incubate *D. salina* extracts at 7-, 15-, and 30-days.

4.1.2 NMR spectroscopy for *D. salina* extracts

4.1.2.1 Liquid media

4.1.2.1.1 Malt extract broth media with and without sea salt:

¹H NMR spectra of extracts afforded by *D. salina* growing on malt extract with and without sea salt showed a huge difference from the blank media (Figure 4.3). Differences could be observed at the aliphatic and hydroxylated region while not significantly perceived at the aromatic region, as shown in Figure 4.3. Differences between chemical profiles of the extracts and blank media were mainly based on the fatty acid yielded by the fungus. In addition, resonances for hydroxyl groups and olefinic hydrogens at 3.50 and 5.50 ppm, respectively, were also observed on the spectra of the fungal extracts. When comparing the extracts in the presence of sea salt with the extract in the absence of the sea salt, no huge difference was observed. Only peaks at aromatic region between 6.00 and 10.00ppm were more intense after 15 days of incubation in the presence of sea salt. On the other hand, for media without sea salt, the intensity of aromatic peaks resonating at >6.00ppm were decreasing with time while the aliphatic region resonances at <6.00ppm had no obvious changes. In the presence of sea salt, intensity of aromatic peaks increased at the 15th day and decreased at the 30th day, while there were no major changes observed in the aliphatic region.

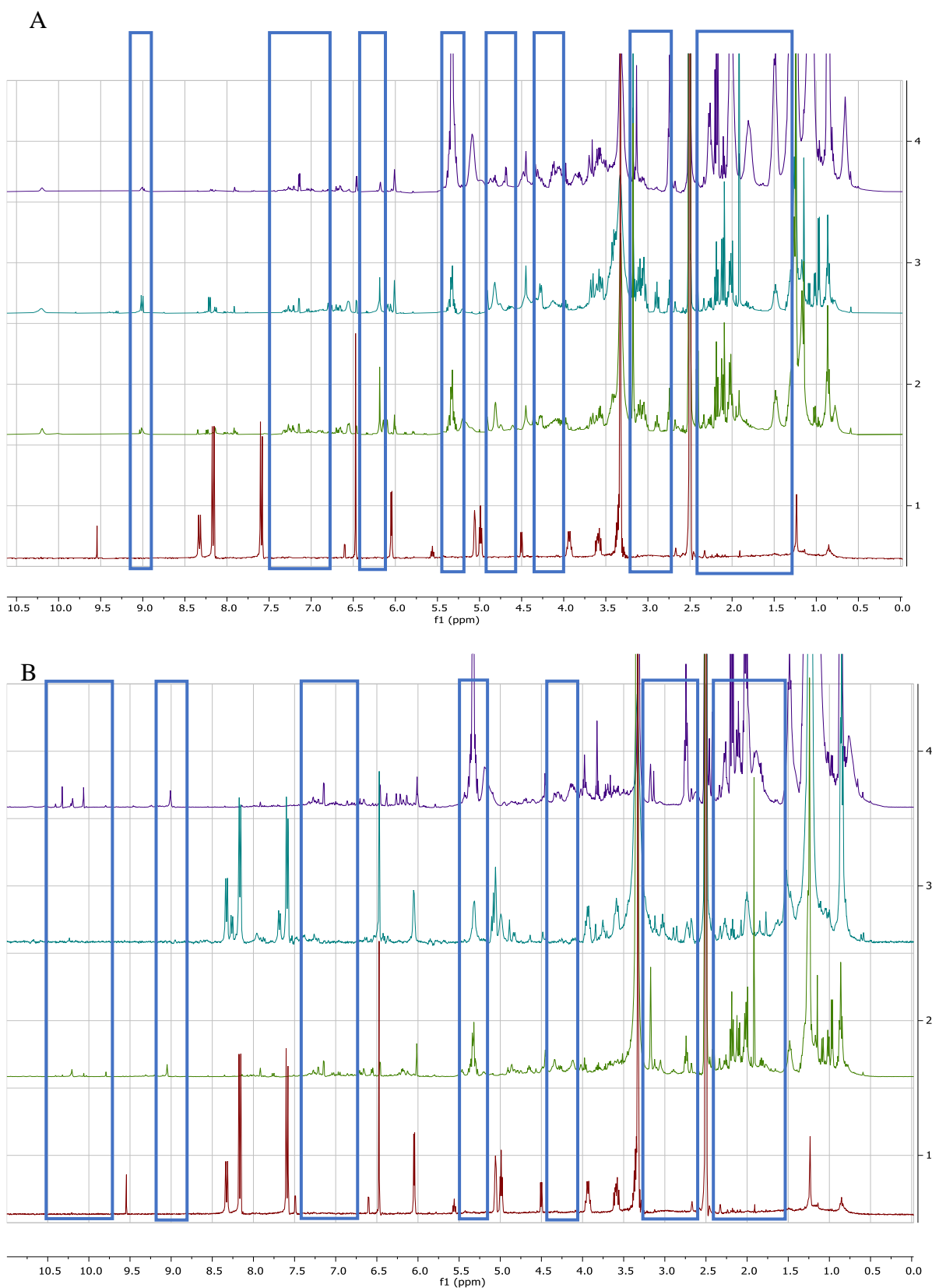


Figure 4.3: Proton NMR spectra of fungal extracts obtained from ME with salt (**A**) and without sea salt (**B**). Spectrum 1 at the bottom of each of the stack represents the blank followed by three incubation periods of 7, 15 and 30 days, respectively. Differences are shown in blue boxes.

4.1.2.1.2 Wickersham media with and without sea salt:

Proton NMR spectra of *D. salina* extracts obtained from Wickersham media with and without sea salt following 7, 15, and 30 days of incubation (Figure 4.4) exhibited great similarity with the blank media, as shown in Figure 4.4. The NMR spectral data afforded identical resonances between the blank media and fungal extracts in the aliphatic region at 1.00 to 1.50 ppm as well as in the double bond region at 6.00 to 6.50 ppm. However, differences between the blank media and fungal extracts were perceived at δ_{H} 6.5 to 7.5 and 8.5 to 9.5. The extract in the presence or in the absence of sea salt showed no huge difference either at the aliphatic or aromatic regions. In addition, the incubation time did not affect the intensity or the incidence of new resonances. This indicated that the incubation period and the presence or the absence of sea salt have no major effect on *D. salina* growing on Wickersham broth.

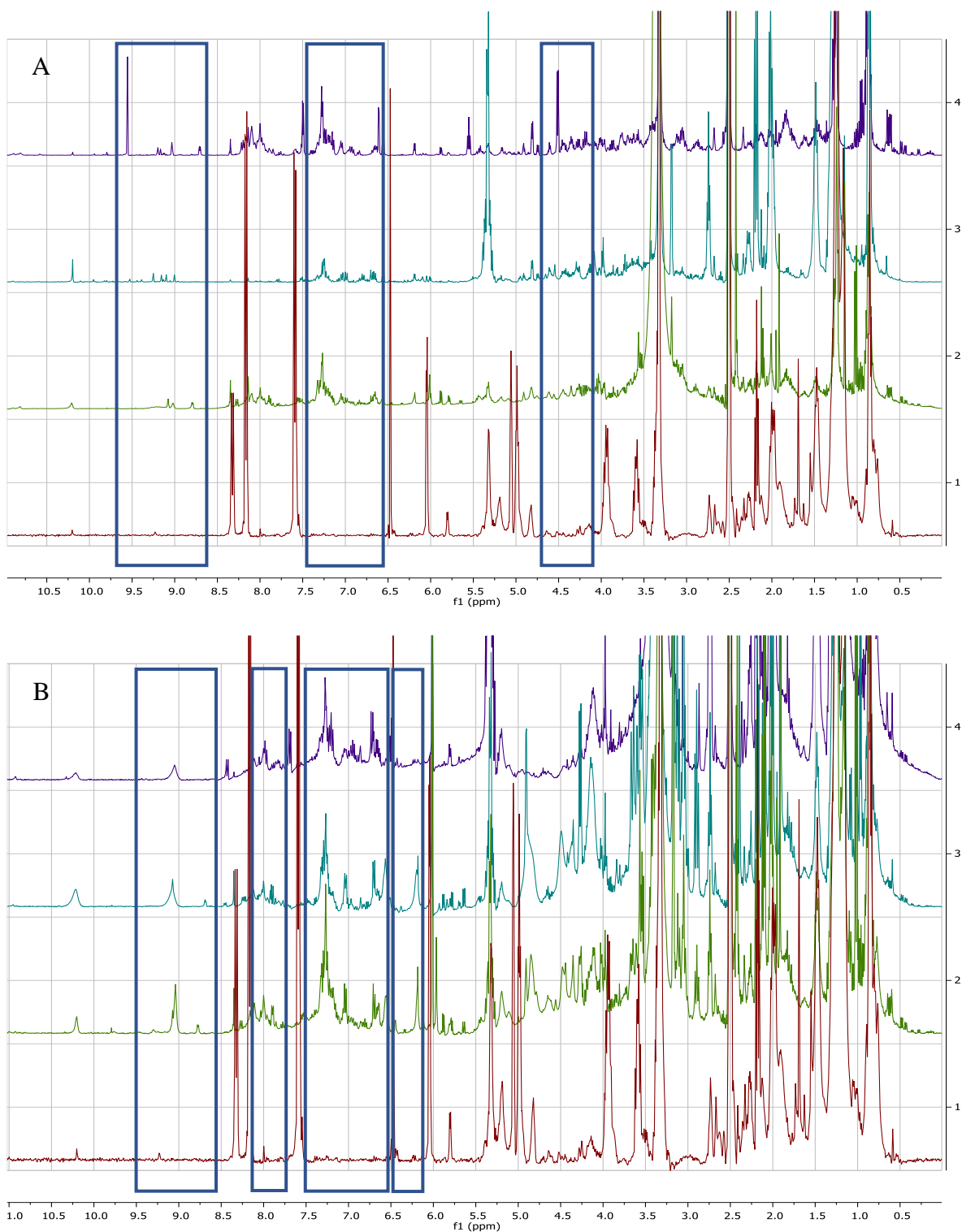


Figure 4.4: Proton NMR spectra for fungal extracts obtained from Wickersham liquid with salt (A) and without sea salt (B). Spectrum 1 at the bottom of each stack represents the blank followed by the three incubations periods of 7, 15 and 30 days, respectively. Differences are indicated in blue boxes.

4.1.2.1.3 Marine broth media:

^1H NMR spectra obtained for the various extracts afforded by *D. salina* after an incubation period of 7, 15 and 30 days, respectively (Figure 4.5), displayed perceivable differences from the blank spectrum especially at the aromatic region. It is noticeable that *D. salina* was producing high amounts of both saturated and unsaturated fatty acids, as shown in Figure 4.4. In addition, a relatively smaller change can be observed between the blank media and extracts at the aromatic region (6.00 to 9.00 ppm) for extracts obtained on the 7th and 30th day of incubation. While a more significant variation can be detected at the aromatic region (6.00 to 9.00 ppm) for the extract afforded on the 15th day of incubation. It seems that the major production of compounds happened at 15 days while it starts to decline after that.

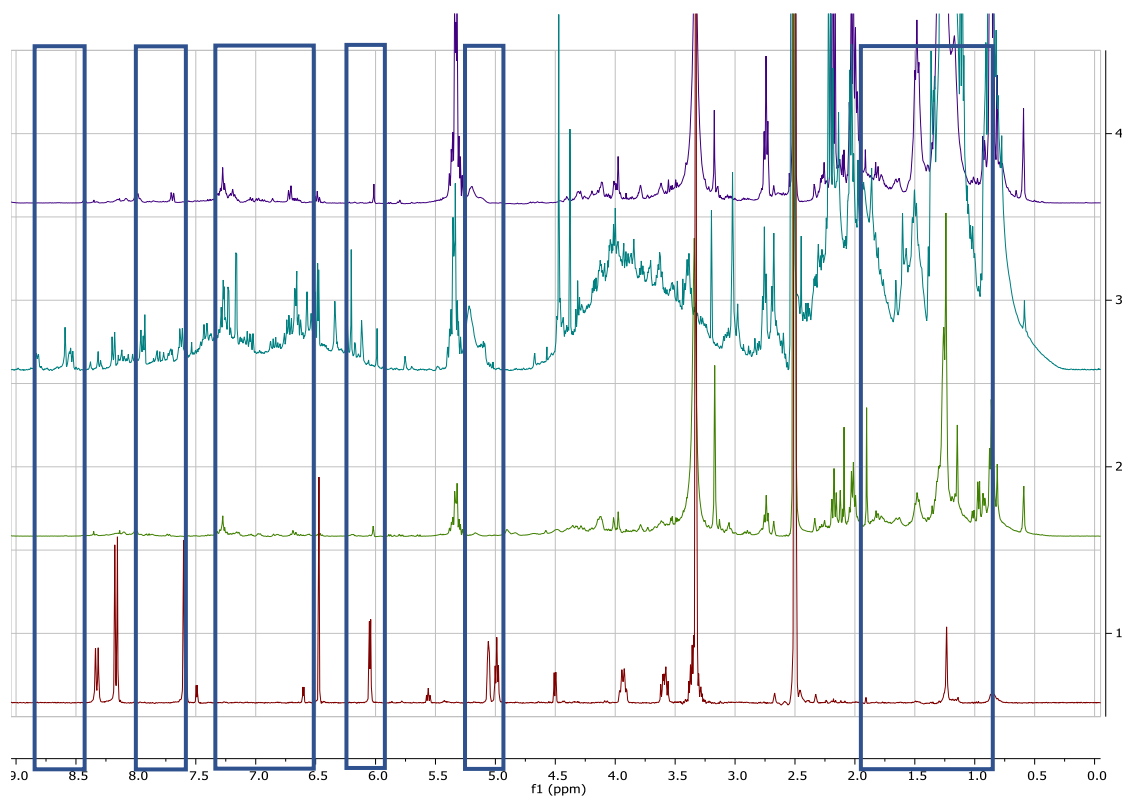


Figure 4.5: Proton NMR spectra of extracts obtained from marine broth extracts and blank media; blank followed by the three incubation periods at 7, 15, and 30 days, respectively. Observed differences are shown in blue boxes.

4.1.2.2 Solid media

4.1.2.2.1 Rice media with and without sea salt:

After growing *D. salina* on rice media with and without sea salt, respectively, small differences between blank media and extracts could be observed on the stacked proton NMR spectra as shown in Figure 4.6. Changes were mainly perceived at the aromatic region particularly between 8.50 and 10.50 ppm. The extract resulted in the presence of sea salt show fewer aromatic peaks especially between 8.50 and 10.50 ppm. While the aliphatic region shows no huge difference from extracts without sea salts. The number of aliphatic peaks between 0.00 and 5.50 ppm are higher in comparison with liquid media. This could be due to the presence of high concentration of carbohydrate provided by the solid media.

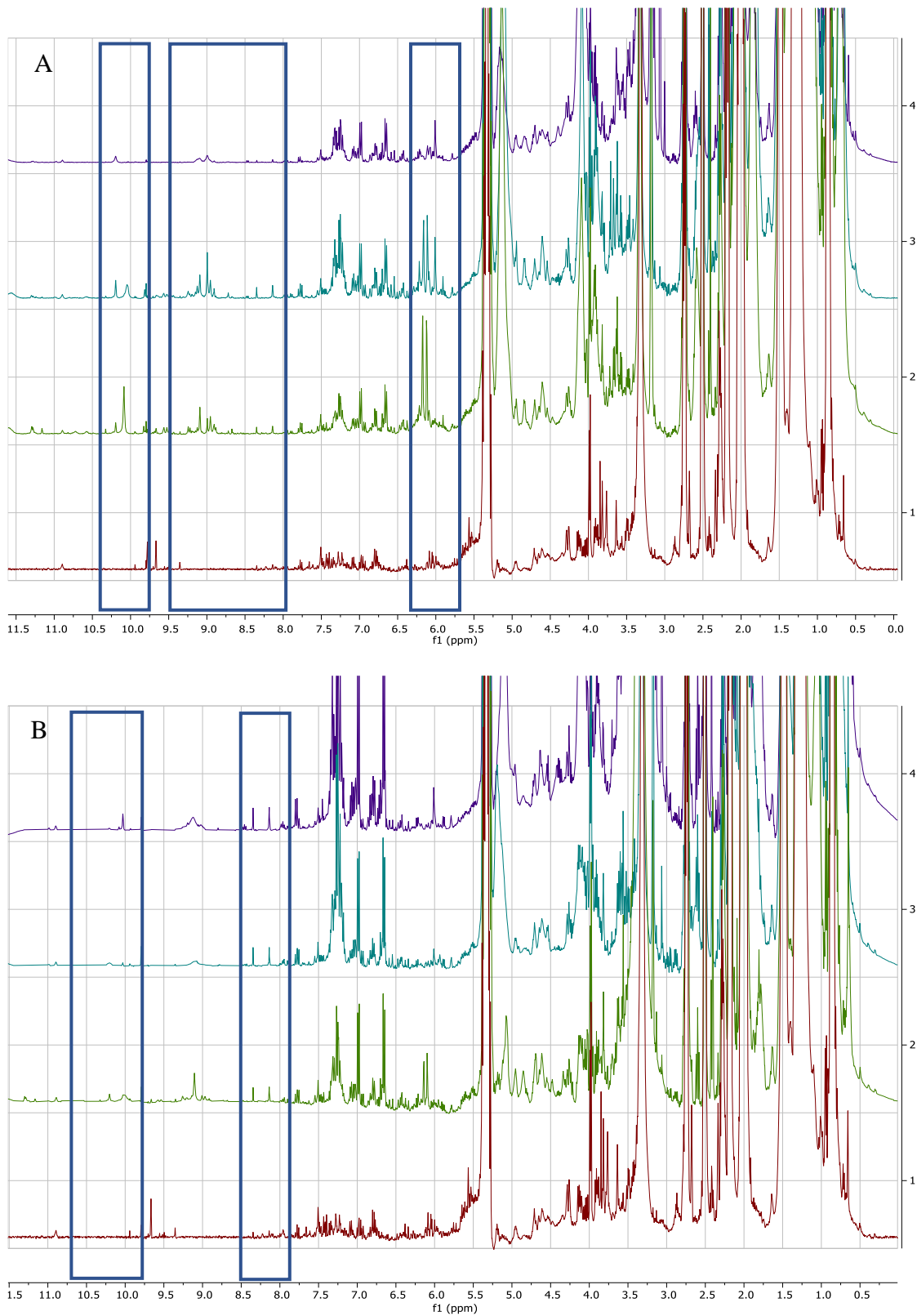


Figure 4.6: Proton NMR spectra of fungal extracts obtained from rice media with salt (A) and without sea salt (B). Spectrum 1 from each stack represents the blank followed by three incubation periods of 7, 15 and 30 days respectively.

4.1.2.2.2 Oat media with and without sea salt:

Proton NMR spectra obtained from oat blank media and fungal extracts prior to an incubation period of 7, 15, and 30 days from both media with and without sea salt (Figure 4.7), showed no perceivable differences except at the aromatic region. Resonances at δ_{H} 6.00 to 6.50 observed in the spectra of the extracts were most prominent at the 7th and 30th days of incubation of *D. salina* on oat media without sea salt as well as at the 7th day on oat media with sea salt. In addition, a small peak started to appear at δ_{H} 9.00 to 9.50 for extracts growing on oat without sea salt incubated for 30 days. Fungal extracts obtained from oat media afforded high yield of aliphatic and hydroxylated compounds as indicated by resonances exhibited at 0.50 and 5.50 ppm, respectively, including various saturated and unsaturated fatty acids. The major difference between extracts in the presence or absence of sea salt is the aromatic region at 9.00-10.50 ppm. Extracts without sea salt show the presence of a small peaks at that region. While extracts with sea salt did not show any peaks. The incubation period showed no major effect on extracts containing sea salt. While in extracts without sea salt the only difference was at the aromatic region between 6.00 and 10.50 ppm.

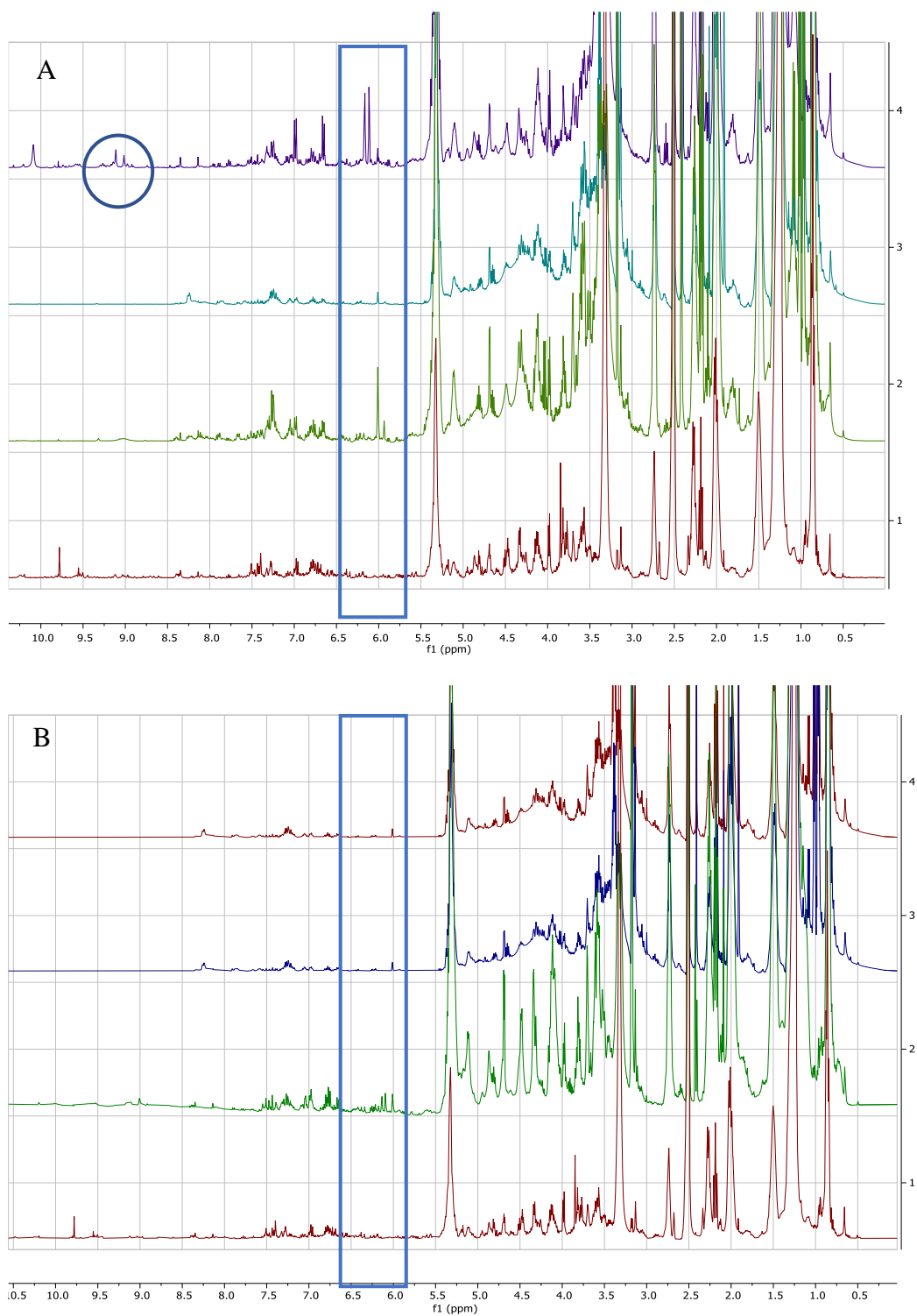


Figure 4.7: Proton NMR spectra obtained from both oat media with salt (A) and without sea salt (B). Spectrum 1 at the bottom of the stack represents the blank followed by the three incubation periods at 7, 15, and 30 days, respectively. Differences are shown in blue boxes.

4.1.3 Anti-biofilm biological assay

4.1.3.1 AlamarBlue® Assay of fungal extracts

Amongst the liquid media used, only extracts obtained after growing *D. salina* for 7, 15, and 30 days on malt extract broth with and without sea salt inhibited the bacterial growth of biofilm-forming *S. aureus* and *P. aeruginosa* by more than 90%. While the second highest inhibition against both biofilms forming bacteria resulted from marine broth extracts gave only 58.3, 57.5 and 55% against *S. aureus* after incubation for 7, 15 and 30 days, respectively. And 52.2, 54.3 and 29.9% against *P. aeruginosa* as shown in figure 4.7-A.

For extracts obtained from solid media, the extract from oat media incubated for 30 days with and without sea salt inhibited bacterial growth at greater than 90%. However, the most potent antimicrobial activity was attained in the presence of sea salt. The biological assay results of Alamarblue® assay, are presented in Table 4.2 and Figures 4.8 and 4.9.

Table 4.2: AlamarBlue® bacterial viability assay results of 100µg/mL of fungal extracts.

Liquid media	% inhibition <i>S. aureus, P. aeruginosa</i>	Solid media	% inhibition <i>S. aureus, P. aeruginosa</i>
Malt extract without sea salt 7 days incubation	100%, 100%	Rice media without sea salt 7 days incubation	58.4%, 37%
Malt extract without sea salt 15 days incubation	100%, 100%	Rice media without sea salt 15 days incubation	65.1%, 63.9%
Malt extract without sea salt 30 days incubation	100%, 100%	Rice media without sea salt 30 days incubation	32.9%, 27.1%
Malt extract with sea salt 7 days incubation	99.4%, 100%	Rice media with sea salt 7 days incubation	68.6%, 66%
Malt extract with sea salt 15 days incubation	100%, 100%	Rice media with sea salt 15 days incubation	70.7%, 69%
Malt extract with sea salt 30 days incubation	100%, 100%	Rice media with sea salt 30 days incubation	68.3%, 64.3%
Wickersham without sea salt 7 days incubation	7.5%, 6.0%	Oat media without sea salt 7 days incubation	75.4%, 68%
Wickersham without sea salt 15 days incubation	15.9%, 25.3%	Oat media without sea salt 15 days incubation	88.9%, 85.4%
Wickersham without sea salt 30 days incubation	50.8%, 31.9%	Oat media without sea salt 30 days incubation	90.4%, 89%
Wickersham with sea salt 7 days incubation	3.4%, 2.4%	Oat media with sea salt 7 days incubation	98.5%, 90.2%
Wickersham with sea salt 15 days incubation	11%, 16.7%	Oat media with sea salt 15 days incubation	98.8%, 93.2%
Wickersham with sea salt 30 days incubation	50.1%, 45.3%	Oat media with sea salt 30 days incubation	99%, 98.9%
Marine broth 7 days incubation	58.3%, 52.2%		
Marine broth 15 days incubation	57.5%, 54.3%		
Marine broth 30 days incubation	55%, 29.9%		

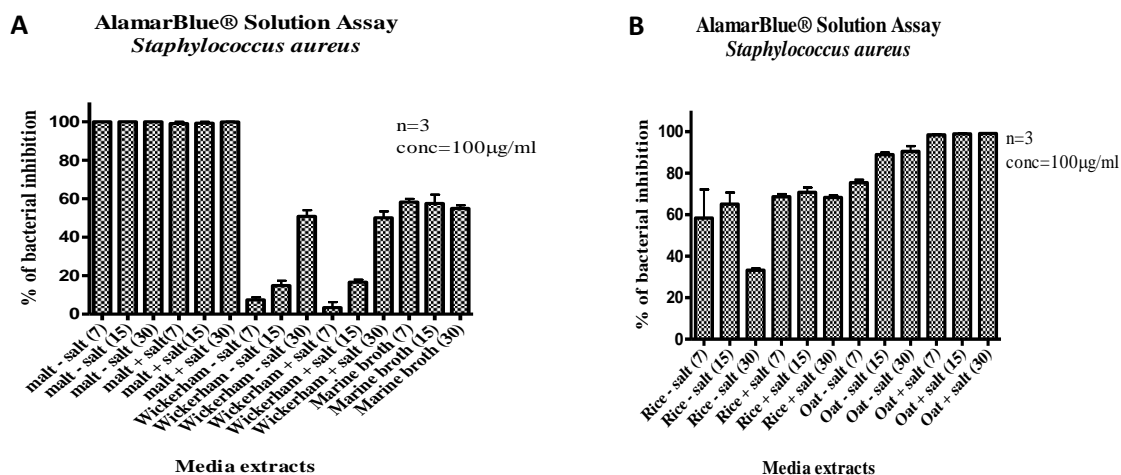


Figure 4.8: Percentage bacterial inhibition of biofilm-forming *S. aureus* with 100µg/mL of *D. salina* extracts obtained from various **A**: liquid and **B**: solid media.

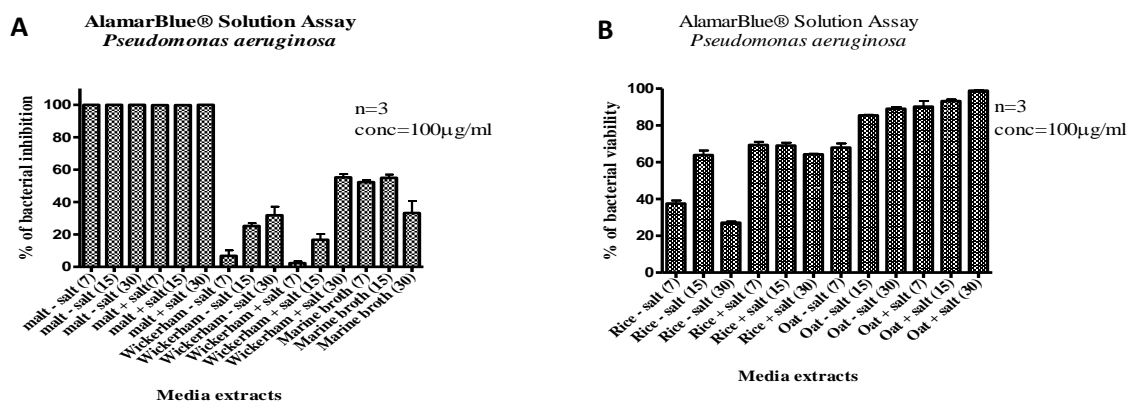


Figure 4.9: Percentage bacterial inhibition of biofilm-forming *P. aeruginosa* with 100µg/mL of *D. salina* extracts obtained from various **A**: liquid and **B**: solid media.

4.1.3.2 Planktonic assay of fungal extracts.

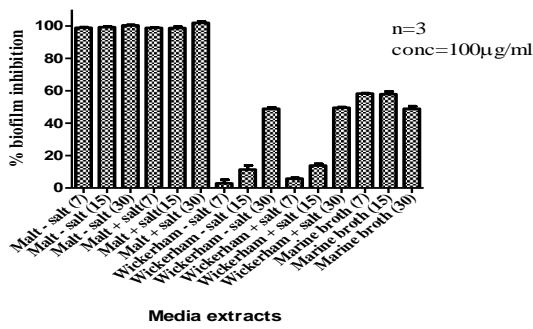
Planktonic assay of *D. salina* extracts after growing on different media confirmed the results obtained from AlamarBlue® assay. The highest biological activity of more than 97.5% against both biofilms, forming *S. aureus* and *P. aeruginosa* was attained for extracts obtained from malt extract media at all incubation periods and in the presence or the absence of sea salt. On the other hand, oat media was able to produce high biological activity of more than 85% for all incubation periods either with or without sea salt except extract obtained after 7 days of incubation without sea salt. While bioactivity was lost or decreased when the fungus was grown on other media. Planktonic assay of *D. salina* extracts against both biofilm-forming *S. aureus*

and *P. aeruginosa* showed the ability of each extract to inhibit biofilm production by both bacteria (*S. aureus* and *P. aeruginosa*).

Table 4.3: Planktonic assay biofilm viability assay results of 100µg/mL of *D. salina* extracts obtained from various media.

Liquid media	% inhibition <i>S. aureus, P. aeruginosa</i>	Solid media	% inhibition <i>S. aureus:P. aeruginosa</i>
Malt extract without sea salt 7 days incubation	99.1%, 97.8%	Rice media without sea salt 7 days incubation	43%, 37.5%
Malt extract without sea salt 15 days incubation	99.2%, 98.1%	Rice media without sea salt 15 days incubation	71%, 63.9%
Malt extract without sea salt 30 days incubation	100%, 99.4%	Rice media without sea salt 30 days incubation	30.1%, 27.1%
Malt extract with sea salt 7 days incubation	98.8%, 98.2%	Rice media with sea salt 7 days incubation	63%, 66%
Malt extract with sea salt 15 days incubation	98.7%, 98.5%	Rice media with sea salt 15 days incubation	71%, 69%
Malt extract with sea salt 30 days incubation	100%, 100%	Rice media with sea salt 30 days incubation	68%, 64.3%
Wickersham without sea salt 7 days incubation	2.9%, 0%	Oat media without sea salt 7 days incubation	72.9%, 68%
Wickersham without sea salt 15 days incubation	11.4%, 6.1%	Oat media without sea salt 15 days incubation	88.6%, 85.4%
Wickersham without sea salt 30 days incubation	48.9%, 45.9%	Oat media without sea salt 30 days incubation	86.1%, 89%
Wickersham with sea salt 7 days incubation	5.8%, 1.8%	Oat media with sea salt 7 days incubation	95.8%, 90.2%
Wickersham with sea salt 15 days incubation	13.9%, 48%	Oat media with sea salt 15 days incubation	100%, 93.2%
Wickersham with sea salt 30 days incubation	49.5%, 46.9%	Oat media with sea salt 30 days incubation	97.5%, 98.9%
Marine broth 7 days incubation	58.3%, 56.1%		
Marine broth 15 days incubation	57.9%, 54.6%		
Marine broth 30 days incubation	48.9%, 45.4%		

A Planktonic Assay Solution Against *Staphylococcus aureus*



B Planktonic Assay Solution Against *Staphylococcus aureus*

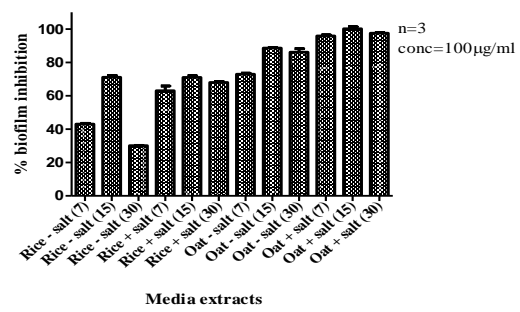
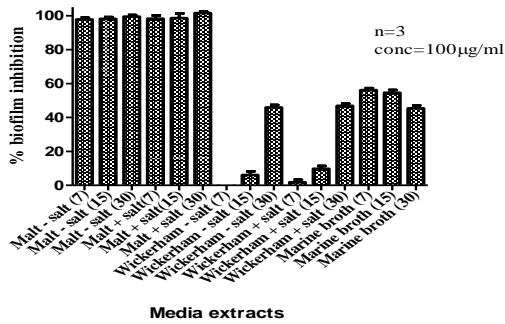


Figure 4.10: Percentage biofilm inhibition for *S. aureus* by 100µg/mL of *D. salina* extracts obtained from various **A:** liquid and **B:** solid media.

A Planktonic Solution Assay *Pseudomonas aeruginosa*



B Planktonic Solution Assay *Pseudomonas aeruginosa*

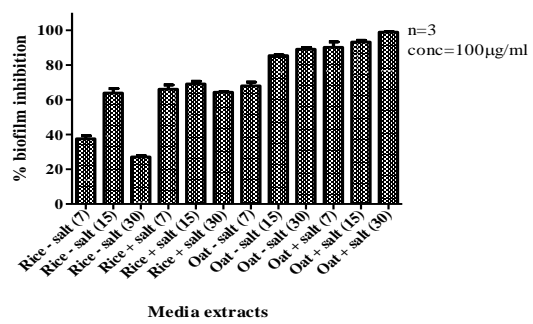


Figure 4.11: Percentage biofilm inhibition of *P. aeruginosa* bacteria against 100µg/mL of *D. salina* extracts obtained from various **A:** liquid and **B:** solid media.

4.1.3.3 Minimum inhibitory concentration (MIC) and Minimum biofilm eradication concentration (MBEC) assays.

D. salina extracts with strong biological activity against biofilm-forming *S. aureus* and *P. aeruginosa* in both AlamarBlue® and planktonic assays were subjected to MIC and MBEC assays. The lowest MIC values against *S. aureus* and *P. aeruginosa* were attained at 17.3µg/mL for fungal extracts obtained from oat and malt extract media, respectively, both incubated for 30 days without sea salt. The rest of the active extracts afforded a biological activity on both biofilm-forming bacteria, with MIC values less than 30µg/mL, which also indicated a strong biological activity, as presented in Table 4.5 and Figure 4.16. Extracts yielded by *D. salina* grown for 30 days on malt extract broth and oat media, both without sea salt obtained a MBEC value of 19.7µg/mL against *S. aureus*, while a higher MBEC value of 36.5µg/mL was exhibited for the extracts obtained from oat media with sea salt incubated for 30 days. On the other hand, *D. salina* growing on malt extract broth with and without sea salt on 30 days incubation yielded an extract with a lower MBEC value of 16.8µg/mL against *P. aeruginosa*. While the highest MBEC value of 30µg/mL was obtained for the extract afforded by growing the fungus on oat media with sea salt incubated for 30 days. MBEC and MIC results are presented in Tables 4.4 and 4.5 and Figures 4.12, 4.13, 4.14 and 4.15.

Table 4.4: MIC of active *D. salina* extracts against *S. aureus* and *P. aeruginosa*.

Media	MIC µg/mL against <i>S. aureus</i>	MIC µg/mL against <i>P. aeruginosa</i>
Malt extract without sea salt 7 days	21.6	20.8
Malt extract without sea salt 15 days	24.8	23.6
Malt extract without sea salt 30 days	18.2	17.3
Malt extract with sea salt 7 days	23.6	24.0
Malt extract with sea salt 15 days	23.9	21.6
Malt extract with sea salt 30 days	20.0	17.5
Oat media without sea salt 7 days	25.9	24.5
Oat media without sea salt 15 days	21.7	22.9
Oat media without sea salt 30 days	17.3	21.1
Oat media with sea salt 7 days	24.1	22.3
Oat media with sea salt 15 days	24.4	21.7
Oat media with sea salt 30 days	35.0	34.5

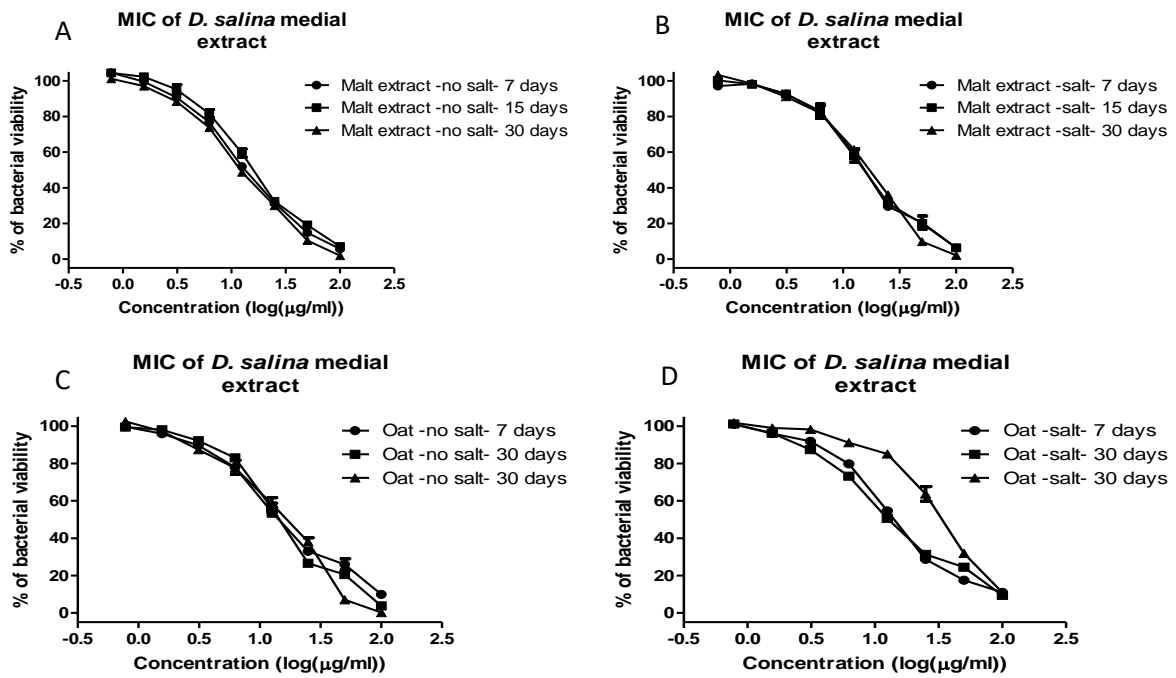


Figure 4.12: MIC results of active *D. salina* extracts against *S. aureus*. **A:** *D. salina* malt extract without sea salt, **B:** *D. salina* malt extract with sea salt, **C:** *D. salina* oat extract without sea salt, and **D:** *D. salina* oat extracts with sea salt. n=3

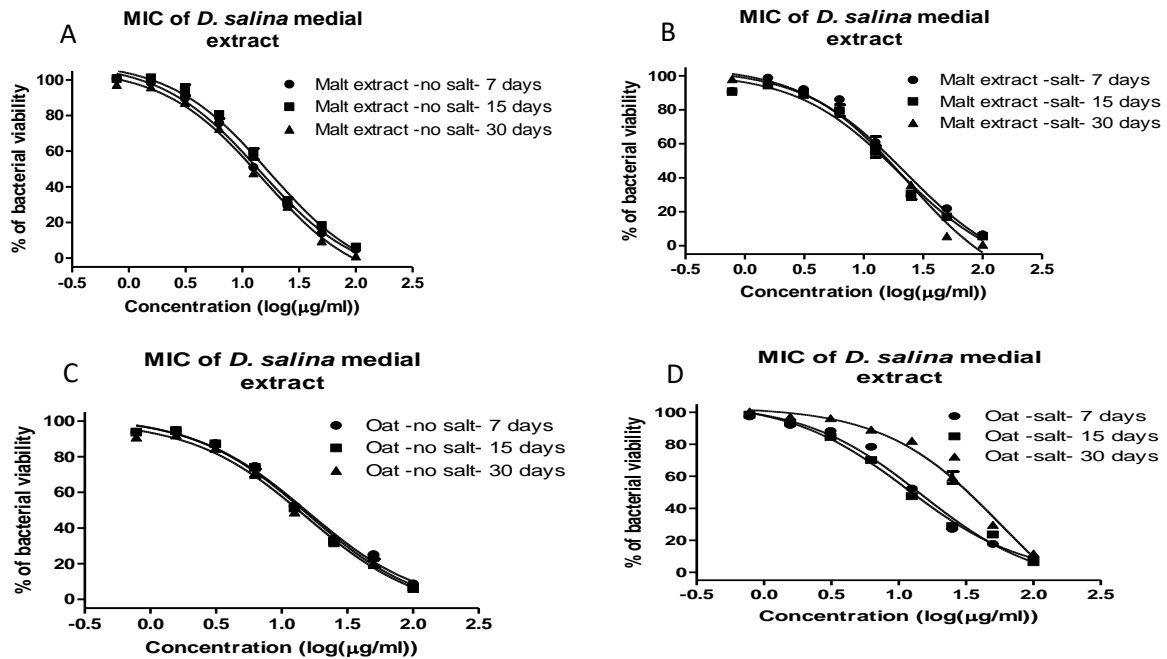


Figure 4.13: MIC results of active *D. salina* extracts against *P. aeruginosa*. **A:** *D. salina* malt extract without sea salt, **B:** *D. salina* malt extract with sea salt, **C:** *D. salina* oat extracts without sea salt, and **D:** *D. salina* oat extracts with sea salt. n=3

Table 4.5: MBEC of active *D. salina* extracts against both biofilm-forming *S. aureus* and *P. aeruginosa*.

Media	MBEC $\mu\text{g/mL}$ against <i>S. aureus</i>	MBEC $\mu\text{g/mL}$ against <i>P. aeruginosa</i>
Malt extract without sea salt 7 days	23.2	21.3
Malt extract without sea salt 15 days	26.2	21.5
Malt extract without sea salt 30 days	19.7	16.8
Malt extract with sea salt 7 days	25.0	24.9
Malt extract with sea salt 15 days	25.4	24.8
Malt extract with sea salt 30 days	21.8	16.8
Oat media without sea salt 7 days	27.6	29.7
Oat media without sea salt 15 days	23.3	22.4
Oat media without sea salt 30 days	19.7	19.4
Oat media with sea salt 7 days	25.6	23.0
Oat media with sea salt 15 days	25.9	21.1
Oat media with sea salt 30 days	36.5	30.0

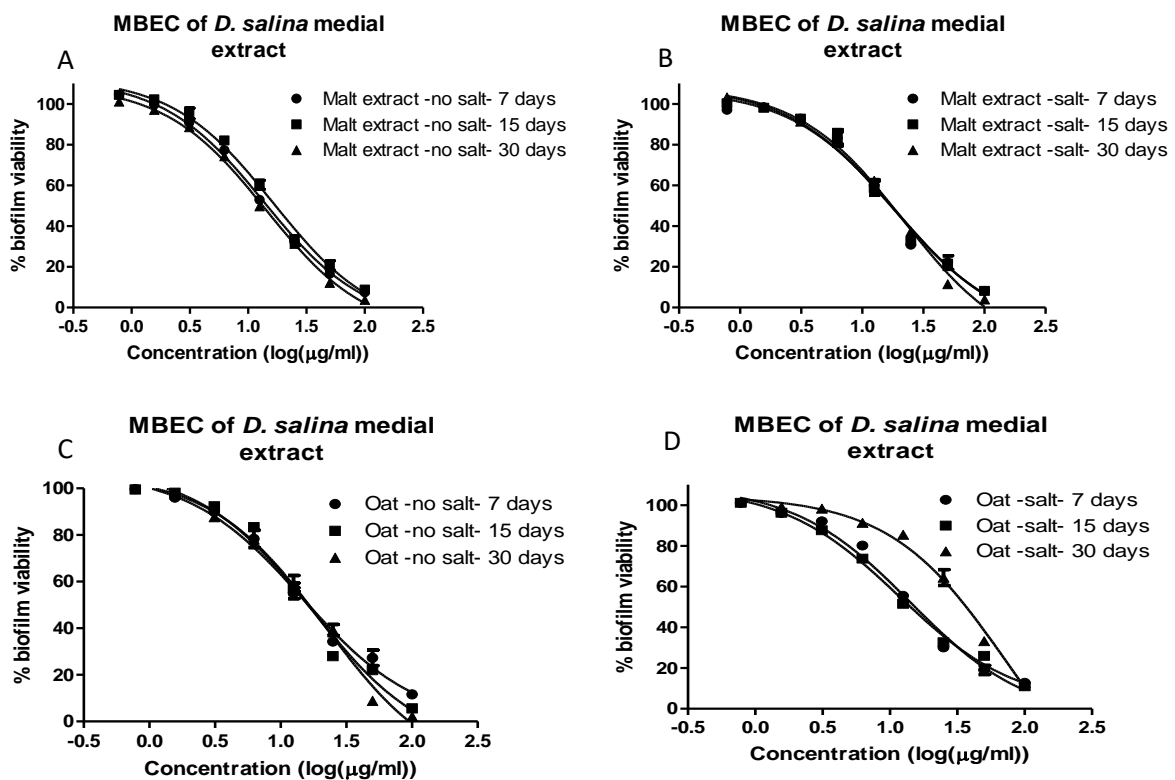


Figure 4.14: MBEC results of active *D. salina* extracts against *S. aureus*. **A:** *D. salina* malt extract without sea salt, **B:** *D. salina* malt extracts with sea salt, **C:** *D. salina* oat extract without sea salt, and **D:** *D. salina* oat extract with sea salt.

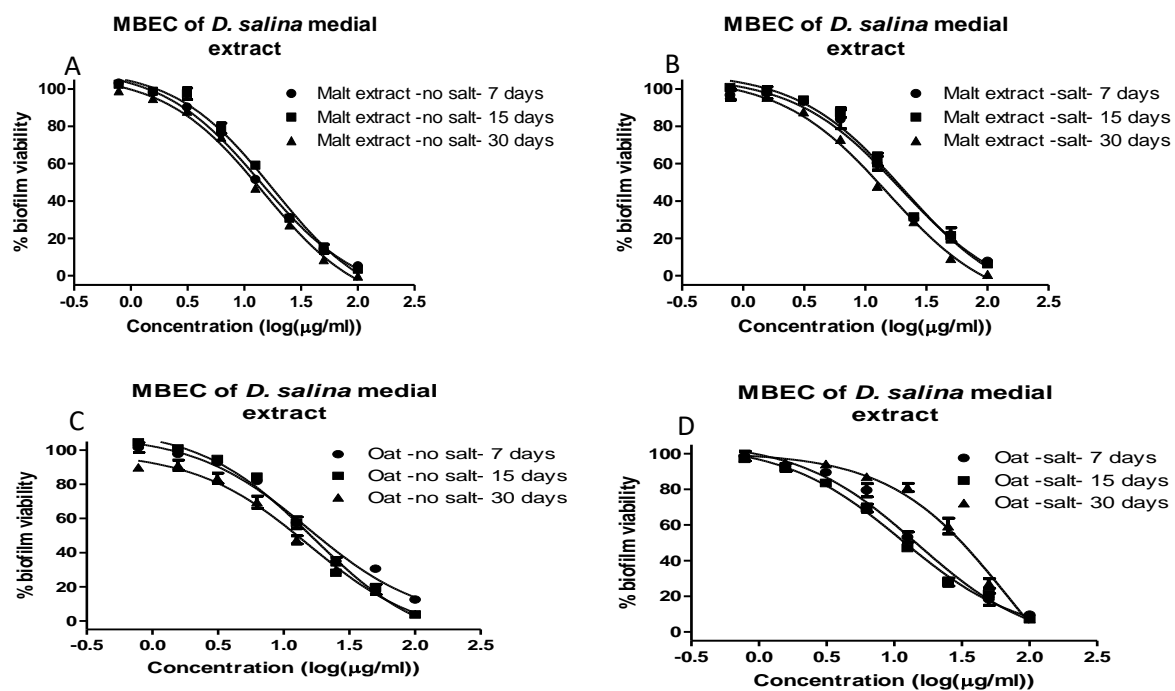


Figure 4.15: MBEC results of active *D. salina* extracts against *P. aeruginosa*. **A:** *D. salina* malt extracts without sea salt, **B:** *D. salina* malt extracts with sea salt, **C:** *D. salina* oat extracts without sea salt, and **D:** *D. salina* oat extracts with sea salt.

4.1.4 Multivariate analysis of ^1H NMR spectral data

PCA scatter plot of the ^1H NMR spectral data of *D. salina* extracts indicated unique chemical profiles for outlying samples obtained from Wickersham media without sea salt incubated for 7 and 30 days (encircled **red**) as shown in Figure 4.16. The ^1H NMR spectral data of malt extract with and without sea salt, Wickersham broth with and without sea salt and marine broth showed high intensity peaks at the aromatic region between 6.00-10.00ppm. While extracts afforded from rice and oat media, both with and without sea salt implied relative similarities in their chemical profiles as they were more closely clustered together in the lower left quadrant (encircled **blue**) and this was also confirmed by their ^1H NMR spectra, which showed high intensity peaks at the olefinic and aliphatic region with chemical shifts between 0.50 and 5.50 ppm. On the other hand, except for the outlying extracts, most of the *D. salina* extracts obtained from the liquid media on the upper right quadrant acquired from marine broth, malt extract and Wickersham with and without sea salt (encircled **orange**) had a more comparable chemical profile. $R^2\text{X}$ and $Q^2\text{X}$ values were 0.79 and 0.53, respectively, with a difference of less than 0.3, which indicates a relatively good model.

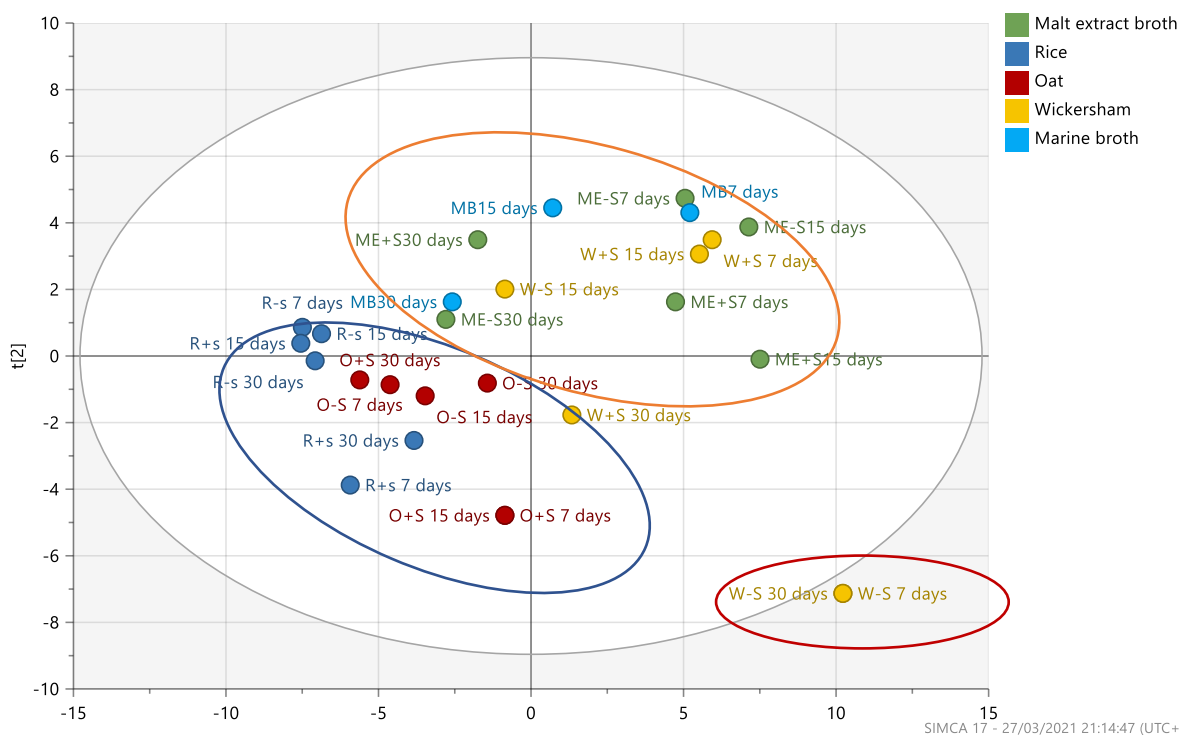


Figure 4.16: PCA scatter plot of proton NMR spectral of *D. salina* extracts from various media incubated at 7, 15, and 30 days. ME-s: malt extract without sea salt, ME+s: malt extract with sea salt, W-s: Wickersham broth without sea salt, W+s: Wickersham with sea salt, MB: marine broth, R-s: rice without sea salt, R+s: rice with sea salt, O-s: oat without sea salt and O+s: oat with sea salt. Each media extract acronym followed by its incubation duration.

Incorporating the results of AlamarBlue® and planktonic assay data for multivariate analysis, the active were positioned on the left and inactive extracts on the right side of the OPLS-DA scatter plot, as shown in Figure 4.17. According to the OPLS-DA loadings plot, the upper left active quadrant entailing the malt extract broth with and without sea salt after incubation for 7- and 15-days were dominated with resonances between 2.00 and 4.00 ppm indicating the occurrence of acylated and hydroxylated active compounds. While the left lower quadrant enclosing the extracts obtained from oat media with and without sea salt at 7, 15, and 30 days incubation and malt extract broth with and without sea salt incubation for after 30 days showed the occurrence of a wider range of resonances between 0.00 and 5.00 ppm indicating the presence of lipids and glycosylated active compounds.

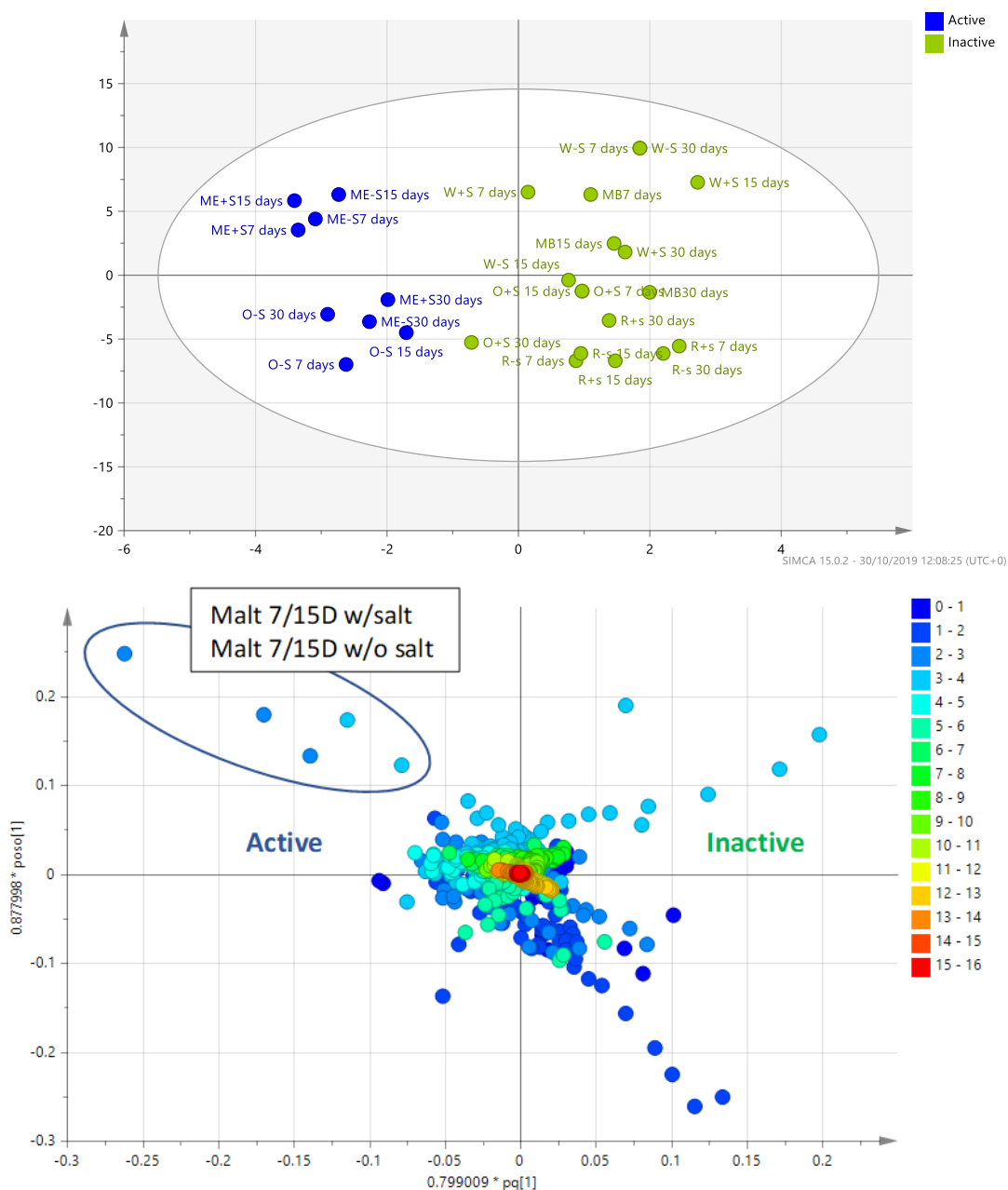


Figure 4.17: OPLS-DA scatter and loadings plots of the NMR spectral data of various fungal extracts classified according to their AlamarBlue® and planktonic assay results.

4.1.5 Multivariate analysis of LC-HRMS data

LC-HRMS data was processed using MZmine 14.1 followed by dereplication of the data using an in-house Macro sheet that is coupled to the DNP. Fungal extracts obtained from various media incubated at 7, 15, and 30 days indicated relatively similar or comparable chemical profiles except for the extracts afforded by marine broth and oat media incubated for 30 days

being designated as outliers as shown in Figure 4.18. The summary fit of the model gave a difference between R^2X (0.997) and Q^2X (0.789) of less than 0.3 which means that it is relatively a good model.

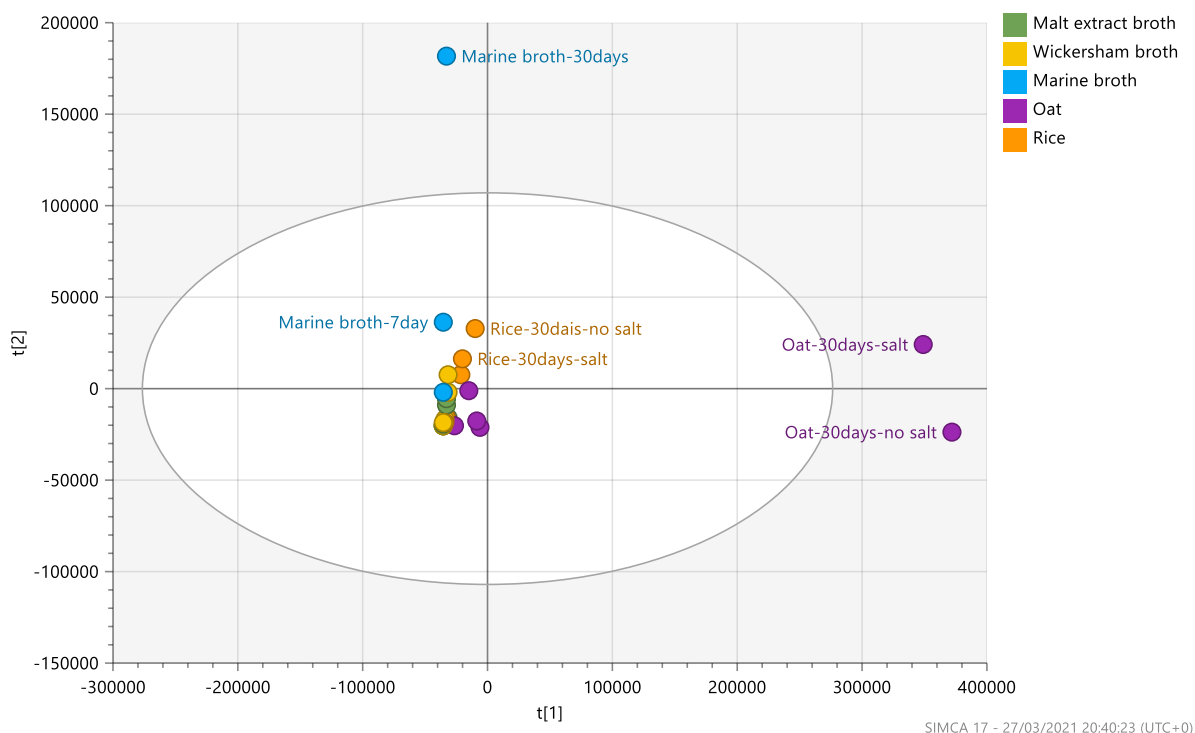


Figure 4.18: PCA scatter plot of LC-HRMS data of fungal extracts from various media.

The extracts were grouped according to their antibacterial bioactivity against biofilm-forming *S. aureus* and *P. aeruginosa* then subjected to OPLS-DA. The active extracts were positioned on the right side of the plot, while the inactive samples were on the left side of the plot. Again, extracts prepared from inoculation of *D. salina* on oat media with and without sea salt as well as marine broth after 30 days of incubation were designated as outliers as shown on OPLS-DA scatter plot presented in (Figure 4.19 A). As indicated by the results shown in the OPLS-DA loadings plot (Figure 4.19 B), *D. salina* growing on oat media for 30 days was able to afford discriminating compounds, with p -values of less than 0.05, as listed in Table 4.6. Four ion peaks with m/z values of 478.293, 520.34, 1006.67 and 1020.68, did not give any hit from the DNP database. The molecular formula representing these m/z values looks comparable to NMR spectra findings, which showed a wide range of resonance between 0.00-5.00 ppm and higher. On the other hand, two of the discriminating compounds with m/z values of 520.34 and 496.34 isolated from marine source were putatively dereplicated as 8,9-dihydroindanomycin, and soraphen A (Figure 4.24) earlier described from *Streptomyces galbus*, and *Sorangium*

cellulosum respectively (Gerth et al., 2003, Li et al., 2009a). According to the DBE values of the discriminating compounds, the compounds contain aliphatic compounds with double bonds or cyclic system and aromatic peaks which also can be seen at the OPLS-DA loading plot of the NMR data.

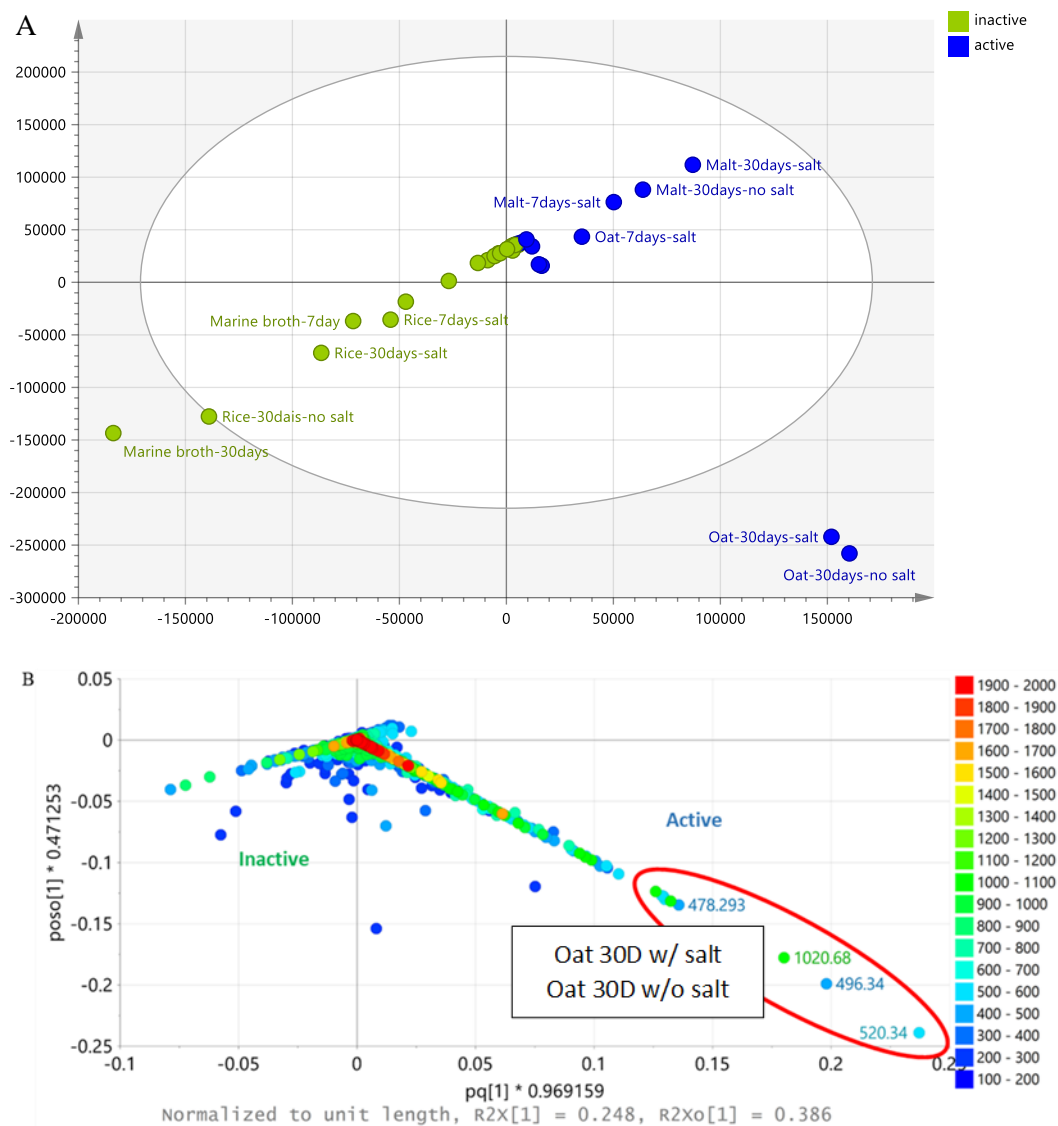


Figure 4.19: OPLS-DA scatter and loading plots of LC-HRMS data of fungal extracts grouped according to their antibacterial activity against both biofilms forming *S. aureus* and *P. aeruginosa*.

Table 4.6: Dereplication of six target bioactive metabolites found in active extracts, with P values < 0.05 as obtained from the OPLS-DA S-plot.

Var ID	p-value	FDR	Molecular weight	Chemical formula prediction (DBE)	Compound hits from DNP and biological source
P_40	0.013638	0.005	477.286	C ₂₆ H ₃₅ N ₇ O ₂ (13) C ₂₁ H ₃₅ N ₉ O ₄ (9)	no hit
P_61	0.032873	0.02	495.335	C ₃₁ H ₄₅ NO ₄ (10)	8,9-dihydroindanomycin <i>Streptomyces galbus</i>
P_19	0.042269	0.025	519.333	C ₃₆ H ₄₅ N ₃ (16) C ₃₁ H ₄₅ N ₅ O ₂ (12)	no hit
P_3635	0.030293	0.015	520.336	C ₂₉ H ₄₄ O ₈ (8)	soraphen A <i>Sorangium cellulosum</i> myxobacteria
N_3742	0.04803	0.03	1007.67	C ₅₆ H ₈₅ N ₁₁ O ₆ (20) C ₅₀ H ₈₅ N ₁₅ O ₇ (16)	no hit
N_3741	0.02339	0.01	1021.69	C ₅₇ H ₈₇ N ₁₁ O ₆ (20) C ₅₁ H ₈₇ N ₁₅ O ₇ (16)	No hit

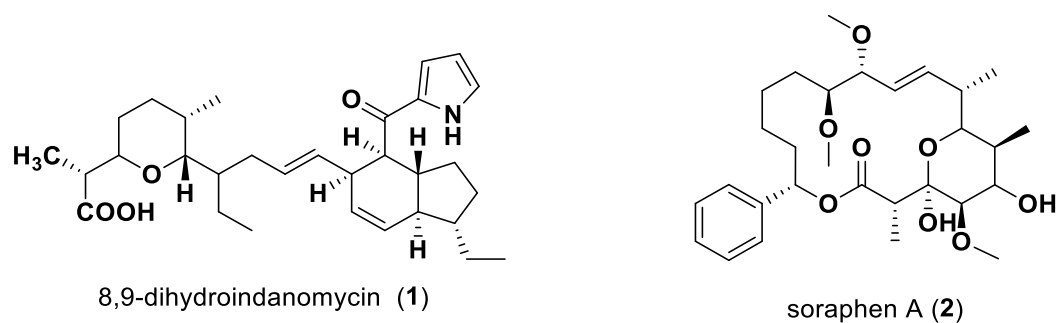


Figure 4.20: Putative structures of dereplicated target bioactive metabolites found in the anti-microbial extracts obtained from the oat media.

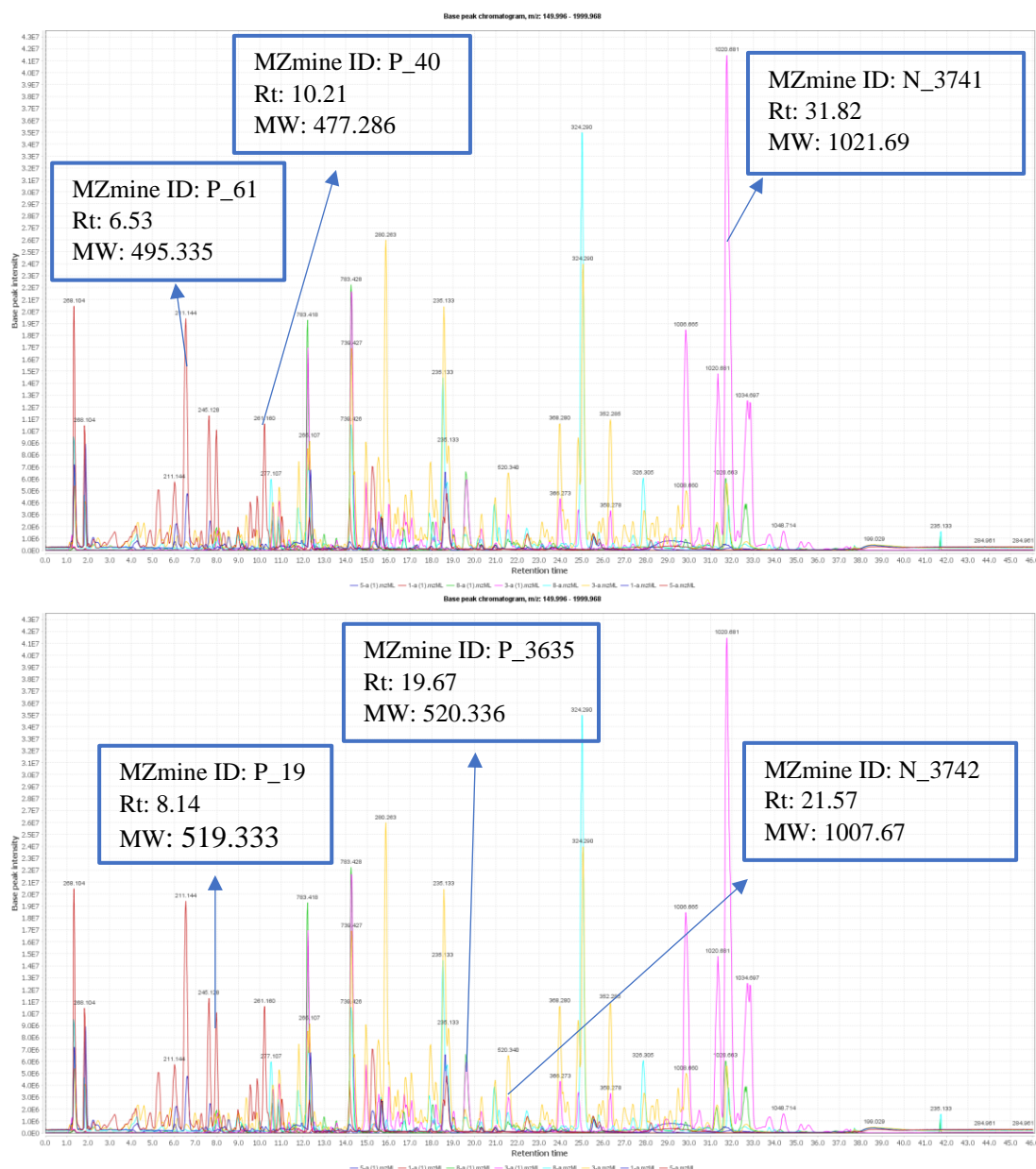


Figure 4.21: Total Ion Chromatogram (TIC) of the active media extracts. The ion peaks that represent the discriminating features listed in Table 4.6 have been labelled

4.2 Optimising the production of anti-biofilm bioactive metabolites produced by *Marianna elegance*.

4.2.1 Extract yields on different media.

M. elegance was unable to show any sign of growth on the 7th day of incubation. Triplicates of the inoculated endophytic fungus grown for 7 days on each of all the media were excluded. One flask from each of the media was extracted and compared with the media blank in terms of their chemical profile. Between all the liquid media used, malt extract without sea salt incubated for 30 days provided the highest extract yield of 239mg for *M. elegance* of all liquid

broth extracts. While the lowest yield was obtained after growing the fungus on marine broth for 15 days. On the other hand, for solid media, the highest yield of 291mg was afforded on oat media without sea salt incubated for 15 days. While the lowest yield obtained after incubation on rice solid media without sea salt after incubation for 15days. The extract yields afforded by *M. elegance* increased with time in all media except on rice with sea salt and oat without sea salt. This indicated that *M. elegance* was on its log growth phase for 15 days. The extract yields of *M. elegance* obtained from various media are presented in Table 4.7 and Figure 4.25.

Table 4.7: Weights of *M. elegans* extracts obtained by cultivation on various media at different incubation periods.

Liquid Media				
Type of Media	Incubation Period Yield			
	7 Days	15 Days	30 Days	Blank
Malt Extract without Sea Salt	-	55.4mg	239mg	4.72mg
Malt Extract with Sea Salt	-	63mg	151mg	11.8mg
Wickersham Media without Sea Salt	-	16.5mg	29.4mg	7.41mg
Wickersham Media with Sea Salt	-	19.4mg	38.5mg	12.3mg
Marine Broth	-	15.1mg	21.1mg	3.35mg
Solid Media				
Type of Media	Incubation Period			
	7 Days	15 Days	30 Days	Blank
Rice Media without Sea Salt	-	127mg	183mg	23.4mg
Rice Media with Sea Salt	-	184mg	175mg	22.7mg
Oat Media without Sea Salt	-	291mg	183mg	81.1mg
Oat Media with Sea Salt	-	203mg	237mg	88.2mg

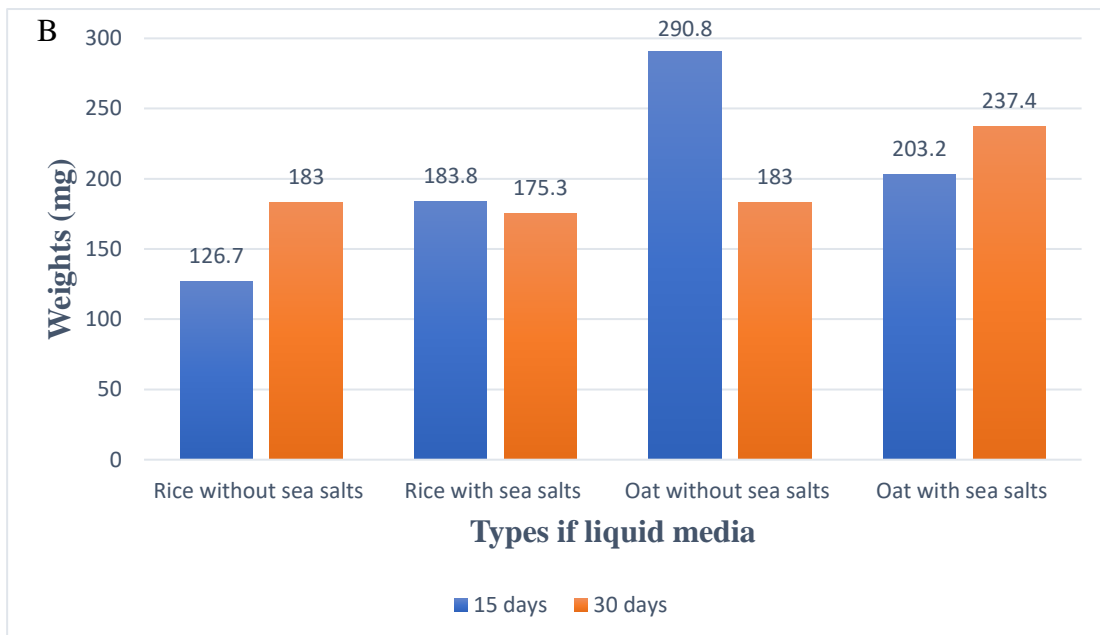
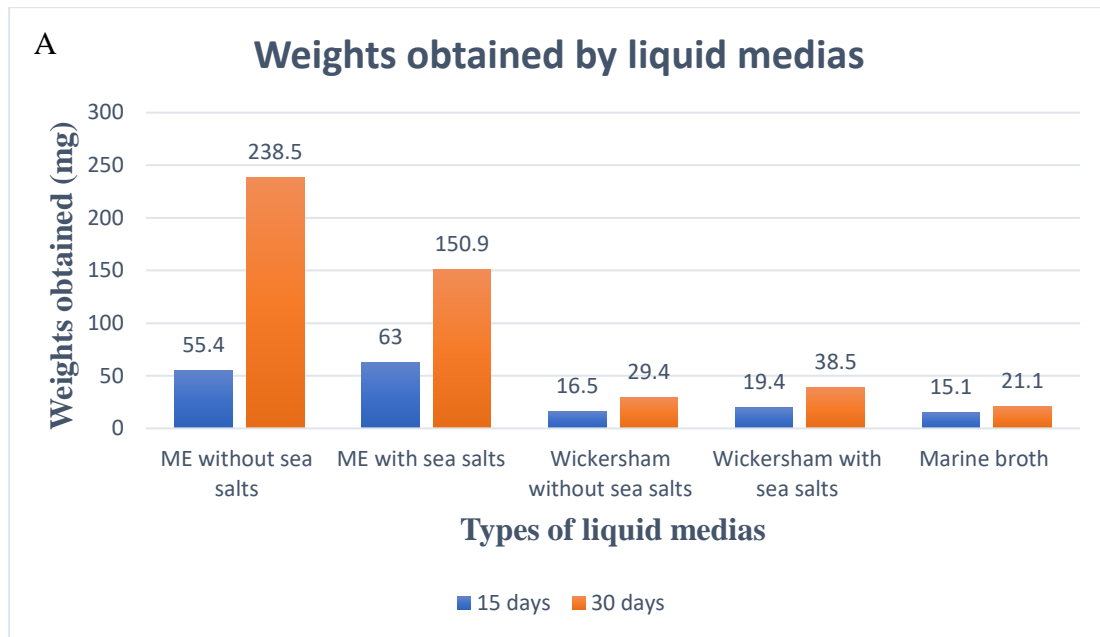


Figure 4.22: Diagrams represent the weights of fungal extracts obtained from : (A) liquid and (B) solid media on 15 and 30 days of incubation periods at 27C°.

4.2.2 NMR spectroscopy for *M. elegance* extracts

4.2.2.1 Liquid media

4.2.2.1.1 Malt extract broth with and without sea salt

The stacked proton NMR spectra of *M. elegance* extracts obtained at 15 and 30 days of incubation periods on malt extract with and without sea salt along with media blanks are presented in Figure 4.23. A few low intensity peaks were observed in the aromatic region at 6.00 to 10.00 ppm. Peaks produced by the extract from the blank media either disappeared or decreased in intensity on 15 and 30 days of incubation, especially those found at the aromatic region indicating the consumption of the media nutrients. The NMR spectra of the extracts afforded on incubation for 15 and 30 days either with or without sea salt showed the presence of high intensity peaks in the aliphatic and hydroxylated regions at δ_H 1.00 to 5.50 ppm, respectively. Like *D. salina*, *M. elegance* was producing a high ratio of saturated and unsaturated fatty acids. When comparing the media with and without sea salt, it seems that media with sea salt had more aromatic peaks between 7.00 and 9.00 ppm. Incubation periods showed no effect on malt extract with sea salt. While the incubation periods have a direct effect on malt extract without sea salt extract. The extract from the fungus incubated for 30days showed the presence of aromatic peaks between 6.00 and 11.00 ppm, while those from 15days, no peaks were shown.

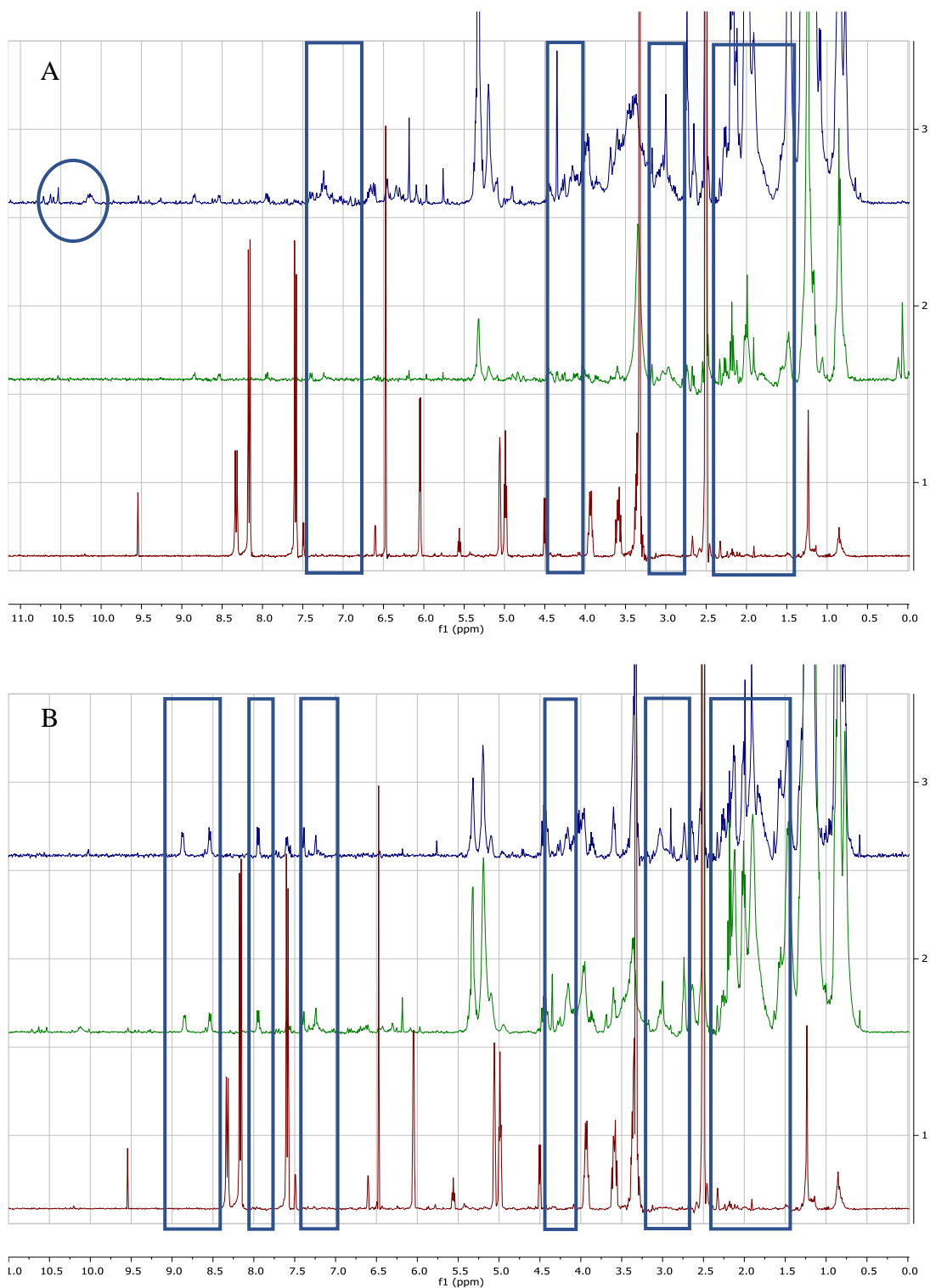


Figure 4.23: Stacked ^1H NMR spectra of fungal extracts obtained from malt extract liquid media with (A) and without sea salt (B). Spectrum 1 at the bottom of each of the stack represents the blank followed by those incubated at 15 and 30 days, respectively. The differences are highlighted in blue boxes.

4.2.2.1.2 Wickersham liquid media with and without sea salt

The stacked ^1H NMR spectra of the extracts afforded by *M. elegance* growing on Wickersham broth with and without sea salt incubated for 15 and 30 days did not show any difference with that obtained from the blank media. Only a small variation could be perceived between blank and the prepared fungal extract derived from the Wickersham broth medium with sea salt. The major difference was observed at chemical shifts between 8.50 and 10.50 ppm. Stacked ^1H NMR spectra of extracts afforded by growing *M. elegance* on Wickersham broth and blank media are presented in Figure 4.24. The incubation periods and the presence or the absence of sea salt did not show any effect on the extract obtained from the fungus grown on Wickersham broth.

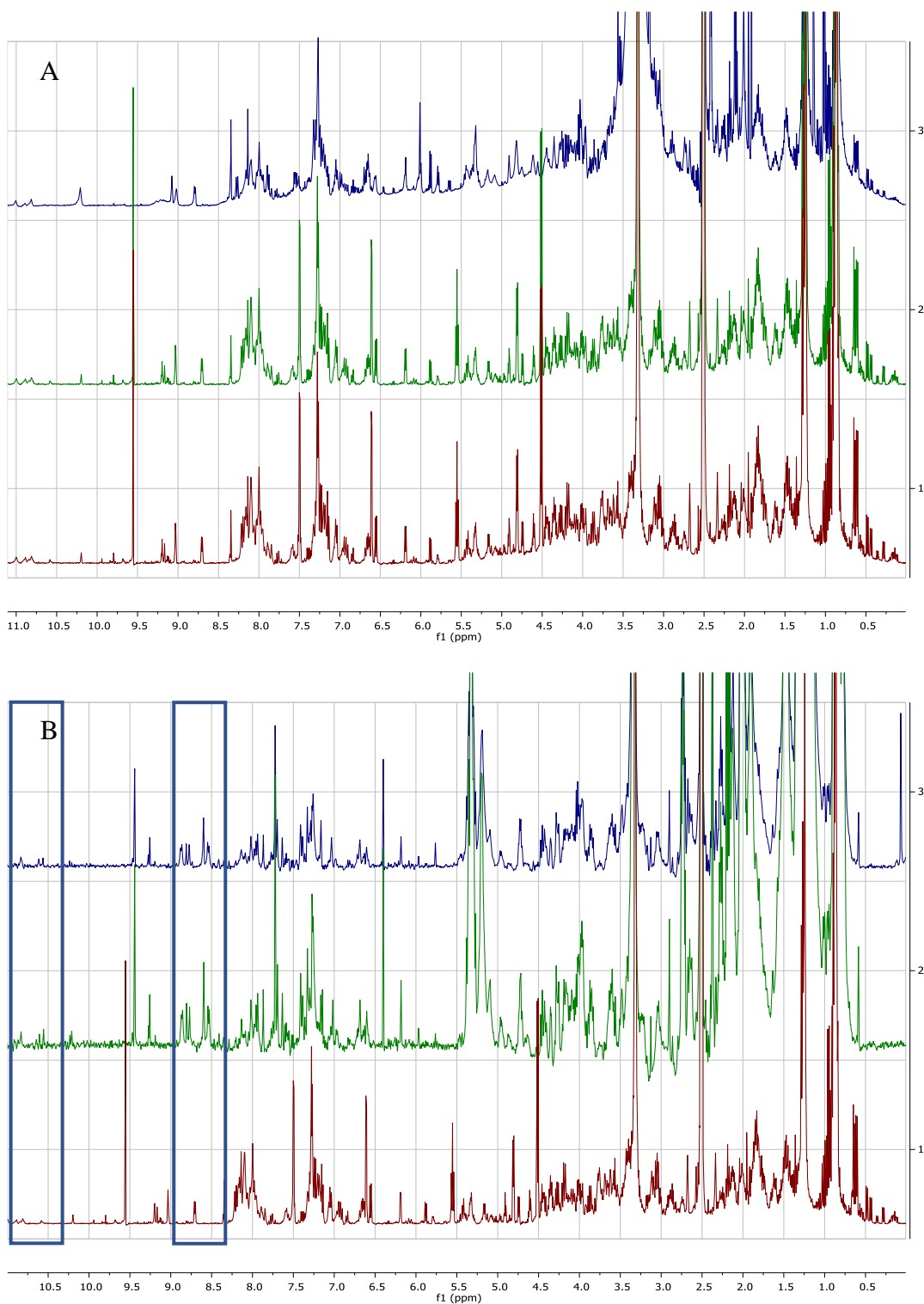


Figure 4.24: Stacked ¹H NMR spectra of fungal extracts obtained from Wickersham liquid media with (A) and without sea salt (B). Spectrum 1 at the bottom of each of the stack represents the blank followed by those incubated at 15 and 30 days, respectively. The differences are highlighted in blue boxes.

4.2.2.1.3 Marine broth media

The stacked ^1H NMR spectra of extracts afforded by *M. elegance* growing on marine broth along with the blank exhibited a high intensity of aliphatic and hydroxylated resonances. When comparing the NMR spectrum of the blank media with those of the fungal extracts, many peaks found in the blank media had disappeared, which also indicated the consumption of primary nutrients provided by the media. Most of these peaks that disappeared were those from the aromatic region at 5.50 to 9.50 ppm. Alternatively, resonances at 0.80 to 5.50ppm signifying the occurrence of aliphatic and hydroxylated compounds, respectively were exhibited after the endophytic fungus was grown on marine broth media. On the other hand, only a few low intensity peaks were observed at the aromatic region at 7.00 to 9.00 ppm. The stacked ^1H NMR spectra of the extracts and blank is presented in Figure 4.25. The incubation periods have minor effect on the chemical profile. This minor effect was observed at the aromatic region between 8.50 and 9.00 ppm after incubating for 30days.

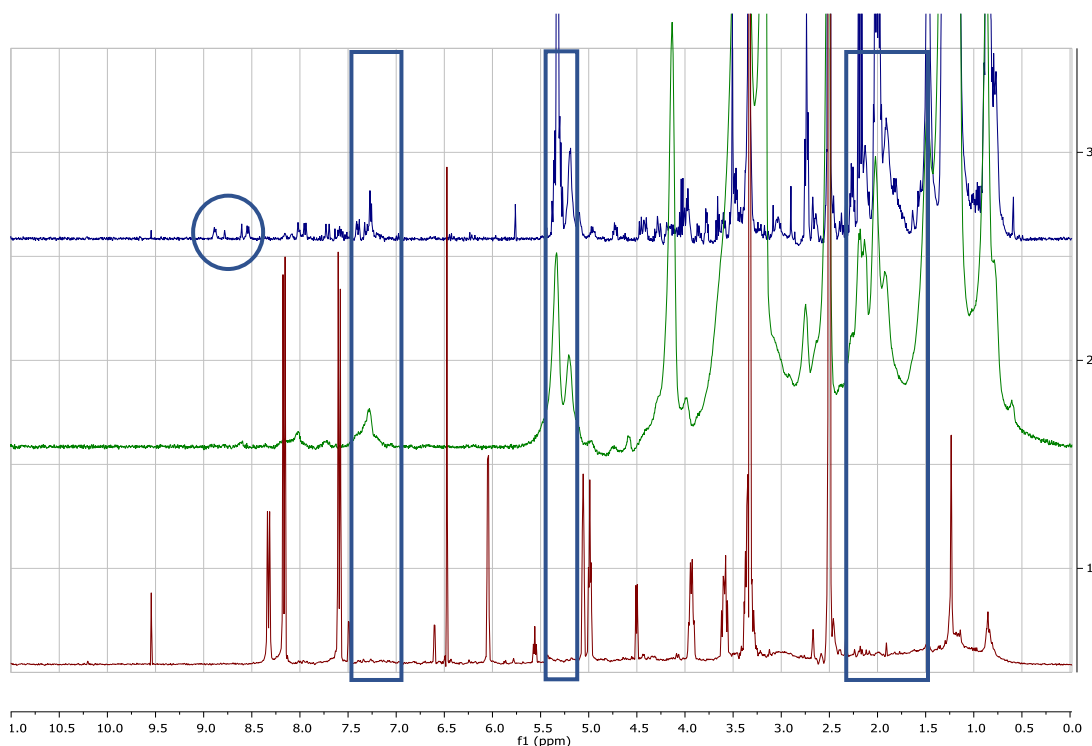


Figure 4.25: Stacked ^1H NMR spectra of *M. elegance* extracts obtained from marine broth media. Spectrum 1 at the bottom of the stack represents the blank followed by those incubated at 15 and 30 days, respectively. The differences are highlighted in blue boxes.

4.2.2.2 Solid media

4.2.2.2.1 Rice media with and without sea salt:

Stacked ^1H NMR spectra of fungal extracts after growing *M. elegance* on rice media with and without sea salt did not exhibit any huge difference to that of the blank media particularly at the aliphatic region. Spectral differences were more perceivable with the occurrence of low intensity peaks in the aromatic region at 6.00 to 10.50 ppm. Again, the higher intensity of aliphatic peaks at 0.80 to 5.50 ppm exhibited in *M. elegance* extracts implied the increasing incidence of saturated and unsaturated fatty acid with some hydroxyl substituents. The stacked ^1H NMR spectra resulted from blank rice media with and without sea salt and extracts afforded by *M. elegance* are presented in Figure 4.26. sea salt has no major effect on the chemical profile of *M. elegance* extracts. Incubation periods have no effect on rice extracts in the absence of sea salt. On the other hand, extracts with sea salt have been affected by incubation periods. In the presence of sea salt, the intensity of aromatic peaks between 6.00 and 10.50 ppm were higher for samples incubated for 30 days than extracts incubated for 15 days.

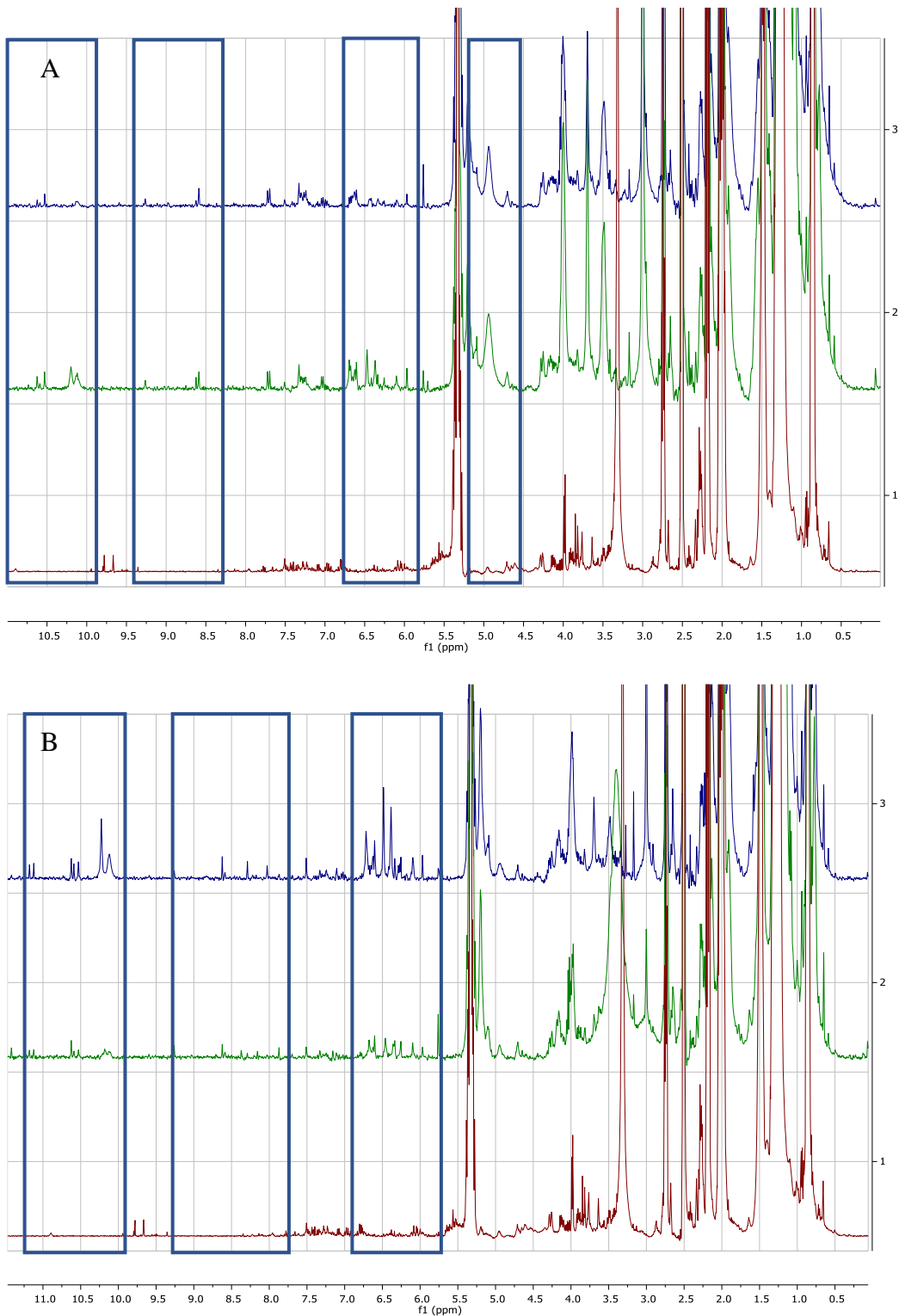


Figure 4.26: Stacked ^1H NMR spectra of fungal extracts obtained from rice media with (A) and without sea salt (B). Spectrum 1 at the bottom of each of the stack represents the blank followed by those incubated at 15 and 30 days, respectively. The differences are highlighted in blue boxes.

4.2.2.2.2 Oat media with and without sea salt:

Stacked ^1H NMR spectra of extracts afforded by *M. elegance* and blank oat media were comparable to those obtained from rice media. No changes in peak resonances were observed at the aliphatic region between the blank media and fungal extracts while a major variation was noticeable at the aromatic region. The contrast between the blank media and the fungal extracts was hard to define due to the complexity at aliphatic and hydroxylated region. The stacked ^1H NMR spectra of fungal extracts and blank media is presented in Figure 4.27. The presence of sea salt displayed no major effect on the on chemical profiles of *M. elegance* extracts growing on oat media. The only difference was the occurrence of peaks between 6.00 and 11.00 ppm in the presence of sea salt. Incubation period showed no major effect on extracts without sea salt. While extract obtained from fungus incubated for 30days with sea salt showed minor differences between 6.00 and 11.00 ppm from those incubated for 15days.

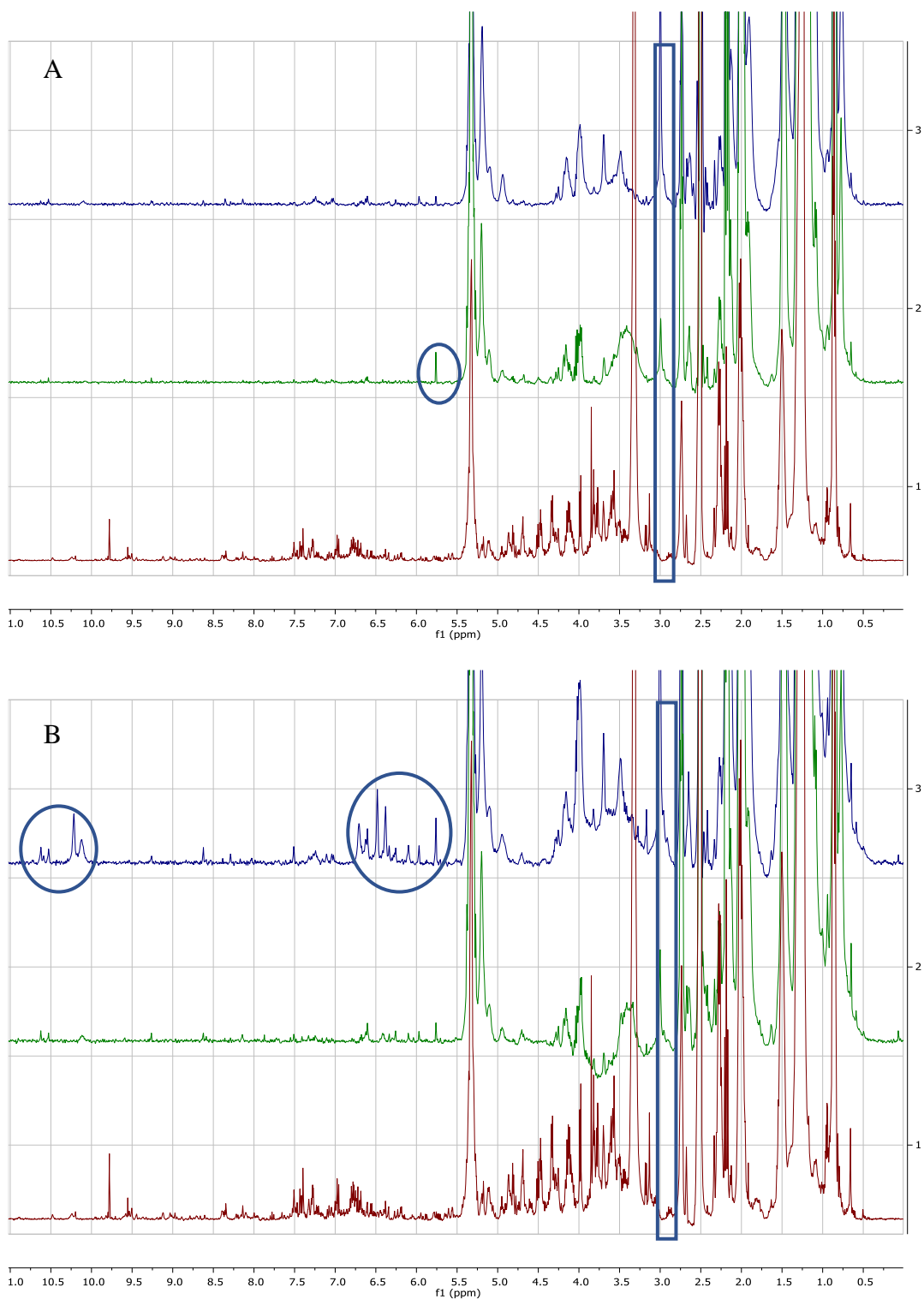


Figure 4.27: Stacked ¹H NMR spectra of fungal extracts obtained from oat media with (A) and without sea salt (B). Spectrum 1 at the bottom of each of the stack represents the blank followed by those incubated at 15 and 30 days, respectively. The differences are highlighted in blue boxes and circles.

4.2.3 Anti-biofilm biological assay

4.3.3.1 AlamarBlue® Assay of *M. elegans* extracts.

M. elegans extracts obtained from malt extract broth and oat media both with and without sea salt incubated at 15 and 30 days afforded potent antimicrobial activity against both biofilm-forming *S. aureus* and *P. aeruginosa*. The extract obtained from the marine broth incubated for 15 days was the only extract found to exert very low antimicrobial activity. The rest of the other extracts exhibited weak biological activity of more than 50% bacterial viability. AlamarBlue® assay results are presented in Table 4.8 and Figures 4.28 and 4.29.

Table 4.8: AlamarBlue® bacterial viability assay results of 100µg/mL of *M. elegans* extracts obtained from various media incubated at 15 and 30 days.

Liquid media	% inhibition <i>S. aureus, P. aeruginosa</i>	Solid media	% inhibition <i>S. aureus:P. aeruginosa</i>
Malt extract without sea salt 15 days incubation	94.9%, 88.9%	Rice media without sea salt 15 days incubation	72.6%, 71.0%
Malt extract without sea salt 30 days incubation	99.7%, 100%	Rice media without sea salt 30 days incubation	88.2%, 85.6%
Malt extract with sea salt 15 days incubation	88.6%, 89.3%	Rice media with sea salt 15 days incubation	77.9%, 70.6%
Malt extract with sea salt 30 days incubation	93%, 95.2%	Rice media with sea salt 30 days incubation	89.3%, 85.9%
Wickersham without sea salt 15 days incubation	51.1%, 50.2%	Oat media without sea salt 15 days incubation	95.4%, 92.1%
Wickersham without sea salt 30 days incubation	60.3%, 64.2%	Oat media without sea salt 30 days incubation	96.9%, 95.8%
Wickersham with sea salt 15 days incubation	52.7%, 55.6%	Oat media with sea salt 15 days incubation	85.9%, 95.2%
Wickersham with sea salt 30 days incubation	60.5%, 56.4%	Oat media with sea salt 30 days incubation	97.2%, 99.7%
Marine broth 15 days incubation	6.2%, 2%		
Marine broth 30 days incubation	68.5%, 91.3%		

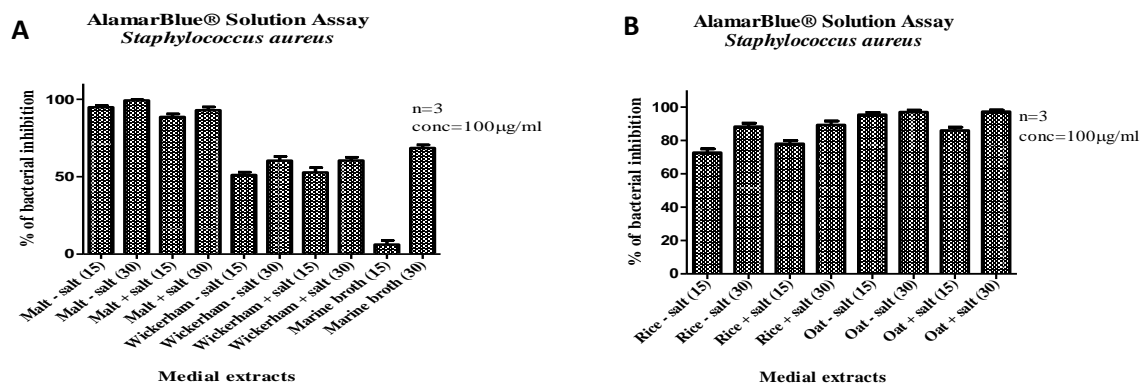


Figure 4.28: Percentage bacterial inhibition of biofilm-forming *S. aureus* with 100µg/mL of *M. elegans* extracts obtained from various **A:** liquid and **B:** solid media.

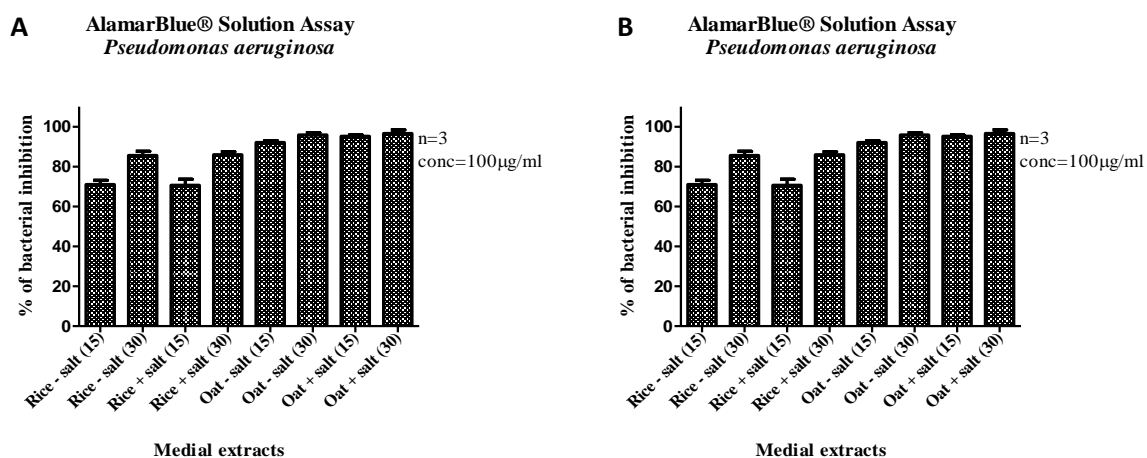


Figure 4.29: Percentage bacterial viability of biofilm-forming *P. aeruginosa* with 100µg/mL of *M. elegans* extracts obtained from various **A:** liquid and **B:** solid media.

4.3.3.2 Planktonic Assay of the *M. elegans* extracts.

The planktonic assay results are presented in Table 4.9 and Figures 4.30 and 4.31. Extracts afforded by inoculation of *M. elegans* on malt extract broth and oat media in the presence or absence of sea salt displayed the highest inhibition of biofilm formation produced by both *S. aureus* and *P. aeruginosa*. As in the AlamarBlue® assay, parallel results were obtained for the rest of the *M. elegans* extracts, inhibiting biofilm production at least ~50%, while the extract obtained from marine broth incubated for 15 days remained inactive.

Table 4.9: Planktonic biofilm viability assay results of 100µg/mL extracts of *M. elegance* inoculated on various media incubated at 15 and 30 days.

Liquid media	% inhibition <i>S. aureus, P. aeruginosa</i>	Solid media	% inhibition <i>S. aureus:P. aeruginosa</i>
Malt extract without sea salt 15 days incubation	90%, 91%	Rice media without sea salt 15 days incubation	67.3%, 71.4%
Malt extract without sea salt 30 days incubation	100%, 98.9%	Rice media without sea salt 30 days incubation	83%, 64%
Malt extract with sea salt 15 days incubation	81.5%, 85.9%	Rice media with sea salt 15 days incubation	75.3%, 74.5%
Malt extract with sea salt 30 days incubation	87.4%, 88.1%	Rice media with sea salt 30 days incubation	83.5%, 87.8%
Wickersham without sea salt 15 days incubation	48.1%, 49.8%	Oat media without sea salt 15 days incubation	92%, 92%
Wickersham without sea salt 30 days incubation	54.1%, 58.5%	Oat media without sea salt 30 days incubation	94.3%, 95.3%
Wickersham with sea salt 15 days incubation	47.5%, 52.1%	Oat media with sea salt 15 days incubation	80.1%, 80.9%
Wickersham with sea salt 30 days incubation	54.9%, 58.6%	Oat media with sea salt 30 days incubation	93.6%, 95.9%
Marine broth 15 days incubation	4.1%, 4%		
Marine broth 30 days incubation	65.1%, 64.2%		

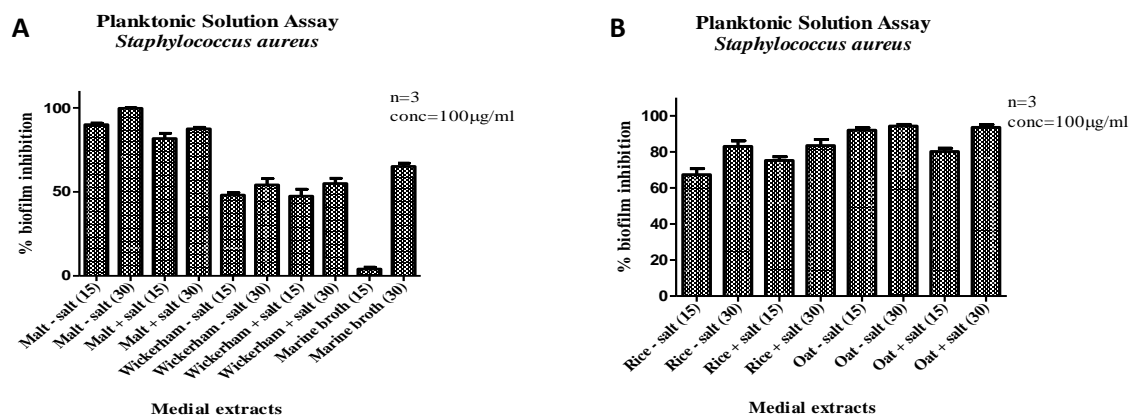


Figure 4.30: Percentage biofilm inhibition of biofilm-forming *S. aureus* with 100µg/mL of *M. elegans* extracts obtained from various **A:** liquid and **B:** solid media.

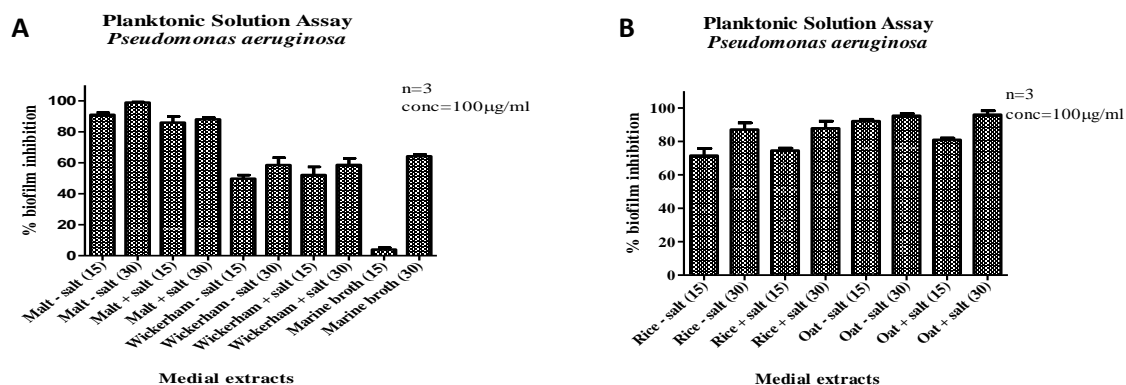


Figure 4.31: Percentage biofilm inhibition of biofilm-forming *P. aeruginosa* with 100µg/mL of *M. elegans* extracts obtained from various **A:** liquid and **B:** solid media.

4.3.3.3 Minimum inhibitory concentration (MIC) and Minimum biofilm eradication concentration (MBEC) assays.

The most bioactive *M. elegans* extracts obtained from malt extract broth and oat media were further tested for their MIC and MBEC values against both biofilm-forming *S. aureus* and *P. aeruginosa*. *M. elegans* growing on malt extract broth for 30 days in the presence of sea salt yielded an extract with the lowest MIC value of 20.9 µg/mL against biofilm-forming *S. aureus*. Alternatively, the highest MIC value of 33.0 µg/mL was exhibited by the extract afforded from *M. elegans* grown for 15 days on oat media with sea salt.

Similarly, the extract afforded by *M. elegans* growing on malt extract broth media with sea salt incubated for 30 days displayed a lowest MIC of 22.3 µg/mL against biofilm-forming *P. aeruginosa*, while a highest MIC value of 34.8 µg/mL was shown by the extract obtained from the oat media with sea salt incubated for 30 days. Most of the extracts obtained from the malt

extract broth gave MIC values of lower or equal to 30ug/mL against both biofilm-forming bacteria. While most of the extracts afforded from the oat media presented MIC values higher than 30ug/mL against both biofilm-forming bacteria. MIC values of the respective active *M. elegance* extracts are presented in Table 4.10 and Figures 4.32 and 4.33.

Table 4.10: MIC of antibacterial *M. elegance* extracts against *S. aureus* and *P. aeruginosa*.

Media	MIC µg/mL against <i>S. aureus</i>	MIC µg/mL against <i>P. aeruginosa</i>
Malt extract without sea salt 15 days	22.8	30.1
Malt extract without sea salt 30 days	21.9	27.9
Malt extract with sea salt 15 days	24.2	25.9
Malt extract with sea salt 30 days	20.9	22.3
Oat media without sea salt 15 days	30.3	30.7
Oat media without sea salt 30 days	28.7	33.9
Oat media with sea salt 15 days	33.0	33.6
Oat media with sea salt 30 days	31.0	34.8

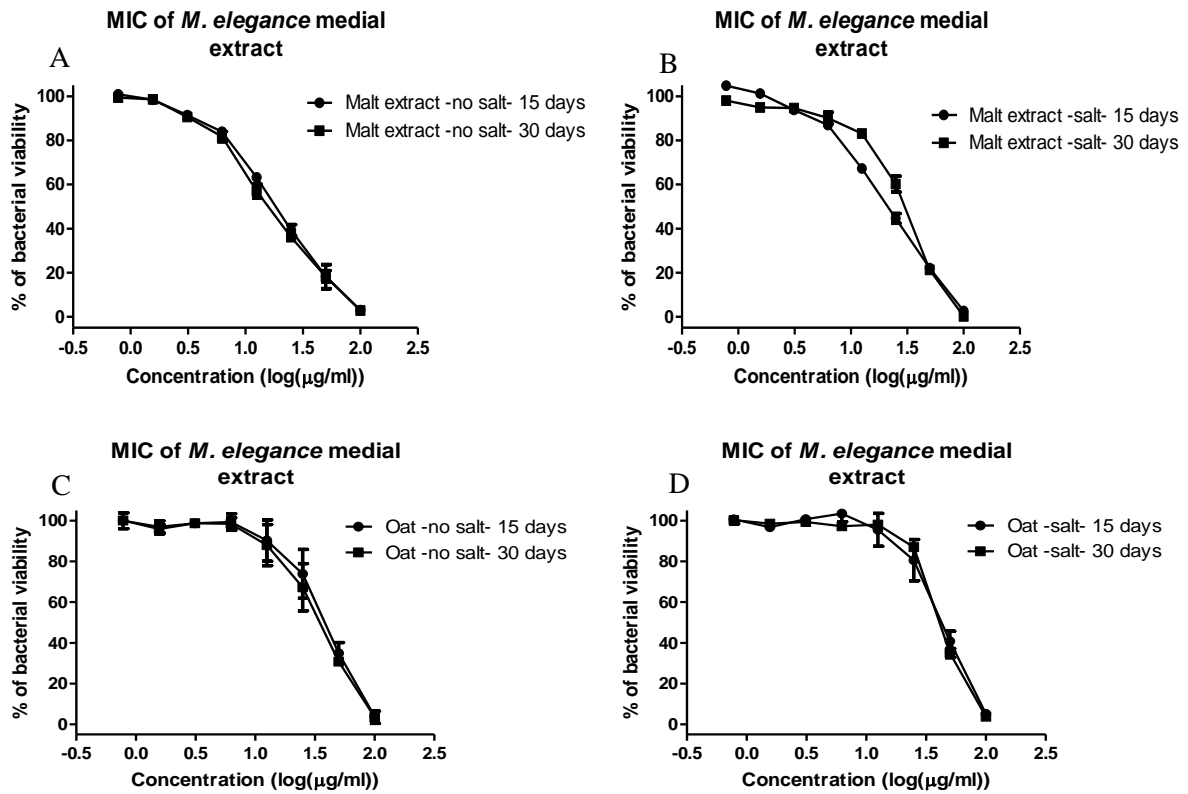


Figure 4.32: MIC results of active *M. elegans* extracts against *S. aureus*. A: MIC of *M. elegans* growing malt extracts without sea salt, B: MIC of *M. elegans* growing on malt extracts with sea salt, C: MIC of *M. elegans* growing on oat extracts without sea salt, and D: MIC of *M. elegans* growing on oat extracts with sea salt.

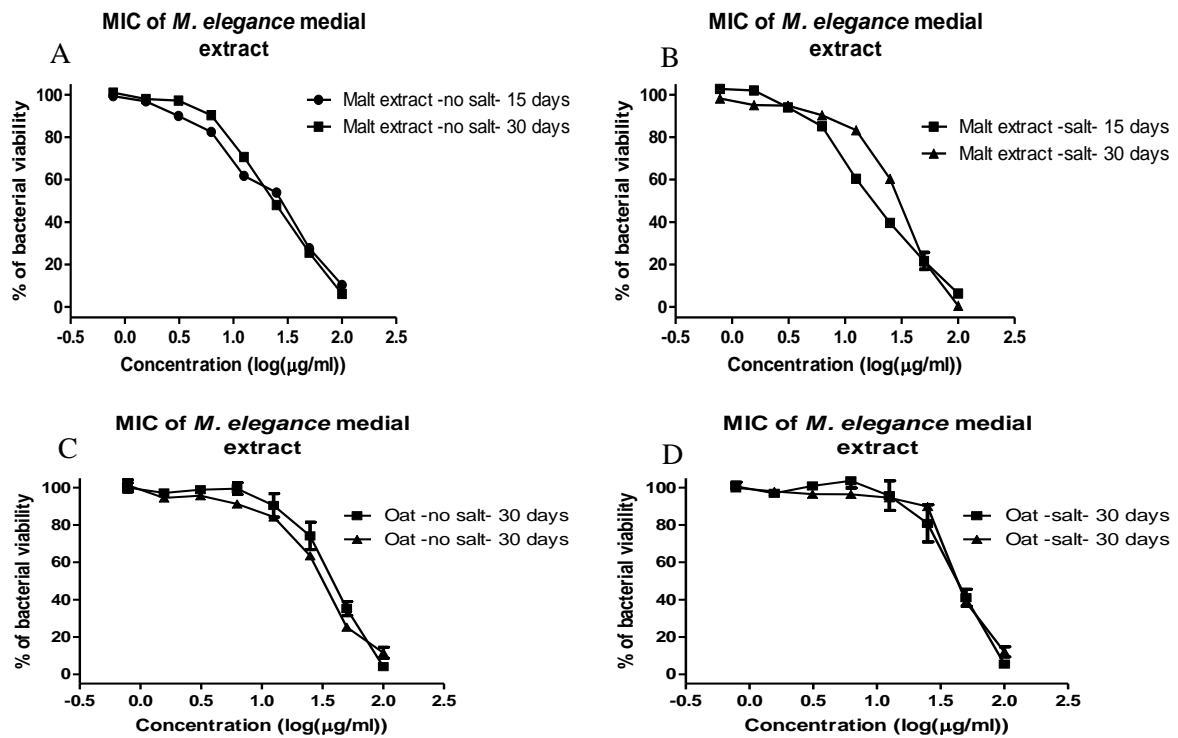


Figure 4.33: MIC results of active *M. elegans* extracts against *P. aeruginosa*. A: MIC of *M. elegans* growing malt extracts without sea salt, B: MIC of *M. elegans* growing on malt extracts with sea salt, C: MIC of *M. elegans* growing on oat extracts without sea salt, and D: MIC of *M. elegans* growing on oat extracts with sea salt.

MBEC results are presented in Table 4.11 and Figures 4.34 and 4.35. *M. elegans* growing on malt extract broth in the presence of sea salt for 30 days yielded the extract with the lowest MIC value of 24.6 $\mu\text{g/ml}$ against biofilm-forming *S. aureus*. On the other hand, the highest MBEC against *S. aureus* was exhibited by the extract obtained from the fungus grown for 30 days on oat media with sea salt. While against *P. aeruginosa*, the lowest MBEC of 18.4 $\mu\text{g/ml}$ was presented by the extract afforded from Malt extract broth media incubated for 30 days while the highest MBEC of 40.7 $\mu\text{g/ml}$ was displayed by the extract obtained from oat media with sea salt incubated for 15 days. *M. elegans* grown for 15 and 30 days on malt extract broth either with or without sea salt yielded extracts with MBEC values of less than 30 $\mu\text{g/ml}$. While extracts obtained from the fungus grown on oat media either with or without sea salt gave MBEC values of more than 30 $\mu\text{g/ml}$.

Table 4.11: MBEC of antibacterial *M. elegans* extracts against *S. aureus* and *P. aeruginosa*.

Media	MBEC $\mu\text{g/mL}$ against <i>S. aureus</i>	MBEC $\mu\text{g/mL}$ against <i>P. aeruginosa</i>
Malt extract without sea salt 15 days	26.1	28.5
Malt extract without sea salt 30 days	25.8	18.4
Malt extract with sea salt 15 days	29.2	27.3
Malt extract with sea salt 30 days	24.6	19.4
Oat media without sea salt 15 days	35.0	35.9
Oat media without sea salt 30 days	33.2	33.2
Oat media with sea salt 15 days	34.5	40.7
Oat media with sea salt 30 days	39.4	35.1

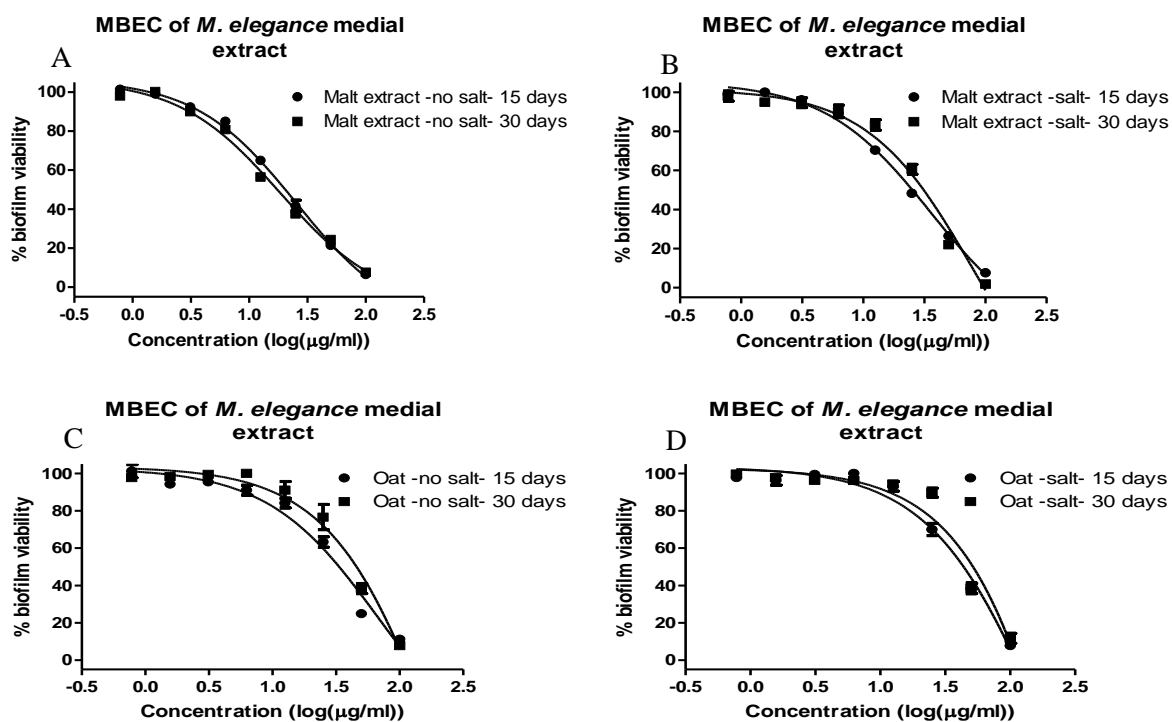


Figure 4.34: MBEC results of active *M. elegans* extracts against *S. aureus*. A: MIC of *M. elegans* growing malt extracts without sea salt, B: MIC of *M. elegans* growing on malt extracts with sea salt, C: MIC of *M. elegans* growing on oat extracts without sea salt, and D: MIC of *M. elegans* growing on oat extracts with sea salt.

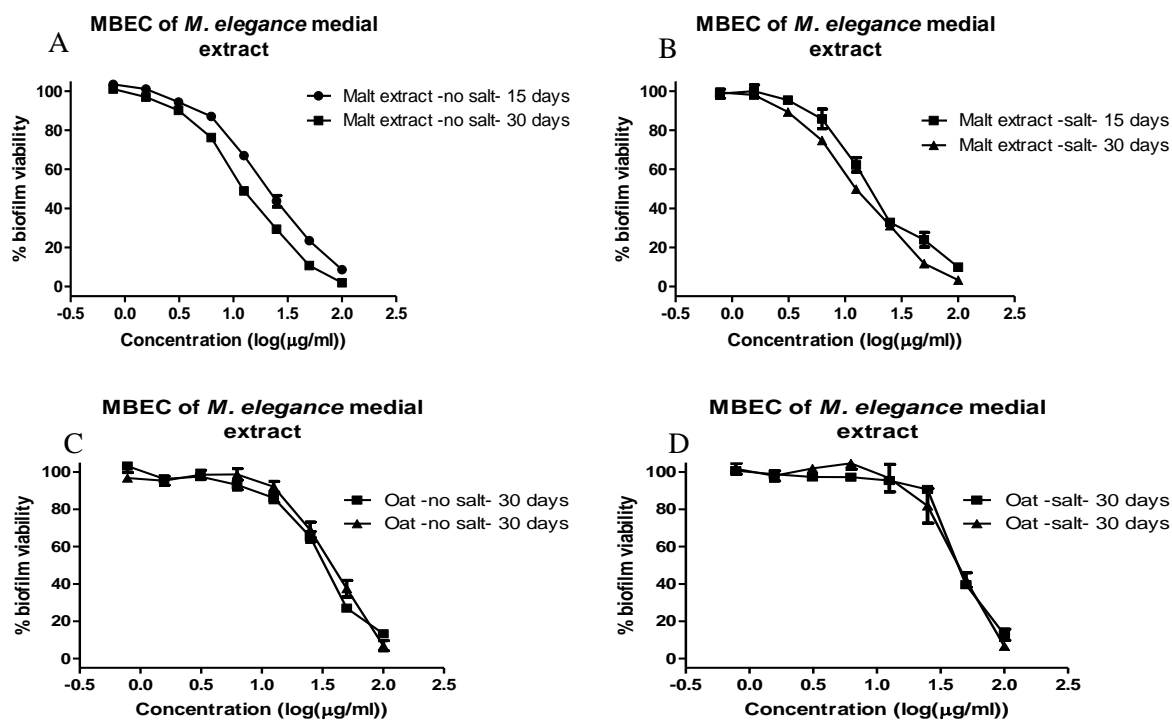


Figure 4.35: MBEC results of active *M. elegans* extracts against *P. aeruginosa*. A: MIC of *M. elegans* growing malt extracts without sea salt, B: MIC of *M. elegans* growing on malt extracts with sea salt, C: MIC of *M. elegans* growing on oat extracts without sea salt, and D: MIC of *M. elegans* growing on oat extracts with sea salt.

4.2.4 Multivariate analysis of NMR data

Multivariate analysis using SIMCA was done on the processed (see section 2.2.7.5) NMR spectral data of fungal extracts and blank media. Extracts from *M. elegans* grown for 15 days on marine broth was the only outlier. Although there are two observed clusters, one on the lower right quadrant and one in the upper right quadrant, most fungal extracts were overlapping except for the extracts obtained from the malt extract with and without sea salt that were incubated for 30 days. However, as the natural groupings of the extracts were based on the relative similarity of their chemical profile, neither of the groups dependently clustered according to the media from where they were obtained nor their incubation periods. R^2X of 1.00 and Q^2X of 0.99.

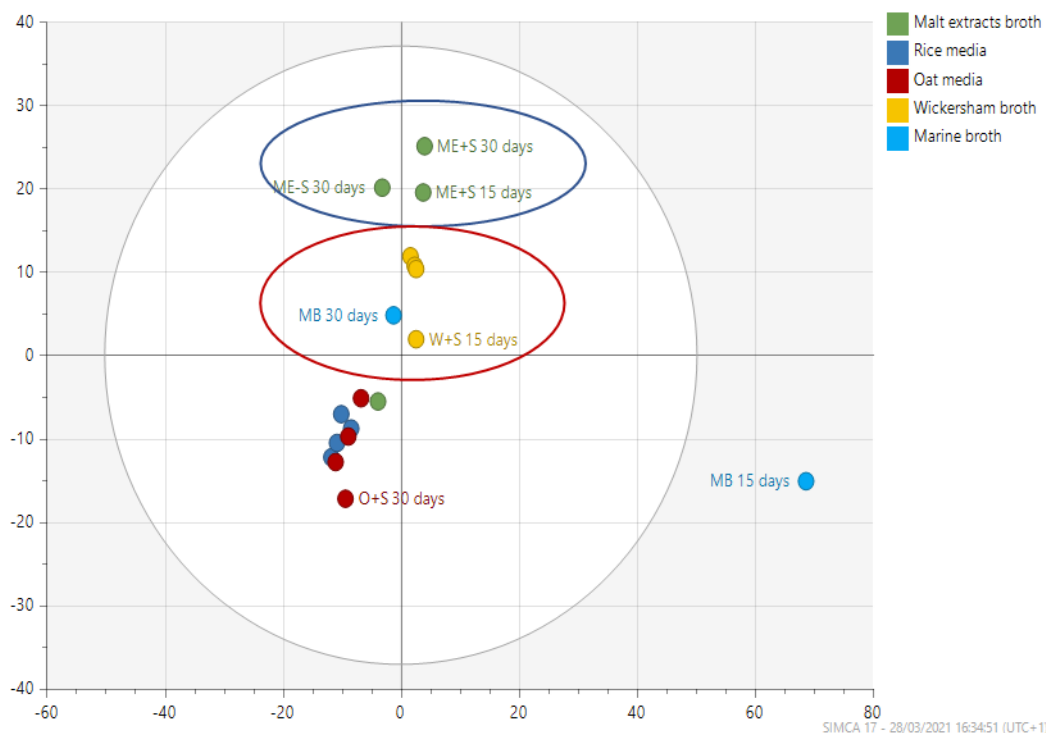


Figure 4.36: PCA scatter plot of NMR spectral data of *M. elegans* extracts obtained from various growth media incubated at 15 and 30 days.

For OPLS-DA, the extracts were classified according to their antimicrobial activity against both biofilm-forming *S. aureus* and *P. aeruginosa*. OPLS-DA positioned the antimicrobial-active extracts on the left side of the scatter plot, while their close collocation implied a comparable chemical profile between the extracts. The OPLS-DA loadings plot revealed that the antimicrobial extracts consisted mainly of peaks from the aliphatic region (1-3ppm) of the spectrum while a smaller numbers of peaks were found at the aromatic region. On the other hand, the inactive extracts exhibited a higher ratio of aromatic peaks and smaller ratio of resonances at the aliphatic region. Interestingly, the outlying inactive extract obtained from the fungus incubated in marine broth (MB) for 15 days yielded highly hydroxylated compounds or saccharides as indicated by peaks from 3 to 5 ppm (encircled in red in Figure 4.37B). OPLS-DA scatter and loading plots are presented in Figure 4.37.

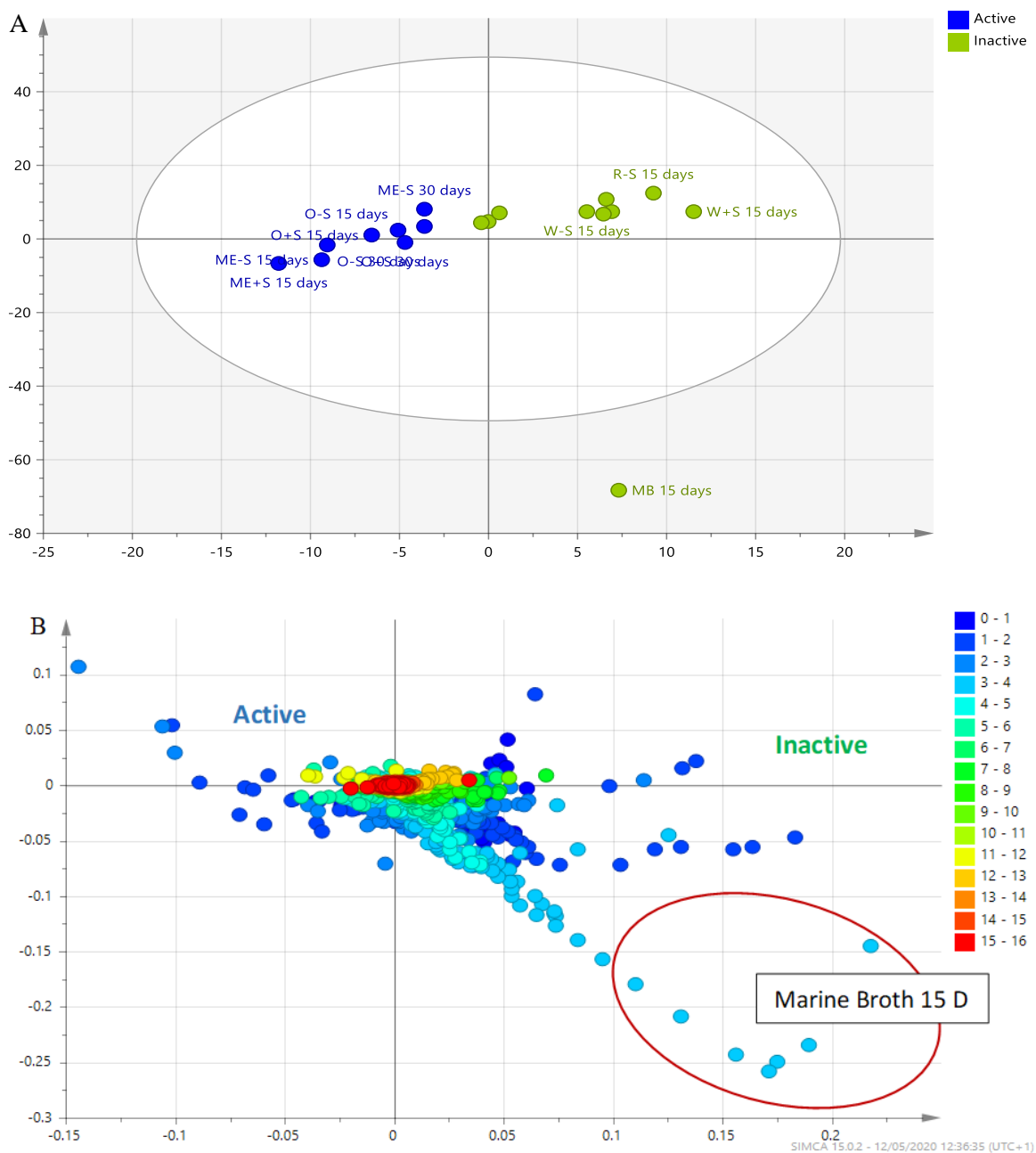


Figure 4.37: OPLS-DA scatter (**A**) and loading (**B**) plots of the NMR spectral data of *M. elegans* extracts obtained from various growth media incubated at 15 and 30 days. Extracts were classified according to their antimicrobial activity against both biofilm-forming *S. aureus* and *P. aeruginosa*.

4.2.5 Multivariate analysis of LC-HRMS data

The LC-HRMS data was processed with Mzmine and dereplicated using an in-house MACRO to couple the spectral data with the DNP. Fungal extract afforded by the malt extract with sea salt incubated for 15 and 30 days, as well as those from the marine broth media incubated for 30 days (encircle **orange**), the extracts were clustered into two main groups (encircled in **blue** and **red**). Comparable to the PCA results of the NMR spectral data, the natural clustering of the fungal extracts or the similarities of the chemical profiles of the extracts were not based on media used to inoculate the fungus or the incubation period. PCA scatter plot of mass spectral data is shown in Figure 4.38. The values of R^2X and Q^2X of the PCA-X scatter plot were 0.738 and 0.542 with a difference of 0.196 which indicates a good model relatively even if Q^2X value is not high.

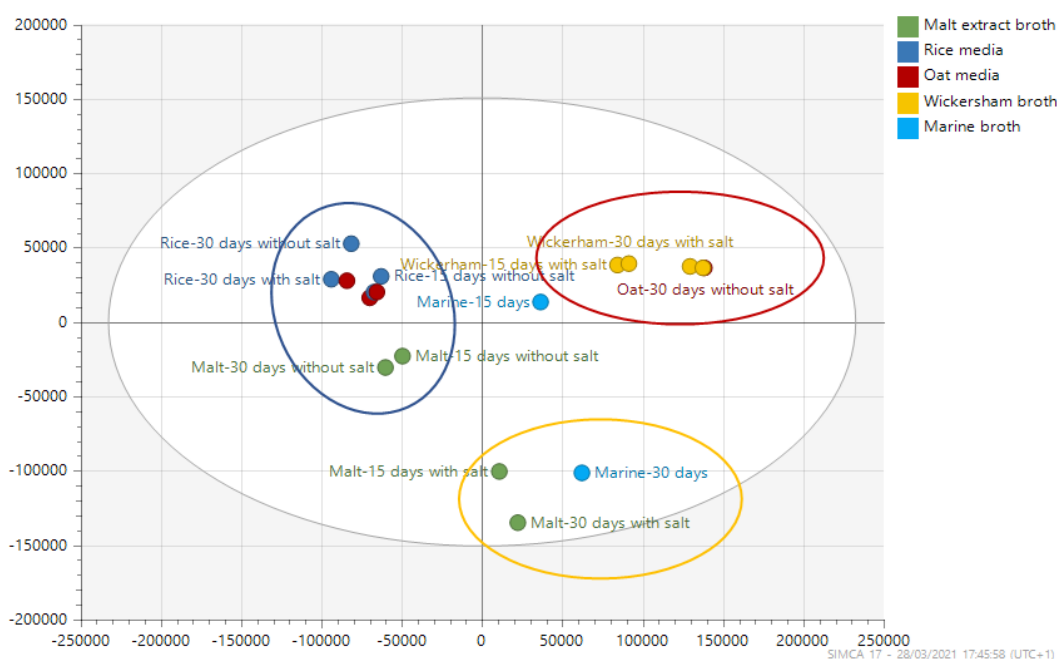


Figure 4.38: PCA scatter plot obtained from LC-HRMS data of *M. elegans* extracts obtained from various media incubated for 15 and 30 days.

The results of the antimicrobial activity against biofilms forming *S. aureus* and *P. aeruginosa* were used to group the extracts for OPLS-DA. In terms of the separation of the extracts between the two pre-designated groups, the variation was comparable to the PCA scatter plot with R^2 of 0.713 and Q^2 value of 0.537 and a difference of 0.176. The active *M. elegans* extracts were

mainly positioned on the upper left quadrant of the OPLS-DA scatter plot, while the inactive extracts covered the entire right side of the plot. The random distribution and overlapping of some of the extracts between the active and inactive groups was indicated by the low separation score. The variation between two groups (R^2X) was 12.3%. While the variation within group (R^2X_0) was slightly higher at 15.7%. The OPLS-DA loadings plot provided the discriminating features at m/z 800 to 900 Da afforded by the fungus inoculated on malt extract with sea salt incubated for 15 and 30 days. Dereplication of the discriminating features did not give any hits from the DNP database. These discriminating features were found to have a p -value less than 0.05. OPLS-DA scatter and loading plots are presented in Figures 4.39 and 4.40. Table 4.12 list the discrimination ion peaks assigned to the antimicrobial extracts.

When comparing the NMR data of the discriminating features provided by multivariate analysis, the active extract showed the presence of a wide range of high intensity resonances between 0.00 and 5.00 ppm but with low intensity resonances between 6.00 and 10.00 ppm. The peaks between 0.00 and 5.00 ppm indicated the presence of acylated and hydroxylated peaks. While the peaks between 6.00 and 10.00 ppm indicated the presence of aromatic peaks as well as exchangeable phenolic OH s or NH peaks of amino acids. These data were comparable to the predicted DBE values for the discriminating compounds encircled with red in the OPLS-DA loadings plot in Figure 4.42.

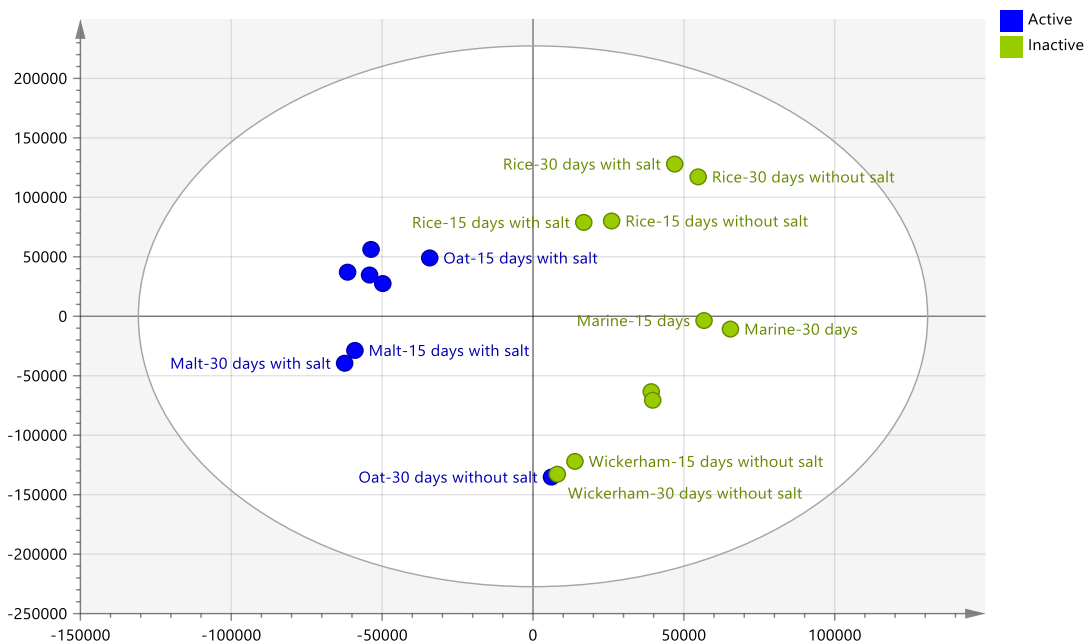


Figure 4.39: OPLS-DA scatter plot of LC-HRMS data of *M. elegans* extracts obtained from various media incubated at 15 and 30 days. Extracts were grouped according to their antimicrobial activity against both biofilm-forming *S. aureus* and *P. aeruginosa*.

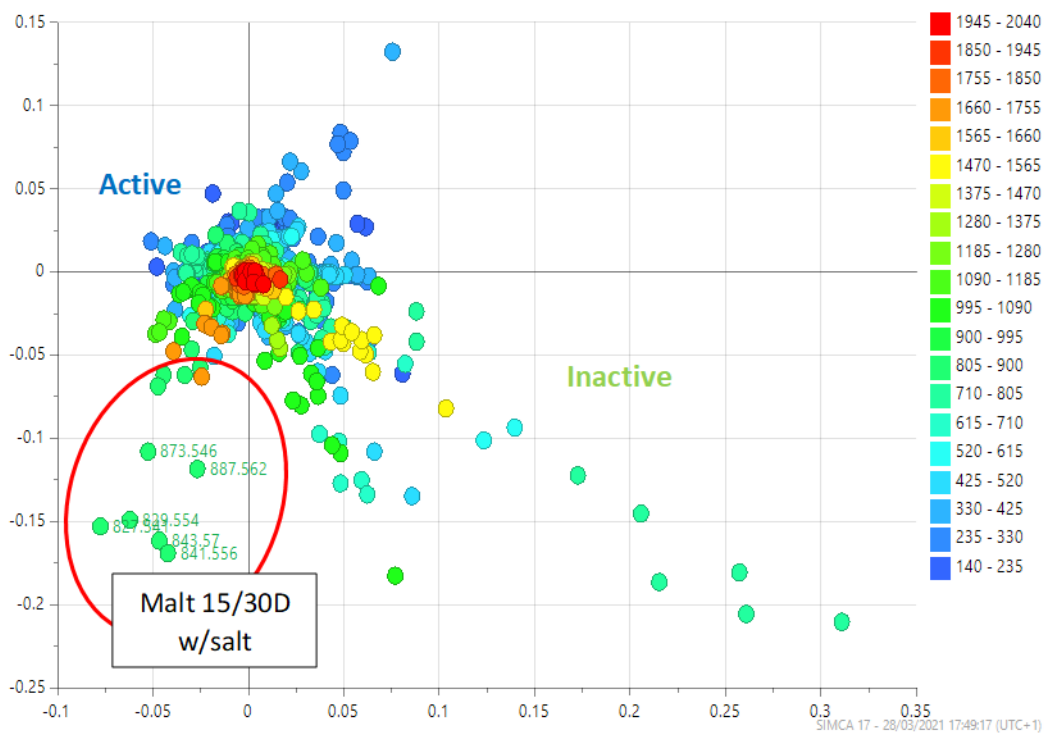


Figure 4.40: OPLS-DA loadings plot of LC-HRMS data of *M. elegans* extracts obtained from various media incubated at 15 and 30 days. Group of discriminating features for antimicrobial active extracts is encircled in red.

Table 4.12: Dereplication of six target bioactive metabolites found in active extracts, with P values < 0.05 as obtained from the OPLS-DA S-plot.

Var ID	p-value	FDR	Molecular weight	Chemical formula prediction (DBE)	Compound hits from DNP and biological source
P_6367	0.049	0.035294118	828.5468	C ₄₄ H ₆₈ N ₁₂ O ₄ (17) C ₄₃ H ₇₂ N ₈ O ₈ (12)	No hit
N_1885	0.0091	0.002941176	828.5485	C ₄₈ H ₇₂ N ₆ O ₆ (16) C ₄₂ H ₇₆ N ₄ O ₁₂ (7)	No hit
P_6366	0.03357	0.029411765	842.5623	C ₄₅ H ₇₀ N ₁₂ O ₄ (17) C ₄₄ H ₇₄ N ₈ O ₈ (12)	No hit
N_558	0.0319	0.011764706	842.5633	C ₄₈ H ₇₈ N ₂ O ₁₀ (11) C ₄₂ H ₈₂ O ₁₆ (2)	No hit
N_1888	0.0265	0.005882353	874.5536	C ₄₄ H ₇₄ N ₈ O ₁₀ (12) C ₄₅ H ₇₀ N ₁₂ O ₆ (17)	No hit
N_1887	0.02767	0.008823529	888.5689	C ₄₆ H ₇₂ N ₁₂ O ₆ (17) C ₄₅ H ₇₆ N ₈ O ₁₀ (12)	No hit

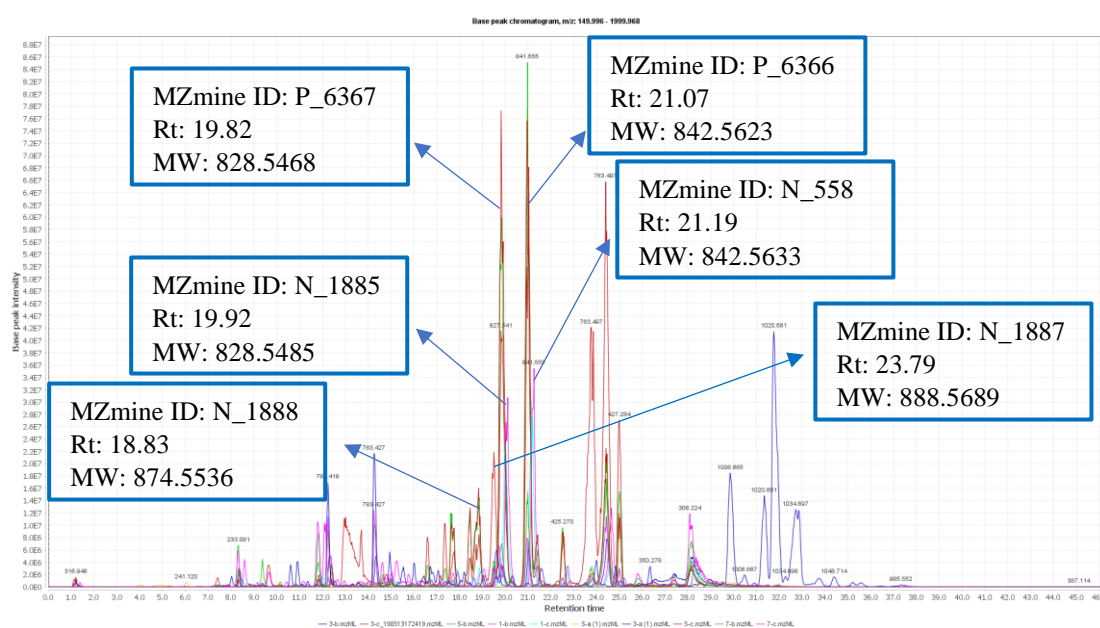


Figure 4.41: Total Ion Chromatogram (TIC) of the active fraction. The ion peaks that represent the discriminating features listed in Table 4.12 have been labelled.

4.3 Optimising the production of anti-biofilm bioactive metabolites produced by *Hypoxylon rubiginosum*.

4.3.1 Extract yields on different media.

H. rubiginosum grown on the different media used in this study showed poor or no growth on 7 days of incubation. Growth was only observed on 15 and 30 days of incubation yielding good biomass. Again, like the previous endophytic fungus, the average yield of extracts afforded by the solid media was higher than the yields from fungus grown on liquid media. Amongst the liquid media, the highest yield of (87.3mg) was achieved by growing the fungus grown on malt extract broth in the presence of sea salt for incubated for 30 days. Alternatively, the fungus inoculated on Wickersham broth without sea salt incubated for 30 days gave the lowest yield of 23.1 mg. On solid media, the highest yield 336 mg of extract was obtained from the fungus grown for 30 days on rice media in the absence of sea salt. While the lowest yield was attained from fungus grown on oat media with sea salt incubated for 15 days. Extract yields obtained from the various media are presented in Table 4.13 and Figure 4.42.

The log growth phase of *H. rubiginosum* was observed between 15 and 30 days on solid media with and without sea salt as well as on malt extract without sea salt. The fungus growing on most of the liquid media seems to reach the stationary phase on the 15th day of the incubation period as shown in Figure 4.42.

Table 4.13: Extract weights of *H. rubiginosum* obtained by cultivation on different media.

Liquid Media				
Type of Media	Incubation Period Yield			Blank
	7 Days	15 Days	30 Days	
Malt Extract without Sea Salt	-	29.5mg	87.3mg	4.52mg
Malt Extract with Sea Salt	-	36.4mg	29.7mg	9.21mg
Wickersham Media without Sea Salt	-	42.2mg	37.1mg	8.11mg
Wickersham Media with Sea Salt	-	52.2mg	23.1mg	15.2mg
Marine Broth	-	46.3mg	46.4mg	4.20mg
Solid Media				
Type of Media	Incubation Period			Blank
	7 Days	15 Days	30 Days	
Rice Media without Sea Salt	-	267mg	336mg	23.4mg
Rice Media with Sea Salt	-	297mg	295mg	22.7mg
Oat Media without Sea Salt	-	61.2mg	67.9mg	33.2mg
Oat Media with Sea Salt	-	57.4mg	73.8mg	29.7mg

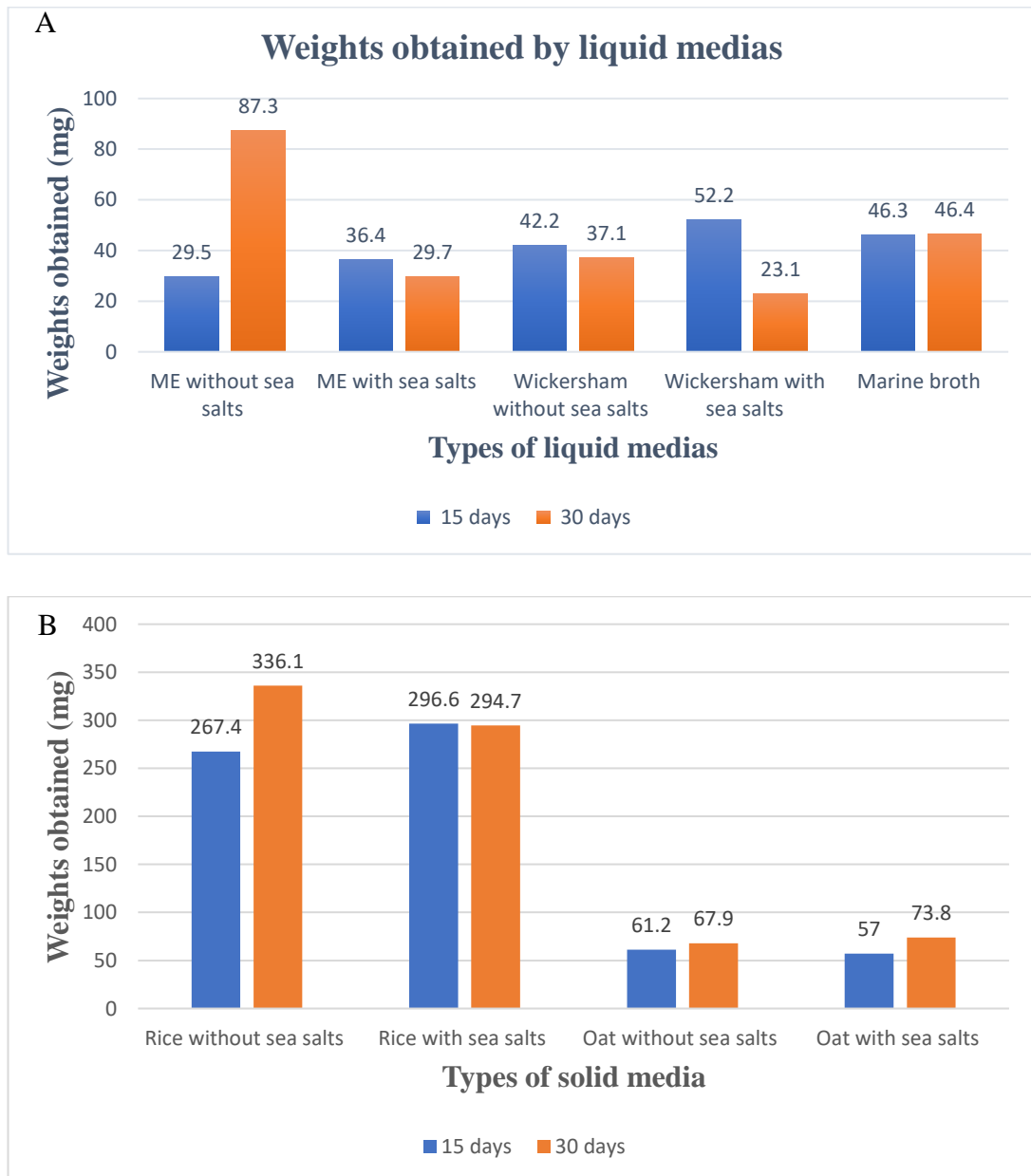


Figure 4.42: Histogram of extract weights of *H. rubiginosum* obtained from various (A) liquid and (B) solid media incubated for 15 and 30 days.

4.3.2 NMR spectroscopy for *H. rubiginosum* extracts

4.3.2.1 Liquid media

4.3.2.1.1 Malt extract broth with and without sea salt:

The stacked ^1H NMR spectra (Figure 4.43) of *H. rubiginosum* extracts obtained from malt extract with and without sea salt, incubated in both 15 and 30 days indicated the production of extracts with wide range of resonance. These resonance peaks are located at aliphatic, hydroxylated, and aromatic regions at 1.50 to 4.50 and 6.00 to 8.50 ppm, respectively). The presence of sea salt did not show any effect on the chemical profile of malt extract broth as no difference between the spectra was indicated. Incubation periods did show to have a major effect on the peaks intensity of the resonances between 4.00 and 8.50 ppm. The intensity of the peaks for samples incubated for 15 days were higher than the peaks of samples from 30 days of incubation.

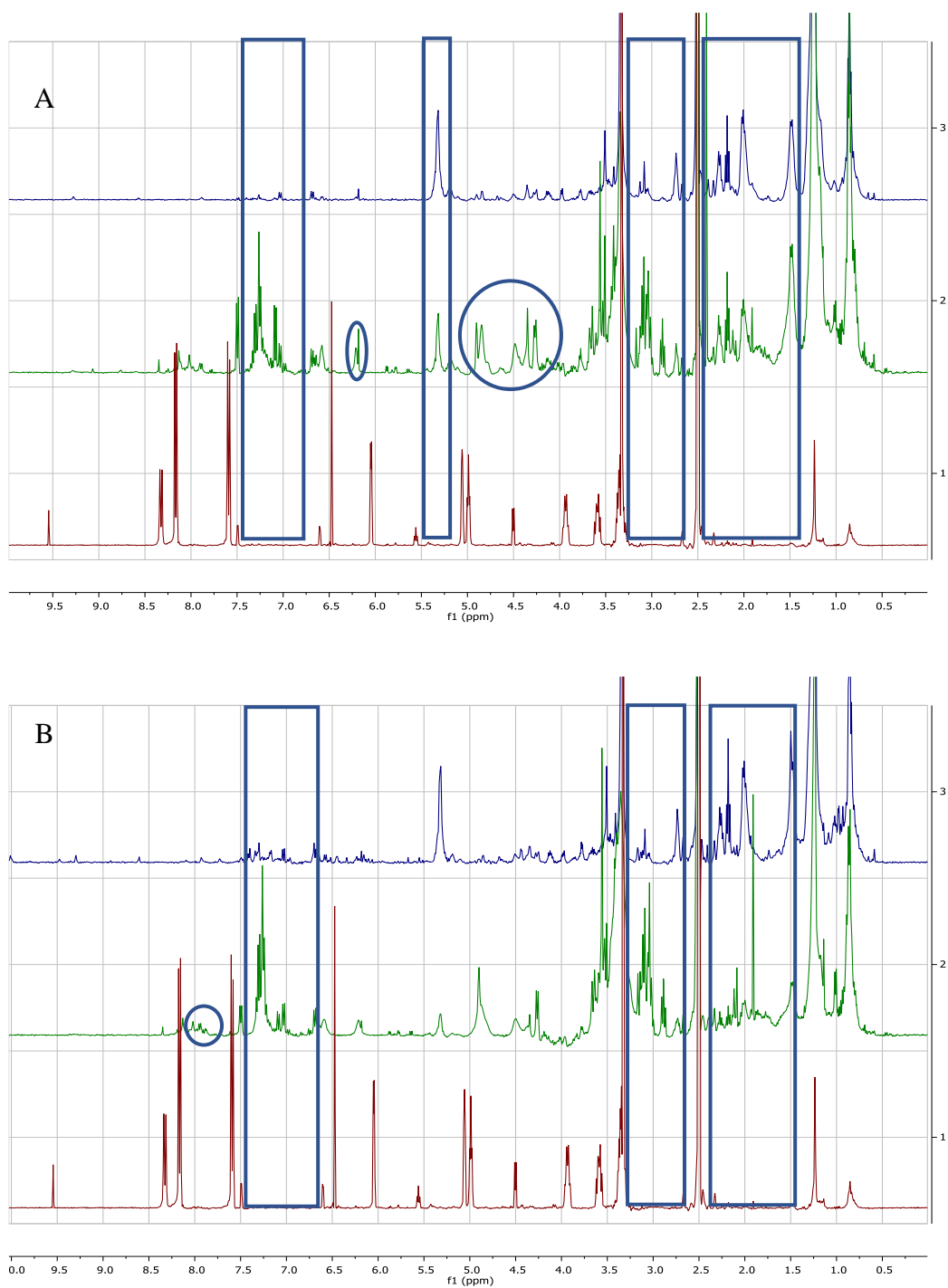


Figure 4.43: Stacked ^1H NMR spectra of *H. rubiginosum* extracts obtained from malt extract liquid media with (A) and without sea salt (B). Spectrum 1 at the bottom of each of the stack represents the blank followed by those incubated at 15 and 30 days, respectively. The differences are highlighted in blue boxes.

4.3.2.1.2 Wickersham liquid media with and without sea salt

Stacked ^1H NMR spectra of *H. rubiginosum* extracts obtained from Wickersham liquid media with and without sea salt both incubated on 15 and 30 days did not show any huge difference to that of the spectrum of the blank media. Most of the intense peaks were found at the aliphatic region designated for saturated and unsaturated fatty acids. In addition, some of the peaks found on the blank media either disappeared or decrease in intensity, while some of the peaks from the extracts were overlapping. Stacked ^1H NMR spectra of *H. rubiginosum* extracts prepared from from Wickersham media are presented in Figure 4.44. Upon comparing the incubation periods and the presence or the absence of sea salt in stacked NMR spectra, it showed that both sea salt and incubation periods have no major effect on the chemical profiles of the extract.

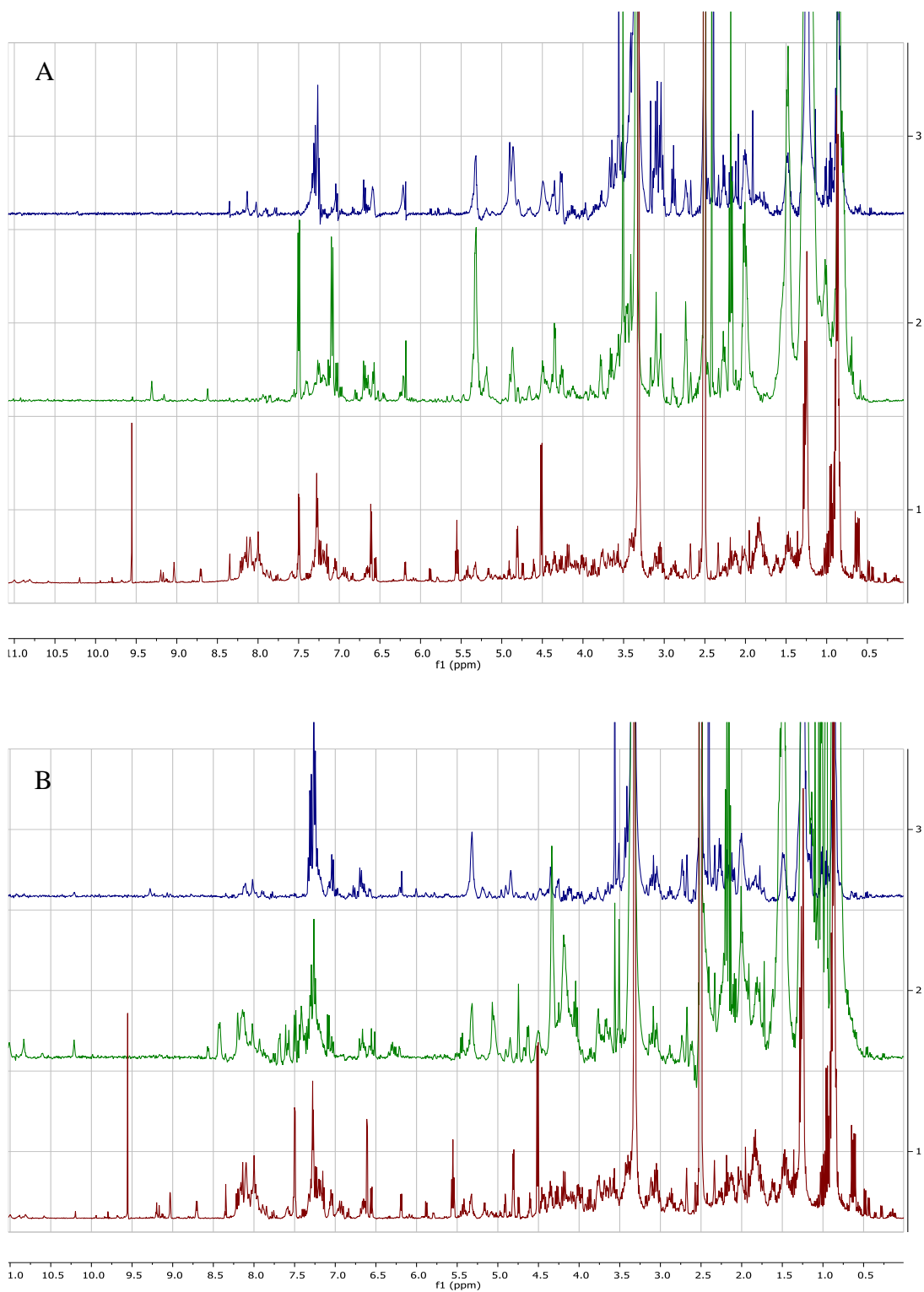


Figure 4.44: Stacked ¹H NMR spectra of *H. rubiginosum* extracts obtained from Wickersham liquid media with (A) and without sea salt (B). Spectrum 1 at the bottom of each of the stack represents the blank followed by those incubated at 15 and 30 days, respectively. The differences are highlighted in blue boxes.

4.3.2.1.3 Marine broth media

Stacked ^1H NMR spectra of *H. rubiginosum* extracts obtained from marine broth showed some differences to that of the extract of the blank media as presented in Figure 4.45. These differences were indicated by peaks resonating at the aliphatic and hydroxylated region between 1.00 and 4.50 ppm, respectively. In addition, some peaks were related to unsaturated fatty at resonances between 5.00 and 5.50 ppm that marine endophytic fungus are known to yield (Certik and Shimizu, 1999). Furthermore, small intensity peaks were observed at the aromatic region between the 6.00 and 8.00 ppm. Some of the ^1H NMR peaks between 4.50 and 10.00ppm found in the extract of the media blank were not found in the spectra of the fungal extracts. The incubation period had no major effect on the chemical profile of the marine broth extracts. The only difference was observed on the intensity of the peaks resonating between 5.00 and 5.50 ppm which increased after incubation for 30 days.

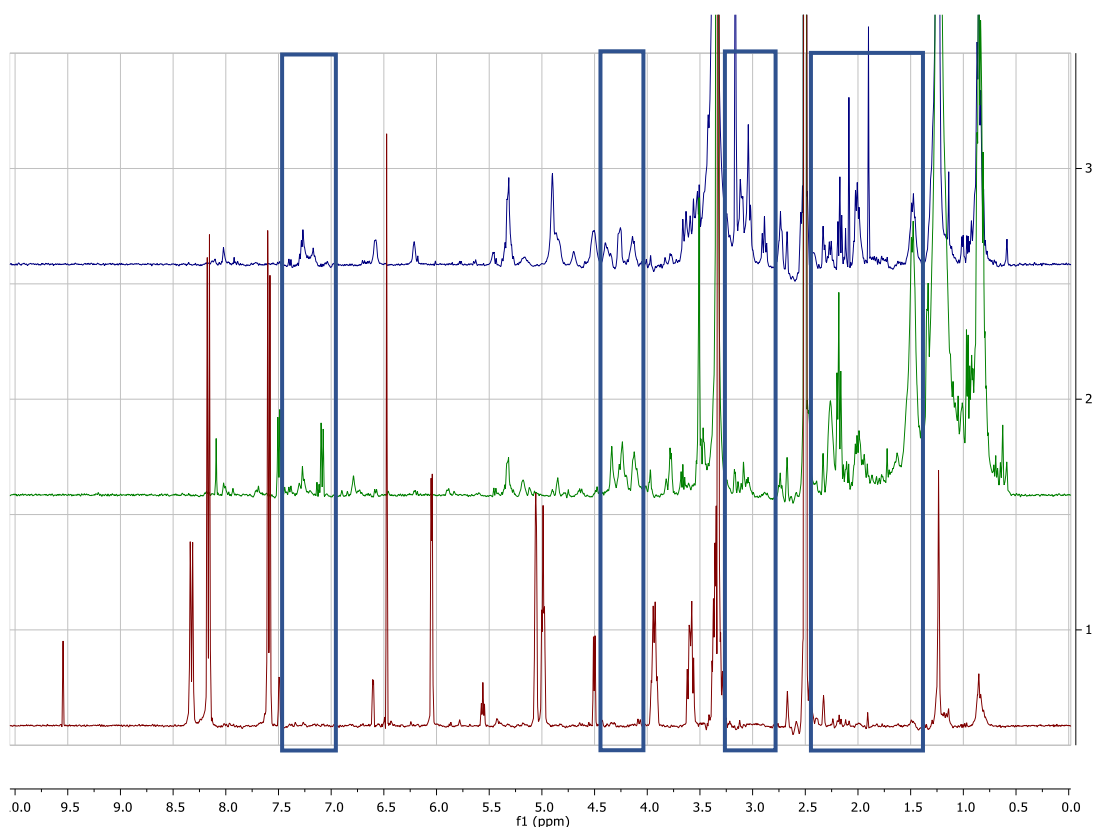


Figure 4.45: Stacked ^1H NMR spectra of *H. rubiginosum* extracts obtained from marine broth media. Spectrum 1 at the bottom of the stack represents the blank followed by those incubated at 15 and 30 days, respectively. The differences are highlighted in blue boxes.

4.3.2.2 Solid media

4.3.2.2.1 Rice media with and without sea salt:

Stacked ^1H NMR spectra of *H. rubiginosum* extracts obtained from rice media with and without sea salt are presented in Figure 4.46. No difference was observable between the extracts afforded after growing *H. rubiginosum* on rice media with and without sea salt. When comparing the fungal extracts with the extract of the blank media, major variations were noticeable at the olefinic and aromatic resonance between 5.50 and 9.50 ppm. The occurrence of saturated or unsaturated fatty acids were also indicated in the spectra of *H. rubiginosum* extracts. In general, the extracts obtained from media incubated for 30 days afforded higher intensity ^1H NMR peaks. In parallel, the extract afforded by the media without sea salt yielded higher intensity peaks particularly those resonating between 5.50 and 9.50 ppm. The intensity of peaks of extracts from 30 days of incubation were higher than the peaks of extracts obtained from 15 days of incubation.

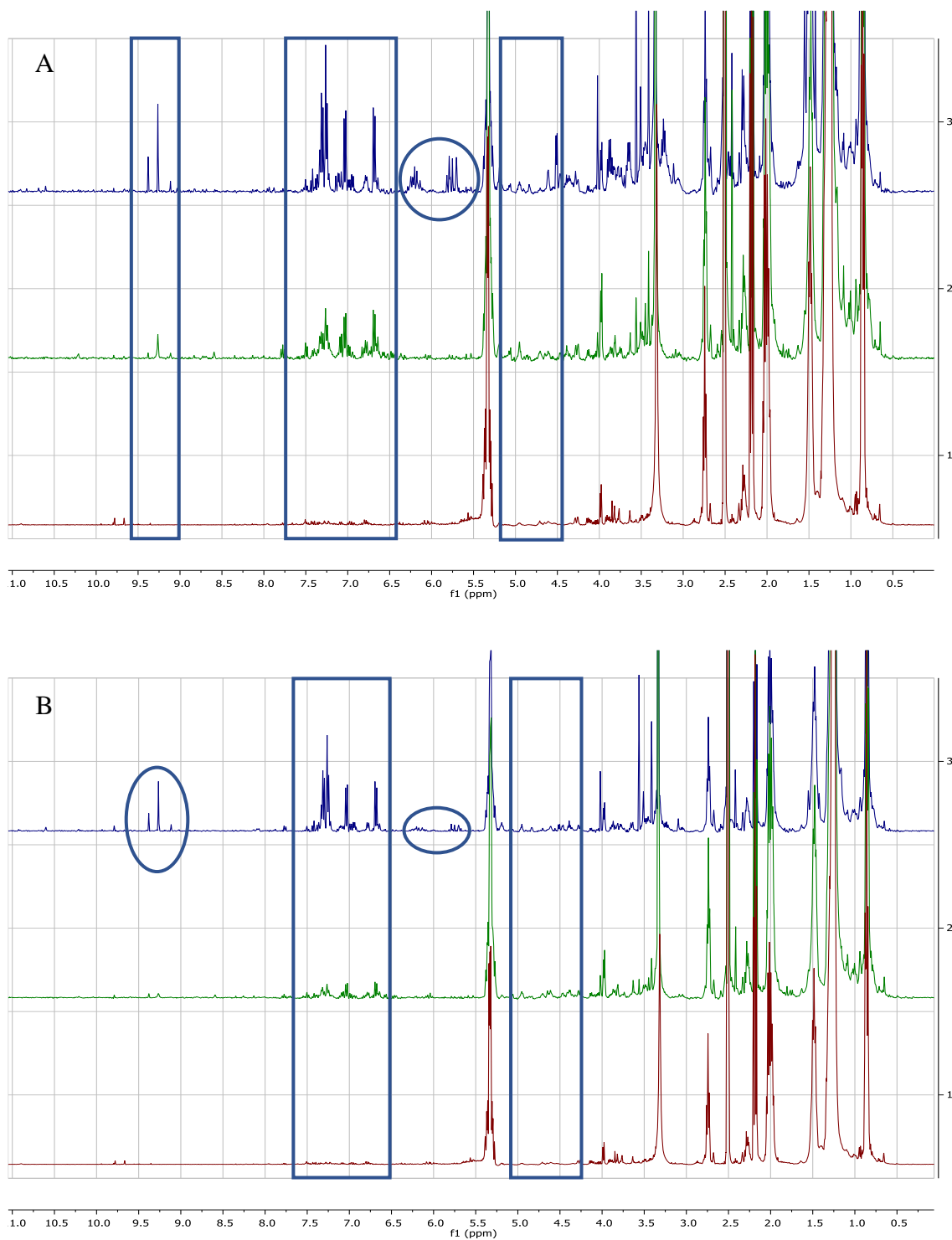


Figure 4.46: Stacked ^1H NMR spectra of *H. rubiginosum* extracts obtained from rice media with (A) and without sea salt (B). Spectrum 1 at the bottom of each of the stack represents the blank followed by those incubated at 15 and 30 days, respectively. The differences are highlighted in blue boxes.

4.3.2.2.2 Oat media with and without sea salt:

Stacked ^1H NMR spectra of *H. rubiginosum* extracts obtained from oat media with and without sea salt did not show any huge differences from the spectrum of the blank media as presented in Figure 4.49. However, extracts afforded by *H. rubiginosum* inoculated on oat media both with and without sea salt incubated for 30 days indicated a weak intensity of NMR peaks resonating between 6.00 and 9.00 ppm. On the other hand, the extracts obtained from the oat media incubated for 15 days showed intense peaks at the aromatic region between 6.00 and 8.50 ppm. ^1H NMR peaks were also observed in the aliphatic and hydroxylated region indicating the occurrence of saturated and unsaturated fatty acids in the fungal extracts. Upon comparing the presence or the absence of sea salt, sea salt had no effect on the chemical profile of the extract. On the other hand, incubation period had a major effect on the aromatic region between 6.00 and 8.50 ppm.

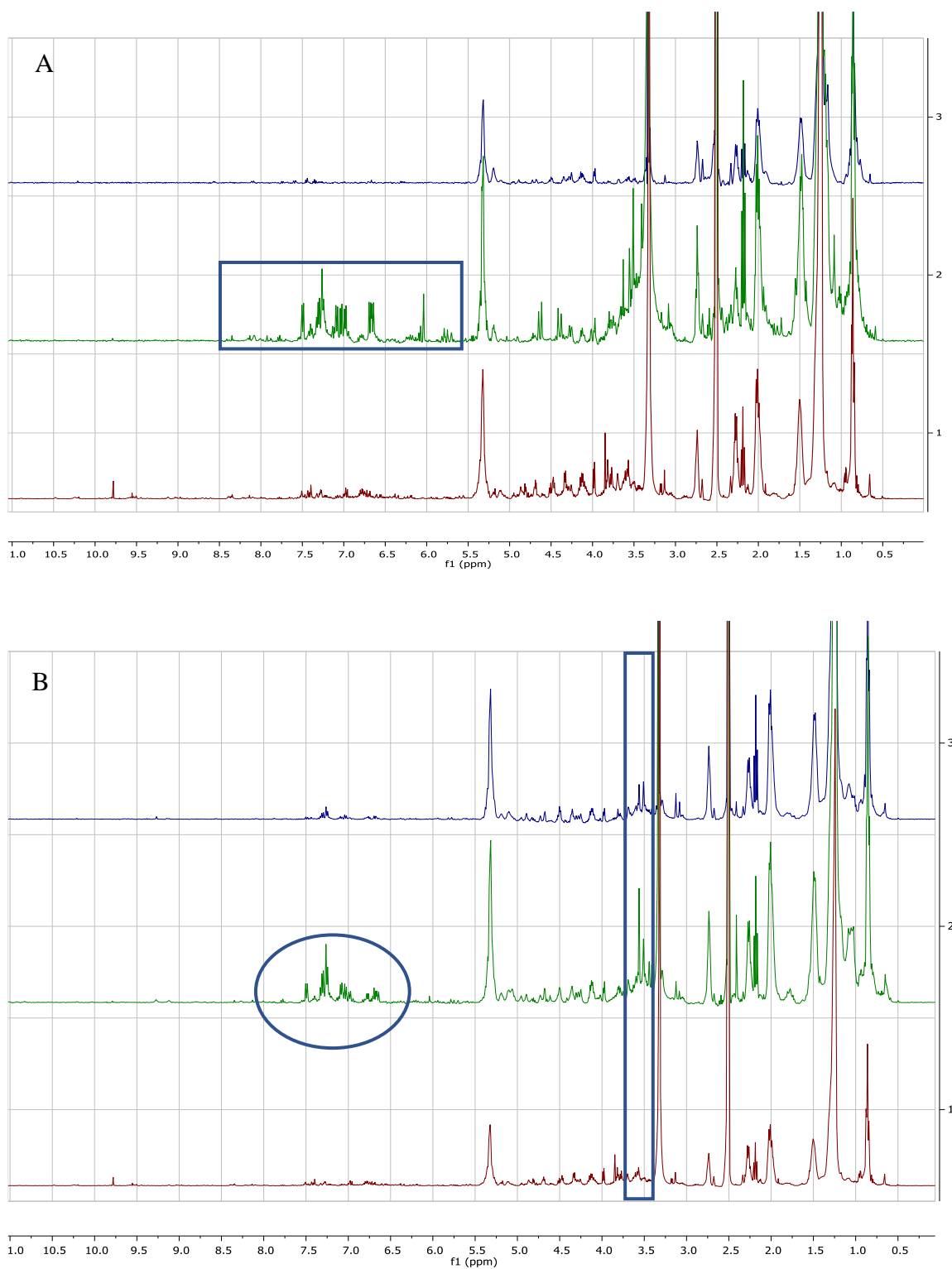


Figure 4.47: Stacked ^1H NMR spectra of *H. rubiginosum* extracts obtained from oat media with (A) and without sea salt (B). Spectrum 1 at the bottom of each of the stack represents the blank followed by those incubated at 15 and 30 days, respectively. The differences are highlighted in blue boxes.

4.3.3 Anti-biofilm biological assay

4.3.3.1 AlamarBlue® Assay of *H. rubiginosum* extracts

AlamarBlue® assay results for *H. rubiginosum* extracts against both biofilm-forming *S. aureus* and *P. aeruginosa* are presented in Table 4.14 as well as Figures 4.48 and 4.49. All *H. rubiginosum* extracts were able to inhibit bacterial growth of at least by 50%. Fungal extracts obtained from rice and oat media with or without sea salt incubated at both 15 and 30 days were able to exhibit biological activity higher than 90% inhibition. The highest biological activity of 100% against *S. aureus* was obtained for extracts of *H. rubiginosum* grown for 15 days on rice media both with and without sea salt, as well as those afforded by rice media with sea salt and oat media with and without sea salt incubated for 30 days. While the lowest biological activity of 60.4% against *S. aureus* was exhibited for extracts deduced from growing on Wickersham liquid media without sea salt incubated for 15 days. On the other hand, the highest biological activity of 100% against *P. aeruginosa* was attained for extracts of *H. rubiginosum* grown on rice media with and without sea salt incubated for 30 days. While the lowest biological activity of 69.6% was obtained after growing the fungus for 15 days on Wickersham broth with sea salt.

Table 4.14: AlamarBlue® bacterial viability assay results of 100µg/mL of *H. rubiginosum* extracts obtained from various media.

Liquid media	% inhibition <i>S. aureus, P. aeruginosa</i>	Solid media	% inhibition <i>S. aureus:P. aeruginosa</i>
Malt extract without sea salt 15 days incubation	83.3%, 83.6%	Rice media without sea salt 15 days incubation	100%, 99.7%
Malt extract without sea salt 30 days incubation	85.3%, 86.4%	Rice media without sea salt 30 days incubation	99.9%, 100%
Malt extract with sea salt 15 days incubation	71.9%, 82.9%	Rice media with sea salt 15 days incubation	100%, 99.6%
Malt extract with sea salt 30 days incubation	84.6%, 83.5%	Rice media with sea salt 30 days incubation	100%, 100%
Wickersham without sea salt 15 days incubation	60.4%, 75.6%	Oat media without sea salt 15 days incubation	99.7%, 98.8%
Wickersham without sea salt 30 days incubation	91.7%, 97.2%	Oat media without sea salt 30 days incubation	100%, 98.8%
Wickersham with sea salt 15 days incubation	77.7%, 69.6%	Oat media with sea salt 15 days incubation	99.9%, 99.2%
Wickersham with sea salt 30 days incubation	80.1%, 96.1%	Oat media with sea salt 30 days incubation	100%, 99%
Marine broth 15 days incubation	71.2%, 76.7%		
Marine broth 30 days incubation	75.9%, 91.3%		

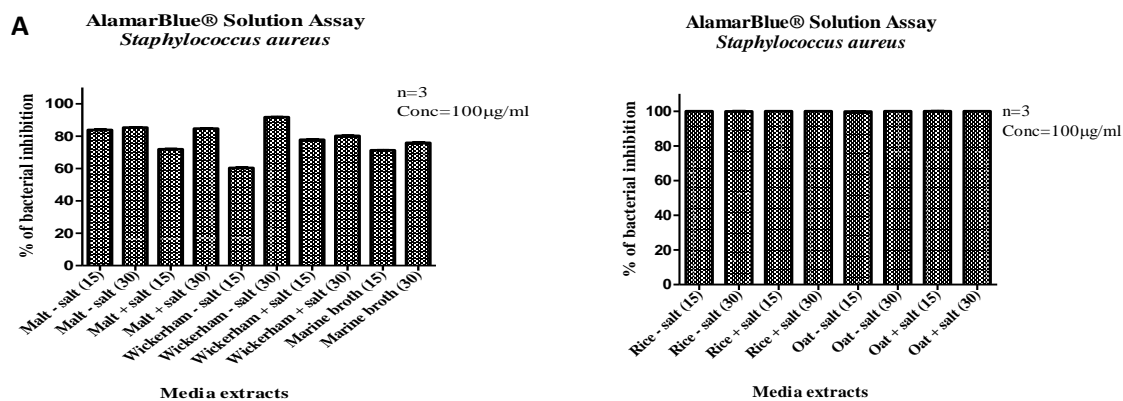


Figure 4.48: Percentage bacterial inhibition of biofilm-forming *S. aureus* with 100µg/mL of *H. rubiginosum* extracts obtained from various **A**: liquid and **B**: solid media.

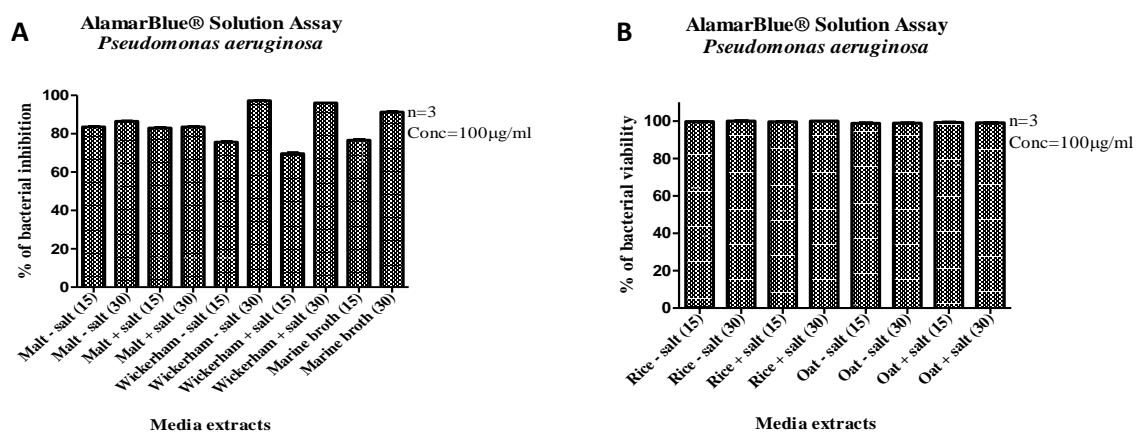


Figure 4.49: Percentage bacterial inhibition of biofilm-forming *P. aeruginosa* with 100µg/mL *H. rubiginosum* extracts obtained from various **A**: liquid and **B**: solid media.

4.3.3.2 Planktonic Assay of the *H. rubiginosum* extracts

The planktonic assay results are presented in Table 4.15 as well as Figures 4.50 and 4.51. Again all *H. rubiginosum* extracts were found to inhibit biofilm formation by at least 50%. Fungal extracts prepared from solid media exhibited higher biological activity with over 95% inhibition. On the other hand, the biological activity of fungal extracts from the liquid media inhibited biofilms formation between 56.8-88.1%. The highest biological activity of 96.5% inhibition against *S. aureus* was obtained after growing the fungus for 15 days on rice media with and without sea salt, on rice media with sea salt incubated for 30 days, and on oat media both with and without sea salt incubated for 30 days. The lowest biological activity of 56.8% inhibition was observed from extracts obtained from the fungus incubated for 15 days on Wickerham broth without sea salt. Additionally, the highest biological activity against biofilm formation by *P. aeruginosa* was 94.9%, that was demonstrated by the fungal extract prepared

from rice media with sea salt incubated for 30 days. The lowest biological activity of 65.6% against biofilms formation was shown by the fungal extract obtained after growing *H. rubiginosum* on Wickersham liquid media with sea salt incubated for 15 days.

Table 4.15: Planktonic biofilm viability assay results of 100µg/mL of *H. rubiginosum* extracts obtained from various media.

Liquid media	% inhibition <i>S. aureus, P. aeruginosa</i>	Solid media	% inhibition <i>S. aureus:P. aeruginosa</i>
Malt extract without sea salt 15 days incubation	80.3%, 79.1%	Rice media without sea salt 15 days incubation	96.5%, 94.5%
Malt extract without sea salt 30 days incubation	81.7%, 81.8%	Rice media without sea salt 30 days incubation	96.3%, 94.8%
Malt extract with sea salt 15 days incubation	68.3%, 78.5%	Rice media with sea salt 15 days incubation	96.5%, 94.5%
Malt extract with sea salt 30 days incubation	81%, 79%	Rice media with sea salt 30 days incubation	96.5%, 94.9%
Wickersham without sea salt 15 days incubation	56.8%, 71.4%	Oat media without sea salt 15 days incubation	96.2%, 93.7%
Wickersham without sea salt 30 days incubation	88.1%, 92.2%	Oat media without sea salt 30 days incubation	96.5%, 93.7%
Wickersham with sea salt 15 days incubation	74.2%, 65.6%	Oat media with sea salt 15 days incubation	96.4%, 94.1%
Wickersham with sea salt 30 days incubation	76.6%, 91%	Oat media with sea salt 30 days incubation	96.5%, 93.9%
Marine broth 15 days incubation	67.7%, 72.4%		
Marine broth 30 days incubation	72.3%, 86.5%		

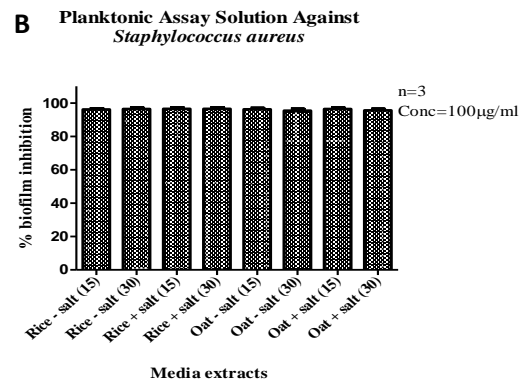
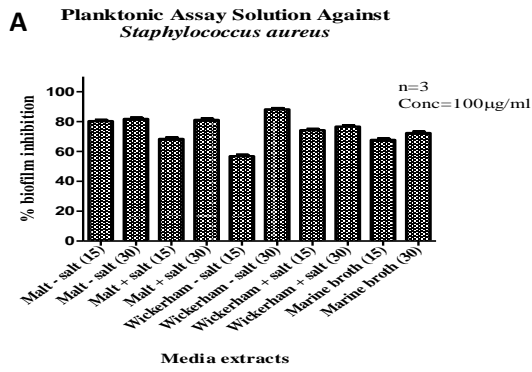


Figure 4.50: Percentage biofilm inhibition of biofilm-forming *S. aureus* with 100µg/mL of *H. rubiginosum* extracts obtained from various **A:** liquid and **B:** solid media.

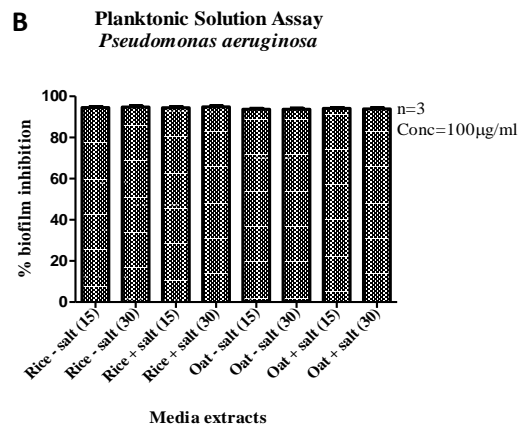
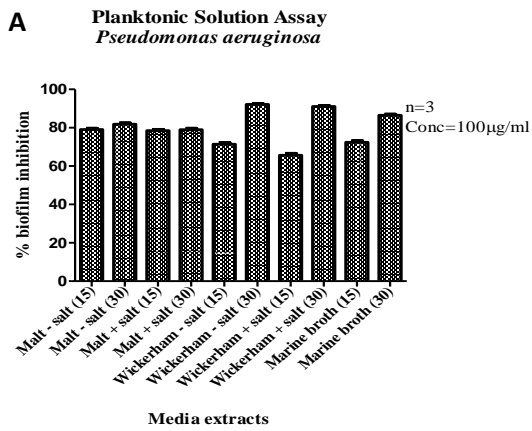


Figure 4.51: Percentage bacterial inhibition of biofilm-forming *P. aeruginosa* with 100µg/mL *H. rubiginosum* extracts obtained from various **A:** liquid and **B:** solid media.

4.3.3.3 Minimum inhibitory concentration (MIC) and Minimum biofilm eradication concentration (MBEC) assays.

Biologically active *H. rubiginosum* extracts prepared from rice and oat media were further assayed to determine their MIC and MBEC values. It was found that the lowest MIC values of 19.4 and 18.5 µg/mL against both biofilm-forming *S. aureus* and *P. aeruginosa*, respectively, were obtained from *H. rubiginosum* grown for 30 days on rice media without sea salt. MIC results are shown in Table 4.16 and Figure 4.52 and 4.53. The highest MIC values of 31.3 and 32.6 µg/mL against biofilm-forming *S. aureus* and *P. aeruginosa*, respectively, were exhibited by extracts deduced from the fungus grown for 15 days on oat media, both with and without sea salt.

Table 4.16: MIC values of antibacterial *H. rubiginosum* extracts against *S. aureus* and *P. aeruginosa*.

Media	MIC µg/mL against <i>S.</i>	MIC µg/mL against <i>P.</i>
	<i>aureus</i>	<i>aeruginosa</i>
Rice without sea salt 15 days	22.3	27.4
Rice without sea salt 30 days	19.4	18.5
Rice with sea salt 15 days	25.5	29.8
Rice with sea salt 30 days	27.0	27.7
Oat media without sea salt 15 days	27.5	32.6
Oat media without sea salt 30 days	19.8	30.6
Oat media with sea salt 15 days	31.3	24.5
Oat media with sea salt 30 days	21.2	23.2

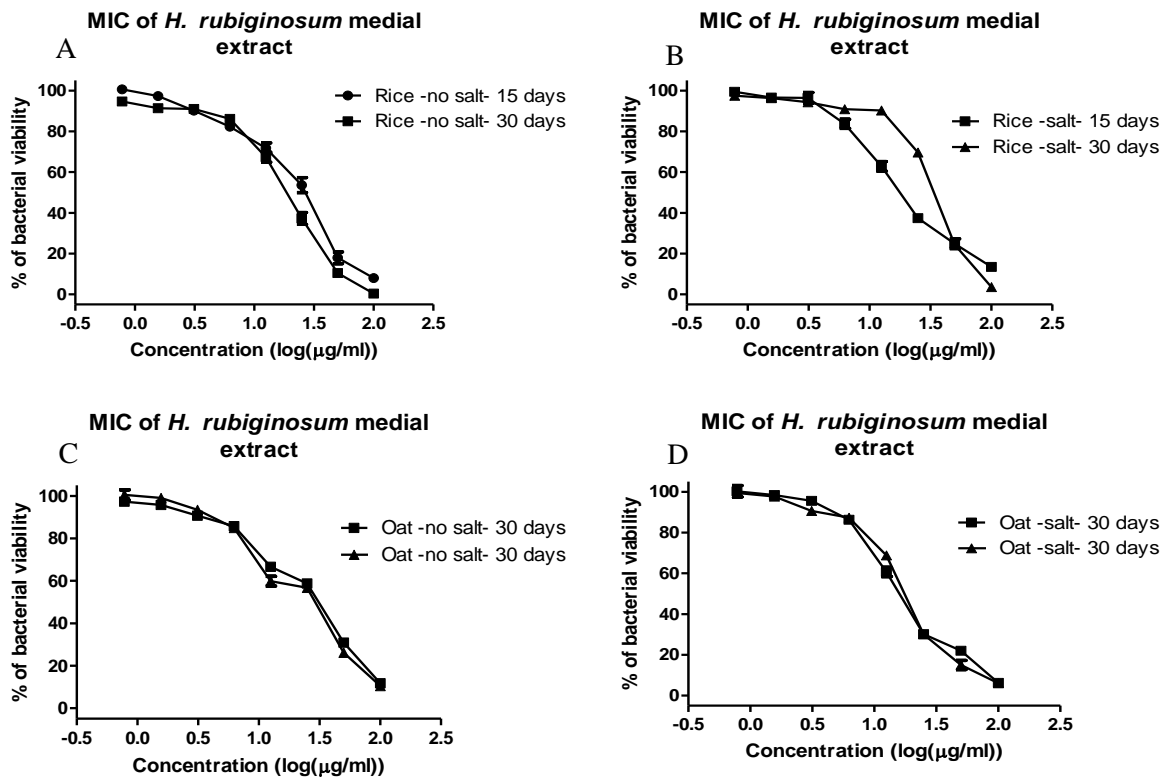


Figure 4.52: MIC results of antibacterial *H. rubiginosum* extracts against *S. aureus*. A: MIC of *H. rubiginosum* growing rice media without sea salt, B: MIC of *H. rubiginosum* growing on rice media with sea salt, C: MIC of *H. rubiginosum* growing on oat extracts without sea salt, and D: MIC of *H. rubiginosum* growing on oat extracts with sea salt.

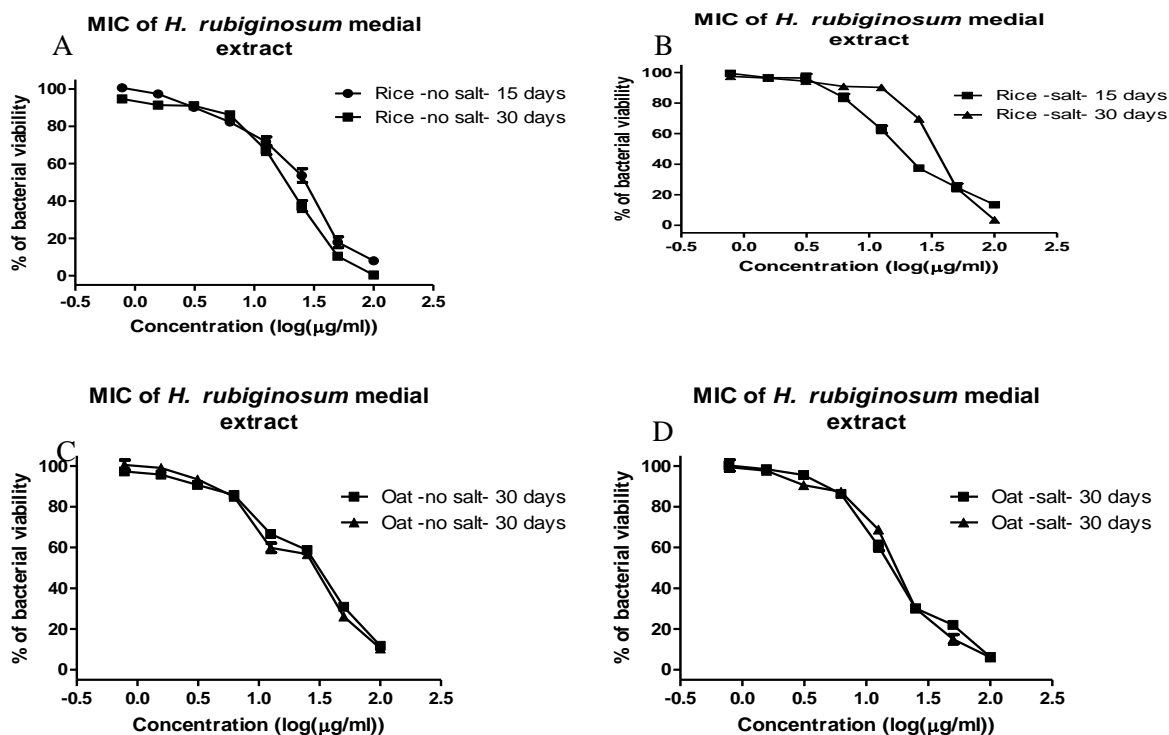


Figure 4.53: MIC results of antibacterial *H. rubiginosum* extracts against *P. aeruginosa*. A: MIC of *H. rubiginosum* growing rice media without sea salt, B: MIC of *H. rubiginosum* growing on rice media with sea salt, C: MIC of *H. rubiginosum* growing on oat extracts without sea salt, and D: MIC of *H. rubiginosum* growing on oat extracts with sea salt.

The MBEC results are presented in Table 4.17 and Figures 4.54 and 4.55. *H. rubiginosum* extracts prepared from rice media without sea salt incubated for 30 days exhibited the lowest MBEC value of 23.3µg/mL against biofilm-forming *S. aureus*. The lowest MBEC value of 26.1µg/mL against *P. aeruginosa* was shown by the extract obtained from the oat media with sea salt incubated for 30 days. On the other hand, the highest MBEC values of 34.5 and 34.4µg/mL against biofilm-forming *S. aureus* and *P. aeruginosa*, were demonstrated by extracts obtained from *H. rubiginosum* grown on oat media with sea salt for 30 days and on oat media without sea salt 15 days, respectively.

Table 4.17: MBEC of antibacterial *H. rubiginosum* extracts against *S. aureus* and *P. aeruginosa*.

Media	MBEC $\mu\text{g/mL}$ against <i>S. aureus</i>	MBEC $\mu\text{g/mL}$ against <i>P. aeruginosa</i>
Rice without sea salt 15 days	28.0	28.6
Rice without sea salt 30 days	23.3	26.8
Rice with sea salt 15 days	28.7	31.1
Rice with sea salt 30 days	24.8	31.4
Oat media without sea salt 15 days	29.1	34.4
Oat media without sea salt 30 days	23.9	29.0
Oat media with sea salt 15 days	26.7	29.0
Oat media with sea salt 30 days	34.5	26.1

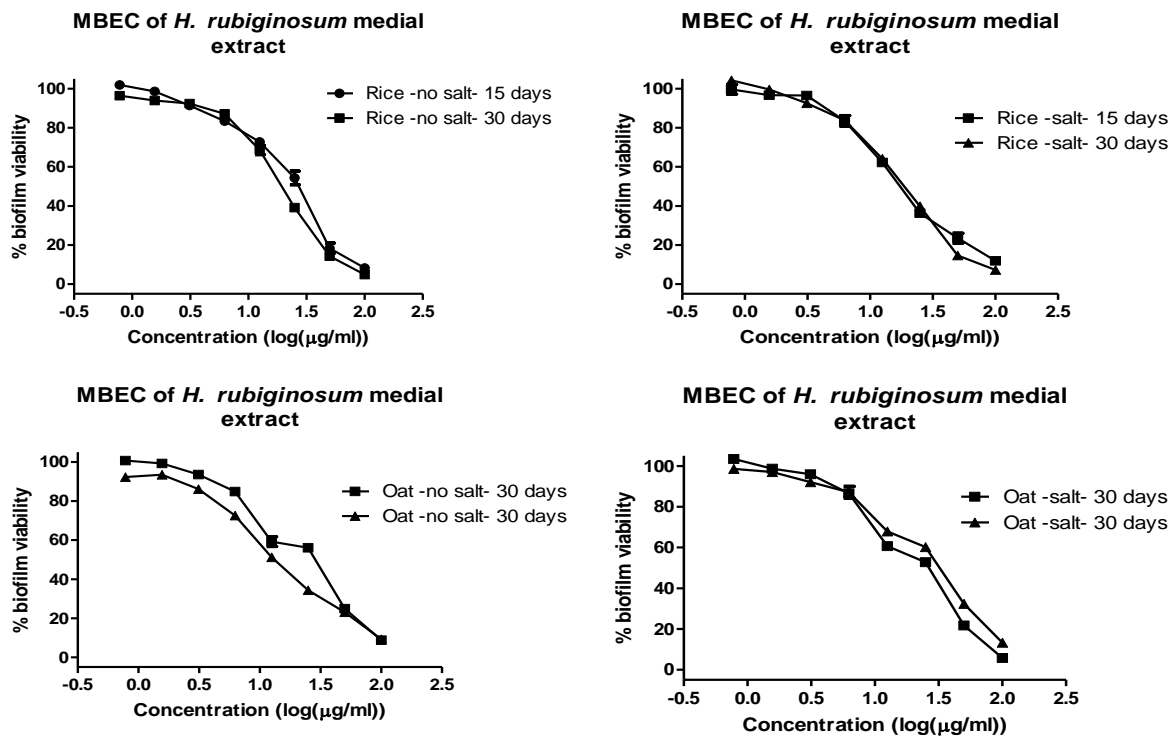


Figure 4.54: MBEC results obtained from antibacterial *H. rubiginosum* extracts against *S. aureus* by planktonic assay. A: MIC of *H. rubiginosum* growing rice media without sea salt, B: MIC of *H. rubiginosum* growing on rice media with sea salt, C: MIC of *H. rubiginosum* growing on oat extracts without sea salt, and D: MIC of *H. rubiginosum* growing on oat extracts with sea salt.

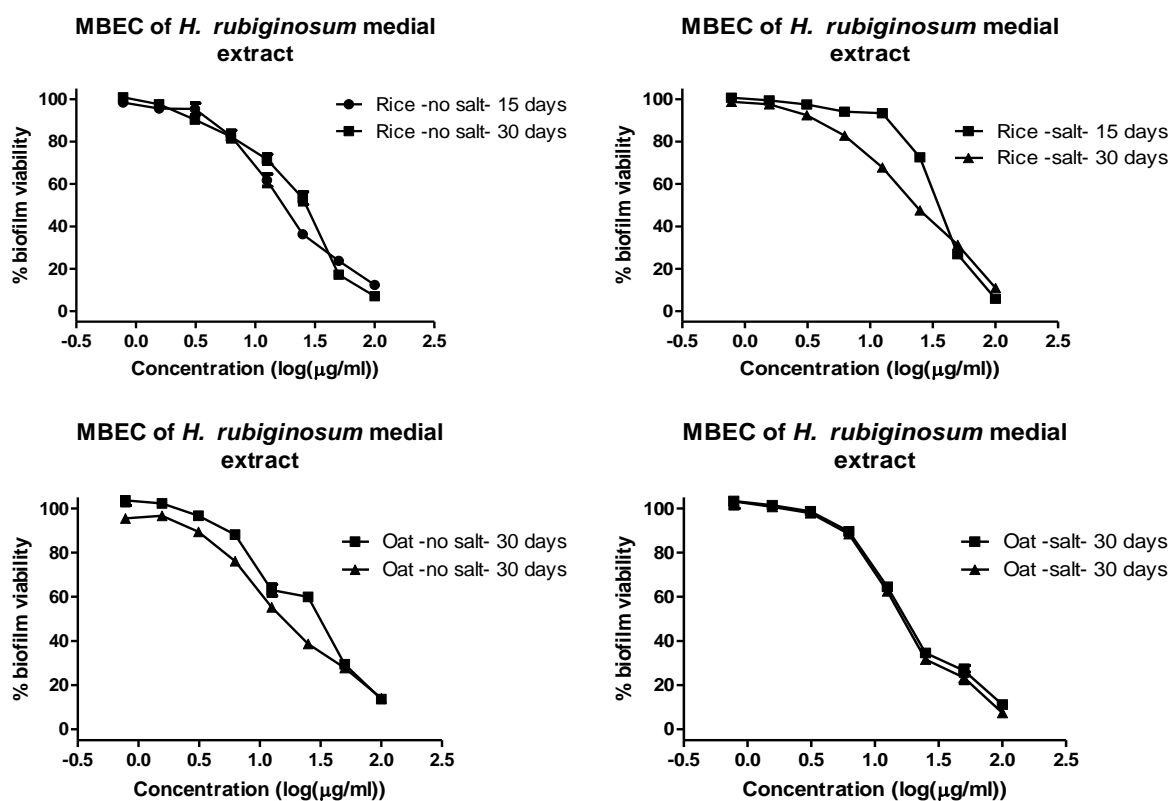


Figure 4.55: MBEC results obtained from antibacterial *H. rubiginosum* extracts against *P. aeruginosa*. A: MIC of *H. rubiginosum* growing rice media without sea salt, B: MIC of *H. rubiginosum* growing on rice media with sea salt, C: MIC of *H. rubiginosum* growing on oat extracts without sea salt, and D: MIC of *H. rubiginosum* growing on oat extracts with sea salt.

4.3.4 Multivariate analysis of NMR data

The PCA scatter plot of the proton NMR spectral data of *H. rubiginosum* extracts is presented in Figure 4.56. Extracts obtained from the solid media (encircled **blue**) were mainly positioned on upper left quadrant of the scatter plot. The nearness in collocation of the sample extracts to each other could imply a relatively more comparable chemical profile. On the other hand, extracts obtained from the liquid media were more widely distributed on both the upper and lower right quadrants along with the extracts obtained from Wickersham, malt extract and marine broth media incubated for 15days at the lower left quadrant. While liquid broth media incubated for 30 days distributed widely at the upper right quadrant. The more dispersed distribution of the extracts from the various liquid media indicated quite a variation in their chemical profiles. However, extracts obtained from the 15-day incubation period (encircled **red**) at the lower right quadrant were separated to those incubated for a 30-day period (encircled **orange**) found at the upper right quadrant. The separation of these two groups

according to their incubation periods indicate a comparable change in chemical profile of the extracts from various media between the growth phases, particularly from the end of the logarithmic phase to the stationary phase. The model gave R^2X and Q^2X values of 1.00 and 0.99, respectively, which indicated a strong model.

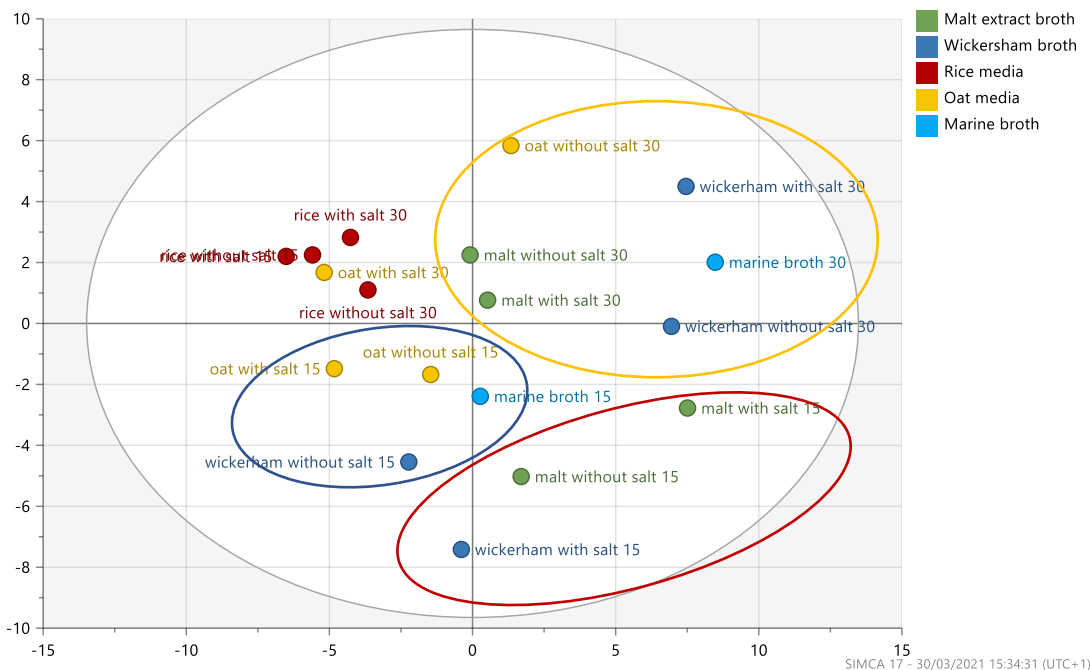


Figure 4.56: PCA scatter plot of proton NMR spectral data of *H. rubiginosum* extracts obtained from various media incubated for 15 and 30 days.

The OPLS-DA scatter plot of the proton NMR spectral data of *H. rubiginosum* extracts were classified according to their antimicrobial activity and is presented in Figure 4.59A. The antimicrobial active extracts were positioned on the left side of the plot, while the inactive extracts were placed on the right side of the plot. Extracts afforded by oat media without sea salt, Wickersham without sea salt and marine broth, which were all incubated for 30 days, implied to have a relatively different chemical profiles from the other active extracts (Figure 4.57A). The OPLS-DA loadings plot (Figure 4.57B), parallelly indicated the unique occurrence of peaks for acylated (2 to 3 ppm) compounds, while there was also the presence of peaks for hydroxylated compounds (3 to 5 ppm)

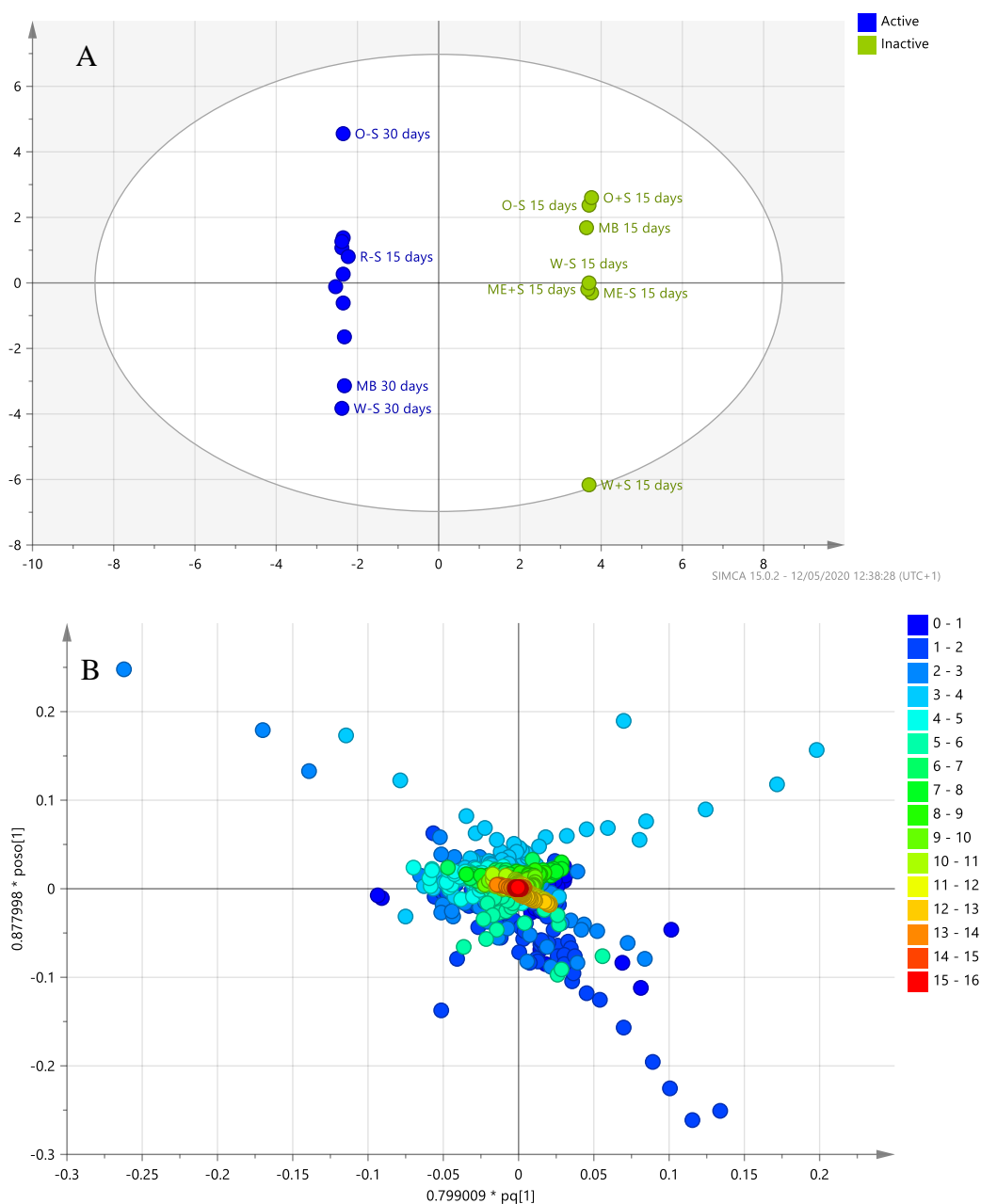


Figure 4.57: OPLS-DA scatter (A) and loadings (B) plots of the ^1H NMR spectral data of *H. rubiginosum* extracts obtained from various media incubated at 15 and 30 days. Extracts were grouped according to their antimicrobial activity against both biofilm-forming *S. aureus* and *P. aeruginosa*.

4.3.5 Multivariate analysis of LC-HRMS data

The PCA scatter plot of the LC-HRMS data of *H. rubiginosum* extracts are presented in Figure 4.60. Extracts accumulated near the centre of the plot while most of the extracts were overlapping on the upper left quadrant indicating a very close similarity of their chemical profiles. Extracts from *H. rubiginosum* grown on rice in general were separated from the cluster

along with extracts obtained from oat media with and without salt, both incubated for 30 days and Wickersham media with salt incubated for 15 days. The extracts obtained from rice media without salt and oat with salt, both incubated for 30 days were indicated as outliers. Dispersion of these latter extracts from the closely accrued cluster signified variations in their chemical profiles. The values of R^2X and Q^2X were 1.00 and 0.99, which indicated a strong model.

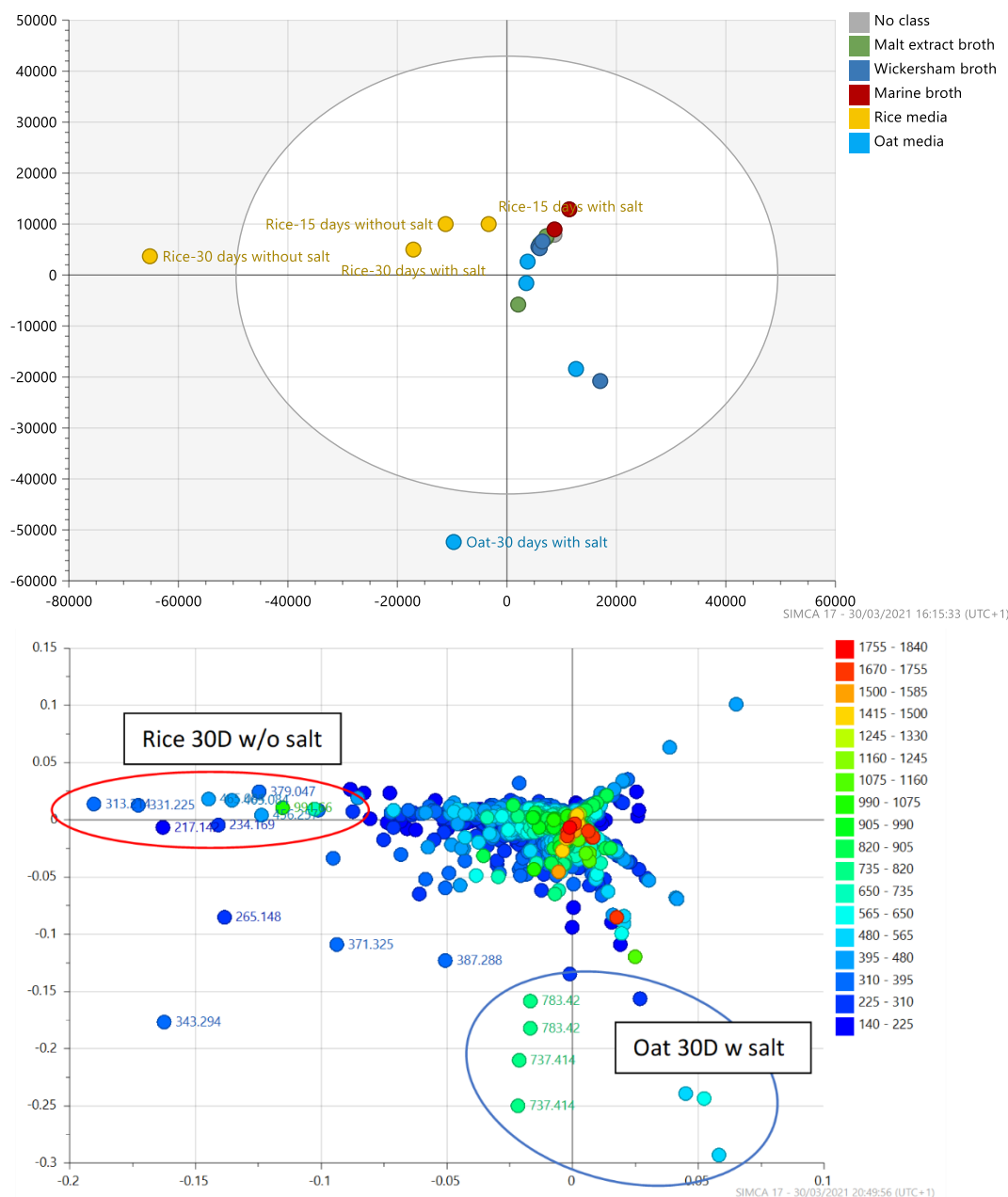


Figure 4.58: (A) PCA scatter and (B) loading plots of the LC-HRMS data of *H. rubiginosum* extracts obtained from various media incubated for 15 and 30 days. For OPLS-DA, the extracts were classified into two groups according to their antimicrobial activity. The OPLS-DA scatter plot is presented in Figure 4.59. The active fungal extract prepared from the rice media without sea salt incubated for 30 days was established as a

strong outlier indicating the occurrence of possible unique bioactive metabolites not found in the other extracts.

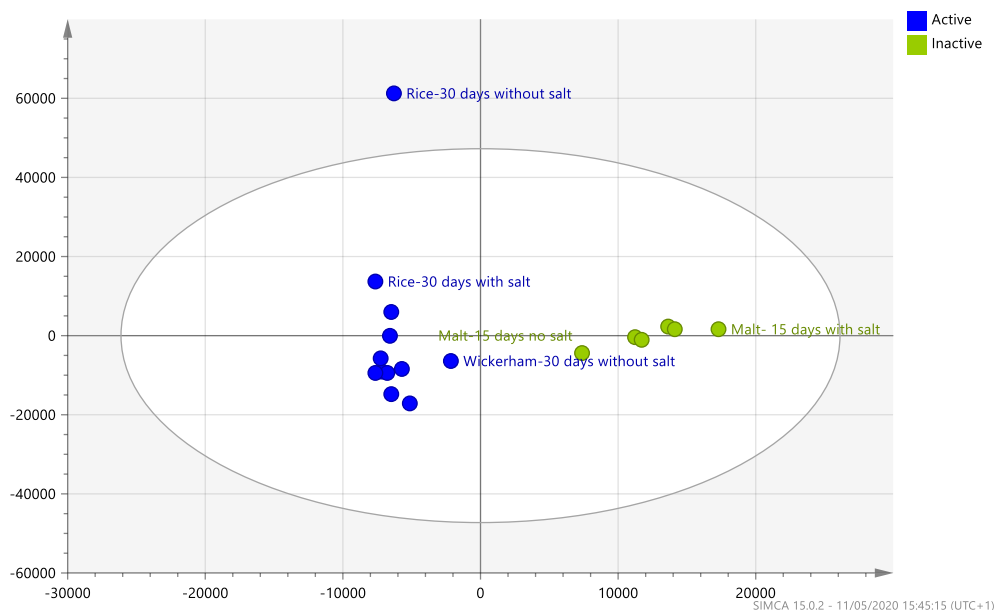


Figure 4.59: OPLS-DA scatter plot of LC-HRMS data of *H. rubiginosum* extracts obtained from various media incubated at 15 and 30 days. Extracts were grouped according to their antimicrobial activity against both biofilm-forming *S. aureus* and *P. aeruginosa*.

In parallel, the OPLS-DA loadings plot (Figure 4.60) revealed the possible types discriminating bioactive metabolites with ion peaks ranging between m/z 100 and 500 Da (encircled in **red**) afforded by *H. rubiginosum* extracts obtained from the rice media incubated for 30 days. Other active extracts also yielded higher molecular weight compounds with ion peaks at m/z 500 to 800 Da (encircled in **blue**). The encircled features or ion peaks were dereplicated using the DNP database. While eleven of the ion peaks remained unidentified, the putatively identified compound hits are listed in Table 4.18 and the structures are shown in Figure 4.61. discriminating features with molecular weight higher than 380 Da show DBE values indicated the presence of aromatic systems resonating between 6.00-9.00ppm with few olefinic signals between 5.00-5.50ppm this was confirmed by the distribution of chemical shift on the OPLS-DS loading plot of the NMR data in figure 4.57 B. While discriminating features with molecular weight of less than 380 Da showed lower DBE values. This is due to the presence of low aromatic systems and high olefinic systems. The OPLS-DA loading plot confirmed this by the presence of high number of olefinic signals resonating between 5.00-5.50ppm especially for those features found in rice extract. This can be also confirmed by the OPLS-DA loadings

plot of the NMR data presented in figure 4.57. which have many peaks between 4.50 and 9.00 ppm.

When comparing loading plots produced from PCA-X and OPLS-DA of the HRMS data of media extracts, the discriminating features were comparable as shown in Figures 4.57 and 4.59. the FDR values of all discriminating features were less than 0.05 except for compound with Var ID of P-51. This indicated a high true possibility of these compounds.

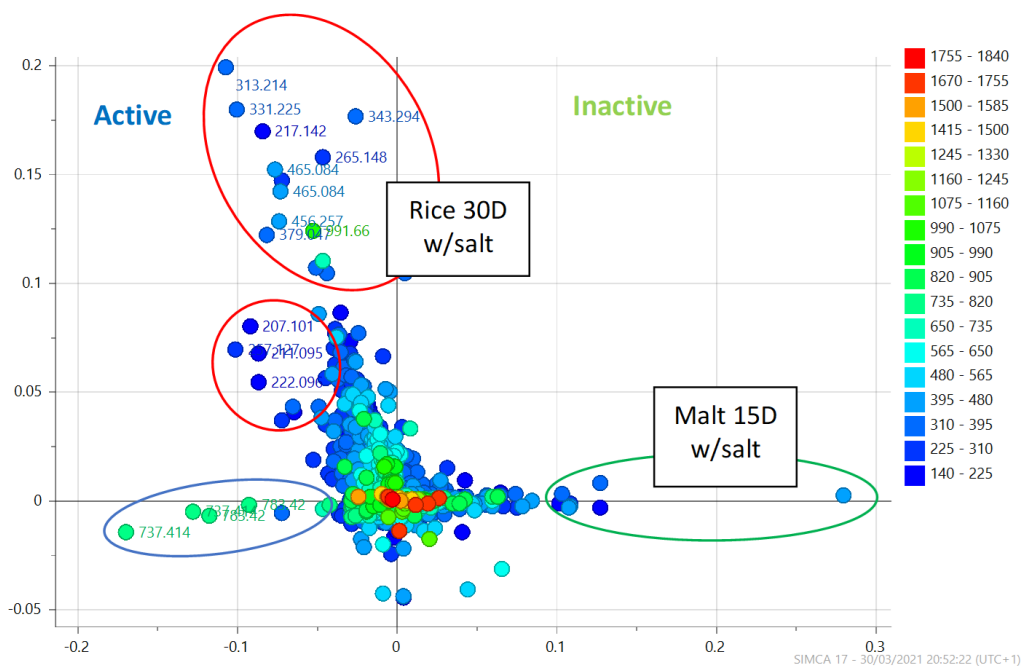


Figure 4.60: OPLS-DA loadings plot of LC-HRMS data of *H. rubiginosum* extracts obtained from various media incubated at 15 and 30 days. Extracts were grouped according to their antimicrobial activity against both biofilms forming *S. aureus* and *P.aeruginosa*.

Table 4.18: Dereplication of six target bioactive metabolites found in active extracts, with P values < 0.05 as obtained from the OPLS-DA S-plot.

Var ID	p-value	FDR	Molecular weight	Chemical formula prediction (DBE)	Compound hits from DNP and biological source
P-50	0.0380602	0.030	216.1351	C ₁₂ H ₁₂ N ₂ O ₂ (8)	No hit
P-51	0.0481968	0.0525	233.1615	C ₉ H ₁₉ N ₃ O ₄ (2)	No hit
N-19	0.0412259	0.0425	266.1557	C ₁₄ H ₂₂ N ₂ O ₃ (5)	2,4,6-trimethyl-1-nonanol; O-sulfate <i>Cucumaria frondosa</i>
N-29	0.0208731	0.02	310.1819	C ₇ H ₂₂ N ₁₀ O ₄ (2)	No hit
P-246	0.0451656	0.0475	330.2174	C ₁₇ H ₂₆ N ₆ O (8)	No hit
P-36	0.0226657	0.0275	342.2864	C ₁₅ H ₃₄ N ₈ O (3)	No hit
N-785	0.0146765	0.0125	380.0542	C ₂₀ H ₁₂ O ₈ (15)	1-(6-hydroxy-4-oxo-4H-1-pyran-2-yl)-4,5,7-trihydroxy-2-methylanthraquinone from <i>Streptomyces coelicolor</i> and tetracenomycin D3 from <i>Streptomyces olivaceus</i>
N-34	0.0472485	0.045	448.3412	C ₂₅ H ₄₄ N ₄ O ₃ (6)	sarcotride C <i>Sarcotragus</i> sp.
P-60	0.0385393	0.0375	455.2496	-	No hit
P-1136	0.00754829	0.0025	660.4349	C ₃₈ H ₅₆ N ₆ O ₄ (14) C ₃₇ H ₆₀ N ₂ O ₈ (9)	No hit
N-73	0.0209009	0.0225	738.4215	C ₄₁ H ₅₄ N ₈ O ₅ (19) C ₄₅ H ₅₈ N ₂ O ₇ (18)	No hit

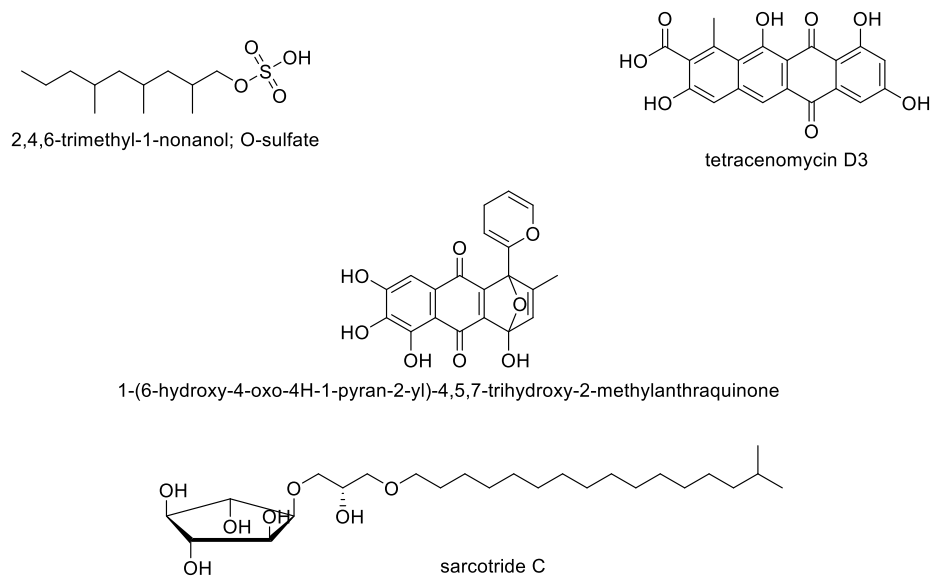


Figure 4.61: Putative structures of dereplicated target bioactive metabolites found in the anti-microbial extracts of *H. rubiginosum*.

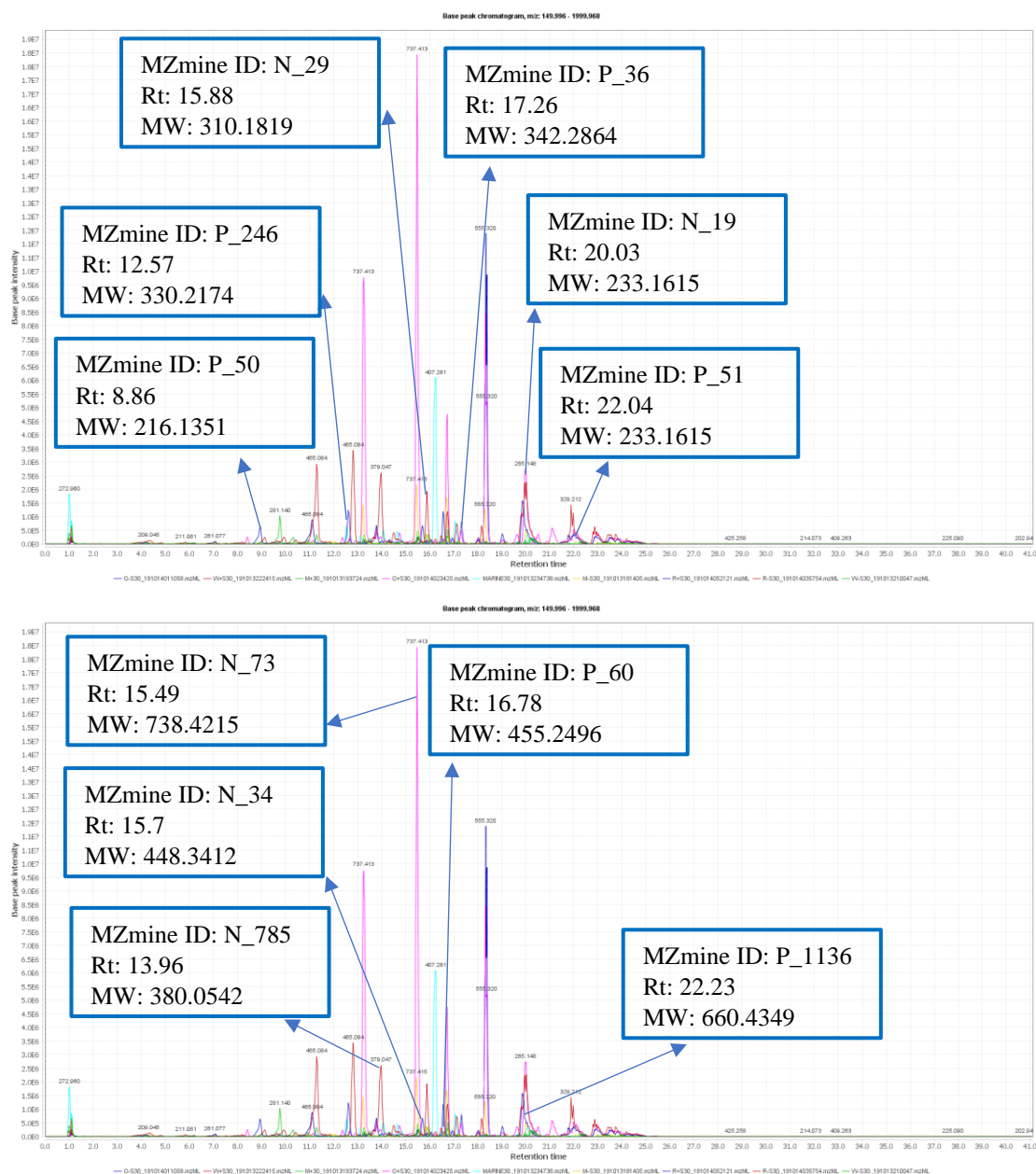


Figure 4.62: Total Ion Chromatogram (TIC) of the active fraction. The ion peaks that represent the discriminating features listed in Table 4.18 have been labelled

4.4 Summary of the media optimisation results for selected fungi

Media optimisation was performed on three anti-microbial endophytic fungi which afforded active fungal extracts against biofilm-forming *S. aureus* and *P. aeruginosa*. Various solid and liquid media were utilised to improve the biomass yield and the potency of the respective fungal extracts. Sea salt was added to the media to mimic the marine environment from where the organisms were primarily collected. However, optimisation was also accomplished with the absence of sea salt for future scale-up that would prevent corrosion on bioreactors. It was then essential to evaluate the effect of the presence or absence of sea salt in the production of the

antimicrobial metabolites. Finally, the active extracts were further bioassayed for their MIC and MBEC values to predict the potency of the extracts. The media used in this study were chosen according to their available nutrients, carbon and/or nitrogen source that could be made accessible to the fungus to survive and biosynthesise a wider range of secondary metabolites.

4.4.1 *Dendryphiella salina* optimisation

A literature review on *D. salina* offered no available information on its chemical profile or biological activity against any specific disease. The only study found on *D. salina* was on carbon consumption of the fungus when grown on malt extract agar media, starch agar, tween agar and urea agar (Clipson and Jennings, 1992). In optimisation of *D. salina* on solid media afforded higher yields of extracts than those inoculated on liquid media.

The limitation associated with analysing the NMR spectral data is its limit of detection and the inability to delete media effects making it difficult to differentiate the spectra of the fungal extract against those of the media blank as reflected by the PCA model. However, OPLS-DA of the LC-HRMS data of *D. salina* extracts revealed the discriminating ion peaks to target the antimicrobial metabolites. Four of these ion peaks at m/z 478.293, 520.34, 1006.67, and 1020.68, did not get any compound hits from the DNP database. Two ion peaks of compounds isolated from marine source at m/z 520.34 and 496.34 were putatively identified as 8,9-dihydroindanomycin, and soraphen A respectively. These two known compounds were earlier described to exhibit antibacterial activity (Naini et al., 2019, Patil et al., 2019). 8,9-dihydroindanomycin is an indonomycin antibiotic related compound with a moderate biological activity against multi-drug resistance *S. aureus* (Lian and Zhang, 2013). While soraphen A has been to exert antifungal activity especially against broad spectrum of yeasts and hyphomycetes strains (Gerth et al., 1994). Inhibition of acetyl CoA carboxylase activity was another biological activity reported for soraphen A (Jump et al., 2011). In addition, soraphen A was described as a broad-spectrum antiviral and potent against hepatitis C virus in nanomolar concentrations (Koutsoudakis et al., 2015).

The oat media without sea salt was chosen to grow *D. salina* for 30 days as it provided a good yield, outlying chemical profile as shown in OPLS-DA scatter plot and antimicrobial activity against biofilm-forming bacteria. The lower MIC of 17.3 and 21.1 $\mu\text{g/ml}$ and the lower MBEC of 19.7 and 19.4 $\mu\text{g/ml}$ against both *S. aureus* and *P. aeruginosa* respectively provided by oat media extract without sea salt incubated for 30 days was the main reason of choosing this oat media extract. For the scale-up, the malt extract broth with sea salt was also chosen to grow *D.*

salina for 30 days as it provided the most potent antimicrobial activity and afforded a different chemical profile to that of *D. salina* grown on oat media.

4.4.2 *Marianna elegance* optimisation

M. elegance has been studied before in 6 previous research articles and several compounds have been isolated from *M. elegance* and their biological activity have been studied (Fabian et al., 2001, Fukuda et al., 2011, Tang et al., 2012, Tani et al., 2013, Hu et al., 2017, Ishiuchi et al., 2020). The chemical compounds recorded to be isolated from *M. elegance* was found to inhibit Thromboxane A₂ with the compound mariannaeapyrone (Fabian et al., 2001). While only mariannamides A was found to exert antimicrobial activity (Ishiuchi et al., 2020). *M. elegance* is a slow-growing fungus that no growth was observed on the 7th day of incubation and required at least 15 days to reach its logarithmic phase. Again, like *D. salina*, the average yield afforded by the solid media is higher than growing the fungus on a liquid media except for those extracts afforded by malt extract broth, which gave a relatively similar yield as those from the solid media.

Albeit, not providing the highest yield but closer to attaining the required yield, the recommended media for a scale up would be malt extract without sea salt for a 30 days incubation period. The NMR spectral data of the extract obtained from the malt extract broth afforded a high density of distinct peaks not found in the blank as well as the occurrence of a lower ratio of fatty acid peaks. The unique spectral data for the extract deduced for the malt extract media was also indicated by the PCA plots. Although, the fungal extract obtained from marine broth incubated for 30 days was a strong outlier, which would indicate a unique chemical profile, extracts afforded by malt extract media with or without sea salt incubated for 30 days, also did show chemical profiles different from most of the other fungal extracts as they were positioned farther out from the two main clusters in the PCA scatter plot.

The most potent antimicrobial activity of 85 to 100% inhibition was exhibited by the extracts afforded by *M. elegance* grown on malt extract broth and oat media with or without sea salt. Due to the higher yield and highly potent antimicrobial activity of the afforded fungal extract, malt extract broth media with sea salt has been chosen to grow *M. elegance* for 30 days mainly because of the simplicity of the provided chemical profile along with the presence of interesting possibly novel bioactive metabolites.

4.4.3 *Hypoxylon rubiginosum* optimisation

Like *M. elegance*, *H. rubiginosum* was also a slow growing fungus that significant growth could be first observed on the 15th day of incubation. Again, like the previous endophytes, the average yield of extracts afforded by the solid media was higher than those grown on liquid media. The highest yield was obtained from the rice media without sea salt and would be recommended to grow *H. rubiginosum* for 30 days.

Multivariate analysis of the NMR spectral data of *H. rubiginosum* extracts did not designate any outlier but did show a clear trend on the change of profile between the incubation periods when the fungus is inoculated on a liquid media. The OPLS-DA loadings plot of the mass spectral data of the extracts indicated 14 discriminating ion peaks. Eleven of these compounds did not give any hit from the DNP database, while three of the ion peaks at m/z 265.14844, 379.04693, and 447.33395 were putatively identified as 2,4,6-trimethyl-1-nonanol; *O*-sulfate, 1-(6-hydroxy-4-oxo-4*H*-1-pyran-2-yl)-4,5,7-trihydroxy-2-methylanthraquinone, or tetracenomyacin D3 and sarcotride C, respectively.

Extracts afforded by *H. rubiginosum* after growing on different media were able to inhibit bacterial growth and biofilm formation of more than 60% and 50%, respectively. Providing an extract with high yield, unique chemical profile, and achieving the most potent antimicrobial activity, rice media without sea salt is the best media to grow *H. rubiginosum* for 30 days.

5 *Dendryphiella salina* scale up and isolation of antimicrobial compounds.

D. salina was chosen for further isolation work, as its extracts afforded the highest yield, which was easiest to work with in terms of chromatographic isolation work and offered the most novelty as to date there no available published literature on its chemical profile or biological activity against any specific disease.

5.1. Literature background on the endophytic fungi *D.salina*

There are twelve species that have been currently listed under the genus *Dendryphiella*, two of them were isolated from marine sources, namely *D. arenaria* and *salina*. Both species have exhibited similar growth response under the abiotic and biotic conditions (dela Cruz et al., 2006). Furthermore, there were no significant differences in the synthesis of degradative enzymes, metabolites (alanine and glutamate, the polyol myo-inositol and the organic acid fumarate as shown under Figure 5.1) or biological activity between the two culture extracts (dela Cruz et al., 2006).

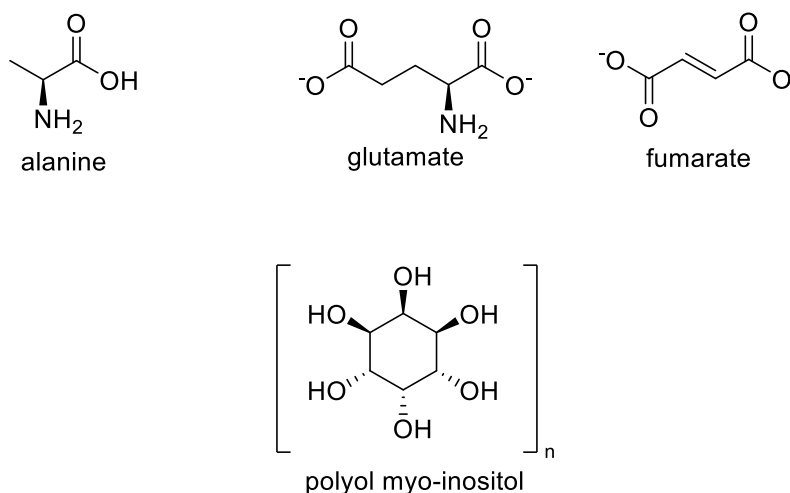


Figure 5.1: Chemical structure of metabolites produced by degradative enzymes in *D. salina* grown on various media.

5.2. *Dendryphiella salina* on Malt Extract Broth Media with Sea Salt

5.2.1 Crude extracts and extract yields

It is well known that marine endophytes produce high concentrations of fatty acids and lipids, which can lead to give a false positive biological activity result due to the nature of those fatty acids (Devi et al., 2006). Indeed, the yield of the crude extract found in n-hexane was 2.6g,

which was 55% of the 4.7g total crude extract. The n-hexane extract was tested against the biofilm-forming *S. aureus* and *P. aeruginosa* and was found to be inactive. The obtained yield for 10% aqueous MeOH extract was 37mg that was 0.74% of the total crude extract and was found to be inactive against the biofilm-forming bacteria. On the other hand, EtOAc extract yield was 2.1g which was 44.7% of the total crude extract. When the EtOAc extract was tested against the biofilm-forming bacteria, it was found to be active and able to inhibit bacterial growth at 86.60 and 95.53 % and biofilm formation at 93.16 and 95.15 % against both biofilm-forming *S. aureus* and *P. aeruginosa* (Table 5.1 and Figure 5.2). EtOAc extract was chosen for further fractionation work to isolate the target bioactive metabolites.

Table 5.1: Antimicrobial assay of liquid-liquid partitioning extracts obtained from *D. salina* grown on malt extract broth media.

Type of extract	% of <i>S. aureus</i> inhibition	% of <i>P. aeruginosa</i> inhibition
AlamarBlue® assay		
n-hexane	3.023	6.27
10% aq MeOH	13.31	15.69
EtOAc	86.60	95.53
Planktonic assay		
n-hexane	3.91	6.18
10% aq MeOH	13.30	12.91
EtOAc	93.16	95.15

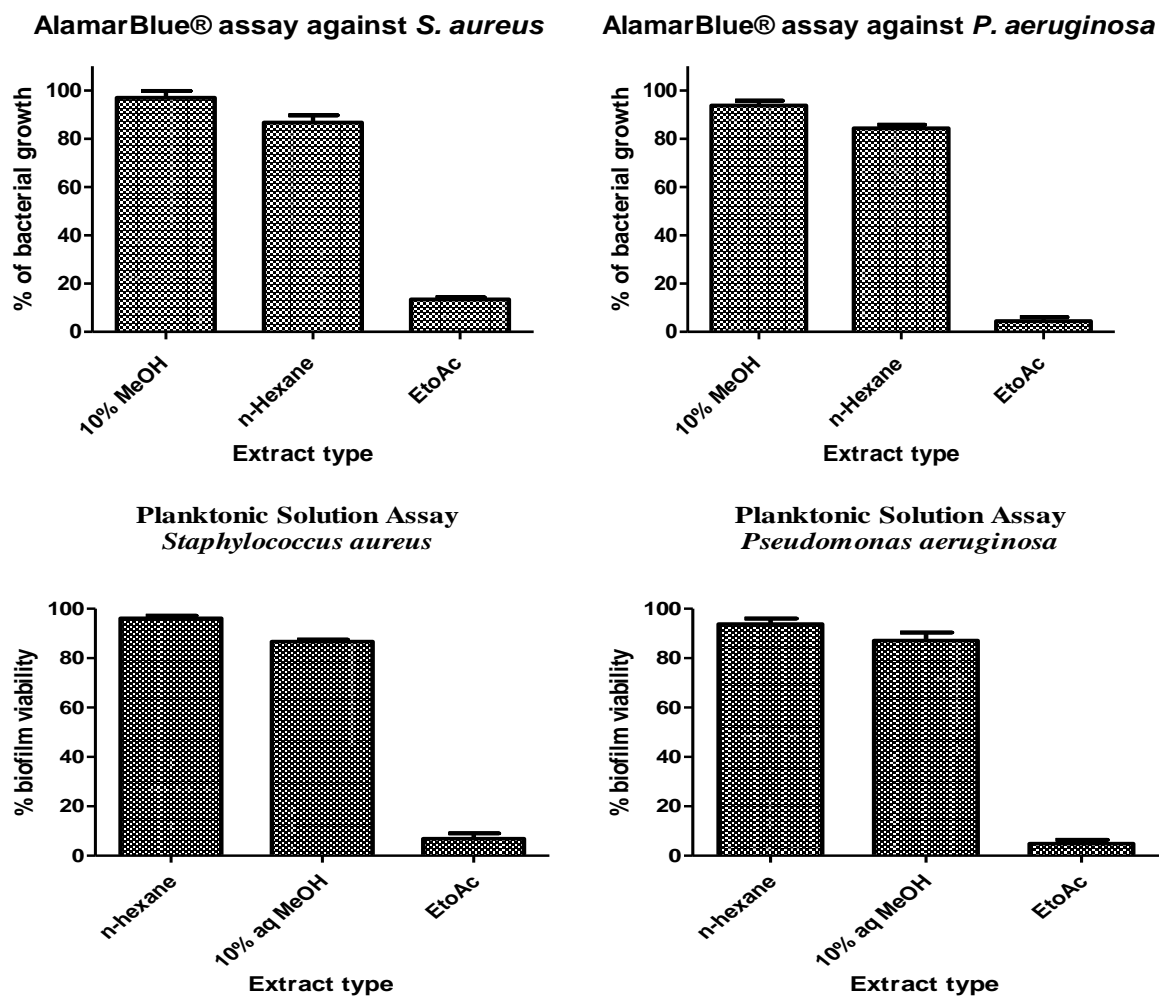


Figure 5.2: Antimicrobial assay of crude fractions from liquid-liquid partitioning of total crude extract of *D. salina* grown on malt extract broth using AlamarBlue® assay and planktonic assay as indicated by the % bacterial growth after treatment with respective extracts shown.

5.2.2 Fractionation of the Extract and Multivariate analysis

The MPLC fractions were collected in Erlenmeyer flasks at volumes 100mL per fraction (Figure 5.3). For monitoring purposes, each fraction was spotted on a TLC plate along with the EtOAc extract sample as reference. As shown in Figure 5.4, the dried sample-loaded TLC plate was developed using a solvent system of 90:10% DCM:MeOH and visualised by spraying with anisaldehyde-H₂SO₄ reagent. Similar fractions in terms of their chromatographic profiles were pooled together resulting to 15 fractions including the washings. The respective fractions were concentrated and dried under *vacuo* then weighed as listed under Table 5.2. The total percentage yield of the collected fractions was 70.1% of the loaded extract weight.



Figure 5.3: MPLC system and flasks used to collect fractions.

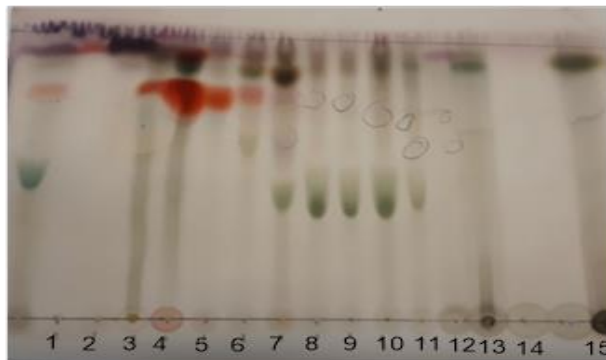


Figure 5.4: Summary TLC plates for the pooled fractions after spraying with anisaldehyde reagent

Table 5.2: Weights of extracts after pooling similar fractions.

Extract No	Weight of extract (mg)	Extract No	Weight of extract (mg)
1	9.6	9	18.2
2	42.2	10	66.6
3	38.2	11	109.1
4	69.1	12	31.6
5	28.0	13	116.9
6	65.6	14	6.4
7	88.8	15	756.2
8	24.8	Total amount	1471.3

5.2.3 Biological assay results of fractions

Fractions 1-7 inhibited bacterial growth and biofilm formation of both *S. aureus* and *P. aeruginosa* at more than 90%. While the rest of the fractions 8-14 showed intermediate or no antimicrobial activity (Table 5.3 and Figure 5.5). For the bioassay, fractions 14 was also pooled together with fraction 15 (washings) due to its low yield and their similar chemical profile on the TLC plate. MIC and MBEC values were not determined for the active fractions to avoid weight loss to have a more manageable quantity for further purification steps.

Table 5.3: AlamarBlue® and planktonic assay results of *D. salina* fractions against biofilm-forming *S. aureus* and *P. aeruginosa*. Highlighted rows represent the bioactive fractions.

<i>S. aureus</i> biological assay results					
Fraction #	% of bacterial viability	% of Biofilms viability	Fraction #	% of bacterial Viability	% of Biofilms viability
1	0.00	0.17	8	46.2	60.7
2	0.88	0.03	9	23.4	26.6
3	0.43	0.75	10	65.5	74.1
4	2.1	0.55	11	86.1	87.1
5	2.0	1.90	12	96.6	101.1
6	0.59	1.88	13	102.2	105.4
7	7.5	4.89	14	95.4	98.1
<i>P. aeruginosa</i> biological assay results					
Fraction #	% of bacterial viability	% of Biofilms viability	Fraction #	% of bacterial Viability	% of Biofilms viability
1	1.02	3.6	8	58.8	75.1
2	0.64	1.5	9	69.0	66.2
3	4.60	10.4	10	68.0	73.3
4	2.2	2.7	11	95.2	100.7
5	4.2	13.1	12	103.8	115.2
6	1.2	1.8	13	106.4	111.1
7	13.8	18.2	14	107.3	102.7

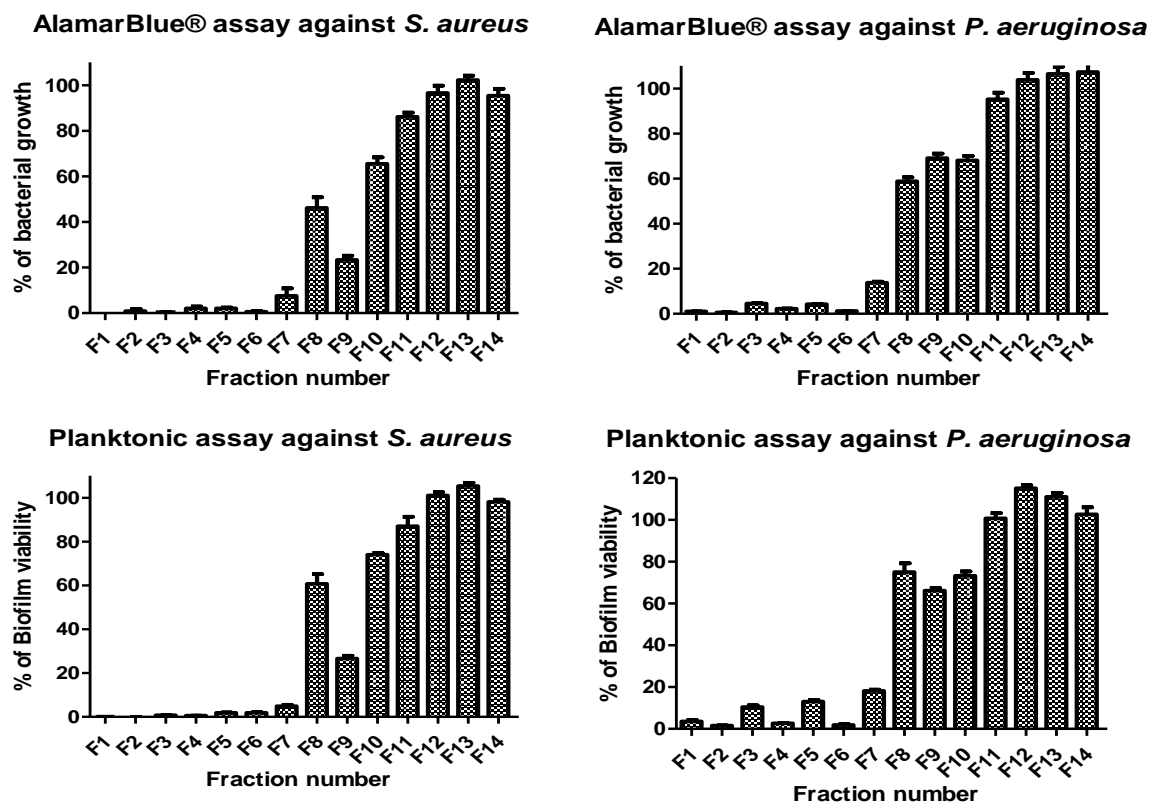


Figure 5.5: AlamarBlue® and planktonic assays of *D. salina* fractions

5.2.4 NMR spectroscopy of *D. salina* fractions

The respective pooled MPLC fractions were subjected to proton NMR measurements to have an overview of the chemical profile and type of compounds expected to be found in each fraction. The ^1H NMR spectra of the fractions were stacked and presented in Figure 5.6.

A high intensity of aliphatic peaks could be observed in the recorded ^1H NMR spectra of the MPLC fractions. Peaks between 6.0 and 9.0 ppm indicated the presence of aromatic compounds. The PCA scatter plot of the spectral NMR data of the MPLC fractions in Figure 5.7 signposted the outlying fraction 2 to have a unique chemical profile. However, when the fractions were tested to see if fraction 2 was a true outlier using DModX fraction 2 gave results of less than 0.05 which indicated that fraction 2 was not a true outlier. As shown by the DModX plot in Figure 5.8, variables above the red line are the true outliers that included Fractions 1, 6, and 13. The proximity of fractions 3 to 12 to each other predicted comparable chemical profiles between fractions. The unique chemical shift provided by fraction 2 is between 1.00-3.00 and 5.00-6.00ppm at aliphatic and olefinic region respectively.

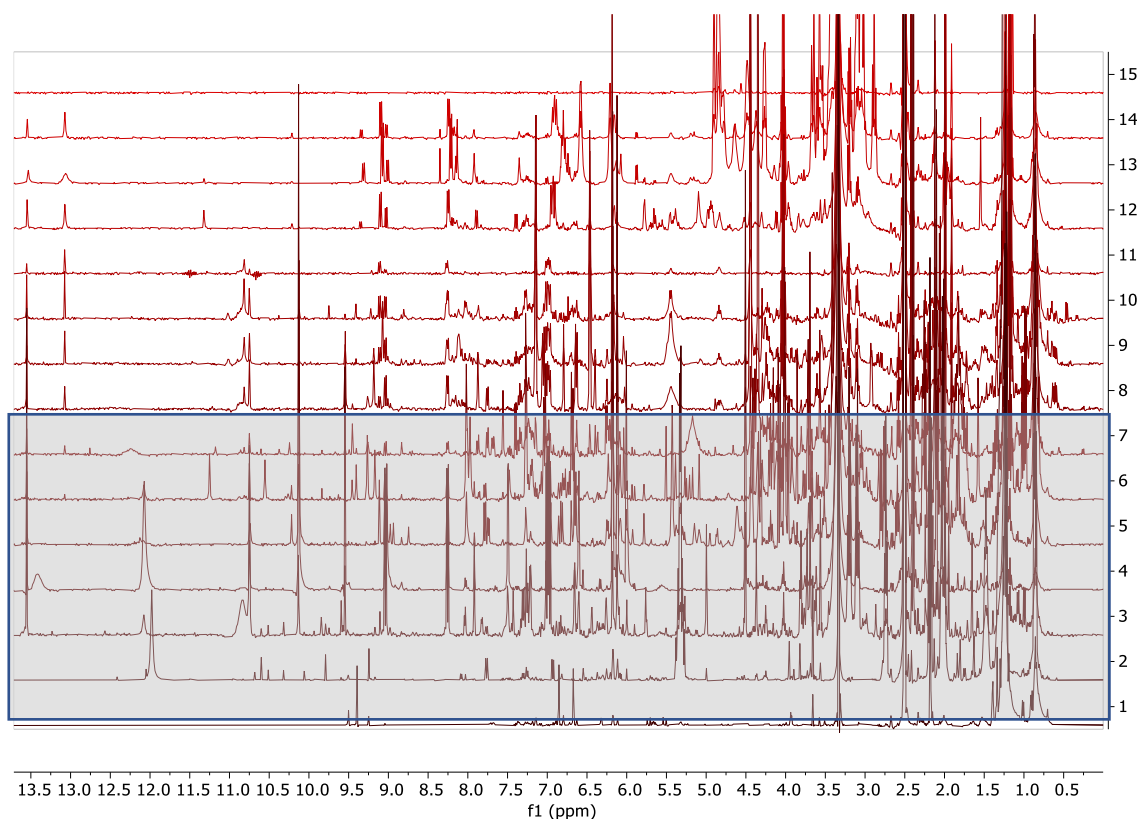


Figure 5.6: Stacked ^1H NMR spectra of 15 MPLC fractions. Highlighted spectra represent the bioactive fractions

However, the OPLS-DA scatter plot presented in Figure 5.9A indicated that the active fractions were more like to each other in terms of their chemical profile as also exhibited by their overlapping features on the corresponding loadings plot in Figure 5.9B. The only fraction that showed some difference was fraction 1, which was positioned slightly farther from the cluster. The OPLS-DA loadings plot displayed a higher ratio of aliphatic peaks (0 to 3 ppm) but a lower ratio of hydroxylated resonances (3 to 6 ppm) in the antimicrobial fractions than in the inactive ones. Aromatic peaks from 6 to 9 ppm seem to similarly occur in both active and inactive fractions

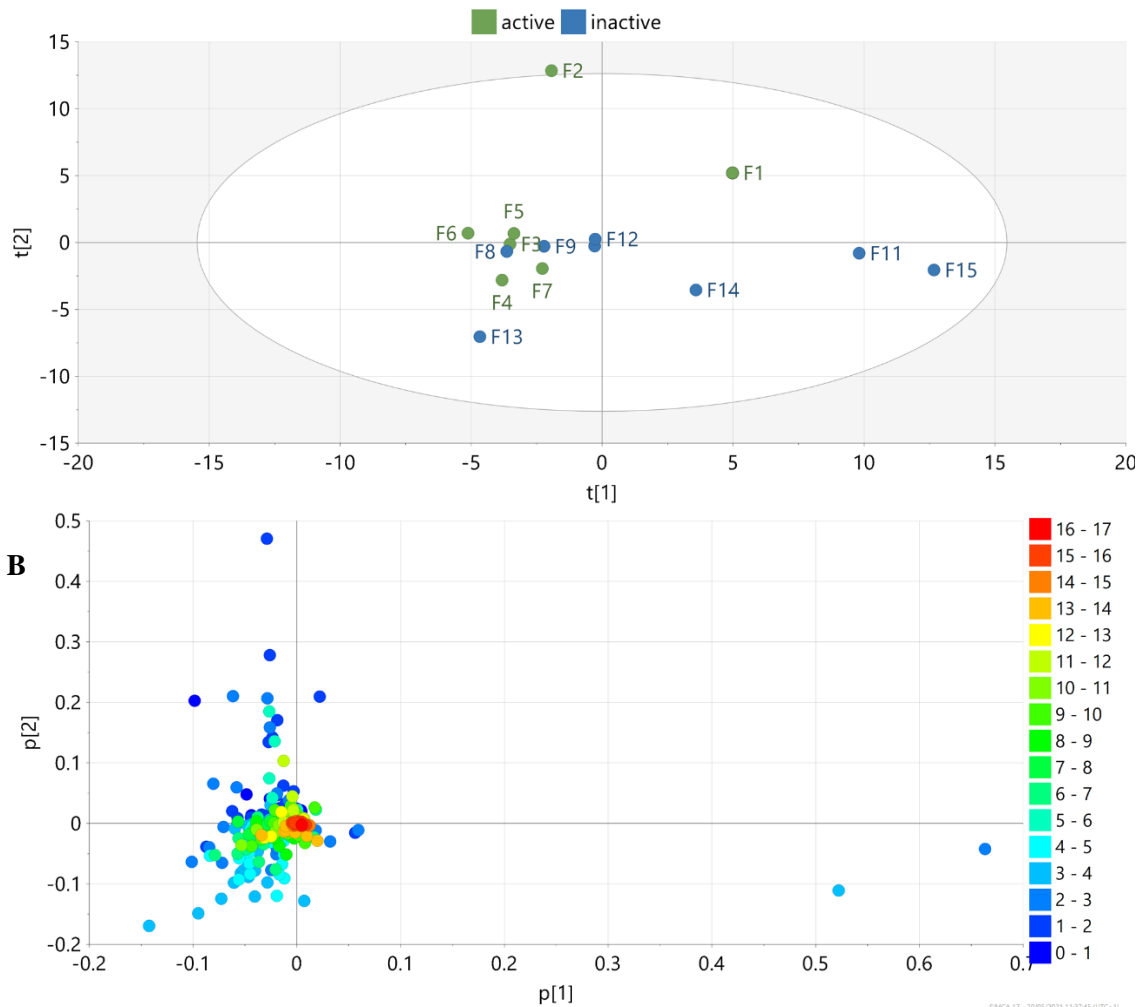


Figure 5.7: (A) PCA scatter and (B) loading plots of the NMR spectral data of the MPLC fractions. The R^2X and Q^2X values were 1.00 and 0.99, respectively.

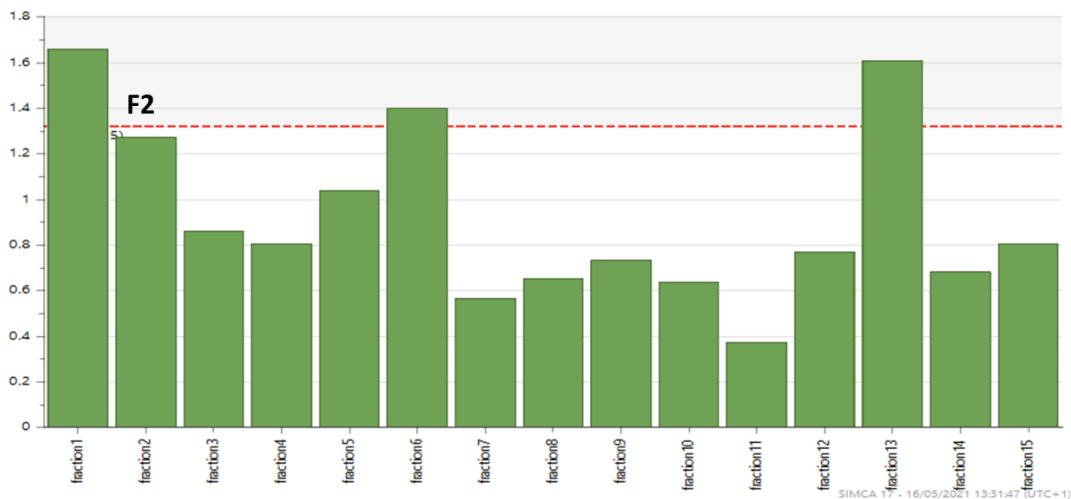


Figure 5.8: DMod X results to test the occurrence of true outliers. Variables above the red line are the true outliers that includes Fractions 1, 6, and 13.

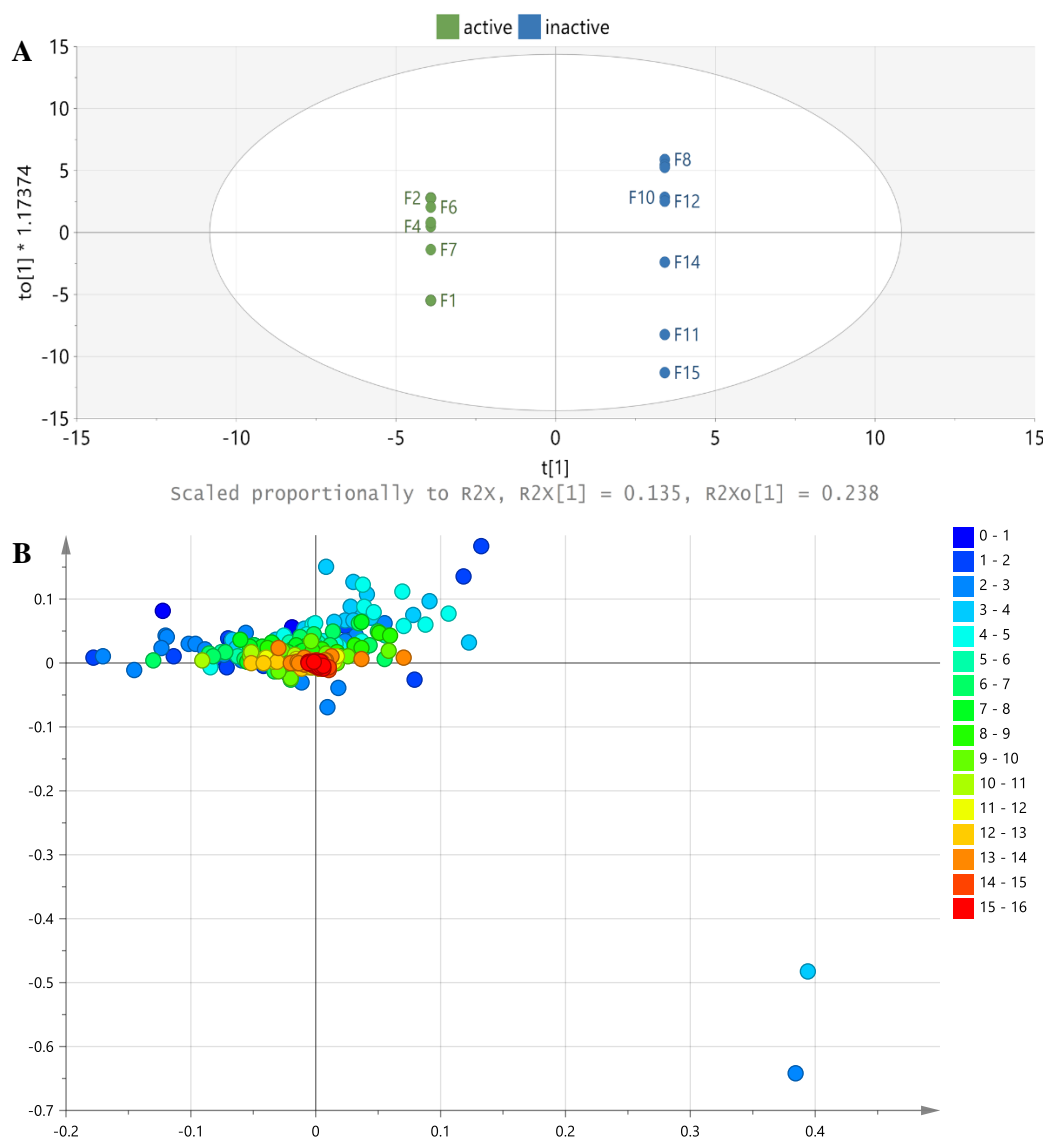


Figure 5.9: OPLS-DA scatter (A) and loadings (B) plots of the NMR spectral data of the MPLC fractions grouped according to their antimicrobial activity against biofilm-forming *S. aureus* and *P. aeruginosa*. R²X and Q²X values were 0.999 and 0.802, respectively. While The difference within group R²Xo is equal to 23% and the difference between groups (R²X[1]) is equal to 13%.

5.2.5 LC-HRMS analysis of *D. salina* MPLC fractions

The PCA scatter plot of the LC-HRMS data of the MPLC fractions in Figure 5.10 showed fractions 11 to 15 overlappingly clustered together that indicated their similar chemical profile. While the rest of the fractions were dispersedly distributed on the scatter plot that exhibited greater diversity between the fractions. In addition, fractions 7-10 show huge similarities with some differences. The fractions could be sub-grouped into three: Fractions 1 to 4 (**blue**), Fractions 5 and 6 (**green**), Fractions 7 to 10 (**yellow**), and Fractions 11 to 15 (**red**). The R²X and Q²X values were quite low at 0.374 and -0.155, respectively, which indicated poor

reproducibility and predictivity. However, the natural groupings of the samples were quite logical as consecutive fractions were classified together albeit the dispersion of the fractions on the scatter plot.

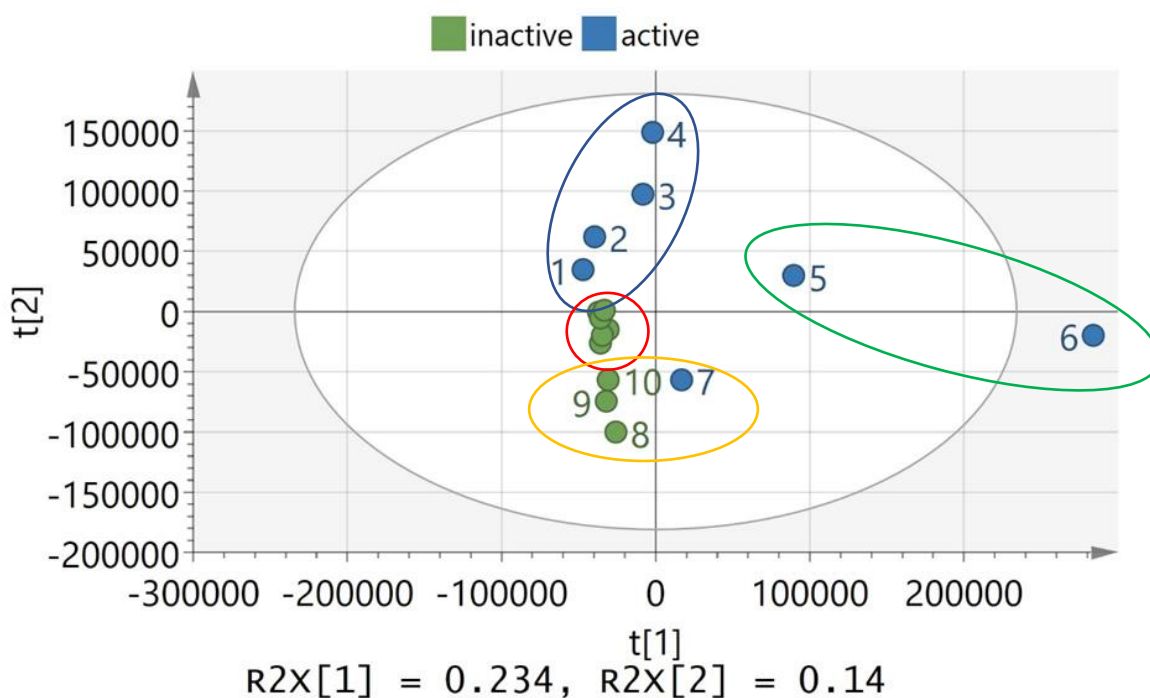


Figure 5.10A: PCA scatter plot of the mass spectral data of the MPLC fractions.

Fraction 6 was displayed as an outlier, which indicated a high possibility of a more unique profile in comparison to the rest of the other fractions. The discriminatory features for Fraction 6 as exhibited by the loadings plot were found at m/z [H⁺] 211.144, 265.107, and 245.128, which were either small peptides or hydroxylated aromatic compounds originating from a polyketide pathway earlier described from various marine-derived microorganisms as shown in Figure 5.10B.

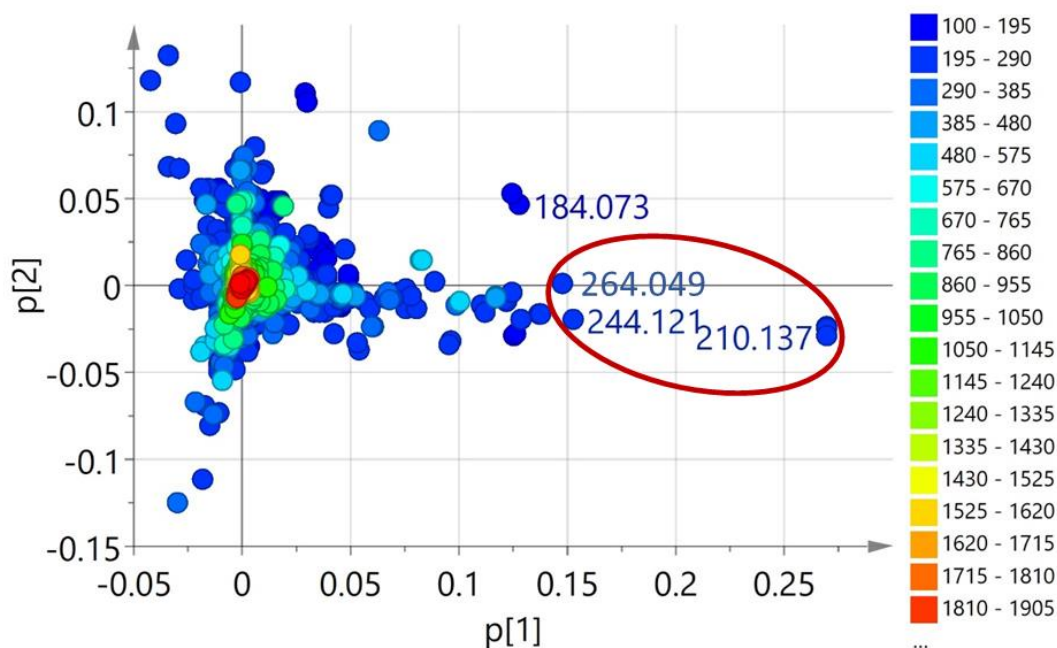
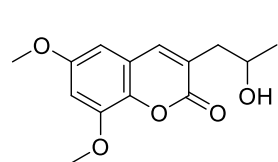


Figure 5.10B: OPLS-DA loadings plot of the mass spectral data of the MPLC fractions. R^2X , R^2Y and Q^2X values are equal to 0.743, 1.00 and 0.759 respectively. Encircled in red are the discriminatory features for the outlying variable Fraction 6, which are listed in the Table below.

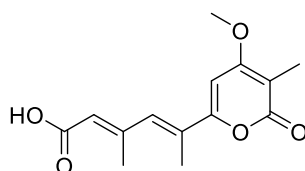
Table 5.4: Discriminatory features for the outlying variable Fraction 6.

Mzmine ID	m/z	RT (min)	MW	MF	Compound hits and sources
P_15251	211.144	7.9	210.137	$C_{11}H_{18}N_2O_2$	cyclo(isoleucylprolyl) from various marine-derived fungi
P_2201	265.107	13.4	264.099	$C_{14}H_{16}O_5$	99 hits, 6 marine-derived*
P_9403	245.128	9.0	244.121	$C_{14}H_{16}N_2O_2$	cyclo(phenylalanylprolyl) from marine-derived bacteria

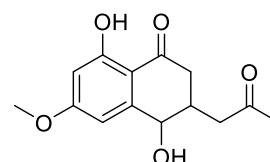
*The 6 marine-derived compounds included: pestalasin A from a mangrove-derived *Pestalotiopsis* sp. JCM2A4 and *Penicillium purpurogenum* MHZ 11; infectopyrone and oxosorbicillinol from various fungi; scytalol D from *Scytalidium* sp. 36-93 and *Biatriospora* sp. 8331; epoxysorbicillinol from sponge-derived *Trichoderma longibrachiatum*; and xestodecalactone A from *Penicillium cf. montanense*.



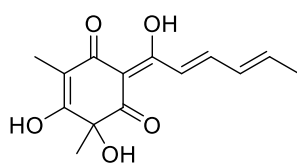
pestalasin A



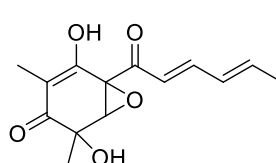
infectopyrone



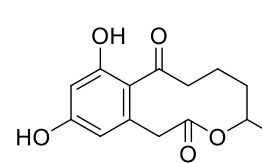
scytalol D



oxosorbicillinol



epoxysorbicillinol



xestodecalactone A

The different outliers indicated by the ^1H NMR and mass spectral data could be due to the sensitivity of the instruments to detect the various metabolites in the fractions. MS would be sensitive to detect highly ionisable compounds independent of their concentration in the samples. The capability of a compound to ionise do not play a role on the sensitivity of the NMR but rather on the respective concentrations of the compounds in a fraction.

The OPLS-DA scatter and loadings plot of the LC-HRMS data of the MPLC fractions were grouped according to their antimicrobial activity against both biofilm-forming *S. aureus* and *P. aeruginosa* (Figures 5.11A and B). The R^2X and Q^2X values were at 0.743 and 0.758, respectively, which indicated relatively good reproducibility and predictivity of the model. The active fractions 1 to 7 on the right quadrants appeared more dispersed while the inactive fractions on the left were overlappingly clustered indicating their similarity. The dispersal of the active variables gave a variation score within the group of 19.9%, which is higher than the variation score between the groups at 12.9%. The diversity in chemical profile of the active fractions were also exhibited by their TLC as shown in Figure 5.12, which indicated that various type of compounds could be responsible for the antimicrobial activity of the extracts. As in the PCA scatter plot, Fraction 6 was an outlier, which indicated the presence of possible novel bioactive compounds that made it an interesting fraction for further purification work.

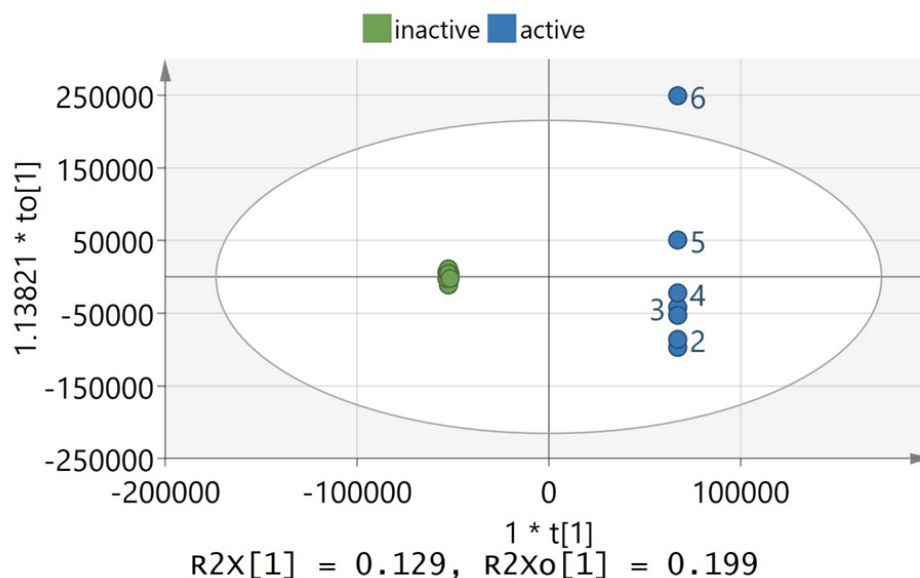


Figure 5.11A: OPLS-DA scatter plot of the mass spectral data of the MPLC fractions. Fractions are grouped according to their antimicrobial activity against both biofilms forming *S. aureus* and *P. aeruginosa*.

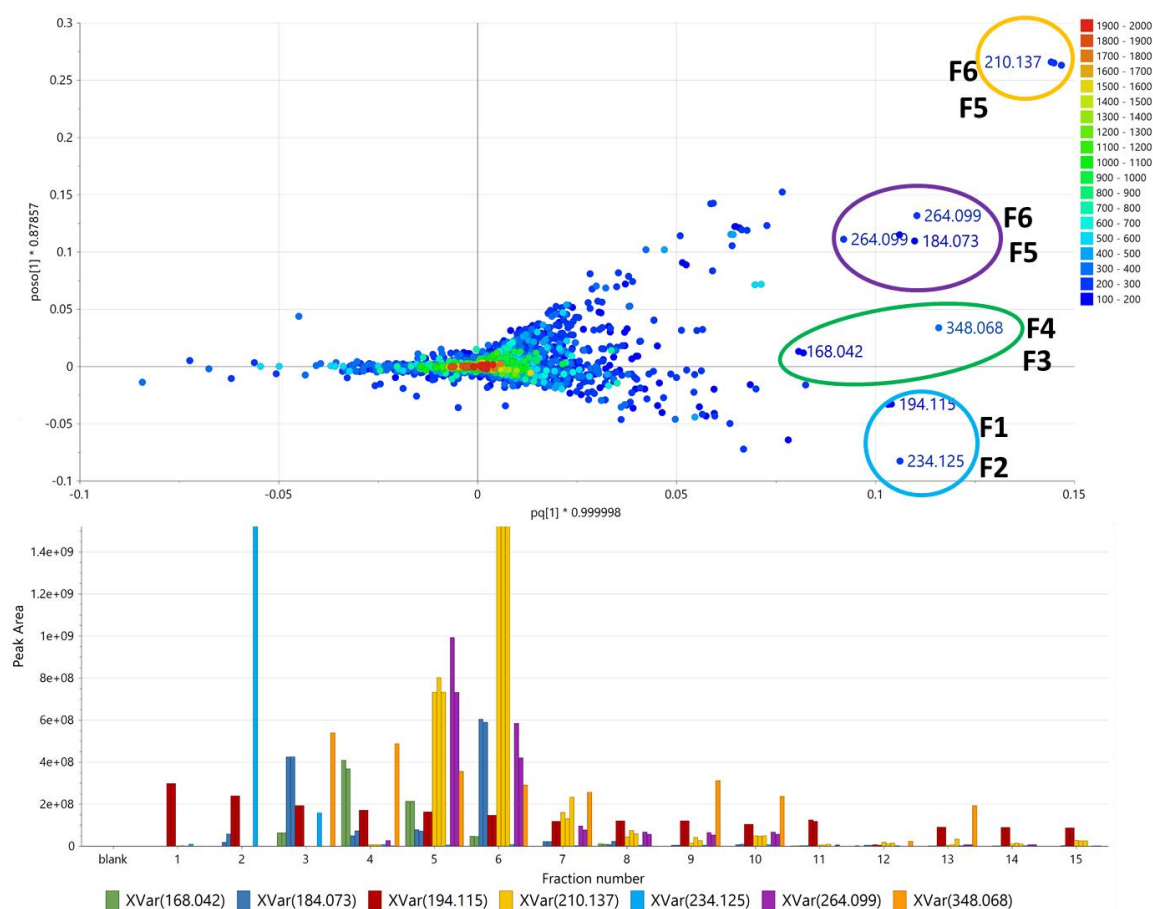


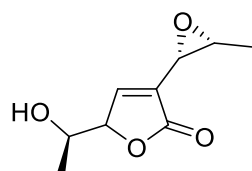
Figure 5.11B: OPLS-DA loadings plot of LC-HRMS data. Discriminatory features for antimicrobial active fractions are encircled and labelled with their MW. Their relative abundance in the respective fractions are shown in the bar graph.

The discriminatory features for the active fractions indicated by the OPLS-DA loadings plot of the LC-HRMS data predicted low molecular weight compounds between 140 and 300 Da, at the most with 264.09 Da. The putatively dereplicated compounds from the DNP are listed in Table 5.5 and shown in Figure 5.12. Similarly, the structures of the putatively dereplicated compounds were small peptides, saccharides and aromatics originating from the polyketide pathway, which are sources of new potential antimicrobials (Magana et al., 2020, Wu et al., 2020). OPLS-DA indicated the top 10 VIP (Variable Importance in Projection) metabolites to predict the discriminating features of the active fractions for antimicrobial activity, which will be targeted for isolation work. However, from this list of compounds, only three features (P_21849, P_2626, and N_842) afforded a p -value <0.05 . N_842 was not identified from the DNP database. N_13086 with a MW 168.042 for a molecular formula of $C_8H_8O_4$ eluting at

9.74 min was dereplicated with 92 hits, 27 of which are microbial metabolites. One of the compound hits was 2,6-dimethoxy-1,4-benzoquinone isolated from *Dendryhiella.salina*.

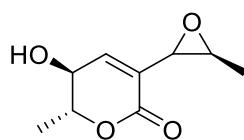
Table 5.5: Top 10 VIP (Variable Importance in Projection) dereplicated metabolites that define the discriminating features of antimicrobial active fractions. The compounds are arranged according to their *p*-values. Similar features with identical MW and a RT difference of less 0.25 minutes were excluded, including only the one with the highest peak area and *p*-value. TIC is shown in Figure 5.13.

Mzmine ID	Rt (min)	MW	MF (DBE)	P-value	FDR	Compound hits (sources)
P_21849	16.28	194.115	C ₈ H ₁₈ O ₅ (1)	0.001	0.007	xylitol (various algal sources)
P_2626	5.91	184.073	C ₉ H ₁₂ O ₄ (4)	0.04	0.014	51 hits, 3 from marine-derived fungi asperlactone and aspyrone from <i>Aspergillus</i> and <i>Exophiala</i> sp. decumbic acid from <i>Lasiodiplodia theobromae</i> and <i>Penicillium decumbens</i>
N_842	16.16	348.068	C ₁₃ H ₁₆ O ₁₁ (6)	0.04	0.021	no hits
N_13086	9.74	168.042	C ₈ H ₈ O ₄ (5)	0.05	0.029	92 hits, 27 are microbial metabolites 2,6-dimethoxy-1,4-benzoquinone from <i>Dendryhiella.salina</i>
P_2201	13.45	264.099	C ₁₄ H ₁₆ O ₅ (7)	0.11	0.036	see Figure 5.12B
P_15251	7.94	210.137	C ₁₁ H ₁₈ N ₂ O ₂ (4)	0.12	0.043	cyclo(isoleucylprolyl) from various marine-derived fungi
P_1491	19.45	234.125	C ₁₄ H ₁₈ O ₃ (6)	0.22	0.050	135 hits, 23 are from marine-derived microorganisms

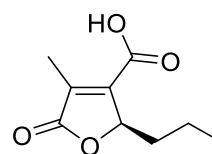


asperlactone

Aspergillus melleus, *Aspergillus ochraceus*
marine-derived *Exophiala* sp



aspyrone



decumbic acid
Lasiodiplodia theobromae
Penicillium decumbens

Figure 5.12A: Compound hits for discriminatory feature P_2626 with a RT of 5.9 min, a molecular weight of 184.073 Da, and a molecular formula of C₉H₁₂O₄.

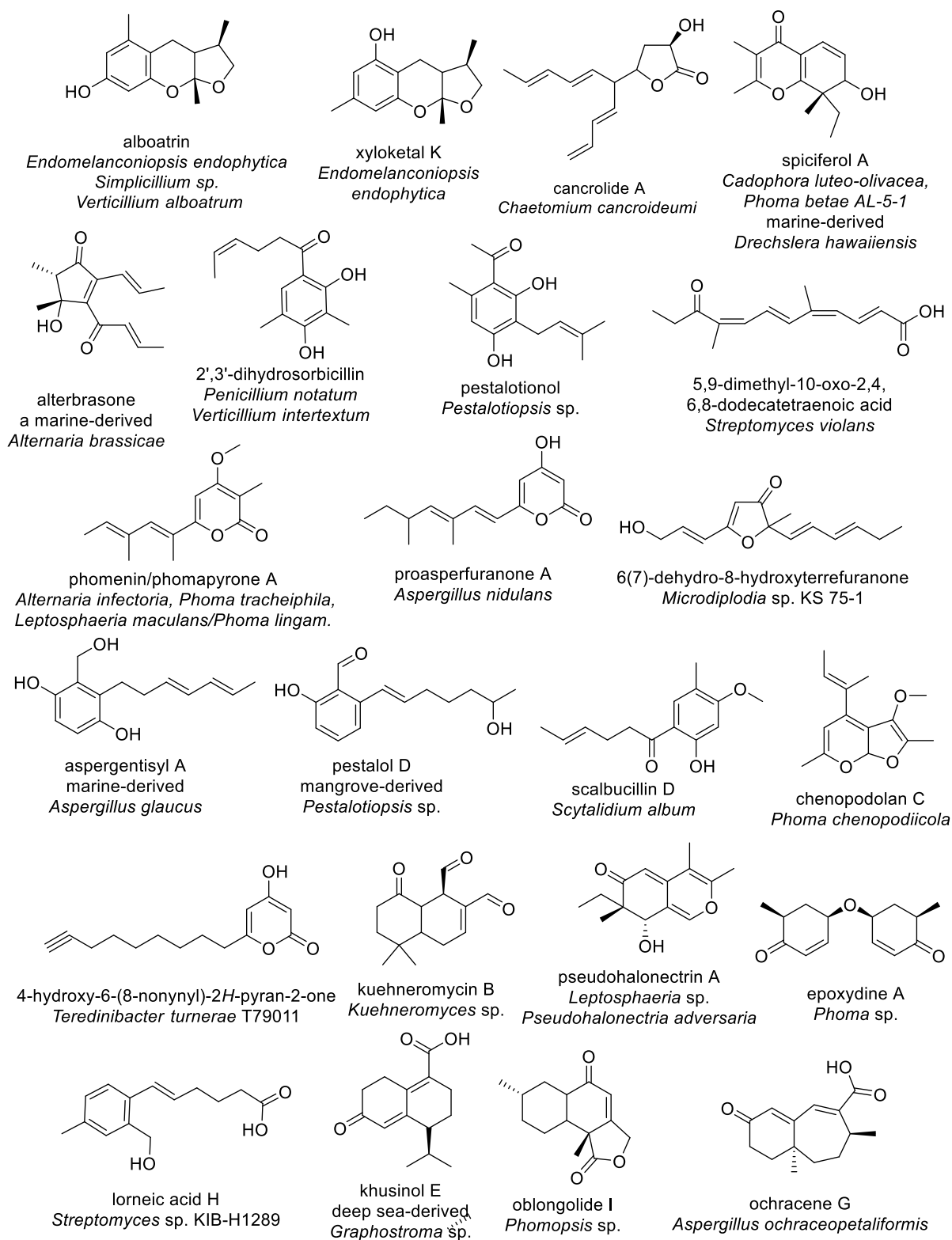


Figure 5.12B: Compound hits for discriminatory feature P_1491 with a RT of 19.4 min, a molecular weight of 234.125 Da, and a molecular formula of C₁₄H₁₈O₃.

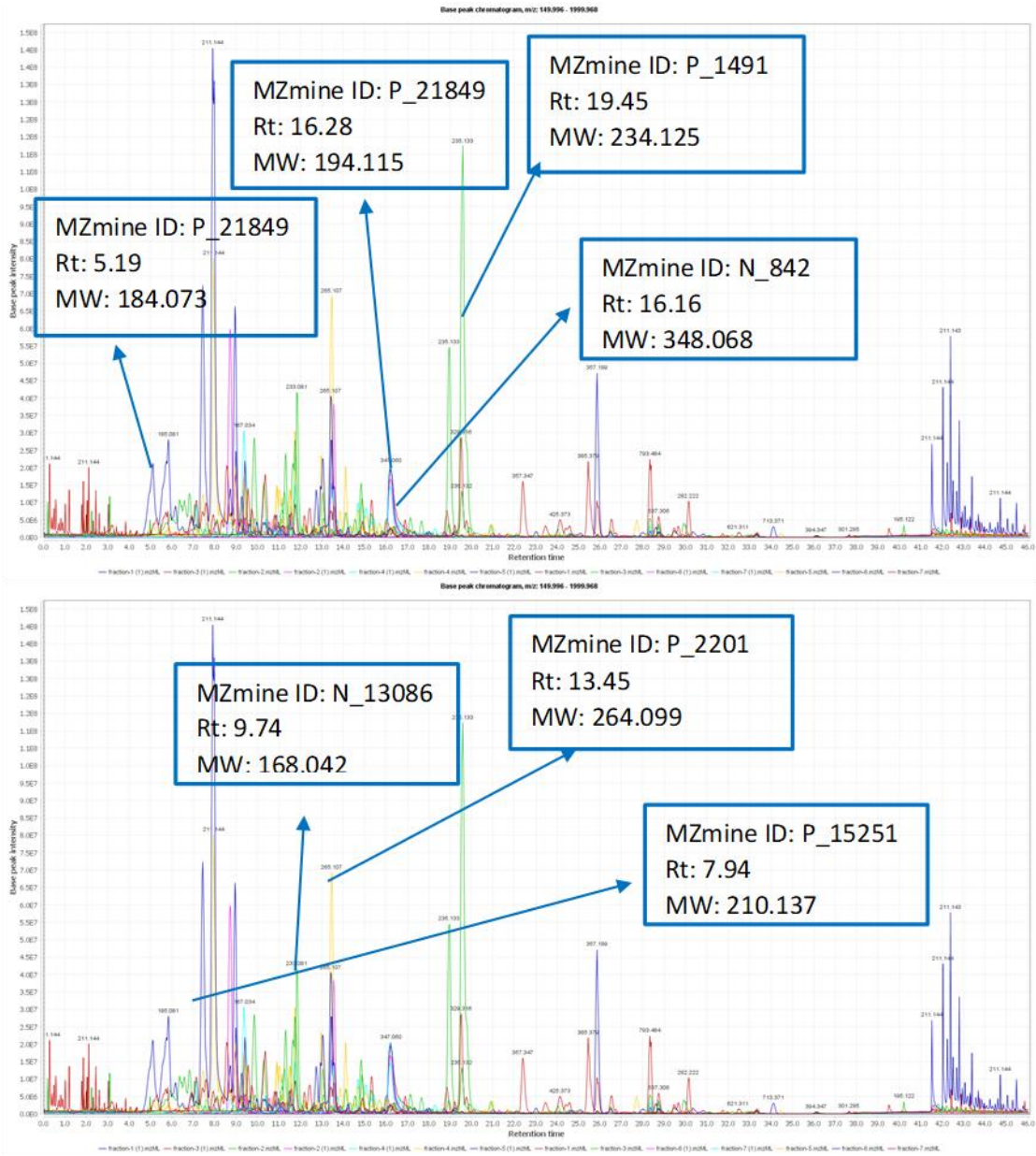


Figure 5.13: Total Ion Chromatogram (TIC) of the active fraction. The ion peaks that represent the discriminating features listed in Table 5.5 have been labelled.

5.2.6 Pure compounds isolation

Fractions 1 to 7 had the potential for further fractionation and purification work. A TLC plate, as shown in Figure 5.14, was run and solvent system was optimised to choose the fractions that will be subjected for extended isolation work using preparative TLC and flash chromatography. The fractions were prioritised for further isolation work depending on the non-complexity but novelty of their chemical profile, fraction yield, and potency of their antimicrobial activity. Using these criteria, Fractions 2 and 4 were chosen for further fractionation with potencies of almost 99% bacterial growth inhibition. Both fractions were subjected to preparative TLC due to their low yields of 42.2 and 69.1mg, respectively. Fraction 2 was the outlier in the multivariate analysis of the NMR spectral data set. Albeit, Fraction 6, with a yield of 65.6 mg, was the outlying variable in the analysis of the mass spectral data, but due to the complexity of its chemical profile with approximately more than two major compounds and more than 5 minor components in the mixture; Fraction 6 was not chosen for further work.

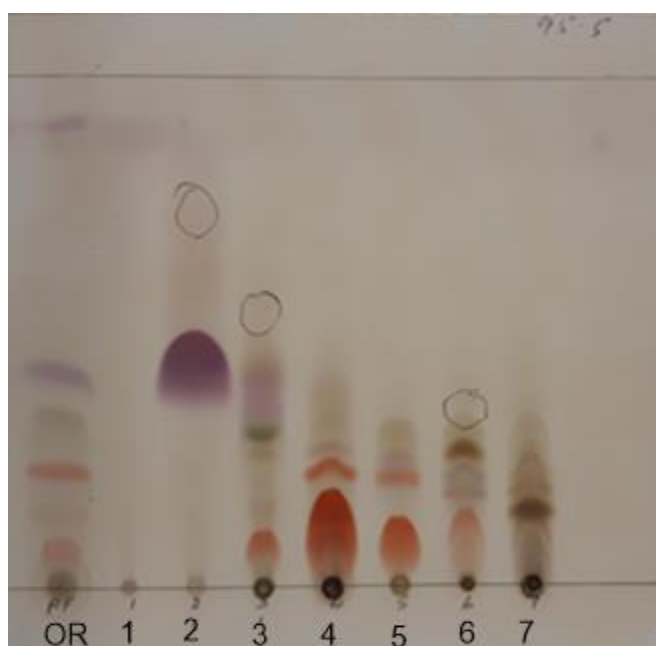


Figure 5.14: TLC of bioactive fractions of *D. salina* grown on malt extract.

5.2.6.1 Fraction 2 purification:

Fraction 2 was solubilized by dissolving each 10mg of extract in 150 μ L of ethyl acetate and loaded on a 20x20cm TLC Si plates. The TLC plates were developed two times with 95:5 DCM:MeOH. Three major bands were observed under UV light (Figure 5.15), and the bands were cut out then extracted from the TLC plates with 50mL acetone. The total percentage yield obtained after fractionation using preparative TLC was 79.46% as shown in Table 5.6.

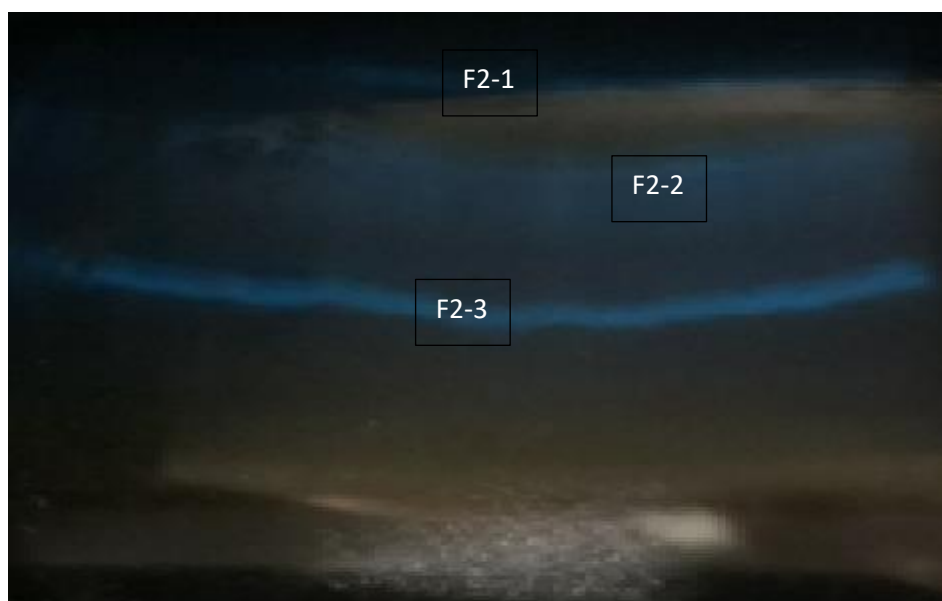


Figure 5.15: Preparative TLC of MPLC fraction 2 from crude extract of *D. salina* grown on malt extract media with sea salts.

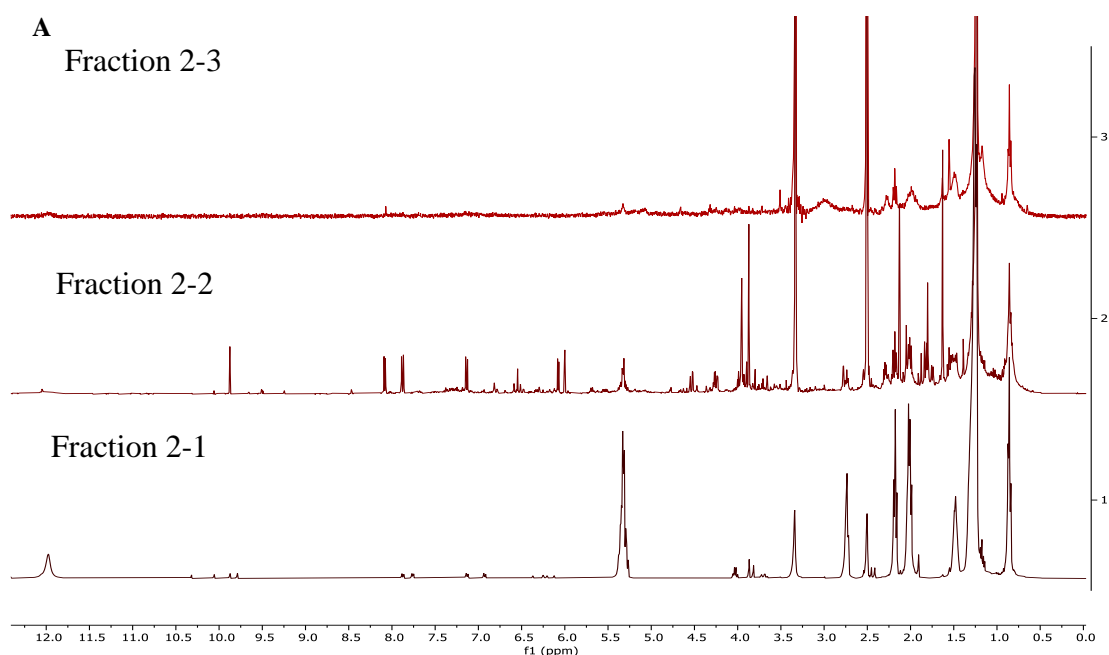
Three major bands were observed under UV light (254nm) and were extracted from the TLC plates using 50mL acetone for each. The total % recovery yield after fractionation using preparative TLC was 79.46% as shown in Table 5.6.

Table 5.6: weights of the three major band from fraction 2.

Fraction #	Weight (mg)
F2-1	23
F2-2	7.5
F2-3	2
Total	32.5
% recovery	79.46

The stacked H^1 NMR spectrum of the collected major bands is shown in Figure 5.16, the highest band with a R_f of 0.82 was an unsaturated fatty acid. While band 2 still contained a

mixture of low yielding compounds, it was possible that the target bioactive metabolite P_1491 with a MW of 234.125 Da ($C_{14}H_{18}O_3$) could be found in this subfraction. However, due to the low yield of F2-2 at 7.5 and yet still a mixture of compounds, it was not feasible to further isolate P_1491. P_1491 afforded compound hits earlier described from marine-derived fungi and these putatively dereplicated compounds have been reported to exhibit potent antimicrobial activities. The structures of these compound hits for P_1491 (Figure 5.13B) consisted mostly of phenyl or lactone ring systems as also could be observed from the 1H spectrum of F2-2 with resonances between 6 and 10 ppm. Band three contained a mixture of low molecular weight fatty acids. According to the proton NMR spectra of fraction F2-1, the integration of the olefinic signals indicated the presence of unsaturated fatty acid with two double bonds (di-unsaturated) due to the presence of 4 hydrogens. While the number of methylene groups according to the integration of F2-1 was approximately to be between 12-14 CH_2 . The number of CH_2 between the two double bond is one with a proton chemical shift of 2.73ppm. According to the integration data the expected molecular weight is between 280.44-308.50 Da.



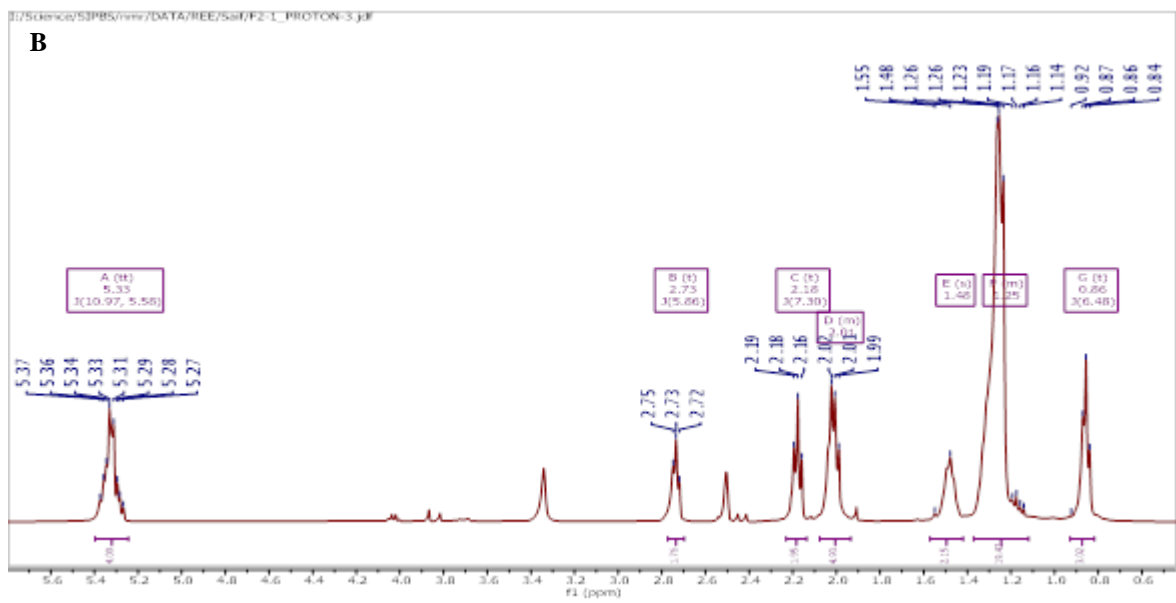
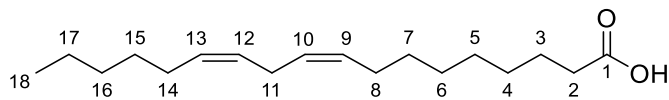


Figure 5.16: (A) Stacked proton NMR spectra of fraction 2 subfractions and (B) fraction F2-1 proton NMR spectra with integration and chemical shifts

Compound 2-1

Linoleic acid



(9Z,12Z)-octadeca-9,12-dienoic acid

Chemical Formula: $C_{18}H_{32}O_2$

Exact Mass: 280.24023

	Formula	Calculated Mass	Target Mass	Double Bond Equivalence	Absolute Error (ppm)	Error (mDa)	Error (ppm)
1	C18 H32 O2	281.24751	281.24752	3.0	0.04	0.01	0.04

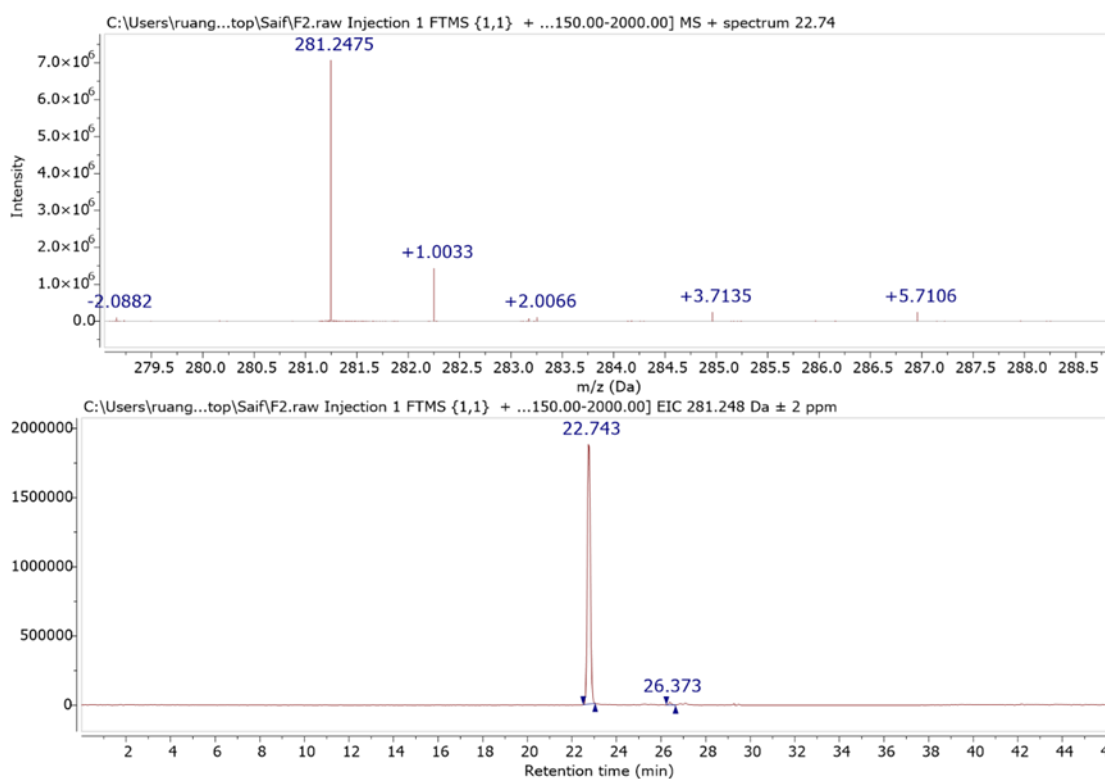


Figure 5.17: High-resolution mass spectral data for linoleic acid.

Compound F2-1 was isolated from fraction 2 as a yellow oily compound. The MW of Compound 2-1 can be deduced from the integration of the peaks representing 32 protons as observed from its 1H NMR spectrum in Figure 5.18. Starting at the utmost downfield region was the exchangeable $COOH$ proton resonance at 11.20 ppm for 1H. At 5.33 ppm, an integration of 4H for two double bonds indicated the occurrence of *cis* olefinic bonds typical for an unconjugated polyunsaturated fatty acid. This was followed by a triplet signal at 2.74 ppm for 2H representing the methylene group between the two olefinic bonds, then another 2H

triplet was observed at 2.18 ppm for the methylene unit adjacent to the COOH unit. At 2.02 ppm was a quartet integrating for 4H in lieu of the two methylene units adjacent to the olefinic double bonds that would further couple with the rest of the alkyl chain units. The 2H multiplet at 1.48 ppm signified the methylene unit next to the CH₂COOH terminal. At 1.27 ppm, a broad high intensity multiplet peak integrated for 18H for nine methylene units. And finally, the 3H triplet at 0.87 ppm indicated the terminal methyl moiety. The described resonances would afford one quaternary carbon, four olefinic methine units, fourteen methylene moieties and one methyl group that would sum up to a molecular formula of C₂₀H₃₆O₂ for an icosanoic or eicosanoic acid diene congener with a MW of 308 Da. However, high resolution mass spectral data (Figure 5.17) gave a mass ion peak at *m/z* [M+H] 281.24752 for C₁₈H₃₂O₂ with 3.0 DBE, which was for linoleic acid or octadeca-9,12-dienoic acid with a MW of 280 Da.

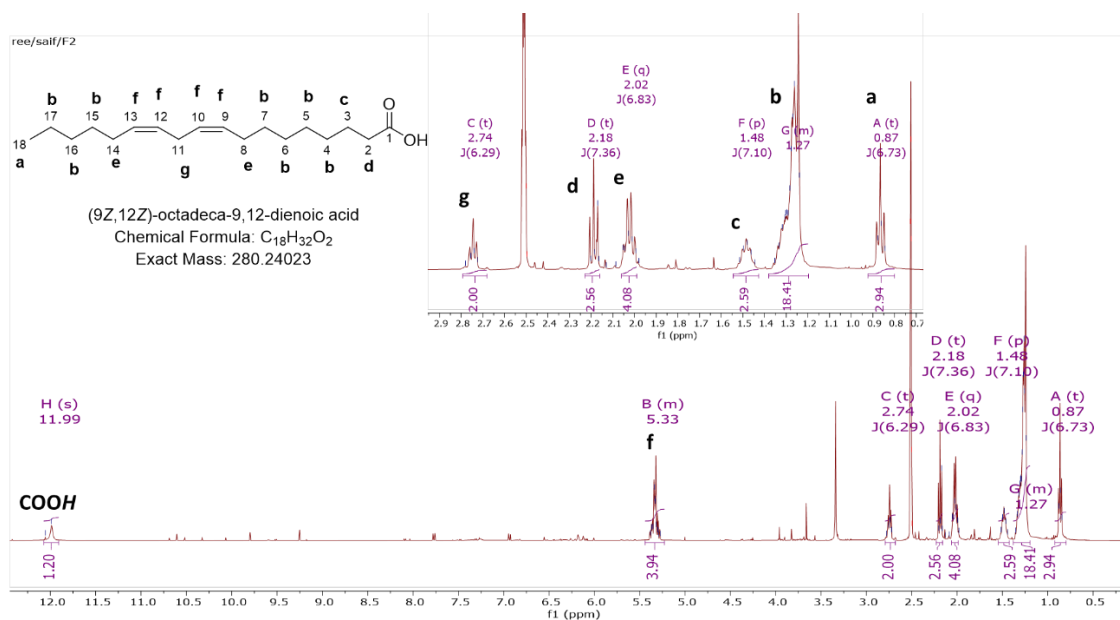


Figure 5.18: ¹H NMR spectrum of Compound 2-1 structurally elucidated as linoleic acid.

The linoleic acid structure of Compound 2-1 was further confirmed by the COSY spectrum in Figure 5.19. To follow the coupling resonances, corresponding peaks were labelled with consecutive letters in lower case. The first system was the terminal methyl unit to the alkyl system CH₃(CH₂)_n- designated as protons **a** to **b**. This was followed by the olefinic system – CH₂CH=CHCH₂CH=CHCH₂- assigned as –**b-e-f-g-f-e-b**-, respectively. Then for the terminal carboxylic unit – CH₂ CH₂COOH, this was specified by –**b-c-d**-. Yet there were more than one possible positions of diene unit, which includes (8Z,11Z); (11Z,14Z); and

(9Z,12Z). The isolated Compound 2-1 was structurally elucidated as (9Z,12Z)-octadeca-9,12-dienoic acid, which was compatible with NMR spectral data of a linoleic acid standard.

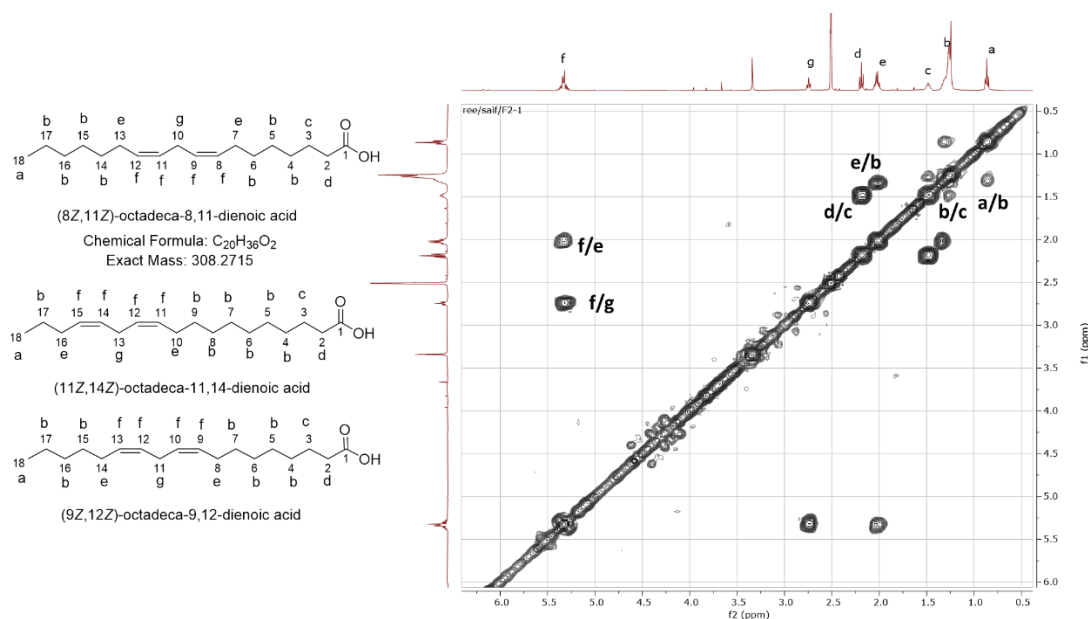


Figure 5.19: COSY NMR spectrum of Compound 2-1 structurally elucidated as linoleic acid

Table 5.7: NMR spectral data for linoleic acid (F2-1) measured in DMSO- d_6 with COSY correlations as indicated by the atom numbers in Figure 5.21.

Atom no	^1H ppm	multiplicity (J in Hz)	COSY (H to H)
1			
1-OH	11.99	br s	
2	2.56	t (7.36)	H-3
3	1.48	br p (7.10)	H-2, H-4
4	1.27	br m	H-3, H-5
5	1.27	br m	H-4, H-6
6	1.27	br m	H-5, H-7
7	1.27	br m	H-6, H-8
8	2.02	q (6.83)	H-7, H-9
9	5.33	m	H-8, H-10
10	5.33	m	H-9, H-11
11	2.74	t (6.29)	H-10, H-12
12	5.33	m	H-11, H-13
13	5.33	m	H-12, H-14
14	2.02	q (6.83)	H-13, H-15
15	1.27	br m	H-14, H-16
16	1.27	br m	H-15, H-17
17	1.27	br m	H-16, H-18
18	0.87	t (6.73)	H-17

5.2.6.2 Fraction 4 purification:

Like Fraction 2, a solvent system of 95:5 DCM:MeOH was used to purify the major bioactive component(s) in Fraction 4 on preparative TLC Silica plates (Figure 5.20) and was developed two times. Six major bands were detected and consequently extracted with acetone. The yield of each band was weighed and presented in Table 5.8.

Table 5.8: Subfraction yield for major bands of fraction 4 of *D. salina* grown on malt extract media crude extract.

Fraction number	Amount (mg)	Fraction number	Amount (mg)
F4-1	11.2	F4-7	1.6
F4-2	5.2	F4-8	0.5
F4-3	2.5	F4-9	1.1
F4-4	1.2	F4-10	2.8
F4-5	1.4	F4-11	3.4
F4-6	5.3	Total	36.2
		% recovery	58.77

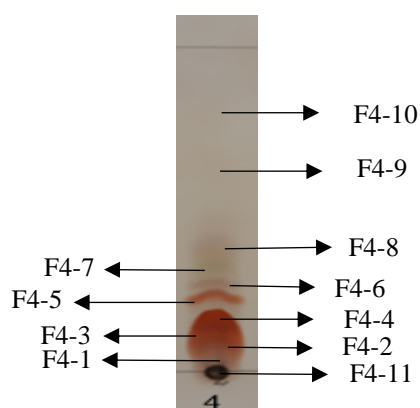


Figure 5.20: TLC of fraction 4 developed in 95:5 DCM and MeOH.

The stacked proton NMR spectrum of the selected fractions are presented in Figure 5.21. Based on the purity of the respective ^1H NMR spectra and yields of the fractions particularly those with higher than 1mg, three fractions (F4-1, F4-2, and F4-6) were selected for structure elucidation work. Fraction 4-6 afforded the highest purity with minor contaminant from another compound. Fraction 4-1 gave the highest yield of 11.2 mg.

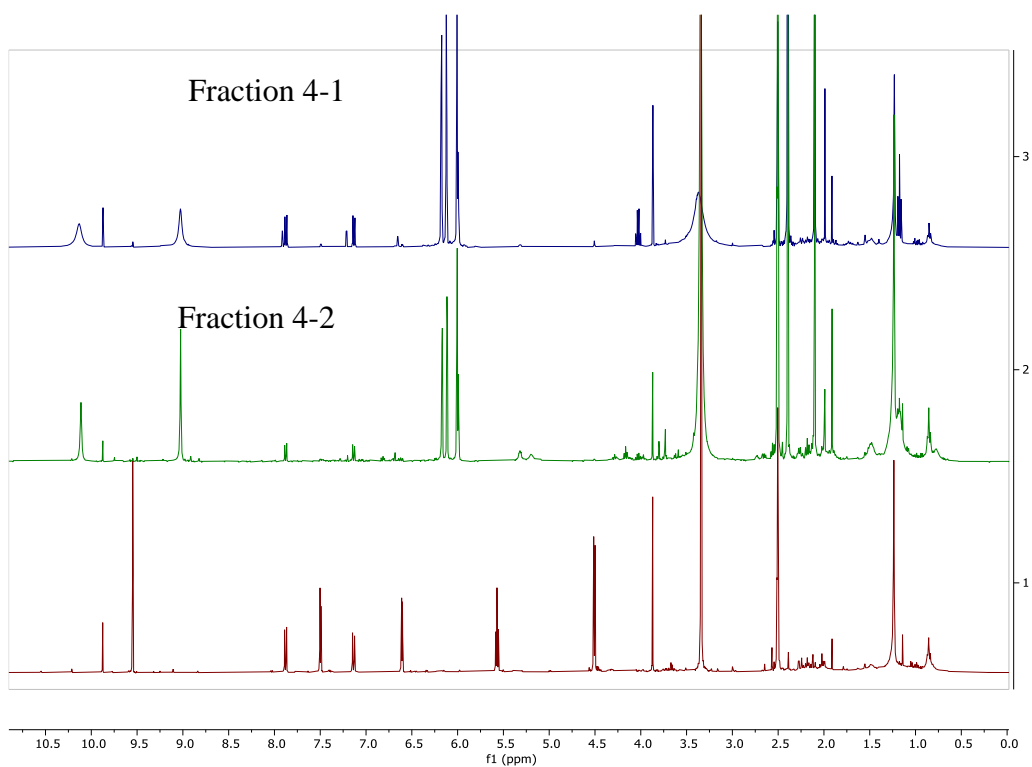


Figure 5.21: Stacked ¹H NMR spectrum of the preparative TLC bands targeted for further analysis and structure elucidation.

5.2.6.2.1 Compound 4-1A and B:

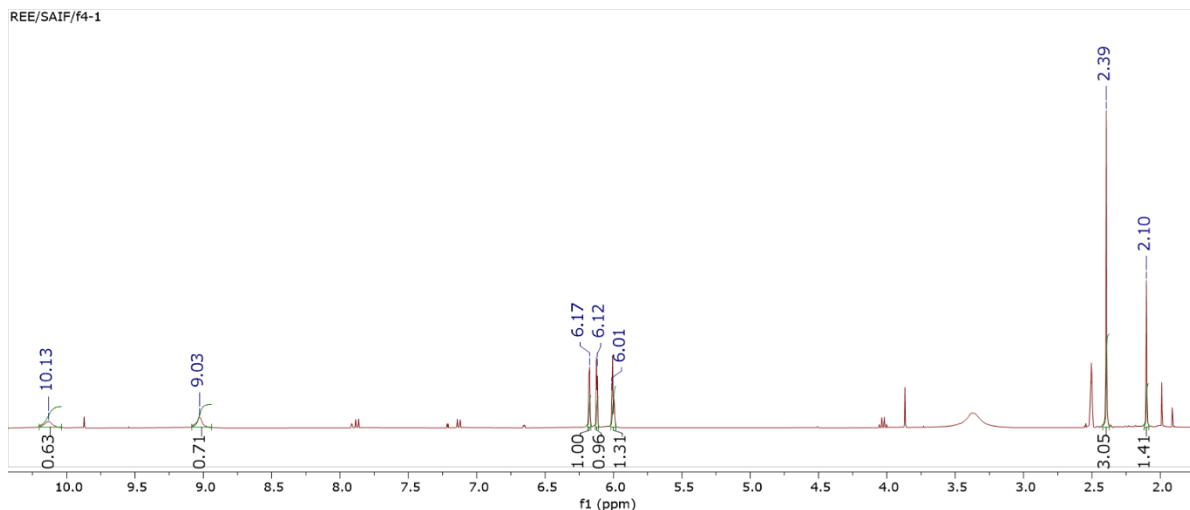
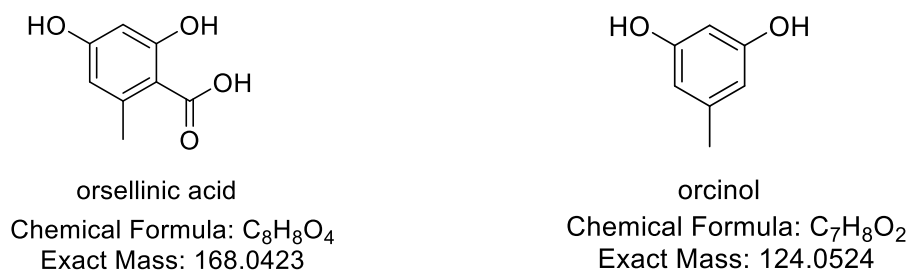


Figure 5.22: ¹H NMR of Fraction 4-1.

Compound F4-1 was isolated from fraction 4 as a white amorphous powder. Fraction 4-1 consisted of two major compounds that were orsellinic acid and orcinol at a ratio of 3:1 as indicated by the integration deduced from the methyl signals at 2.39 and 2.10 ppm of the ¹H NMR spectrum in Figure 5.22. Orsellinic acid has the molecular formula C₈H₈O₄, which was deduced from the high-resolution ion peak at m/z [M+H]⁺ 169.04943 (calc. 169.04954, Δ 0.63 ppm) eluting at 9.38 min (Figure 5.23). However, orcinol was not detected due to the lower cut off mass range of 140 Da used. Orcinol has an expected MW of 124 Da for a molecular formula of C₇H₈O₂.

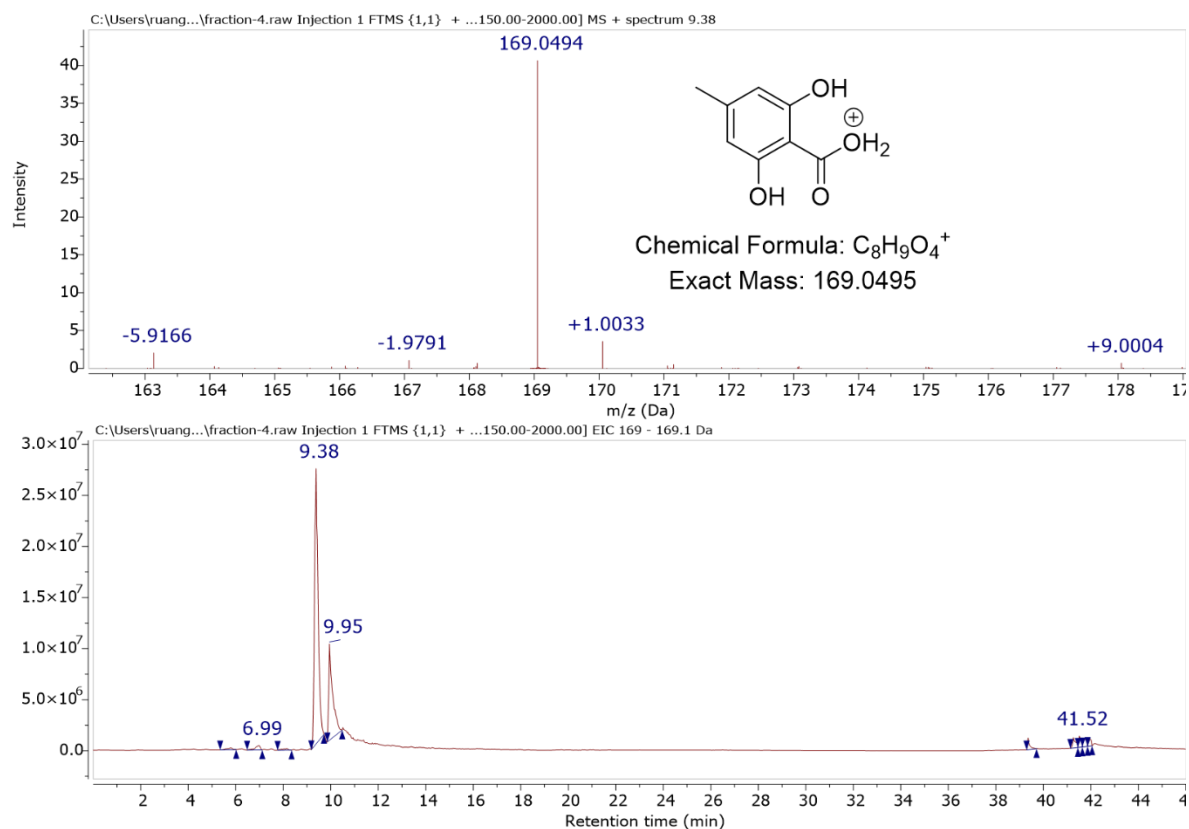


Figure 5.23: High-resolution mass spectral data for orsellinic acid.

¹H and ¹³C NMR spectra of orsellinic acid is presented in Figure 5.24. NMR spectral data is shown in Table 5.9 and is compatible to those found in the literature (Sanchez et al., 2010). Orsellinic acid was distinguished from orcinol by its 2D HMBC NMR (Figure 5.25 and Table 5.9). Typical for orsellinic acid was the presence of the *meta* doublet pair with coupling constants of 2.4 Hz at 6.12 (H-3) and 6.18 (H-5) ppm, while ³J cross peaks were observed with their respective carbons at 101.03 (C-3) and 111.52 (C-5) ppm. CH-3 gave ²J correlations with two hydroxyl bearing carbons at 165.01 (C-2) and 162.50 (C-4) ppm. A ³J correlation was also observed with C-1 at 105.04 ppm. In addition, CH-5 correlated further with the methyl carbon unit at 24.0 ppm. The methyl proton at 2.40 ppm showed cross peaks with C-6 for a ²J as well as ³J correlations with C-1 and C-5. The CH direct resonances were observed by the cross-peak pairs as illustrated with **blue** connecting lines on the HMBC spectrum.

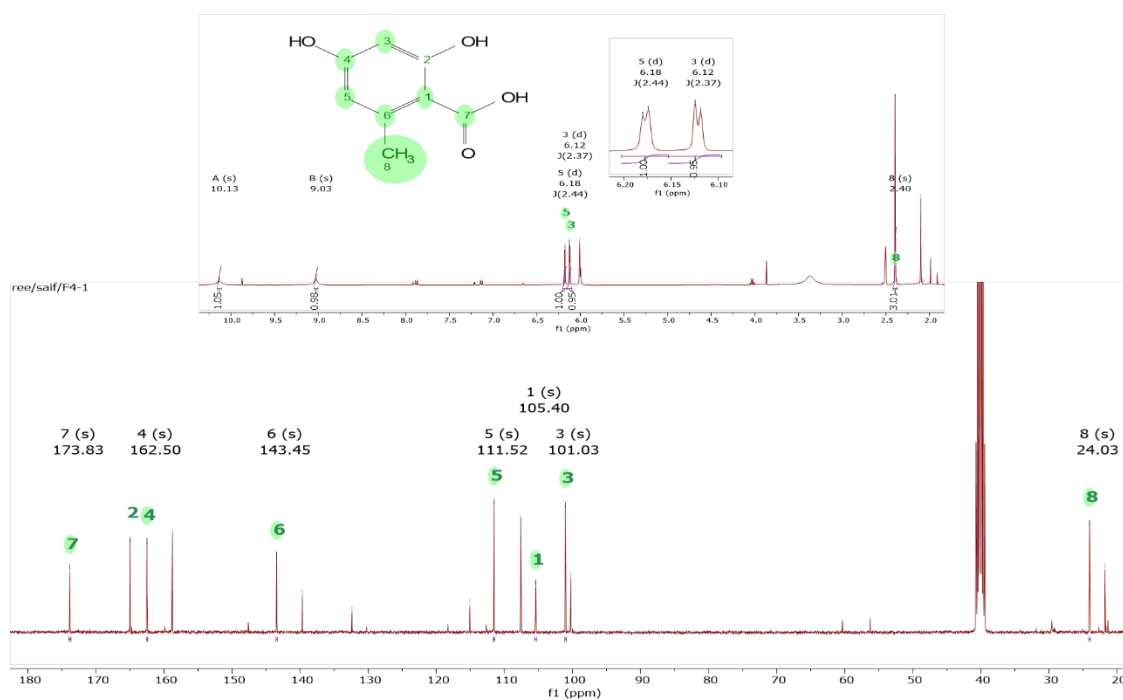
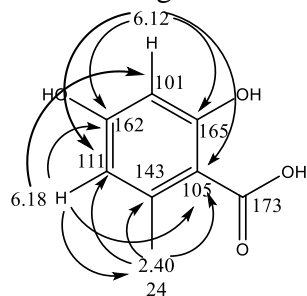


Figure 5.24: ^1H and ^{13}C NMR spectra of orsellinic acid in DMSO-d_6 at 400 and 100 MHz, respectively.

Table 5.9: NMR spectral data for orsellinic acid (F4-1A) measured in DMSO-d_6 with HMBC correlations as indicated by the arrows in the figure below.



Atom no	^{13}C ppm,	multiplicity	^1H ppm	multiplicity (J in Hz)	HMBC (H to C)
1	105.40	C			
2	165.01	C			
2-OH			10.13	br s	
3	101.03	CH	6.12	d (2.4)	C-1, C-2, C-4, C5
4	162.50	C			
4-OH			9.03	br s	
5	111.52	CH	6.18	d (2.4)	C-1, C-3, C-4, C-8
6	143.45	C			
7	173.83	C			
8	24.03	CH_3	2.40	s	C-1, C-5, C-6

Legend: br s = broad singlet, s = singlet, d = doublet,

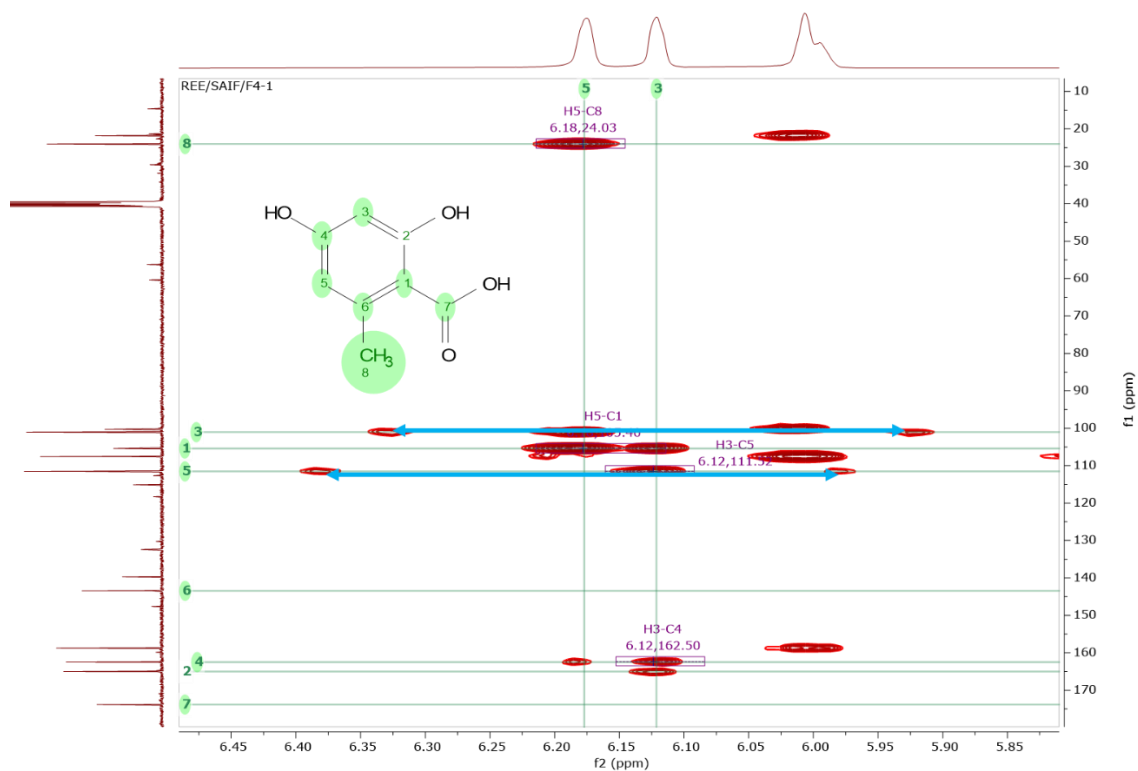
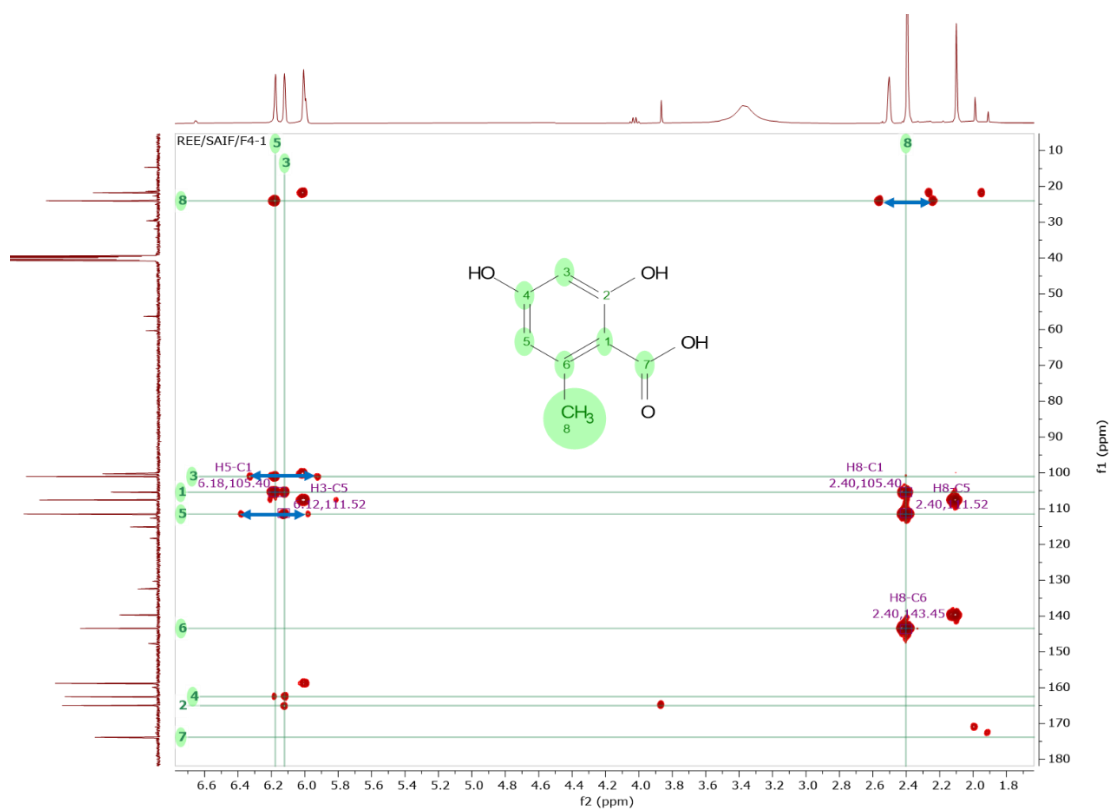


Figure 5.25: HMBC spectrum of orsellinic acid in DMSO-d₆. Blue connecting lines represent the CH direct signals.

Orcinol is a smaller molecule with overlapping *meta*-coupling proton peaks at 6.00 ppm due to its symmetry in addition to one methyl singlet at 2.10 ppm observed in ^1H NMR spectrum of F4-1 (Figure 5.26). Using the remaining unassigned peaks, the carbon resonances on the ^{13}C NMR spectrum (Figure 5.26) for orcinol were designated with the aid of the CH direct signals from the HMBC as well as the HMQC spectrum (Figure 5.27). The three overlapping *meta* doublet protons exhibited two carbon resonances at 100.26 ppm for C-2 along with 107.59 ppm for C-4 and C-6, which were equivalent. The hydroxyl-bearing carbons at 158.77 for C-1 and C-3 were also equivalent. The methyl carbon unit was assigned at 21.78 ppm as evidenced by the CH direct signals. C-5 at 143.45 ppm was the methyl-bearing carbon, which was perceived through its 2J HMBC correlation with the methyl signal at 2.10 ppm. The methyl proton further exhibited 2J correlations with the methine protons at 6.00 ppm, which gave cross-peaks with the hydroxyl-bearing carbons as well as with C-2. No HMBC correlations was observed from H-2 due to its weaker signal intensity. Full proton and carbon assignments are presented in Table 5.10.

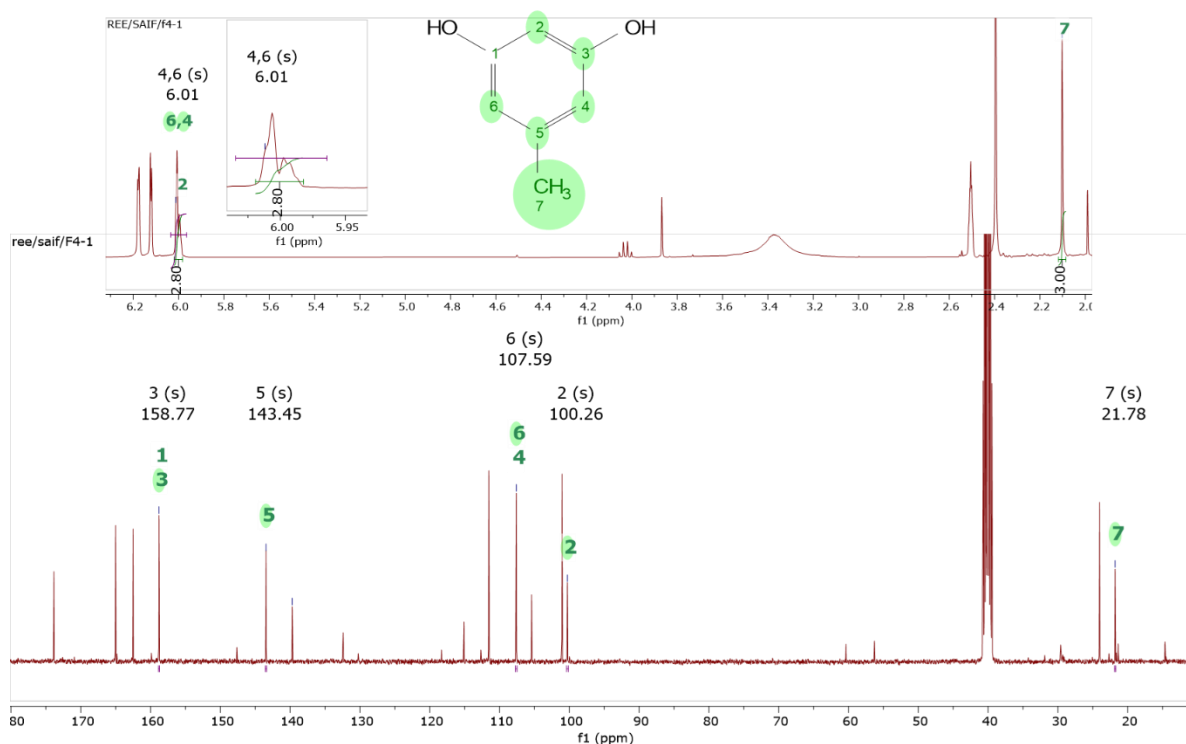


Figure 5.26: ^1H and ^{13}C NMR spectra of orcinol in DMSO-d_6 at 400 and 100 MHz, respectively.

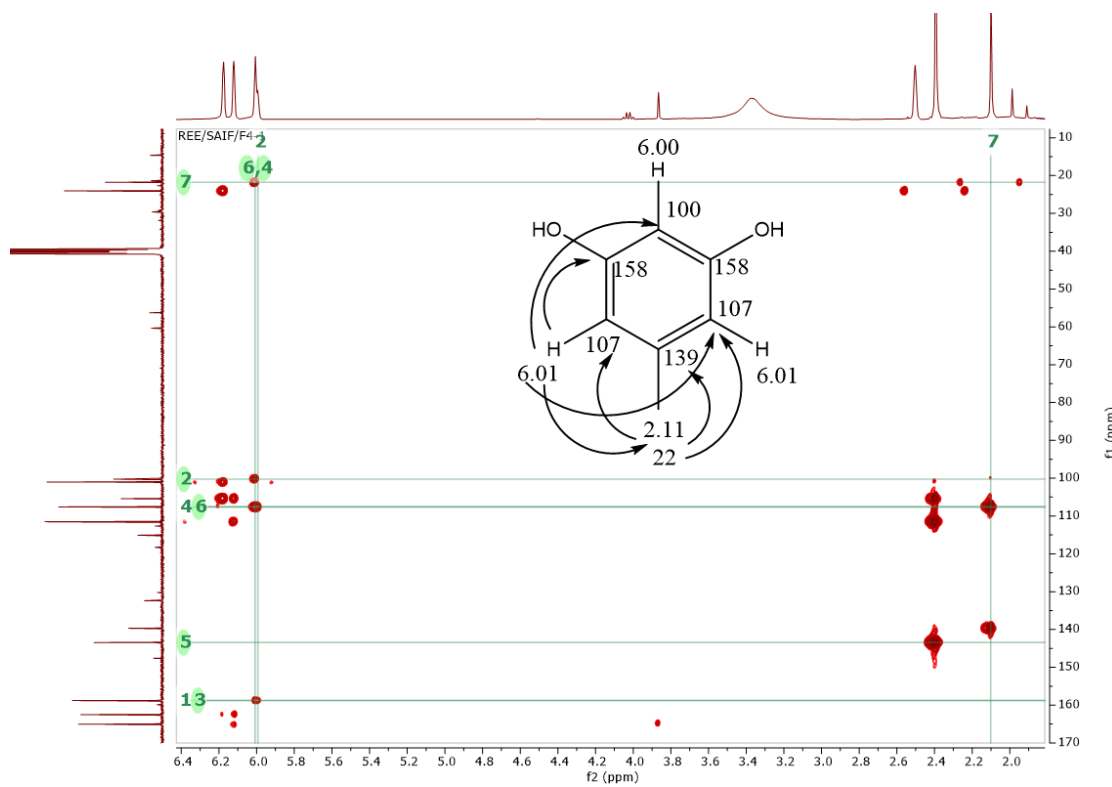
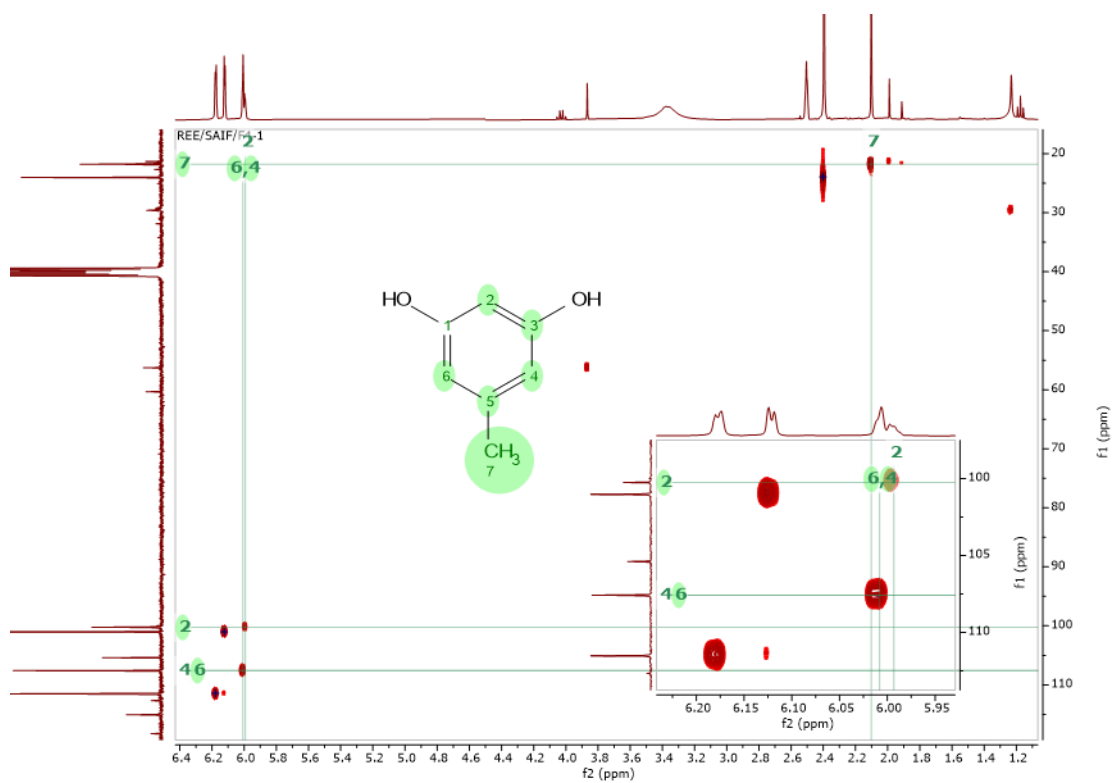


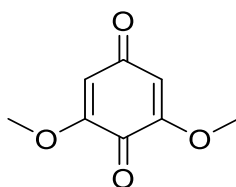
Figure 5.27. HMQC (above) and HMBC (below) spectrum of orcinol in DMSO-d₆.

Table 5.10: NMR data for orcinol (F4-1B) of Fraction 4-1 measured in DMSO-d₆

Atom no	¹³ C ppm,	multiplicity	¹ H ppm	multiplicity	HMBC (H to C)
1	158.77	C			
2	100.26	CH	6.00	br s	
3	158.77	C			
4	107.59	CH	6.01	br s	C-3, C-2, C-6, C-7
5	143.45	C			
6	107.59	CH	6.01	br s	C-1, C-2, C-4, C-7
7	21.78	CH ₃	2.10	s	C-4, C-5, C-6

Legend: br s = broad singlet, s = singlet

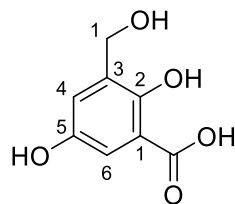
Orsellinic acid has been widely distributed in lichens. But it has also been isolated from cultures of *Penicillium* spp., *Hypoxylon* spp. and other microorganisms such as the marine-derived *Chaetomium* sp. Gö 100/9, *Aspergillus versicolor* SCSIO 41502 and an ascomycete culture LL-W1278 (Bashyal et al., 2005, Hellwig et al., 2005, Sanchez et al., 2010, Abdelmohsen et al., 2015). Interestingly, the ion peak found at m/z 169.04943 was amongst the top 10 VIP metabolites predicted for antimicrobial metabolite. Amongst the dereplicated hits was 2,6-dimethoxy-1,4-benzoquinone (Figure 5.28) isolated from *Dendryhiella.salina* (Bramhachari et al., 2019). However, the *D. salina* used in this study did not afford a similar compound.



2,6-dimethoxy-1,4-benzoquinone

Figure 5.28: 2,6-dimethoxy-1,4-benzoquinone chemical previously reported from *D. salina* (Bramhachari et al., 2019)

5.2.6.2 Compound 4-6:



2,5-dihydroxy-3-(hydroxymethyl)benzoic acid

Chemical Formula: $C_8H_8O_5$

Exact Mass: 184.0372

	Formula	Calculated Mass	Target Mass	Double Bond Equivalence	Absolute Error (ppm)	Error (mDa)	Fitness
1	C ₈ H ₈ O ₅	185.04445	185.04469	5.0	1.32	0.24	0.977

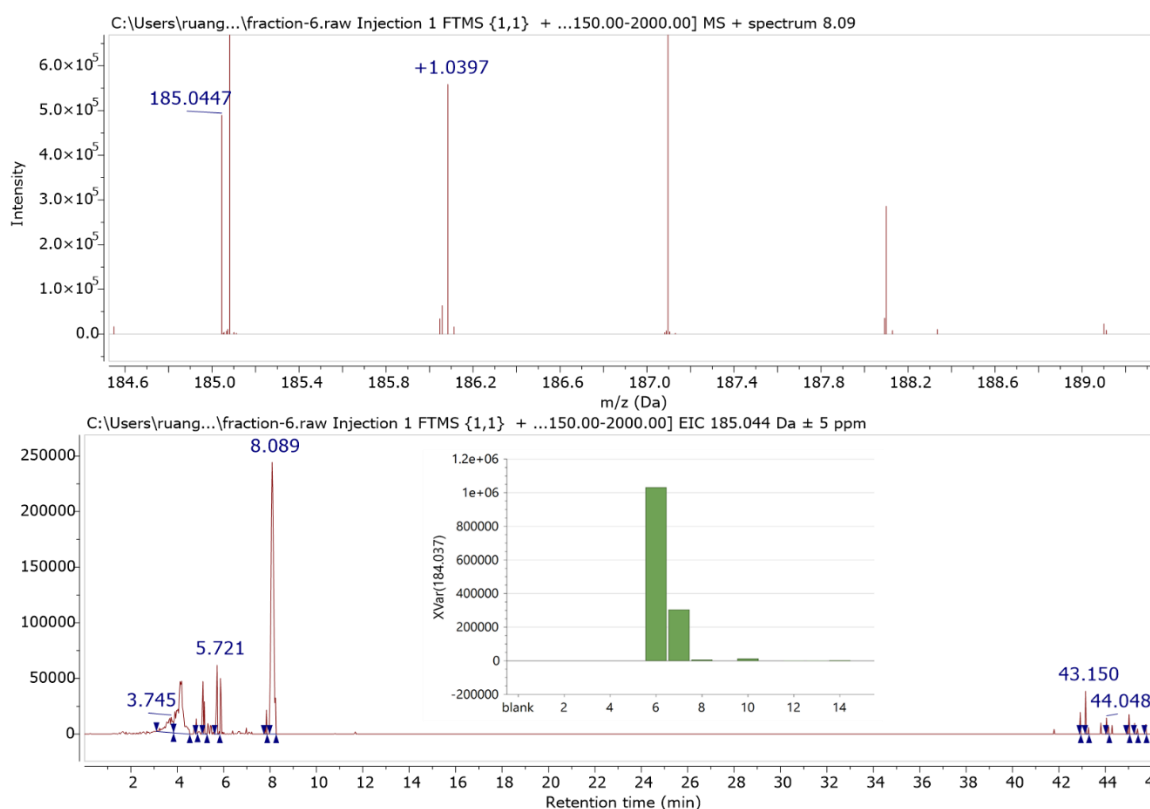


Figure 5.29. High-resolution mass spectral data for F4-6. Inset shows the relative abundance of F4-6 in the different fractions that is highest in Fraction 6.

Compound F4-6 was isolated from fraction 4 as a white amorphous powder. Fraction 4-6 afforded a very low yield at 5.6 mg. The MW data of 184.0372 Da with an expected molecular formula $C_8H_8O_5$ was deduced from the NMR data, which was not found in the mass spectral dataset of the afforded fractions. As high-resolution data was used to predict the target metabolite, the elucidated compound was indeed different from the target bioactive metabolite P_2626 found at m/z $[M+H]^+$ 185.080 Da (MW = 184.0736) for $C_9H_{12}O_4$ eluting at 5.91 min, which is one methyl group more while the isolated compound 4-6 (F4-6) had an additional oxygen atom. The expected MW of 184.0372 Da for the isolated compounds was not detected in the loaded MPLC Fractions 4. However, relative abundance of F4-6 was highest in the antimicrobial active Fraction-6 although its concentration was also down to the instrument's limit of detection. It could have been possible that the targeted metabolite underwent oxidation during the isolation work (Figure 5.30).

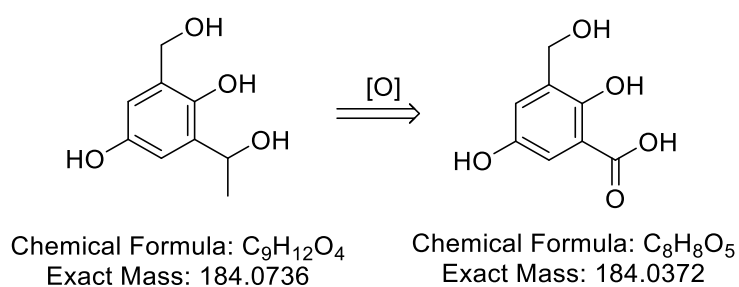


Figure 5.30: Hypothetical oxidation of compound F4-6 during isolation work.

The 1H NMR spectrum of F4-6 (Figure 5.31A) displayed two coupling pairs of resonances and a downfield singlet at 9.56 ppm. The coupling proton signals included two meta-doublets ($J = 3.5$ Hz) at 6.61 and 7.50 ppm that indicated the protons were adjacent to electron-donating and -withdrawing groups, respectively. The second coupling pair was more upfield and consisted of a 1H triplet and a 2H doublet at 5.56 and 4.51 ppm, respectively with coupling constant of 6.0 Hz. The chemical shifts of the triplet-doublet pair signified their occurrence in a benzylic and/or heteroatom environment. The coupling protons were confirmed by COSY as shown in Figure 5.31B.

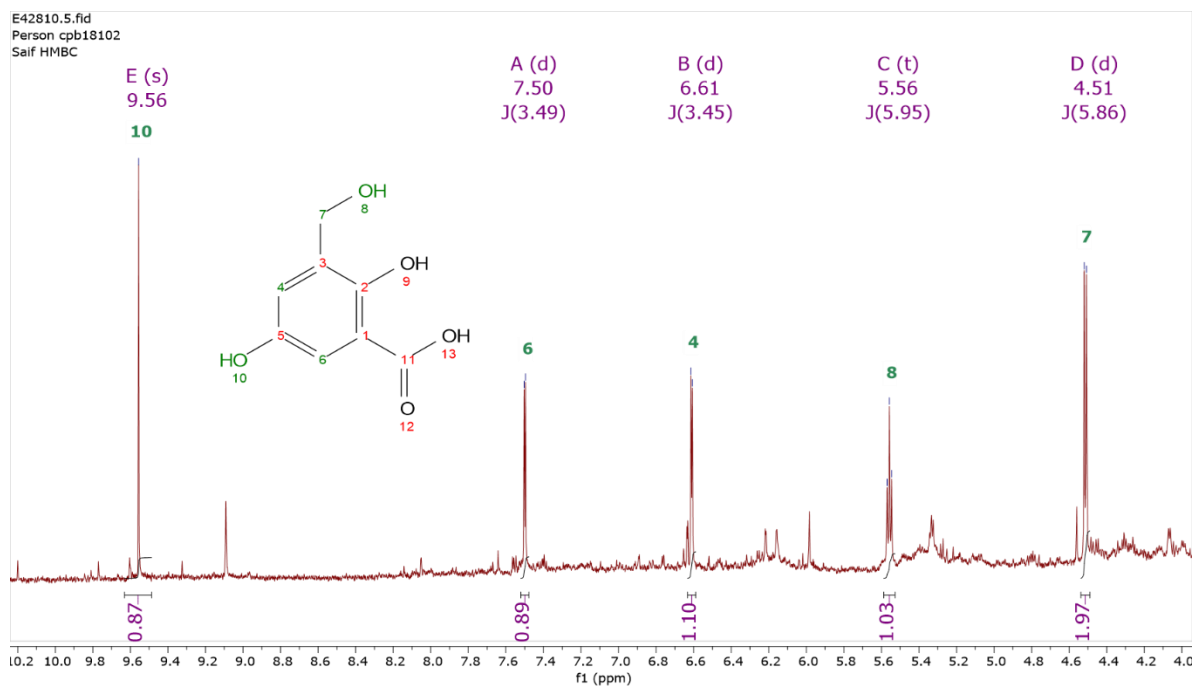


Figure 5.31A: ^1H NMR spectrum of F4-6 in DMSO-d_6 at 500 MHz.

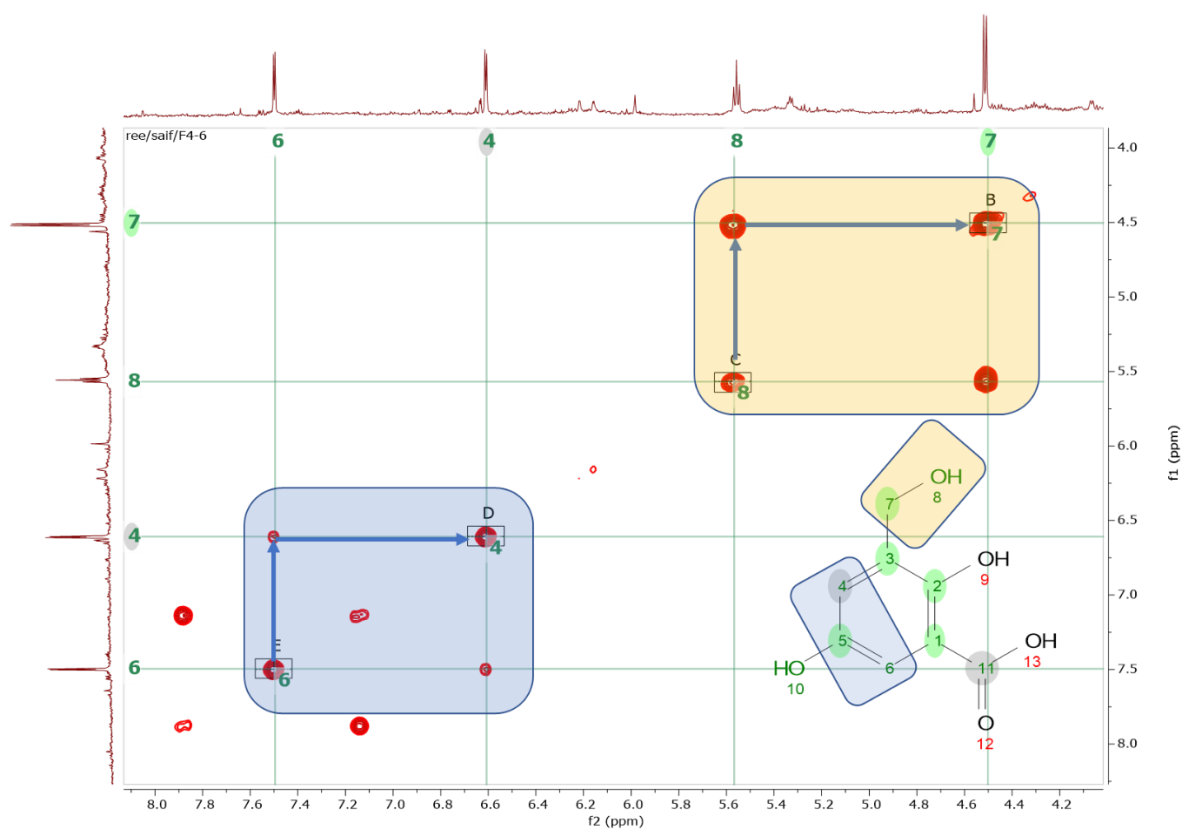


Figure 5.31B: ^1H - ^1H COSY NMR spectrum of F4-6 in DMSO-d_6 at 400 MHz.

The ^{13}C NMR spectrum in Figure 5.32 revealed the presence of three oxygen bearing-carbons at 152.32, 162.77, and 178.57 ppm, two of which were hydroxyl units and a carboxylic acid moiety. These resonances were comparable but not identical to those found in orsellinic acid. Quite a difference to the spectral data of orsellinic acid was the heteroatom-bearing carbon in the aliphatic region at 56.51 ppm. Complimentary to the ^1H NMR spectrum of F4-6, four aromatic carbons were observed at 110.27, 115.11, which were shielded due to adjacent electron donating substituents like a hydroxyl unit as well as more deshielded carbons at 125.0 and 132.4 ppm.

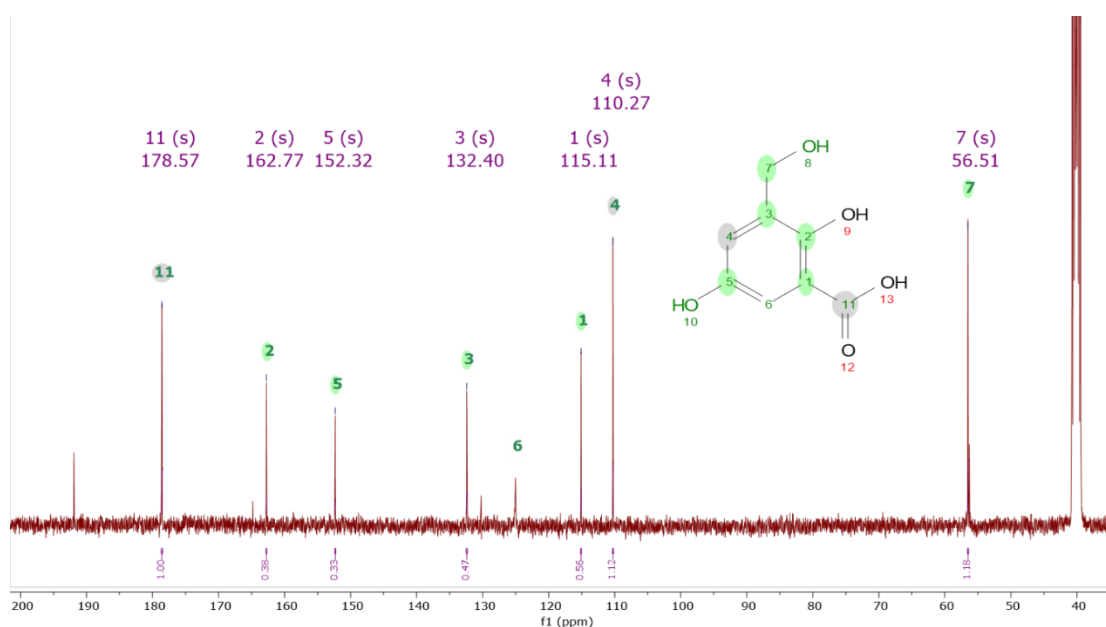


Figure 5.32: ^{13}C NMR spectrum of F4-6 in DMSO-d_6 at 500 MHz.

Assignments for the non-quaternary carbons were accomplished by HMQC (Figure 5.33). However, there were only three cross-peaks observed instead of the expected four for the two pairs of coupling protons observed in the COSY spectrum. The two meta-doublets at 6.61 and 7.50 ppm directly correlated with carbons at 110.27 and 125.0 ppm, respectively. The methylene doublet at 4.51 gave a cross peak with the carbon at 56.51 ppm while the triplet 1H proton did not correlate with any carbons, which indicated that it was indeed an exchangeable proton either an OH or NH . The signal at 9.56 ppm was also considered an exchangeable proton and did not exhibit any CH direct correlation.

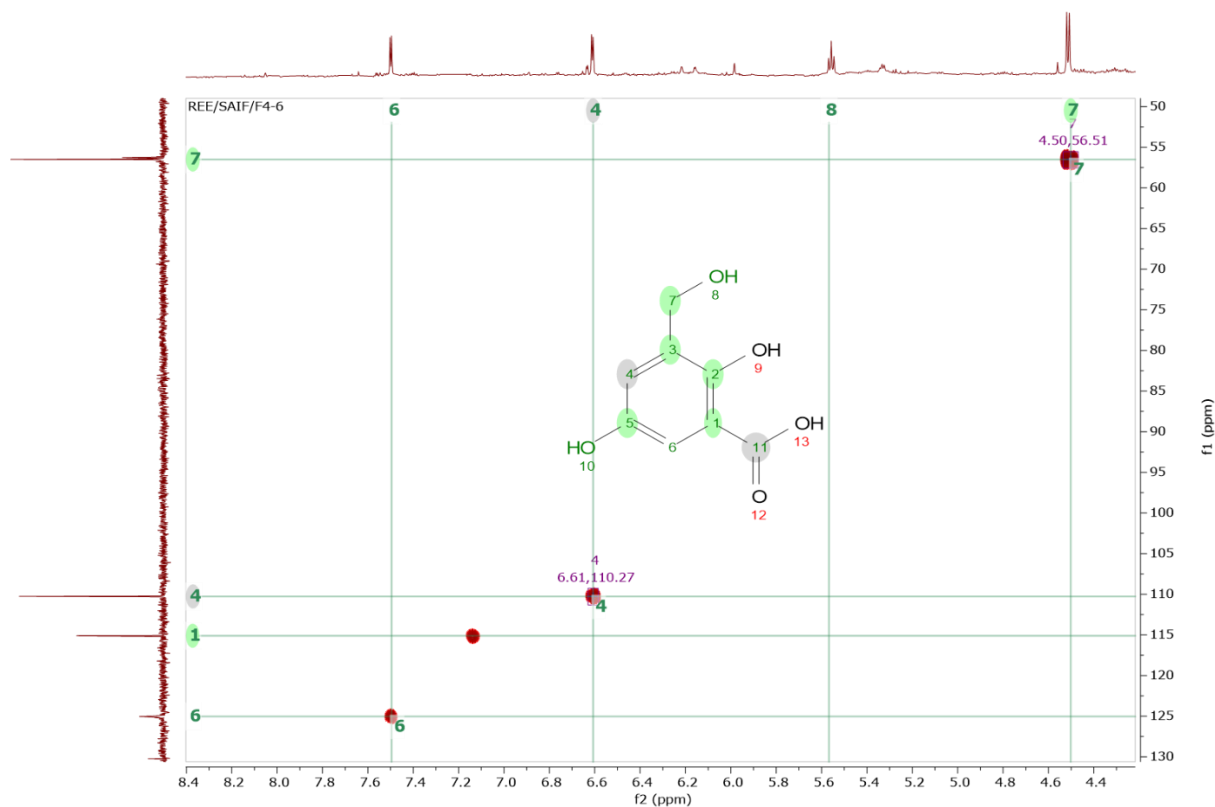


Figure 5.33: HMBC spectrum of F4-6 in DMSO- d_6 at 500 MHz.

Full assignment and the connectivity of the quaternary carbons with the rest of the units were achieved by HMBC in Figure 5.34. Commencing with the methylene doublet proton at 4.51 ppm, 3J -correlations were observed with the hydroxyl-bearing carbon at 162.77 ppm (C-2) and a shielded methine carbon at 110.27 ppm (C-4) indicating the position of the hydroxymethylene unit on C-3. At this stage, the hydroxyl moiety was preferred over an amine group as a terminal unit. An amine (NH_2) would afford a methylene triplet while a hydroxyl group would give a methylene doublet as observed in the 1H spectrum of F4-6. The hydroxyl triplet proton at 5.56 ppm gave a 2J -cross peak with the methylene carbon at 56.51 ppm (C-7) as well as a 4J -correlation with C-2. Further, the methine doublet proton at 6.61 ppm on C-4 also correlated with C-2 and to 125.0 ppm (C-6) bearing its meta-coupling proton partner at 7.50 ppm. Continuing with H-6, it showed 3J -cross peaks with C-2 and C-4 along with the second hydroxyl-bearing carbon at 152.32 ppm for C-5. The culminating correlation was observed between the hydroxyl proton singlet at 9.56 ppm with C-5. However, no HMBC cross peaks were detected to quaternary carbon signals at 132.40 (C-3), 115.11 (C-1), and 178.57 (COOH). Their assignments were completed by comparison with the spectral data afforded by orsellinic acid. Full 1H and ^{13}C assignments for F4-6 is presented in Table 5.11.

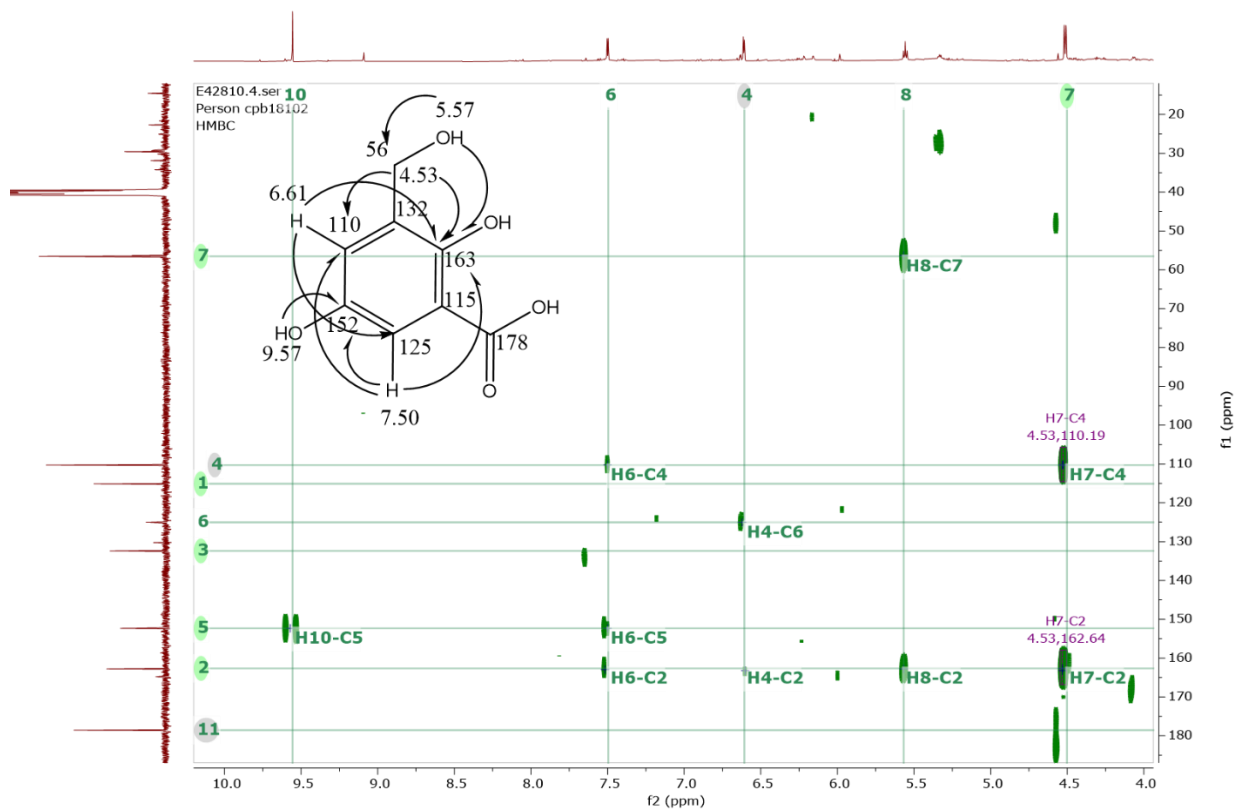


Figure 5.34: HMBC spectrum of F4-6 in DMSO-d₆ at 500 MHz.

Table 5.11: NMR spectral data for compound F4-6 measured in DMSO-d₆ with HMBC correlations as indicated by the arrows in the figure below.

Atom no	¹³ C ppm,	multiplicity	¹ H ppm	multiplicity (<i>J</i> in Hz)	HMBC (H to C)
1	115.11	C			
2	162.77	C			
3	132.40	C			
4	110.27	CH	6.61	d (3.5)	C-2, C-6
5	152.32	C			
5-OH			9.56	s	C-5
6	125.0	CH	7.50	d (3.5)	C-2, C-4, C-5
7	56.51	CH ₂	4.51	d (6.0)	C-2, C-4
7-OH			5.56	t (6.0)	C-2, C-7
11 (COOH)	178.57	C			

Legend: br s = broad singlet, s = singlet, d = doublet, t = triplet

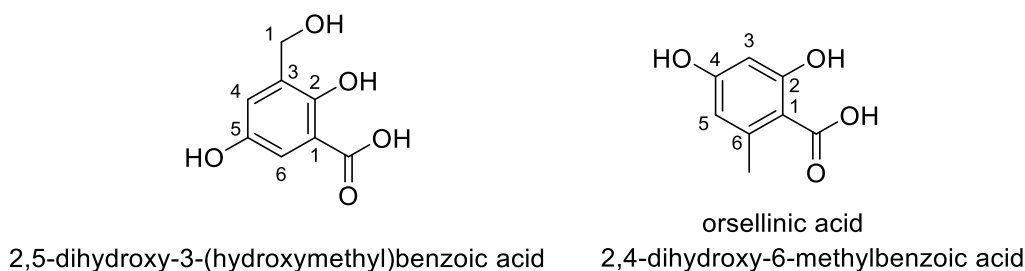


Figure 5.35: Chemical structure of 2,5-dihydroxy-3-(hydroxymethyl) benzoic acid (F4-6) and orsellinic acid.

The structure of compound F4-6 was elucidated as 2,5-dihydroxy-3-(hydroxymethyl)benzoic acid and was comparable to orsellinic acid (Figure 5.35). Using the systematic chemical nomenclature of naming compounds, orsellinic acid is known as 2,4-dihydroxy-6-methylbenzoic acid. In both structures, the carboxylic acid moiety is *ortho* to one of the hydroxy units. In orsellinic acid, the hydroxyl and alkyl substituents are all *meta* to each other. In F4-6, the hydroxyl groups are *para* oriented while the alkyl substituent also *ortho* to one of the hydroxyl moiety.

A similarity search was done for the elucidated structure of F4-6 on SciFinder© library database. With no exact match found, a compound with 86% similarity was retrieved, which was used as a precursor in the synthesis of antimicrobial oenostacin active against *S. aureus* and *epidermis* (Monde et al., 1998, Srivastava et al., 2007). The synthetic precursor analogue (Figure 5.36) was 5x less active than oenostacin.

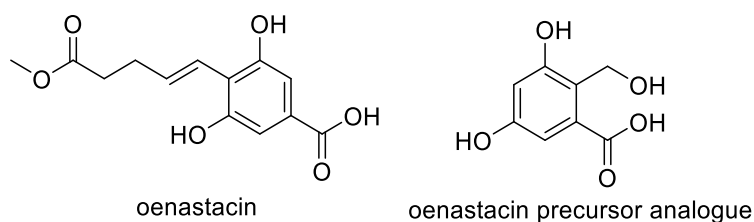


Figure 5.36: Structures of oenostacin and a synthetic precursor analogue (Srivastava et al., 2007).

5.3 Dendryphiella salina on Oat Solid Media without sea salt.

5.3.1 Crude extracts and extract yields.

Oat solid media without sea salt was also chosen as a media for scaling up the production of antimicrobial secondary metabolites produced by *D. salina*. The scale-up was achieved by inoculating *D. salina* in twelve 2L flasks of oat solid media and incubated for 30 days at 27C°. The total yield of the attained crude EtOAc extract was 19.299g. After solvent partitioning, the n-hexane extract yield was 14.599g with a 75.6% yield, which indicated a high production of lipids and fatty acids. In parallel, only 0.3g of aqueous methanolic and 4.4g of EtOAc extract were obtained at 1.55 and 22.8%. yield.

The EtOAc extract exhibited the highest biological antimicrobial activity with 90% of bacterial growth inhibition followed by n-hexane extract at 50-60% inhibition at concentrations of 100µg/mL while the aqueous methanolic extract did not show any activity. The bioassay result is presented in Table 5.12 and Figure 5.37.

Table 5.12: Antimicrobial assay of liquid-liquid partitioning extracts obtained from *D. salina* grown on oat solid media.

Type of extract	% of <i>S. aureus</i> inhibition	% of <i>P. aeruginosa</i> inhibition
AlamarBlue® assay		
n-hexane	48.47	42.49
10% Aq MeOH	-4.14	1.07
EtOAc	99.10	98.13
Planktonic assay		
n-hexane	3.46	8.638
10% Aq MeOH	48.31	42.38
EtOAc	98.79	97.82

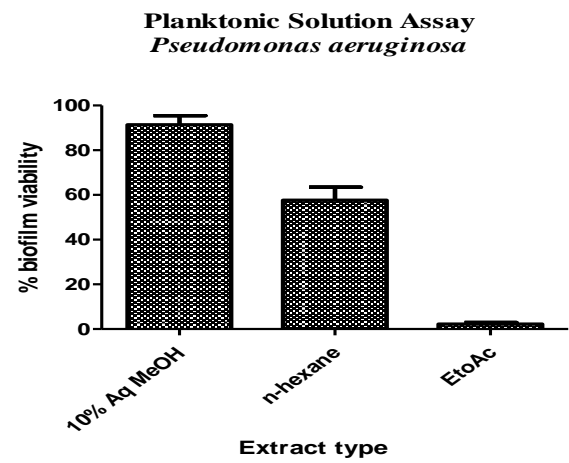
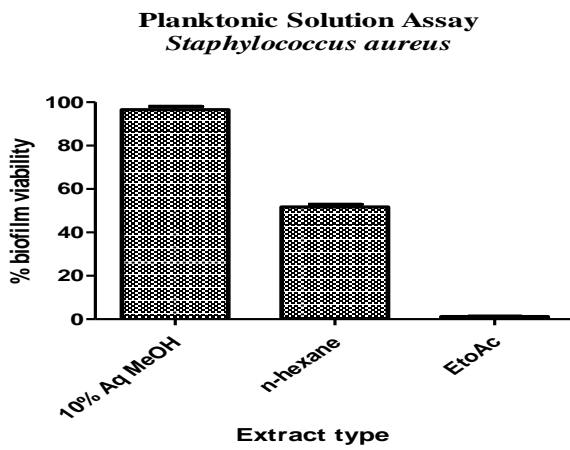
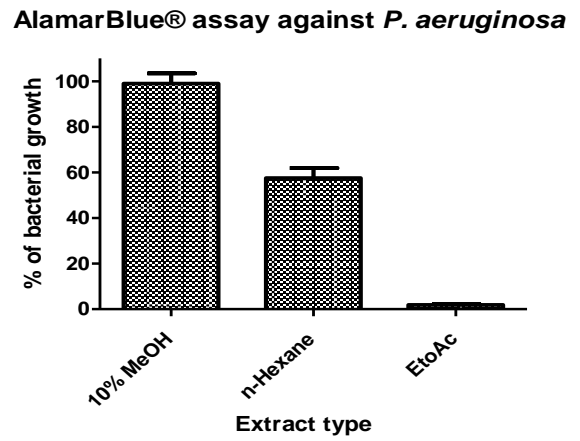
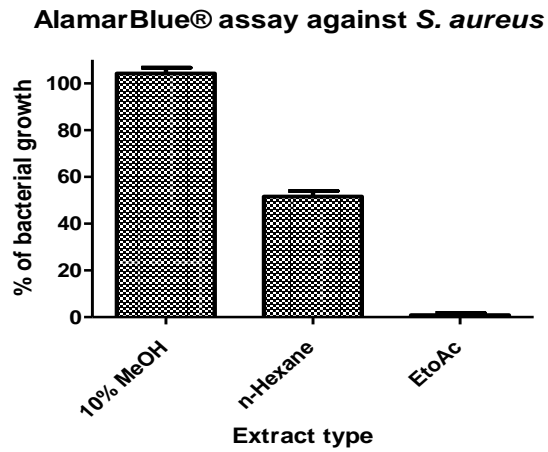


Figure 5.37: AlamarBlue® and planktonic assays of liquid-liquid partitioning extracts against biofilm-forming *S. aureus* and *P. aeruginosa*.

5.3.2 Fractionation of the Extract

The EtOAc extract was subjected to MPLC fractionation and similar fractions were pooled together (Figure 5.38). The yield of pooled fractions afforded 66.6% recovery as shown in Table 5.13.

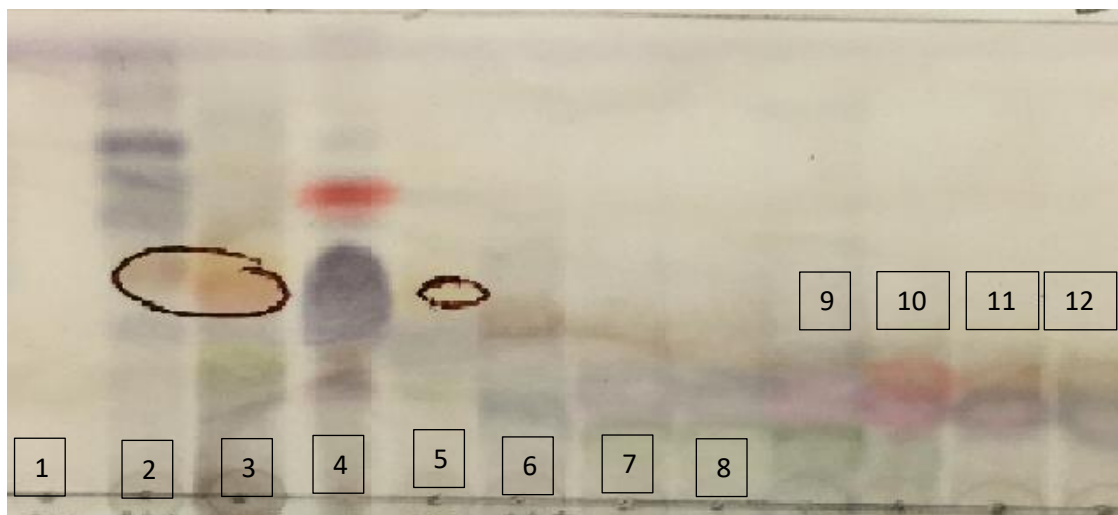


Figure 5.38: Summary TLC plate of MPLC fractions of fungal extract obtained from the oat media. TLC was developed in MeOH:DCM 2:98.

Table 5.13: Fraction weights obtained after fractionation of crude extracts produced from *D. salina* grown on oat solid media.

Fraction #	Fraction Weight	Fraction #	Fraction Weight
F1	290	F8	35.5
F2	77.8	F9	68.5
F3	70.7	F10	490
F4	2.3	F11	18.8
F5	93.6	F12	1404.8
F6	38.7	Fraction wash	310.2
F7	28	Total yield	2928.9
		% recovery	66.6%

5.3.3 Antimicrobial assay results

In the antimicrobial assay results against both biofilm-forming *S. aureus* and *P. aeruginosa*, fractions 2, 3, 5, 9 and 10 inhibited the growth of both microorganisms at more than 75%. Fractions 4 and 6 were able to produce an antimicrobial activity of at least 40%. The rest of the fractions were found inactive and therefore excluded for further fractionation work. The antimicrobial assay results are presented in Figure 5.39 and Table 5.14.

Table 5.14: AlamarBlue® and planktonic assay results of *D. salina* fractions against both biofilm-forming *S. aureus* and *P. aeruginosa*. Highlighted rows are the antimicrobial active fractions at a threshold of 75% growth inhibition or 25% bacterial viability.

<i>S. aureus</i> biological assay results					
Fraction #	% of bacterial viability	% of Biofilms viability	Fraction #	% of bacterial viability	% of Biofilms viability
1	93.27	89.90	7	93.98	93.91
2	25.90	23.78	8	83.65	85.29
3	13.65	10.80	9	14.47	18.41
4	48.51	45.79	10	10.09	11.81
5	5.73	7.3577	11	89.38	91.02
6	56.78	56.91	12	91.31	92.95
Washing				96.91	96.49
<i>P. aeruginosa</i> biological assay results					
Fraction #	% of bacterial viability	% of Biofilms viability	Fraction #	% of bacterial Viability	% of Biofilms viability
1	93.33	86.63	7	95.42	94.39
2	25.75	24.75	8	81.61	80.58
3	13.45	12.47	9	21.86	23.09
4	48.44	47.44	10	8.16	7.18
5	5.53	4.56	11	92.278	91.25
6	56.74118	55.7349	12	89.52	88.49
Washing				99.14	98.11

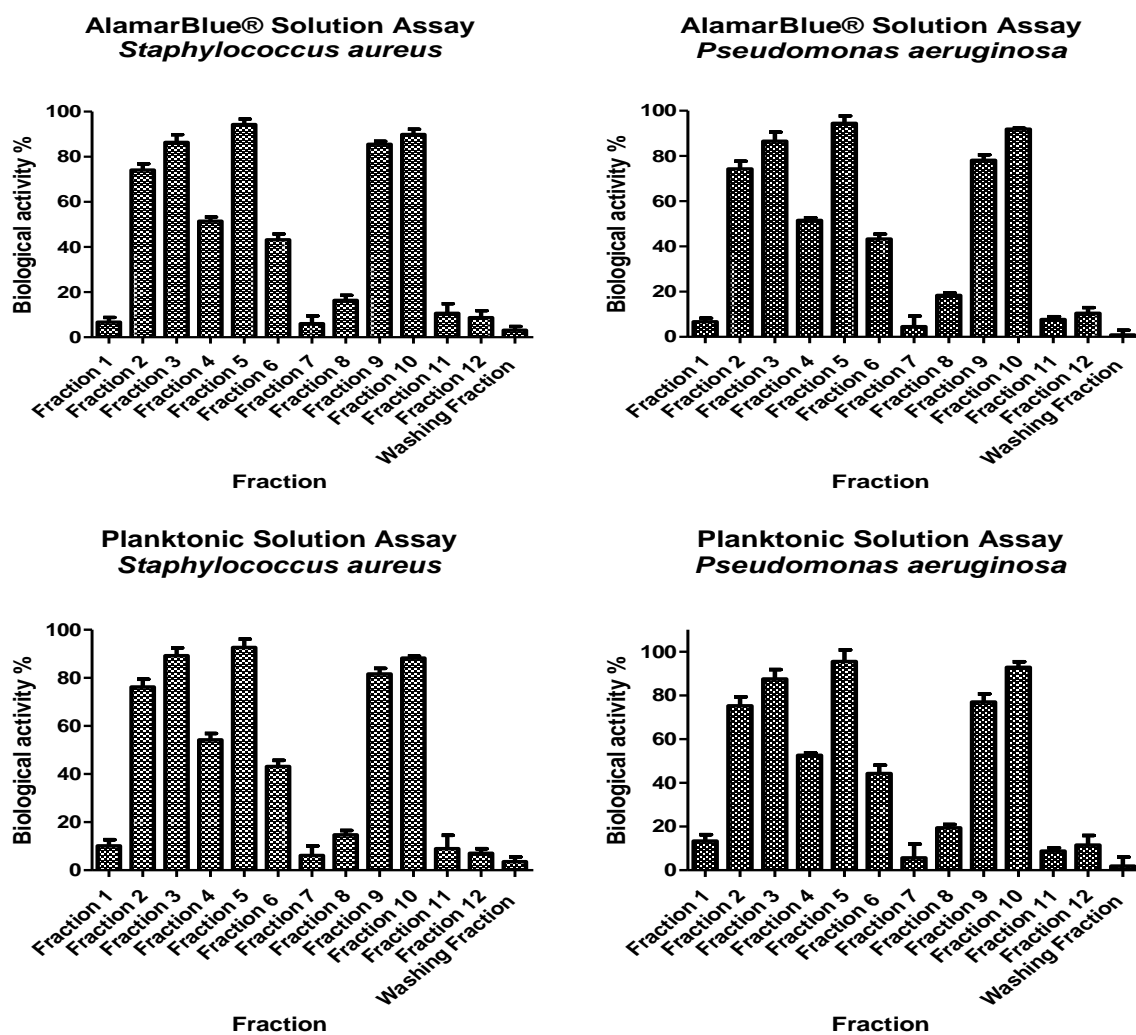


Figure 5.39: AlamarBlue® and planktonic assay results of MPLC fractions of *D. salina* grown on oat solid media fractions.

5.3.4 ¹H NMR spectroscopy.

As indicated by the ¹H NMR spectral data of the MPLC fractions in Figure 5.40, the compounds produced by *D. salina* grown on oat solid media were comparable to the compounds produced by the endophyte grown on malt extract liquid media. The major difference was the ratio of fatty acids and the aliphatic compounds, which was higher when the fungus was grown in oat solid media as shown in Figure 5.40.

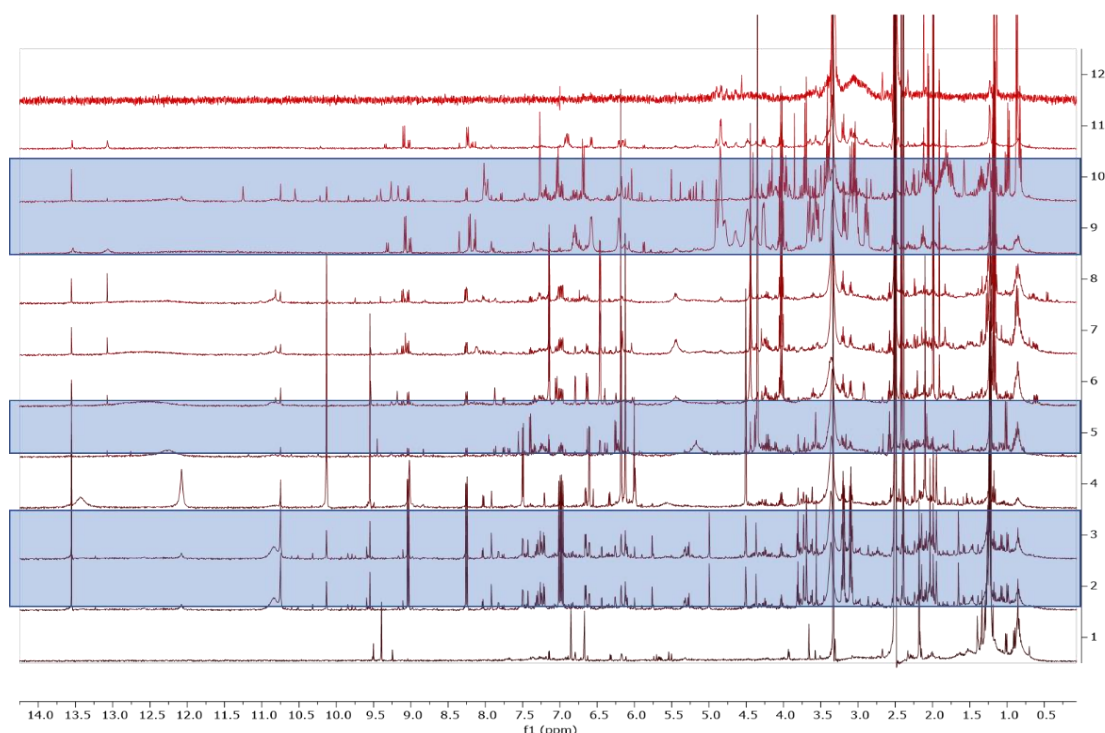


Figure 5.40: Stacked ¹H NMR spectrum of MPLC fractions of *D. salina* grown on oat solid media. Highlighted spectra represent the bioactive fractions.

The ¹H NMR spectral data of fractions 2, 9, and 12 revealed a different chemical profile from the rest of the other fractions. However, fraction-3 looked more like fraction-2. The ¹H NMR spectrum of fraction-12 showed the absence of any signals found from the earlier fractions indicating the exhaustive elution of all metabolites. Many signals from both the aliphatic to the aromatic region could be perceived in fractions 2 and 9. Such differences were also reflected on the PCA scatter plot of their NMR spectral data that is presented in Figure 5.41. The model gave a goodness of fit R^2 at 0.966 but a very poor predictivity Q^2 of 0.356 after 8 components (Figure 5.41A). To improve the predictivity score, fraction-12 was removed and the model gave a R^2 and Q^2 at 0.99 and 0.515, respectively, which made the model valid, while emphasising the uniqueness of fractions 2 and 9 (Figure 5.41B). The PCA loadings plot (Figure 5.42A) revealed the discriminating peaks and the type of compounds unique or most abundant in the respective fractions. Fraction-2 afforded the highest abundance of phenolic aromatic (6-7ppm) and acetylated (2-3ppm) peaks (Figure 5.42B). On the other hand, fraction-9 yielded a higher profusion of hydroxylated aliphatics (3-4ppm) as well as acetylated (2-3ppm) peaks, although not unique to the fraction (Figure 5.42C).

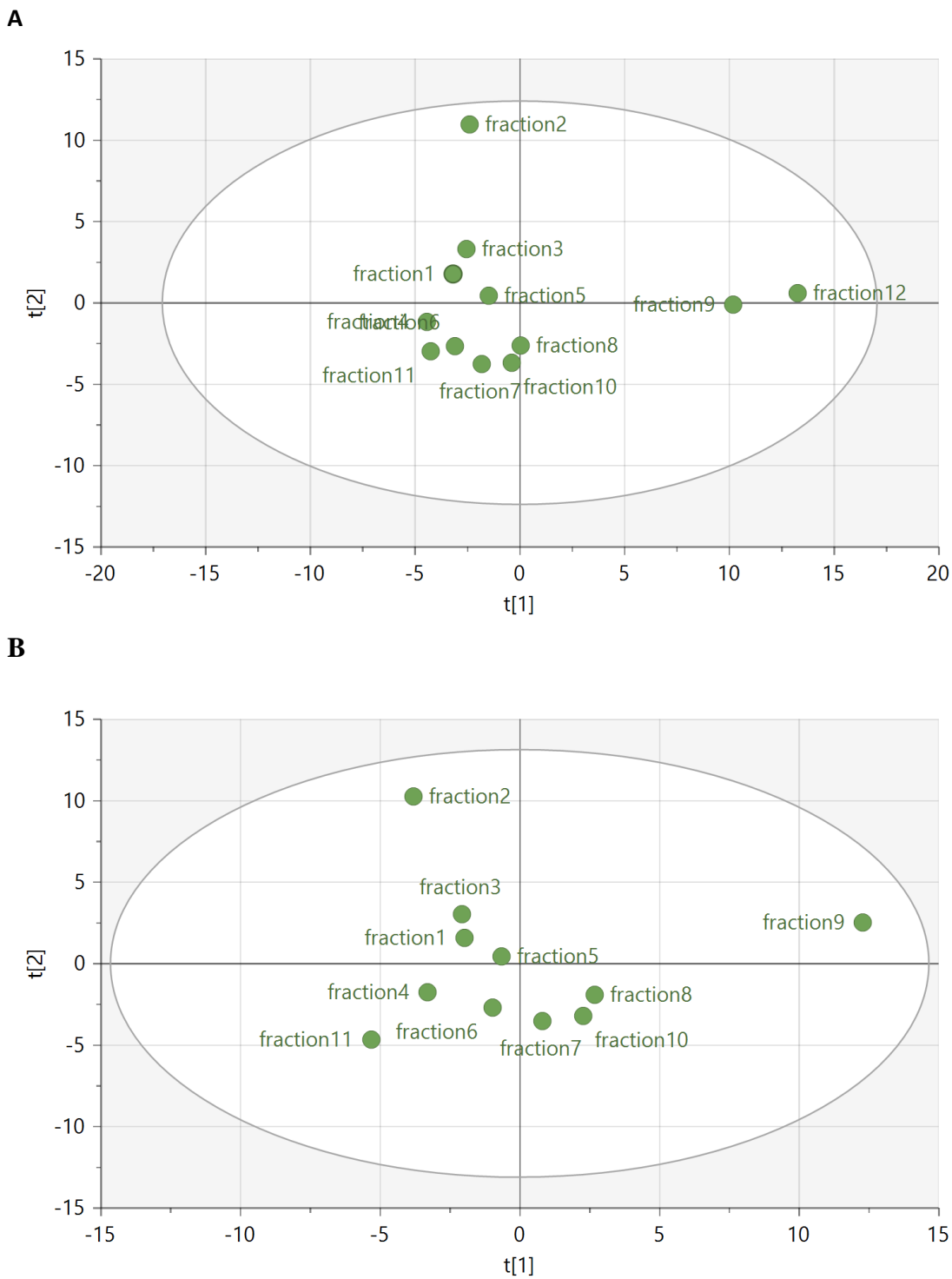


Figure 5.41: PCA scatter plot of the ^1H NMR spectral data of (A) all MPLC fractions and (B) with the exception fraction-12 of the EtOAc extract of *D. salina* grown on oat solid media.

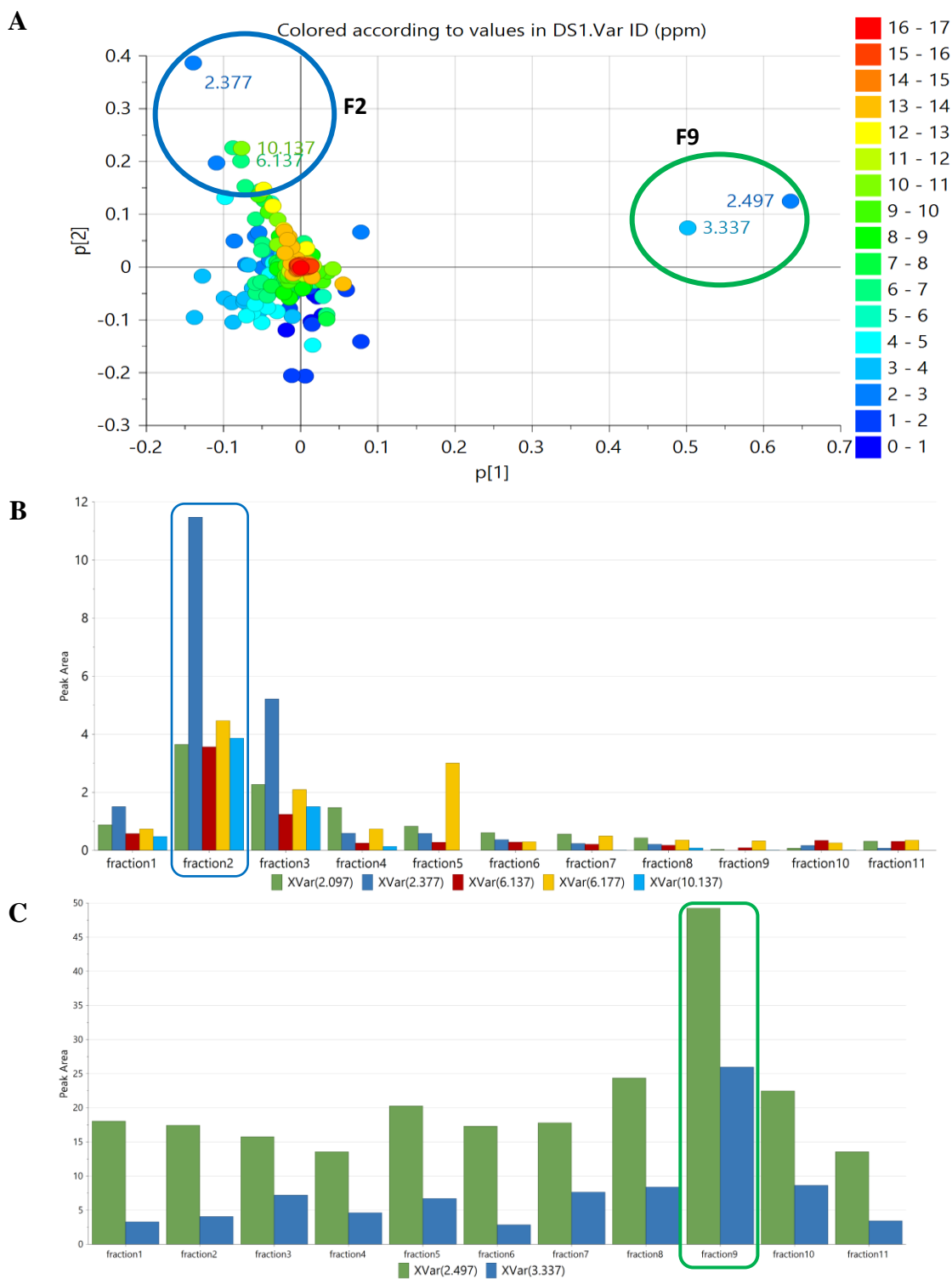


Figure 5.42. PCA loadings plot (A) of the ^1H NMR spectral data of the MPLC fractions with the exception fraction-12 of the EtOAc extract of *D. salina* grown on oat solid media. The relative abundance of the discriminating peaks for Fraction-2 (B) and Fraction-9 (C).

When coupling the biological assay results to the ^1H NMR spectral data, the chemical profiles of the active and inactive fractions can be differentiated. The active fractions were located on the left quadrants of the OPLS-DA scatter plot (Figure 5.43A), where fractions 9 and 2 were separated on the upper left quadrant. The inactive fractions were positioned at the right quadrants of the OPLS-DA scatter plot while only fraction 12 was separated on the upper right quadrant due to the absence of ^1H NMR signals in its spectrum. The variation within group was obviously higher at 27.6% due to the dispersal of some of the sample fractions within the respective classes. On the other hand, the variation score between groups was only 5.79%, which indicated their poor separation. By excluding Fraction -12, R^2 and Q^2 are 1.00 and 0.37, respectively, for 9 components. R^2 value was improved to 1.00 but the predictivity was still poor due to the weak separation of the variables between the active and inactive groups.

The OPLS-DA loadings plots (Figure 5.43B) revealed that the active fractions could afford compounds with various types of functional groups such as hydroxyl, carbonyl and nitrogen substituents as indicated by occurrence of peaks between 2 and 10ppm. However, it was also observed that discriminatory peaks (encircled in **red**) at the aromatic region between 6 and 9 ppm while for fractions 2 and 9, it was between 2 and 4 ppm, indicative for the acetylated compounds and presence of heteroatom units in the predicted active metabolites.

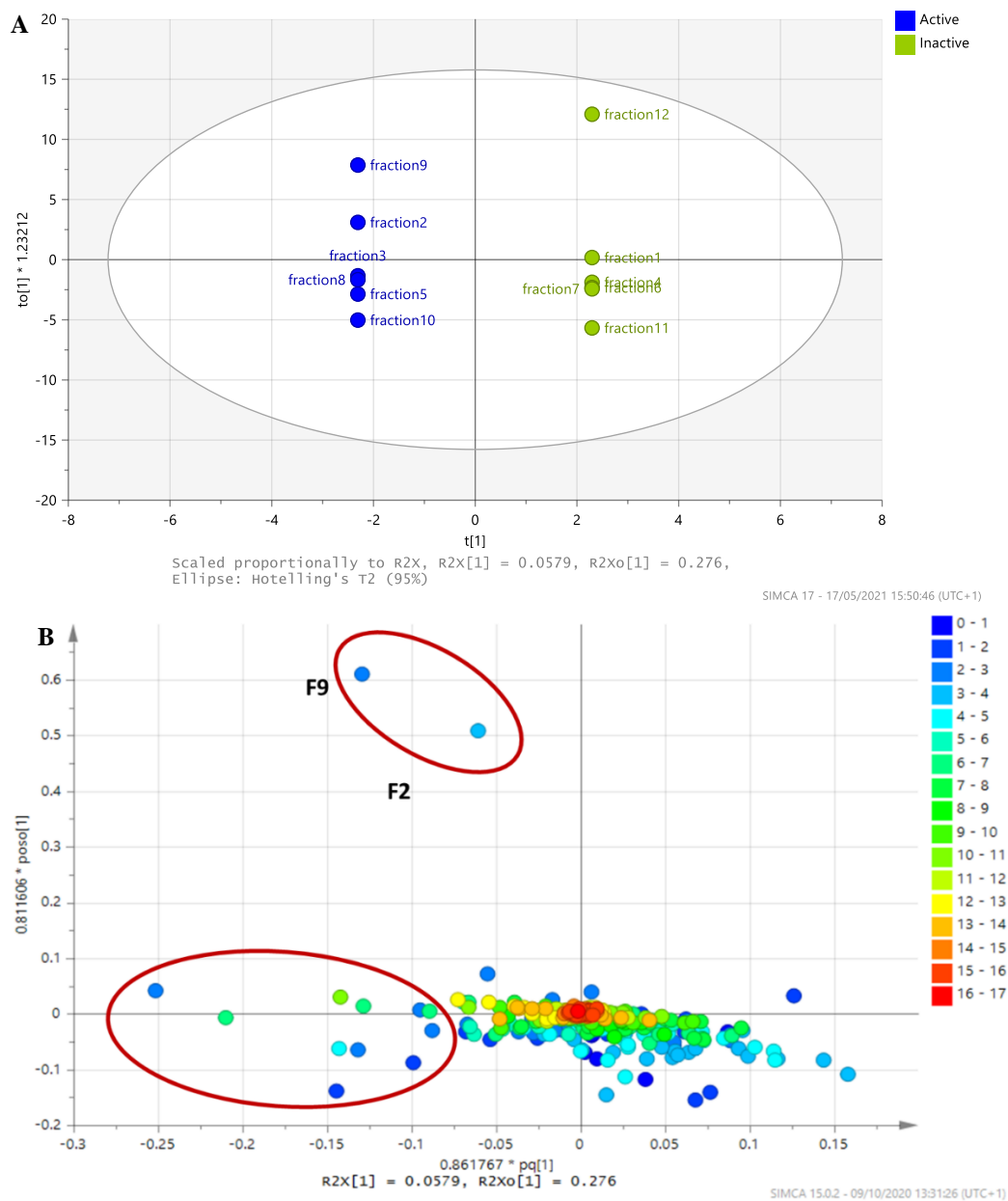


Figure 5.43: OPLS-DA scatter (A) and loadings (B) plots of ^1H NMR spectral data of the MPLC fractions grouped according to their antimicrobial activity. Encircled in red are the discriminatory features for the antimicrobial-active fractions. R^2 and Q^2 are 1.00 and 0.37, respectively, for 9 components.

5.3.5 LC-HRMS data analysis.

The PCA scatter plot of the mass spectral data of the MPLC fractions in Figure 5.44 indicated that fractions 4, 5, and 6 could have a somewhat different chemical profile from the other fractions, with the outlying Fraction-5 as probably unique. The model gave a goodness of fit at 0.74 but a very poor predictivity score of -0.329 after 4 components. Again, adding on the antimicrobial assay results to the mass spectral data, the fractions were classified as either active or inactive for OPLS-DA. The model gave a goodness of fit at 1.0 and a predictivity at 0.922 after 13 components, which indicated a very good model. The active fractions were located at the left side of the OPLS-DA scatter plot while fraction-5 remained separated from the main cluster on the upper right quadrant, which indicated the presence of possible unique bioactive feature. Unlike in the multivariate analysis of the NMR data, fraction-5 stayed within the cluster of active fractions, while fractions 2 and 9 were separated

The OPLS-DA loadings plot in Figure 5.45A indicated the discriminatory features projected for their antimicrobial activity to have molecular weights between 250 and 350 Da. These are the features encircled in **red**. Dereplication of these predicted antimicrobial metabolites afforded oxygenated or heteroatom-bearing compounds. Hence, the high ratio of resonances between 2 and 4 ppm region in the NMR data of the antimicrobial fractions. The antimicrobial compounds were distributed mainly in fraction-5 as presented on the bar graph of the peak areas of the discriminating x-variables (Figure 5.45B). Amongst these predicted active compounds, five were found to be included in the top 10 VIP features (Figure 5.47c) to discriminate the active from the inactive features. However, none of these features gave a p -value <0.05 .

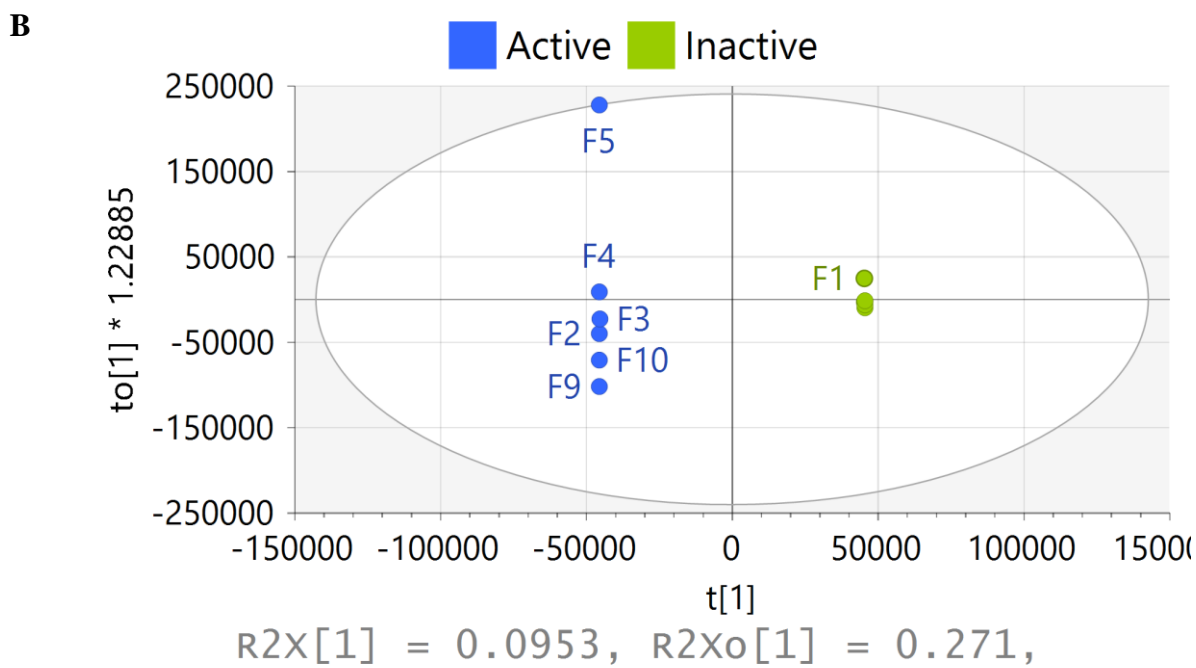
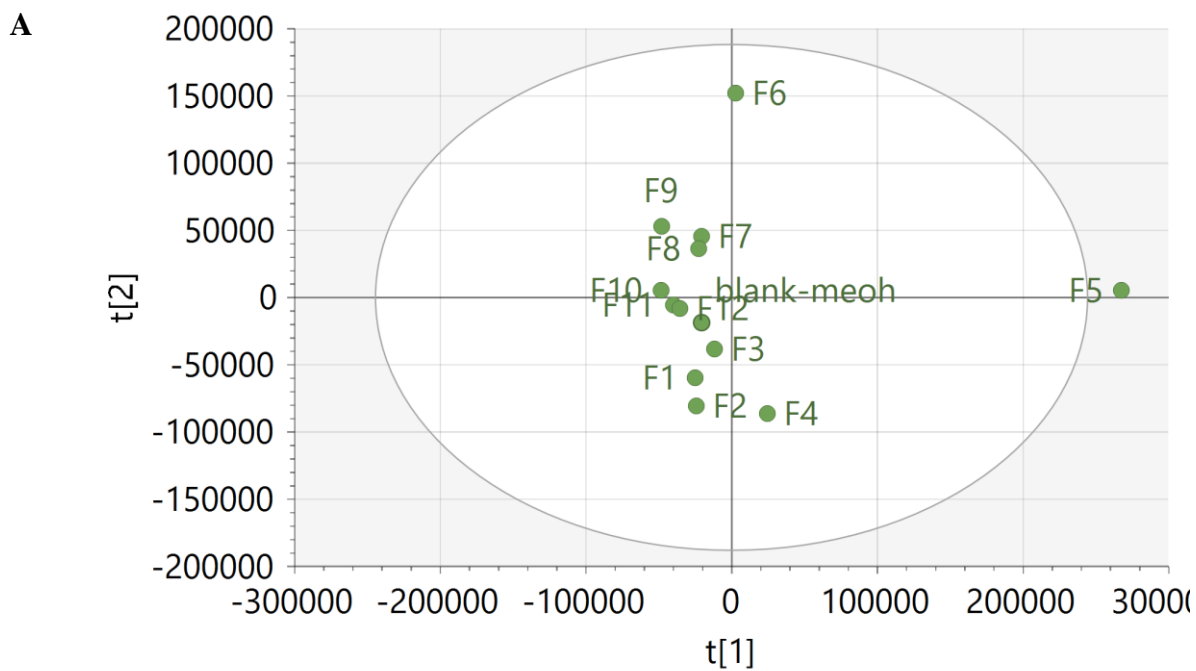


Figure 5.44: PCA (A) and OPLS-DA (B) scatter plot of the LC-HRMS data of the MPLC fractions of the extracts of *D.salina* grown on oat solid media.

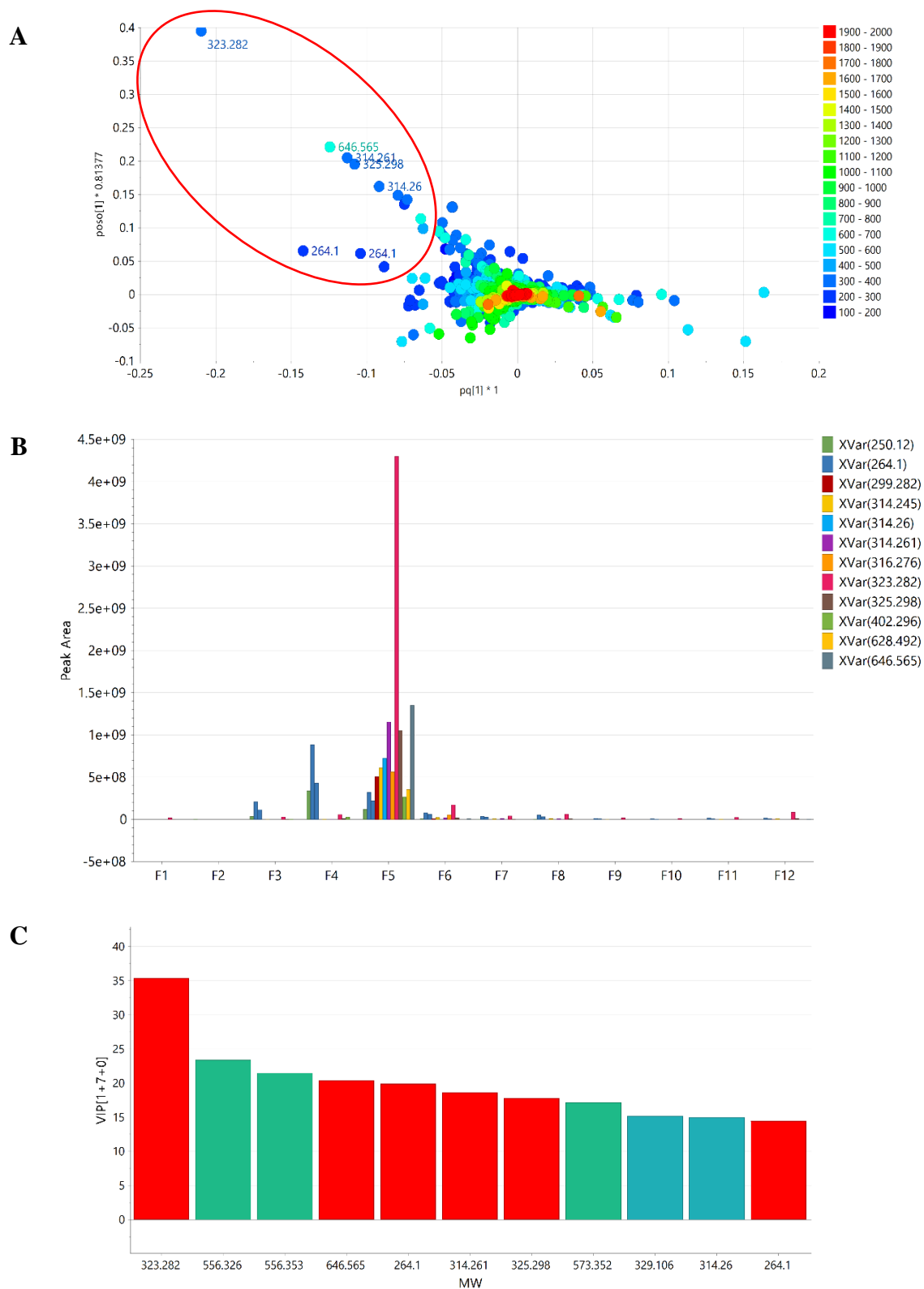
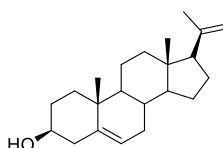
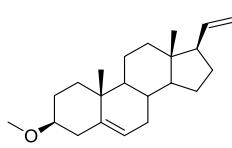
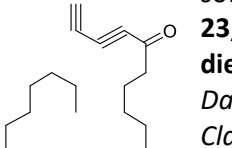
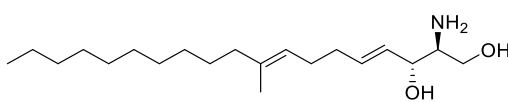
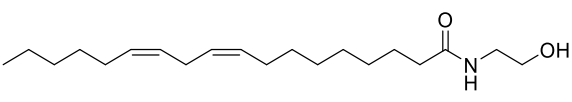


Figure 5.45: (A) OPLS-DA loadings of the LC-HRMS data of the MPLC fractions obtain from the extract of *D.salina* grown on oat solid media crude extracts fractions. (B) Peak areas showing the relative abundance of discriminatory features of the antimicrobial fractions. (C) VIP plot of top 10 features differentiating the active and inactive fractions. The red bars represent the features from the antimicrobial fractions.

Table 5.15: Discriminatory features for the antimicrobial active fractions under the top 10 VIP (Variable Importance in Projection. Features are arranged according to increasing FDR (False Discovery Rate).

Mzmine ID	Rt (min)	MW	MF (DBE)	p-value	FDR	Compound hits (sources)
P_3600	12.22	264.100	C ₁₄ H ₁₆ O ₅ (7)	0.17214	0.01	99 hits, 20 were of fungal origin, 6 of which were marine-derived See P_2201 in Figure 5.11B
N_2865	19.24	314.260	C ₂₂ H ₃₄ O (6)	0.34150	0.02	12 hits from sponges and soft corals 23,24-bisnorchola-5,20-dien-3-ol (sponge <i>Damiriana hawaiiiana</i> , <i>Cladophora vagabunda</i> and brown alga <i>Cystoseira crinata</i>) debromorenierin 1 (sponge <i>Reniera fulva</i>) pregna-5,20-dien-3-methoxy (Cnidaria <i>Scleronephthya flexilis</i>)
						
						
						
P_3798	25.00	646.565	2[C ₂₀ H ₃₇ NO ₂]	0.34480	0.03	Complex of P_2438
P_3483	27.82	325.298	C ₂₀ H ₃₉ NO ₂ (2)	0.35254	0.04	12 hits, 1 from a soft coral 2-amino-9-methyl-4,8-nonadecadiene-1,3-diol (<i>Cespitularia cocerulea</i>)
						
P_2438	24.97	323.282	C ₂₀ H ₃₇ NO ₂ (3)	0.37093	0.05	N-(2-hydroxyethyl)linoleamide Found in plants N-(1 <i>H</i> -pyrrole-2-carbonyl) derivative was isolated from the sponge <i>Agelas nakamurai</i> (Chu et al., 2017)
						

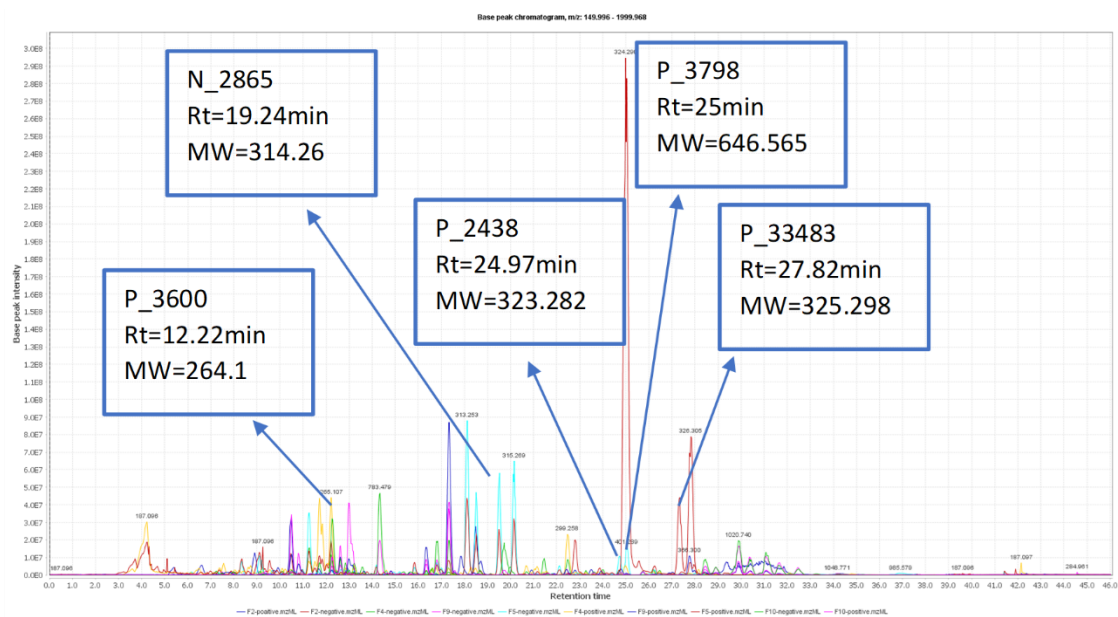


Figure 5.46: Total Ion Chromatogram (TIC) of the active fraction. The ion peaks that represent the discriminating features listed in Table 5.15 have been labelled.

The five predicted antimicrobial compounds were dereplicated and listed in Table 5.15 and their TIC is shown in Figure 5.46. Amongst these features was P_3798, which was a complex or a $2M^+$ of P_2438. Like the antimicrobial compounds dereplicated from the fungal extract incubated in malt extract, hydroxylated phenyl or lactone congeners were also detected for the feature P_3600 with a RT of 12.22 min. P_2201 from the extract grown in malt extract has a RT of 13.4 min, which was almost in the comparable elution time range as P_3600. However, the extract obtained from the fungus incubated in oat media afforded a higher concentration of non-polar compounds that were initially revealed from the NMR spectral data, which was also perceived in the dereplication data of the bioactive features. This included long unsaturated alkyl chains and steroids. The fungal extract obtained from the malt extract broth showed more compounds originating from the polyketide pathway.

5.3.6 Pure compounds isolation and structure elucidation

Four fractions were subjected for further fractionation depending on their antimicrobial activity, metabolomic profile, and fraction yield. There were five active fractions (F-2, F-3, F-5, F-9, and F-10) when considering a 75% bacterial growth inhibition threshold. Fraction-5 was the most active with an average inhibition of 95%, followed by Fractions-10 and-3 at 90%, then Fraction-9 at 80% and lastly, Fraction-2 at 75%. Fraction-10 gave the highest yield of 490 mg, Fraction-5 at 93.6 mg, Fraction-2 and-3 at *ca.* 75 mg. The lowest yield was afforded by

Fraction-9 at 63 mg. In terms of the chemical profile as defined by the target antimicrobial metabolites predicted by multivariate analysis, Fraction-5 was the most interesting.

5.3.6.1 Fraction 2 sub fractionation

Fraction 2 (77.8 mg) was fractionated using the Reveleris flash chromatography instrument equipped with an evaporative light scattering detector (ELSD) due to the presence of non-chromophore compounds. Fraction 2 was still a complex mixture of various compounds as shown in Figure 5.47. DCM and EtOAc were used as the solvent system for gradient elution. Fraction-2 was loaded over a 12g silica column. Elution started with 100% DCM to 100% of EtOAc in 2hrs. The collected fractions were pooled into six (Figure 5.48), then were dried and weighed as recorded in Table 5.16.

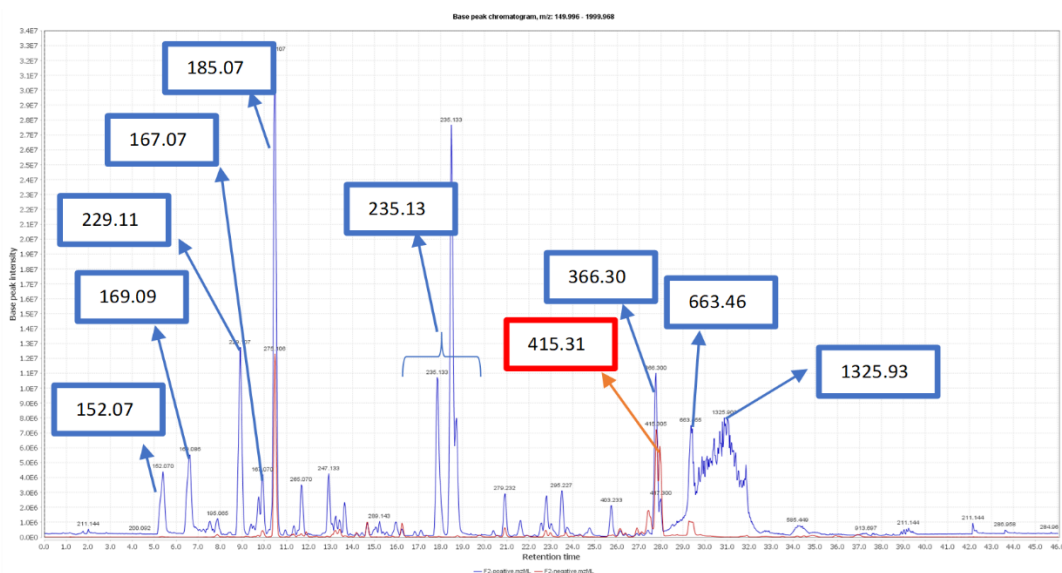


Figure 5.47: Total Ion Chromatogram (TIC) of fraction 2 with assigned [M+H] and [M-H] of the major peaks: [M+H] values are in blue boxes and [M-H] value in red box.

Table 5.16: Yields of subfractions of fraction 2 obtained by Reveleris flash chromatography.

Fraction #	Weight (mg)	Fraction #	Weight (mg)
1	7.2	4	11.4
2	12.2	5	13.7
3	12.7	6	7.2
Wash			11.4
% recovery			99.7%

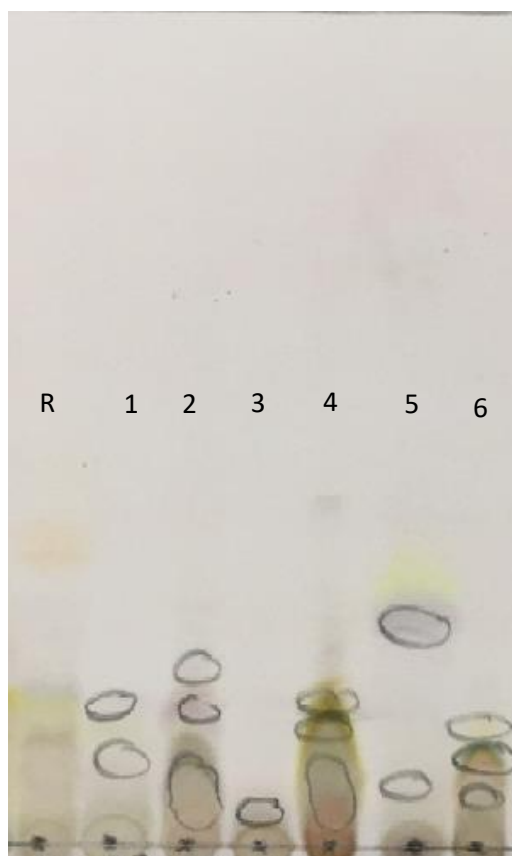


Figure 5.48: Summary TLC plate developed with MP of DCM:MeOH 99:1.

After comparing the stacked ^1H NMR spectra of fraction-2-subfractions as shown in Figure 5.49, only subfractions-1, -2 and -3 were found interesting for further purification and elucidation work. Subfractions-1 and -2 were quite similar and could entail the same compounds, as well as with their low yields, the two subfractions were therefore pooled together for preparative-TLC purification.

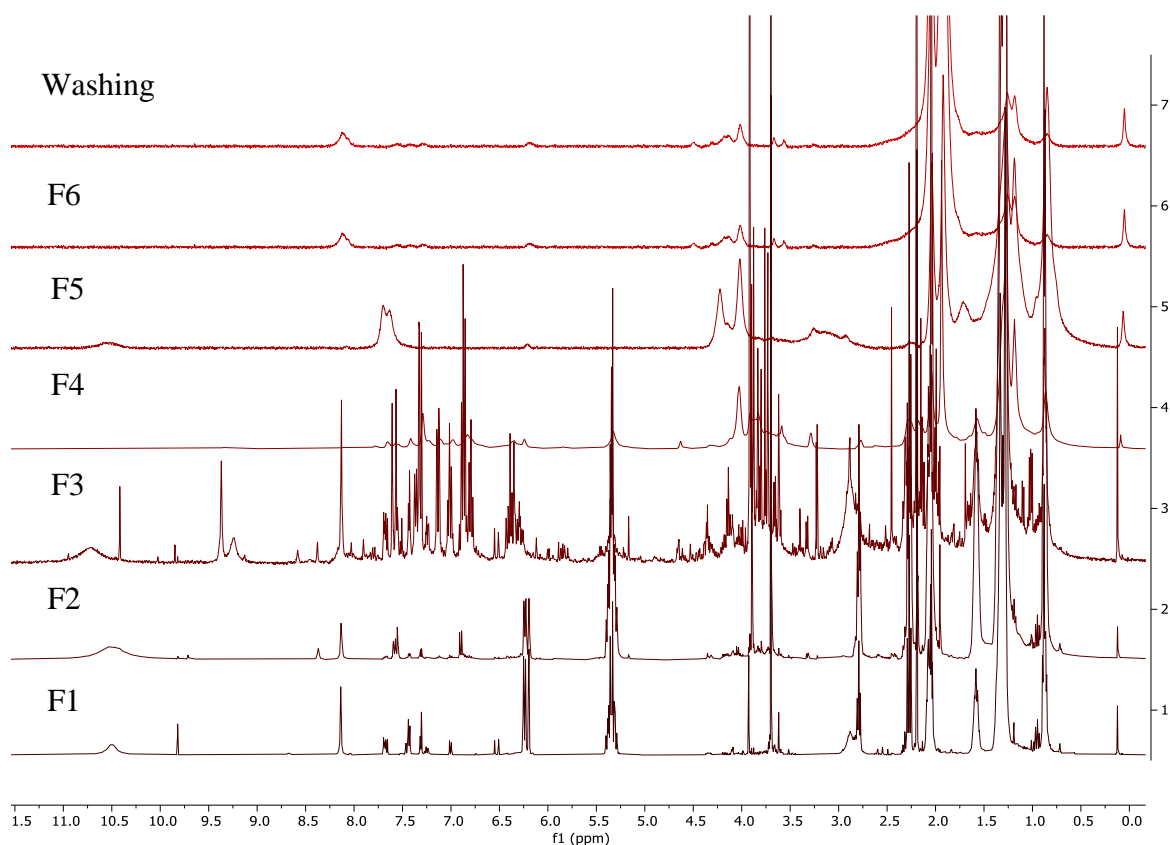


Figure 5.49. Stacked ^1H NMR spectra of the fraction-2-subfractions obtained by flash chromatography equipped with an evaporative light scattering detector (ELSD).

5.3.6.2 Fraction 2-2 purification.

The pooled subfractions 2-1 and 2-2 gave a total yield of 19.4 mg, which was further purified by preparative-TLC afforded five subfractions. The yields of the subfractions are presented in Table 5.17. From the stacked ^1H NMR spectra of the preparative-TLC subfractions (Figure 5.50), fraction-2-2-2 was the purest and was subjected to structure elucidation work using different 2D-NMR techniques that included COSY, HMBC and HMQC.

Table 5.17: Yields of preparative-TLC subfractions from the pooled fractions 2-1 and 2-2.

Fraction #	Weight (mg)	Fraction #	Weight (mg)
F2-2-1	1.2	F2-2-6	1.1
F2-2-2	2.1	F2-2-7	1.3
F2-2-3	0.9	F2-2-8	0.8
F2-2-4	1.4	F2-2-9	1.7
F2-2-5	1.1	Loading zone	2.1
		% recovery	70.6

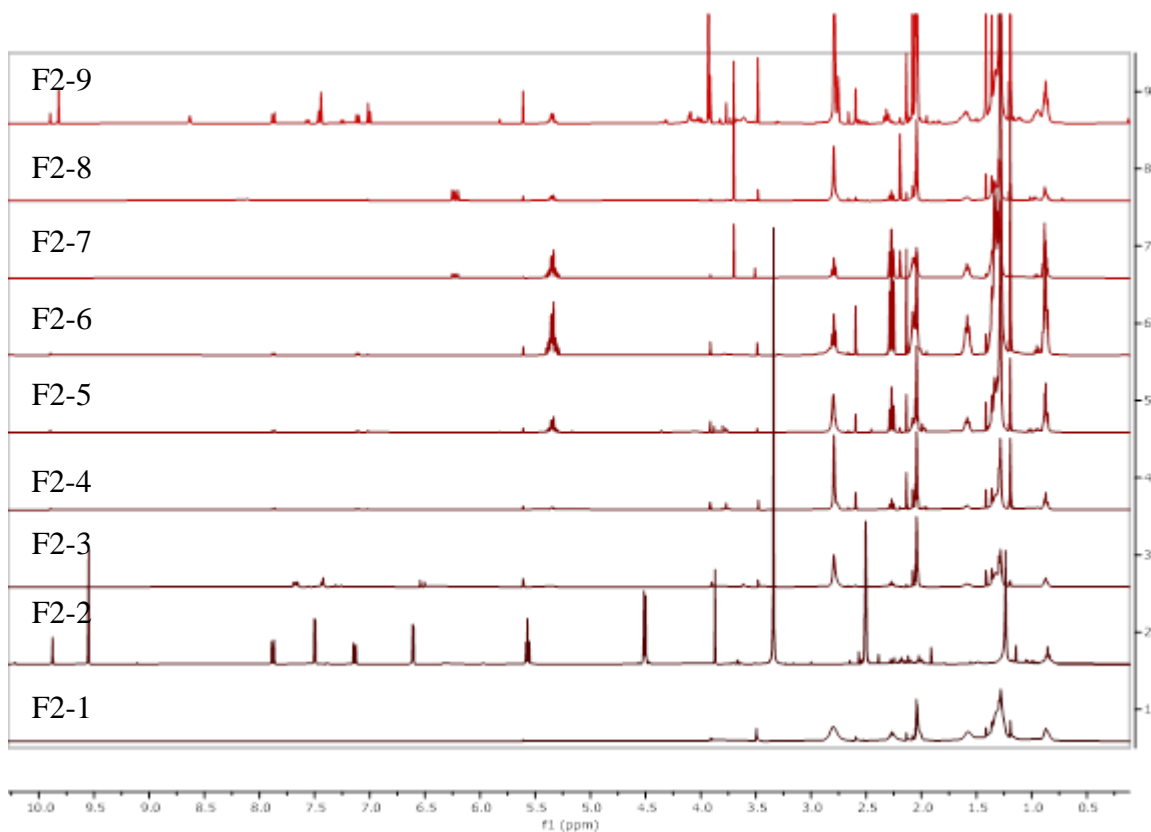


Figure 5.50: Stacked ¹H NMR spectra of preparative-TLC subfractions from the pooled fractions 2-1 and 2-2.

5.3.6.2.1 Fraction 2-2-2 structure elucidation.

The ^1H NMR spectrum of compound F2-2-2 in Figures 5.53 was identical to that for compound F4-6 isolated from *D. salina* grown on malt extract broth. For ^1H and ^{13}C NMR full assignments, see Table 5.10. The structure elucidation of these identical compounds was discussed under section 5.2.7.2.2.

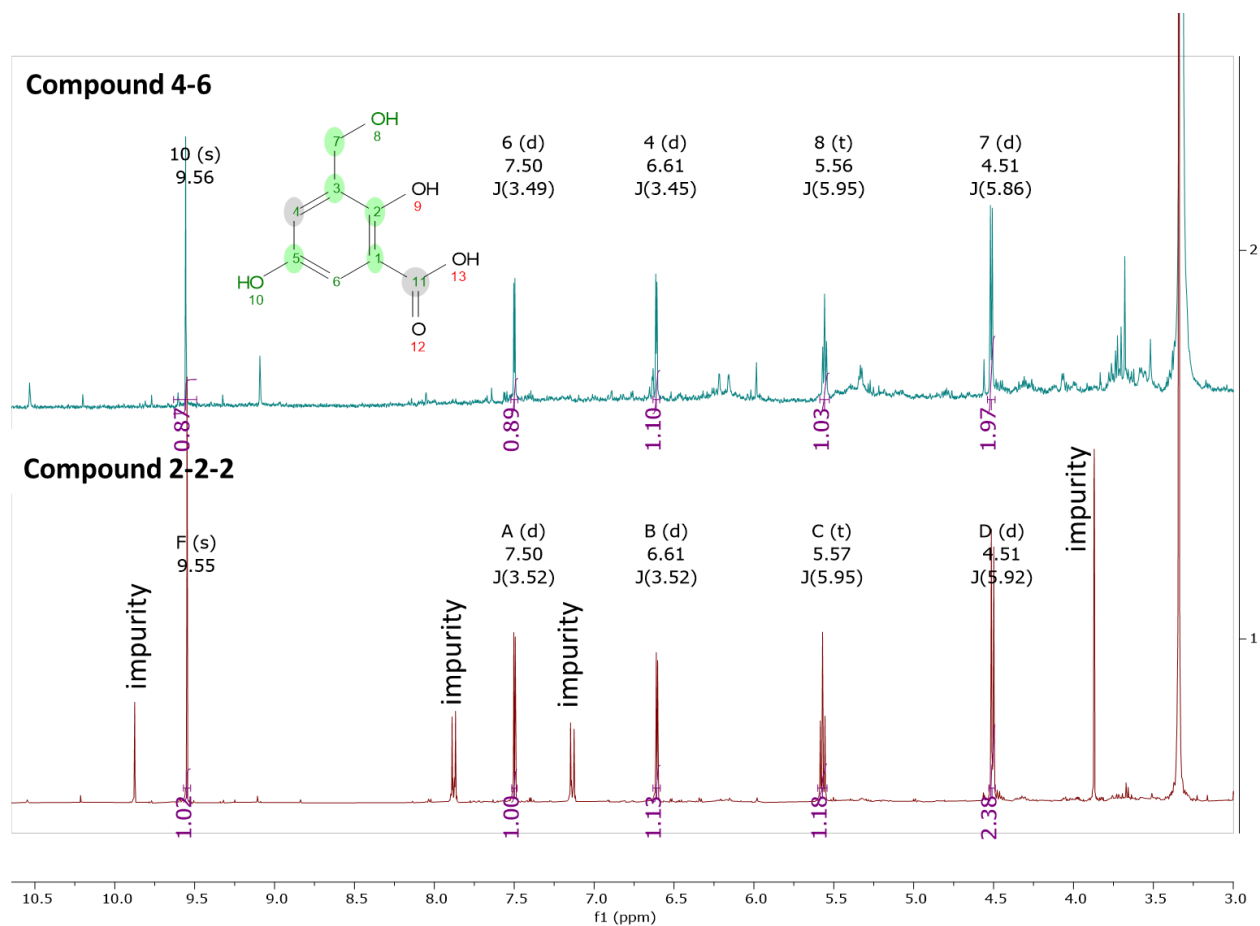


Figure 5.51: ^1H spectra of compounds F2-2-2 and F4-6.

5.3.6.3 Fraction 3 subfractionation.

Fraction 3 (70.7 mg) was also subjected to flash chromatography for further fractionation. Fraction 3 was loaded on a 12g silica column. The number of pooled fractions afforded five subfractions along with one fraction wash. Yields of the respective subfractions and % total recovery are presented in Table 5.18.

Table 5.18: Yields of subfractions of fraction 3 obtained by flash chromatography.

Fraction #	Weight (mg)	Fraction #	Weight (mg)
F3-1	1.8	F3-4	14.2
F3-2	18.3	F3-5	12.7
F3-3	7.2	Washing	15.4
% recovery	98.44		

As presented in the stacked NMR spectra in figure 5.52, Subfractions 3-1, 3-3 and 3-4 were of highest purity as indicated by their ^1H NMR spectra. Subfraction 3-2 consisted of at least two compounds that was one minor and a major compound. Subfraction 3-5 and the fraction wash still entailed a mixture of compounds.

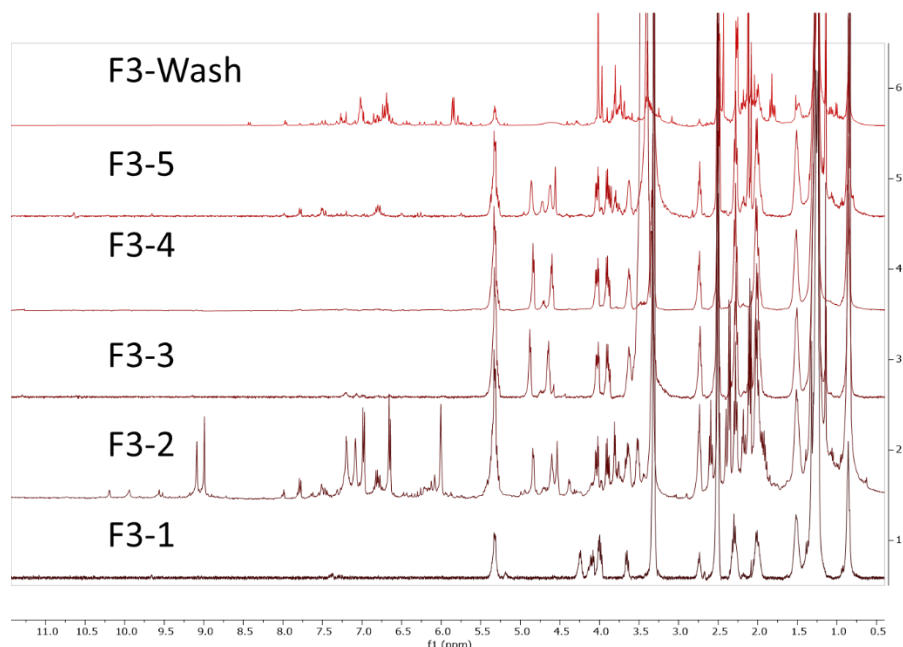
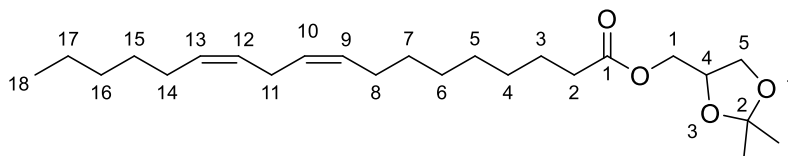


Figure 5.52: Stacked ^1H NMR spectra of fraction-3-subfractions obtained by flash chromatography.

5.3.6.3.1 Compound F3-1 structure elucidation.

1,2-acetonide-3-(9,12- octadecadienoyl)glycerol



(2,2-dimethyl-1,3-dioxolan-4-yl)methyl (9Z,12Z)-octadeca-9,12-dienoate

Chemical Formula: C₂₄H₄₂O₄

Exact Mass: 394.3083

Figure 5.53: Chemical structure of compound F3-1

Formula	Calculated Mass	Target Mass	Double Bond Equivalence	Absolute Error (ppm)	Error (mDa)	Fitness
C ₂₄ H ₄₁ O ₄	393.30103	393.29934 [M-H]	4	4.30	-1.69	0.998

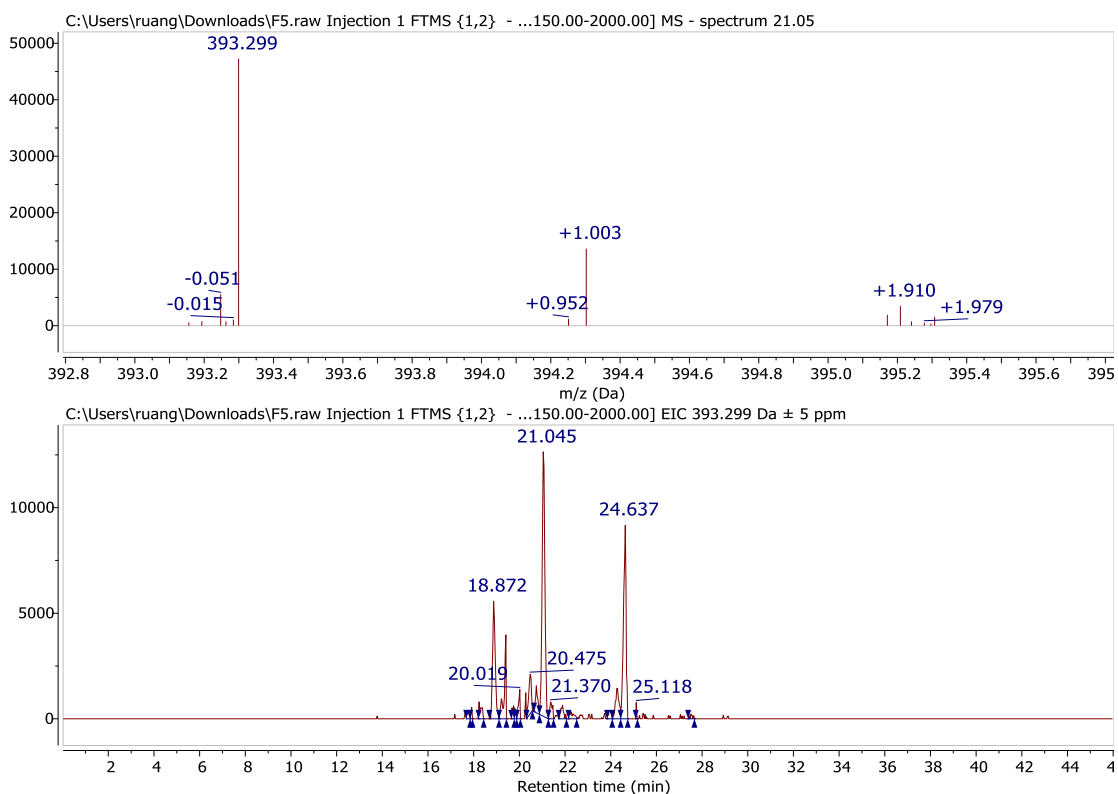


Figure 5.54. Extracted ion chromatogram for the mass spectral data of F3-1 at the ion peak m/z 393.29934 [M-H].

Compound F3-1 was isolated from Fraction 3 as a yellow amorphous powder. Fraction 3 was a non-polar eluate at higher concentration of DCM that was greater than 95% along with a low ratio of MeOH. Mass spectral data revealed a DBE of 4 while the number of hydrogens is almost double the number of carbons less than six, which could account for three double bonds. Ionisation could be better observed in the negative mode (Figure 5.54) at the ion peak m/z 393.29934 [M-H] for the molecular formula $C_{24}H_{41}O_4$ that would indicate a lipid-like structure. However, this target ion peak eluting at ca. 21 min afforded a higher intensity peak in Fraction 5, where the compound occurred at a higher concentration.

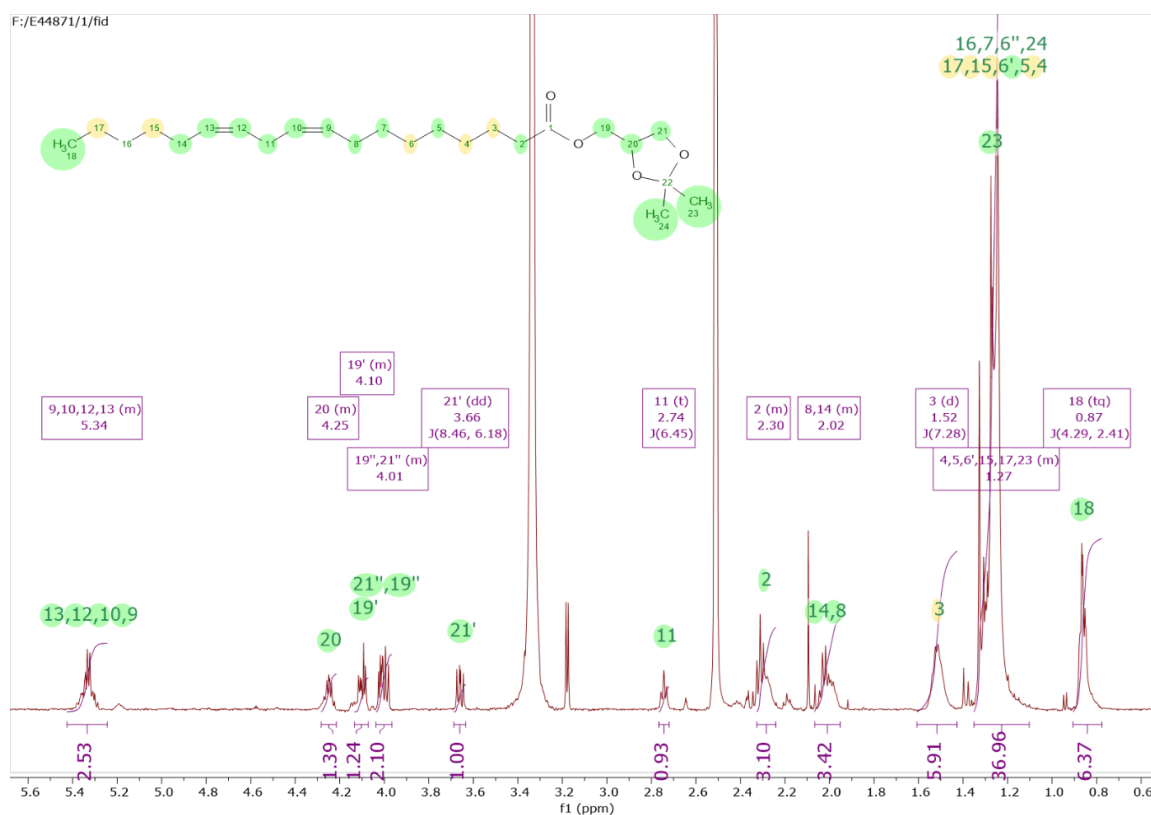


Figure 5.55. ^1H NMR spectrum of compound F3-1 in $\text{DMSO-}d_6$ measured at 400 MHz.

The occurrence of a polyunsaturated compound was evident in the ^1H spectrum of F3-1 (Figure 5.55) with a characteristic unconjugated *cis* olefinic multiplet at 5.34 ppm along with the high intensity broad signal at 1.2 ppm for long alkyl chain and the terminal methyl unit at 0.80 ppm. However, the integration was double the length of the expected alkyl and methyl units implying a possible mixture of fatty acids with either two different lengths or terminating branching units. Nevertheless, the major compound has a glycerol moiety as implicated by characteristic

signals between 3 and 5 ppm for oxygenated alkyl groups with an integral ratio of 2:2:1 that would equate to 5 protons. The occurrence of a triglyceryl group cleared the possibility of having a terminal carboxylic group.

Using a COSY spectrum designated the various spin systems in the major compound for Fraction 3-1 as exhibited in Figure 5.56. The olefinic unit at 5.4 ppm coupled to the triplet at 2.74 ppm ($J = 6.45\text{Hz}$), which was typical for a methylene unit positioned between two double bonds while the olefinic methines gave cross peaks with the multiplets at 2.0 ppm, which further correlated into the broad high intensity peak for the long chain saturated alkyl unit that then went out to the methyl terminal unit at 0.8 ppm. The olefinic system is designated with orange arrows as shown in the Figure 5.56 On the other hand, the alkyl units also correlated with broad singlet at 1.6 ppm and further down field at 2.4 ppm, which can be adjacent to a ketone moiety. The third spin system that could be observed in the COSY spectrum and highlighted in a blue box in Figure 5.56 showed typical correlating resonances for a glyceryl unit.

The HSQC spectrum in Figure 5.57 sorted the proton signals into methines, methylenes, and methyl units. It is from the HSQC spectrum that two methyl groups were found overlapping underneath the broad multiplet for the long alkyl chain. However, at this stage of the analysis, F3-1 could be a triglyceride compound with two or three different fatty acids attached to the glycerol unit.

The HMBC spectrum in Figure 5.58 was used to conform the connectivity of the substructures and to define the different structural units attached to the glyceride moiety. Since it was not feasible to measure a ^{13}C NMR spectrum for F3-1, due to its very low yield, it was only possible to detect the quaternary carbons through HMBC. As for a triglyceride structure, correlations between carboxylic units and the oxygenated methine and methylene groups were expected. However, there was only one correlation that was observed with a carboxylic signal at 173 ppm. While the glyceryl protons gave cross peaks between their carbons within its moiety, these correlations signified the absence of other fatty acid system attached to the system. The glyceryl methylene protons $\text{CH}_2\text{-21}$ correlated with an oxygenated quaternary carbon at ca. 105 ppm, which further correlated with deshielded methyl protons at 1.33 and 1.29 ppm. These correlations signified ring closure of the glycerol unit to form an acetonide structure. Compound F3-1 was elucidated as 1,2-acetonide-3-(9,12- octadecadienoyl)glycerol, a linoleic acid congener. This is the first that the compound has been isolated as a natural product. The compound is known as a precursor in the synthesis of docosahexaenoic acid (DHA, 22:6n-3)

that protects against a range of degenerative disease conditions. The NMR spectral data of isolated compound F3-1 was compatible with the literature data presented in Table 5.19.

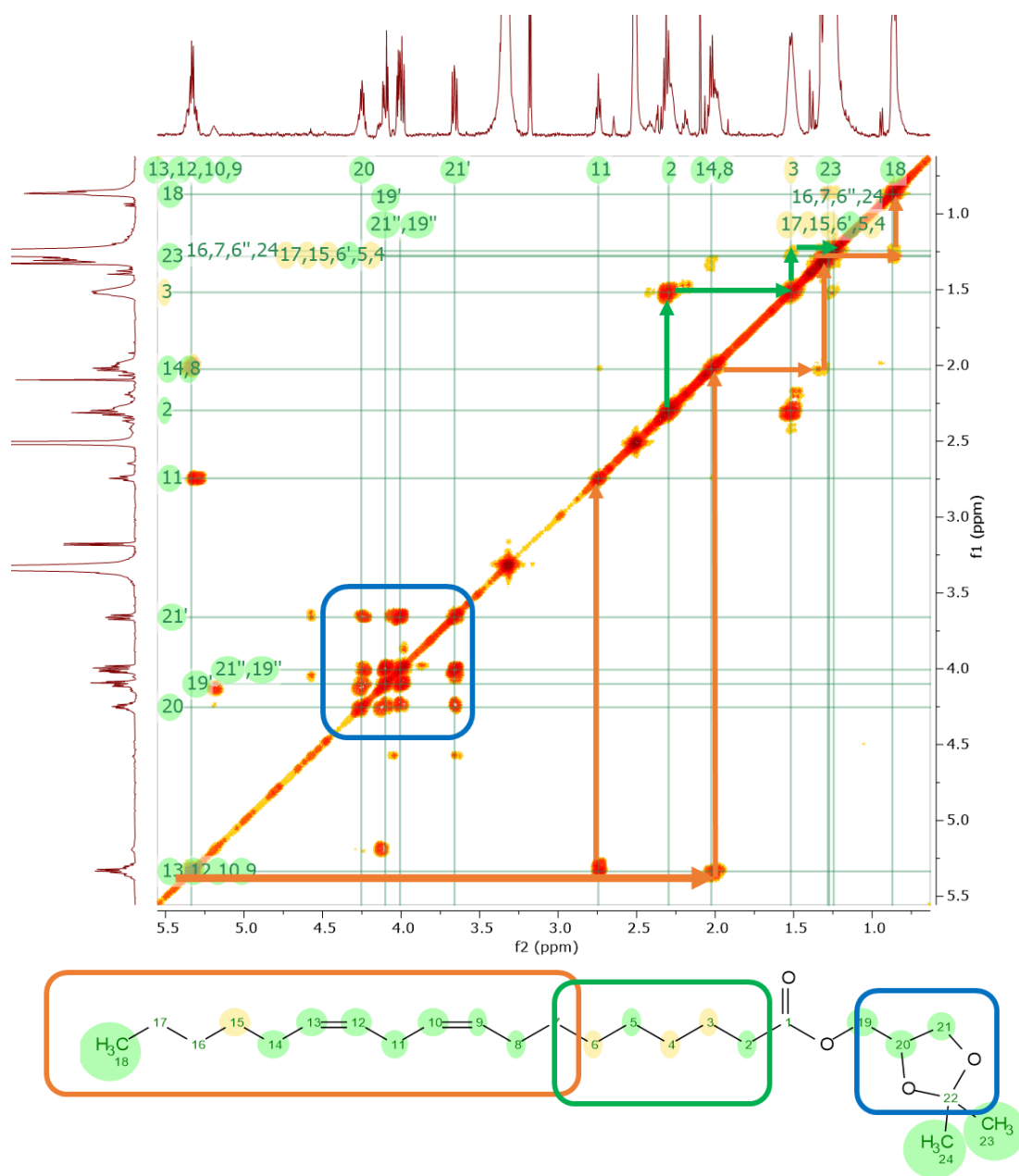


Figure 5.56. Correlation (2D-COSY) NMR spectrum of compound F3-1 in DMSO-d₆.

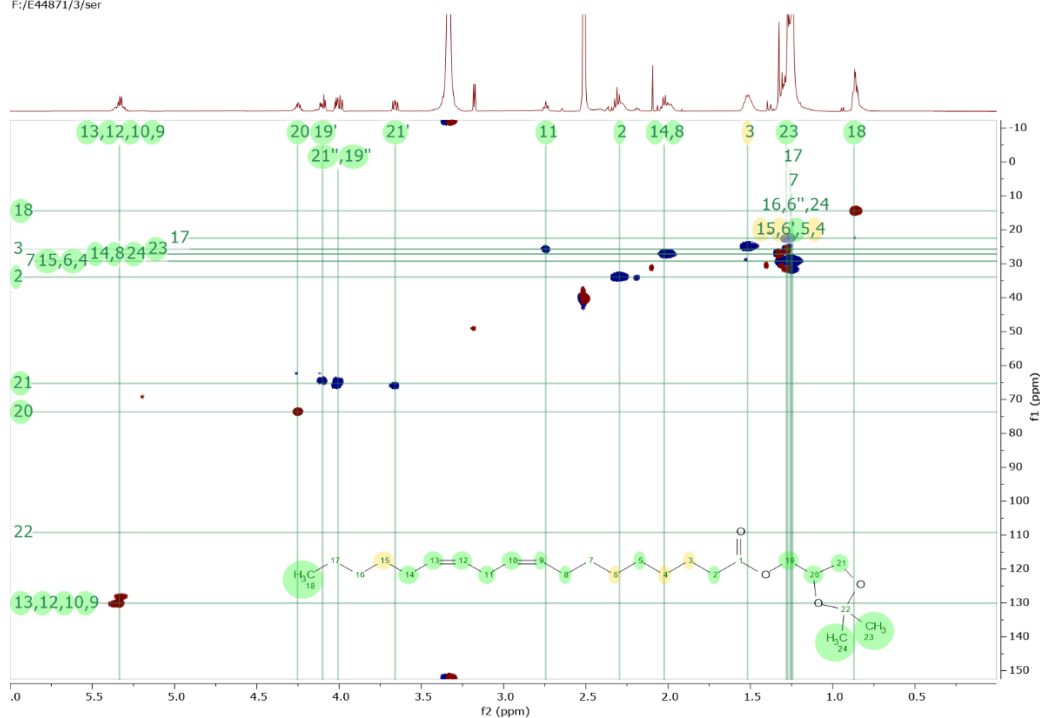


Figure 5.57. HSQC NMR spectrum of compound F3-1 in DMSO- d_6 at 500 MHz.

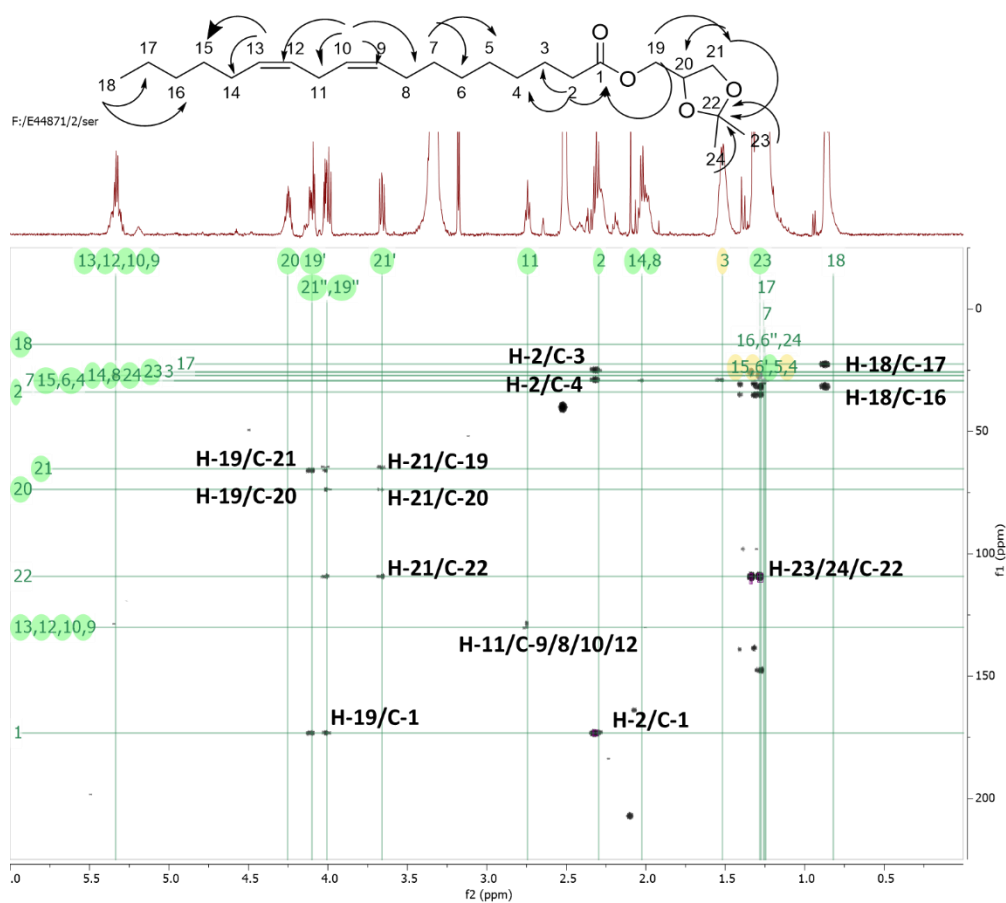


Figure 5.58. HMBC NMR spectrum of compound F3-1 in DMSO- d_6 at 500 MHz.

Table 5.19: NMR spectral data for compound F3-1 in comparison to synthesized 1,2-acetonide-3-(9,12-octadecadienoyl)glycerol (Fraser et al., 2007).

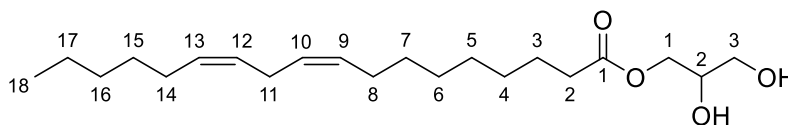
Atom no	F3-1 in DMSO-d6		Lit. in CDCl ₃	
	¹³ C _δ * 500 MHz multiplicity	¹ H _δ 400 MHz multiplicity (<i>J</i> in Hz)	¹³ C _δ 75 MHz	¹ H _δ 300 MHz
1	173.2 C		173.6	
2	33.9 CH ₂	2.30 m	34.2	2.09
3	25.7 CH ₂	1.52 br t (7.3)	26.8	1.58
4	29.2 CH ₂	1.27 m	25.0	1.27
5	29.2 CH ₂	1.27 m	31.6	1.27
6	29.2 CH ₂	1.27 m	34.2	1.27
7	29.2 CH ₂	1.27 m	29.2	1.27
8	27.5 CH ₂	2.02 m	29.7	1.27
9	130.1 CH	5.34 m	130.3	5.42
10	128.2 CH	5.34 m	128.2	5.42
11	25.7 CH ₂	2.74 t (6.5)	25.8	2.75 t (5.7)
12	128.2 CH	5.34 m	128.0	5.42
13	130.1 CH	5.34 m	130.1	5.42
14	27.5 CH ₂	2.02 m	25.5	2.00
15	29.2 CH ₂	1.27 m	29.8	1.27
16	29.2 CH ₂	1.27 m	25.0	1.27
17	22.5 CH ₂	1.27 m	22.7	1.27
18	14.4 CH ₃	0.87 t (6.7)	14.2	0.88t (7.0)
19A	68.3 CH ₂ A	4.10 m	66.5	4.18
19B	CH ₂ B	4.01 m		4.03
20	73.7 CH	4.25 m	73.8	4.29
21A	65.3 CH ₂ A	4.01 m	64.7	4.03
21B	CH ₂ B	3.66 dd(8.5, 6.2)		3.72 dd(8.5, 6.2)
22	105.2 C		109.9	
23	27.0 CH ₃	1.33 s	26.8	1.42
24	25.9 CH ₃	1.29 s	25.5	1.36

Legend: br s = broad singlet, s = singlet, d = doublet, t = triplet, q = quartet, m = multiplet

*Data taken from HMQC and HMBC experiments.

5.3.6.3.2 Compound F3-3 structure elucidation.

1-*O*-(9*Z*,12*Z*-octadecadienyl)glycerol



2,3-dihydroxypropyl (9*Z*,12*Z*)-octadeca-9,12-dienoate

Chemical Formula: C₂₁H₃₈O₄

Exact Mass: 354.2770

Figure 5.59: Chemical structure of Compound F3-3

Formula	Calculated Mass	Target Mass	Double Bond Equivalence	Absolute Error (ppm)	Error (mDa)	Fitness
C ₂₁ H ₃₈ O ₄	355.28429	355.28425 [M+H]	3.0	0.11	-0.04	0.993

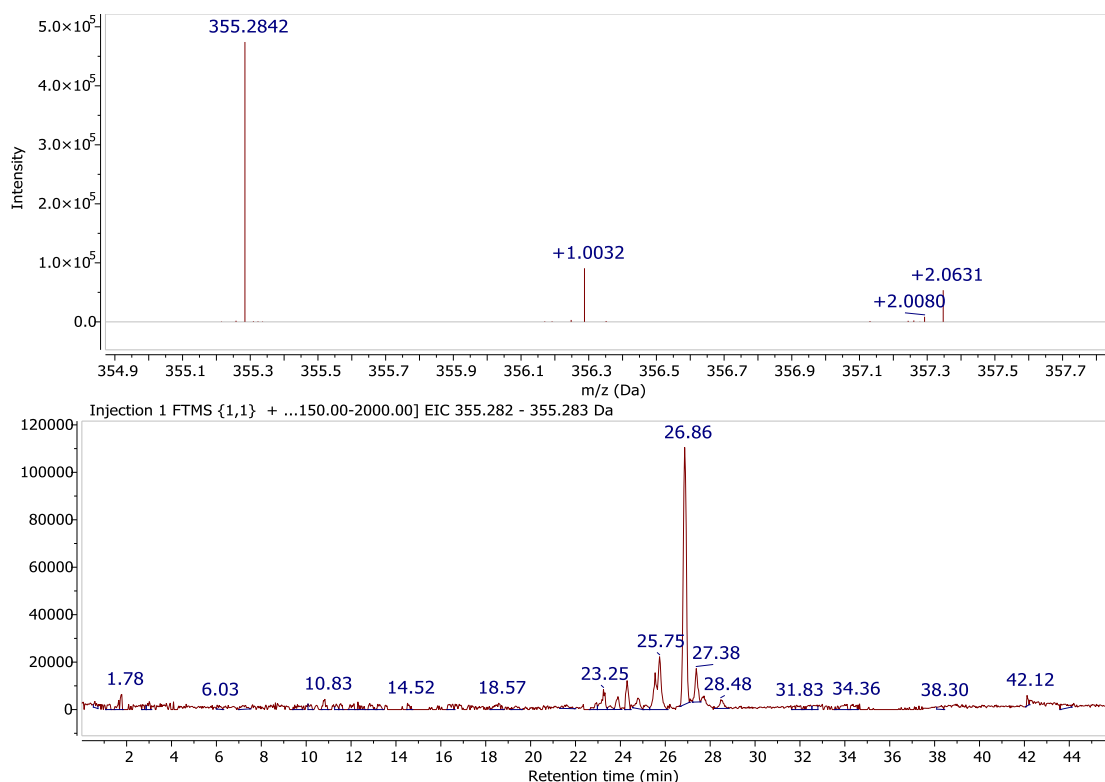


Figure 5.60. Extracted ion chromatogram for the mass spectral data of F3-3 at the ion peak m/z 355.28425 [M+H].

Compound F3-3 was isolated from fraction 3 as a yellow amorphous powder. Along with the non-polar eluate was Compound F3-3. It gave a MW of 354.28 Da that is 40 mass units less than that of F3-1. High-resolution data (as shown in Figure 4.60) afforded an ion peak at m/z 355.28425 $[M+H]$ for the molecular formula $C_{21}H_{38}O_4$. The DBE of 3.0 would signify either one double-bond less or loss of the acetonide ring when compared to that of F3-1.

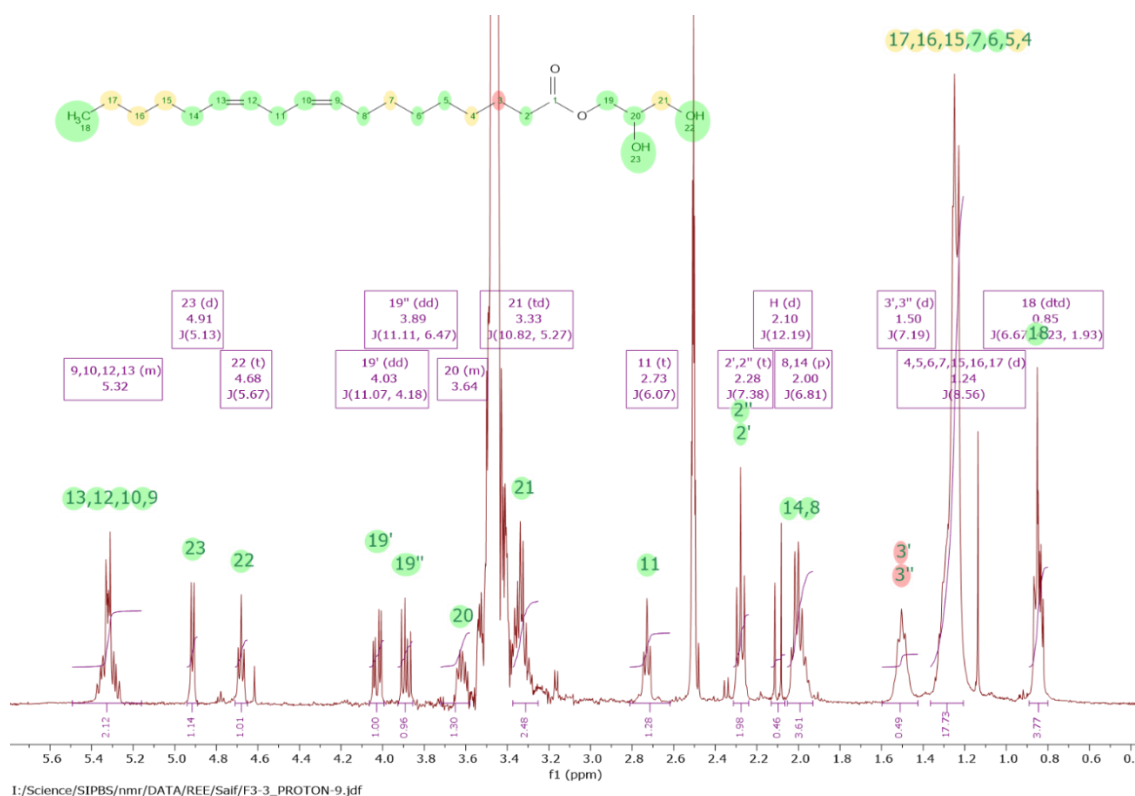


Figure 5.61. ^1H NMR spectrum of compound F3-3 in $\text{DMSO}-d_6$ at 400 MHz.

The ^1H NMR spectrum of F3-3 in Figure 5.61 was also comparable to that of F3-1. Major changes were observed between the 3 and 5 ppm region for the glycerol unit. There was the appearance two extra oxygenated bearing units, a doublet at 4.9 and a triplet at 4.7 ppm. The COSY NMR spectrum of F3-3 in Figure 5.62 again revealed the three spin systems comparable to those found in F3-1. The resonances within the 3 to 5 ppm region did correlate with each other, which were distinctive for a glycerol or a sugar unit as highlighted in a blue box in Figure 5.62. The linoleic or 9Z,12Z-octadecadienoyl moiety remained very similar to that in F3-1 as shown by the orange and green lines in the spectrum below.

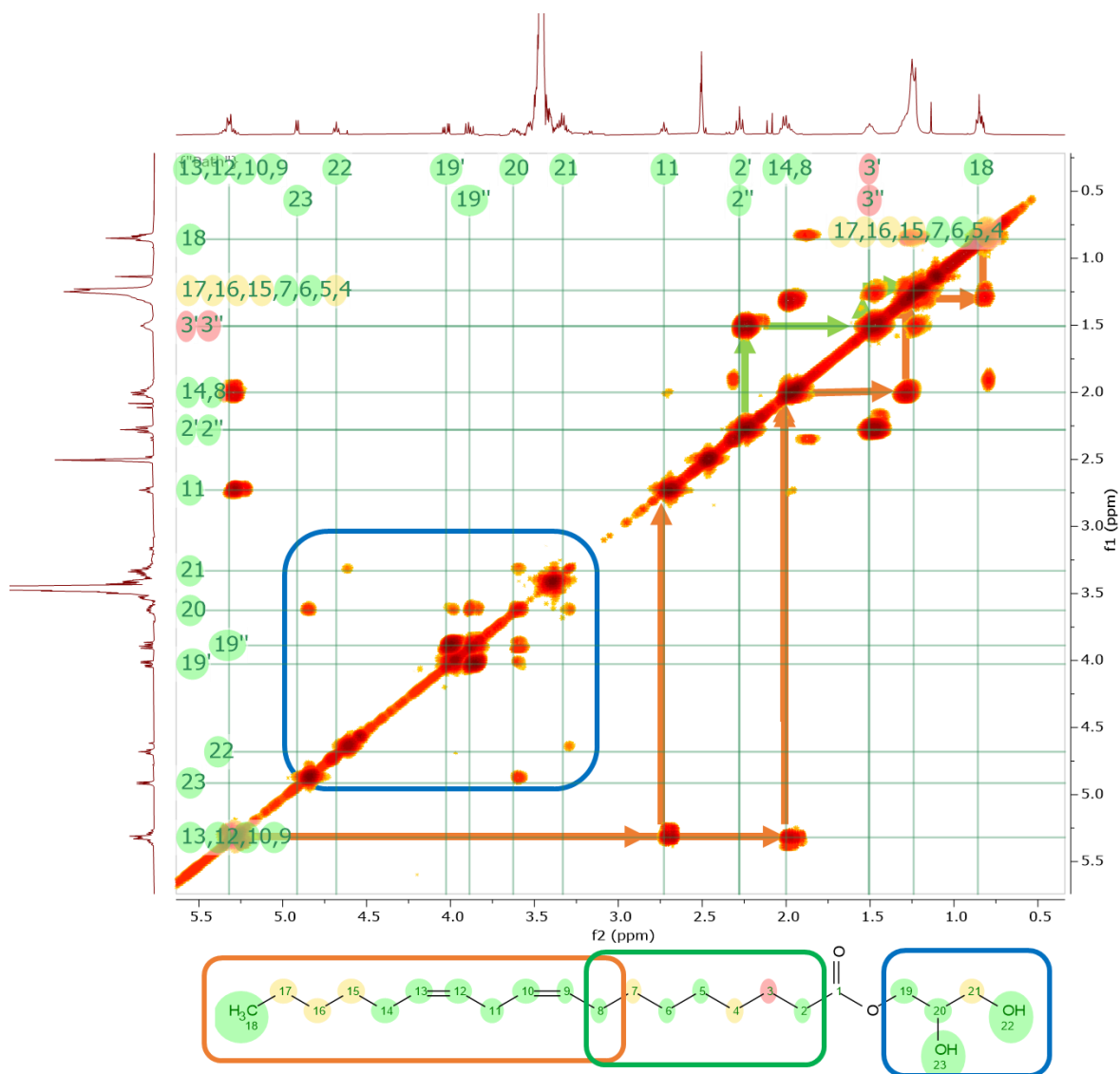


Figure 5.62. Correlation (2D-COSY) NMR spectrum of compound F3-3 in DMSO-d₆.

Further information was obtained on the protons in the 3 to 5 ppm region through a combination of ¹³C, DEPT and HMQC experiments (Figure 5.63). The ¹³C and DEPT spectra only showed three instead of the expected five oxygen-bearing carbons between 60 and 70 ppm. The DEPT spectrum confirmed that two of the peaks were methylene groups and there was only one methine unit like in a glycerol structure. This eliminated the possible presence of a sugar unit in the structure F3-3. Again, the rest of the ¹³C resonances were more identical to those found in F3-1. The HMQC spectrum further established that the doublet and triplet protons at 4.9 and 4.7 ppm, respectively, were indeed exchangeable hydrogens that indicated the opening of the acetonide ring. Both the DEPT and HMQC spectra verified the loss as well of two downfield methyl units found in F3-1.

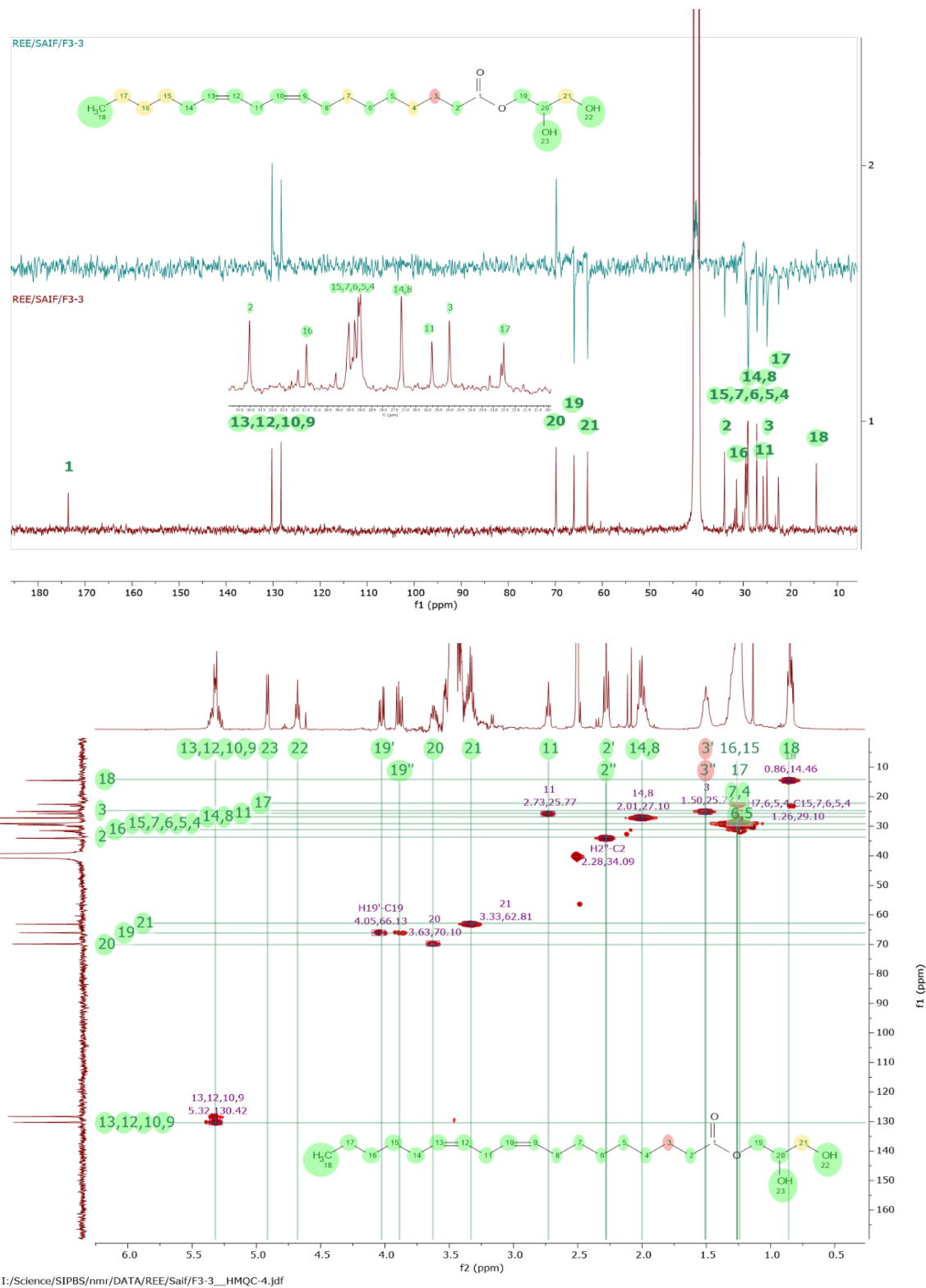


Figure 5.63. ¹³C, DEPT and HMQC NMR spectra of compound F3-3 in DMSO-*d*₆.

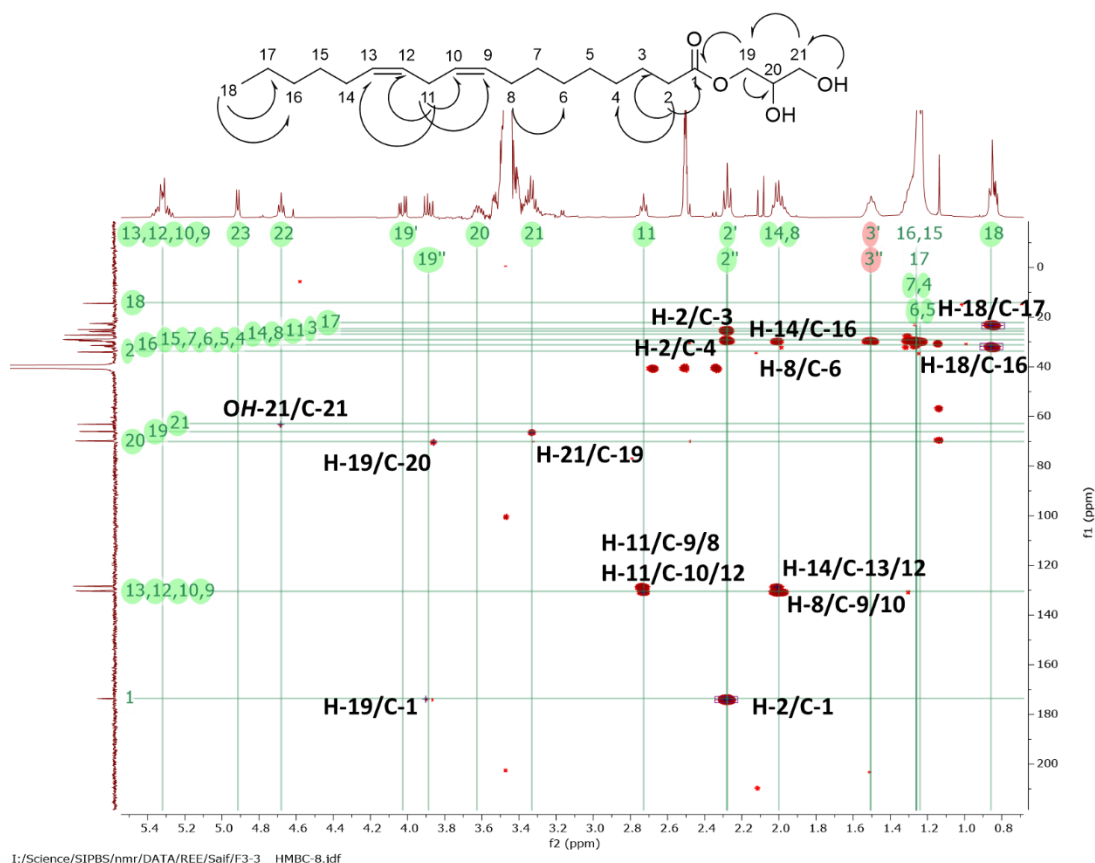


Figure 5.64. HMBC NMR spectrum of compound F3-3 in DMSO- d_6 .

The HMBC NMR spectrum of F3-3 in Figure 5.64 also afforded similar correlations observed for F3-1. The HMBC correlations further established the structure of F3-3 as well as validated the opening of the acetonide ring and the attachment of the glycerol moiety to the carboxy unit. The hydroxyl triplet gave a $2J$ correlation with C-21. $\text{CH}_2\text{B-19}$ at 3.89 ppm had a cross peak with C-20 methine at 70 ppm and C-1 of the carboxyl group at 173 ppm.

The structure of F3-3 was therefore elucidated as 1-*O*-(9*Z*,12*Z*-octadecadienyl)glycerol also known as 1-monolinolein, which was earlier isolated from the fungus *Sclerotinia fructicola* and the roots of *Cymbidium* (Orchidaceae). Monolinolein was also described as an antifungal agent (Stoessl et al., 1980, Sola et al., 1986). Monolinolein was also earlier reported to inactivate ASF virus and inhibited its replication in Vero cells at 25 $\mu\text{g/ml}$ while at 10 $\mu\text{g/ml}$ no inactivation occurred but inhibition of viral replication in the tissue culture was observed (Stoessl et al., 1980, Sola et al., 1986). However, synthesised 1-monolinolein did not give any antibacterial activity against *Staphylococcus aureus* and *Escherichia coli* (Jumina et al., 2019). The full assignments for the ^1H and ^{13}C spectral data is listed in Table 5.20.

Table 5.20: NMR spectral data for compound F3-3 in comparison to F3-1 in DMSO-d₆ in 400 MHz for ¹H_δ and 100 MHz for ¹³C_δ.

Atom no	F3-3		F3-1	
	¹³ C _δ multiplicity	¹ H _δ multiplicity (J in Hz)	¹³ C _δ * multiplicity	¹ H _δ multiplicity (J in Hz)
1	173.9 C		173.2 C	
2	34.0 CH ₂	2.28 t (7.4)	33.9 CH ₂	2.30 m
3	25.0 CH ₂	1.51 br t (7.2)	25.7 CH ₂	1.52 br t (7.3)
4	29.4 CH ₂	1.24 m	29.2 CH ₂	1.27 m
5	29.4 CH ₂	1.24 m	29.2 CH ₂	1.27 m
6	29.4 CH ₂	1.24 m	29.2 CH ₂	1.27 m
7	29.4 CH ₂	1.24 m	29.2 CH ₂	1.27 m
8	27.4 CH ₂	2.00 dd (6.8, 7.0)	27.5 CH ₂	2.02 m
9	130.8 CH	5.32 m	130.1 CH	5.34 m
10	128.2 CH	5.32 m	128.2 CH	5.34 m
11	25.8 CH ₂	2.73 t (6.1)	25.7 CH ₂	2.74 t (6.5)
12	128.2 CH	5.32 m	128.2 CH	5.34 m
13	130.8 CH	5.32 m	130.1 CH	5.34 m
14	27.4 CH ₂	2.00 m	27.5 CH ₂	2.02 m
15	29.4 CH ₂	1.24 m	29.2 CH ₂	1.27 m
16	31.5 CH ₂	1.24 m	29.2 CH ₂	1.27 m
17	22.5 CH ₂	1.24 m	22.5 CH ₂	1.27 m
18	14.5 CH ₃	0.86 t (6.7)	14.4 CH ₃	0.87 t (6.7)
19A	66.5 CH ₂ A	4.03 dd (4.2, 11.1)	68.3 CH ₂ A	4.10 m
19B	CH ₂ B	3.89 dd (6.5, 11.1)	CH ₂ B	4.01 m
20	70.4 CH	3.63 m	73.7 CH	4.25 m
20-OH		4.91 d (5.13)		
21A	63.2 CH ₂	3.33 td (5.7, 11.0)	65.3 CH ₂ A	4.01 m
21B			CH ₂ B	3.66 dd (8.5, 6.2)
21-OH		4.68 t (5.7)		
22			105.2 C	
23			27.0 CH ₃	1.33 s
24			25.9 CH ₃	1.29 s

Legend: br s = broad singlet, s = singlet, d = doublet, t = triplet, q = quartet, m = multiplet

*Data taken from HMQC and HMBC experiments.

5.3.6.4 Fraction 10 sub-fractionation:

Fraction 10 afforded 490mg and was the highest yield amongst the active MPLC fractions. The fraction components were all not detectable under UV and were visualised by spraying with anisaldehyde reagent. For further fractionation and purification work on the MPLC, an ELSD detector was utilised. Fraction was loaded on a 40g silica pre-packed column..

Table 5.21: Yield of pooled MPLC sub-fractions of fraction 10

Fraction #	Weight (mg)	Fraction #	Weight (mg)
F10-1	2.3	F10-6	249.8
F10-2	1.2	F10-7	92.7
F10-3	4.8	F10-8	19.7
F10-4	5.2	F-wash	13.2
F10-5	43.7	% recovery	88.3%

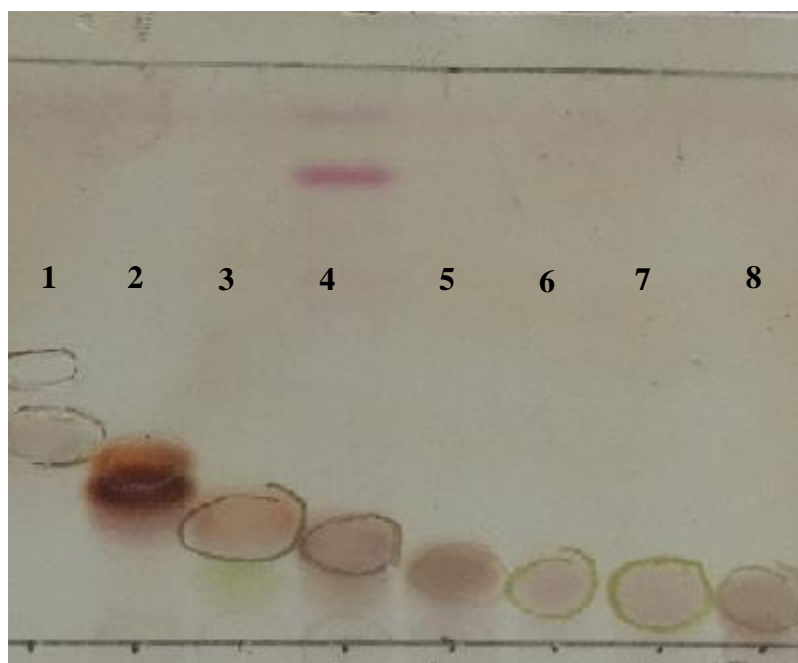


Figure 5.65: Summary TLC plate for fraction 10 fractionation.

Sub-fractionation of fraction 10 by MPLC afforded a recovery of 88.3% (Table 5.21). A ^1H NMR was recorded for each of the subfractions. The stacked NMR spectra of the MPLC sub-fractions are presented in Figure 5.66. Sub-fractions 10-1 and 10-2 showed a different chemical profile from the rest of the other eluted fractions. Sub-fractions F10-3 to F10-8 did exhibit identical spectra that were highly hydroxylated as revealed by the peaks between 3 to 6 ppm. F10-7 and the fraction wash did not reveal anything of interest. F10-2 and F10-8 were chosen

for further structure elucidation work using both 1D and 2D NMR experiment such as COSY, TOCSY, HSQC and HMBC.

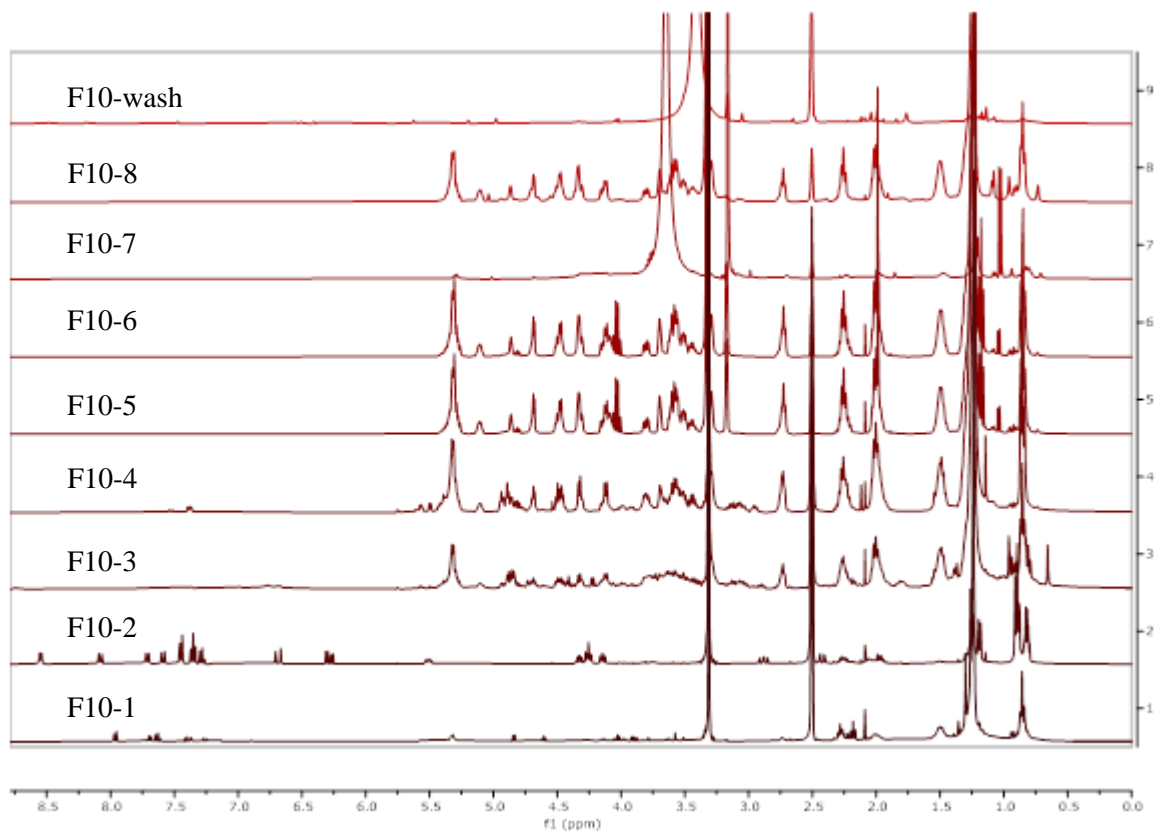
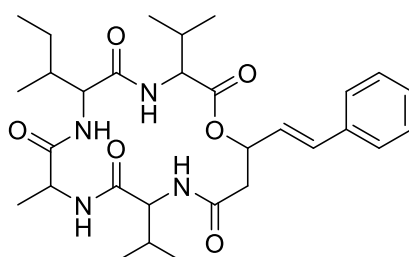


Figure 5.66: Stacked ¹H NMR spectra of the MPLC sub-fractions of fraction 10 in DMSO-*d*₆ recorded at 400 MHz.

5.3.6.4.1 Compound 10-2



Chemical Formula: C₃₀H₄₄N₄O₆
Exact Mass: 556.3261

turnagainolide A

Figure 5.67: Chemical structure of compound F10-2 (turnagainolide A)

	Formula	Calculated Mass	Target Mass	Double Bond Equivalence	Absolute Error (ppm)	Error (mDa)	Fitness
1	C ₃₀ H ₄₄ N ₄ O ₆	557.33336	557.33406	11.0	1.26	0.70	1.000

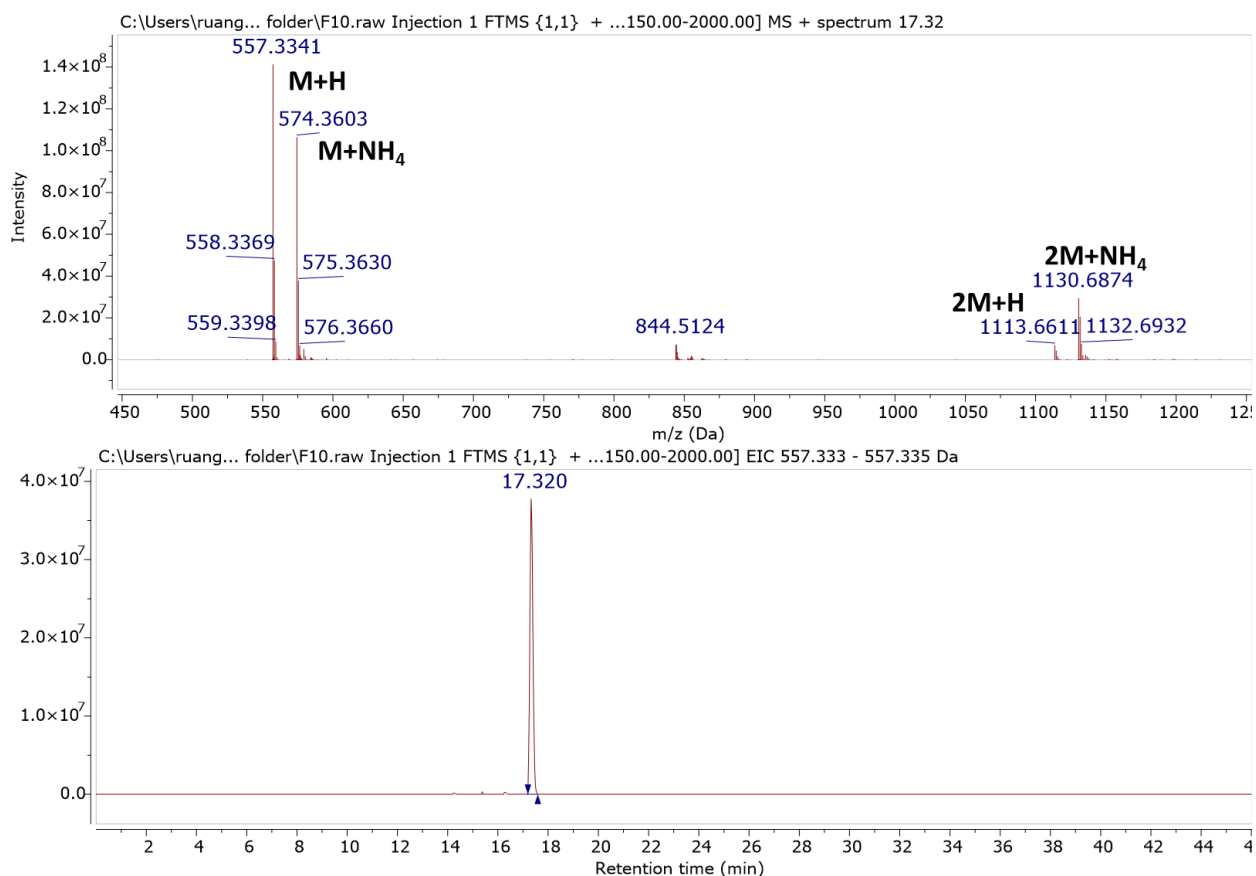


Figure 5.68. Extracted ion chromatogram for the mass spectral data of F10-2 at the ion peak m/z 557.33406 [M+H].

Compound 10-2 was isolated from fraction 10 as a white crystalline powder. Despite the low yield of Compound 10-2 (F10-2) at only 1.2mg, it was the major ion peak found in fraction 10 and was isolated at 90% purity. The mass feature was however not amongst the targeted antimicrobial compound. Compound 10-2 gave an ion peak at m/z 557.33406 [M+H] for the molecular formula C₃₀H₄₄N₄O₆ with DBE of 11 (Figure 5.68). Dereplication found five compound hits from the DNP: FR235222, streptolide, turnagainolides A, B, and C. All earlier reported natural products were tetrapeptides. The isolated turnagainolides were epimer derivatives. FR235222 was a fungal metabolite from *Acremonium* sp. No. 2708 (Mori et al., 2003).

Streptolide was described from *Streptomyces* (Rong et al., 2015) and turnagainolides were isolated from marine-derived *Bacillus* sp. RJA2194 (Li et al., 2011) and *Microascus* sp. and produced by *Arthrobacter* sp. PGVB1 (Igarashi et al., 2015) and *Streptomyces rutgersensis* T009 (Zhou et al., 2016a). The turnagainolides derivatives were simply epimers at the site of macrolactonization where (*E*)-3-hydroxy-5-phenylpent-4-enoic acid moiety was attached. The peptolide was also described as EGM-556 from the marine sediment-derived fungus *Microascus* sp. 098059A, which was encoded from a silent biosynthetic gene (Vervoort et al 2011). Interestingly, congeners of the peptolide were reported to inhibit quorum sensing in *Staphylococcus aureus* (Igarashi et al., 2015).

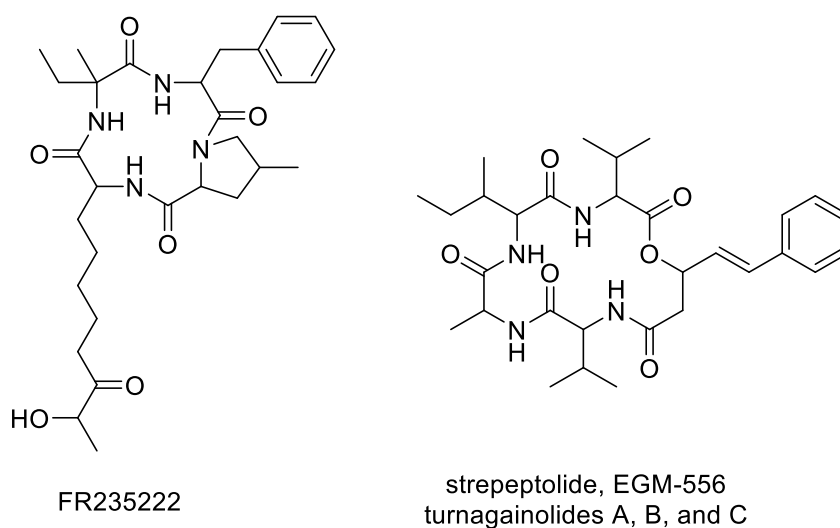


Figure 5.69: Structures of dereplicated compound hits for ion peak at m/z 557.33406 [M+H] for the molecular formula $C_{30}H_{44}N_4O_6$.

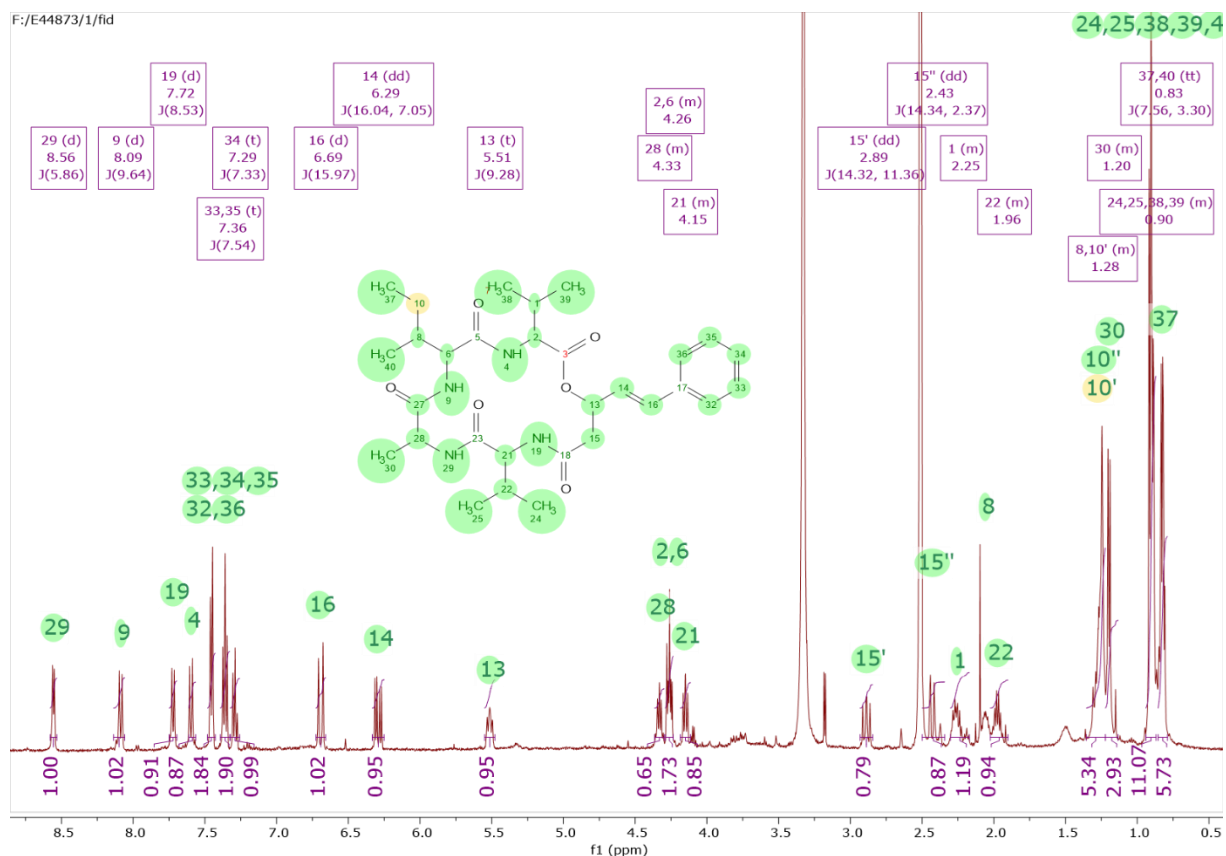


Figure 5.70. ¹H NMR spectrum of Compound 10-2 in DMSO-*d*₆ at 500 MHz.

The ¹H NMR spectrum of Compound 10-2 in Figure 5.70 did reveal the presence of a monosubstituted phenyl unit at 7.0 to 7.5 ppm similar to the structures of the derplicated compounds, FR235222 and the peptolides. In comparison to FR235222, the occurrence of a long alkyl chain was not evident in the ¹H NMR spectrum of F10-2. However, the ¹H NMR spectrum of F10-2 was comparable or identical to those of the peptolides. The COSY spectrum of F10-2 disclosed the presence of the *trans* 3-hydroxy-pent-4-enoic acid moiety in the structure, which is highlighted in a blue box in Figure 5.71. The *trans* coupling proton pairs at 6.71 (d) and 6.30 (dd) exhibited a coupling constant of 16.0 Hz and further coupled to an oxygen-bearing methine unit at 5.52 ppm then to an AB methylene group at 2.89 (dd 14.0, 11.0) and 2.43 (dd 14.0, 2.4) ppm. The *trans* 3-hydroxy-pent-4-enoic acid was established to be attached to a monosubstituted benzene ring by HMBC as illustrated in Figure 5.72.

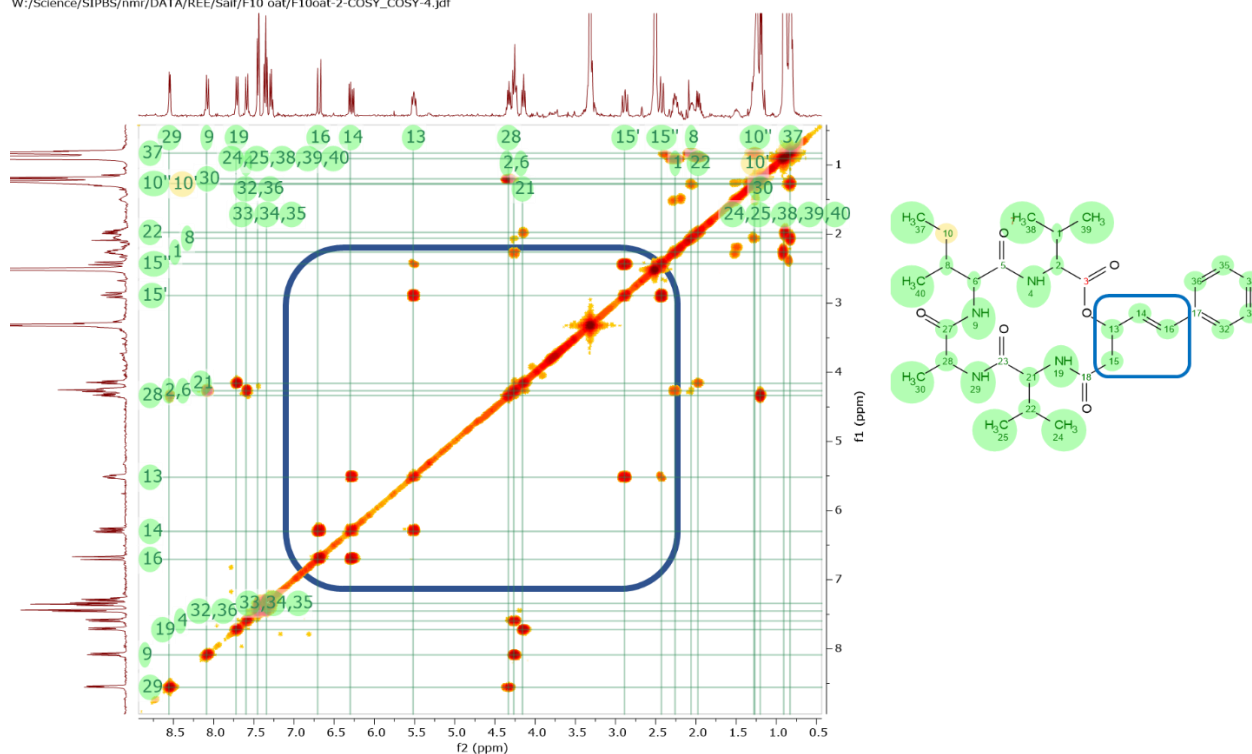


Figure 5.71. COSY spectrum of Compound 10-2 in DMSO-*d*₆ at 400 MHz.

F:/E44873/2/ser

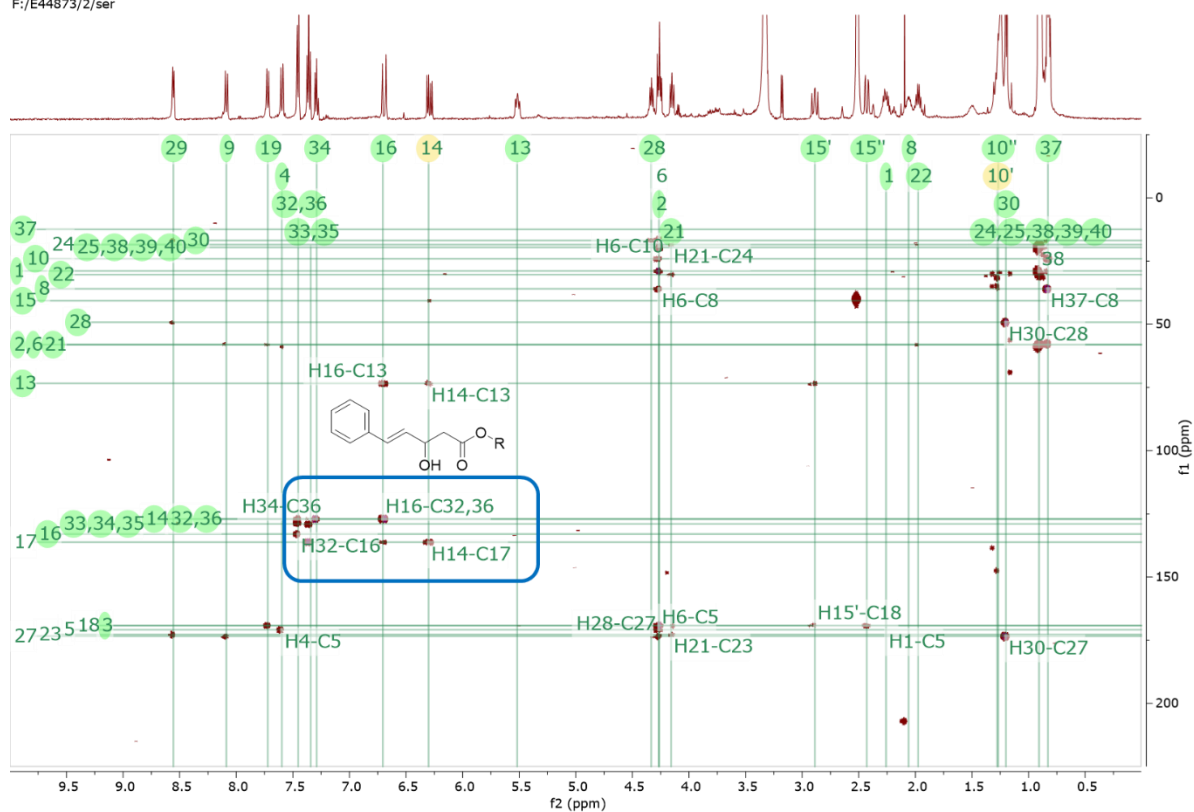


Figure 5.72. HMBC spectrum of Compound 10-2 in DMSO-*d*₆ at 500 MHz.

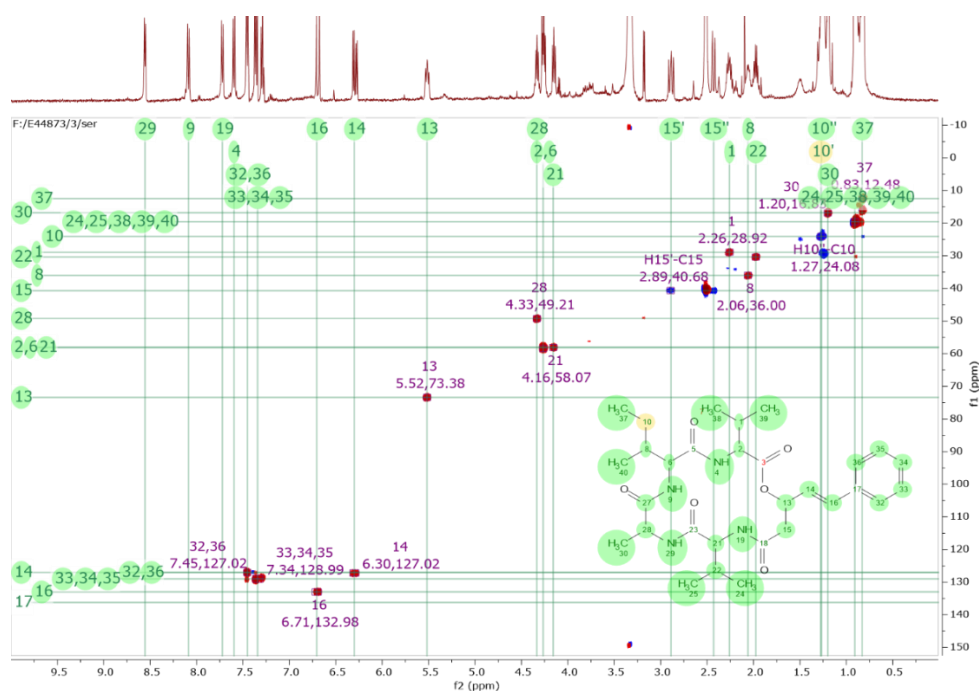


Figure 5.73. HSQC spectrum of Compound 10-2 in DMSO- d_6 at 500 MHz. Red correlations are CHs and CH₃s while blue are CH₂s.

An HSQC experiment was accomplished to assign the protons to their respective carbons as well as to sort the methine and methyl protons from the methylene units. The HSQC spectrum in Figure 5.73 revealed four exchangeable doublet protons between 7.5 and 9.0 ppm in addition two or three CH₂s, six CH₃s, which were also compatible to the integrals deduced from the ¹H NMR spectrum, and lastly 15 methine units totalling to 24 carbons with a remaining six unassigned quaternary carbons. Since six DBE was already assumed for the *E*)-3-hydroxy-5-phenylpent-4-enoic acid moiety, five could be accounted for four amide units and a ring.

The four amino acids were elucidated by 2D total correlation spectroscopy (TOCSY) as shown in Figure 5.74A. Each of the amino acids was ascertained by following the correlation peaks within their respective spin systems from the NH (7 to 9 ppm) to the α-CH (4 to 5 ppm) to the β-CH or CH₂ (ca. 2ppm) to the γ-CH₂ or CH₃ (ca. 1ppm). TOCSY pattern of amino acids have been widely used in the structure elucidation of peptides (Wüthrich, 1986). The same standard protocol was used to identify the four amino acids found in F10-2, which were alanine, isoleucine and two valine units. Alanine was the easiest to detect as the correlating peaks commenced from 8.5 (NH) to 4.3 (α-CH) and culminated on the methyl doublet at 1.20 ppm. The two valine units were perceived through the methine units at ca. 2 ppm prior to the geminal methyl units. Isoleucine was the only amino acid that has a methylene unit at 1.28 pp, and terminating with two methyl units.

The amino acid sequence was established by looking into the HMBC correlations of the carbonyl units with the respective *NH*s for each of the identified amino acids as illustrated in Figures 5.76B and C. The *NH* of val-4 at 7.60 ppm had a cross peak with the C=O of ile-2 at 170.8, while the *NH* of ile-2 at 8.09 ppm correlated with the C=O of ala-1 at 173.4. Onwards, the *NH* of ala-1 at 8.56 ppm linked with the C=O of val-3 at 172.6, and finally, the *NH* of val-3 at 7.72 ppm linked with the C=O of HPE-5 at 169.2 ppm. The resulting amino acid sequence was val-4, ile-2, ala-1, val-3, and HPE-5.

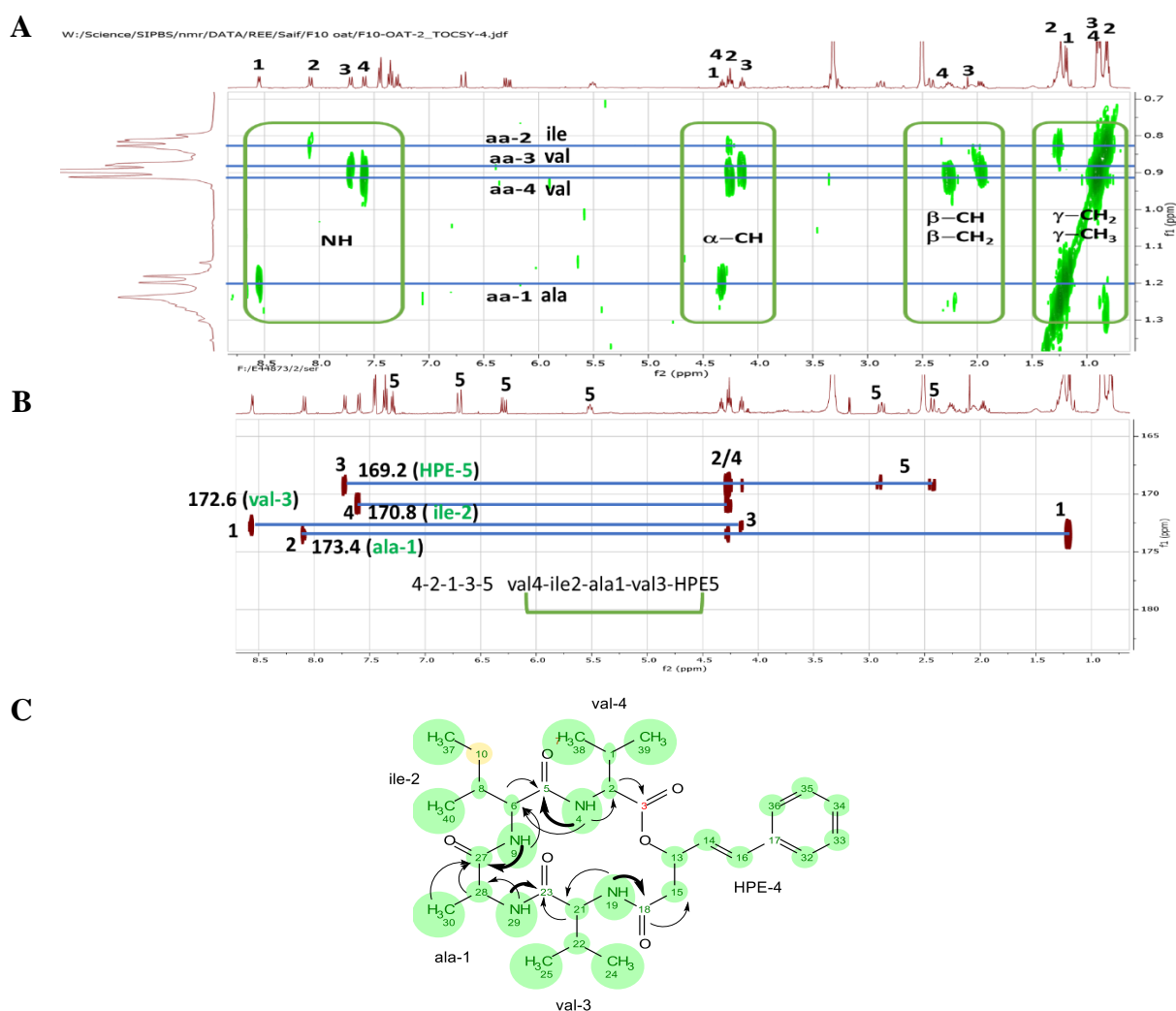


Figure 5.74: (A) TOCSY spectrum of F10-2 in DMSO-*d*₆ at 400 MHz. (B) Carbonyl region of the HMBC spectrum of F10-2 at 500 MHz. (C) Important HMBC correlations to establish the amino acid sequence in the peptide structure of F10-2.

Table 5.22. NMR spectral data for compound F10-2 in DMSO-d₆ in 500 MHz.

Atom	δ C (ppm)	δ H (ppm), multiplicity (<i>J</i> in Hz)	HMBC (H to C)
Val-4			
1 CH	28.9	2.26 1H, m	
2 CH	58.1	4.27 1H, m	C-3, C-38, C-39
4 NH		7.60 1H, d (9.5)	C-2, C-5, C-6
3 CO	169.2		
38 CH ₃	19.6	0.91 3H, br.s (overlap)	C-1, C-2
39 CH ₃	19.6	0.91 3H, br.s (overlap)	C-1, C-2
Ile-2			
5 CO	170.8		
6 CH	58.1	4.27 1H, m	C-5, C-8, C-10, C-27, C-40
8 CH	36.0	2.06 1H, m	
9 NH		8.09 1H, d (9.5)	C-6, C-27
10 CH ₂	24.1	1.28 1H, m	
		1.27 1H, m	
37 CH ₃	12.5	0.83 3H, br.s (overlap)	C-8, C-10
40 CH ₃	19.6	0.91 3H, br.s (overlap)	C-6, C-28
Ala-1			
27 CO	173.4		
28 CH	49.2	4.33 1H, t (4.0)	C-27, C-30
29 NH		8.56 1H, d (5.9)	C-23, C-28
30 CH ₃	16.8	1.20 3H, d (6.8)	C-27, C-28
Val-3			
19 NH		7.72 1H, d (8.55)	C-18, C-21
21 CH	58.1	4.16 1H, t (4.0)	C-18, C-22, C-23, C-24, C-25
22 CH	30.4	1.98 1H, m	C-21, C-24, C-25
23 CO	172.6		
24 CH ₃	19.6	0.91 3H, br.s (overlap)	
25 CH ₃	19.6	0.91 3H, br.s (overlap)	
HPE-5			
13 CH	73.4	5.52 1H, br t (9.2)	
14 CH	127.0	6.30 1H, dd (16.0, 7.0)	C-13, C-15, C-17
15 CH ₂	40.7	2.89 1H, dd (14.0, 11.0)	C-13, C-18
		2.43 1H, dd (14.0, 2.4)	C-18
16 CH	133.0	6.71 1H, d (16.0)	C-13, C-17, C-32, C-36
17 C	136.2		
18 CO	169.2		
32 CH	127.0	7.45 1H, d (7.6)	C-16, C-34, C-36
33 CH	129.0	7.34 1H, t (7.5)	C-17, C-34, C-35
34 CH	129.0	7.28 1H, t (7.2)	C-32, C-36
35 CH	129.0	7.34 1H, t (7.5)	C-17, C-33, C-34
36 CH	127.0	7.45 1H, d (7.6)	C-16, C-32, C-34

The ^1H and ^{13}C spectral data of F10-2 presented in Table 5.22 were compared to those reported in the literature and were found to be identical to turnagainolide A. The geminal methylene protons of the (*E*)-3-hydroxy-5-phenylpent-4-enoic acid moiety afforded an identical sets of coupling constants of as those found in turnagainolide A. However, due to the very low yield of the isolated F10-2, it was not possible to establish the configuration of the respective amino acids.

The ^1H and ^{13}C spectral data of F10-2 presented in Table 5.22 were compared to those reported in the literature and were found to be identical to turnagainolide A. The geminal methylene protons of the (*E*)-3-hydroxy-5-phenylpent-4-enoic acid moiety afforded an identical sets of coupling constants of as those found in turnagainolide A. However, due to the very low yield of the isolated F10-2, it was not possible to establish the configuration of the respective amino acids.

5.3.6.4.2 Compound F10-8

1-*O*-(9*Z*,12*Z*-octadecadienoyl)glycerol-3-*O*-[*D*-galactopyranosyl-(1→6) α -*D*-galactopyranoside]

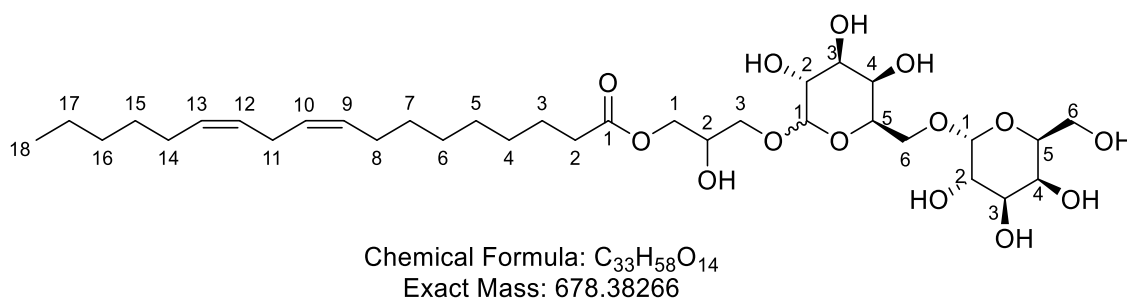


Figure 5.75: Chemical structure of compound F10-8 (1-*O*-(9*Z*,12*Z*-octadecadienoyl)glycerol-3-*O*-[*D*-galactopyranosyl-(1→6)α -*D*-galactopyranoside])

Formula	Adduct	Charge State	<i>m/z</i>	Calculated Mass	Double Bond Equivalence	Absolute Error (ppm)
C ₃₃ H ₅₈ O ₁₄	H +	+1	679.3900	679.3899	5.0	-0.03
C ₃₃ H ₅₈ O ₁₄	NH ₄ +	+1	696.4164	696.4165	5.0	0.05

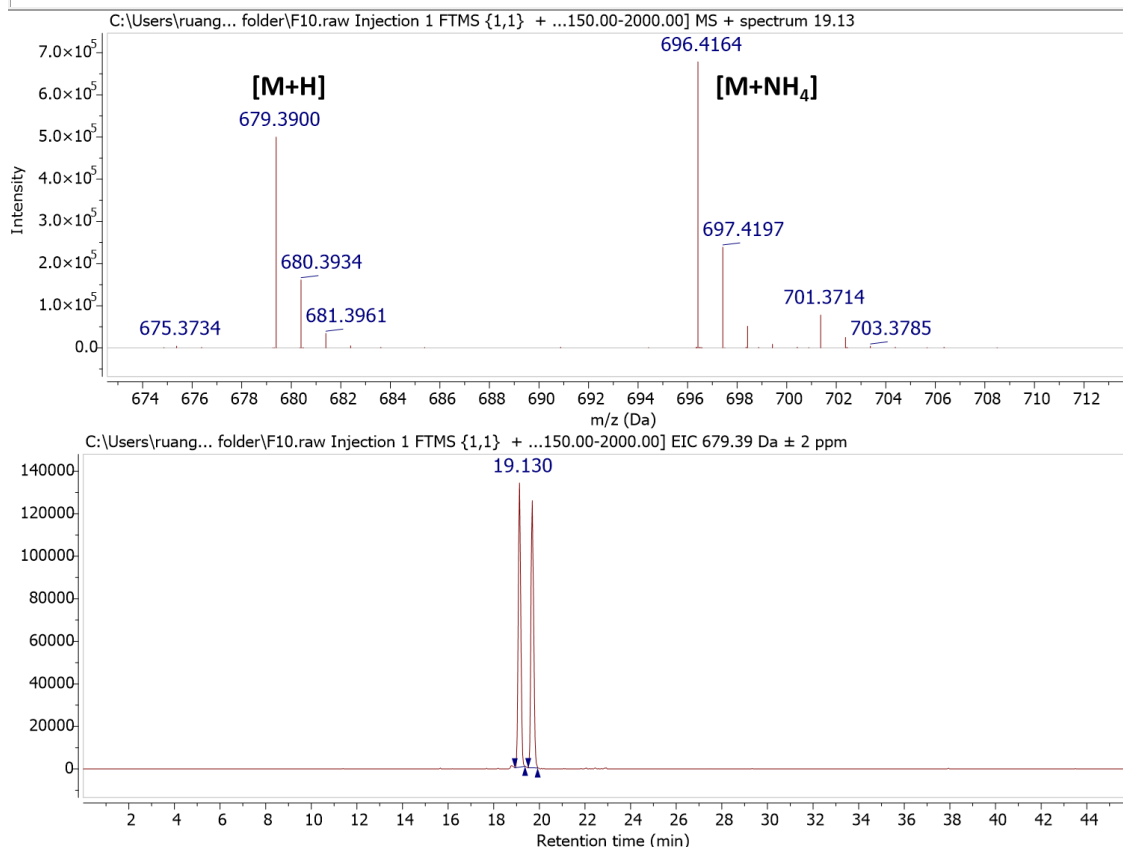
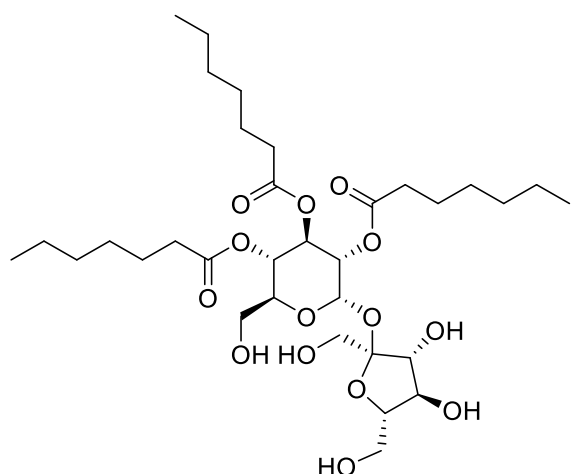


Figure 5.76. Extracted ion chromatogram for the mass spectral data of F10-8 at the ion peak *m/z* 679.3900 [M+H].

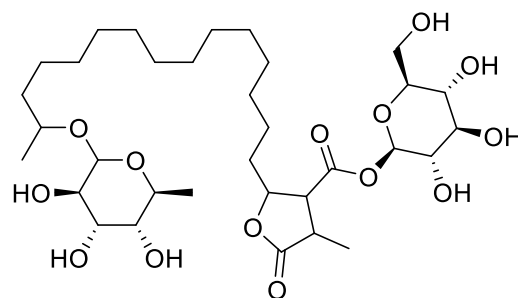
Compound F10-8 was isolated from Fraction 10 as a yellow oily compound. The compound has very poor solubility in water but is soluble in methanol and EtOAc. However, at this stage the optical rotation has not been measured. Compound 10-8 (F10-8) was afforded from a polar fraction. It gave mass ion peaks at m/z 679.3899 [M+H] and 696.4165 [M+NH₄] for the molecular formula C₃₃H₅₈O₁₄ with a DBE of 5 (Figure 5.76). F10-8 is highly oxygenated and the number of hydrogen almost double the number of carbons, this would signify a glycolipid structure. Dereplication of the molecular formula C₃₃H₅₈O₁₄ gave five hits. Structurally, the compound hits were indeed glycolipids as shown in Figure in 5.79. They were all earlier isolated from plants except for the murolic acid glycosides that were widely distributed in lichens (Yoshikawa et al., 1994, Řezanka and Guschina, 2000, Singh et al., 2003). Glycerol-1-alkanoate derivatives have been reported from the marine green algae *Codium iyengaraii* algae as well as marine sponges and soft corals (Yu et al., 1996, Ali et al., 2001, Zhao et al., 2003, Liu et al., 2006, Li et al., 2009b). A congener has also been described from the fungus *Microsphaeropsis olivacea* (Yu et al., 1996).

Interestingly, gingerglycolipid B (did match the linoleic acid moiety that were found in the structures of the isolated compounds F3-1 and F3-3. The ¹H and ¹³C NMR spectra of Compound 10-8 in Figure 5.78 were comparable to those of F3-1 and F3-3, with a noticeable increase of the number of peaks between the 3 and 5 ppm region as well as between 60 and 100 ppm in its ¹H and ¹³C NMR spectra, respectively. Both spectra were typical for a glycolipid structure. Albeit a change in solvent from DMSO-*d*₆ to MeOD to get rid of the OH peaks for a less complex spectrum, the obtained sets of 1D and 2D spectra comparable were still comparable to those of F3-1 and particularly with F3-3.

The ¹³C *J*-mod NMR spectrum of F10-8 in Figure 5.78 revealed 33 high-intensity carbons with one carbonyl carbon at 173 ppm; the two usual olefinic methine carbons at ca. 130 ppm; two new methine resonances at ca. 100 ppm that is a typical chemical shift for anomeric carbons of two sugar units along with the 9 methine carbons between ca. 70 and 80 ppm; one of which belongs to the glycerol moiety. At 60 to 70 ppm, four methylene peaks were recorded, two for glycerol and two for the two predicted sugar elements in the compound, The rest of the methylene peaks found between 20 and 40 ppm were identical to those of the octadecanoyl chain in F3-3 that terminated with a methyl group at 15 ppm.

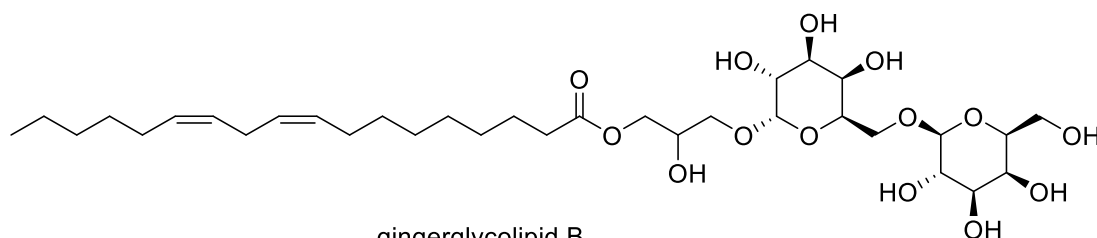


2,3,4-triheptanoylacylsucrose



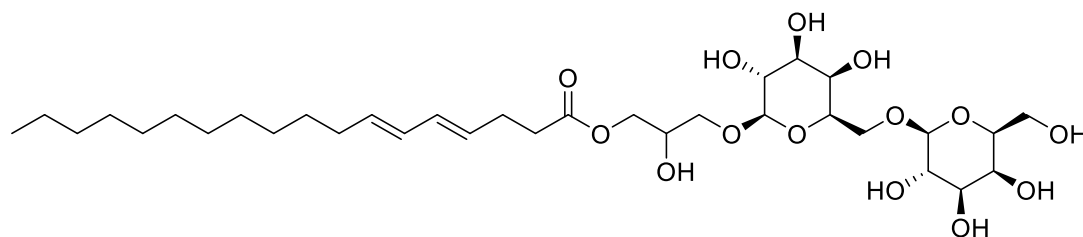
2,3,4-tris(5-methylhexanoyl)sucrose

constituents. of the epigeal parts of *Petunia nyctaginiflora*

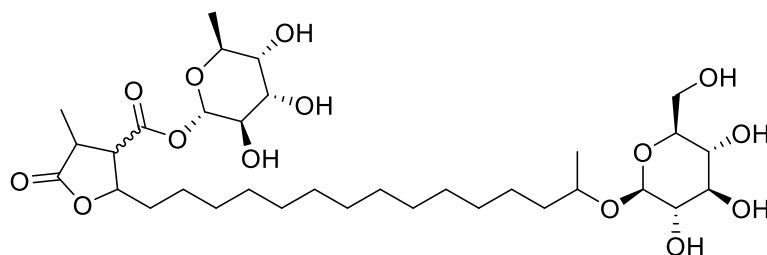


gingerglycolipid B

(2'S)-3'-O--linelenoylglycerol-6-O-(α -D-galactopyranosyl)- β -D-galactopyranoside
from *Zingiber officinale* (ginger), *Sonchus arvensis* and *Stellera chamaejasme*



glycerol-1-(4E,6E-octadecadienoate)-3-O-[β -D-galactopyranosyl-(1-6)- β -D-galactopyranoside]
from the roots of *Aganope balansae*



4R,20-dihydro, O- α -L-rhamnopyranoside- β -D-glucopyranosyl-murolic ester
from various lichens

Figure 5.77. Compound hits for the molecular formula $C_{33}H_{58}O_{14}$ dereplicated from the DNP.

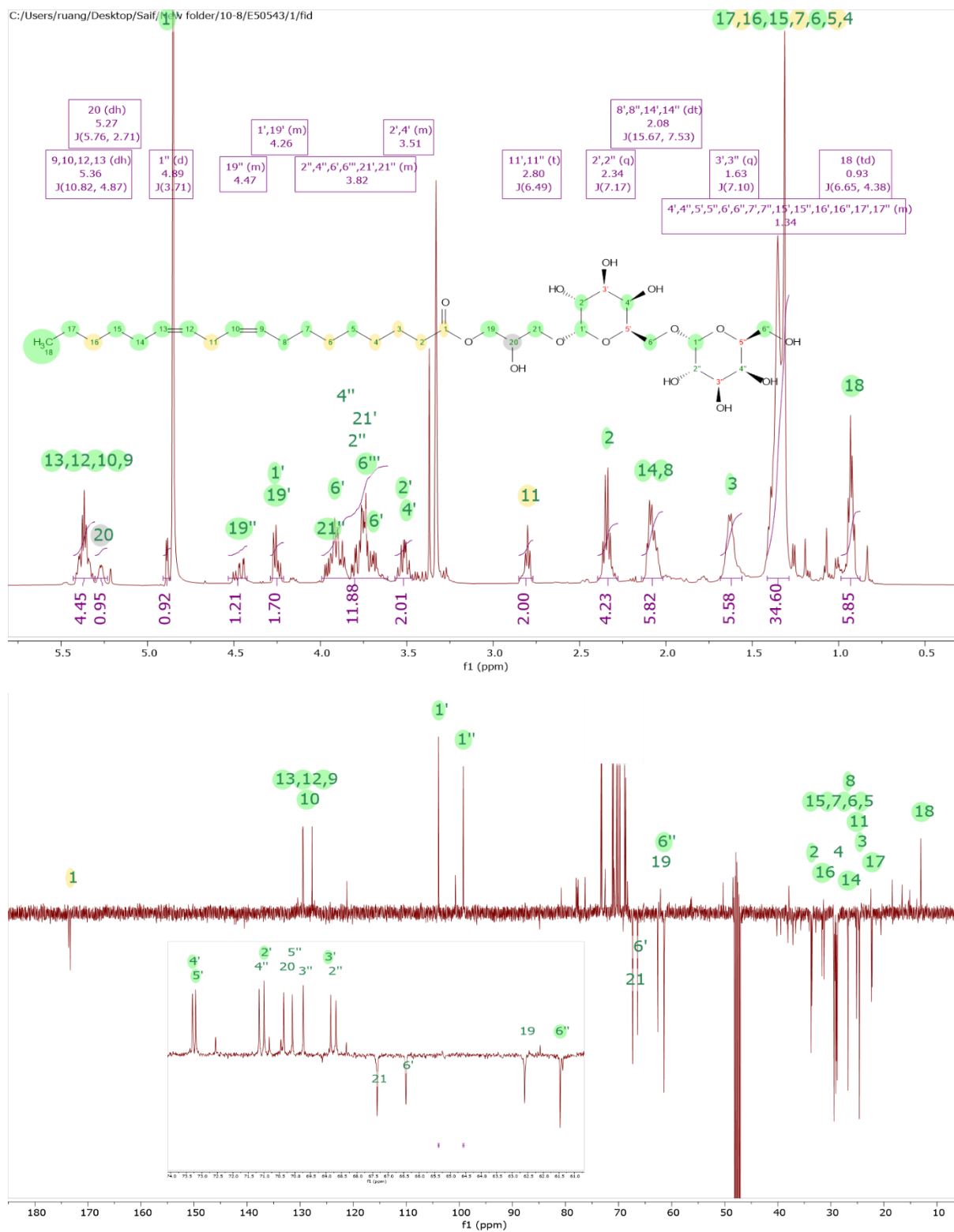


Figure 5.78. ¹H and ¹³C NMR spectra of Compound 10-8 in DMSO-*d*₆ at 500 MHz

Inspection of the 2D COSY spectrum of F10-8 in Figure 5.79 exhibited the same correlation peaks for the 9Z,12Z-octadecadienoyl unit, which were even superimposable to those found in F3-3. A similar pattern of cross peaks was also observed for the glycerol unit although the characteristic peaks shifted more downfield. However, a full assignment of the proton peaks in the sugar region was quite difficult to achieve after determining H-2 from the anomeric H-1 protons at 4 to 5 ppm, the cross peaks enter the region of overlapping peaks at 3 to 4 ppm. Furthermore, the anomeric protons were also half underneath the solvent HDO peak and one of the glycerol methylene protons that it was not feasible to determine their configurations at C-1. Although a doublet at 4.89 ppm with a coupling constant of 3.7 could be observed for one of the anomeric protons that indicated its equatorial position for an α -sugar.

Therefore, TOCSY was used to separate the correlation peaks for each respective sugar unit. This was a similar strategy that was utilised in the structure elucidation of the peptolide F10-2. But due to the overlapping peaks of the sugar units with those of the glycerol and the water peak, it was not feasible to decipher the peaks for each spin system. This is illustrated below in Figure 5.79.

The HMBC spectrum of F10-8 (Figure 5.80) also did display identical correlation peaks for the (9Z,12Z-octadecadienoyl)glycerol despite the change in chemical shifts for the two methylene carbons of the glycerol unit at 62.6 and 67.4 ppm. Both ^{13}C shifts deviated by 4 ppm when compared to those of F3-3. CH_2 -19 went upfield while CH_2 -21 was downfield for F10-2. On the other hand, all of the glycerol ^1H resonances were deshielded in the spectrum of F10-2. The HMBC correlations of the sugar protons in F10-2 were used to fully assign their chemical shifts and most essential their connectivity as exemplified in Figure 5.80. The methylene protons of the glycerol unit CH_2 -21 at 3.76 and 3.96 correlated with the anomeric carbon at 103.9 ppm for Gal1 while the methylene protons of Gal1 (CH_2 -6') at 3.69 and 3.93 ppm gave a cross peak with anomeric carbon of Gal2 at 99.2 ppm. These correlations established the connectivity of Gal1 to the glycerol unit from the anomeric carbon to CH_2 -21 (Gly-3) and a 1 \rightarrow 6 linkage between Gal2 and Gal1. The more isolated cross peaks were able to reveal the 3J correlations between the protons within the respective sugar units. Strong correlations were observed between H-1 and C-3, H-2 and C-4, and H-2-6 to C-4.

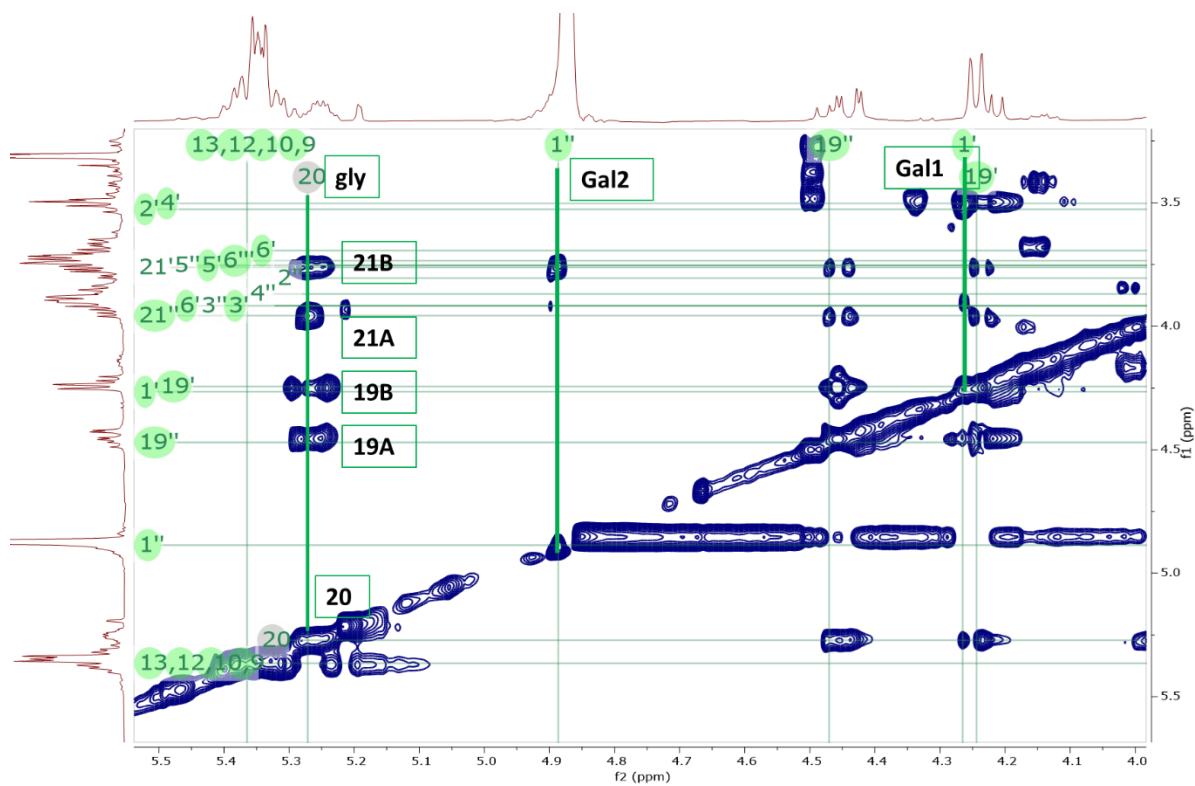
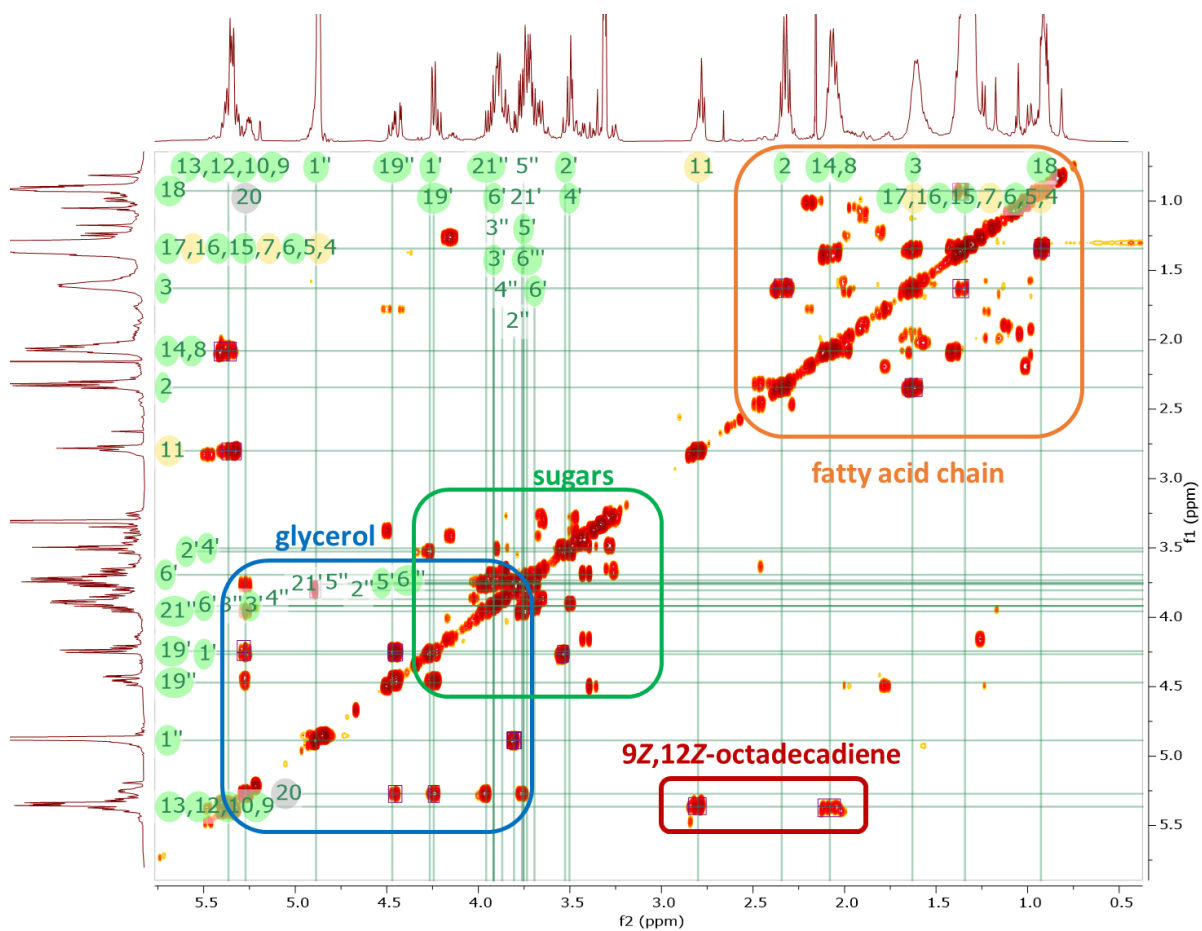


Figure 5.79. 2D COSY (above) and TOCSY (below) spectra of Compound 10-8 in DMSO- d_6 at 500 MHz

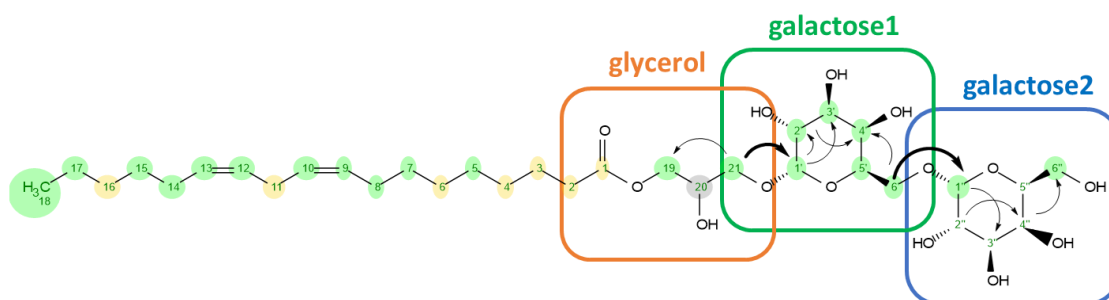
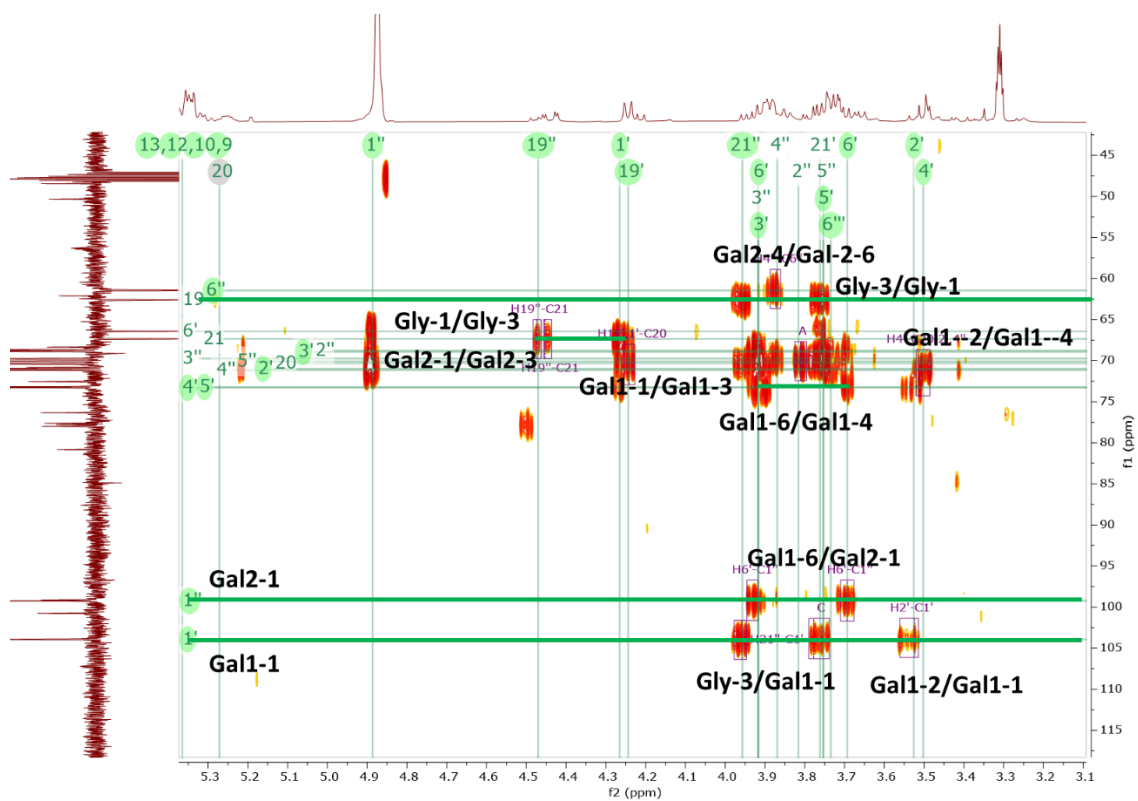


Figure 5.80. 2D HMBC spectrum of Compound 10-8 in DMSO- d_6 at 500 MHz illustrating the connectivity (H to C) of the three moieties in its structure with bold arrows.

While the ^1H and ^{13}C NMR shifts for the 9Z,12Z-octadecadienoyl moiety were almost superimposable to that of F3-3 despite the change in NMR solvents, full assignments for the glyceryl-sugar part were confirmed with a HSQC spectrum in Figure 5.81 and recorded in Table 5.23. The resulting spectral data was comparable to those of gingerglycolipid B isolated from the dried rhizomes of *Zingiber officinale* (Yoshikawa et al 2004) as presented in Table 5.24. However, the published ^{13}C NMR shifts had an average of a 2-ppm downfield shift while those reported for the glycerol methylene carbons deviated at almost 5 ppm along with the CH-3 for Gal1 with a 6-ppm difference. The reported ^1H NMR spectral data for gingerglycolipid B was identical to that of F10-8 but the ^1H chemical shifts for the glycerol unit was not reported in the publication. It was indeed plausible that there was a change in stereochemistry in the glycerol moiety that could have affected these larger differences. For instance, it has been reported that glycosylmonoacylglycerols (monogalactosyl-, digalactosyl-, and sulfoquinovosylmonoacylglycerols) isolated from coralline red alga *Corallina pilulifera* showed that the glycerol moieties in all the glycoylglycerolipids examined have the S-configuration *sn*-1,2-diacyl- and *sn*-1-monoacylglycerols (Takahashi et al., 2001).

Since it was not feasible to use the coupling constants to determine the configuration of each proton unit, the carbon shifts were compared to those found in the literature (Shashkov et al., 1993, Duus et al., 2000, Bubb, 2003). From the number of the carbon resonances between 60 to 100 ppm region, a set of 12 carbons could be assigned to two sugar units after subtracting the three carbon peaks for glycerol. The two sugar units were further evident by the two sets of anomeric at 100 ppm and two methylene units for CH₂-6 between 60 and 70 ppm. These chemical shifts were compared on the Glycosciences.DB database (<http://www.glycosciences.de/>), which generated a galactopyranosyl-(1→6) α -D-glucopyranoside unit at 72.50% match (Table 5.25). Albeit to date, the occurrence of digalactosyl among glycerol-1-alkanoate derivatives had been more common in the DNP database version 2021.

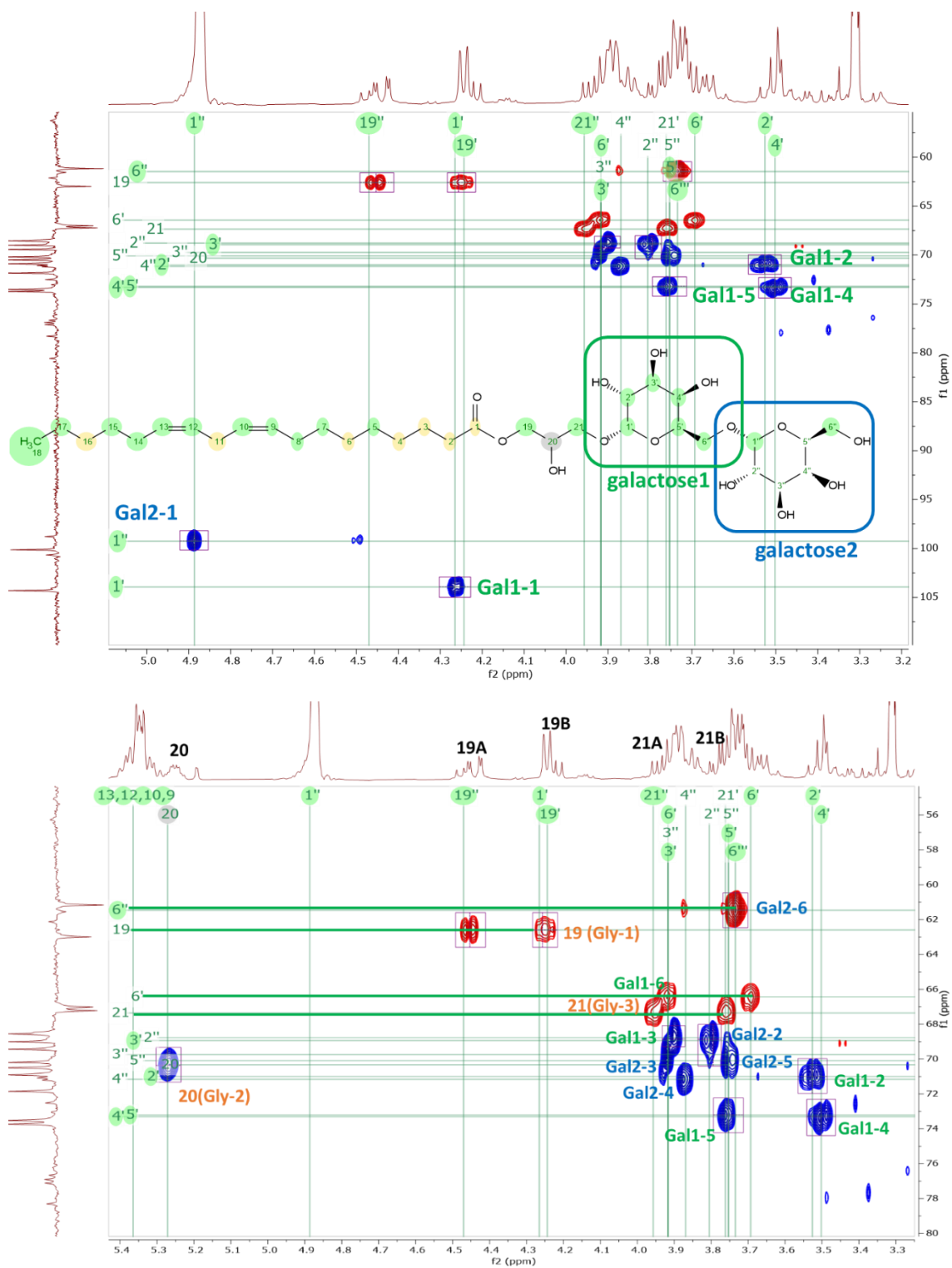


Figure 5.81. 2D HSQC spectrum of Compound 10-8 in DMSO-*d*₆ at 500 MHz highlighting the sugar region.

Table 5.23. NMR spectral data for compound F10-8 in MeOD at 500 MHz for δH and at 125 MHz for δC .

Atom	δC (ppm)	δH ppm (<i>J</i> in Hz)	Gal-1	δC (ppm)	δH ppm (<i>J</i> in Hz)
1 C	173.3		1' CH	103.9	4.23 - 4.30 m
2 CH ₂	33.7	2.34 q (7.2)	2' CH	71.0	3.49 - 3.57 m
3 CH ₂	24.6	1.63 q (7.2)	3' CH	68.9	3.87 - 3.93 m
4 CH ₂	29.1	1.29 - 1.41 m	4' CH	73.3	3.46 - 3.54 m
5 CH ₂	29.1	1.29 - 1.41 m	5' CH	73.2	3.71 - 3.79 m
6 CH ₂	29.1	1.29 - 1.41 m	6' CH ₂	66.4	3.68 - 3.71 m
7 CH ₂	29.1	1.29 - 1.41 m			3.92 - 3.95 m
8 CH ₂	26.8	2.02 - 2.14 m			
9 CH	129.5	5.30 - 5.43 m	Gal-2	δC (ppm)	δH ppm (<i>J</i> in Hz)
10 CH	128.8	5.30 - 5.43 m	1" CH	99.2	4.89 d (3.7)
11 CH ₂	25.21	2.8 t (6.5)	2" CH	68.8	3.72 - 3.84 m
12 CH	128.8	5.30 - 5.43 m	3" CH	69.7	3.91 - 3.92 m
13 CH	129.5	5.30 - 5.43 m	4" CH	71.2	3.87 m
14 CH ₂	26.8	2.02 - 2.14 m	5" CH	70.1	3.75 - 3.76 m
15 CH ₂	29.1	1.29 - 1.41 m	6" CH ₂	61.5	3.70 - 3.77 m
16 CH ₂	31.7	1.29 - 1.41 m			3.87 m
17 CH ₂	22.2	1.29 - 1.41 m			
18 CH ₃	13.0	0.93 t (6.6)			
19 CH ₂	62.6	4.21 - 4.29 m			
		4.42 - 4.53 m			
20 CH	70.3	5.23 - 5.30 m			
21 CH ₂	67.3	3.76 m			
		3.95 - 3.98 m			

Table 5.24. ^{13}C NMR spectral data for compound F10-8 measured at 125 MHz in comparison to literature at 67.5 MHz (Yoshikawa et al 1994).

linoleic	F10-2	Lit. Data	Diff.	Gly	F10-2	Lit. Data	Diff.
1 C	173.3	176.2	-2.90	19 CH ₂	62.6	67.4	-4.81
2 CH ₂	33.7	35.7	-2.04	20 CH	70.3	70.4	-0.08
3 CH ₂	24.6	26.8	-2.23	21 CH ₂	67.4	72.9	-5.55
4 CH ₂	29.1	31.1	-2.00			Average	-3.48
5 CH ₂	29.1	31.1	-2.01	Gal-1			
6 CH ₂	29.1	31.3	-2.21	1' CH	103.9	106.1	-2.17
7 CH ₂	29.1	31.3	-2.21	2' CH	71.0	73.3	-2.30
8 CH ₂	26.8	29.0	-2.18	3' CH	68.9	75.3	-6.37
9 CH	129.5	131.7	-2.23	4' CH	73.3	71.0	2.30
10 CH	128.8	129.9	-1.14	5' CH	73.2	75.3	-2.10
11 CH ₂	25.2	27.3	-2.09	6' CH ₂	66.4	68.5	-2.07
12 CH	128.8	129.9	-1.14	Gal-2			
13 CH	129.5	131.7	-2.23	1" CH	99.3	101.3	-2.05
14 CH ₂	26.8	29.0	-2.20	2" CH	68.8	70.8	-2.03
15 CH ₂	29.1	31.3	-2.21	3" CH	69.7	72.2	-2.46
16 CH ₂	31.7	33.5	-1.84	4" CH	71.2	71.8	-0.64
17 CH ₂	22.3	24.4	-2.15	5" CH	70.1	73.3	-3.21
18 CH ₃	13.0	15.3	-2.33	6" CH ₂	61.5	63.5	-2.04
		Average	-2.07			Average	-2.10

Table 5.25. ^{13}C NMR spectral comparison from Glycosciences.DB with a match score of 72.50% (<http://www.glycosciences.de/>).

$\alpha\text{-D-Glcp-(1-6)}$ + D-Gal $\alpha\text{-L-Rhap-(1-3)}$ +	Shift	Residue	Atom	Linkage	PPM	ERROR (PPM)
	1: 103.9	$\alpha\text{-L-Rhap}$	C1	3	103.599998	0.30000200000001
	2: 71.0	D-Gal	C5A		70.800003	0.199997
	3: 68.9	D-Gal	C4B		68.900002	1.9999999949505E-6
	4: 73.3	$\alpha\text{-D-Glcp}$	C5	6	73.099998	0.200002
	5: 73.2	$\alpha\text{-D-Glcp}$	C5	6	73.099998	0.100002
	7: 99.3	$\alpha\text{-D-Glcp}$	C1	6	99.5	0.2
	8: 68.8	D-Gal	C4B		68.900002	0.100002
	9: 69.7	D-Gal	C4A		69.800003	0.100003
	10: 71.2	D-Gal	C5A		70.800003	0.399997
	11: 70.1	D-Gal	C4A		69.800003	0.299996999999999
	12: 61.5	$\alpha\text{-D-Glcp}$	C6	6	61.799999	0.299999

5.4 Biological assay results for purified fractions and isolated compounds

Purified fractions obtained from *D. salina* grown on malt extract broth afforded antimicrobial activity against biofilm-forming *S. aureus* and *P. aeruginosa*. Fraction 2-2 exhibited the most potent activity with 95% growth inhibition of *P. aeruginosa* while under the viability threshold of 30%, F4-1 was found to be only antimicrobial against *S. aureus* but was able to inhibit biofilm formation of *P. aeruginosa*. The rest of the purified fractions exhibited moderate to weak antimicrobial activity with a bacterial and biofilm viability from 30 to 50% and more than 50%, respectively. AlamarBlue® and planktonic assay results are presented in Table 5.26.

On the other hand, chromatographic purification of antimicrobial-active fractions obtained from *D. salina* grown on oat solid media afforded several bioactive subfractions with bacterial growth and/or biofilm inhibition of greater 70% as highlighted in grey in Table 5.27. This included F2-2-2, F2-2-9, F 3-1, F3-2, F10-1, F10-2, F10-3, F10-5, F10-6 and F10-8. Further isolation and structure elucidation work were done on F2-2-2, F 3-1, F10-2, and F10-8, which were chosen according to their respective yield and purity. However, none of these subfractions were as potent as F2-2, which was obtained from the fungal extract incubated on malt extract broth media.

Table 5.26: AlamarBlue® and planktonic assay results against biofilm-forming *S. aureus* and *P. aeruginosa* for 100µg/ml concentration of bioactive subfractions obtained from *D. salina* grown on malt extract broth. Highlighted rows represent bioactive fractions at a threshold of less than 30% viability.

Sub-Fraction	AlamarBlue® results % of bacteria viability		Planktonic results % of biofilm viability	
	<i>S. aureus</i>	<i>P. aeruginosa</i>	<i>S. aureus</i>	<i>P. aeruginosa</i>
F2-1	85.27	88.61	91.58	95.81
F2-2	14.51	4.91	16.29	21.08
F2-3	96.43	93.72	97.38	97.71
F4-1	29.84	31.27	39.47	28.91
F4-2	31.23	36.81	42.53	38.25
F4-3	34.66	38.76	56.48	69.61
F4-4	52.97	52.27	62.52	67.51
F4-5	51.21	51.31	56.59	43.32
F4-6	35.28	39.02	27.37	18.65
F4-7	53.46	52.93	47.08	50.85
F4-8	86.81	87.21	83.38	86.18
F4-9	87.35	90.04	84.07	93.73
F4-10	95.37	94.17	94.18	92.68
F4-11	99.38	98.51	99.47	99.02

Table 5.27: AlamarBlue® and planktonic assay results against biofilm-forming *S. aureus* and *P. aeruginosa* for 100µg/ml concentration of subfractions obtained from *D. salina* grown on oat solid media. Highlighted rows represent bioactive fractions at a threshold of less than 30% viability.

Sub-Fraction	AlamarBlue® results % of bacteria viability		Planktonic results % of biofilm viability	
	<i>S. aureus</i>	<i>P. aeruginosa</i>	<i>S. aureus</i>	<i>P. aeruginosa</i>
F2-2-1	83.71	93.71	86.82	86.34
F2-2-2	29.44	34.48	25.84	22.35
F2-2-3	74.14	67.32	96.58	68.25
F2-2-4	85.81	92.65	95.17	57.89
F2-2-5	44.32	36.78	54.12	53.71
F2-2-6	84.76	57.13	51.49	58.62
F2-2-7	78.19	63.92	84.92	75.19
F2-2-8	34.58	31.98	34.54	38.58
F2-2-9	22.37	24.92	33.17	27.18
F3-1	43.65	54.19	27.15	24.49
F3-2	27.18	24.49	18.32	21.26
F3-3	65.26	65.28	76.46	85.46
F3-4	76.16	75.26	83.16	94.18
F3-5	79.25	89.46	89.79	96.86
F3-wash	22.78	19.68	18.62	27.15
F10-1	21.85	26.54	43.75	42.17
F10-2	27.18	28.12	17.46	20.85
F10-3	50.13	48.13	33.45	25.13
F10-4	54.76	51.41	36.59	30.76
F10-5	52.19	57.37	34.76	27.47
F10-6	55.48	54.89	41.27	29.85
F10-7	58.14	61.14	35.82	34.84
F10-8	54.37	56.74	34.45	27.46

MIC and MBEC were determined for the isolated compounds from the purified sub-fractions and the results are presented in Table 5.28. F10-2 (turnagainolide A) and F10-8 (gingerglycolipid B stereoisomer) displayed the highest potency against both biofilm-forming *S.aureus* and *P.aeruginosa* with MIC and MBEC values between 45 and 75 μ M concentrations. F2-1 and F3-3, which were identified as linoleic acid and its glycerol congener were both deemed inactive with MIC and MBEC values of greater than 100 μ g/ml. Subfraction F3-3 was already found inactive in the viability assay but due to its spectral similarity to F3-1 as shown in Figure 5.52, it was noteworthy to do further elucidation work on this inactive subfraction. Amongst the linoleate derivatives, the glycolipid F10-8 was the most active while the acetone congener F3-1 was less active with MIC and MBEC values between 75 and 145 μ M concentrations. In contrast, the isolated phenolic compounds; F4-1, which is a mixture of orsellinic acid and orcinol at a ratio of 3:1, and 2,5-dihydroxy-3-(hydroxymethyl)benzoic acid (F4-6 and F2-2-2) were less active with MIC and MBEC values between 145 and 360 μ M concentrations.

Table 5.28: MIC and MBEC results of isolated compounds from *D. salina* extracts against biofilm-forming *S. aureus* and *P. aeruginosa*. Gentamicin was used as positive control.

Compounds isolated from <i>D. salina</i> growing on malt extract broth				
Compound Code	MIC (μ g/ml) against <i>S. aureus</i> *	MIC (μ g/ml) against <i>P. aeruginosa</i> *	MBEC (μ g/ml) against <i>S. aureus</i> *	MBEC (μ g/ml) against <i>P. aeruginosa</i> *
F2-1	>100	>100	>100	>100
F4-1**	37.94 (225:305)	44.29 (264:357)	41.81 (249:337)	31.89 (190:257)
F4-6	29.10 (158)	33.28 (181)	31.82 (173)	39.38 (214)
Compounds isolated from <i>D. salina</i> growing on oat solid media				
Compound Code	MIC (μ g/ml) against <i>S. aureus</i> *	MIC (μ g/ml) against <i>P. aeruginosa</i> *	MBEC (μ g/ml) against <i>S. aureus</i> *	MBEC (μ g/ml) against <i>P. aeruginosa</i> *
F2-2-2	27.07 (147)	29.31 (159)	29.35 (159)	34.03 (212)
F3-1	47.16 (119)	47.21 (120)	56.17 (143)	30.04 (76)
F3-3	>100	>100	>100	>100
F10-2	31.53 (57)	37.28 (67)	25.18 (45)	34.85 (63)
F10-8	38.46 (57)	42.93 (63)	31.73 (47)	30.91(46)
Positive control				
Drug tested	MIC (μ g/ml) against <i>S. aureus</i> *	MIC (μ g/ml) against <i>P. aeruginosa</i> *	MBEC (μ g/ml) against <i>S. aureus</i> *	MBEC (μ g/ml) against <i>P. aeruginosa</i> *
Gentamicin	4.98 (10)	10.08 (21)	5.45 (11)	10.76 (22)
Gentamicin-SO ₄	4.98 (10)	10.08 (19)	5.45 (11)	10.76 (21)

*In parenthesis is the μ M concentration. **Mixture of orsellinic acid and orcinol at a ratio of 3:1.

6 General Discussion

6.1 Metabolomics-guided and bioassay-assisted isolation of antimicrobial compounds

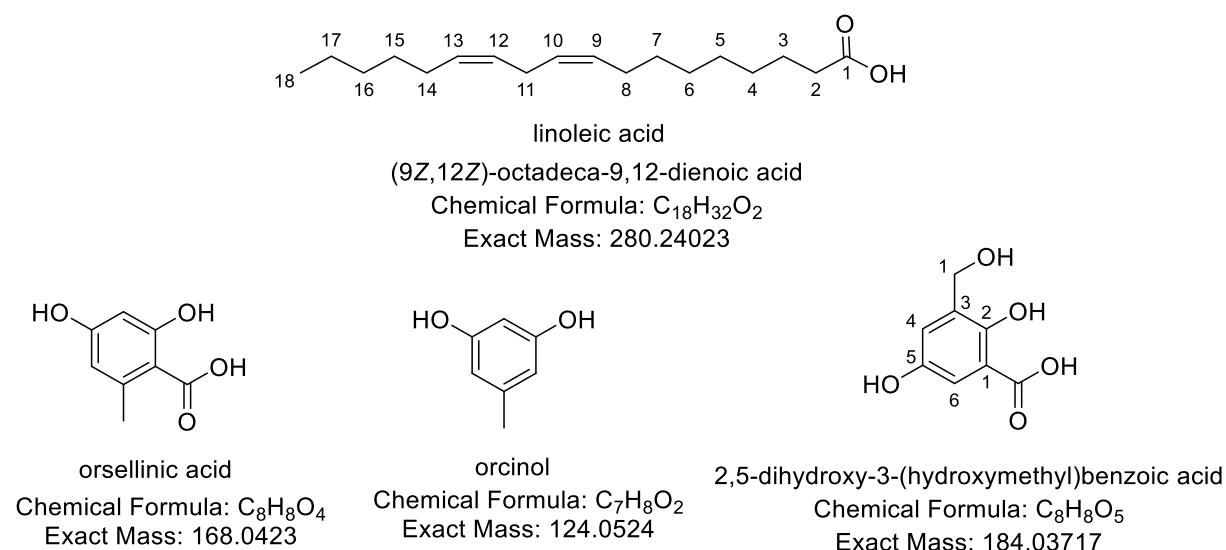


Figure 6.1A. Compounds isolated from the fungal extract of *D. salina* grown on malt extract broth media with sea salt.

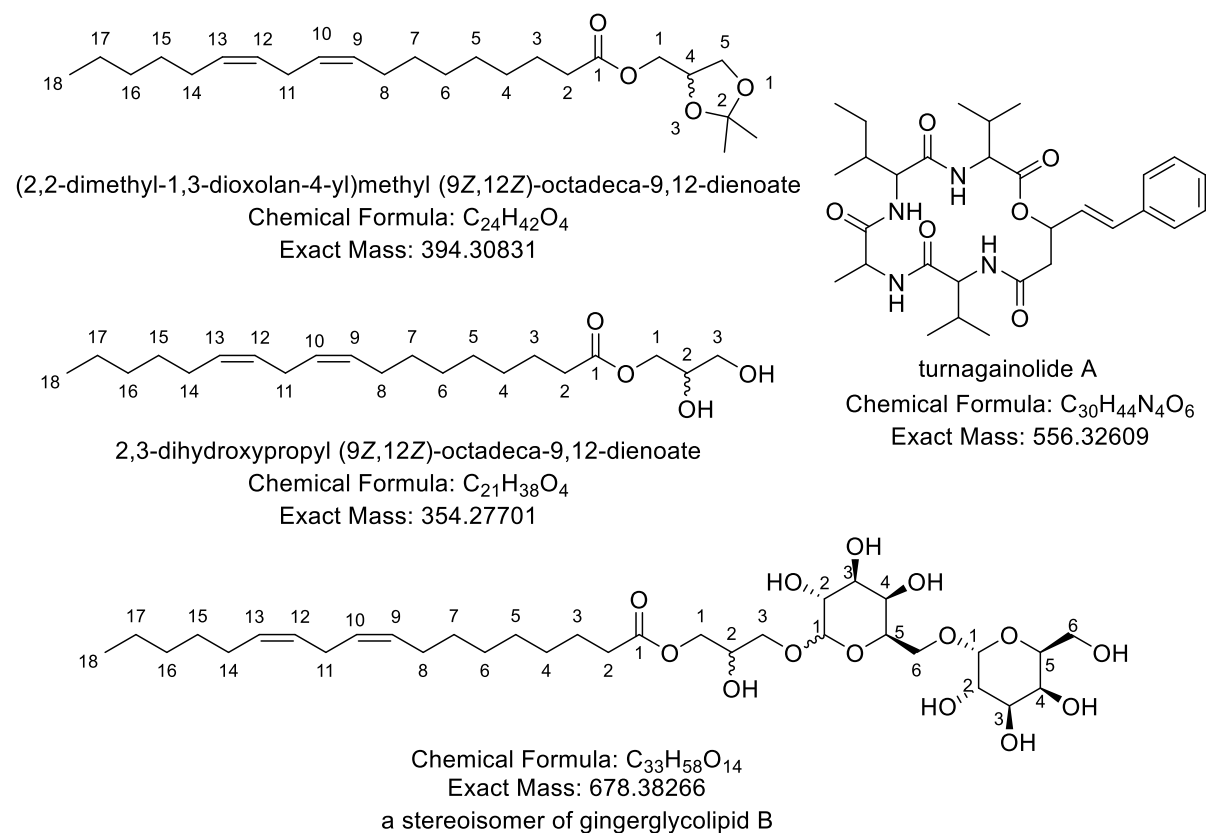


Figure 6.1B. Compounds isolated from the fungal extract of *D. salina* grown on oat media without sea salt.

The dereplicated secondary metabolites produced by *D.salina* incubated in malt extract broth and oat media were quite different. However, there was one common target antimicrobial active metabolite found at the ion peak m/z 265.107 [M+H] for $C_{14}H_{16}O_5$, which was exhibited by P_2201 from the extract obtained from malt extract broth media and P_3600 from the fungus grown in oat media. Extracts afforded from the malt extract yielded low molecular weight aromatic compounds that included substituted phenyl units and lactone derivatives while the extract obtained from oat afforded aliphatic compounds such as di-unsaturated lipids, glycolipids and small peptides.

Amongst the targeted compounds, only one compound was achieved to be isolated, which was F4-1A from the *D. salina* extract obtained from malt extract media. It was a small molecule with a MW of 168 Da and a structure related to those predicted for P_2201 and P_3600. However, the compound is known, which is orsellinic acid that has been widely described in lichens and was also reported to be antimicrobial (Rowe et al., 1999). Orsellinic acid in F4-1 was isolated with another lichen metabolite known as orcinol with a MW of 124 Da, which was outside the range of detection of the MS parameter set-up used in this study. Four compounds were isolated from two active fractions, Fractions F-2 and F-4, derived from the *D. salina* extract obtained from malt extract media. However, the isolated compound F2-1 was merely (9Z,12Z)-octadeca-9,12-dienoic acid, which is linoleic acid. Inspection of the 1H NMR data of the subfraction F2-2 at 7mg, also derived from Fraction 2 but remains a mixture, it could be said from the perceivable resonances that the target metabolite was still in this subfraction. F4-6 with a MW of 184 Da was near that of the target antimicrobial feature P_2626 at m/z [M+H]⁺ 185.080 Da (MW = 184.0736 for $C_9H_{12}O_4$). F4-6 had a molecular formula of $C_8H_8O_5$, with an extra oxygen atom and loss of an alkyl unit, it was hypothesised that the isolated compound could be a product of an oxidation reaction during the isolation work.

From the oat media, five compounds were obtained from three active fractions F-2, F-3, and F-10. Further work on Fraction 5, which was amongst the highlighted fraction due to its interesting chemical profile, was not successful due to instrument leakage during fractionation, Fraction F-5 was loss. This included the re-isolation of the 2,5-dihydroxy-3-(hydroxymethyl)benzoic acid, the compound with a MW 185 Da (F4-6) from F-2. The isolation work of the fungal extract from the oat media afforded three glyceryl linoleate derivatives and a peptolide. Included amongst the predicted and dereplicated antimicrobial compounds from the extract derived from the oat media were 2-amino-9-methyl-4,8-nonadecadiene-1,3-diol for P_3483 and *N*-(2-hydroxyethyl)linoleamide for P_2438, which were structurally related to the

isolated glyceryl linoleate in this study. It seems that in the oat media, the fungus utilised linoleic acid for further derivatization. On the other hand, the peptolide (F10-2) that was known as turnagainolides have been isolated by several research groups and was given other trivial names such as EGM-56 and strepeptolide (Li et al., 2011, Vervoort et al., 2011). The afforded peptolide F10-2 could also be detected in the other neighbouring fractions.

Since only one target antimicrobial compound was isolated from the selected active fractions, all the isolated compounds were revisited on their position on the OPLS-DA loadings plot for their predicted bioactivity as shown in Figure 6.2. Amongst the isolated compound, F2-1 (linoleic acid) and F3-1 (1,2-acetonide-3-(9,12- octadecadienoyl)glycerol) were classified in the inactive quadrant. The presence of linoleic acid could actually be deduced in all of the fractions as shown in Figure 6.3. The occurrence of the 168 Da compound or orsellinic acid could also be observed in its active neighbouring fractions (Figure 6.3).

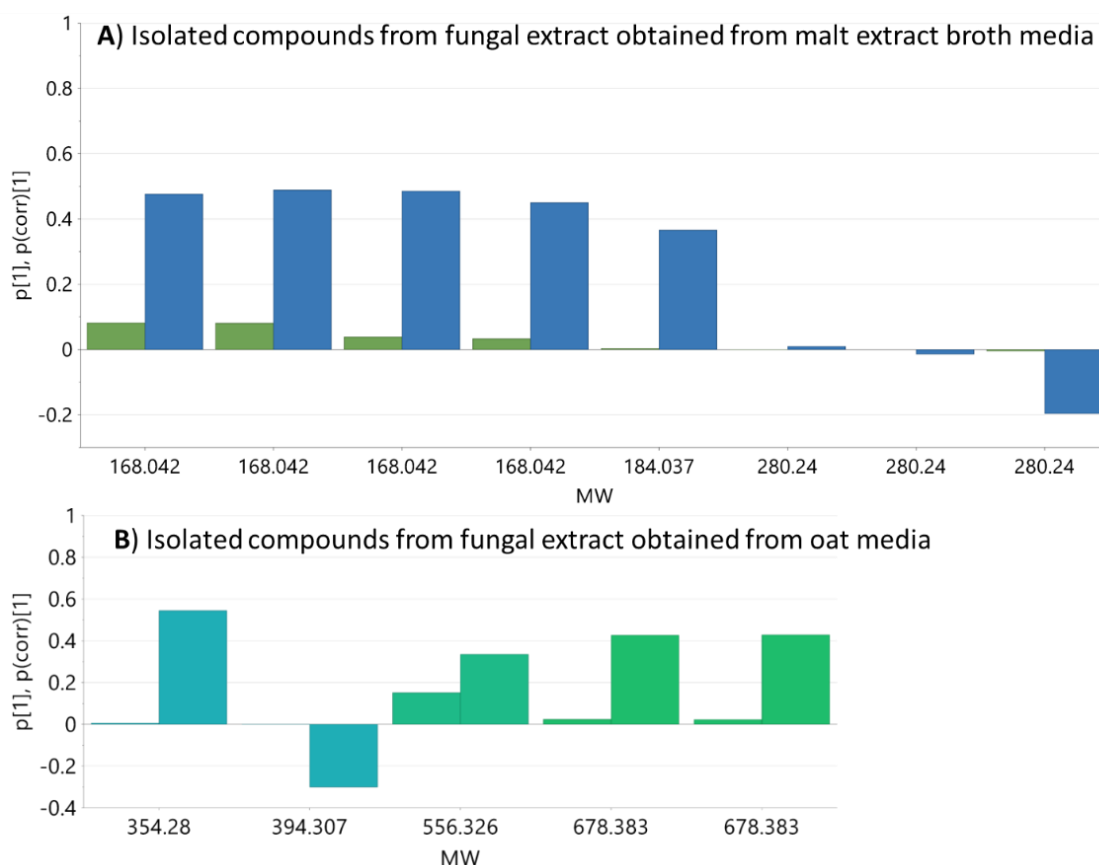
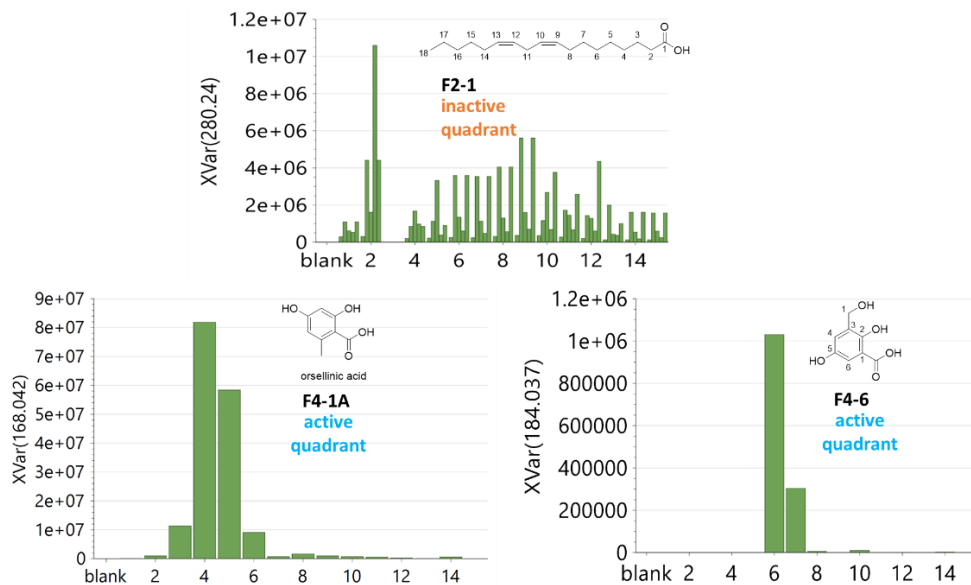


Figure 6.2. Distribution of the isolated compounds between the active and inactive quadrant by OPLS-DA. Positive projection are the predicted compounds with antimicrobial activity and compounds on the negative projection are predicted to be inactive. Ion peaks with the same retention time but ionises in both modes were plotted twice.

D. salina grown on malt extract broth media with sea salt yielded antimicrobial active non-polar fractions F-1 to F-7. *D. salina* inoculated on oat solid media without sea salt afforded active fractions F-2, F-3, F-5, F-9, and F-10. However, the relative abundance of the isolated bioactive compounds in the various fractions from the fungal extract obtained from the oat solid media indicated their distribution in the active fractions as generated by the X-variant plot (Figure 6.3). For instance, the phenolic acid derivatives, F4-1 and F4-6, were highly abundant in the active fractions F-2 to F-7, while the inactive linolenic acid F2-1 widely occurred in fractions F-8 to F-14. In the case of acetonide linoleate (F3-1), which was located in the inactive quadrant of the OPLS-DA plot, it was actually most abundant in the active fraction F-5. Alternatively, the inactive glycerol ester of linolenic acid situated in the active quadrant was distributed in the inactive fractions F-6, F-7, and F-8. The limitation of the metabolomics approach in predicting the biologically active metabolites is the incapability to isolate low-yielding compounds (Rowe et al., 1999).

Compound F4-6 (2,5-dihydroxy-6-hydroxymethyl) benzoic acid afforded the most potent antimicrobial activity with MIC values of 27.07 and 29.31 μ g/ml against both biofilm forming *S. aureus* and *P. aeruginosa*, respectively. On the other hand, compound F10-2 (turnagainolide A) and F3-1 (1,2-acetonide-3-(9,12-octadecadienoyl) glycerol) exhibited the lowest MBEC values against biofilm forming *S. aureus* and *P. aeruginosa* at 25.18 and 30.04 μ g/ml, respectively. However, the antimicrobial activity of F3-1 and inactivity of F3-3 were mispredicted by the OPLS-DA plot but their actual distribution in the active and inactive fractions could be validated from the x-variant plot as mentioned above.

A) Compounds isolated from the *D. salina* extract obtained from malt extract broth media



B) Compounds isolated from the *D. salina* extract obtained from oat media

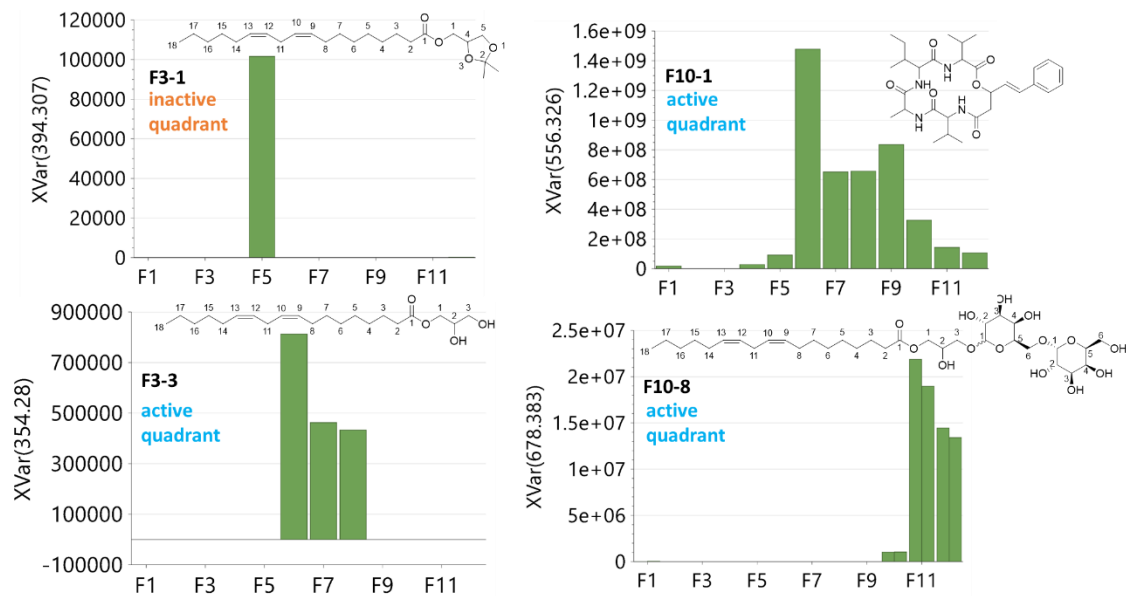


Figure 6.3: Relative abundance of the isolated compounds in various MPLC fractions.

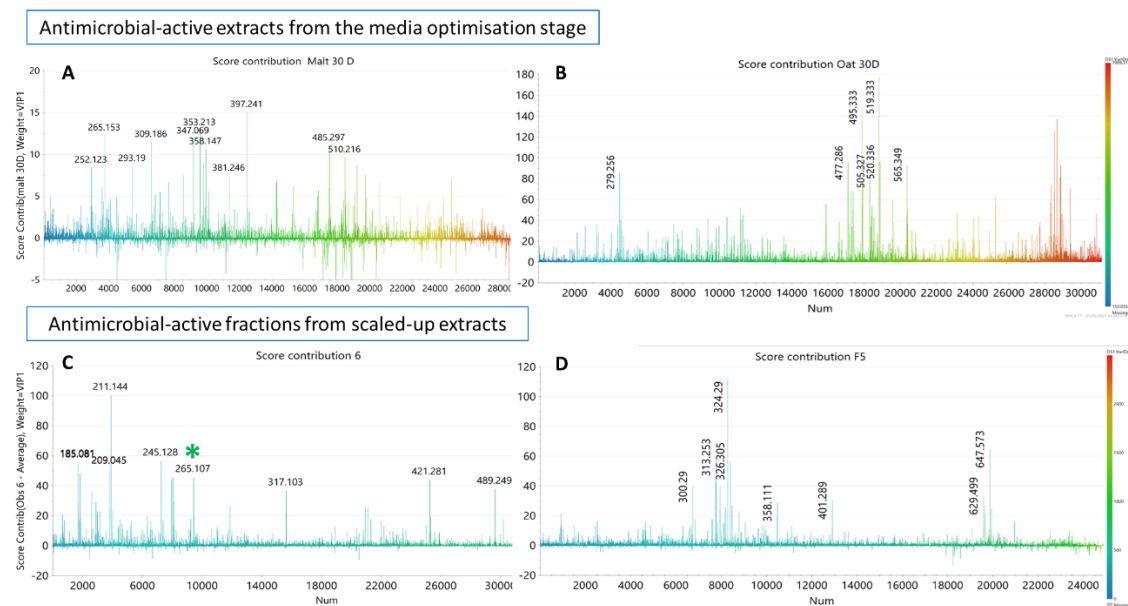


Figure 6.4: OPLS-DA score contribution plot of active features in antimicrobial extracts and corresponding outlying fractions. Y-axis is the weighed VIP scores in the active quadrant. X-axis is the feature number arranged according to m/z . Colour range blue to red is from low to high m/z . **A)** Active extract obtained from *D. salina* incubated for 30 days on malt extract media with sea salt. **B)** Active extract obtained from *D. salina* incubated for 30 days on oat media without sea salt. **C)** Outlying active Fraction-6 obtained from scaled-up fungal extract derived from malt extract media. **D)** Outlying active Fraction-5 obtained from scaled-up fungal extract derived from oat media. Asterisk (*) on ion peak at m/z 265.107 signifies similar ion peak detected from antimicrobial-active fungal extract obtained malt extract agar plates.

The chemical profiles of the active features of the antimicrobial extracts and outlying active fractions were compared. As shown in Figure 6.4, the chemical profiles of the fungal extracts derived from different media were different. However, scaling-up also resulted to a change in chemical profile. During scale-up, indeed there was still a change in the fermentation environment such as the amount of oxygen in the fermentation vessel while any other variation would affect the chemical profile of the afforded extracts. Nevertheless, some generalizations could be put together. *D. salina* incubated in malt extract with sea salt tend to yield low MW compounds, while incubating the fungus in oat media without sea salt produced higher MW compounds. Remarkably, the ion peak at m/z 265.107 [M+H] for $C_{14}H_{16}O_5$, which was putatively dereplicated for pestalasin A from a mangrove-derived *Pestalotiopsis* sp. JCM2A4 and *Penicillium purpurogenum* MHZ 11 (Xu et al., 2009, Shaaban et al., 2016); infectopyrone and oxosorbicillinol from various fungi (Abe et al., 2000, Larsen et al., 2003); scytalol D from *Scytalidium* sp. 36-93 and *Biatriospora* sp. 8331 (Thines et al., 1998, Zhou et al., 2016b); epoxysorbicillinol from sponge-derived *Trichoderma longibrachiatum* (Sperry et al., 1998);

and xestodecalactone A from *Penicillium cf. montanense* (Edrada et al., 2002), was the similar ion peak initially detected from the antimicrobial-active fungal extract obtained from the malt extract agar plates. But again, the occurrence of this specific bioactive metabolite at low concentrations remained unachievable to isolate.

6.2 Proposed biosynthetic pathways of the isolated compounds

6.2.1 Polyketide biosynthetic pathway for orcinol, orsellinic acid and 2,5-dihydroxy-6-hydroxymethyl) benzoic acid.

Polyketides are diverse compounds divided to three main groups: type 1 polyketide includes macrolides, type 2 polyketide comprises of small aromatic compounds produced by iterative reaction of dissociated enzymes and type 3 polyketides are small aromatic molecules produced usually by fungi species. Orsellinic acid, orcinol and (2,5-dihydroxy-6-hydroxy methyl)benzoic acid are examples of compounds synthesised through the polyketide pathway. One mole of acetyl-CoA interacts with three moles of malonyl-CoA in the presence of β -ketoacylsynthase (KS) and acyltransferase (AT) would afford the intermediate 2,4,6-trioxoheptanoic acid (Chooi et al., 2008). Sequentially, cyclisation of 2,4,6-trioxoheptanoic acid occurs in the presence of Claisen cyclase (CYC) (Chooi et al., 2008). Finally, Claisen condensation will take place to form orsellinic acid (Chooi et al., 2008). Orcinol is further synthesized through decarboxylative aldol condensation of 2,4,6-trioxoheptanoic acid followed by aromatization (Taura et al., 2016). While the new compound (2,5-dihydroxy-6-hydroxy methyl)benzoic acid could have been synthesized by subsequent condensation and reduction of another plausible quinone intermediate 6-methyl-2,5-dioxocyclohex-6-ene-2-carboxylic acid followed by oxidation of its methyl unit as shown in Figure 6.5.

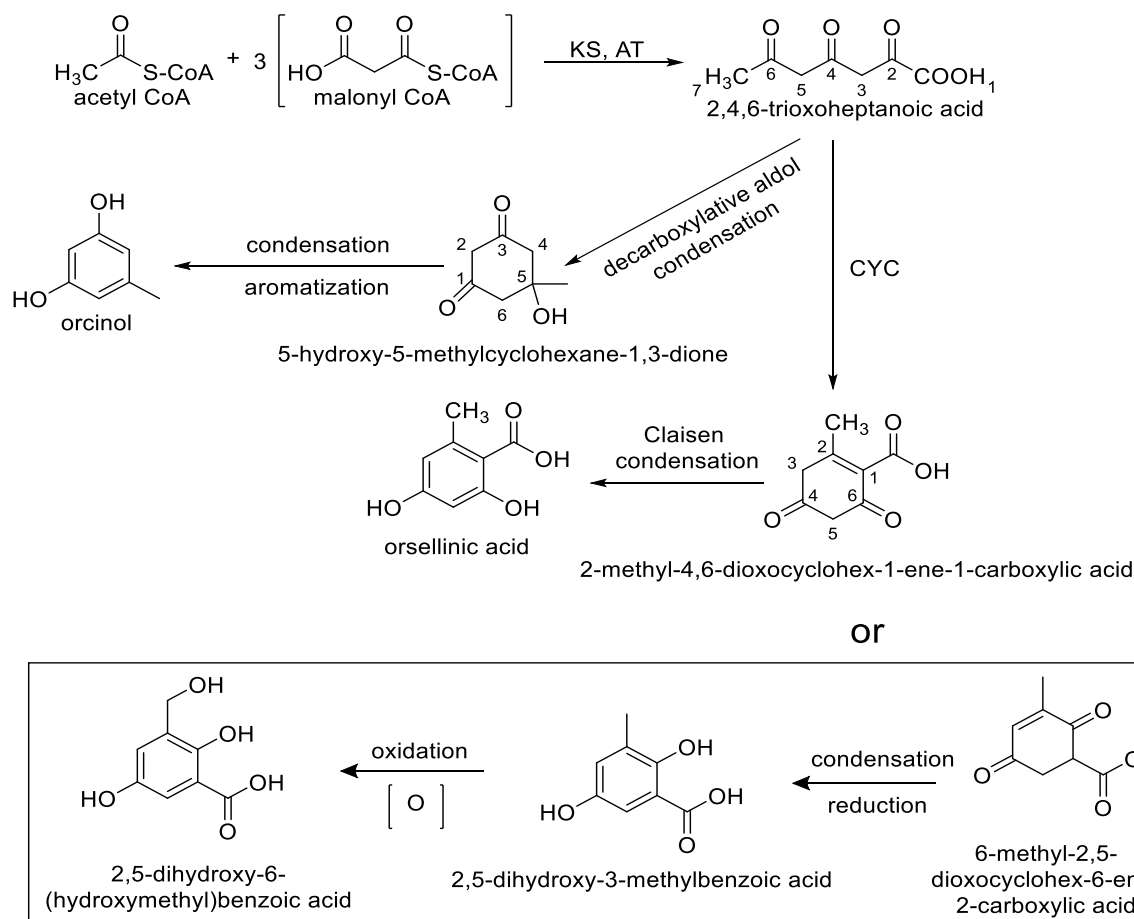


Figure 6.5: Proposed biosynthetic pathway of orsellinic acid, orcinol and 2,5-dihydroxy-6-(hydroxymethyl)benzoic acid isolated from *D. salina* grown on malt extract broth with sea salt (adapted from Chooi et al., 2008).

6.2.2 Proposed biosynthetic pathway of linoleic acid and its derivatives

The proposed biosynthetic pathway of linoleic acid as shown in Figure 6.6A basically starts with one mole of acetyl-CoA and seven moles of malonyl-CoA as precursors for fatty acid (FA) synthesis (Akpınar-Bayizit, 2014). As was proposed in *Saccharomyces cerevisiae* (Gajewski et al., 2017), the precursors enter the FA cycle, where the acyl substrate (either as the acetyl molecule or ACP-bound) with malonyl undertake condensation in the presence of ketoacyl synthase (KS). The resulting β -ketoacyl intermediate is then processed in a repetitive sequence of reaction steps that involve reduction with ketoacyl reductase (KR), dehydrogenation with a dehydratase (DH) enzyme, and again another reduction step with enoyl reductase (ER) in the presence of NADPH, to a fully reduced acyl-chain. The resulting acyl-chain would be the precursor for the next cycle.. The process is repeated until the final FA is cleaved off from its thio-CoA moiety by hydrolysis with a thioesterase. The FA product

that is C₁₆ (palmitic acid) would be elongated to C₁₈ (stearic acid) elongase enzyme then a sequence of desaturation reactions occurs to add double bonds to the FA structure. Commencing with Δ⁹ desaturase would form oleic acid (18:1(9)) then followed with Δ¹² desaturase to yield linoleic acid (18:2(9,12)).

The proposed biosynthesis of 2,3-dihydroxypropyl (9Z,12Z)-octadeca-9,12-dienoate also trivially known as glycerol linoleate continues with an esterification reduction reaction of linoleic acid in the presence of glycerol. Otherwise, the biosynthesis of 1,2-acetonide-3-(9,12-octadecadienoyl) glycerol could result with the reduction of glycerol linoleate in the presence of acetone. This will lead to the cyclization and the formation of acetonide with two methyl substitution provided by the acetone substrate as presented in Figure 6.6A.

Finally, the proposed biosynthesis of gingerglycolipid B stereoisomer shown in in Figure 6.6B could be accomplished by glycosylation of glycerol linoleate with uridine diphosphate (UDP)-galactose in the presence of UDP-glycosyltransferases (Hori et al., 2016). This step will be done twice to add two galactose units attached to the terminal hydroxyl group of the glycerol moiety.

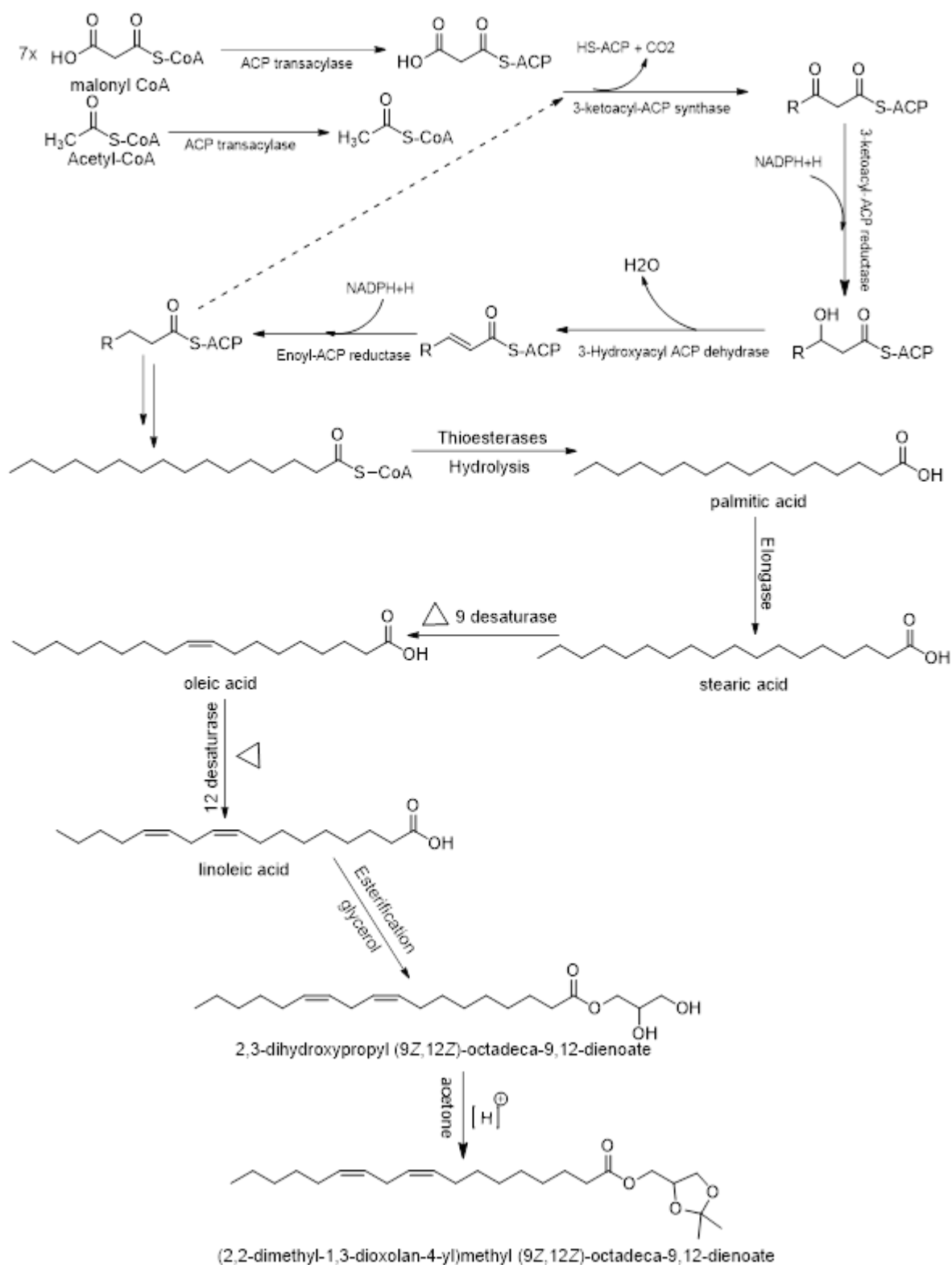


Figure 6.6A: Proposed biosynthetic pathway of linoleic acid and its derivatives isolated from *D. salina* grown on malt extract broth and oat solid media, respectively. (adapted from Akpinar-Bayazit, 2014 and Gajewski et al., 2017)

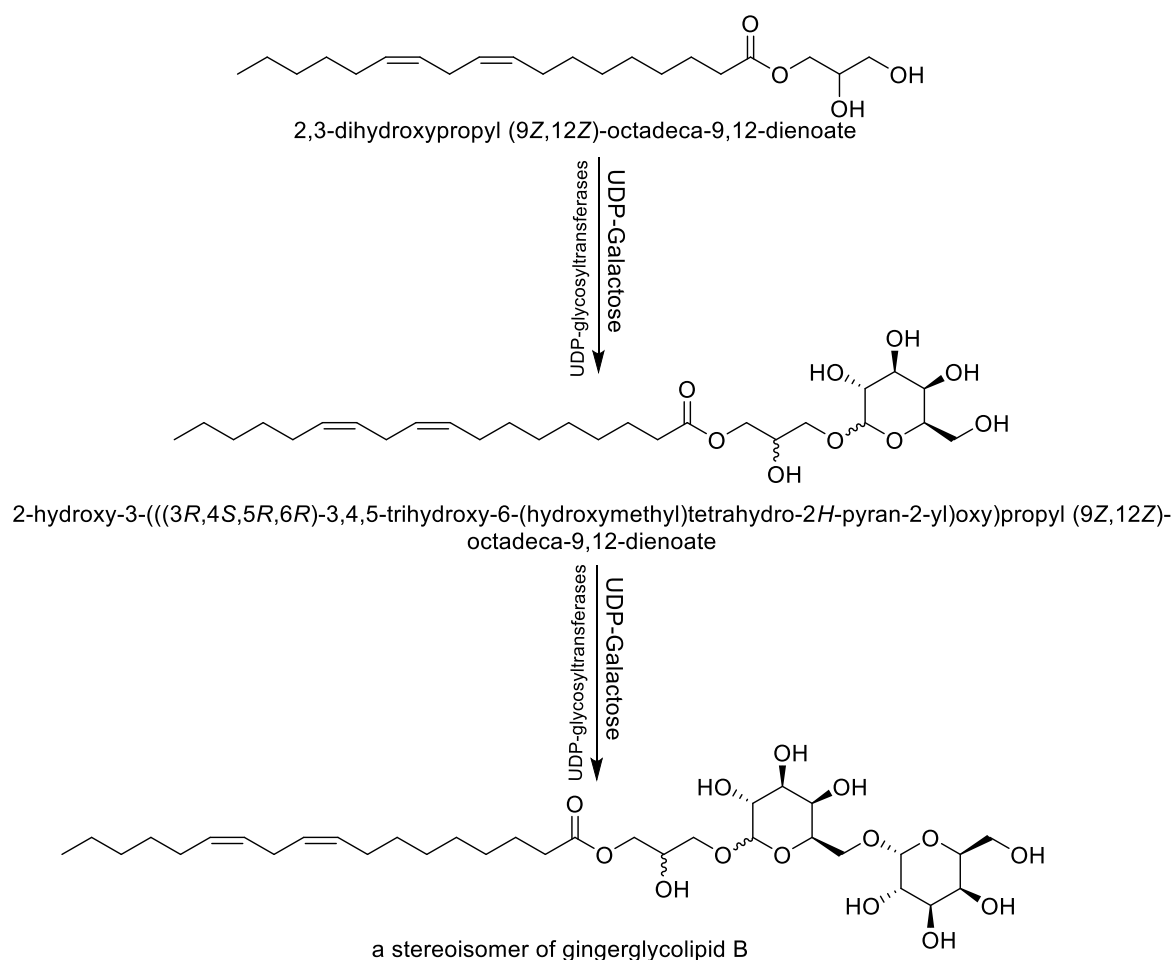


Figure 6.2-B: Proposed biosynthetic pathway of linoleic acid and its derivatives isolated from *D. salina* grown on malt extract broth and oat solid media, respectively.

6.2.3 Proposed biosynthetic pathway of turnagainolide A

Cyclic peptides are compounds composed of two or more amino acids. Cyclic peptides are formed from linear peptides in the presence of protease-like enzymes (Barber et al., 2013). Protease-like enzymes will push the interaction between the NH_2 and COOH backbone of a linear peptide (Barber et al., 2013). The proposed biosynthetic pathway of turnagainolide A involves the preliminary formation of a linear peptide composed of four amino acids (Val-Ile-Ala-Val) *via* a messenger-RNA translation. This is followed by an esterification reduction reaction with (*E*)-3-hydroxy-5-phenylpent-4-enoic acid (HPPE) between the COOH end of the valine (Val-1) of the linear backbone and the hydroxyl group at position **a**, as illustrated in Figure 6.7. Then an amide linkage is formed between the NH_2 of the second valine (Val-2) of the linear backbone with the hydroxyl group of HPPE at position **a'**. These two interactions will cause the cyclization and formation of turnagainolide A

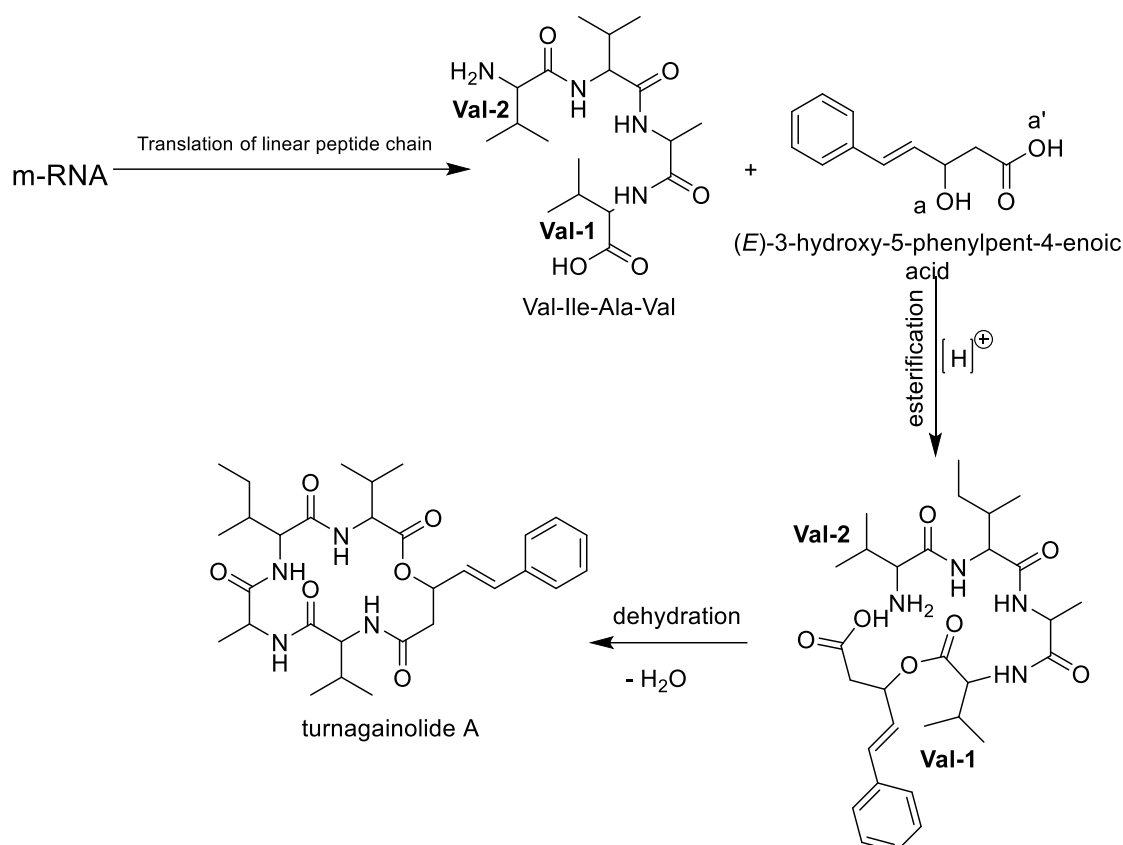


Figure 6.7: Proposed biosynthetic pathway of turnagainolide A isolated from *D. salina* grown on oat solid media.

6.3 Significance of anti-biofilm activity

Biofilms are multi-microbial communities enclosed or protected by a polymeric matrix synthesised by these microbes. The attachments of these communities can be either on a biotic or abiotic surface (Miquel et al., 2016). These bacterial communities express phenotypes with an adherent planktonic counterparts to aid the colonization of new surfaces and to overcome any exogenous stress produced by anti-infective agents (Donlan and Costerton, 2002, Macfarlane and Dillon, 2007). Such microbial communities can be either beneficial or detrimental for humans depending on the species responsible for producing these biofilms and their localization, which could be environmental, industrial or biomedical (Miquel et al., 2016). Usually, microbial communities colonising on certain environmental niches such as in a marine coastline or on the surface of a microorganism can be considered beneficial if the colonies are not damaging to the organism and its environment. While bacterial colonization on medical or industrial devices (especially those employed for the food industry) are a detrimental to human utilisation. According to the National Institute of Health, 75% of

microbial infections are caused by biofilm forming microbes. Nevertheless, some bacterial colonization that leads to biofilm formation in the in healthy people like those that occur in an intestinal microbiota have been beneficial resulting to protection and functional roles as in homeostasis (Wrzosek et al., 2013, Miquel et al., 2016). However, this beneficial colonization of a microbiota could be imbalanced in a diseased-state, which could be detrimental to an individual's health (Martín et al., 2014).

Biofilms are ubiquitous while most micro and macroorganisms like bacteria, fungi, algae, protozoa and viruses can cling on surfaces and enhance their adherence by forming biofilms (Wingender and Flemming, 2011). Biofilms produced by pathogenic bacteria like *Klebsiella pneumoniae* have been extensively and well documented especially due to their increase infections (Donlan and Costerton, 2002, Wingender and Flemming, 2011). These biofilms forming pathogenic bacteria are responsible for mild but chronic infectious diseases such as osteomyelitis, otitis media, and periodontitis, as well as in dental caries (Costerton et al., 1999). While pulmonary infections such as cystic fibrosis is also one of the more chronic cases (Miquel et al., 2016). In addition, biofilms can results in opportunistic infections in the urinary tract, lower respiratory tract, and surgical site infections and bacteraemia, and mostly when invasive medical devices are being used (Miquel et al., 2016). The main concern on infections caused by biofilm-forming bacteria are the clinically-associated complications with sessile bacterial cells that are inherently recalcitrant to antimicrobial agents (Lebeaux et al., 2014). Several factors are responsible for resistance associated with biofilm formation that include density and physiological state of the cells as well as some physical structural related issues (Miquel et al., 2016). Biofilms are exopolysaccharide and extracellular DNA matrix forming a barrier between bacterial cells and antibiotics (Miquel et al., 2016). This barrier has a various effects on antibiotic penetration (Miquel et al., 2016). Usually, the penetration of tetracyclines, rifamycins, fluoroquinolones, and daptomycin is better than those of beta-lactams, aminoglycosides, and glycopeptides (Stewart et al., 2009, Singh et al., 2010, Cha et al., 2011, Doroshenko et al., 2014). Furthermore, the micro-environment produced by the aggregation of biofilms like an acidic pH and low oxygen level can have a major effect on antibiotic activity (Siala et al., 2014). Bacterial cells within biofilms are metabolically less active than planktonic cells that antimicrobial agents targeting macromolecular synthesis, like beta-lactams and quinolones, have less activity on bacterial cells (Xie et al., 2005, Mascio et al., 2007).

Two types of antibiofilm classes namely; synthetic and natural products, have been used to overcome biofilm formation depending on the localization capacity of the biofilm.

Synthetic type of antibiofilm agents:

- 1- Non-thermal Plasma (NTP) Technology: depending on the unique state of matter of the plasma resulting from rapid ionization of gas such as nitrogen through extremely high temperatures or high-voltage electricity (Scholtz et al., 2015). NTP exert antimicrobial activity with low toxicity and absence of residual toxic compounds, which makes it a promising biofilm decontamination tool, especially for food and biological materials (Ermolaeva et al., 2015).
- 2- Photodynamic Substances: photodynamic therapy against microorganisms has three major components that includes light, an oxygen source and a photosensitizer (Miquel et al., 2016). Light excites the photosensitizer, which will cause the production of active oxygen species that will oxidise biomolecules and would lead to cell damage and death (Hamblin and Hasan, 2004).

Natural products:

Natural source is providing the world with a wide diverse bioactive compounds with diverse chemical structure. Plants and microbial source of active antibacterial compounds have been extensively studied due to the emergence of microbial resistance (Strobel, 2003, Ncube et al., 2008).

- 1- Plant products: plants are considered to be a huge source of bioactive compounds (Miquel et al., 2016). Some plants contain antibiofilm secondary metabolites with the ability to inhibit bacterial growth, interrupt quorum sensing and/or prevent bacterial adhesion (Husain et al., 2015).
- 2- Microorganism-derived biofilm inhibitors: the high competition between different microorganisms within a biofilm is affected by ecological and evolutionary parameters (Rendueles and Ghigo, 2015).

Antibiofilm compounds from marine sources.

As shown in Table 6.1, many antibiofilm compounds were isolated from marine sources and were found to be active against either biofilm-forming bacteria or fungi (Jiang et al., 2011, Sayem et al., 2011, Arai et al., 2013, Salta et al., 2013, Scopel et al., 2014, Buseti et al., 2015, Estrela and Abraham, 2016).

Table 6.1: List of active antibiofilm compounds isolated from marine environment. Structures of compounds are illustrated in Figures 6.8-A and -B

Bioactive compounds isolated from bacterial source		
Source	Compound	Reported activity on
<i>Bacillus licheniformis</i>	α -D-galactopyranosyl-(1→2)-glycerol-phosphate	<i>Escherichia coli</i> and <i>Pseudomonas fluorescens</i>
<i>Vibrio sp. QY101</i>	Exopolysaccharide A101	<i>Pseudomonas aeruginosa</i> FRD1
Bioactive compounds isolated from fungal source		
<i>Emericella varicolor</i>	ophiobolin K	<i>Mycobacterium bovis</i>
<i>Emericella varicolor</i>	6-epi-ophiobolin	<i>Mycobacterium smegmatis</i>
Unidentified fungus	mevalonolactone	<i>Staphylococcus epidermidis</i>
<i>Penicillium sp</i>	cyclo(L-Tyr-L-Leu)	<i>Staphylococcus epidermidis</i>
<i>Penicillium commune</i>	cyclo(L-Leu-L-Pro)	<i>Staphylococcus aureus</i>
<i>Cladosporium sp.</i>	cyclo-(L-Phe-L-Pro)	<i>Loktanella hongkongensis</i> , <i>Micrococcus luteus</i> and <i>Ruegeria sp.</i>
<i>Cladosporium sp.</i>	cyclo-(Val-Pro)	<i>Loktanella hongkongensis</i>
<i>Aspergillus flavipes</i>	flavipesin A	<i>Staphylococcus aureus</i> and <i>Bacillus subtilis</i>
Bioactive compounds isolated from algae source		
<i>Chondrus crispus</i>	usnic acid	<i>Cobetia marina</i> and <i>Marinobacter hydrocarbonoclasticus</i>
<i>Chondrus crispus</i>	juglone	<i>Cobetia marina</i> and <i>Marinobacter hydrocarbonoclasticu</i>

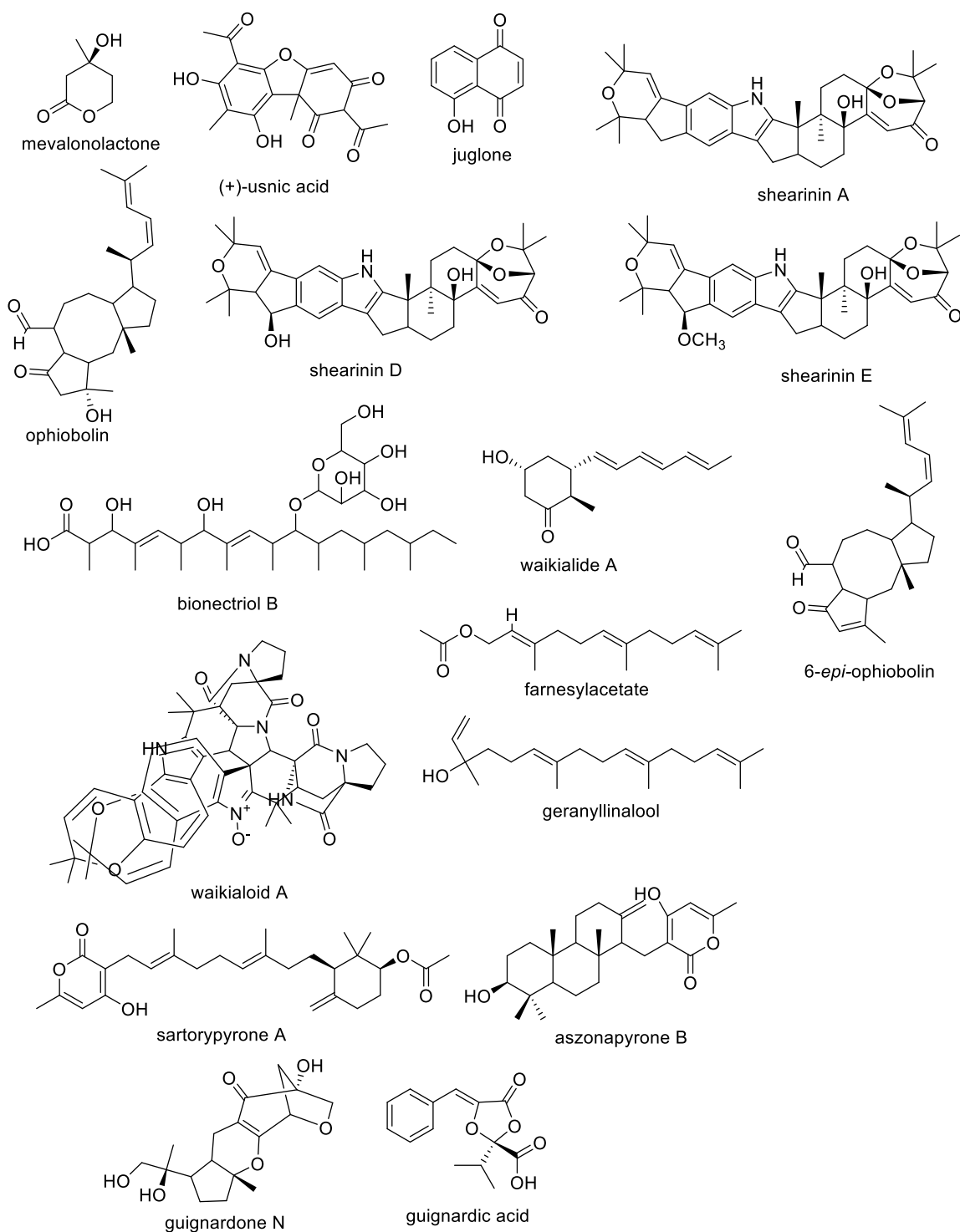


Figure 6.8A: Chemical structure of bioactive compounds isolated from marine source against biofilm-forming microbes.

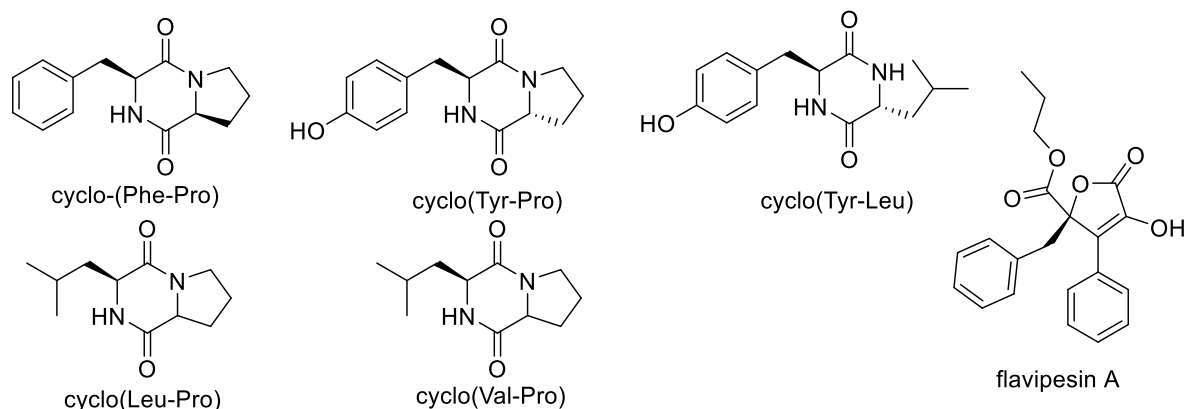


Figure 6.8-B: Chemical structures of bioactive compounds isolated from marine source against biofilm-forming microbes.

Biofilm formation in microbes is determined by their cell density and coordinated by population behaviour (Estrela and Abraham, 2016). This is controlled by small molecules (Figure 6.9) released by microbes to the environment to act as an autoinducer to start the formation of biofilm (Camilli and Bassler, 2006). Once the autoinducers reaches the threshold, microbes will start producing virulence factors for intracellular communication (Estrela and Abraham, 2016). This kind of intracellular communication used by many microbes is called quorum sensing (Schauder and Bassler, 2001). To date, more than 100 different inducers are known to be used by bacteria, archaea and fungi for quorum sensing (Estrela and Abraham, 2016).

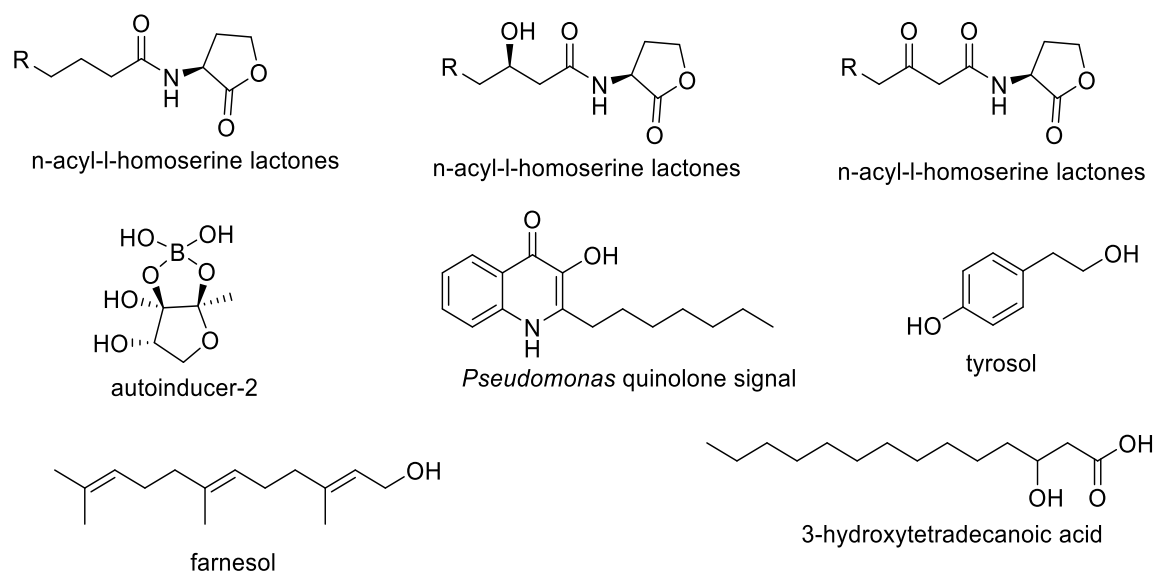


Figure 6.9: Some compounds responsible for quorum sensing in biofilm-forming microbes.

Due to the complications associated with biofilm formation by bacteria, several approaches have been developed like the search for novel antibiotics that have the ability to penetrate the biofilm layer or disrupt quorum sensing communication to enhance the penetration of antibiotics through biofilms formed by the bacteria (Zhu and Kaufmann, 2013, Worthington et al., 2014, Wright, 2014). Mevalonolactone is a simple terpene compound isolated from an unidentified endophytic fungi derived from *Mycale magnirhaphidifera* reported to show biofilm modulating activity to prevent the formation of biofilm by *S. epidermidis* (Scopel et al., 2014). Three novel sesterterpene compounds, namely; ophiobolin K, 6-*epi*- ophiobolin K and 6-*epi*- ophiobolin G isolated from the fungus *Emericella varicolor*, found to exhibit antibiofilm activity with MBEC range of 4.1 to 65 μ M against *Mycobacterium smegmatis* (*M. smegmatis*) and *M. bovis* (Arai et al., 2013). However, these three compounds did not exhibit any antimicrobial activity. Small peptides isolated from various marine fungi have also played a major role in antibiofilm activity. Examples of these small peptides are cyclo(L-Phe-L-Pro) produced by *Rosellinia necatrix* and cyclo(L-Tyr-L-Pro) produced by *Alternaria alternate*, which were found to exhibit antibiofilm activity by interfering with quorum sensing of some bacteria and inhibiting the action of acyl-homoserine lactones (Chen, 1960, Stierle et al., 1988, Ryan and Dow, 2008). Cyclo(l-Tyr-l-Leu) is another small peptide produced by an endophytic *Penicillium sp.* from *Axinella corrugata* was found to inhibit biofilm formation by *S. epidermidis* (Scopel et al., 2013). Dipeptides cyclo(l-Leu-l-Pro), cyclo-(Phe-Pro) and cyclo-(Val-Pro) that were also isolated from marine fungi were also found to be active against biofilm forming bacteria (Qi et al., 2009, Diblasi et al., 2015). Cyclo(l-Leu-l-Pro) was isolated from *Penicillium commune* and found to be antibacterial against biofilm-forming *S. aureus* (Diblasi et al., 2015). Additionally, cyclo-(Phe-Pro) and cyclo-(Val-Pro) from *Cladosporium sp.*, were also active against biofilm-forming *Loktanella hongkongensis* (Qi et al., 2009). Furthermore, cyclo-(Phe-Pro) was found to be active as an antimicrobial compound against *Micrococcus luteus* and *Ruegeria sp* (Qi et al., 2009). Flavipesin A is another antimicrobial compound produced by the endophytic *Aspergillus flavipes* from the mangrove plant *Acanthus ilicifolius* (Bai et al., 2014). Flavipesin A was able to penetrate the mature biofilms of *S. aureus* and *B. subtilis* to exert its antimicrobial activity (Bai et al., 2014). These compounds are polyhydroxylated polyketide or polyoxygenated compounds, which mainly disrupts the biofilm layer (Estrela and Abraham, 2016). Some of these compounds have both antibiofilm with antimicrobial activity, while some will only have antibiofilm activity, which indicates the need for these compounds to be used in combination with other antimicrobial compounds. Moreover, antibiofilm compounds especially; ophiobolin K, 6-*epi*- ophiobolin K and 6-*epi*-

orphibolin G, possess aliphatic chains with a small degree of unsaturation, which could be a primary part of its chemical structural system that could be required to exhibit antibiofilm activity. When comparing some of the examples of antibiofilm compounds mentioned in Figures 6.8-A and 6.8-B with those isolated from *D. salina*, there could be basic structural similarity of some compounds such as usnic acid and juglone with orsellinic acid. orcinol (F4-1A and B, respectively), and 2,5-dihydroxy-3-(hydroxymethyl)benzoic acid (F4-6 and F2-2-2). Furthermore, 1,2-acetonide-3-(9Z,12Z- octadecadienoyl)glycerol (F3-1), and glycerol-3-O-[D-galactopyranosyl-(1→6)α-D-galactopyranoside linoleate (F10-8) could be related to farnesylacetate and geranilinalool as well as a quorum sensing compound 3-hydroxytetradecanoic acid (Figure 5.9). Additionally, the bioactivity of turnagainolide A (F10-2) could be compared to dipeptides shown in Figure 6.8-B (Qi et al., 2009, Scopel et al., 2013, Diblasi et al., 2015).

Amongst these isolated antibiofilm compounds, the isolated phenolic acid compounds displayed the least potent antimicrobial activity. The predicted biological activity of these compounds could have resulted from the interference with autoinducers or compounds responsible for quorum sensing due to structural similarity (Zhu and Kaufmann, 2013, Worthington et al., 2014). This can either lead to prevent microbes to form their biofilms or disrupt the already formed biofilms.

7 General Conclusion, Future Work, and Recommendations

The primary aim of this project is to isolate antimicrobial-active metabolites against biofilm-forming bacteria from marine endophytic fungi obtained from the Scottish Ayrshire coast. This section would summarise the result chapters: 3, 4 and 5. The objective was to determine the antimicrobial activity of fungal extracts against both biofilm-forming *S. aureus* and *P. aeruginosa* via AlamarBlue® and planktonic assays. The possible bioactive discriminating metabolites were pinpointed through a metabolomics approach and the known metabolites were identified through a dereplication EXCEL MACRO coupled with the DNP database ([Macintyre et al., 2014](#)). Fungi that afforded antimicrobial-active extracts were taxonomically identified by ITS gene sequencing. These fungi included *Dendryphiella salina* (*D. salina*), *Hypoxyton rubiginosum* (*H. rubiginosum*), and *Mariannaea elegans* (*M. elegance*) and *Galactomyces candidum* (*G. candidum*). However, *G. candidum* did not produce enough extract yield and was discontinued for further scale-up and isolation work.

The three good-yielding, antimicrobial-active fungi; *D. salina*, *M. elegance*, and *H. rubiginosum*; were then further optimised on nine different media namely, malt extract (ME) broth with and without sea salt, Wickersham broth with and without sea salt and marine broth as liquid media. For solid media, rice and oat with and without sea salt were employed. According to the AlamarBlue® and planktonic assay results, in addition to the uniqueness chemical profiles of the various fungal extracts determined by multivariate analysis; *D. salina* incubated for 30 days at 27C° on malt extract with sea salt and oat media without sea salt were chosen for the scale-up experiments. Both fungal extracts inhibited bacterial growth at greater than 90%. The extract obtained from *D. salina* grown on malt extract gave an MIC of 20 and 17.5 µg/ml and MBEC of 19.7 and 16.8 µg/ml against *S. aureus* and *P. aeruginosa*, respectively. While the *D. salina* extract derived from the oat media exhibited an MIC of 17.3 and 21.1 µg/ml and MBEC of 19.7 and 19.4 µg/ml against *S. aureus* and *P. aeruginosa*, respectively. Inspection of the chemical profiles of the two fungal extract revealed that they were quite different. Dereplication study revealed that the fungal extract derived from the oat media afforded a higher concentration of non-polar compounds, included long unsaturated alkyl chains and steroids. The fungal extract obtained from the malt extract broth showed the occurrence of low MW compounds originating from the polyketide pathway.

The scaled-up crude extracts of *D. salina* were subjected to solvent partitioning with n-hexane and EtOAc to remove lipids and small fatty acids from the respective extracts. The EtOAc

extracts exhibited antimicrobial activity and were further fractionated by MPLC. The EtOAc extract derived from malt gave an average bacterial growth inhibition of 93% while the extract obtained from the oat media exhibited an average of 99% inhibition, both at a concentration of 100µg/ml.

The MPLC fractions were again assayed, and the antimicrobial-active fractions were chosen for further purification work. Outlying bioactive fractions did represent a unique chemical profile as established by multivariate analysis and were given priority for further analysis. In this case, this was Fraction-6 from the extract derived from the malt extract with an average bacterial growth inhibition of 99% at 100µg/ml and a fraction yield of 65mg. However, due to the complexity of its chemical profile in terms of the occurrence of a higher number of components, Fractions-2 and -4 with comparable potencies to Fraction-6 and with a smaller number of components were chosen for purification work. Despite this, Fraction 2 yielded the inactive linoleic acid while the target antimicrobial compound remained in the neighbouring sub-fraction. Alternatively, compounds F4-1 and F4-6, were isolated from Fraction-4. Both compounds found with a MW of 168 and 184 Da were found on the active quadrant of the OPLS-DA plot. F4-1 was identified as orsellinic acid and was amongst the top 10 VIP metabolites predicted for antimicrobial activity. Orsellinic acid was isolated as a mixture together with its close derivative orcinol. F4-6 was elucidated as 2,5-dihydroxy-3-(hydroxymethyl) benzoic acid and a congener of orsellinic acid. Nevertheless, F4-6 did not have any matching hit from the SCiFinder library database and is plausibly a new compound. Hypothetically, F4-6 could also be the oxidised congener of the target ion peak P_2626 found at m/z $[M+H]^+$ 185.080 Da (MW = 184.0736) for C₉H₁₂O₄.

On the other hand, Fraction-5 was the outlier and most active fraction from *D. salina* extract obtained from oat media. It had a relatively good yield of 94mg but the most complex chemical profile amongst the active fractions. However, due to a stroke of instrument misfortune, the sample was lost, and no further work could be achieved. Albeit windfall, isolation work was continued on active Fractions-2, -3, and -10. Fraction-10 was the highest yielding fraction and had a relatively comparable bioactivity to Fraction-5. Five compounds; F2-2-2, F3-1, F3-3, F10-2 and F10-8; were isolated from *D. salina* grown on oat media without sea salts. F2-2-2 was identical to F4-6. Despite the difference in chemical profiles between the two fungal extracts, it seems that there was still the incidence of a common metabolite in the two extracts. F3-1, F3-3, and F10-8 were elucidated as glyceryl linoleate derivatives; 1,2-acetonide-3-(9,12-octadecadienoyl)glycerol, 1-O-(9Z,12Z-octadecadienoyl)glycerol, and glycerol-3-O-[D-

galactopyranosyl-(1→6) α -D-galactopyranoside] linoleate, respectively. *D. salina* seems to upregulate the further derivatisation of linoleic acid when incubated in the oat media without sea salt, which was alternatively downregulated when the fungus was grown in malt extract with sea salt. F3-1 along with F2-1 (linoleic acid) were both found in the inactive quadrants of the OPLS-DA plots. F10-8 was identified as a new stereoisomer of gingerglycolipid B. F10-2 was elucidated as the antimicrobial turnagainolide A, earlier described from marine-derived *Bacillus* and encoded from a silent biosynthetic gene of a marine sediment-derived fungus *Microascus* ([Vervoort et al., 2011](#)).

MIC and MBEC were determined for all the isolated compounds. F10-2 (turnagainolide A) and F10-8 (gingerglycolipid B stereoisomer) displayed the highest antimicrobial activity against both biofilm-forming *S. aureus* and *P. aeruginosa* with MIC and MBEC values between 45 and 75 μ M concentrations. F2-1 and F3-3, which were identified as linoleic acid and its glycerol congener were both rendered inactive with MIC and MBEC values of greater than 100 μ g/ml. Moreover, it is noteworthy mentioning in line with structure-activity relationships of the isolated linoleate congeners, the glycolipid F10-8 was the most active while the acetone congener F3-1 was less active with MIC and MBEC values between 75 and 145 μ M concentrations. On the other hand, the isolated phenolic compounds were less active with MIC and MBEC values between 145 and 360 μ M concentrations.

Due to the Covid-19 situation and the national lockdown associated with the pandemic, it was not possible to perform further physical analytical experiments that need to be done outside of the institute. Because of travel limitation and Covid-19 rules, this prevented the submission of samples to another institution for further analysis. This includes the measurement of optical rotation for the isolated glyceryl linoleate derivatives. F10-8 was elucidated as a stereoisomer of gingerglycolipid B with a different stereochemistry at the glycerol unit, so further derivatisation experiment will be needed for this compound as well.

My future work will be based on the following six further research questions hypothetically based on evidence from my current PhD work, which I would like to develop for innovative applications that could be corroborated to my scientific career plans in my country. Part of this future work would involve collaboration with my PhD supervisors working on Scottish Seaweeds, which would as well require signing a Material Transfer Agreement to continue part of the work in my home University in Jordan. In parallel to this, I would be establishing my research laboratory in Jordan using resources from my home country.

First question: Would scaling-up the endophytic fungi, *M. elegance* and *H. rubiginosum*, on malt extract without sea salt and rice solid media without sea salt, respectively, going to yield novel bioactive compounds against biofilm-forming *S. aureus* and *P. aeruginosa*?

M. elegance and *H. rubiginosum* will be grown in a suitable media according to the media optimisation results done in this study (Chapter 4). Extract obtained from *M. elegance* grown on malt extract media would be fractionated and the antimicrobial compounds would be targeted by employing a metabolomics approach. The antimicrobial compounds will be elucidated using LC-HRMS and NMR that could be assisted by GC-MS if needed and optical rotation to decide on the stereochemistry in the occurrence of chiral centres. *H. rubiginosum* will be scaled up, subjected to fractionation, and bioactive compounds elucidated in the same manner as *M. elegance*. This should take from 4 to 6 months depending on the availability of the instruments and the complexity of the crude extract. The reason of starting with *M. elegance* is the simplicity of the chemical profile of crude extract as determined during the media optimisation stage, which resulted in two major compounds and few minor compounds to target. In contrast, *H. rubiginosum* extract showed a more complex chemical profile, which indicated the need for more time to undergo more steps in chromatographic fractionation and purification.

All compounds will be tested against the methicillin sensitive and biofilm forming *S. aureus* and *P. aeruginosa* to calculate the MIC and MBEC of the isolated compounds. The structures of the isolated compounds from *D. salina*, *M. elegance* and *H. rubiginosum* extracts will be correlated with the possible mechanism of action for their antimicrobial and/or antibiofilm activity. The biological activity of these compounds will take between 2 to 4 months depending on the availability of the bacteria, materials like media and colouring reagents (AlamarBlue®) and instruments (plate readers and incubators).

Second question: Would the isolated compounds from the algal endophytic fungi, *D. salina*, *M. elegance*, and *H. rubiginosum* safe to use to obtain the desired biological activity *in vivo*?

Different concentrations of the isolated antimicrobial-active compounds would be tested on normal cell lines. The concentration range would be paralleled to the antimicrobial activity based on their MIC and MBEC values. Toxic concentrations will be calculated to determine the safety of the compounds *in vitro*. An *in vivo* bioassay for the isolated compounds could be done in Jordan using mice infected with biofilm-forming bacteria. The toxicity experiments will take between 6 to 10 months to accomplish.

Third question: Could *D. salina*, *M. elegance*, and *H. rubiginosum* be subjected to a biotechnological industrial scale-up to target the production of the isolated antimicrobial compounds from my PhD work as potential new drugs?

Industrial scale-up is done in a huge 500 to 50000L fermentation tanks made of double stainless-steel jacket. These stainless-steel jackets could corrode in the presence of sea salt. Thus, scale-up that employs sea salt-containing media will be high risk, which will have a direct effect on the running cost of the scale-up. *D. salina*, *M. elegance* and *H. rubiginosum* could only be industrially scaled-up in the absence of sea salt. Albeit, *D. salina* yielded more compounds when grown in malt extract media with sea salt, *D. salina* cannot be industrially scaled-up in this media.

A pilot industrial scale-up of 500L will be subjected to the same procedure of metabolomics-guided fractionation and purification. Chromatographic fractionation will be done at a larger scale with a larger silica column and a rational flowrate should be used to mimic the fractionation procedure performed in the lab previously. However, at an industrial scale, the use of larger volumes of organic is not recommendable. New chromatographic method must be developed such as the employment of Sequential Simulated Moving Resin Beds that are passed through lower volumes of solvent (<https://www.novasep.com/technologies/chromatography-for-large-scale-bio-industrial-applications.html>) or the use of supercritical fluid chromatography (([Schmidtsdorff et al., 2021](#))). As a quality control protocol to confirm the production of the targeted antimicrobial compounds, aliquots of extracts and fractions will be assayed against methicillin-sensitive biofilm-forming *S. aureus* and *P. aeruginosa* along with a standardised LCMS SOP.

The industrial scale-up of the production of isolated compounds should take 2 to 3 years. I or we will need to collaborate with institutes with biotechnological and chemical process engineering expertise. In addition, a collaboration with a biotechnological company in Scotland like Ingenza (<https://www.ingenza.com/>), who are known to work with academics for technological transfer and translation will be necessary. The latter collaboration will make it possible to arrange the scale-up work on pilot industrial fermenters reservation. However, such arrangements with companies will take a lot of preparation experiments that must avoid time waste for an industrial partner because for companies “times mean money”. Such pilot fermentation work could only be booked with the company for not more than three months. Background experiments will need to be done in consultation with the industrial partner. The industrial scale-up of the production of these compounds from Scottish algal endophytic fungi

will be a future project by itself and would be done in collaboration with the country of origin that is the UK in due process of the Nagoya Protocol and the United Nations Convention on the Law of the Sea (UNCLOS).

Fourth question: Could the isolated compounds from algal endophytic fungi, such as *D. salina*, *M. elegance* and *H. rubiginosum*, be alternatively scaled-up by chemical synthesis using green chemistry that would be less expensive but must be ecologically friendly?

F3-1 (1,2-acetonide-3-(9,12-octadecadienoyl)glycerol and F10-8 (gingerglycolipid B stereoisomer) are two derivatives of linoleic acid. F3-1 is already known to be chemically synthesised. However, the challenge lies on the synthesis of the compound with a similar stereochemistry to that biosynthetically afforded by *D. salina*. While chemical synthesis of such chiral compounds could yield an end product of mixed stereoisomers, considerations must be accounted for a stereoselective pathway. Otherwise, stereoisomeric mixtures could also be purified by employing chiral columns, which however, would be quite expensive for a future scale-up work and may not be economically sustainable or feasible at all.

Compound F10-8, on the other hand, entails 9 chiral centres. Thus, synthesising compound F10-8 will be more difficult and this will depend on the availability of the galactose with a similar stereocentre. Finally, for compound 10-2 (turnagainolides A), there is no reports about its chemical synthesis while many peptide derivatives, even larger ones, are already known to be scale-up by chemical synthesis. Such examples include ziconotide, an N-type calcium channel antagonist, which is now used to treat chronic pain. Ziconotide, derived from the conotoxin of *Conus magus*, with a MW of 2639 Da has 25 amino acids in its structure and is commercially produced solely by total synthesis. This indicates the possibility for turnagainolide A to be chemically synthesised as well, which could be less expensive than a biotechnological method or fermentation.

As in the case of *M. elegance*, dereplication of its LC-HRMS data gave two peptides with MWs greater than 800 Da as its major compounds. Again, the chemical synthesis of these peptides simply depend on the commercial availability of suitable amino acids as starting material while the synthetic pathway will follow a standard protocol for peptide synthesis.

In contrast, the chemical profile of *H. rubiginosum* extract is highly diverse which means the economical success of chemical synthesis of its secondary metabolites or natural products largely depend on the complexity of the stereochemistry of the structures of the targeted antimicrobial compounds. Designing and accomplishing a synthetic pathway module could

take a period between 1 to 2 years depending more on the diversity and complexity of the compounds. This will be done in collaboration with a medicinal chemistry lab and/or a CBBD (Computer-Based Drug Discovery) group.

Fifth question: Could the targeted antimicrobial compounds from the endophytic fungi, *D. salina*, *M. elegance*, and *H. rubiginosum* be formulated to improve their biological activity through optimum bioavailability and efficacy?

Formulation of the compounds depend on their location on the Biopharmaceutics Classification System (BCS), which is categorised according to a compound's solubility and permeability. Formulation design would be achieved around the different solubility and diffusibility of the isolated compound using various simulated media and membrane to mimic and simulate human physiological condition. In addition, intrinsic solubility of the isolated compounds can be measured to have an idea about the behaviour of the compounds when dissolved in water. For the more lipophilic linoleate compounds of *D. salina*, which would have good permeability but poor water solubility, could be formulated in liposomes to improve the compounds' solubility prior to their absorption. In contrast, hydrophilic phenolic compounds, such as orsellinic acid and its congeners that are more water soluble, their drug formulations should be determined by their permeability properties. Similarly, antimicrobial compounds afforded from *M. elegance* and *H. rubiginosum*, will be subject to solubility and permeability studies to design the best formulation to achieve their optimum bioavailability.

Biopharmaceutical studies will take from 6 to 12 months, which will be accomplished in collaboration with research groups from Pharmaceutical Technology institutes with expertise in Drug Delivery, like those led by Professors Y. Perrie and A. Mullen at Strathclyde University.

Sixth question: Could endophytic fungi derived from Scottish seaweeds afford compounds with anticancer and antidiabetic activity?

Cancer and diabetes are the leading cause of death in Jordan. According to the Ministry of Health (MOH) report in 2009¹, more than one third of the deaths in Jordan are caused by cancer illness with 14.6% while macro and micro complications associated with diabetes is 13.1%. According to the Cancer Incidence in Jordan-2014 report, number of registered cancer cases in

¹ Ministry of Health Annual Statistical Book., 2011, Amman. Hashemite Kingdom of Jordan: Ministry of Health

Jordan from 2004 to 2014 has increased from 3591 to 5695 cases. This indicates an increase of 2004 cases in 10 years period. While the number of diabetes mellitus type two cases in Jordan in 2020 is 702,326 with 36,941 new cases between 2019 and 2020 ([Awad et al., 2020](#)). Thus, all these data urged the importance of finding a new promising pipeline of anticancer and antidiabetic active compounds with higher potential to be produced commercially.

Stored fungal vouchers under glycerol in liquid nitrogen will be reinoculated in various media. The resulting fungal extracts will be tested for anticancer activity against various cancer cell lines by employing 2,2-diphenyl-1-picrylhydrazyl (DPPH), and AlamarBlue® assays. In addition, α -amylase assay will be utilised to test for antidiabetic activity. Although chemical profiles of these algal endophytic fungi have already been recorded during my PhD study, chemical analysis using NMR and LC-HRMS must be done on the fungal extracts to quality control the stability of the chemical profiles afforded by the endophytes after long cold storage. Like what has been earlier established in my PhD research study, media optimisation and chromatographic isolation procedures will be guided *via* a metabolomics approach on collected spectral data of the extracts and fractions to target the bioactive compounds. Fungi yielding the most potent bioactive extracts will be scaled-up to isolate the anticancer and antidiabetic compounds for structure elucidation and further EC₅₀ determination. *In vivo* animal and/or zebra fish assays would be performed for efficacy and cytotoxicity studies, which could be done in collaboration with the group of Professor T. Henry of Heriot Watt University.

To date, mass spectrometry has advanced to detect compounds at nanogram-level concentration and multivariate analysis was able to pick out these compounds as discriminatory features even at their nanogram concentrations ([Gowda and Djukovic, 2014](#)). Such low-yielding features could be used to explore and encode “silent” biosynthetic gene information that could be exploited to increase the yield of these bioactive target metabolites ([Harvey et al., 2015](#)).

The richness of the natural ecosystem has a major contribution on the diversity of natural products, which has evolved today’s drug discovery approach. Albeit the occurrence of a wide broad range of natural resources affording new natural products, their production of biologically and pharmacologically active compounds with unique mode of action is still being underestimated ([Brakhage et al., 2011](#), [Newman and Cragg, 2012](#)). However, the diversity of bioactive compounds will bring its own challenges like when replacing the biosynthetic source organism of these potentially bioactive compounds with other host producers ([Reen et al., 2015](#)). Thus, providing a closed system production pipeline, isolation of secondary metabolites

from living organisms need a full and detailed understanding of the organism's physiological and environmental features ([Reen et al., 2015](#)). The occurrence of biosynthetic gene clusters (BGCs) provides organisms the capacity to synthesise and yield small molecules within discrete localized sections of the microbial genome ([Reen et al., 2015](#)). BGCs consist of repeating units or molecules controlling the biosynthesis of the final chemical structure of a secondary metabolite ([Reen et al., 2015](#)). The chemical diversity of natural products would result from the variation in number and order of these units incorporated to a certain molecular structure ([Berti et al., 2007](#)). Despite the advances in culturing technologies of these various producer organisms, the number of biosynthetic genes in many organisms still greatly outnumbers the known metabolites already described from these respective organisms ([Berti et al., 2007](#)) indicating the existence of unexpressed "silent genes". The development of innovative approaches to stimulate the production of unknown or novel secondary metabolites from these cryptic systems of "silent genes" is currently the key challenge ([Reen et al., 2015](#)). Endophytic fungi like *D. salina*, *M. elegance*, and *H. rubiginosum* could be subjected to different cultivational approaches like OSMAC (One Strain Many Compounds), environmental cues and co-cultivation or molecular approaches like ribosome engineering, activator awakeners or elicitors, deleting suppressors and artificial promoters to activate such silent genes to increase the production of a targeted compounds and/or increase the chemical diversity of bioactive compounds as presented in Figure 7.1. This will need intensive collaboration with groups working with molecular biology and gene clustering to improve the identification of the silent genes and activate them by a suitable approach. This would envisage collaborative work with Professor A Dobson (Cork University in Ireland) and/or the Alberti Lab at the University of Warwick who works with the biosynthesis of terpenoid natural products from fungi. I would aim to get a postdoc position in such research teams to learn new skills and aspects of drug discovery.

In parallel, my home country Jordan has the deepest point on earth which is the Dead Sea. This place is a protected marine environment with high concentration of salts. The studies on the Dead Sea microorganisms are very limited especially regarding the chemical profile of these species. Thus, due to the high salinity of the Dead Sea, its environment is a very promising source of novel microorganisms that would be potential producers of unique secondary metabolites. The ecological system of the Dead Sea will cause stress on its thriving microorganisms, which could lead to genetical changes to adapt to its challenging environment and cause the possible production of unique secondary metabolites.

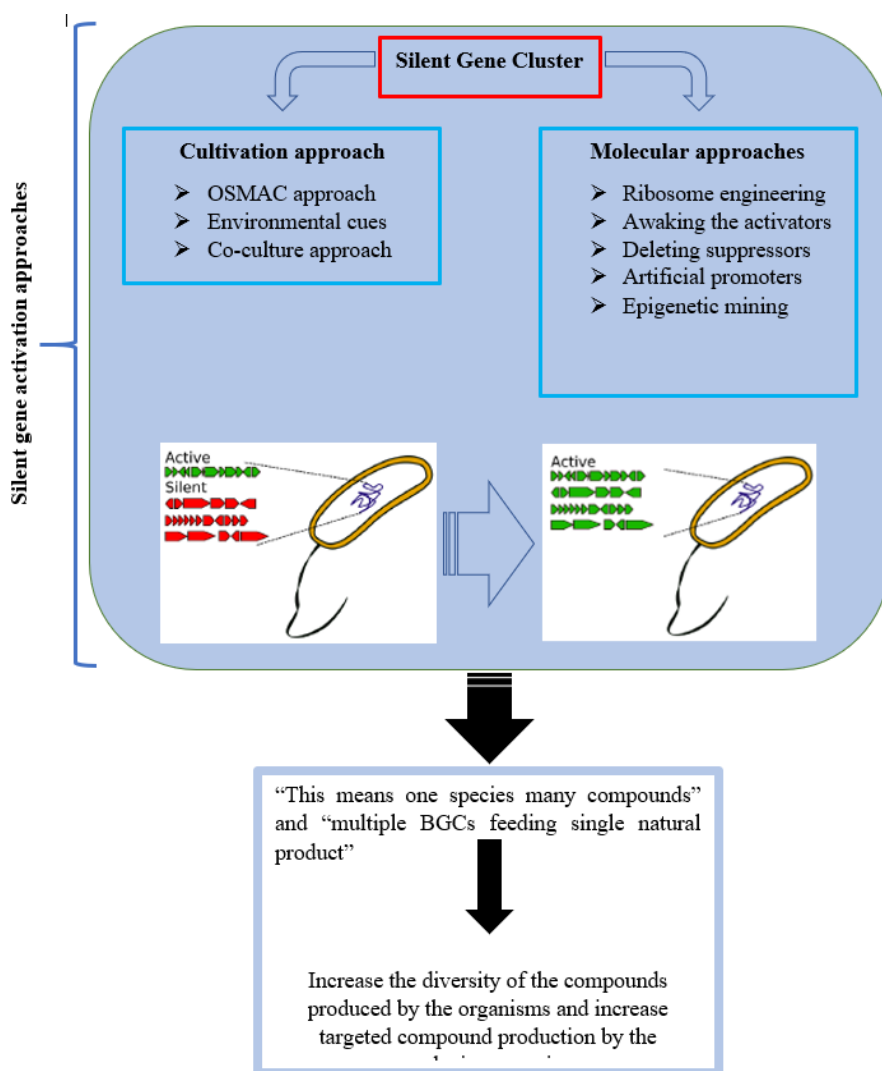


Figure 7.1: Schematic diagram representing the integration of molecular and cultivational approaches on silent gene cluster to increase the biodiversity and the yield of the produced compounds (Reen et al., 2015).

8 References

- ABAGYAN, R., TOTROV, M. & KUZNETSOV, D. 1994. Icm—a new method for protein modeling and design: Applications to docking and structure prediction from the distorted native conformation. *J Comput Chem*, 15, 488-506.
- ABDEL-LATEFF, A., FISCH, K. M., WRIGHT, A. D. & KONIG, G. M. 2003. A new antioxidant isobenzofuranone derivative from the algicolous marine fungus *epicoccum* sp. *Planta Med*, 69, 831-834.
- ABDELMOHSEN, U. R., CHENG, C., VIEGELMANN, C., ZHANG, T., GRKOVIC, T., AHMED, S., QUINN, R. J., HENTSCHEL, U. & EDRADA-EBEL, R. 2014. Dereplication strategies for targeted isolation of new antitypanosomal actinosporins a and b from a marine sponge associated-actinokineospora sp. Eg49. *Mar Drugs*, 12, 1220-1244.
- ABDELMOHSEN, U. R., GRKOVIC, T., BALASUBRAMANIAN, S., KAMEL, M. S., QUINN, R. J. & HENTSCHEL, U. 2015. Elicitation of secondary metabolism in actinomycetes. *Biotechnol Adv*, 33, 798-811.
- ABE, N., YAMAMOTO, K. & HIROTA, A. 2000. Novel fungal metabolites, demethylsorbicillin and oxosorbicillinol, isolated from *trichoderma* sp. Usf-2690. *Biosci Biotechnol Biochem*, 64, 620-622.
- AGRANOFF, B. W., DAVIES, J., HAHN, F. E., MANDEL, H. G., SCOTT, N. S., SMILLIE, R. M. & WOESE, C. R. 1969. *Progress in molecular and subcellular biology*, Berlin, Springer-Verlag
- AKPINAR-BAYIZIT, A. 2014. Fungal lipids: The biochemistry of lipid accumulation. *International Journal of Chemical Engineering and Applications*, 5, 409-414.
- ALI, K., IQBAL, M., YULIANA, N. D., LEE, Y.-J., PARK, S., HAN, S., LEE, J.-W., LEE, H.-S., VERPOORTE, R. & CHOI, Y. H. 2013. Identification of bioactive metabolites against adenosine a1 receptor using nmr-based metabolomics. *Metabolomics*, 9, 778-785.
- ALI, M. S., SALEEM, M., AHMAD, V. U. & SHAMEEL, S. 2001. Phytol and glycerol derivatives from the marine green alga *codium iyengarii* of the karachi coast (arabian sea). *Zeitschrift für Naturforschung B*, 56, 837-841.
- ALLEN, V., POND, K., SAKER, K., FONTENOT, J., BAGLEY, C., IVY, R., EVANS, R., SCHMIDT, R., FIKE, J. & ZHANG, X. 2001. Tasco: Influence of a brown seaweed on antioxidants in forages and livestock—a review. *Journal of Animal Science*, 79, E21-E31.
- ALMEIDA, C., EGUEREVA, E., KEHRAUS, S., SIERING, C. & KONIG, G. M. 2010. Hydroxylated sclerosporin derivatives from the marine-derived fungus *cadophora malorum*. *J Nat Prod*, 73, 476-478.
- ALTMANN, K.-H. 2017. Drugs from the oceans: Marine natural products as leads for drug discovery. *J CHIMIA* 71, 646-652.
- ALVIN, A., MILLER, K. I. & NEILAN, B. A. 2014. Exploring the potential of endophytes from medicinal plants as sources of antimycobacterial compounds. *Microbiol Res*, 169, 483-495.
- ARAI, M., NIKAWA, H. & KOBAYASHI, M. 2013. Marine-derived fungal sesterterpenes, ophiobolins, inhibit biofilm formation of mycobacterium species. *J Nat Med*, 67, 271-275.
- ARUNPANICHLERT, J., RUKACHAISIRIKUL, V., SUKPODMA, Y., PHONGPAICHT, S., TEWTRAKUL, S., RUNGJINDAMAI, N. & SAKAYAROJ, J. 2010. Azaphilone and isocoumarin derivatives from the endophytic fungus *penicillium sclerotiorum* psu-a13. *Chem Pharm Bull* 58, 1033-1036.
- AWAD, S. F., HUANGFU, P., DARGHAM, S. R., AJLOUNI, K., BATIEHA, A., KHADER, Y. S., CRITCHLEY, J. A. & ABU-RADDAD, L. J. 2020. Characterizing the type 2 diabetes mellitus epidemic in Jordan up to 2050. *Sci Rep*, 10, 21001.
- BACON, C. W. & WHITE, J. 2000. *Microbial endophytes*, New York, Marcel Dekker, Inc.
- BAI, Z. Q., LIN, X., WANG, Y., WANG, J., ZHOU, X., YANG, B., LIU, J., YANG, X., WANG, Y. & LIU, Y. 2014. New phenyl derivatives from endophytic fungus *aspergillus flavipes* ail8 derived of mangrove plant *acanthus ilicifolius*. *Fitoterapia*, 95, 194-202.
- BAJPAI, V. K. 2016. Antimicrobial secondary metabolites from marine fungi: A mini review. *Indian J Geo-Mar Sci*, 45, 1067-1075.

- BARBER, C. J., PUJARA, P. T., REED, D. W., CHIWOCHA, S., ZHANG, H. & COVELLO, P. S. 2013. The two-step biosynthesis of cyclic peptides from linear precursors in a member of the plant family caryophyllaceae involves cyclization by a serine protease-like enzyme. *J Biol Chem*, 288, 12500-12510.
- BARRY, C. E., 3RD & BLANCHARD, J. S. 2010. The chemical biology of new drugs in the development for tuberculosis. *Curr Opin Chem Biol*, 14, 456-466.
- BASHYAL, B. P., WIJERATNE, E. K., FAETH, S. H. & GUNATILAKA, A. L. 2005. Globosumones a– c, cytotoxic orsellinic acid esters from the sonoran desert endophytic fungus *chaetomium globosum*. *J Nat Prod*, 68, 724-728.
- BECCUTI, G., MONAGHEDDU, C., EVANGELISTA, A., CICCONE, G., BROGLIO, F., SOLDATI, L. & BO, S. 2017. Timing of food intake: Sounding the alarm about metabolic impairments? A systematic review. *J Pharmacol Res*, 125, 132-141.
- BERGMANN, W. & BURKE, D. C. 1955. Contributions to the study of marine products. Xxxix. The nucleosides of sponges. Iii. 1 spongothymidine and spongouridine2. *J Org Chem*, 20, 1501-1507.
- BERTI, A. D., GREVE, N. J., CHRISTENSEN, Q. H. & THOMAS, M. G. 2007. Identification of a biosynthetic gene cluster and the six associated lipopeptides involved in swarming motility of *pseudomonas syringae* pv. Tomato dc3000. *J Bacteriol*, 189, 6312-6323.
- BHADURY, P. & WRIGHT, P. C. 2004. Exploitation of marine algae: Biogenic compounds for potential antifouling applications. *Planta*, 219, 561-578.
- BHATTACHARYYA, P. & JHA, D. 2011. Optimization of cultural conditions affecting growth and improved bioactive metabolite production by a subsurface aspergillus strain tsf 146. *Int J Appl Biol Pharm Technol*, 2, 133-143.
- BOCHNER, B. R. 2009. Global phenotypic characterization of bacteria. *FEMS Microbiol Rev*, 33, 191-205.
- BRADING, J. W., GEORG-PLANT, M. M. & HARDY, D. M. 1954. The polysaccharide from the alga *ulva lactuca*. Purification, hydrolysis, and methylation of the polysaccharide. *J Chem Soc*, 319-324.
- BRAKHAGE, A. A., SCHROECKH, V. & BIOLOGY 2011. Fungal secondary metabolites—strategies to activate silent gene clusters. *Fungal Genetics*, 48, 15-22.
- BRAMHACHARI, P., ANJU, S., SHEELA, G. M., KOMARAIHAH, T. R., VENKATAIAH, P. & PRATHYUSHA, A. 2019. Secondary metabolites from marine endophytic fungi: Emphasis on recent advances in natural product research. *Adv Endophytic Fungal Res*, 339-350.
- BROADBENT, D., MABELIS, R. P. & SPENCER, H. 1975. 3, 6, 8-trihydroxy-1-methylxanthone--an antibacterial metabolite from *penicillium patulum*. *Phytochem Rev*.
- BUBB, W. A. 2003. Nmr spectroscopy in the study of carbohydrates: Characterizing the structural complexity. *Concepts Magn Res A: An Educational Journal*, 19, 1-19.
- BUCHANAN, M., HASHIMOTO, T., YASUDA, A., TAKAOKA, S., KAN, Y. & ASAKAWA, Y. 37th symposium on the chemistry of natural products. 1995. Symposium Papers Tokushima, Japan.
- BUEDENBENDER, L., ASTONE, F. A. & TASDEMIR, D. 2020. Bioactive molecular networking for mapping the antimicrobial constituents of the baltic brown alga *fucus vesiculosus*. *Mar Drugs*, 18, 311.
- BUGNI, T. S. & IRELAND, C. M. 2004. Marine-derived fungi: A chemically and biologically diverse group of microorganisms. *Nat Prod Rep*, 21, 143-163.
- BUSETTI, A., THOMPSON, T. P., TEGAZZINI, D., MEGAW, J., MAGGS, C. A. & GILMORE, B. F. 2015. Antibiofilm activity of the brown alga *halidrys siliquosa* against clinically relevant human pathogens. *Mar Drugs*, 13, 3581-3605.
- BUTLER, M. S. 2008. Natural products to drugs: Natural product-derived compounds in clinical trials. *Nat Prod Rep*, 25, 475-516.
- BYLESJÖ, M., RANTALAINEN, M., CLOAREC, O., NICHOLSON, J. K., HOLMES, E. & TRYGG, J. 2006. Opls discriminant analysis: Combining the strengths of pls-da and simca classification. *Journal of Chemometrics: A Journal of the Chemometrics Society*, 20, 341-351.
- CAMILLI, A. & BASSLER, B. L. 2006. Bacterial small-molecule signaling pathways. *Science*, 311, 1113-1116.

- CATARINO, M. D., SILVA, A. M. S. & CARDOSO, S. M. 2017. Fucaceae: A source of bioactive phlorotannins. *Int J Mol Sci*, 18, 1327.
- CERTIK, M. & SHIMIZU, S. 1999. Biosynthesis and regulation of microbial polyunsaturated fatty acid production. *J Biosci Bioeng*, 87, 1-14.
- CHA, J. O., PARK, Y. K., LEE, Y. S. & CHUNG, G. T. 2011. In vitro biofilm formation and bactericidal activities of methicillin-resistant staphylococcus aureus clones prevalent in korea. *Diagn Microbiol Infect Dis*, 70, 112-118.
- CHANG, M. C. & KEASLING, J. D. 2006. Production of isoprenoid pharmaceuticals by engineered microbes. *Nature Chem Biol*, 2, 674-681.
- CHATZIKONSTANTINOOU, A. V., CHATZIATHANASIADOU, M. V., RAVERA, E., FRAGAI, M., PARIGI, G., GEROTHANASSIS, I. P., LUCHINAT, C., STAMATIS, H. & TZAKOS, A. G. 2018. Enriching the biological space of natural products and charting drug metabolites, through real time biotransformation monitoring: The nmr tube bioreactor. *Biochim Biophys Acta Gen Subj*, 1862, 1-8.
- CHEN, J., LI, W., YAO, H. & XU, J. 2015. Insights into drug discovery from natural products through structural modification. *Fitoterapia*, 103, 231-241.
- CHEN, S., JIANG, H., WU, X. & FANG, J. 2016. Therapeutic effects of quercetin on inflammation, obesity, and type 2 diabetes. *Mediators Inflamm*, 2016, 9340637.
- CHEN, Y.-S. 1960. Studies on the metabolic products of *rosellinia necatrix berlese*: Part i. Isolation and characterization of several physiologically active neutral substances. *J Agri Chem Soc Japan*, 24, 372-381.
- CHEN, Y., DE BRUYN KOPS, C. & KIRCHMAIR, J. 2017. Data resources for the computer-guided discovery of bioactive natural products. *J Chem Inf Model*, 57, 2099-2111.
- CHOOI, Y. H., STALKER, D. M., DAVIS, M. A., FUJII, I., ELIX, J. A., LOUWHOFF, S. H. & LAWRIE, A. C. 2008. Cloning and sequence characterization of a non-reducing polyketide synthase gene from the lichen *xanthoparmelia semiviridis*. *Mycol Res*, 112, 147-161.
- CHU, M. J., TANG, X. L., QIN, G. F., SUN, Y. T., LI, L., DE VOOGD, N. J., LI, P. L. & LI, G. Q. 2017. Pyrrole derivatives and diterpene alkaloids from the south china sea sponge *agelas nakamura*. *Chem Biodivers*, 14, e1600446.
- CLIPSON, N. & JENNINGS, D. 1992. *Dendryphiella salina* and *debaryomyces hansenii*: Models for ecophysical adaptation to salinity by fungi that grow in the sea. *Can J Botany*, 70, 2097-2105.
- COSTELLO, M. J., BOUCHET, P., BOXSHALL, G., FAUCHALD, K., GORDON, D., HOEKSEMA, B. W., POORE, G. C., VAN SOEST, R. W., STÖHR, S. & WALTER, T. C. 2013. Global coordination and standardisation in marine biodiversity through the world register of marine species (worms) and related databases. *PloS One*, 8, e51629.
- COSTERTON, J. W., STEWART, P. S. & GREENBERG, E. P. 1999. Bacterial biofilms: A common cause of persistent infections. *Science*, 284, 1318-1322.
- COVINGTON, B. C., MCLEAN, J. A. & BACHMANN, B. O. 2017. Comparative mass spectrometry-based metabolomics strategies for the investigation of microbial secondary metabolites. *Nat Prod Rep*, 34, 6-24.
- CRAGG, G. M. & NEWMAN, D. 2005a. Plants as a source of anti-cancer agents. *J Ethnopharmacol*, 100, 72-79.
- CRAGG, G. M. & NEWMAN, D. J. 2005b. Biodiversity: A continuing source of novel drug leads. *Pure Appl Chem*, 77, 7-24.
- CRAGG, G. M., NEWMAN, D. J. & WEISS, R. B. Coral reefs, forests, and thermal vents: The worldwide exploration of nature for novel antitumor agents. *Seminars in Oncology*, 1997. 156-163.
- CRAIGIE, J. S., MCINNES, A. G., RAGAN, M. A. & WALTER, J. A. 1977. Chemical constituents of the physodes of brown algae. Characterization by ¹h and ¹³c nuclear magnetic resonance spectroscopy of oligomers of phloroglucinol from *fucus vesiculosus* (L.). *Can J Chem*, 55, 1575-1582.
- CREEMERS, G. J., BOLIS, G., GORE, M., SCARFONE, G., LACAVE, A. J., GUASTALLA, J. P., DESPAX, R., FAVALLI, G., KREINBERG, R., VAN BELLE, S., HUDSON, I., VERWEIJ, J. & TEN BOKKEL HUININK,

- W. W. 1996. Topotecan, an active drug in the second-line treatment of epithelial ovarian cancer: Results of a large european phase ii study. *J Clin Oncol*, 14, 3056-3061.
- DA ROCHA, A. B., LOPES, R. M. & SCHWARTSMANN, G. 2001. Natural products in anticancer therapy. *Curr Opin Pharmacol*, 1, 364-369.
- DEBBAB, A., ALY, A. H., LIN, W. H. & PROKSCH, P. 2010. Bioactive compounds from marine bacteria and fungi. *Microb Biotechnol*, 3, 544-563.
- DEBBAB, A., ALY, A. H. & PROKSCH, P. 2011. Bioactive secondary metabolites from endophytes and associated marine derived fungi. *Fungal Diversity*, 49, 1.
- DEKA, D. & JHA, D. K. 2018. Optimization of culture parameters for improved production of bioactive metabolite by endophytic geosmithia pallida (ku693285) isolated from brucea mollis wall ex. Kurz, an endangered medicinal plant. *J Pure Appl. Microbiol*, 12, 1205-1213.
- DELA CRUZ, T. E. E., SCHULZ, B. E., KUBICEK, C. P. & DRUZHININA, I. S. 2006. Carbon source utilization by the marine dendryphiella species d. Arenaria and d. Salina. *FEMS Microbiology Ecology*, 58, 343-353.
- DETTMER, K., ARONOV, P. A. & HAMMOCK, B. D. 2007. Mass spectrometry-based metabolomics. *Mass Spec Rev*, 26, 51-78.
- DEVI, P., SHRIDHAR, M., D'SOUZA, L. & NAIK, C. 2006. Cellular fatty acid composition of marine-derived fungi. *Indian J Mar Sci*, 35, 359-363.
- DI CAMILLO, C. G., CERRANO, C., ROMAGNOLI, T. & CALCINAI, B. 2017. Living inside a sponge skeleton: The association of a sponge, a macroalga and a diatom. *Symbiosis*, 71, 185-198.
- DIAS, D. A., URBAN, S. & ROESSNER, U. 2012. A historical overview of natural products in drug discovery. *Metabolites*, 2, 303-336.
- DIBLASI, L., ARRIGHI, F., SILVA, J., BARDÓN, A. & CARTAGENA, E. 2015. Penicillium commune metabolic profile as a promising source of antipathogenic natural products. *Nat Prod Res*, 29, 2181-2187.
- DING, L., LI, J., SONG, B., XIAO, X., HUANG, W., ZHANG, B., TANG, X., QI, M., YANG, Q., YANG, Q., YANG, L. & WANG, Z. 2014. Andrographolide prevents high-fat diet-induced obesity in c57bl/6 mice by suppressing the sterol regulatory element-binding protein pathway. *J Pharmacol Exp Ther*, 351, 474-483.
- DONLAN, R. M. & COSTERTON, J. W. 2002. Biofilms: Survival mechanisms of clinically relevant microorganisms. *Clin Microbiol Rev*, 15, 167-193.
- DOROSHENKO, N., TSENG, B. S., HOWLIN, R. P., DEACON, J., WHARTON, J. A., THURNER, P. J., GILMORE, B. F., PARSEK, M. R. & STOODLEY, P. 2014. Extracellular DNA impedes the transport of vancomycin in staphylococcus epidermidis biofilms preexposed to subinhibitory concentrations of vancomycin. *Antimicrob Agents Chemother*, 58, 7273-7282.
- DOS SANTOS, R. M. G., RODRIGUES-FO, E., ROCHA, W. C. & TEIXEIRA, M. F. S. 2003. Endophytic fungi from melia azedarach. *World J Microbiol Biotechnol*, 19, 767-770.
- DOSHI, G., AGGARWAL, G., MARTINS, E. & SHANBHAG, P. 2011. Novel antibiotics from marine sources. *Int. J. Pharm. Sci. Nanotech*, 4, 1446-1461.
- DREWRY, D. H. & MACARRON, R. 2010. Enhancements of screening collections to address areas of unmet medical need: An industry perspective. *Curr Opin Chem Biol*, 14, 289-298.
- DUUS, J., GOTFREDSSEN, C. H. & BOCK, K. 2000. Carbohydrate structural determination by nmr spectroscopy: Modern methods and limitations. *Chem Rev*, 100, 4589-4614.
- EDRADA, R. A., HEUBES, M., BRAUERS, G., WRAY, V., BERG, A., GRÄFE, U., WOHLFARTH, M., MÜHLBACHER, J., SCHAUMANN, K. & SUDARSONO 2002. Online analysis of xestodecalactones a– c, novel bioactive metabolites from the fungus penicillium cf. M ontanense and their subsequent isolation from the sponge xestospongia e xigua. *J Nat Prod*, 65, 1598-1604.
- EDWARDS, J., CHAMBERLAIN, D., BROSNAN, G., WEST, D., STANLEY, M., CLIPSON, N. & HOOLEY, P. 1998. A comparative physiological and morphological study of dendryphiella salina and d. Arenaria in relation to adaptation to life in the sea. *Mycol Res*, 102, 1198-1202.
- EL-BEIH, A. A., KATO, H., OHTA, T. & TSUKAMOTO, S. 2007. (3r,4ar,5s,6r)-6-hydroxy-5-methylramulosin: A new ramulosin derivative from a marine-derived sterile mycelium. *Chem Pharm Bull (Tokyo)*, 55, 953-954.

- ELSEBAI, M. F., KEHRAUS, S., GÜTSCHOW, M. & KÖNIG, G. M. 2010. Spartinoxide, a new enantiomer of a82775c with inhibitory activity toward hle from the marine-derived fungus phaeosphaeria spartinae. *Nat Prod Comm*, 5, 1934578X1000500718.
- ELSEBAI, M. F., KEHRAUS, S., LINDEQUIST, U., SASSE, F., SHAABAN, S., GUTSCHOW, M., JOSTEN, M., SAHL, H. G. & KONIG, G. M. 2011. Antimicrobial phenalenone derivatives from the marine-derived fungus coniothyrium cereale. *Org Biomol Chem*, 9, 802-808.
- ERMOLAEVA, S. A., SYSOLYATINA, E. V. & GINTSBURG, A. L. 2015. Atmospheric pressure nonthermal plasmas for bacterial biofilm prevention and eradication. *Biointerphases*, 10, 029404.
- ESTRELA, A. B. & ABRAHAM, W.-R. 2016. Fungal metabolites for the control of biofilm infections. *Agriculture*, 6, 37.
- FABIAN, K., ANKE, T. & STERNER, O. 2001. Mariannaeapyrone-a new inhibitor of thromboxane a₂ induced platelet aggregation. *Zeitschrift für Naturforschung C*, 56, 106-110.
- FATIMA, N., MUKHTAR, U., IHSAN UL, H., AHMED QAZI, M., JADOON, M. & AHMED, S. 2016. Biological evaluation of endophytic fungus chaetomium sp. Nf15 of justicia adhatoda l.: A potential candidate for drug discovery. *Jundishapur J Microbiol*, 9, e29978.
- FERNANDES, A. A., NOVELLI, E. L., OKOSHI, K., OKOSHI, M. P., DI MUZIO, B. P., GUIMARAES, J. F. & FERNANDES JUNIOR, A. 2010. Influence of rutin treatment on biochemical alterations in experimental diabetes. *Biomed Pharmacother*, 64, 214-219.
- FERNANDO, I. P., KIM, M., SON, K. T., JEONG, Y. & JEON, Y. J. 2016. Antioxidant activity of marine algal polyphenolic compounds: A mechanistic approach. *J Med Food*, 19, 615-628.
- FOTEDAR, R. 2011. Integration of western king prawn (penaeus latisulcatus kishinouye, 1896) and green seaweed (ulva lactuca linnaeus, 1753) in a closed recirculating aquaculture system. *Aquaculture*, 322, 201-209.
- FRASER, B. H., PERLMUTTER, P. & WIJESUNDERA, C. 2007. Practical syntheses of triacylglycerol regioisomers containing long-chain polyunsaturated fatty acids. *J Am Oil Chemists' Soc*, 84, 11.
- FU, Y., LUO, J., JIA, Z., ZHEN, W., ZHOU, K., GILBERT, E. & LIU, D. 2014. Baicalein protects against type 2 diabetes via promoting islet beta-cell function in obese diabetic mice. *Int J Endocrinol*, 2014, 846742.
- FUKUDA, T., SHIMOYAMA, K., NAGAMITSU, T. & TOMODA, H. 2014. Synthesis and biological activity of citridone a and its derivatives. *J Antibiot (Tokyo)*, 67, 445-450.
- FUKUDA, T., SUDOH, Y., TSUCHIYA, Y., OKUDA, T., FUJIMORI, F. & IGARASHI, Y. 2011. Marianins a and b, prenylated phenylpropanoids from mariannaea camptospora. *J Nat Prod*, 74, 1327-1330.
- FUKUDA, T., TOMODA, H. & ŌMURA, S. 2005. Citridones, new potentiators of antifungal miconazole activity, produced by penicillium sp. Fki-1938. *The J Antibiotics*, 58, 315-321.
- GAJEWSKI, J., PAVLOVIC, R., FISCHER, M., BOLES, E. & GRININGER, M. 2017. Engineering fungal de novo fatty acid synthesis for short chain fatty acid production. *Nature Comm*, 8, 14650.
- GALLOP, M. A., BARRETT, R. W., DOWER, W. J., FODOR, S. P. & GORDON, E. M. 1994. Applications of combinatorial technologies to drug discovery. 1. Background and peptide combinatorial libraries. *J Med Chem*, 37, 1233-1251.
- GAMAL-ELDEEN, A. M., ABDEL-LATEFF, A. & OKINO, T. 2009. Modulation of carcinogen metabolizing enzymes by chromanone a; a new chromone derivative from algicolous marine fungus penicillium sp. *Environ Toxicol Pharmacol*, 28, 317-322.
- GAO, C., BOURKE, E., SCOBIE, M., FAMME, M. A., KOOLMEISTER, T., HELLEDAY, T., ERIKSSON, L. A., LOWNDES, N. F. & BROWN, J. A. 2014. Rational design and validation of a tip60 histone acetyltransferase inhibitor. *Sci Rep*, 4, 5372.
- GELADI, P. 2003. Chemometrics in spectroscopy. Part 1. Classical chemometrics. *Spectrochim Acta B: Atomic Spectroscopy*, 58, 767-782.
- GERTH, K., BEDORF, N., IRSCHIK, H., HÖFLE, G. & REICHENBACH, H. 1994. The soraphens: A family of novel antifungal compounds from sorangium cellulosum (myxobacteria) i. Soraphen a 1α: Fermentation, isolation, biological properties. *J Antibiotics*, 47, 23-31.
- GERTH, K., PRADELLA, S., PERLOVA, O., BEYER, S. & MÜLLER, R. 2003. Myxobacteria: Proficient producers of novel natural products with various biological activities—past and future

- biotechnological aspects with the focus on the genus sorangium. *J Biotechnology*, 106, 233-253.
- GIDDINGS, L.-A. & NEWMAN, D. J. 2015. Bioactive compounds from marine extremophiles. *Bioactive compounds from marine extremophiles*. Springer.
- GILLESPIE, D. E., BRADY, S. F., BETTERMANN, A. D., CIANCOTTO, N. P., LILES, M. R., RONDON, M. R., CLARDY, J., GOODMAN, R. M. & HANDELSMAN, J. 2002. Isolation of antibiotics turbomycin a and b from a metagenomic library of soil microbial DNA. *Appl Environ Microbiol*, 68, 4301-4306.
- GOMES, N. M., DETHOUP, T., SINGBURAUDOM, N., GALES, L., SILVA, A. M. & KIJOA, A. 2012. Eurocristatine, a new diketopiperazine dimer from the marine sponge-associated fungus eurotium cristatum. *Phytochem Lett*, 5, 717-720.
- GOPALAKRISHNAN, B., APARNA, V., JEEVAN, J., RAVI, M., DESIRAJU, G. & MODELING 2005. A virtual screening approach for thymidine monophosphate kinase inhibitors as antitubercular agents based on docking and pharmacophore models. *J Chem Inf*, 45, 1101-1108.
- GOWDA, G. A. & DJUKOVIC, D. 2014. Overview of mass spectrometry-based metabolomics: Opportunities and challenges. *Methods Mol Biol*, 1198, 3-12.
- GRAY, A. I., IGOLI, J. O. & EDRADA-EBEL, R. 2012. Natural products isolation in modern drug discovery programs. *Methods Mol Biol*, 864, 515-534.
- GRIFFITHS, W. J., KOAL, T., WANG, Y., KOHL, M., ENOT, D. P. & DEIGNER, H. P. 2010. Targeted metabolomics for biomarker discovery. *Angew Chem Int Edn*, 49, 5426-5445.
- GUAN, M., YAO, W., LIU, R., LAM, K. S., NOLTA, J., JIA, J., PANGANIBAN, B., MENG, L., ZHOU, P., SHAHNAZARI, M., RITCHIE, R. O. & LANE, N. E. 2012. Directing mesenchymal stem cells to bone to augment bone formation and increase bone mass. *Nature Med*, 18, 456-462.
- HABBU, P., WARAD, V., SHASTRI, R., MADAGUNDI, S. & KULKARNI, V. H. 2016. Antimicrobial metabolites from marine microorganisms. *Chin J Nat Med*, 14, 101-116.
- HAMBLIN, M. R. & HASAN, T. 2004. Photodynamic therapy: A new antimicrobial approach to infectious disease? *Photochem Photobiol Sci*, 3, 436-450.
- HARPER, J. K., ARIF, A. M., FORD, E. J., STROBEL, G. A., PORCO JR, J. A., TOMER, D. P., ONEILL, K. L., HEIDER, E. M. & GRANT, D. M. 2003. Pestacin: A 1, 3-dihydro isobenzofuran from pestalotiopsis microspora possessing antioxidant and antimycotic activities. *Tetrahedron*, 59, 2471-2476.
- HARVEY, A. L. 2007. Natural products as a screening resource. *Curr Opin Chem Biol*, 11, 480-484.
- HARVEY, A. L. 2008. Natural products in drug discovery. *Drug Discov Today*, 13, 894-901.
- HARVEY, A. L., EDRADA-EBEL, R. & QUINN, R. J. 2015. The re-emergence of natural products for drug discovery in the genomics era. *Nature Rev Drug Discov*, 14, 111-129.
- HASHIMOTO, T. & ASAKAWA, Y. 1998. Biologically active substances of japanese inedible mushrooms. *Heterocycles*, 2, 1067-1110.
- HASHIMOTO, T., TAHARA, S., TAKAOKA, S., TORI, M. & ASAKAWA, Y. 1994. Structures of daldining a~c, three novel azaphilone derivatives from ascomycetous fungus kalkinia concentrica. *Chem Pharm Bull*, 42, 2397-2399.
- HATFIELD, G. 1994. *Country remedies: Traditional east anglian plant remedies in the twentieth century*, Woodbridge, Boydell Press.
- HELLWIG, V., JU, Y.-M., ROGERS, J. D., FOURNIER, J. & STADLER, M. 2005. Hypomiltin, a novel azaphilone from hypoxylon hypomiltum, and chemotypes in hypoxylon sect. Hypoxylon as inferred from analytical hplc profiling. *Mycol Prog*, 4, 39-54.
- HORI, K., NOBUSAWA, T., WATANABE, T., MADOKA, Y., SUZUKI, H., SHIBATA, D., SHIMOJIMA, M. & OHTA, H. 2016. Tangled evolutionary processes with commonality and diversity in plastidial glycolipid synthesis in photosynthetic organisms. *Biochim Biophys Acta*, 1861, 1294-1308.
- HOUGHTEN, R. A. 1985. General method for the rapid solid-phase synthesis of large numbers of peptides: Specificity of antigen-antibody interaction at the level of individual amino acids. *Proc Nat Acad Sci*, 82, 5131-5135.

- HU, D.-M., WANG, M. & CAI, L. 2017. Phylogenetic assessment and taxonomic revision of mariannaea. *Mycol Prog*, 16, 271-283.
- HUANG, H., SONG, Y., LI, X., WANG, X., LING, C., QIN, X., ZHOU, Z., LI, Q., WEI, X. & JU, J. 2018. Abyssomicin monomers and dimers from the marine-derived streptomyces koyangensis scsio 5802. *J Nat Prod*, 81, 1892-1898.
- HUBERT, J., NUZILLARD, J.-M., PURSON, S., HAMZAOU, M., BORIE, N., REYNAUD, R. & RENAULT, J.-H. 2014. Identification of natural metabolites in mixture: A pattern recognition strategy based on 13c nmr. *Anal Chem*, 86, 2955-2962.
- HUSAIN, F. M., AHMAD, I., KHAN, M. S. & AL-SHABIB, N. A. 2015. Trigonella foenum-graceum (seed) extract interferes with quorum sensing regulated traits and biofilm formation in the strains of pseudomonas aeruginosa and aeromonas hydrophila. *Evid Based Complement Alternat Med*, 2015, 879540.
- HYDE, K. D. 2001. Where are the missing fungi? *Mycol Res*, 105, 1409-1412.
- IGARASHI, Y., YAMAMOTO, K., FUKUDA, T., SHOJIMA, A., NAKAYAMA, J., CARRO, L. & TRUJILLO, M. E. 2015. Arthroamide, a cyclic depsipeptide with quorum sensing inhibitory activity from arthrobacter sp. *J Nat Prod*, 78, 2827-2831.
- ISAKA, M., CHINTHANOM, P., BOONRUANGPRAPA, T., RUNGJINDAMAI, N. & PINRUAN, U. 2010. Eremophilane-type sesquiterpenes from the fungus xylaria sp. Bcc 21097. *J Nat Prod*, 73, 683-687.
- ISHIUCHI, K., HIROSE, D., KONDO, T., WATANABE, K., TERASAKA, K. & MAKINO, T. 2020. Mariannamides a and b, new cyclic octapeptides isolated from mariannaea elegans nbr102301. *Bioorg Med Chem Lett*, 30, 126946.
- JADULCO, R., BRAUERS, G., EDRADA, R. A., EBEL, R., WRAY, V., SUDARSONO & PROKSCH, P. 2002. New metabolites from sponge-derived fungi curvularia lunata and cladosporium herbarum. *J Nat Prod*, 65, 730-733.
- JAYAPRAKASHA, G. K. & RAO, L. J. 2000. Phenolic constituents from the lichen parmotrema stuppeum (nyl.) hale and their antioxidant activity. *Zeitschrift für Naturforschung C*, 55, 1018-1022.
- JIANG, P., LI, J., HAN, F., DUAN, G., LU, X., GU, Y. & YU, W. 2011. Antibiofilm activity of an exopolysaccharide from marine bacterium vibrio sp. Qy101. *PLoS One*, 6, e18514.
- JIMÉNEZ, J. T., O'CONNELL, S., LYONS, H., BRADLEY, B. & HALL, M. 2010. Antioxidant, antimicrobial, and tyrosinase inhibition activities of acetone extract of ascophyllum nodosum. *Chem Papers*, 64, 434-442.
- JORDÀ, J., JOUHTEN, P., CÁMARA, E., MAAHEIMO, H., ALBIOL, J. & FERRER, P. 2012. Metabolic flux profiling of recombinant protein secreting pichia pastoris growing on glucose: Methanol mixtures. *Microbial cell factories*, 11, 57.
- JUMINA, J., LAVENDI, W., SINGGIH, T., TRIONO, S., KURNIAWAN, Y. S. & KOKETSU, M. 2019. Preparation of monoacylglycerol derivatives from indonesian edible oil and their antimicrobial assay against staphylococcus aureus and escherichia coli. *Sci Rep*, 9, 1-8.
- JUMP, D. B., TORRES-GONZALEZ, M. & OLSON, L. K. 2011. Soraphen a, an inhibitor of acetyl coa carboxylase activity, interferes with fatty acid elongation. *Biochem Pharmacol*, 81, 649-660.
- JUNG, U. J., LEE, M. K., PARK, Y. B., KANG, M. A. & CHOI, M. S. 2006. Effect of citrus flavonoids on lipid metabolism and glucose-regulating enzyme mrna levels in type-2 diabetic mice. *Int J Biochem Cell Biol*, 38, 1134-1145.
- KADAM, S. U., O'DONNELL, C. P., RAI, D. K., HOSSAIN, M. B., BURGESS, C. M., WALSH, D. & TIWARI, B. K. 2015. Laminarin from irish brown seaweeds ascophyllum nodosum and laminaria hyperborea: Ultrasound assisted extraction, characterization and bioactivity. *Mar Drugs*, 13, 4270-4280.
- KAPETANOVIC, I. 2008. Computer-aided drug discovery and development (cadd): In silico-chemico-biological approach. *Chemico-biological interactions*, 171, 165-176.
- KAUL, S., GUPTA, S., AHMED, M. & DHAR, M. K. 2012. Endophytic fungi from medicinal plants: A treasure hunt for bioactive metabolites. *Phytochem Rev*, 11, 487-505.

- KELLAND, L. R. 2000. Flavopiridol, the first cyclin-dependent kinase inhibitor to enter the clinic: Current status. *Expert Opin Investig Drugs*, 9, 2903-2911.
- KESSNER, D., CHAMBERS, M., BURKE, R., AGUS, D. & MALLICK, P. 2008. Proteowizard: Open source software for rapid proteomics tools development. *Bioinformatics*, 24, 2534-2536.
- KJER, J., DEBBAB, A., ALY, A. H. & PROKSCH, P. 2010. Methods for isolation of marine-derived endophytic fungi and their bioactive secondary products. *Nature Prot* 5, 479-490.
- KOHLMEYER, J. & KOHLMEYER, E. 1979. *Marine mycology: The higher fungi*, NY, USA, Academic Press.
- KÖNIG, G. M., KEHRAUS, S., SEIBERT, S. F., ABDEL-LATEFF, A. & MÜLLER, D. 2006. Natural products from marine organisms and their associated microbes. *ChemBioChem*, 7, 229-238.
- KOPP, F. & MARAHIEL, M. A. 2007. Where chemistry meets biology: The chemoenzymatic synthesis of nonribosomal peptides and polyketides. *Curr Opin Biotechnol*, 18, 513-520.
- KOUR, A., SHAWL, A. S., REHMAN, S., SULTAN, P., QAZI, P. H., SUDEN, P., KHAJURIA, R. K., VERMA, V. & BIOTECHNOLOGY 2008. Isolation and identification of an endophytic strain of fusarium oxysporum producing podophyllotoxin from juniperus recurva. *World J Microbiol Biotechnol*, 24, 1115-1121.
- KOUTSOUDAKIS, G., ROMERO-BREY, I., BERGER, C., PÉREZ-VILARÓ, G., MONTEIRO PERIN, P., VONDRAN, F. W. R., KALESSE, M., HARMROLFS, K., MÜLLER, R., MARTINEZ, J. P., PIETSCHMANN, T., BARTENSCHLAGER, R., BRÖNSTRUP, M., MEYERHANS, A. & DÍEZ, J. 2015. Soraphen a: A broad-spectrum antiviral natural product with potent anti-hepatitis c virus activity. *J Hepatology*, 63, 813-821.
- KRABEL, D., MORGENSTERN, K., HERZOG, S. & FORESTRY 2013. Endophytes in changing environments- do we need new concepts in forest management? *iForest-Biogeosciences*, 6, 109.
- KRUG, D. & MÜLLER, R. 2014. Secondary metabolomics: The impact of mass spectrometry-based approaches on the discovery and characterization of microbial natural products. *Nat Prod Rep*, 31, 768-783.
- KUMAR, A., PATIL, D., RAJAMOCHANAN, P. R. & AHMAD, A. 2013. Isolation, purification and characterization of vinblastine and vincristine from endophytic fungus fusarium oxysporum isolated from catharanthus roseus. *PLoS one*, 8, e71805.
- KUSARI, S., SINGH, S. & JAYABASKARAN, C. 2014. Biotechnological potential of plant-associated endophytic fungi: Hope versus hype. *Trends Biotechnol*, 32, 297-303.
- KUSARI, S., ZÜHLKE, S., KOSUTH, J., CELLAROVA, E. & SPITELLER, M. 2009. Light-independent metabolomics of endophytic thielavia subthermophila provides insight into microbial hypericin biosynthesis. *J Nat Prod*, 72, 1825-1835.
- LARSEN, T. O., PERRY, N. B. & ANDERSEN, B. 2003. Infectopyrone, a potential mycotoxin from alternaria infectoria. *Tetrahedron Lett*, 44, 4511-4513.
- LARSSON, C., AXELSSON, L., RYBERG, H. & BEER, S. 1997. Photosynthetic carbon utilization by enteromorpha intestinalis (chlorophyta) from a swedish rockpool. *Eur J Phycol*, 32, 49-54.
- LE TUTOUR, B., BENSLIMANE, F., GOULEAU, M., GOUYGOU, J., SAADAN, B. & QUEMENEUR, F. 1998. Antioxidant and pro-oxidant activities of the brown algae, laminaria digitata, himanthalia elongata, fucus vesiculosus, fucus serratus and ascophyllum nodosum. *J Appl Phycol*, 10, 121.
- LEBEAUX, D., GHIGO, J.-M. & BELOIN, C. 2014. Biofilm-related infections: Bridging the gap between clinical management and fundamental aspects of recalcitrance toward antibiotics. *Microbiol Mol Biol Rev*, 78, 510.
- LEE, Y. S., KIM, W. S., KIM, K. H., YOON, M. J., CHO, H. J., SHEN, Y., YE, J.-M., LEE, C. H., OH, W. K. & KIM, C. T. 2006. Berberine, a natural plant product, activates amp-activated protein kinase with beneficial metabolic effects in diabetic and insulin-resistant states. *Diabetes*, 55, 2256-2264.
- LI, C., ROEGE, K. E. & KELLY, W. L. 2009a. Analysis of the indanomycin biosynthetic gene cluster from streptomyces antibioticus nrrl 8167. *ChemBioChem*, 10, 1064-1072.
- LI, D., CARR, G., ZHANG, Y., WILLIAMS, D. E., AMLANI, A., BOTTRIELL, H., MUI, A. L.-F. & ANDERSEN, R. J. 2011. Turnagainolides a and b, cyclic depsipeptides produced in culture by a bacillus sp.: Isolation, structure elucidation, and synthesis. *J Nat Prod*, 74, 1093-1099.

- LI, L., WANG, C. Y., SHAO, C. L., GUO, Y. W., LI, G. Q., SUN, X. P., HAN, L., HUANG, H. & GUAN, H. S. 2009b. Sarcoglycosides a–c, new o-glycosylglycerol derivatives from the south china sea soft coral sarcophyton infundibuliforme. *Helv Chim Acta*, 92, 1495-1502.
- LIAN, X.-Y. & ZHANG, Z. 2013. Indanomycin-related antibiotics from marine streptomyces antibioticus ptz0016. *Nat Prod Res*, 27, 2161-2167.
- LIN, C. L. & LIN, J. K. 2008. Epigallocatechin gallate (egcg) attenuates high glucose-induced insulin signaling blockade in human hepg2 hepatoma cells. *Mol Nutr Food Res*, 52, 930-939.
- LIU, F., CAI, X.-L., YANG, H., XIA, X.-K., GUO, Z.-Y., YUAN, J., LI, M.-F., SHE, Z.-G. & LIN, Y.-C. 2010. The bioactive metabolites of the mangrove endophytic fungus talaromyces sp. Zh-154 isolated from kandelia candel (l.) druce. *Planta Med*, 76, 185-189.
- LIU, L. F., ZHANG, H., QI, H., WANG, X. M., WANG, J. D. & TAN, G. S. 2017a. A new androstanoid metabolite from a soil fungus curvularia borrierae strain hs-fg-237. *Nat Prod Res*, 31, 1080-1084.
- LIU, R., LI, X. & LAM, K. S. 2017b. Combinatorial chemistry in drug discovery. *Curr Opin Chem Biol*, 38, 117-126.
- LIU, Y., JUNG, J. H., JI, H. & ZHANG, S. 2006. Glycerolipids from a sarcotragus species sponge. *Molecules*, 11, 714-719.
- LIU, Y., LI, X.-M., MENG, L.-H. & WANG, B.-G. 2015. Polyketides from the marine mangrove-derived fungus *aspergillus ochraceus* ma-15 and their activity against aquatic pathogenic bacteria. *Phytochem Lett*, 12, 232-236.
- MACFARLANE, S. & DILLON, J. F. 2007. Microbial biofilms in the human gastrointestinal tract. *J Appl Microbiol*, 102, 1187-1196.
- MACINTYRE, L., ZHANG, T., VIEGELMANN, C., MARTINEZ, I. J., CHENG, C., DOWDELLS, C., ABDELMOHSEN, U. R., GERNERT, C., HENTSCHEL, U. & EDRADA-EBEL, R. 2014. Metabolomic tools for secondary metabolite discovery from marine microbial symbionts. *Mar Drugs*, 12, 3416-3448.
- MAGANA, M., PUSHPANATHAN, M., SANTOS, A. L., LEANSE, L., FERNANDEZ, M., IOANNIDIS, A., GIULIANOTTI, M. A., APIDIANAKIS, Y., BRADFUTE, S. & FERGUSON, A. L. 2020. The value of antimicrobial peptides in the age of resistance. *Lancet Infect Dis*.
- MAGNONE, M., AMERI, P., SALIS, A., ANDRAGHETTI, G., EMIONITE, L., MURIALDO, G., DE FLORA, A. & ZOCCHI, E. 2015. Microgram amounts of abscisic acid in fruit extracts improve glucose tolerance and reduce insulinemia in rats and in humans. *The FASEB Journal*, 29, 4783-4793.
- MAJOR, A. P. 1977. *The book of seaweed*, London, Gordon & Cremonesi.
- MALMSTRØM, J., CHRISTOPHERSEN, C., BARRERO, A. F., OLTRA, J. E., JUSTICIA, J. & ROSALES, A. 2002. Bioactive metabolites from a marine-derived strain of the fungus *emericella varicolor*. *J Nat Prod*, 65, 364-367.
- MANDAL, S., MOUDGIL, M. & MANDAL, S. K. 2009. Rational drug design. *Eur J Pharmacol*, 625, 90-100.
- MARCON, L., BATTERSBY, B. J., RÜHMANN, A., FORD, K., DALEY, M., LAWRIE, G. A. & TRAU, M. 2010. 'On-the-fly' optical encoding of combinatorial peptide libraries for profiling of protease specificity. *Molecular bioSystems*, 6, 225-233.
- MAREE, J., KAMATOU, G., GIBBONS, S., VILJOEN, A. & VAN VUUREN, S. 2014. The application of gc–ms combined with chemometrics for the identification of antimicrobial compounds from selected commercial essential oils. *Chemomet Intell Lab Syst*, 130, 172-181.
- MARTÍN, R., MIQUEL, S., LANGELLA, P. & BERMÚDEZ-HUMARÁN, L. G. 2014. The role of metagenomics in understanding the human microbiome in health and disease. *Virulence*, 5, 413-423.
- MASCIO, C. T., ALDER, J. D. & SILVERMAN, J. A. 2007. Bactericidal action of daptomycin against stationary-phase and nondividing staphylococcus aureus cells. *Antimicrob Agents Chemother*, 51, 4255.
- MAZLAN, N. W., TATE, R., YUSOFF, Y. M., CLEMENTS, C. & EDRADA-EBEL, R. 2020. Metabolomics-guided isolation of anti-trypanosomal compounds from endophytic fungi of the mangrove plant *avicennia lanata*. *Curr Med Chem*, 27, 1815-1835.

- MCCHESENEY, J. D., VENKATARAMAN, S. K. & HENRI, J. T. 2007. Plant natural products: Back to the future or into extinction? *Phytochemistry*, 68, 2015-2022.
- MEENUPRIYA, J. & THANGARAJ, M. 2011. Analytical characterization and structure elucidation of metabolites from *Aspergillus ochraceus* mp2 fungi. *Asian Pacific J Trop Biomed*, 1, 376-380.
- MIQUEL, S., LAGRAFEUILLE, R., SOUWEINE, B. & FORESTIER, C. 2016. Anti-biofilm activity as a health issue. *Frontiers in Microbiol*, 7, 592.
- MOK, D. K. & CHAU, F.-T. 2006. Chemical information of chinese medicines: A challenge to chemist. *Chemomet Intell Lab Syst*, 82, 210-217.
- MOLINSKI, T. F., DALISAY, D. S., LIEVENS, S. L. & SALUDES, J. P. 2009. Drug development from marine natural products. *Nature Rev Drug Discov*, 8, 69-85.
- MONDE, K., SATOH, H., NAKAMURA, M., TAMURA, M. & TAKASUGI, M. 1998. Organochlorine compounds from a terrestrial higher plant: Structures and origin of chlorinated orcinol derivatives from diseased bulbs of *Lilium maximowiczii*. *J Nat Prod*, 61, 913-921.
- MORI, H., URANO, Y., ABE, F., FURUKAWA, S., FURUKAWA, S., TSURUMI, Y., SAKAMOTO, K., HASHIMOTO, M., TAKASE, S. & HINO, M. 2003. Fr235222, a fungal metabolite, is a novel immunosuppressant that inhibits mammalian histone deacetylase (hdac). *J Antibiotics*, 56, 72-79.
- MÜHLBAUER, A., TRIEBEL, D., PERSOH, D., WOLLWEBER, H., SEIP, S. & STADLER, M. 2002. Macrocarpones, novel metabolites from stromata of *hypoxylon macrocarpum*, and new evidence on the chemotaxonomy of *hypoxylon* species. *Mycol Prog*, 1, 235-248.
- MULLER, B. A. 2009. Imatinib and its successors--how modern chemistry has changed drug development. *Curr Pharm Des*, 15, 120-133.
- MURPHY, P., DAL BELLO, F., O'DOHERTY, J., ARENDT, E., SWEENEY, T. & COFFEY, A. 2013. Analysis of bacterial community shifts in the gastrointestinal tract of pigs fed diets supplemented with β -glucan from *Laminaria digitata*, *Laminaria hyperborea* and *Saccharomyces cerevisiae*. *Animal*, 7, 1079-1087.
- NAINI, A., SASSE, F. & BRÖNSTRUP, M. 2019. The intriguing chemistry and biology of soraphens. *Nat Prod Rep*, 36, 1394-1411.
- NARAYANI, C. G. S., ARULPRIYA, M., RUBAN, P., ANANTHARAJ, K. & SRINIVASAN, R. 2011. In vitro antimicrobial activities of seaweed extracts against human pathogens. *J Pharm Res*, 4, 2076-2077.
- NCUBE, N., AFOLAYAN, A. & OKOH, A. 2008. Assessment techniques of antimicrobial properties of natural compounds of plant origin: Current methods and future trends. *Afr J Biotechnol*, 7.
- NETO, A., TITTLE, I. & RAPOSEIRO, P. 2006. Flora marinha do litoral dos açores= rocky shore marine flora of the azores. Secretaria Regional do Ambiente e do Mar, Horta.
- NEWMAN, D. J. & CRAGG, G. M. 2007. Natural products as sources of new drugs over the last 25 years. *J Nat Prod*, 70, 461-477.
- NEWMAN, D. J. & CRAGG, G. M. 2012. Natural products as sources of new drugs over the 30 years from 1981 to 2010. *J Nat Prod*, 75, 311-335.
- NEWMAN, D. J. & CRAGG, G. M. 2016. Natural products as sources of new drugs from 1981 to 2014. *J Nat Prod*, 79, 629-661.
- NEWTON, G. & ABRAHAM, E. 1955. Cephalosporin c, a new antibiotic containing sulphur and d- α -amino adipic acid. *Nature*, 175, 548-548.
- NISA, H., KAMILI, A. N., NAWCHOO, I. A., SHAFI, S., SHAMEEM, N. & BANDH, S. A. 2015. Fungal endophytes as prolific source of phytochemicals and other bioactive natural products: A review. *Microb Pathog*, 82, 50-59.
- OLIVEIRA, A. L. L. D., FELÍCIO, R. D. & DEBONSI, H. M. 2012. Marine natural products: Chemical and biological potential of seaweeds and their endophytic fungi. *Rev Bras Farmacog*, 22, 906-920.
- OSTERHAGE, C., KAMINSKY, R., KÖNIG, G. M. & WRIGHT, A. D. 2000. Ascosalipyrrolidinone a, an antimicrobial alkaloid, from the obligate marine fungus *ascochyta s alicorniae*. *J Org Chem*, 65, 6412-6417.

- OSTERHAGE, C., KÖNIG, G. M., HÖLLER, U. & WRIGHT, A. D. 2002. Rare sesquiterpenes from the algicolous fungus *drechslera dematioides*. *J Nat Prod*, 65, 306-313.
- OWEN, N. L. & HUNDLEY, N. 2004. Endophytes—the chemical synthesizers inside plants. *Sci Prog*, 87, 79-99.
- PAIVA, L., LIMA, E., NETO, A. I. & BAPTISTA, J. 2016. Angiotensin i-converting enzyme (ace) inhibitory activity of *fucus spiralis* macroalgae and influence of the extracts storage temperature—a short report. *J Pharm Biomed Anal*, 131, 503-507.
- PAIVA, L., LIMA, E., NETO, A. I. & BAPTISTA, J. 2017. Angiotensin i-converting enzyme (ace) inhibitory activity, antioxidant properties, phenolic content and amino acid profiles of *fucus spiralis* l. Protein hydrolysate fractions. *Mar Drugs*, 15, 311.
- PAIVA, L., LIMA, E., NETO, A. I. & BAPTISTA, J. 2018. Seasonal variability of the biochemical composition and antioxidant properties of *fucus spiralis* at two azorean islands. *Mar Drugs*, 16, 248.
- PATIL, A., MANE, A., KAMAT, S., LOHAR, T. & SALUNKHE, R. 2019. Aqueous hydrotropic solution: Green reaction medium for synthesis of pyridopyrimidine carbonitrile and spiro-oxindole dihydroquinazolinone derivatives. *Res Chem Intermed*, 45, 3441-3452.
- PAZ, Z., KOMON-ZELAZOWSKA, M., DRUZHININA, I., AVESKAMP, M., SHNAIDERMAN, A., ALUMA, Y., CARMELI, S., ILAN, M. & YARDEN, O. 2010. Diversity and potential antifungal properties of fungi associated with a mediterranean sponge. *Fungal Diversity*, 42, 17-26.
- PEAY, K. G., KENNEDY, P. G. & BRUNS, T. D. 2008. Fungal community ecology: A hybrid beast with a molecular master. *AlBs Bull*, 58, 799-810.
- PÉREZ, M. J., FALQUÉ, E. & DOMÍNGUEZ, H. 2016. Antimicrobial action of compounds from marine seaweed. *Mar Drugs*, 14, 52.
- PIMENTEL, M. R., MOLINA, G., DIONÍSIO, A. P., MARÓSTICA JUNIOR, M. R. & PASTORE, G. M. 2011. The use of endophytes to obtain bioactive compounds and their application in biotransformation process. *Biotechnol Res Int*, 2011.
- PLUSKAL, T., CASTILLO, S., VILLAR-BRIONES, A. & OREŠIČ, M. 2010. Mzmine 2: Modular framework for processing, visualizing, and analyzing mass spectrometry-based molecular profile data. *BMC Bioinformatics*, 11, 1-11.
- PURI, S. C., VERMA, V., AMNA, T., QAZI, G. N. & SPITELLER, M. 2005. An endophytic fungus from nothapodytes foetida that produces camptothecin. *J Nat Prod*, 68, 1717-1719.
- PYE, C. R., BERTIN, M. J., LOKEY, R. S., GERWICK, W. H. & LININGTON, R. G. 2017. Retrospective analysis of natural products provides insights for future discovery trends. *Proc Nat Acad Sci*, 114, 5601-5606.
- QI, S.-H., XU, Y., XIONG, H.-R., QIAN, P.-Y. & ZHANG, S. 2009. Antifouling and antibacterial compounds from a marine fungus *cladosporium* sp. F14. *World J Microbiol Biotechnol*, 25, 399-406.
- QUINN, R. J., CARROLL, A. R., PHAM, N. B., BARON, P., PALFRAMAN, M. E., SURAWEEERA, L., PIERENS, G. K. & MURESAN, S. 2008. Developing a drug-like natural product library. *J Nat Prod*, 71, 464-468.
- RAHEEM, D. J., TAWFIKE, A. F., ABDELMOHSEN, U. R., EDRADA-EBEL, R. & FITZSIMMONS-THOSS, V. 2019. Application of metabolomics and molecular networking in investigating the chemical profile and antitrypanosomal activity of british bluebells (*hyacinthoides non-scripta*). *Sci Rep*, 9, 1-13.
- RAJALAHTI, T. & KVALHEIM, O. M. 2011. Multivariate data analysis in pharmaceuticals: A tutorial review. *International journal of pharmaceuticals*, 417, 280-290.
- RATEB, M. E. & EBEL, R. 2011. Secondary metabolites of fungi from marine habitats. *Nat Prod Rep*, 28, 290-344.
- REEN, F. J., ROMANO, S., DOBSON, A. D. & O'GARA, F. 2015. The sound of silence: Activating silent biosynthetic gene clusters in marine microorganisms. *Mar Drugs*, 13, 4754-4783.
- RENDUELES, O. & GHIGO, J.-M. 2015. Mechanisms of competition in biofilm communities. *Microb Biofilms*, 319-342.
- ŘEZANKA, T. & GUSCHINA, I. A. 2000. Glycosidic compounds of murolic, protoconstipatic and allo-murolic acids from lichens of central asia. *Phytochemistry Reviews*, 54, 635-645.

- RIOUX, L.-E., TURGEON, S. L. & BEAULIEU, M. 2007. Characterization of polysaccharides extracted from brown seaweeds. *Carb Polymers*, 69, 530-537.
- ROCHFORT, S. 2005. Metabolomics reviewed: A new “omics” platform technology for systems biology and implications for natural products research. *J Nat Prod*, 68, 1813-1820.
- ROEPKE, J., SALIM, V., WU, M., THAMM, A. M., MURATA, J., PLOSS, K., BOLAND, W. & DE LUCA, V. 2010. Vinca drug components accumulate exclusively in leaf exudates of madagascar periwinkle. *Proc Nat Acad Sci*, 107, 15287-15292.
- RONG, H., HAN, L., LI, Y.-Q., ZHAO, L.-X., ZHENG, D., WU, L.-X., XU, L.-H., HUANG, X.-S. & JIANG, Y. 2015. New cyclic depsipeptide from an endophytic actinomycete. *Chem Nat Prod*, 51, 926-928.
- ROWE, J. G., GIMENEZ, M. G. & RODRIGUEZ, M. S. 1999. Some lichen products have antimicrobial activity. *Zeitschrift für Naturforschung C*, 54, 605-609.
- RYAN, R. P. & DOW, J. M. 2008. Diffusible signals and interspecies communication in bacteria. *Microbiology*, 154, 1845-1858.
- RYZHIK, I., MAKAROV, M. & VOSKOBOINIKOV, G. 2014. The physiological state of intertidal brown seaweeds *fucus serratus* linnaeus, 1753 and *fucus distichus* linnaeus, 1767 cultivated on a biofiltration system in the barents sea. *Russian J Mar Biol*, 40, 119-124.
- SACKS, P., JACOBS, P., GALE, D., LYNCH, S. R., BOTHWELL, T. H. & STEVENS, K. 1973. Combination chemotherapy in the treatment of advanced hodgkin's disease. *S Afr Med J*, 47, 903-907.
- SAHA, M., REMPT, M., GROSSER, K., POHNERT, G. & WEINBERGER, F. 2011. Surface-associated fucoxanthin mediates settlement of bacterial epiphytes on the rockweed *fucus vesiculosus*. *Biofouling*, 27, 423-433.
- SAHNOUNI, F., BENATTOUCHE, Z., MATALLAH-BOUTIBA, A., BENCHOHRA, M., MOUMEN CHENTOUF, W., BOUHADI, D. & BOUTIBA, Z. 2016. Antimicrobial activity of two marine algae *ulva rigida* and *ulva intestinalis* collected from arzew gulf (western algeria). *J Appl Environ Biol Sci*, 6, 242-248.
- SALTA, M., WHARTON, J. A., DENNINGTON, S. P., STOODLEY, P. & STOKES, K. R. 2013. Anti-biofilm performance of three natural products against initial bacterial attachment. *Int J Mol Sci*, 14, 21757-21780.
- SÁNCHEZ-MACHADO, D., LÓPEZ-HERNÁNDEZ, J., PASEIRO-LOSADA, P. & LÓPEZ-CERVANTES, J. 2004. An hplc method for the quantification of sterols in edible seaweeds. *Biomed Chrom*, 18, 183-190.
- SANCHEZ, J. F., CHIANG, Y. M., SZEWCZYK, E., DAVIDSON, A. D., AHUJA, M., ELIZABETH OAKLEY, C., WOO BOK, J., KELLER, N., OAKLEY, B. R. & WANG, C. C. 2010. Molecular genetic analysis of the orsellinic acid/f9775 gene cluster of *aspergillus nidulans*. *Mol Biosyst*, 6, 587-593.
- SANDSDALEN, E., HAUG, T., STENSVÅG, K. & STYRVOLD, O. B. 2003. The antibacterial effect of a polyhydroxylated fucophlorethol from the marine brown alga, *fucus vesiculosus*. *World J Microbiol Biotechnol*, 19, 777-782.
- SANTIAGO, K. A. A., EDRADA-EBEL, R., CHEOW, Y. L. & TING, A. S. Y. 2021. Biodiscovery of potential antibacterial diagnostic metabolites from the endolichenic fungus *xylaria venustula* using lc–ms-based metabolomics. *Biology*, 10, 191.
- SARASAN, M., PUTHUMANA, J., JOB, N., HAN, J., LEE, J. S. & PHILIP, R. 2017. Marine algicolous endophytic fungi - a promising drug resource of the era. *J Microbiol Biotechnol*, 27, 1039-1052.
- SARKER, S. D. & NAHAR, L. 2012. An introduction to natural products isolation. *Methods Mol Biol*, 864, 1-25.
- SAYEM, S. M. A., MANZO, E., CIAVATTA, L., TRAMICE, A., CORDONE, A., ZANFARDINO, A., DE FELICE, M. & VARCAMONTI, M. 2011. Anti-biofilm activity of an exopolysaccharide from a sponge-associated strain of *bacillus licheniformis*. *Microbial Cell Factories*, 10, 74.
- SCHAUDER, S. & BASSLER, B. L. 2001. The languages of bacteria. *Genes Dev*, 15, 1468-1480.
- SCHERLACH, K. & HERTWECK, C. 2009. Triggering cryptic natural product biosynthesis in microorganisms. *Org Biomol Chem*, 7, 1753-1760.

- SCHMID, M., GUIHÉNEUF, F. & STENGEL, D. 2017. Ecological and commercial implications of temporal and spatial variability in the composition of pigments and fatty acids in five irish macroalgae. *Mar Biol*, 164, 158.
- SCHMIDTSDORFF, S., NEUMANN, J., SCHMIDT, A. H. & PARR, M. K. 2021. Analytical lifecycle management for comprehensive and universal nitrosamine analysis in various pharmaceutical formulations by supercritical fluid chromatography. *J Pharm Biomed Anal*, 197, 113960.
- SCHOLTZ, V., PAZLAROVA, J., SOUSKOVA, H., KHUN, J. & JULAK, J. 2015. Nonthermal plasma—a tool for decontamination and disinfection. *Biotechnol Adv*, 33, 1108-1119.
- SCHULZ, B. & BOYLE, C. 2005. The endophytic continuum. *Mycol Res*, 109, 661-686.
- SCHULZ, B., BOYLE, C., DRAEGER, S., RÖMMERT, A.-K. & KROHN, K. 2002. Endophytic fungi: A source of novel biologically active secondary metabolites. *Mycol Res*, 106, 996-1004.
- SCHWARTSMANN, G. 2000. Marine organisms and other novel natural sources of new cancer drugs. *Ann Oncol*, 11, 235-244.
- SCHWARTSMANN, G., DA ROCHA, A. B., BERLINCK, R. G. & JIMENO, J. 2001. Marine organisms as a source of new anticancer agents. *Lancet Oncol*, 2, 221-225.
- SCOPEL, M., ABRAHAM, W.-R., ANTUNES, A. L., TEREZINHA HENRIQUES, A. & JOSE MACEDO, A. J. 2014. Mevalonolactone: An inhibitor of *staphylococcus epidermidis* adherence and biofilm formation. *J Med Chem*, 10, 246-251.
- SCOPEL, M., ABRAHAM, W.-R., HENRIQUES, A. T. & MACEDO, A. J. 2013. Dipeptide cis-cyclo (leucyl-tyrosyl) produced by sponge associated penicillium sp. F37 inhibits biofilm formation of the pathogenic staphylococcus epidermidis. *Bioorg Med Chem Lett*, 23, 624-626.
- SEBAK, M., SAAFAN, A. E., ABDELGHANI, S., BAKEER, W., EL-GENDY, A. O., ESPRIU, L. C., DUNCAN, K. & EDRADA-EBEL, R. 2020. Bioassay-and metabolomics-guided screening of bioactive soil actinomycetes from the ancient city of ihnasia, egypt. *PLoS One*, 15, e0228901.
- SHAABAN, M., EL-METWALLY, M. M. & LAATSCH, H. 2016. New bioactive metabolites from penicillium purpurogenum mm. *Zeitschrift für Naturforschung B*, 71, 287-295.
- SHAH, U., SHAH, R., ACHARYA, S. & ACHARYA, N. 2013. Novel anticancer agents from plant sources. *Chin J Nat Med*, 11, 16-23.
- SHASHKOV, A. S., NIFANT'EV, N. E., AMOCHAEVA, V. Y. & KOCHETKOV, N. K. 1993. 1h and 13c nmr data for 2-o-, 3-o-and 2, 3-di-o-glycosylated methyl α -and β -d-galactopyranosides. *J Magn Res Chem*, 31, 599-605.
- SIALA, W., MINGEOT-LECLERCQ, M.-P., TULKENS, P. M., HALLIN, M., DENIS, O. & VAN BAMBEKE, F. 2014. Comparison of the antibiotic activities of daptomycin, vancomycin, and the investigational fluoroquinolone delafloxacin against biofilms from staphylococcus aureus clinical isolates. *J Antimicrob Agents Chemother*, 58, 6385.
- SIMOBEN, C., NTIE-KANG, F. & SIPPL, W. Development of a drug-like natural product library from the east african flora. ABSTRACTS OF PAPERS OF THE AMERICAN CHEMICAL SOCIETY, 2018. AMER CHEMICAL SOC 1155 16TH ST, NW, WASHINGTON, DC 20036 USA.
- SINGH, A. P., SINGH, A. K., BEGUM, A. S. & SAHAI, M. 2003. Two acyl sucroses from petunia nyctaginiflora. *Phytochemistry*, 63, 485-489.
- SINGH, R., RAY, P., DAS, A. & SHARMA, M. 2010. Penetration of antibiotics through staphylococcus aureus and staphylococcus epidermidis biofilms. *J Antimicrob Chemother*, 65, 1955-1958.
- SINGH, S. B. & BARRETT, J. F. 2006. Empirical antibacterial drug discovery—foundation in natural products. *Biochem Pharmacol*, 71, 1006-1015.
- SLIWOSKI, G., KOTHIWALE, S., MEILER, J. & LOWE, E. W. 2014. Computational methods in drug discovery. *Pharmacol Rev*, 66, 334-395.
- SÖDERSTRÖM, B. E. & BÅÅTH, E. 1978. Soil microfungi in three swedish coniferous forests. *Ecography*, 1, 62-72.
- SOLA, A., RODRÍGUEZ, S., GANCEDO, A. G., VILAS, P. & GIL-FERNÁNDEZ, C. 1986. Inactivation and inhibition of african swine fever virus by monoolein, monolinolein, and γ -linolenyl alcohol. *Arch Virol*, 88, 285-292.

- SOYOUNG, K., YOOJEONG, J., YOUNGSHIM, C. & TAESUN, P. 2011. Resveratrol exerts anti-obesity effects via mechanisms involving down-regulation of adipogenic and inflammatory processes in mice. *Proc Nutr Soc*, 70.
- SPERRY, S., SAMUELS, G. J. & CREWS, P. 1998. Vertinoid polyketides from the saltwater culture of the fungus trichoderma longibrachiatum separated from a haliclona marine sponge. *J Org Chem*, 63, 10011-10014.
- SRIVASTAVA, V., DAROKAR, M. P., FATIMA, A., KUMAR, J., CHOWDHURY, C., SAXENA, H. O., DWIVEDI, G. R., SHRIVASTAVA, K., GUPTA, V. & CHATTOPADHYAY, S. 2007. Synthesis of diverse analogues of oenostacin and their antibacterial activities. *Bioorg Med Chem*, 15, 518-525.
- STEINBERG, P. D. & DE NYS, R. 2002. Chemical mediation of colonization of seaweed surfaces1. *J Phycol*, 38, 621-629.
- STEWART, P. S., DAVISON, W. M. & STEENBERGEN, J. N. 2009. Daptomycin rapidly penetrates a staphylococcus epidermidis biofilm. *Antimicrob Agents Chemother*, 53, 3505.
- STIERLE, A. C., CARDELLINA, J. H. & STROBEL, G. A. 1988. Maculosin, a host-specific phytotoxin for spotted knapweed from alternaria alternata. *Proc Nat Acad Sci* 85, 8008-8011.
- STOESSL, A., FISCH, M. H. & ARDITTI, J. 1980. Monolinolein as a selective fungus inhibitor from cymbidium, orchidaceae. *Mycopathologia*, 70, 131-134.
- STONE, J. K., BACON, C. W. & WHITE, J. 2000. An overview of endophytic microbes: Endophytism defined. *Microb Endophytes*, 3, 29-33.
- STROBEL, G. & DAISY, B. 2003. Bioprospecting for microbial endophytes and their natural products. *Microbiol Mol Biol Rev*, 67, 491-502.
- STROBEL, G., FORD, E., WORAPONG, J., HARPER, J. K., ARIF, A. M., GRANT, D. M., FUNG, P. C. & CHAU, R. M. W. 2002. Isopestacin, an isobenzofuranone from pestalotiopsis microspora, possessing antifungal and antioxidant activities. *Phytochem Rev*, 60, 179-183.
- STROBEL, G. A. 2002. Rainforest endophytes and bioactive products. *Crit Rev Microbiol*, 22, 315-333.
- STROBEL, G. A. 2003. Endophytes as sources of bioactive products. *Microbes Infect*, 5, 535-544.
- STUART, K. A., WELSH, K., WALKER, M. C. & EDRADA-EBEL, R. 2020. Metabolomic tools used in marine natural product drug discovery. *Expert Opin Drug Discovery*, 15, 499-522.
- STURZ, A. & NOWAK, J. 2000. Endophytic communities of rhizobacteria and the strategies required to create yield enhancing associations with crops. *Appl Soil Ecol*, 15, 183-190.
- SUMNER, L. W., MENDES, P. & DIXON, R. A. 2003. Plant metabolomics: Large-scale phytochemistry in the functional genomics era. *Phytochemistry*, 62, 817-836.
- SUN, P., XU, D.-X., MANDI, A., KURTAN, T., LI, T.-J., SCHULZ, B. & ZHANG, W. 2013. Structure, absolute configuration, and conformational study of 12-membered macrolides from the fungus dendrodochium sp. Associated with the sea cucumber holothuria nobilis selenka. *J Org Chem*, 78, 7030-7047.
- SÜNTAR, I. 2019. Importance of ethnopharmacological studies in drug discovery: Role of medicinal plants. *Phytochem Rev*, 1-11.
- SURYANARAYANAN, T. S. 2012. Fungal endosymbionts of seaweeds. In: RAGHUKUMAR, C. (ed.) *Biology of marine fungi*. Berlin: Springer-Verlag.
- SWANTON, E. 1914. Economic and folk lore notes. *Trans British Mycol Soc*, 5, 408-409.
- SWANTON, E. 1932. Sussex county magazine. *Eastbourne: TR Beckett*.
- TAKAHASHI, Y., ITABASHI, Y., SUZUKI, M. & KUKSIS, A. 2001. Determination of stereochemical configuration of the glycerol moieties in glycolipids by chiral phase high-performance liquid chromatography. *Lipids*, 36, 741-748.
- TANG, L., HYUN, M. W., YUN, Y. H., SUH, D. Y., KIM, S. H. & SUNG, G. H. 2012. New record of mariannaea elegans var. Elegans in korea. *Mycobiology*, 40, 14-19.
- TANI, Y., NAKAMURA, K., SAWA, R., NISHIO, M., SAITO, S., ITO, M., ITONORI, S. & MIHARA, H. 2013. Novel neogala-series glycosphingolipids with a terminal glucose residue from the fungus mariannaea elegans. *Biosci Biotechnol Biochem*, 77, 754-759.
- TAURA, F., IJIMA, M., YAMANAKA, E., TAKAHASHI, H., KENMOKU, H., SAEKI, H., MORIMOTO, S., ASAKAWA, Y., KUROSAKI, F. & MORITA, H. 2016. A novel class of plant type iii polyketide

- synthase involved in orsellinic acid biosynthesis from rhododendron dauricum. *Front Plant Sci*, 7, 1452.
- TAVERNIER, M., DELATTRE, C., PETIT, E. & MICHAUD, P. 2008. B-(1, 4)-polyglucuronic acids—an overview. *Open Biotechnol J*, 2.
- TAWFIKE, A. F., ROMLI, M., CLEMENTS, C., ABBOTT, G., YOUNG, L., SCHUMACHER, M., DIEDERICH, M., FARAG, M. & EDRADA-EBEL, R. 2019. Isolation of anticancer and anti-trypanosome secondary metabolites from the endophytic fungus aspergillus flocculus via bioactivity guided isolation and ms based metabolomics. *J Chromatogr B Analyt Technol Biomed Life Sci*, 1106-1107, 71-83.
- TAWFIKE, A. F., VIEGELMANN, C. & EDRADA-EBEL, R. 2013. Metabolomics and dereplication strategies in natural products. *Methods Mol Biol*, 1055, 227-244.
- TAYLOR, W. R. & RAO, Q. 1957. *Marine algae of the northeastern coast of north america*, Ann Arbor, University of Michigan Press
- TENGURIA, R. K., KHAN, F. N. & QUERESHI, S. 2011. Endophytes-mines of pharmacological therapeutics. *World J Sci Technol*, 1, 127-149.
- TERRETT, N. K., GARDNER, M., GORDON, D. W., KOBYLECKI, R. J. & STEELE, J. 1995. Combinatorial synthesis—the design of compound libraries and their application to drug discovery. *Tetrahedron*, 51, 8135-8173.
- THAKUR, D., BORA, T., BORDOLOI, G. & MAZUMDAR, S. 2009. Influence of nutrition and culturing conditions for optimum growth and antimicrobial metabolite production by streptomyces sp. 201. *J Mycol Med*, 19, 161-167.
- THINES, E., ANKE, H. & STERNER, O. 1998. Scytalols a, b, c, and d and other modulators of melanin biosynthesis from scytalidium sp. 36-93. *J Antibiot (Tokyo)*, 51, 387-393.
- TOYA, Y. & SHIMIZU, H. 2013. Flux analysis and metabolomics for systematic metabolic engineering of microorganisms. *Biotechnol Adv*, 31, 818-826.
- TURNER, J. L., DRITZ, S., HIGGINS, J. J. & MINTON, J. E. 2002. Effects of ascophyllum nodosum extract on growth performance and immune function of young pigs challenged with salmonella typhimurium. *J Animal Sci*, 80, 1947-1953.
- V SIMOBEN, C., IBEZIM, A., NTIE-KANG, F., N NWODO, J. & L LIFONGO, L. 2015. Exploring cancer therapeutics with natural products from african medicinal plants, part i: Xanthenes, quinones, steroids, coumarins, phenolics and other classes of compounds. *Anti-Cancer Agents Med Chem*, 15, 1092-1111.
- VERVOORT, H. C., DRAŠKOVIĆ, M. & CREWS, P. 2011. Histone deacetylase inhibitors as a tool to up-regulate new fungal biosynthetic products: Isolation of egm-556, a cyclodepsipeptide, from microascus sp. *Organic Lett*, 13, 410-413.
- WALL, P. E. 2005. *Thin-layer chromatography: A modern practical approach*, Cambridge, Royal Society of Chemistry.
- WALSH, C. 2003. Where will new antibiotics come from? *Nature Rev Microbiol*, 1, 65-70.
- WANG, J.-M., DING, G.-Z., FANG, L., DAI, J.-G., YU, S.-S., WANG, Y.-H., CHEN, X.-G., MA, S.-G., QU, J. & XU, S. 2010. Thiodiketopiperazines produced by the endophytic fungus epicoccum nigrum. *J Nat Prod*, 73, 1240-1249.
- WATANABE, K. & OIKAWA, H. 2007. Robust platform for de novo production of heterologous polyketides and nonribosomal peptides in escherichia coli. *Org Biomol Chem*, 5, 593-602.
- WERNER, A. & KRAAN, S. 2004. *Review of the potential mechanisation of kelp harvesting in ireland*, Galway, Ireland, Marine Inst.
- WIKLUND, S. 2008. Multivariate data analysis for omics. *Umeå: Umetrics AB*.
- WILLIAMS, S. D., BIRCH, R., EINHORN, L. H., IRWIN, L., GRECO, F. A. & LOEHRER, P. J. 1987. Treatment of disseminated germ-cell tumors with cisplatin, bleomycin, and either vinblastine or etoposide. *New England J Med*, 316, 1435-1440.
- WINGENDER, J. & FLEMMING, H.-C. 2011. Biofilms in drinking water and their role as reservoir for pathogens. *Int J Hygiene Environl Health*, 214, 417-423.

- WOLD, S. & SJÖSTRÖM, M. 1998. Chemometrics, present and future success. *Chemomet Intell Lab Syst*, 44, 3-14.
- WORTHINGTON, R. J., RICHARDS, J. J. & MELANDER, C. 2014. Non-microbicidal control of bacterial biofilms with small molecules. *J Anti-Infective Agents*, 12, 120-138.
- WRIGHT, G. D. 2014. Something old, something new: Revisiting natural products in antibiotic drug discovery. *Can J Microbiol*, 60, 147-154.
- WRZOSEK, L., MIQUEL, S., NOORDINE, M. L., BOUET, S., JONCQUEL CHEVALIER-CURT, M., ROBERT, V., PHILIPPE, C., BRIDONNEAU, C., CHERBUY, C., ROBBE-MASSELOT, C., LANGELLA, P. & THOMAS, M. 2013. Bacteroides thetaiotaomicron and faecalibacterium prausnitzii influence the production of mucus glycans and the development of goblet cells in the colonic epithelium of a gnotobiotic model rodent. *BMC Biol*, 11, 61.
- WU, C., KIM, H. K., VAN WEZEL, G. P. & CHOI, Y. H. 2015. Metabolomics in the natural products field—a gateway to novel antibiotics. *Drug Discov Today: Technologies*, 13, 11-17.
- WU, C., TAN, Y., GAN, M., WANG, Y., GUAN, Y., HU, X., ZHOU, H., SHANG, X., YOU, X. & YANG, Z. 2013. Identification of elaiophylin derivatives from the marine-derived actinomycete streptomyces sp. 7-145 using pcr-based screening. *J Nat Prod*, 76, 2153-2157.
- WU, Y.-H., ZHANG, Z.-H., ZHONG, Y., HUANG, J.-J., LI, X.-X., JIANG, J.-Y., DENG, Y.-Y., ZHANG, L.-H. & HE, F. 2017. Sumalactones a–d, four new curvularin-type macrolides from a marine deep sea fungus penicillium sumatrense. *J RSC advances*, 7, 40015-40019.
- WU, Y., XIA, G., ZHANG, W., CHEN, K., BI, Y., LIU, S., ZHANG, W. & LIU, R. 2020. Structural design and antimicrobial properties of polypeptides and saccharide-polypeptide conjugates. *J Mater Chem B*, 8, 9173-9196.
- WU, Z., LIU, D., HUANG, J., PROKSCH, P., ZHU, K. & LIN, W. 2018. Hansforesters a–m, polyesters from the sponge-associated fungus hansfordia sinuosae with antibacterial activities. *RSC Adv*, 8, 39756-39768.
- WÜTHRICH, K. 1986. Nmr with proteins and nucleic acids. *Europhysics News*, 17, 11-13.
- XIE, Z., SIDDIQI, N. & RUBIN, E. J. 2005. Differential antibiotic susceptibilities of starved mycobacterium tuberculosis isolates. *Antimicrob Agents Chemother*, 49, 4778-4780.
- XU, J., KJER, J., SENDKER, J., WRAY, V., GUAN, H., EDRADA, R., MÜLLER, W. E., BAYER, M., LIN, W. & WU, J. 2009. Cytosporones, coumarins, and an alkaloid from the endophytic fungus pestalotiopsis sp. Isolated from the chinese mangrove plant rhizophora mucronata. *J Bioorganic medicinal chemistry*, 17, 7362-7367.
- XU, L., LI, Y., DAI, Y. & PENG, J. 2018. Natural products for the treatment of type 2 diabetes mellitus: Pharmacology and mechanisms. *Pharmacol Res*, 130, 451-465.
- YAICH, H., GARNA, H., BESBES, S., PAQUOT, M., BLECKER, C. & ATTIA, H. 2011. Chemical composition and functional properties of ulva lactuca seaweed collected in tunisia. *J Food Chem*, 128, 895-901.
- YOSHIKAWA, M., YAMAGUCHI, S., KUNIMI, K., MATSUDA, H., OKUNO, Y., YAMAHARA, J. & MURAKAMI, N. 1994. Stomachic principles in ginger. Iii. An anti-ulcer principle, 6-gingesulfonic acid, and three monoacyldigalactosylglycerols, gingerglycolipids a, b, and c, from zingiberis rhizoma originating in taiwan. *Chem Pharm Bull (Tokyo)*, 42, 1226-1230.
- YU, C.-M., FATHI-AFSHAR, Z. R., CURTIS, J. M., WRIGHT, J. L. C. & AYER, S. W. 1996. An unusual fatty acid and its glyceride from the marine fungus microsphaeropsis olivacea. *Can J Chem*, 74, 730-735.
- YU, H., ZHANG, L., LI, L., ZHENG, C., GUO, L., LI, W., SUN, P. & QIN, L. 2010. Recent developments and future prospects of antimicrobial metabolites produced by endophytes. *Microbiol Res*, 165, 437-449.
- YULIANA, N. D., KHATIB, A., CHOI, Y. H. & VERPOORTE, R. 2011. Metabolomics for bioactivity assessment of natural products. *Phytother Res*, 25, 157-169.
- ZAINUDDIN, N., ALIAS, S. A., LEE, C. W., EBEL, R., OTHMAN, N. A., MUKHTAR, M. R. & AWANG, K. 2010. Antimicrobial activities of marine fungi from malaysia. *Botanica Marina*, 53, 507-513.

- ZAVARZINA, A. & ZAVARZIN, A. 2006. Laccase and tyrosinase activities in lichens. *Microbiology*, 75, 546-556.
- ZHANG, H. W., SONG, Y. C. & TAN, R. X. 2006. Biology and chemistry of endophytes. *Nat Prod Rep*, 23, 753-771.
- ZHANG, L., AN, R., WANG, J., SUN, N., ZHANG, S., HU, J. & KUAI, J. 2005. Exploring novel bioactive compounds from marine microbes. *Curr Opin Microbiol*, 8, 276-281.
- ZHANG, Y., MU, J., FENG, Y., KANG, Y., ZHANG, J., GU, P. J., WANG, Y., MA, L. F. & ZHU, Y. H. 2009. Broad-spectrum antimicrobial epiphytic and endophytic fungi from marine organisms: Isolation, bioassay and taxonomy. *Mar Drugs*, 7, 97-112.
- ZHAO, J., FU, Y., LUO, M., ZU, Y., WANG, W., ZHAO, C. & GU, C. 2012. Endophytic fungi from pigeon pea [*cajanus cajan* (L.) millsp.] produce antioxidant cajaninstilbene acid. *J Agric Food Chem*, 60, 4314-4319.
- ZHAO, Q., MANSOOR, T. A., HONG, J., LEE, C. O., IM, K. S., LEE, D. S. & JUNG, J. H. 2003. New lysophosphatidylcholines and monoglycerides from the marine sponge *stelletta* sp. *J Nat Prod*, 66, 725-728.
- ZHOU, H., YANG, Y.-B., DUAN, R.-T., YANG, X.-Q., ZHANG, J.-C., XIE, X.-G., ZHAO, L.-X. & DING, Z.-T. 2016a. Neopeapyran, an unusual furo [2, 3b] pyran analogue and turnagainolide c from a soil streptomycetes sp. S2236. *J Chin Chem Lett*, 27, 1044-1047.
- ZHOU, Y.-H., ZHANG, M., ZHU, R.-X., ZHANG, J.-Z., XIE, F., LI, X.-B., CHANG, W.-Q., WANG, X.-N., ZHAO, Z.-T. & LOU, H.-X. 2016b. Heptaketides from an endolichenic fungus *biatriospora* sp. And their antifungal activity. *J Nat Prod*, 79, 2149-2157.
- ZHU, F., CAI, J., WU, X., HUANG, J., HUANG, L., ZHU, J., ZHENG, Q., CEN, P. & XU, Z. 2013. The main byproducts and metabolic flux profiling of γ -PGA-producing strain *b. Subtilis* zju-7 under different pH values. *Journal of biotechnology*, 164, 67-74.
- ZHU, J. & KAUFMANN, G. F. 2013. Quo vadis quorum quenching? *Curr Opin Pharmacol*, 13, 688-698.
- ZHU, T. J., DU, L., HAO, P. F., LIN, Z. J. & GU, Q. Q. 2009. Citrinal a, a novel tricyclic derivative of citrinin, from an algicolous fungus *penicillium* sp. I-1-1. *J Chin Chem Lett*, 20, 917-920.
- ZILLA, M. K., QADRI, M., PATHANIA, A. S., STROBEL, G. A., NALLI, Y., KUMAR, S., GURU, S. K., BHUSHAN, S., SINGH, S. K., VISHWAKARMA, R. A., RIYAZ-UL-HASSAN, S. & ALI, A. 2013. Bioactive metabolites from an endophytic cryptosporiopsis sp. Inhabiting *clidemia hirta*. *Phytochemistry*, 95, 291-297.

9 Appendix

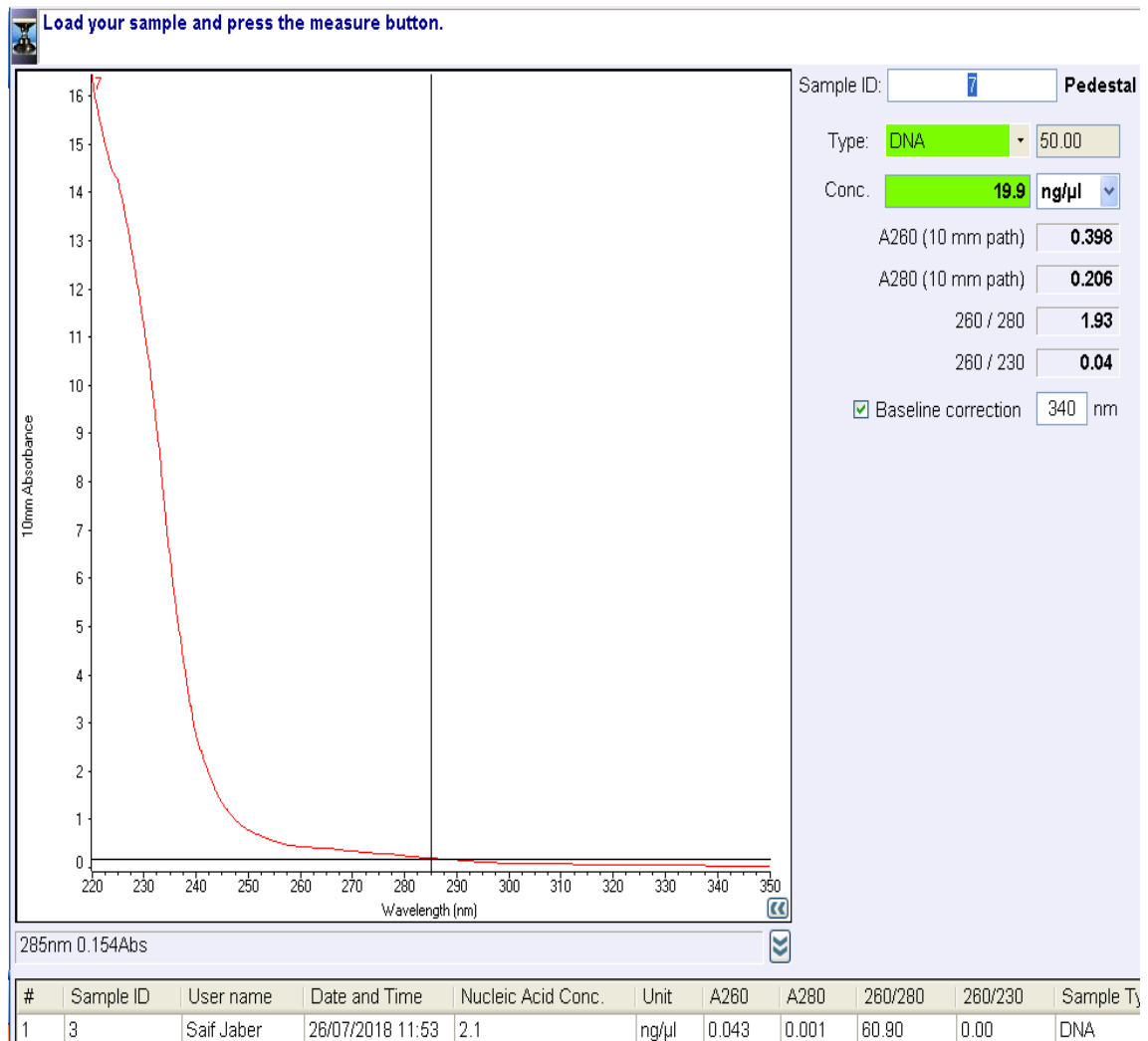


Figure 9.1: Nanodrop spectrophotometry for the calculation of *D. salina* DNA concentration.

sequence; and internal transcribed spacer 2, partial sequence

Sequence ID: [DQ307322.1](#) Length: 541 Number of Matches: 1

Range 1: 16 to 539 [GenBank](#) [Graphics](#)

[▼ Next Match](#) [▲ Previous Match](#)

Score	Expect	Identities	Gaps	Strand
968 bits(524)	0.0	524/524(100%)	0/524(0%)	Plus/Plus
Query 2	CCTCATCTCGGTGGGGGCTCCAGCTTGTCTGAATTATTCACCCATGTCTTTTGCGCACTT	61		
Sbjct 16	CCTCATCTCGGTGGGGGCTCCAGCTTGTCTGAATTATTCACCCATGTCTTTTGCGCACTT	75		
Query 62	CTTGTTCCTGGGCGGGTTCGCCCGCCACCAGGACCCAACCATAAACCTTTTTTGTAAAT	121		
Sbjct 76	CTTGTTCCTGGGCGGGTTCGCCCGCCACCAGGACCCAACCATAAACCTTTTTTGTAAAT	135		
Query 122	TGCAATCAGCGTCAGTAAACAATGTAATTATTACAACTTTCAACAACGGATCTCTTGGTT	181		
Sbjct 136	TGCAATCAGCGTCAGTAAACAATGTAATTATTACAACTTTCAACAACGGATCTCTTGGTT	195		
Query 182	CTGGCATCGATGAAGAACGCAGCGAAATGCGATACGTAGTGTGAATTGCAGAATTCAGTG	241		
Sbjct 196	CTGGCATCGATGAAGAACGCAGCGAAATGCGATACGTAGTGTGAATTGCAGAATTCAGTG	255		
Query 242	AATCATCGAATCTTTGAACGCACATTGCGCCCTTTGGTATTCCAAAGGGCATGCCTGTTC	301		
Sbjct 256	AATCATCGAATCTTTGAACGCACATTGCGCCCTTTGGTATTCCAAAGGGCATGCCTGTTC	315		
Query 302	GAGCGTCATTTGTACCCTCAAGCTTTGCTTGGTGTGGGCGTCTTTGTCTCTCACGAGAC	361		
Sbjct 316	GAGCGTCATTTGTACCCTCAAGCTTTGCTTGGTGTGGGCGTCTTTGTCTCTCACGAGAC	375		
Query 362	TCGCCTTAAAATGATTGGCAGCCGCGCTACTGGTTTCGGAGCGCAGCACAATCTTGCACT	421		
Sbjct 376	TCGCCTTAAAATGATTGGCAGCCGCGCTACTGGTTTCGGAGCGCAGCACAATCTTGCACT	435		
Query 422	TCTGATCAGCCATGGTTGAGCATCCATCAAGACCACATTTTCTCACTTTTGACCTCGGA	481		
Sbjct 436	TCTGATCAGCCATGGTTGAGCATCCATCAAGACCACATTTTCTCACTTTTGACCTCGGA	495		
Query 482	TCAGGTAGGGATACCCGCTGAACCTAAGCATATCAATAAGCGGA	525		
Sbjct 496	TCAGGTAGGGATACCCGCTGAACCTAAGCATATCAATAAGCGGA	539		

Figure 9.2: *D. salina* identification using NCBI blast database.

<input checked="" type="checkbox"/>	Dendryphiella salina strain TUBS den92 internal transcribed spacer 1, partial sequence; 5.8S ribosomal RNA gen... Paradendryphiell...	968	968	99%	0.0	100.00%	541
<input checked="" type="checkbox"/>	Dendryphiella salina strain TUBS Den90 internal transcribed spacer 1, partial sequence; 5.8S ribosomal RNA gen... Paradendryphiell...	968	968	99%	0.0	100.00%	533
<input checked="" type="checkbox"/>	Dendryphiella salina strain TUBS Den88 internal transcribed spacer 1, partial sequence; 5.8S ribosomal RNA gen... Paradendryphiell...	968	968	99%	0.0	100.00%	539
<input checked="" type="checkbox"/>	Dendryphiella salina strain TUBS Den82 internal transcribed spacer 1, partial sequence; 5.8S ribosomal RNA gen... Paradendryphiell...	968	968	99%	0.0	100.00%	535
<input checked="" type="checkbox"/>	Dendryphiella salina strain TUBS Den53 internal transcribed spacer 1, partial sequence; 5.8S ribosomal RNA gen... Paradendryphiell...	968	968	99%	0.0	100.00%	540
<input checked="" type="checkbox"/>	Dendryphiella arenaria strain TUBS Den37 internal transcribed spacer 1, partial sequence; 5.8S ribosomal RNA g... Paradendryphiell...	968	968	99%	0.0	100.00%	542
<input checked="" type="checkbox"/>	Dendryphiella arenaria strain TUBS Den32 internal transcribed spacer 1, partial sequence; 5.8S ribosomal RNA g... Paradendryphiell...	968	968	99%	0.0	100.00%	543
<input checked="" type="checkbox"/>	Dendryphiella salina strain TUBS 21 internal transcribed spacer 1, partial sequence; 5.8S ribosomal RNA gene, c... Paradendryphiell...	968	968	99%	0.0	100.00%	553
<input checked="" type="checkbox"/>	Dendryphiella salina strain TUBS 17 internal transcribed spacer 1, partial sequence; 5.8S ribosomal RNA gene, c... Paradendryphiell...	968	968	99%	0.0	100.00%	544
<input checked="" type="checkbox"/>	Dendryphiella salina strain TUBS 05 internal transcribed spacer 1, partial sequence; 5.8S ribosomal RNA gene, c... Paradendryphiell...	968	968	99%	0.0	100.00%	541

Figure 9.3: Blast results of the processed ITS sequenced using FinchTV

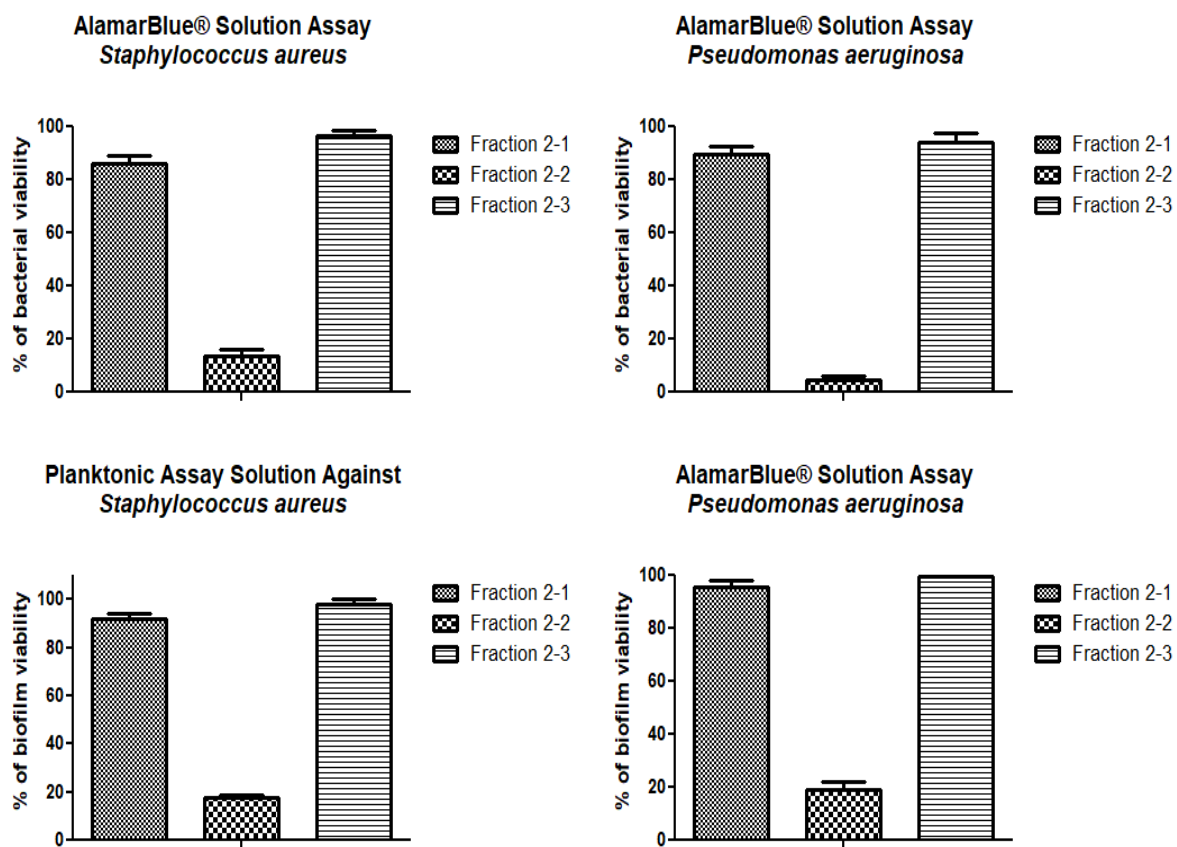


Figure 9.4: AlamarBlue® and planktonic assay results of fraction 2 subfractions of *D. salina* grown on malt extract broth against both biofilms forming *S. aureus* and *P. aeruginosa*.

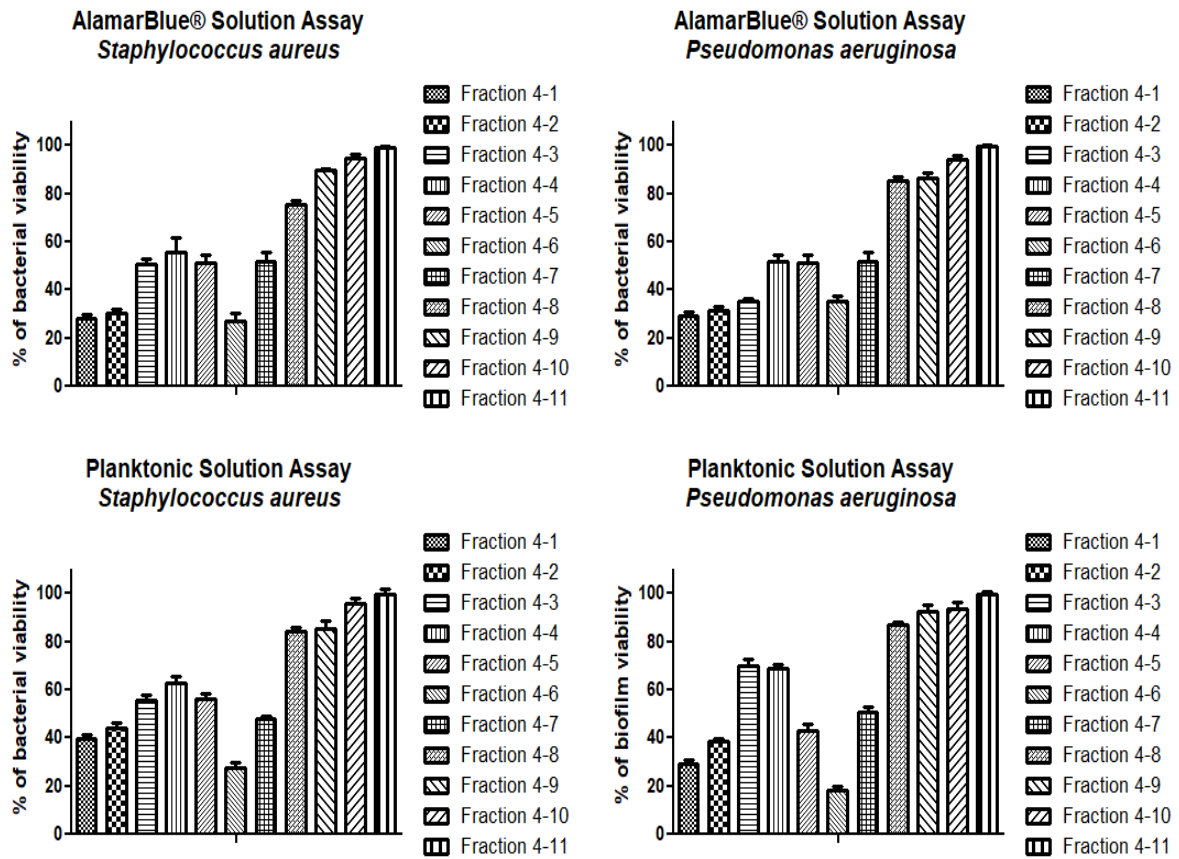


Figure 9.5: AlamarBlue® and planktonic assay results of fraction 4 subfractions of *D. salina* grown on malt extract broth against both biofilms forming *S. aureus* and *P. aeruginosa*.

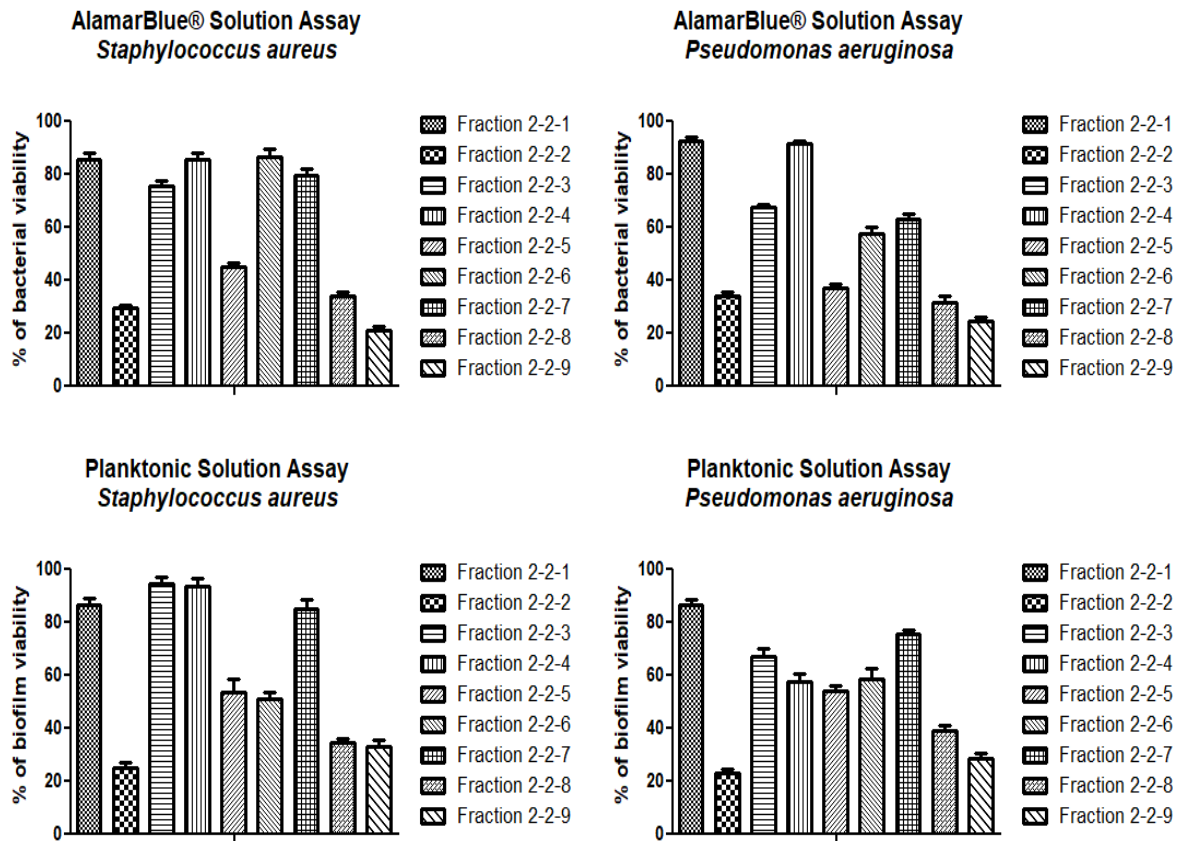
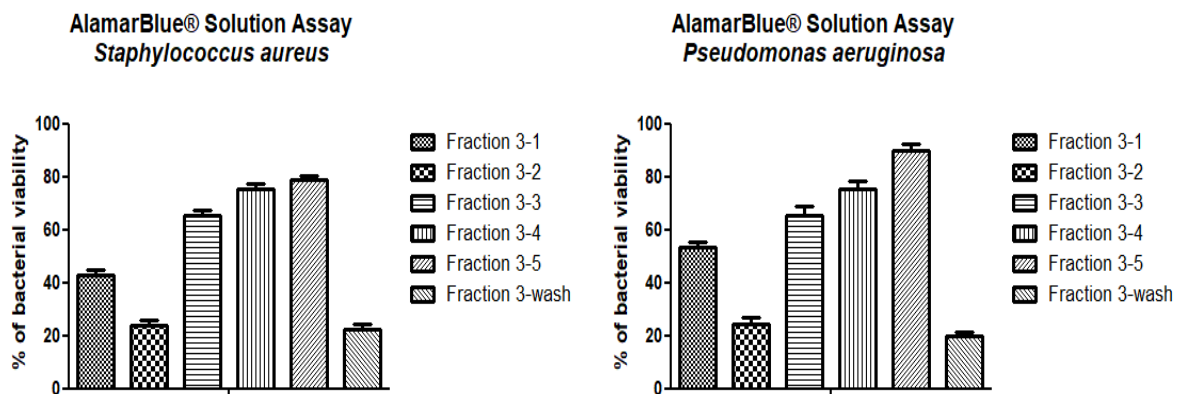


Figure 9.6: AlamarBlue® and planktonic assay results of fraction 2-2 subfractions of *D. salina* grown on Oat solid media against both biofilms forming *S. aureus* and *P. aeruginosa*.



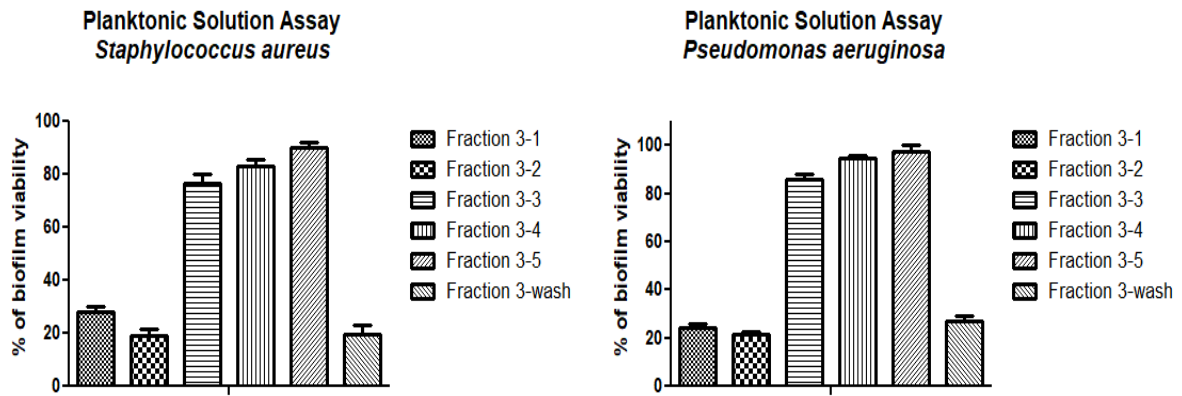


Figure 9.7: AlamarBlue® and planktonic assay results of fraction 3 subfractions of *D. salina* growing on Oat solid media against both biofilms forming *S. aureus* and *P. aeruginosa*.

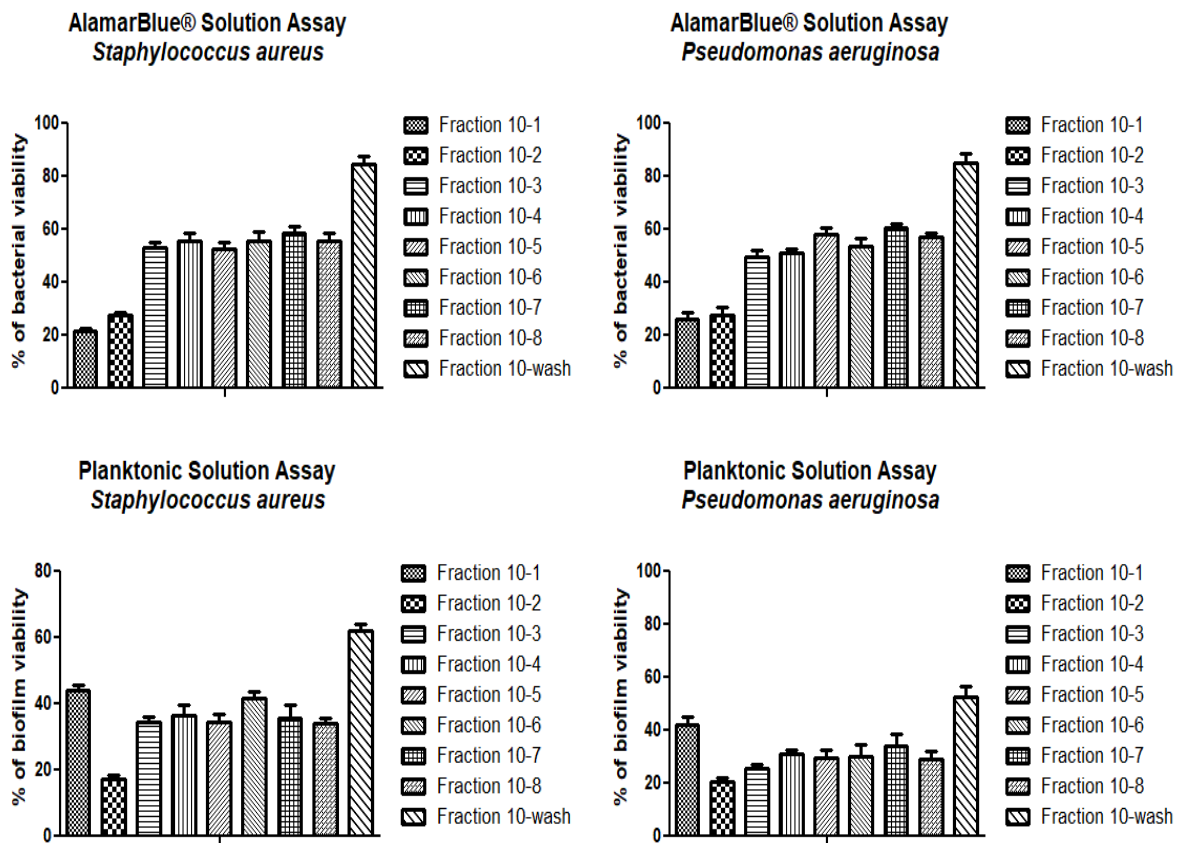


Figure 9.8: AlamarBlue® and planktonic assay results of fraction 10 subfractions of *D. salina* growing on Oat solid media against both biofilms forming *S. aureus* and *P. aeruginosa*.

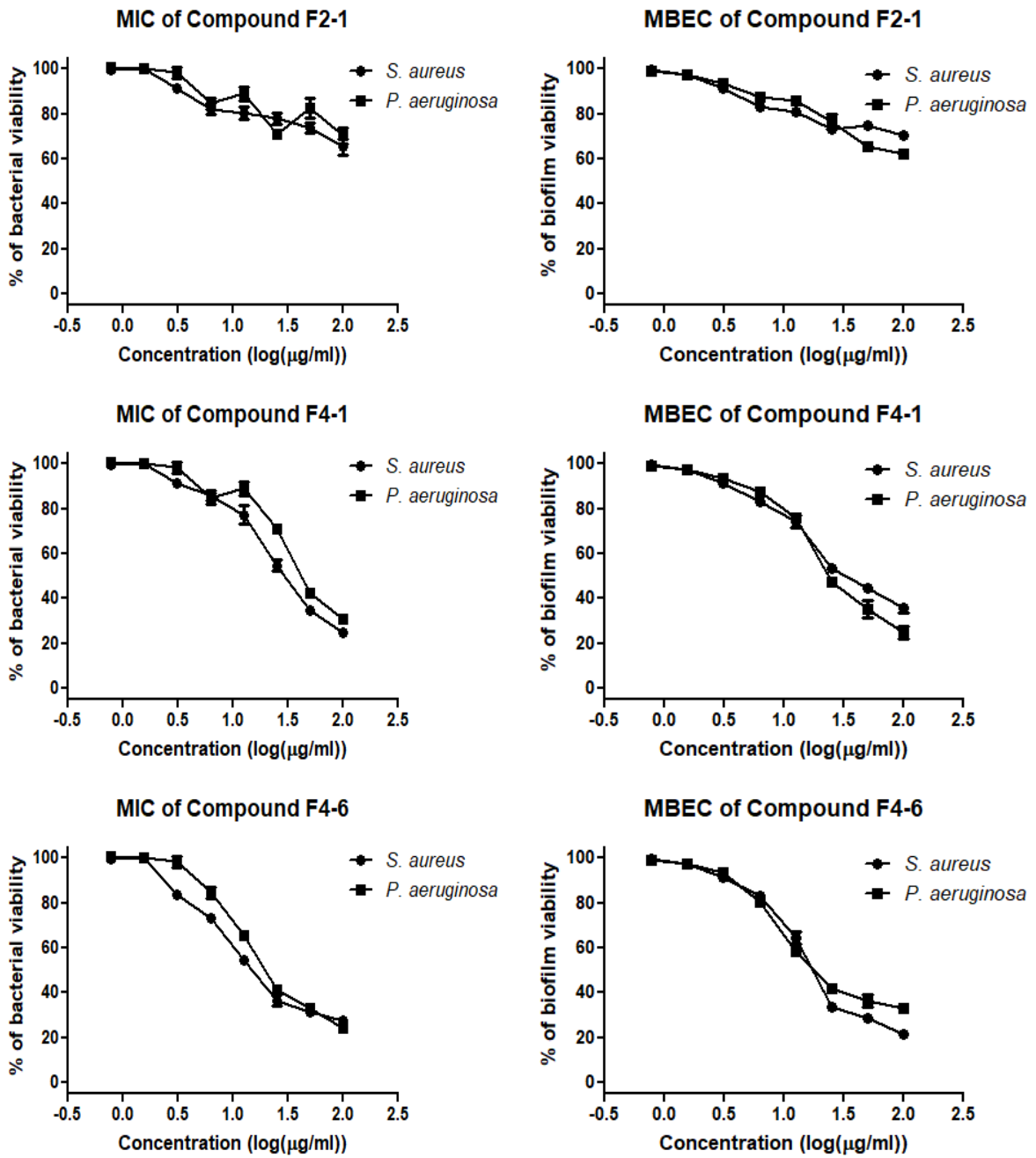


Figure 9.9: MIC and MBEC results of compound F2-1, F4-1 and F4-6 isolated from *D. salina* growing in Malt extract broth against both biofilms forming *S. aureus* and *P. aeruginosa*.

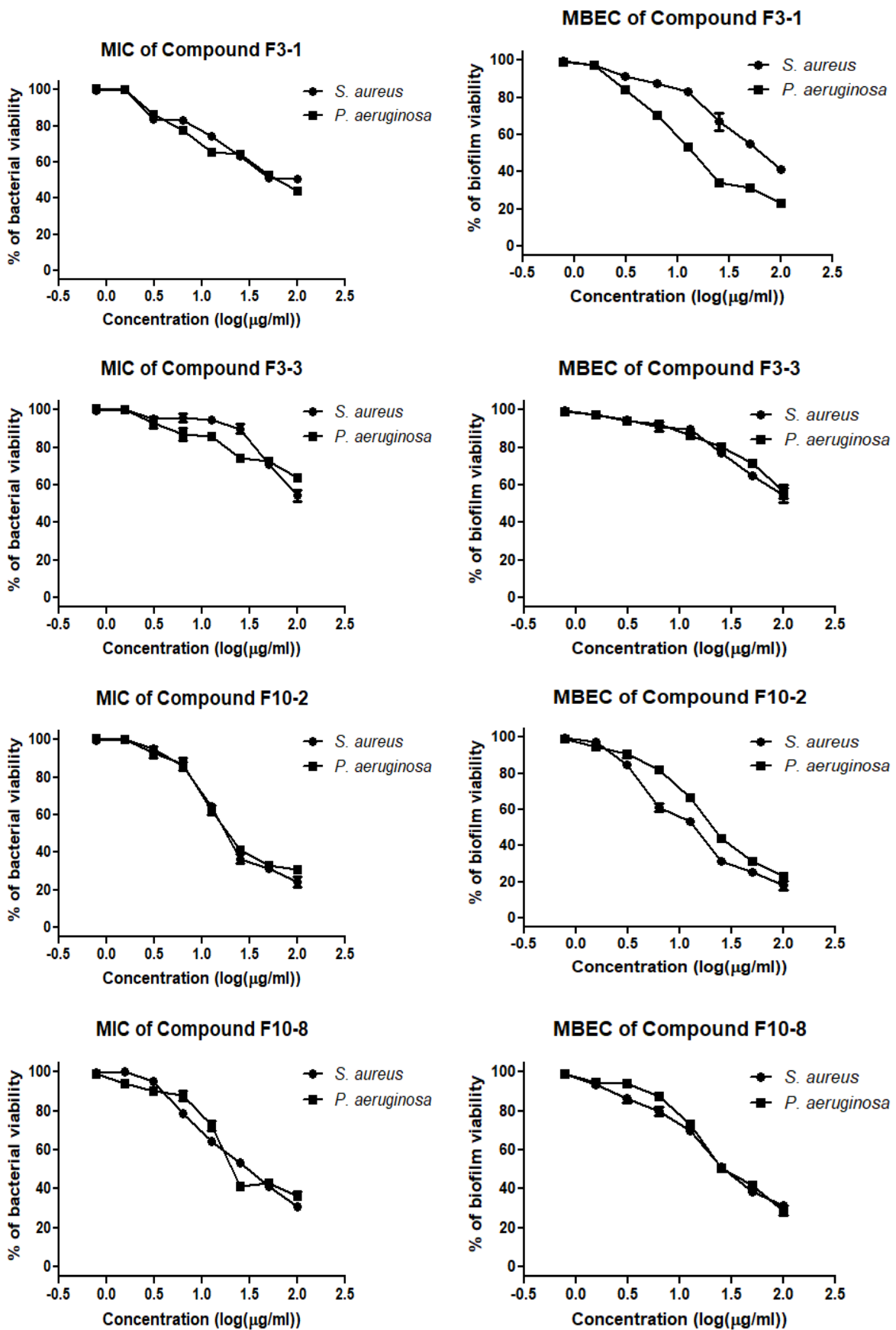


Figure 9.10: MIC and MBEC results of compounds F3-1, F3-3, F10-2 and F10-8 isolated from *D. salina* growing in oat solid media against both biofilms forming *S. aureus* and *P. aeruginosa*.

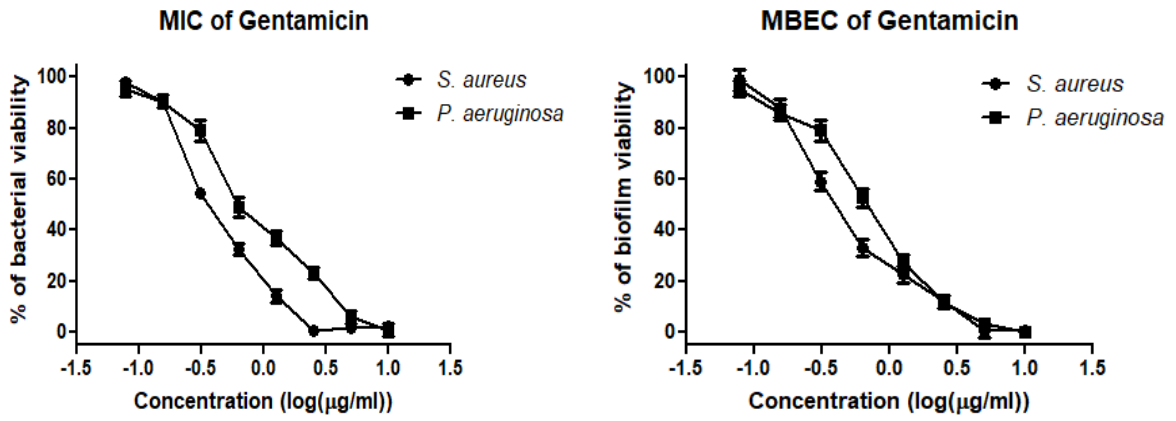


Figure 9.11: Gentamicin MIC and MBEC results against biofilm forming *S. aureus* and *P. aeruginosa*. Gentamicin used as a positive control.